DE GRUYTER
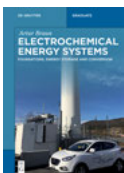
Thomas Zell, Robert Langer (Eds.)

HYDROGEN
STORAGE

BASED ON HYDROGENATION AND
DEHYDROGENATION REACTIONS OF
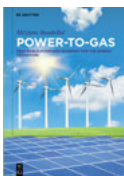## SMALL MOLECULES
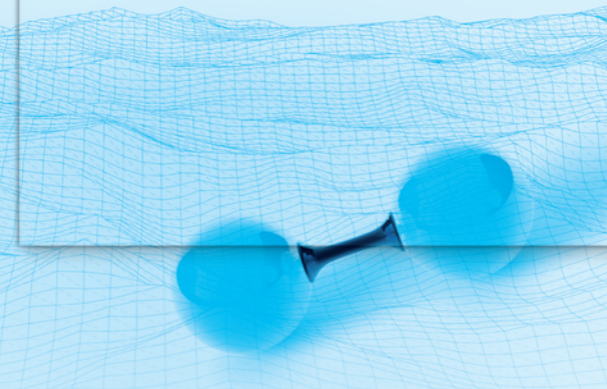
Thomas Zell, Robert Langer (Eds.)

Hydrogen Storage

Also of interest

Electrochemical Energy Systems.
Foundations, Energy Storage and Conversion
Braun, 2019
ISBN 978-3-11-056182-1, e-ISBN 978-3-11-056183-8

Power-to-Gas.
Renewable Hydrogen Economy for the Energy Transition
Boudellal, 2018
ISBN 978-3-11-055881-4, e-ISBN 978-3-11-055981-1

Hydrogen Storage Alloys.
With RE-Mg-Ni Based Electrodes
Han, Li, Liu, 2017
ISBN 978-3-11-050116-2, e-ISBN 978-3-11-050148-3
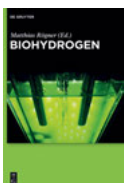
Biohydrogen.
Rögner (Ed.), 2015
ISBN 978-3-11-033645-0, e-ISBN 978-3-11-033673-3)

Chemical Energy Storage.
Schlögl (Ed.), 2012
ISBN 978-3-11-026407-4, e-ISBN 978-3-11-026632-0

Hydrogen Storage

Based on Hydrogenation and Dehydrogenation Reactions
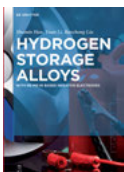of Small Molecules

Edited by
Thomas Zell, Robert Langer

DE GRUYTER

Editors
Dr. Thomas Zell
Team Leader and Project Manager
ADAMA Makhteshim Ltd.
PO Box 70
8410001 Beer Sheva
Israel
dr.zell@web.de

Dr. Robert Langer
Philipps-Universität Marburg
Fachbereich Chemie
Hans-Meerwein-Str. 4
35032 Marburg
Germany
robert.langer@chemie.uni-marburg.de

Preface

Today, more than ever before, the increasing change of our climate demands an immediate action. Consequently, changing demands on the global energy system require new innovative technologies. The development of new sustainable technologies for the production of energy is desirable. Besides focusing on the production step, also new and improved energy storage systems are needed to cope with peak energy productions and also provide an alternative to fossil fuels in the transportation sector. Requirements for these storage solutions will strongly depend on their application. In this context, storing energy by producing and consuming hydrogen is a very attractive approach. It may be suitable for storage of energy for transportation and also for the bulk energy storage. Due to physical restrictions of high pressure hydrogen storage, alternative techniques are developed. This is, in turn, an ongoing task with multidisciplinary aspects, which combines chemistry, physics, material science, and engineering.

This book provides overview on the concept of hydrogen storage based on hydrogenation and dehydrogenation reactions of small molecules. This is a promising approach, which is in most cases based on the use of Liquid Organic Hydrogen Carriers, so called LOHCs. We present selected examples of different types of hydrogen carriers. The book is structured according to functional groups in which the hydrogen can be stored. For each functional group at least one chapter is discussing the hydrogenation and the dehydrogenation steps. Different (potential) storage systems are in different development states and the authors critically discuss advantages and disadvantages of the storage systems.

We are very pleased that the book is composed of chapters written by the most outstanding scientists in the field. The authors, who are representatives from industry and from the most prestigious academic research institutes worldwide, were carefully chosen according to their expertise and all of them have an outstanding track record in the field. We would like to take the opportunity and express our gratitude to each and every contributor of this book. We are convinced that the passion and thought put into each chapter of this book will make it valuable for the education of graduate students and also for scientist of the field.

Beer Sheva, September 2018, Thomas Zell and
Marburg, September 2018, Robert Langer

Contents

Andrés Suárez

Jesús Campos

List of contributing authors

Thomas Schaub
Synthesis and Homogeneous
Catalysis
BASF SE
Carl-Bosch-Str. 38
67056 Ludwigshafen
Germany
thomas.schaub@basf.com

Monica Trincado
Department for Chemistry and Applied
Biosciences
ETH Zürich
Vladimir-Prelog-Weg 1
8093 Zürich
Switzerland
trincado@inorg.chem.ethz.ch

Hansjörg Grützmacher
Department for Chemistry and Applied
Biosciences
ETH Zürich
Vladimir-Prelog-Weg 1
8093 Zürich
Switzerland
hgruetzmacher@ethz.ch

Martin H. G. Prechtl
Department of Chemistry
Universität zu Köln
Greinstr. 6
50939 Köln
Germany
martin.prechtl@uni-koeln.de

Matthias Vogt
Institut für Anorganische Chemie und
Kristallographie
Universität Bremen
Fachbereich 2 Biologie/Chemie
Leobener Str. 7
28359 Bremen
Germany
mavogt@uni-bremen.de

Andrés Suárez
Instituto de Investigaciones Químicas
Consejo Superior de Investigaciones
Científicas
Avda. Américo Vespucio 49
41092 Sevilla
Spain
andres.suarez@iiq.csic.es

Jesús Campos
Instituto de Investigaciones Químicas
Consejo Superior de Investigaciones
Científicas
Avda. Américo Vespucio 49
41092 Sevilla
Spain
jesus.campos@iiq.csic.es

Moran Feller
Weizmann Institute of Science
Department of Organic Chemistry
76100 Rehovot
Israel
moran.feller@weizmann.ac.il

Daniël L. J. Broere
Universiteit Utrecht
Organic Chemistry & Catalysis
Debye Institute for Nanomaterials Science
Universiteitsweg 99
3584 CG Utrecht
Netherlands
d.l.j.broere@uu.nl

Zhuofeng Ke
School of Materials Science and Engineering
PCFM Lab
Sun Yat-sen University
510275 Guangzhou
PR China
kezhf3@mail.sysu.edu.cn

Yinwu Li
School of Materials Science and Engineering
PCFM Lab

Sun Yat-sen University
510275 Guangzhou
PR China

Cheng Hou
School of Materials Science
and Engineering
PCFM Lab
Sun Yat-sen University

510275 Guangzhou
PR China

Yan Liu
School of Materials Science and Engineering
PCFM Lab
Sun Yat-sen University
510275 Guangzhou
PR China

Thomas Zell and Robert Langer

1 Introduction: hydrogen storage as solution for a changing energy landscape

Abstract: The expansion of sustainable technologies and infrastructures for the production and delivery of energy to the final consumer and the development of new technologies for energy production, storage and distribution, are challenging and inevitable tasks. Power plants based on the combustion of fossil fuel resources or nuclear power plants are not suitable to provide energy in the future due to significant disadvantages and dangers associated with these outdated technologies. The development of new sustainable technologies for the production of energy is desirable. Besides focusing on the production step, the change in global energy landscape requires also new and improved energy storage systems. Requirements for these storage solutions will strongly depend on the application. Storing energy by producing and consuming hydrogen is in this context a very attractive approach. It may be suitable for storage of energy for transportation and also for the bulk energy storage. Due to physical restrictions of high pressure hydrogen storage, alternative techniques are developed. This is, in turn, an ongoing task with multidisciplinary aspects, which combines chemistry, physics, material science and engineering. Herein, we review the production and consumption of energy, different energy storage applications, and we introduce the concept of hydrogen storage based on hydrogenation and dehydrogenation reactions of small molecules.

Keywords: Energy Storage, Energy Transportation, Greenhouse Gases, Hydrogen Generation, Hydrogen Storage

1.1 Introduction

The continuously growing world population and dwindling resources of fossil fuels, raise the demand for alternative sources of energy. In addition, the combustion of those fossil fuels is the main source for the greenhouse gas carbon dioxide (CO_2) [1, 2]. Besides CO_2, depending on the combustion conditions, also other greenhouse gases such as methane (CH_4) and nitrous oxide (N_2O) may be formed in substantial amounts [3].

In this context it seems unfortunate that the world's energy demand is accommodated to a large extend by the combustion of fossil fuels such as coal, oil, and natural gas [3]. In the following paragraph, the distribution of the different energy sources is discussed on the example of the United States of America (US), one of the leading economies. It should be noted that the statistics on the energy may vary strongly in other countries.

1.2 Current energy landscape – US statistics

In 2016, for example, the overall energy production of the US was based to 33% on natural gas, to 28% on petroleum (which includes crude oil and natural gas liquids), to 17% on coal, to 12% on renewable energy, and to 10% on nuclear energy, Figure 1.1 [4]. Similar numbers are found for the US energy consumption of 2016, Figure 1.2. Taking a closer look at the electric energy generation shows that the relative percentage of renewable energy here slightly higher, but still underrepresented, Figure 1.3. The total electric energy produced in the US in 2016 was based to 30% on coal, to 34% natural gas, to 20% nuclear power, and to 15% on renewable energy, whereas oil/petroleum contributed less than 1% [4].

Total primary energy production, US, 2016: 8.39·10^{16} Btu

■ Natural gas (33%)   ■ Oil, petroleum* (28%)   ■ Coal (17%)
■ Renewable (12%)   ■ Nuclear (10%)
*includes crude oil and natural gas plant liquids
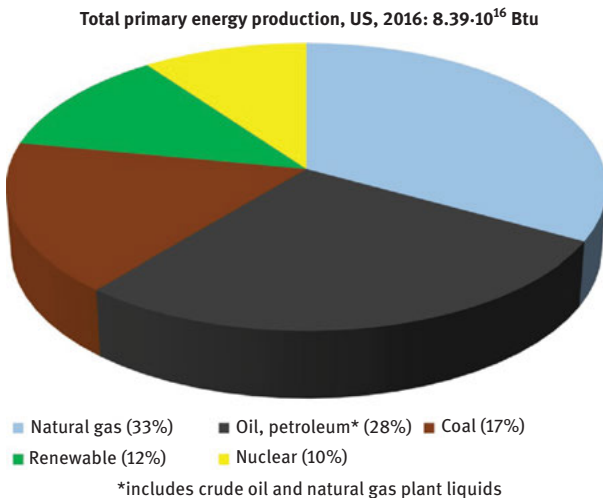
Figure 1.1: US overall energy production in 2016.

Interestingly, the CO_2 emissions of the residential sector are significantly smaller as one may expect. The statistics for the US of 2016 show that only 20% of the CO_2 emissions are attributed to the residential sector, whereas the vast majority stems from other sectors such as the transportation (36%), industrial (27%), and commercial sector (17%), Figure 1.4 [4].

For transforming to a more sustainable energy landscape, the reduction of CO_2 emissions is essential. This so called "Decarbonization" can be achieved by using CO_2-neutral technologies [5]. Attempts of CO_2 capture and subsequent transformation to useful chemical raw materials were discussed as possible solution for decreasing atmospheric CO_2 [6–17]. Especially over the last decades a wide array of synthetic methods for transforming CO_2 into various value-added products have been

Energy consumption, US, 2016: 9.74·10¹⁶ Btu

- Natural gas (29%) ■ Oil, petroleum* (37%) ■ Coal (15%)
- Renewable (10%) ■ Nuclear (9%)

*includes crude oil and naturl gas plant liquids
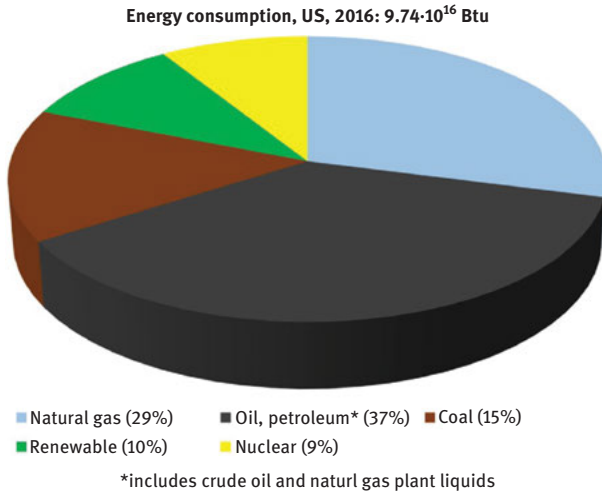
Figure 1.2: US energy consumption in 2016.

Total electricity production, US, 2016: 4.08·10¹⁶ kW-h

- Natural gas (34%) ■ Coal (30%) ■ Nuclear (20%)
- Renewable (15%) ■ Oil, petroleum* (<1%)
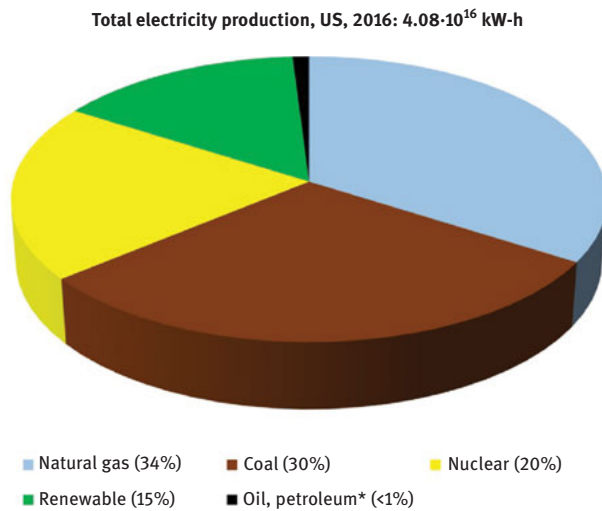
Figure 1.3: US overall electricity production in 2016.

developed [16]. Besides using CO_2 as C_1 building block this concept could in principle also reduces atmospheric CO_2, simply by the fact that no fossils feedstocks need to be consumed.

The use of nuclear energy as transition technology is often discussed in the context of reducing CO_2 emissions. The generation of electric energy by nuclear power plants is not sustainable and associated with risks for humanity and

CO2 emisssions according to sectors, US, 2016: 5.17·10^{12} kg

■ Transportation (36%)   ■ Industrial (27%)
■ Residential (20%)   ■ Commercial (17%)
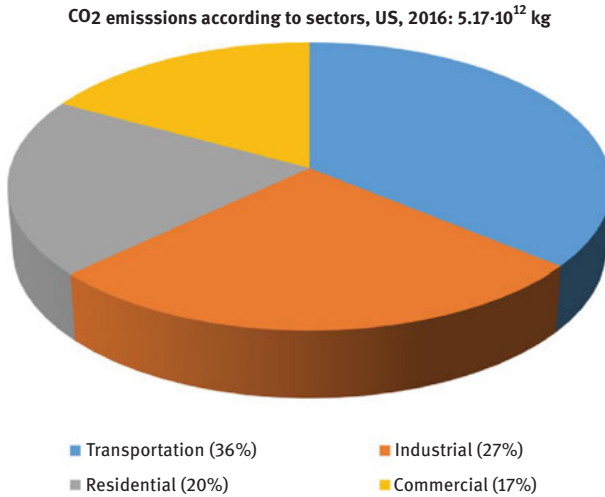
Figure 1.4: CO_2 emissions of the US in 2016 according to sectors.

environment [18]. Although supporters of this technology may claim that it can reduce global warming [19] by reduced green-house gas emissions and that the technology is getting safer year by year [20], the tremendous effects of accidents are disastrous, Fukushima being a recent example [21–25].

Along these lines, the US federal government defines as major energy accidents, incidents which either result in the loss of human lives or in the damage of property of over 50,000 US\$ [26]. In the years 1952–2009, worldwide 99 of those incidents have been reported, which fulfill the aforementioned criterion. The overall damage is summing up to an estimated 20.5 billion US\$. In terms of fatal incidents in that period (1952–2009), the nuclear energy sector lies on second place of all energy sources, number one being hydroelectric dams.

Besides the running facility, also the storage of nuclear waste is dangerous. Although deep geological disposal is thought to be the best solution for the final disposal of radioactive waste, it by far cannot be considered green or sustainable. Notably, there is and will not be a 100% safe solution for the storage of radioactive waste. It remains questionable, if this technology may currently be used during a transition period until the infrastructure for the use of renewable resources is fully developed.

However, given the clear disadvantages of nuclear energy, it is imperative that the infrastructure green, safe and sustainable alternative energies are developed.

Different technologies contribute to renewable energies. The 2016 statistics of the US' energy consumption show that in total 1.02×10^{16} BTU (=3.516×10^9 MWh) were in 2016 attributed to renewable energy consumption, Figure 1.5. This mix consists of hydroelectric power (24%), wind energy (21%), solar energy (6%),

geothermal energy (2%). In addition, biomass contributes 46%, out of which biofuels contribute 22%, wood contributes 19% and biomass waste contributes 5%. With 55%, a large part of the renewable energy is transformed to electric energy. In turn, ca. 15% of the electric energy produced in 2016 in the US stems from renewable energy, Figure 1.2.

Consuption of renewable energy, US, 2016: 1.02·10^{16} BTU

■ hydroelectric (28%)　■ wind (21%)　■ solar (6%)
■ geothermal (2%)　■ biofuels (22%)　■ biomass waste (5%)
■ wood (19%)
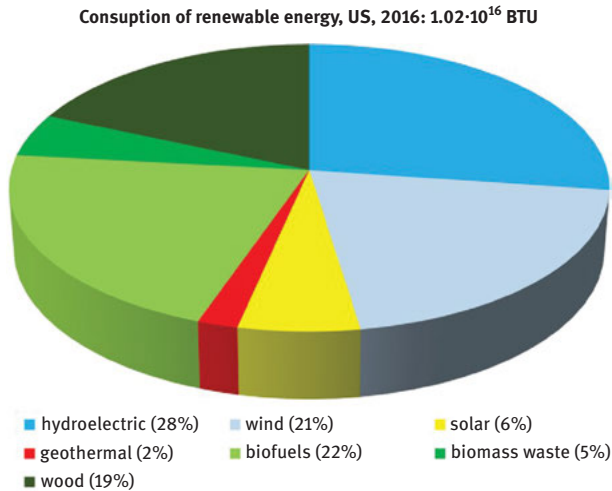
Figure 1.5: US energy consumption from renewable resources in 2016. Note, biomass (= biofuels + wood + biomass waste) is colored green.

1.3 Energy storage systems

There is no doubt that the production of energy from renewable resources needs to be expanded and that a shift towards green and sustainable energy sources is necessary. This change is essential in reducing the emissions of greenhouse gases and thereby reducing global warming.

　Whereas combustion of biomaterials (biofuels, wood, biomass waste) can be timed, some renewable energy sources which depend on the weather cannot be influenced (e. g. solar and wind energy can only be harvested when there is a sufficient amount of sunlight or wind). In order to compensate the gaps between demand and supply of energy, technologies for the storage of energy become important [27]. In practice, mismatches between the demand of electricity and the available electricity, for example from solar energy, necessitate cost effective energy storage solutions [28], as fluctuations of the energy supply can compromise the stability of the grid and the quality of the electricity from the grid.

　Although, the extensive discussion on different energy storage applications is beyond the scope of this work, knowledge of other storage systems is important as

they provide a benchmark for hydrogen storage. Notably, the best-suited storage system for a certain case is depending on the boundary conditions, and there is no ultimate solution for energy storage.

When discussing energy storage, one need to distinguish between stationary centralized storage, for large scale applications and stationary decentralized storage for smaller grids or distributed energy storage and mobile storage applications used for example in transportation or smaller portable devices.

Large scale centralized energy storage is best performed by pumped hydroelectric energy storage (PHES) or compressed air energy storage (CAES) but both have geographical constrains.

1.3.1 Large scale centralized energy storage

1.3.1.1 Pumped hydroelectric energy storage (PHES)

PHES stores potential energy of water and later on uses the kinetic energy of the falling or flowing water. In principle, this is hydropower that works like a battery [27, 29]. Off-peak electric energy may be used to pump water from a low-elevation reservoir to an elevated reservoir. This step transforms electric energy to gravitational potential energy. The resulting energy may be reused during periods of peak demand, by releasing the water again. The water flow is spinning a turbine, which generated electricity along the way. Interestingly, state of the art PHES facilities use pump turbines, which are bidirectional devices for pumping and electricity generation at the same time. This technique is highly efficient, reaching round-trip efficiencies of up to 85% [29, 30]. PHES is used to store energy from intermittent sources, such as wind, solar, and other renewables or excess electricity form continuous production. PHES facilities are with >96% of all tracked storage installation worldwide by far the most common energy storage solution with an overall storage capacity of 168 GW [31]. It may be mentioned, that as a rule of thumb ca. 50 km^2 are needed per 100 MW storage capacity [32]. Round trip efficiencies for this technology lie in the range of 70 – 75% [33].

1.3.1.2 Compressed air energy storage (CAES)

CAES is used mainly for storing excess energy of wind farms [34], but could in principle also be used, analogous to PHES, to store off-peak or excess stemming from different sources. Usually, the extra energy is used to compress air in preexisting underground caverns, such as salt domes or depleted gas fields. In practice operating pressures of 50 – 80 bar and an operation volume of 200 – 300 m^3 are needed for storing per 1 MWh [34]. Recently, CEAS systems successfully operating at >100 MWh were built. The drawbacks of this technology are the limited availability of sufficiently large and suited natural caverns necessary for large scale applications. Smaller scale storage can naturally be conducted using smaller caverns or storage cylinders. Using this technology, system

efficiencies of >50% can be achieved. In addition, for smaller storage applications the cycle lifetime is limited by the deterioration of the cylinders. In practice, life cycles in the order of magnitude of 10^4 can be achieved.

1.3.2 Smaller scale grids and distributed energy storage systems

1.3.2.1 Flywheel energy storage(FES)

Various technologies are available for energy storage in smaller scale grids and distributed energy storage systems. Flywheels are used to store kinetic energy in a rotating mass (called rotor). In FES energy can be transferred from and to the device as needed. The rotor is located either in a helium atmosphere or under vacuum, in order to reduce energy losses due to friction. The energy is transferred to the rotor via a power interface consisting of an electrical motor and generator. Technically, two classes of flywheels exist, conventional flywheels operating at frequencies around ca. 6,000 rev. min^{-1}, and advanced flywheels, rotating at frequencies up to 50,000 rev. min^{-1}. Steel FES has specific energies of ca. 5 Wh/kg, whereas highly sophisticated composite rotor achieve energy densities of up to ca. 100 Wh/kg. These systems employ magnetic bearings, a high speed magnetic lift system, and the flywheel is located in a vacuum sealed steel container. FES is a robust technology, allowing for fast energy uptake and release, many lifecycles (100,000 – 2,000,000), long lifetime (15 – 25 years), relatively high storage capacities (0 – 1,000 MW) and energy efficiencies of up to 90% can be achieved. The drawback of FES is the relatively high investment costs. For a system with 1 MW and 0.25 MWh, the total investment is about 750,000 – 2,000,000 US$. The high self-discharge rates limit FES to short term storage applications, such as uninterruptible power supplies (UPS) that involve frequent charging and discharging.

1.3.2.2 Superconducting magnetic energy storage (SMES)

An additional storage system is based on storage of electric energy in superconducting magnets. The storage is based on storing DC electricity in cryogenically cooled coils of the magnet at temperatures of –270°C. SMES has >97% efficiency (ohmic resistance in the coils) and can be charged and discharged instantaneously with a response time of milliseconds [30, 35]. Most SMESs, today, are used for mid-sized application and have capacities are in a range of 280 – 830 MWh and power outputs up to 2.5 MWh [36]. The obvious major drawback of SEMS is the relatively high operational costs due to the need for cooling to very low temperatures.

1.3.2.3 Electrochemical storage: batteries

Electrical energy can also be stored electrochemically, the most prominent examples being batteries. The development of various types of batteries is an ongoing field of

research. For selected review on batteries see [30, 37–43]. The storage of electric energy in rechargeable batteries is based on electro chemical half-cell reactions occurring at the cathode and anode, respectively. The common principle is that during the discharge, electrons flow from the anode to the cathode in an external circuit. In turn, cations flow within the electrolyte of the battery cell in the same direction, in order to maintain electro-neutrality. Depending on the materials varying energy densities can be achieved, but overall batteries are considered low density energy carriers, with energy densities in a range of ca. 30 – 300 Wh/kg [28]. Commercial high end batteries based on lithium carbon monofluoride reach energy densities somewhat below 500 Wh/kg [44].

1.3.2.4 Electrochemical capacitators (ECs)

Electrochemical capacitators (ECs) store energy in form of an electric field, which is generated by physical separation of charge between the two electrodes. Those systems are also called supercapacitors or ultracapacitors. For selected reviews on ECs see [45–49]. Notably, in contrast to batteries no chemical reactions take place. Contrary to conventional capacitors, in which the charge is stored on metallic sheets which are separated from each other by a dielectric membrane, in ECs there is an electrolyte which allows ion movement between the electrolyte and the electrode. The interface between electrolyte and electrode has a high surface area. This technique allows for a significant increase in storage capacity in comparison to conventional capacitors. Although this technology offers only low energy densities, the clear advantage of those systems is the possibility of extremely fast charging and recharging, as no chemical reactions take place. This leads to high power densities. A comparison with state of the art lithium ion batteries shows that in terms of storage capacity ECs are with ca 10 – 20 $/Wh ca. 10-fold more expensive than for Li ion batteries, however the cost per kW is lower [28]. The costs for ECs are lie in a range of 25 – 50 $/kW, whereas for Li-ion batteries it is 75 – 100 $/kW [28]. Due to moderately high discharge rates of ECs (ca. 5% per day), these systems are best suited for short terms storage.

1.3.2.5 Gravimetric battery

Besides using water as medium for storage also the potential gravimetric energy of solid masses can also be stored. Several pilot projects have been developed in this field, but so far these technologies do not have a significant commercial impact. Potential storage capacities of such systems vary depending on the size [33, 50–54].

1.3.2.6 Thermal energy storage systems

Energy is also stored in form of heat energy by warming up or melting a material. The energy stored can later on be reused by cooling down the storage medium. In other words, heating and cooling of a storage medium resembles charging and recharging

of the system with energy, respectively. This technique may have applications for waste heat recovery, solar energy utilization, energy saving in buildings, and electronic device management [30, 55].

1.3.2.7 Phase change materials (PCMs)

Phase change energy storage systems are a subcategory of thermal energy storage systems, which are suitable for latent heat storage. PCMs allow charging and recharging of the energy system with thermal energy during their phase change process. Advantages of this technique are higher energy storage capacities and small temperature alteration during the charging/recharging process. In principle, PCMs can be classified into solid/solid and solid/liquid systems depending on the phase change. Notably solid/solid absorbs or release heat during their crystal transition. Prominent examples of PCMs include polyalcohols, macromolecules, perovskites, and inorganic salts. For selected reviews on phase change energy storage, see [56–62].

1.3.2.8 Thermal chemical energy storage (TCES)

Similar to PCM systems, where the heat exchange is accompanied by a phase transition, also the heat energy of reversible reactions can also be used for energy storage [30]. TCES rely on different reversible chemical coordination processes, such as the absorption of the coordinating solvent (water, ammonia, or alcohol) to a metal salt. This can include liquid and solid absorption-desorption processes. Examples for the absorbate/absorbent couples are: $CaCl_2/H_2O$, Glycerin/H_2O, KOH/H_2O, LiBr/H_2O, LiCl/H_2O, NaOH/H_2O, and H_2O/NH_3 [63]. Advantages of this technology are high storage densities and robust systems with long lifetimes. These systems are used for the storage of electric energy. Thermal energy in a combined heat and power plant can be stored, when there is few demand on electricity and released to the grid at peak demands [64]. The corresponding energy storage cycle is based on: electric energy -> thermal (heat) energy -> chemical energy -> thermal (heat) energy -> electric energy. For selected reviews on this topic, see [62, 65–76].

1.4 Energy transportation

Besides storage, also the transportation and distribution of energy to the consumer is an important aspect. Often favorable renewable resources are located in remote areas, where the demand on energy is low and the energy needs to be transported. Building electricity lines from the places of renewable energy sources to populated cities, with a high demand on energy can be costly. In this context, the DESERTEC program may be mentioned here as selected example [77]. This program promotes the large scale production of solar and wind power in the desert regions of the world. This

energy should then be combined in a smart mix of the most efficient and abundant renewable energy sources (photovoltaic, hydropower, biomass, and geothermal energy). Whether the overall system is then to be distributed in a trans-national super grid using high voltage direct current lines is unclear due to the high investment costs.

One also needs to take into account mobile applications, which require energy. These include a wide variety of appliances, ranging from traditional electricity based appliances, such as cell phones, to large equipment like cars, trucks, boats, airplanes, and even space missiles. Air traffic is especially problematic due to the requirement for extremely high energy densities of the energy storage systems. Today's electric batteries simply do not offer high enough energy/weight ratios to make commercialization of electric flying feasible [78–80].

The current batteries have roughly 2% of the energy density of liquid fuels. Taking into account the low efficiency of combustion engines vs. the high efficiencies of electro motors, the relative energy density improves to ca. 7%. This means per kg of traditional fuel one would need to accommodate ca. 14 kg of battery in an airplane. This seems almost impossible and experts estimate that it will take 10 of years until the commercialization of such systems.

1.5 H$_2$ storage – production of hydrogen

For energy storage, in any case, energy needs to be transformed into so called secondary energy sources, which are namely electricity and hydrogen. Notably, secondary energy sources are produced from other energy sources, ideally from renewable ones.

The storage of energy in form of hydrogen (H$_2$) is a promising approach, which will contribute to a changing energy landscape [81]. H$_2$, like electricity, can be produced from various primary energy sources, such as water, fossil fuels, or biomass. In addition, it is a (by)product of some chemical reactions. There is a diverse portfolio of different technologies to produce hydrogen from non-renewable and renewable sources. In practice, three relevant technologies and combination thereof are used nowadays to for the industrial scale production of H$_2$ [82]. These processes are namely, steam reforming (for selected reviews see [83–86]), dry reforming (also called carbon dioxide reforming, for selected reviews see [83, 86–93]) and partial oxidation (for selected reviews see [83, 86, 94]). The majority of H$_2$ is today produced from steam reforming, which is probably the most established and practical technology [95]. Here, hydrocarbon fuels (such as natural gas) serve as starting materials for the production of H$_2$. The chemical equations of the process are given in Figure 1.6, using the example of methane. In the first reaction step, methane and water are transformed at high temperatures (700 – 1100°C) to syngas, a 3:1 mixture of hydrogen along with carbon monoxide (CO). This reaction is endothermic by ΔH^0(298K) = +206

Steam reforming:

$$CH_4 \;+\; H_2O \;\longrightarrow\; 3\,H_2 \;+\; CO$$

$$\Delta H_0(298K) = +\,206 \text{ kJ/mol}$$

Carbon dioxide (dry) reforming:

$$CH_4 \;+\; CO_2 \;\longrightarrow\; 2\,H_2 \;+\; 2\,CO$$

$$\Delta H_0(298K) = +\,247 \text{ kJ/mol}$$

Partial oxidation:

$$CH_4 \;+\; 0.5\,O_2 \;\longrightarrow\; 2\,H_2 \;+\; CO$$

$$\Delta H_0(298K) = -\,35 \text{ kJ/mol}$$

Water gas shift reaction:

$$CO \;+\; H_2O \;\longrightarrow\; H_2 \;+\; CO_2$$

$$\Delta H_0(298K) = -\,41 \text{ kJ/mol}$$
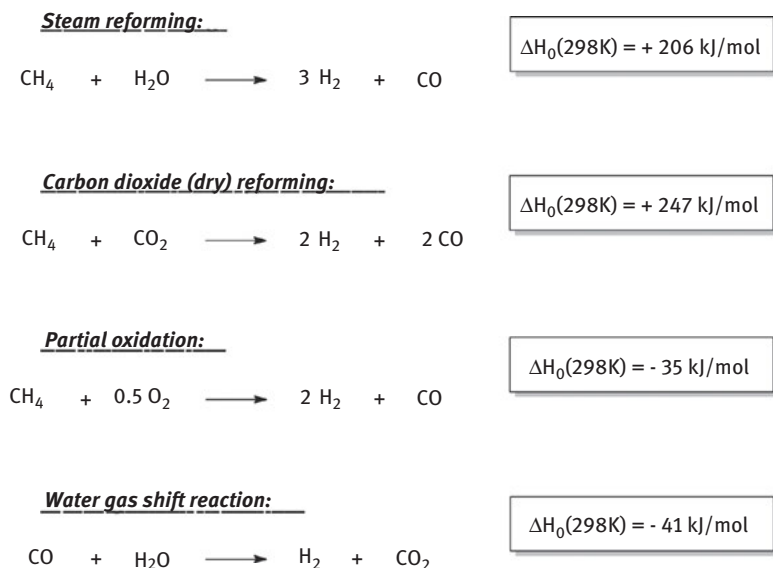
Figure 1.6: Different reactions for the production of H$_2$ gas from hydrocarbons (examples are shown for methane as starting material) and from carbon monoxide.

kJ/mol [82]. Similarly, for the dry reforming reaction, using not H$_2$O as oxygen source but CO$_2$, the reaction is highly endothermic with $\Delta H^O(298K) = +247$ kJ/mol, Figure 1.6 [82]. For both processes, the resulting CO can be converted in a second reaction to additional H$_2$ and CO$_2$ via the so called water gas shift reaction (WGSR). This reaction is exothermic, $\Delta H^O(298K) = -41$ kJ/mol, and is conducted at milder temperatures of around 360°C. Partial oxidation of natural gas or heating oil is an additional technique for the production of H$_2$ (Figure 1.6). Similar to the aforementioned steam and dry reforming to the reforming processes a CO/H$_2$ mixture is by combustion with a substoichiometric amount of oxygen (O$_2$). In case of methane as starting material this reaction is exothermic, $\Delta H^O(298K) = -35$ kJ/mol, but requires oxygen or air. Interestingly, these techniques for the production of hydrogen are not limited to fossil source but also biomass can be converted to H$_2$, for recent reviews on biomass conversion to H$_2$ see [96–100].

Much less common, due to an increased price, is the production of H$_2$ by electrolysis of water [95]. The primary source of energy for this process is electrical energy, which is with the current technologies too expensive to serve as source for H$_2$. More direct approaches, without paying the D-tour costs of electricity production, are economically more attractive. In the future, hydrogen would ideally be generated by electrolysis based on renewable energy sources [101].

Depending on the feedstocks and the technologies employed for the H$_2$ production, its commercial price varies strongly [95]. In addition, different

technologies have strongly varying carbon footprints [102]. Estimations for the production cost of coal-based H_2 lie in a range of 0.36 – 1.83 US\$/kg, whereas the costs for natural gas-based H_2 are estimated to be in a higher range of 2.48 – 3.17 US\$/kg. Hydrogen produced from coal has the highest carbon footprint of all technologies. Per ton of H_2 produced from coal, ca. 25 ton of CO_2 are emitted [102]. For comparison, other technologies such as electrolysis using electricity (ca. 16 – 18 ton(CO_2)/ton(H_2)) methane steam reforming (ca. 10 – 12 ton(CO_2)/ton(H_2)), biogasification (ca. 5 – 7 ton(CO_2)/ton(H_2)) or electrolysis using wind energy (ca. 0 – 2 ton(CO_2)/ton(H_2)) result in lower CO_2 emissions. Biomass as starting material is expected to result in costs of 1.44 – 2.83 US\$/kg, depending on cost and type of raw material. Wind energy-based H_2, depending on the specific set-up (size of wind turbines and type of electrolyzers) is estimated to cost around 5.50 US\$/kg. Electrolysis of water is with ca. 8.00 US\$/kg somewhat more expensive. Interestingly, based on current technologies, H_2 from solar energy is supposed to be three orders of magnitude more expensive than conventional H_2 produced from fossil fuels. From all the different technologies, which are available today, steam reforming of methane is supposed to be the most economic way to obtain H_2. Here the commercial price for the production is expected to vary in a range of 1.25 – 3.50 US\$/kg, depending on the size of the production plant.

Today, the worldwide production of H_2 is mainly based on fossil feedstocks (96%) [103]. Although with 4% underrepresented on commercial production scale, technologies for the H_2 production from renewable feedstocks exist. In practice most of the H_2 is produced in large centralized facilities with natural gas being the most common feedstock, being responsible for the production of 49% of H_2 worldwide. Natural gas is followed by oil (29%) and coal (18%). It is worth mentioning, however, that nonfossil resources could in principle be sufficient for the production of hydrogen in the US. If used only for this purpose, the amount of energy from biogas, biomass, nuclear power, wind, solar energy digester gas, and other waste streams would be enough to fuel 10 times the US vehicle fleet. This prognosis would hold true for the foreseeable future [104].

It becomes apparent that H_2 is available from a large variety of different feedstocks, which in principle allow H_2 production almost everywhere on the globe. H_2 as a new possible energy vector may also help to also circumvent the dependencies on other energy sources, such as fossil fuels, which come primarily from politically unstable regions [105]. It is even speculated that H_2, based on matured technologies may be the most ubiquitous fuel in the future.

1.6 Efficiencies of hydrogen economy

Already in 1972, Bockris has suggested to use hydrogen a source for energy transportation instead of electricity. With this visionary work the author has coined the expression "hydrogen economy" [106].

The biggest problem associated with the hydrogen economy today is the mediocre round-trip efficiencies [107]. The energy efficiency of typical electrolyzes lies currently around 70% energy efficiency. In practice however this is reduced significantly and 60% efficiency seems a still optimistic number. In 2008, the National Renewable Energy Laboratory conducted a market analysis and based on a questionnaire for manufacturers 53% efficiency was assumed [108]. For storage under pressure it can be estimated that the compression of H_2 to 100 bar costs about 10% of its energy content. Taken into account the 10% loss results in a 54% efficiency of energy to stored H_2.

In addition, the reconversion of H_2 to energy also needs to be considered [107]. Reconversion to electric energy is performed with fuel cells but could in principle also performed using gas/steam turbines. Good estimations for the corresponding efficiencies are 50% and 60%, respectively. This very optimistic estimation gives ca. 30% overall energy efficiency for electric energy storage as H_2.

An additional approach would be using the produced hydrogen and feeding it to the existing natural gas system [109]. Alternatively, the hydrogen could also be used for fuel cell based transportation by FCEVs. From an economical point of view, however, running electrolyzes at less than full capacity is in many cases unattractive due to their high initial investments.

1.7 Hydrogen storage – why hydrogen?

There are various reasons for hydrogen as new energy carrier [107]. Hydrogen has the highest energy content of all compounds and it can be converted to energy either by fuel cells or by combustion in internal combustion engines, leading to water as the sole byproduct. If air is used for the combustion of H_2 instead of oxygen, depending on the combustion conditions, beside water also nitrogen oxide (NO) can be formed at high temperatures.

Hydrogen's lower heating value at 25°C and 1 atm. is 119.93 kJ/g. Table 1.1 summarizes gravimetric heat contents of selected compounds (fuels) in comparison to H_2 [110].

Whereas H_2 features high gravimetric energy content its volumetric energy content is comparatively low at ambient pressure. Table 1.2 summarizes the volumetric energy densities of selected fuels. At 1 atm. pressure and 15°C, H_2 has only 31% of the energy content of methane and only 12% of the energy content of propane. This makes storage of energy in form of hydrogen problematic.

The low gravimetric energy content of gaseous H_2 necessitates storage under high pressure, cryogenic cooling, by absorption techniques or other means of storage such as storage in chemical reactions [107, 111]. Current fuel cell electric vehicles (FCEVs), such as hydrogen fueled cars [112–117], busses [115, 116, 118, 119], or trucks

Table 1.1: Heating values of selected compounds (fuels). Note, the lower and higher heating values are experimental results. The energy difference between the higher heating value and lower heating value is the sum of vaporization energies, needed to evaporate the fuel and water gas to liquid [110].

Fuel	Higher heating value (at 25°C and 1 atm), [kJ/g]	Lower heating value (at 25°C and 1 atm), [kJ/g]
Hydrogen	141.9	119.9
Methane	55.5	50.0
Propane	50.4	45.6
Gasoline	47.5	44.5
Diesel	44.8	42.5
Methanol	20.0	18.1

Table 1.2: Energy densities of selected compounds (fuels). Values for gases are given at different pressures [110].

Fuel	Energy densities, [MJ/m^3]
Hydrogen	10.05 (gas at 1 atm and 15°C)
	1825 (gas at 200 bar and 15°C)
	4500 (gas at 690 bar and 15°C)
	8491 (liquid)
Methane	32.56 (gas at 1 atm and 15°C)
	6860 (gas at 200 bar and 15°C)
	20920 (liquid)
Propane	86.67 (gas at 1 atm and 15°C)
	23489 (liquid)
Gasoline	31150 (liquid)
Diesel	31436 (minimum, liquid)
Methanol	15800 (liquid)

[120, 121], use mainly compressed hydrogen tanks systems in combination with fuel cell technology.

Interestingly, in September 2016, the first four-seater airplane, HY4, developed by the German Aerospace Center took off in Stuttgart, Germany [122]. This is the first example for a hydrogen fueled plane designed for the transportation of passengers. This prototype system works with a hybrid fuel cell/battery system. During a steady flight mode, only the hydrogen fuel cells deliver the energy for flying, and the battery systems assists only during take-off and landing, when more energy is needed. Independently also aircraft systems based hydrogen combustion have been tested [123]. Usually these prototypes use liquid hydrogen tanks.

Large scale hydrogen storage is less problematic compared to mobile applications. Systems, using subterranean caverns, such as salt domes, are used today commercially

already [107]. The Clemens Dome (TX, USA) with a volume of 580,000 m^3 is used to store H_2 with minimal losses (<0.01% loss/year) [124]. The middle range of pressure used in Texas is 100 bar. Assuming this pressure, the cavern would hold around 170 GWh of energy. Similar to the concept of energy storage by compressed air, CAES, also this technology is limited by the availability of the caverns.

1.8 Demands on hydrogen storage systems

Various governmental agencies and companies work on developing hydrogen storage systems for commercial applications. The US department of energy's (DOE) fuel cell technology office (= FTCO) [125], for instance, conducts in conjunction with the US Drive Partnership initiative[126] an applied research development program in order to meet a 300 – 500 mile driving range for light-duty vehicles, while meeting packaging, cost, safety, and performance targets [127]. From a commercial point of view, the 300 mile (or 500 km) barrier is considered as the minimum entry point into the market [128]. Whereas this collaborative research effort has already led to prototype vehicles exceeding the driving range of 300 miles, significant efforts must still be directed to cost and packaging. Thus, it is obvious that applied hydrogen storage systems need to be improved in order to provide a viable alternative for commercialization.

The FTCO is running a research development and demonstration program for hydrogen storage application, and defining regularly technical system targets to be reached [129]. This includes requirements on system gravimetric and volumetric capacities, system costs, charging and discharging rates, conditions for charging and discharging, fuel quality and environmental, health, and safety aspects. Selected parameters defined as targets for 2020 and defined as ultimate targets are shown for light duty fuel cell vehicles in Table 1.3. Notably, these targets are system targets and take into account the overall weight of all components in the storage system, including, material, valves, regulators, piping, mounting brackets, insulation, added cooling capacity, and all other balance-of-plant components. Furthermore, all targets are estimated to be met at the end of service life, this is equivalent to 1500 charge-discharge cycles/5,000 h operation/150,000 miles.

Besides targets for light duty fuel cell vehicles also targets for other applications including light and medium portable power equipment have been defined by the FTCO [129]. Naturally, depending on the application the technical targets vary, but general trends are clear if hydrogen systems need to compete with traditional ones. The goal is achieving low cost, high efficiency hydrogen storage systems, which operate safely under ideally ambient temperatures with long lifetimes.

Table 1.3: Selected technical systems targets by the fuel cell technology office (FTCO) of the US department of energy's (DOE) for onboard hydrogen storage for light duty fuel cell vehicles [129].

Specific target	Targets for 2020	Ultimate target
System gravimetric capacity, [kWh/kg]	1.8	2.5
System gravimetric capacity, [kg of hydrogen/kg of system]	0.055	0.075
System volumetric capacity, [kWh/L]	1.3	2.3
System volumetric capacity, [kg of hydrogen/L of system]	0.040	0.070
Storage system cost, [$/kWh net]	10	8
Storage system cost, [$/kg of hydrogen stored]	333	266
Operating ambient temperature, [°C]	−40/+60	−40/+60
Min./Max delivery temperature, [°C]	−40/+85	−40/+85
Operational cycle life (1 cycle = 1/4 tank to full tank), [Cycle]	1500	1500
Min. delivery pressure from storage system, [bar]	5	3
Max. delivery pressure from storage system, [bar]	12	12
Onboard efficiency, [%]	90	90
Overall (onboard + off-board) efficiency with respective to power plant, [%]	60	60
Max. system fill time during charging (5 Kg hydrogen), [min]	3.3	2.5
Min. full flow rate, [(g/s)/kW]	0.02	0.02
Start time to full flow (at 20°C), [s]	5	5
Start time to full flow (at −20°C), [s]	15	15
Loss of usable hydrogen during storage, [(g/h)/kg hydrogen stored]	0.05	0.05

It needs to be emphasized here, that practical hydrogen storage systems need to comply with these requirements in order to be candidates for improved applications.

1.9 Classification of hydrogen storage systems

Various systems for the storage of hydrogen have been developed. In the literature, there are several ways to classify different hydrogen storage systems according to the storage principles; Figure 1.7 represents one possible classification, which serves as basis for this work. In general, one can distinguish between physical and material-based hydrogen storage [111, 130]. By definition in physical hydrogen storage systems no chemical bonds are newly formed or broken. This, in turn, is the case for material based systems, especially for chemical hydrogen storage systems. Physical methods for hydrogen storage include liquefaction, pressure storage and a combination of both compression
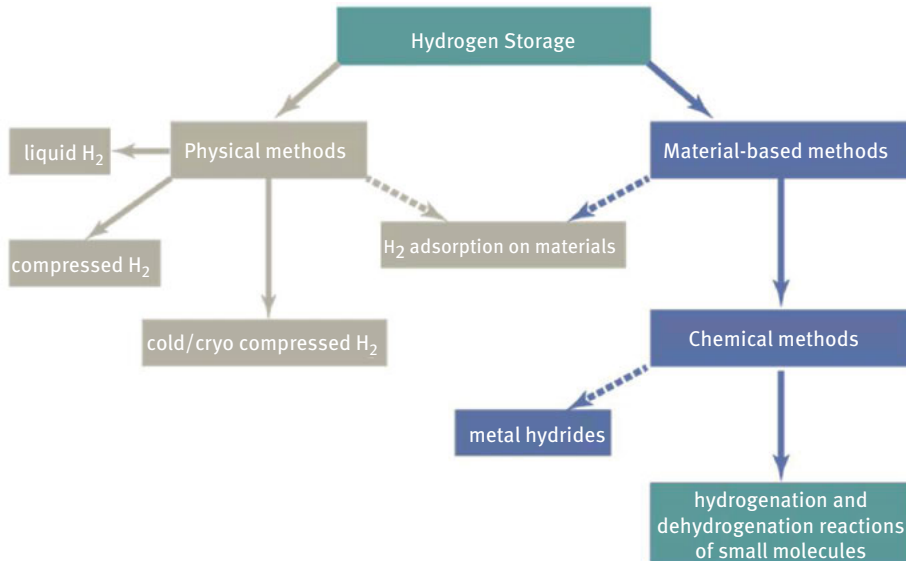
Figure 1.7: Classification of hydrogen storage systems.

of H_2 under cooling . Adsorption techniques are classified as material-based methods, in the interface between chemical and physical storage. In fact, for most adsorbing materials, the hydrogen is adsorbed molecularly, as intact H_2 molecule, and not dissociated. Therefore, this method is commonly classified as physical storage. This dissociation of H_2 is the difference between adsorption and chemical storage of hydrogen as metal hydrides.

1.10 Physical methods for hydrogen storage

As shown in Figure 1.7, physical hydrogen storage consists of three sub-technologies [111]:
i.   Storage of compressed gaseous hydrogen (350 – 700 bar, room temperature)
ii. Liquefaction of hydrogen (1 – 10 bar, ca. –252°C)
iii. Cryo-absorption on high surface area materials (2 – 5 bar, ca. –193°C)

1.10.1 Compressing gaseous hydrogen (CGH2)

As mentioned above, the low volumetric energy content of H_2 makes its storage unpractical for most applications. Compression of H_2 is one possibility to overcome this limitation. Most common gas cylinders for H_2 storage operate at a pressure of up to 200 bar [131]. However, when increasing the tensile strength of

the cylinders, significantly higher pressures can be reached. In this context, small and medium sized storage tanks are ideal for constructing high pressure tank vessels. New lightweight composite cylinder allows storage at almost 800 bar, so that a volumetric density of 36 kg/m^3 (of the overall system) can be reached, which is almost half the density of liquid H$_2$ at its boiling point. Notably these systems are technically highly sophisticated and have high demands on the building materials. The development of new pressure tanks is an ongoing engineering challenge. This is of outmost importance for reaching requirements of practical hydrogen storage on commercial scale. For example, an advanced three-vessel carbon composite unit which allows storing of 4.2 kg H$_2$ at 700 bar was designed, with an overall weight of only 135 kg. In comparison the weight of similar steel system would be around 600 kg [111, 132]. For the automotive industry, probably the most important application of H$_2$ storage today, the state of the art system is based on CGH2 at 700 bar [133].

Hydrogen is not an ideal gas. Thus its volumetric density does not behave linear with increasing pressure, Table 1.4 and Figure 1.8. For instance, at 25°C the H$_2$ density raises from 0.08 to 0.8 to 7.7 to 49 kg H$_2$ per m^3 at pressures of 1, 10, 100, and 1,000 bars, respectively, see Figure 1.8.

Table 1.4: H$_2$ density as function of pressure and temperature [135].

T in °C	H$_2$ density ρ(H$_2$) at different H$_2$ pressures p(H$_2$) in kg/m^3						
	p(H$_2$) = 1 bar	p(H$_2$) = 10 bar	p(H$_2$) = 50 bar	p(H$_2$) = 100 bar	p(H$_2$) = 300 bar	p(H$_2$) = 500 bar	p(H$_2$) = 10^3 bar
−255	73.284	74.252					
−250	1.1212	68.747	73.672				
−225	0.5081	5.5430	36.621	54.812	75.287		
−200	0.3321	3.3817	17.662	33.380	62.118	74.261	
−175	0.2471	2.4760	12.298	23.483	51.204	65.036	
−150	0.1968	1.9617	9.5952	18.355	43.079	57.343	
−125	0.1636	1.6271	7.9181	15.179	37.109	51.090	71.606
−100	0.1399	1.3911	6.7608	12.992	32.614	46.013	66.660
−75	0.1223	1.2154	5.9085	11.382	29.124	41.848	62.322
−50	0.1086	1.0793	5.2521	10.141	26.336	38.384	58.503
−25	0.0976	0.9708	4.7297	9.1526	24.055	35.464	55.123
0	0.0887	0.8822	4.3036	8.3447	22.151	32.968	52.115
25	0.0813	0.8085	3.9490	7.6711	20.537	30.811	49.424
50	0.0750	0.7461	3.6490	7.1003	19.149	28.928	47.001
75	0.0696	0.6928	3.3918	6.6100	17.943	27.268	44.810
100	0.0649	0.6465	3.1688	6.1840	16.883	25.793	42.819
125	0.0609	0.6061	2.9736	5.8104	15.944	24.474	41.001
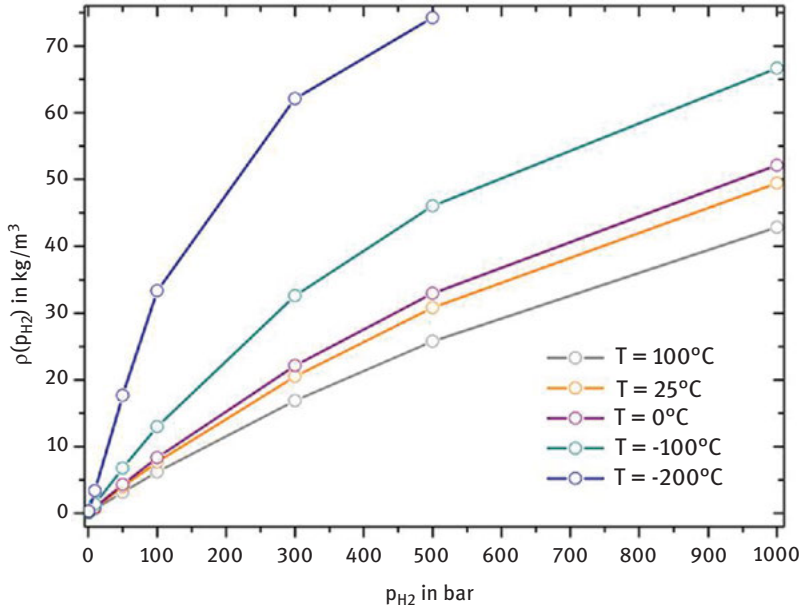
Figure 1.8: Hydrogen density as function of pressure at different temperatures, generated from data of Table 1.4.

When compressing gases mechanical energy is needed (Figure 1.9). This compression energy is substantial for systems operating at high pressure. For instance, in order to compress H_2 to 350 bar, 12% of his lower heating value needs to be used, for 700 bar
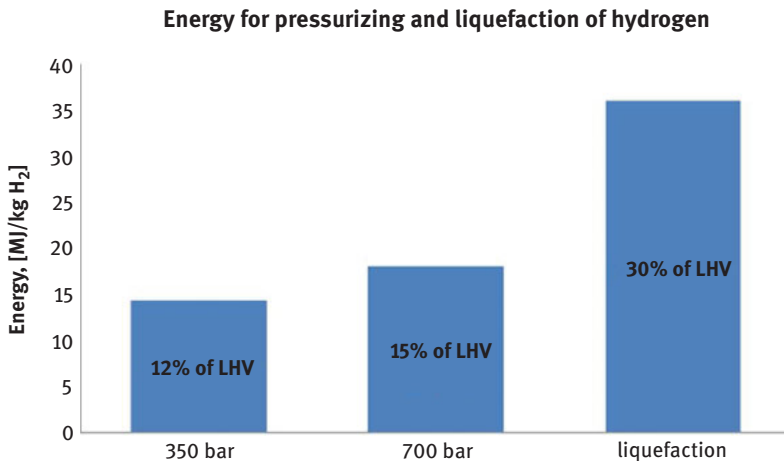
Figure 1.9: Energy necessary for pressurizing and liquefaction of hydrogen. With LHV = lower heating value of hydrogen: 120 MJ/kg H_2.

even 15% are needed. In comparison, the liquefaction energy of hydrogen amount to 30% of its lower heating value [111]. With the lower heating value for H_2 being 120 MJ/kg H_2, the energies need to compress hydrogen to 350 bar, to 700 bar or for its liquefaction are 14.4, 18.0, and 36.0 MJ/kg H_2, respectively.

1.10.2 Liquid hydrogen (LH2)

Although liquefaction of H_2 demands a relative high energy, it is highly attractive in terms of volumetric storage density. The density of liquid hydrogen is 70.8 kg/m^3 and its energy density is 8.5 GJ/m^3 [134]. However, the handling of liquid hydrogen has other operational disadvantages. When storing liquid H_2 (–252.9°C boiling point of H_2 at 1 atm.) [135], heat flowing from the environment to the H_2 tank leads to evaporation of H_2. The critical temperature of H_2 is 241°C, this means above this temperature H is gaseous [134]. Due to heat transfer the internal pressure of the tank increases, which makes periodic venting of the storage vessel necessary when a critical maximum pressure is reached. This maximum pressure is typically around 10 bar [111]. The losses of hydrogen, resulting from releasing it to the environment (so called boil-off gas) are significant. The phase change enthalpy for the evaporation of H_2 (liquid -> gaseous state) is with 452 kJ per kg of H_2 [134] too small to effectively cool the system in high efficiency. Therefore, even advanced engineering concepts were so far not able to address this challenge.

In contrast to H_2 storage under pressure, the storage of liquefied hydrogen is best suited for larger tank systems. Larger tanks have smaller surface to volume ratios, which allow for decreased heat transfer and, therefore, decreased boil-off losses. Systems for cryogenic storage of H_2 use multilayer vacuum superinsulation techniques and are technically highly sophisticated [136]. However, losses stemming from boiling-off of H_2 both storage and transferring (filling the liquid H_2 tank) of the H_2 are significantly limiting the use of this technique.

In space technology, where high energy density fuels are essential during lift-off and ascent are more important than energy efficiencies, systems based on cryotechniques and superinsulation have proved themselves to be capable of storing liquid H_2. Space shuttles are equipped with liquid hydrogen tanks and liquid O_2 [137, 138]. This application poses enormous technical challenges, as the hydrogen must be insulated from all sources of heat, including the rocket engine exhaust, heat resulting from friction, and radiation heat of the sun.

1.11 Material based methods for hydrogen storage

1.11.1 Hydrogen storage by absorption on solids with large surface area

Hydrogen can be stored by adsorption on surfaces; the efficiency of storage in such sorbent systems depends on the applied pressures and the temperature [134, 139].

Hydrogen can be bound to surfaces via weak van-der Waals forces, as intact H_2 molecule. Alternatively, depending on the surface forces (which are a function of distance) [140], also splitting of the H_2 molecules can take place and hydrogen can be stored in form of H atoms/ions. The first method, where no bonds are broken, is called physisorption, whereas the latter one, where the H-H bonds are cleaved is called chemisorption. For physisorption processes the interaction energies are very low and they are reversible as no activation energy is involved [141]. In contrast, chemisorption processes may not be reversible, or not fully reversible and one commonly need to overcome high activation energies for absorption and desorption.

The most stable position for an absorbed H_2 molecule is in a distance of one molecular radius, meaning in the first monolayer. Full coordination of a surface with H_2 leads to one monolayer of hydrogen and surface saturation. Maximum absorption of one full monolayer corresponds to around 1.3×10^{-5} mol hydrogen per square meter. If more hydrogen is to be placed on the surface, gas molecules interact with the adsorbate and attractive forces strongly resemble interactions of pure hydrogen. In other words condensation on the condensate. This means the conditions need to be similar to liquefaction of hydrogen. Consequently, absorption to solid surfaces can facilitate hydrogen storage above its boiling temperature, up to one monolayer of adsorbate, only. Hence, ultrahigh surface area materials are developed with the goal of maximizing the reversible storage capacity. One class of materials investigated as hydrogen carriers are for example metal organic frameworks (MOFs), which have high porosity and allow modification of porous size and absorption energy. Those parameters can be tuned by changes of the composition of the MOF, meaning by the choice of ligands and metal centers. A benchmark capacity of hydrogen storage reported to date in MOFs is a surface excess hydrogen uptake of 86 mg/g, at 77 K and 80 bar pressure [142]. For the same material, MOF-210, a maximum gravimetric hydrogen density (which corresponds to the maximum amount of hydrogen that can be embedded in the system) of 176 mg/g was calculated. Similarly, for a different MOF, namely NU-100, a total uptake of 164 mg/g was determined (excess uptake = 99.5 mg/g) at 70 bar and 77 K [143]. For selected reviews on MOFs as hydrogen storage materials see [128, 141, 144–151]. Covalent organic frameworks, so called COFs, are organic analogue of MOFs and are crystalline porous polymers which can be used for gas adsorption platforms as well (for selected reviews on COFs see [152–156]). The COF with the largest hydrogen storage capacity is the three-dimensional COF-102, which can take up 72 mg H_2 per gram of COF at 1 bar pressure and 77 K [156]. This is very close to the capacities of leading MOFs. Under identical conditions MOF-177 has a uptake capacity of 75 mg/g, MOF-5 76 mg/g and the porous aromatic framework PAF-1 75 mg/g [156].

Other porous materials, which are commonly used for physisorption of hydrogen include carbon materials and doped carbon materials (for selected reviews see [128, 157–161]), organic polymers (for selected reviews see [162–166]), zeolites (for selected reviews see [167–169]), and clathrate hydrates (for selected reviews see [170–172]). In

general, for these systems nanostructured material are investigated, which allow high surface area to weight ratios.

An analysis of data on hydrogen storage reveals that only moderate storage capacities can be achieved by absorption on porous high surface materials at room temperature (max. ca. 3 wt.% even at very high pressures of >500 bar) [157]. In many cases, however, the storage capacity can be increased by cooling. Therefore, cryogenic hydrogen storage by porous materials is significantly favored. In case of activated carbons, for instance, at 1 atm. storage capacities of 1 – 3 wt.% can be reached and at moderate pressure of 10 – 100 bar, 2 – 7 wt.% can be achieved [157].

It remains questionable whether too much research efforts should be spent on the development of porous materials [133]. Naturally, due to the scaling of the hydrogen storage capacity with the surface area there are clearly limitations of the maximum capacities as increasing the surface cannot be performed infinitely. Surely higher capacities can be achieved under more forced conditions, such as extreme cooling and/or high pressure. This however raises the question whether such systems can be sufficiently energy efficient. Furthermore, the technical requirements for cooling to those temperatures and reaching these high pressures are enormous. This makes practical filling of potential tanks very difficult.

1.12 Chemical methods for hydrogen storage

By definition, chemical methods for hydrogen storage have in common that the hydrogen-hydrogen bond of the H_2 molecule is cleaved. As a consequence, in most cases new chemical bonds with carrier molecules or materials are formed. For storage in condensed materials, hydrogen is then stored either as proton (H^+), as atomic hydrogen radical ($H\cdot$) or as hydride (H^-) [173]. Whether hydrogen is getting reduced to H^- or oxidized to a H^+ or remains formally atomic, depends on the nature of the bonding partner and/or host structure (see below). In addition to storage in condensed materials chemical methods for hydrogen storage also include systems based on hydrogenation and dehydrogenation reactions of small molecules (see below).

1.12.1 Hydride materials

After cleavage, the resulting hydrogen atoms can take up an electron from a more electropositive element, and can subsequently be embedded in a solid state structure as a hydride (H^-). This is the case for hydrogen storage materials based on hydride formation. A large variety of different hydride based hydrogen storage materials have been reported and this area of research has been the focus of several comprehensive reviews (for a selection see [173–187]). In general, the focus here naturally lies on hydrides of light weight elements (= HLEs), in order to achieve high storage capacities. Besides getting embedded in crystal structures in some cases also molecular

hydrides and molecularly defined hydrides are formed. There is no clear borderline separating ionic interactions from covalent ones this is rather a continuous spectrum. Hence one distinguishes between (i) ionic hydrides, (ii) covalent hydrides, and (iii) interstitial hydrides.

Ionic hydrides, with high or only ionic bonding interactions are obtained for very electropositive bonding partners, generally an alkali metal or alkaline earth metal. Synthetically, this type of compound is very often used as strong bases and occasionally as reducing agents.

Covalent hydrides are compounds where the hydrogen is bound covalently. Examples for covalent hydrides include hydrocarbons, compounds with true non-metal p-block elements and compounds where the hydrogen is bound to metallic p-block elements (e. g. Al, Ga, Sn, Pb, Bi, and Po). Complex metal hydrides are an important subcategory of covalent hydrides. These are compound with the general composition of $M_xM'_yH_n$ where the anion contains hydrogen bound in form of hydrides. Typical examples are group 13 based compounds such as $NaBH_4$, $LiAlH_4$, $LiBH_4$ but also include transition metal compounds including hydride containing anions such as $[FeH_6]^{4-}$, $[RuH_4]^{4-}$, $[RuH_6]^{4-}$, $[RuH_7]^{3-}$, $[OsH_6]^{4-}$, $[OsH_7]^{3-}$, $[NiH_4]^{4-}$ [188]. Notably, especially complex hydrides of light elements are very valuable due their synthetic applications in organic transformations as reducing agents.

Interstitial hydrides may be defined by their metal bonding character, which exists most commonly within metals or metallic alloys. This means that the electron of the hydrogen is delocalized over the solid state structure (within the band structure of the metal) and the proton is diffused in the lattice. Most importantly, hydrogen can exist in these structures as atomic hydrogen or as diatomic molecule.

Historically, in the last century the first examples of hydrides were based on magnesium [184, 186] and transition metals. Magnesium hydride, MgH_2, exists in different crystal structures and has, depending on the structure solely ionic or ionic/covalent interactions. Reversible storage of hydrogen in magnesium can be partially achieved by ball milling to very small particles or by doping. But the thermodynamic stability as well as the kinetic stabilization do not allow to release the theoretical hydrogen storage capacity of 7.66 wt.% for MgH_2. Also recharging of the hydrogen-depleted magnesium to regenerate magnesium hydride is challenging. A patent application, which was recently granted in the United States (US8651268B2), claims the use of controlled laser beams for this purpose. It, however, is questionable how practical and cost efficient this system in fact is. In this context, a theoretical system where MgH_2 is reacted with water to form H_2 and $Mg(OH)_2$ is conceivable, however the regeneration of MgH_2 from $Mg(OH)_2$ is highly energy intensive and, therefore, technically not feasible.

Transition metals store atomic hydrogen which is embedded in the metal framework. Depending on the metal and the type of compound, delocalization of the valence electron of the hydrogen can lead to a partially metallic bonding character. The most popular example here is probably hydrogen storage in palladium, which

has the ability to absorb rather large volumes hydrogen gas at ambient pressure and temperature [189, 190]. During this adsorption process atomic hydrogen "dissolves" in the cubic lattice of palladium and occupies the octahedral sites of the face centered cubic lattice. This process forms a palladium hydrogen compound with the composition of PdH_X (X ≤ 1), which are often misleadingly called palladium hydrides as the hydrogen is not bound as H^-. Overall, this results in a hydrogen storage capacity of max. 0.93 wt.%. The dissociation of H_2 is the initial step in the adsorption process. Whereas for other metals substantial activation energy is needed to achieve this for Pd the adsorption and dissociation of H_2 takes place with almost no barrier [191]. This means whereas hydrogen dissolution can take place for Pd at ambient conditions, other metals necessitate high pressures or elevated temperatures. Given the high price, low abundancy and the relatively low storage capacity of Pd, its use for H storage applications is not a cost effective.

In 1997, seminal work of Bogdanović [192] prompted a significant interest in alanates (for selected reviews on the topic see [176, 193–195]:) which later-on also resulted in extensive research efforts in boron compounds and borohydrides as hydrogen carriers (for selected reviews see [196–206]:).

One the one hand HLEs are the most promising candidates for achieving practical hydrogen storage in hydride materials due to their high volumetric and gravimetric storage potential [173]. The most severe drawbacks of these systems are: slow kinetics, unwanted by-product formation, and irreversibility and high operating temperatures for the hydrogen release step [173]. These drawbacks make the use of current state of the art HLEs as hydrogen carriers in reversible hydrogen storage systems impossible. An ideal material which possess not only a high hydrogen storage capacity, but also stability and reversibility of the H_2 uptake remains elusive. The development of such a system demands a significant conceptual breakthrough. The development of such a game-changing material or material class is highly desirable and may represent one of the most challenging task facing todays solid state chemists and other material scientists.

1.12.2 Hydrogenation and dehydrogenation reactions of small molecules

This book focuses on a different concept of hydrogen storage, which is hydrogen storage based on reversible *hydrogenation and dehydrogenation reactions of small molecules*. This concept is based on a reaction in which substrates are (catalytically) hydrogenated in order to store hydrogen and on demand dehydrogenated to release hydrogen. The first and second reaction correspond to charging and discharging of the system with hydrogen, respectively. The principle of this storage concept is depicted in Figure 1.10 which illustrates the concept based on the acetone/isopropanol couple.
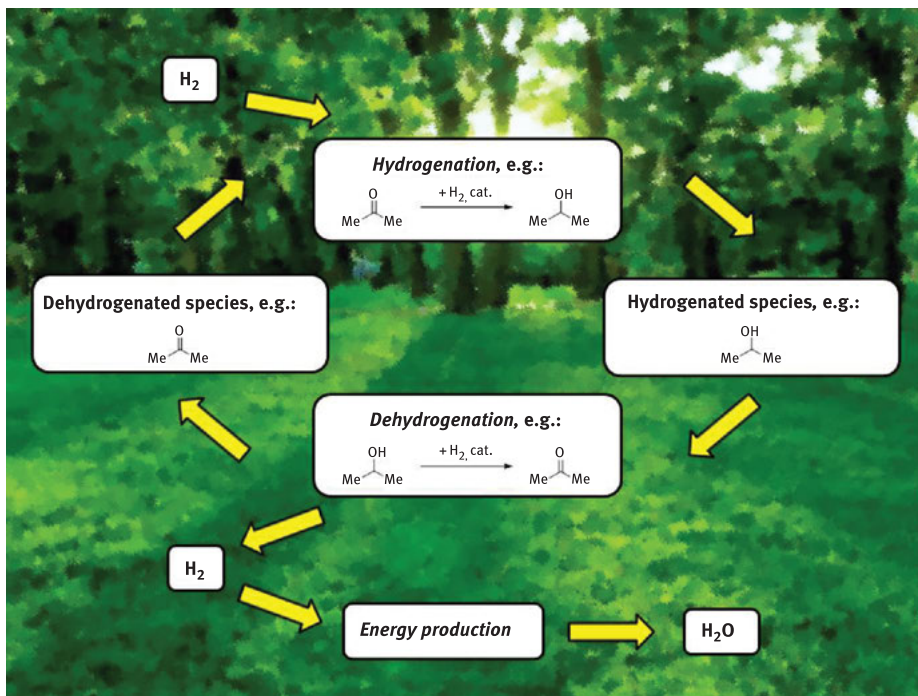
Figure 1.10: Principle of hydrogen storage by reversible *hydrogenation and dehydrogenation reactions of small molecules*, exemplified by the acetone/isopropanol couple.

Systems which work according to this principle have in the literature been described as hydrogen batteries. There are several chemical systems capable for this application. Throughout the book, we have decided to organize storage systems according to substrates. Notably, for many storage systems reversible hydrogen storage has not been demonstrated yet. Each storage system or possible storage system, which is described, has advantages and disadvantages. Most importantly, none of them is ideal and fulfill all requirements for broad commercialization today. The field of hydrogen storage is broad, multidisciplinary, and extraordinary vivid. Every year, novel and exciting new approaches for (possible) hydrogen storage are presented in the literature. Especially in the field of hydrogen storage by hydrogenation and dehydrogenation reactions of small molecules a tremendous progress can be observed in the last years. This includes on the one hand new substrates as platform molecules for hydrogen storage but also developing improved catalytic protocols for known hydrogenation and dehydrogenation processes.

Ideally, in order to obtain a sustainable energy storage cycle, the hydrogen should be produced from green, regenerative resources. We have no doubt that the implementation of this concept will certainly play a major role in navigating today's society towards a green and environmentally friendly and therefore responsible future energy

landscape. It is clear that not all applications can be fueled by this concept and alternative concepts for energy storage, transportation and distribution may be used in combination with this one in order to achieve a viable solution for the challenges facing us today.

References

[1] https://www.epa.gov/ghgemissions/global-greenhouse-gas-emissions-data.

[2] https://www.eia.gov/energyexplained/index.cfm?page=environment_where_ghg_come_from.

[3] Sathre, R. Comparing the heat of combustion of fossil fuels to the heat accumulated by their lifecycle greenhouse gases. Fuel. 2014;115:674–7.

[4] https://www.eia.gov/energyexplained/?page=us_energy_home.

[5] Schüth F. Guest editorial: paving the way to new energy systems: the key role of the chemical sciences. Chem Sus Chem. 2010;3:6–8.

[6] Dibenedetto A, Angelini A, Stufano P. Use of carbon dioxide as feedstock for chemicals and fuels: homogeneous and heterogeneous catalysis. J Chem Technol Biotechnol. 2014;89:334–53.

[7] Yang L, Wang H. Recent advances in carbon dioxide capture, fixation, and activation by using N-heterocyclic carbenes. Chem Sus Chem. 2014;7:962–98.

[8] Appel AM. Frontiers, opportunities, and challenges in biochemical and chemical catalysis of CO_2 fixation. Chem Rev. 2013;113:6621–58.

[9] Aresta M, Dibenedetto A, Angelini A. Catalysis for the valorization of exhaust carbon: from CO_2 to chemicals, materials, and fuels. Technological use of CO_2. Chem Rev. 2014;114:1709–42.

[10] Anker MD. Selective reduction of CO_2 to a methanol equivalent by $B(C6F5)3$-activated alkaline earth catalysis. Chem Sci. 2014;5:2826–30.

[11] Perathoner S, Centi G. CO_2 recycling: a key strategy to introduce green energy in the chemical production chain. Chem Sus Chem. 2014;7:1274–82.

[12] Fernández-Alvarez FJ. CO_2 activation and catalysis driven by iridium complexes. Chem Cat Chem. 2013;5:3481–94.

[13] Martens JA. The chemical route to a carbon dioxide neutral world. Chem Sus Chem. 2017;10:1039–55.

[14] Meier B, Ruoss F, Friedl M. Investigation of carbon flows in Switzerland with the special consideration of carbon dioxide as a feedstock for sustainable energy carriers. Energy Technol. 2017;5:864–76.

[15] Al-Mamoori A. Carbon capture and utilization update. Energy Technol. 2017;5:834–49.

[16] Artz J. Sustainable conversion of carbon dioxide: an integrated review of catalysis and life cycle assessment. Chem Rev. 2018;118:434–504.

[17] Klankermayer J. Selective catalytic synthesis using the combination of carbon dioxide and hydrogen: catalytic chess at the interface of energy and chemistry. Angew Chem Ed. 2016;55:7296–343.

[18] https://www.wiseinternational.org/nuclear-monitor.

[19] https://www.ucsusa.org/nuclear-power/nuclear-power-and-global-warming#.WmMTZXnLi70, s.e.g.

[20] http://www.world-nuclear.org/information-library/safety-and-security/safety-of-plants/ safety-of-nuclear-power-reactors.aspx, s.e.g.

[21] For a comprehensive summary impactful research from a multidisciplinary perspective on the incident, s., e.g.: https://www.elsevier.com/connect/5-years-after-fukushima-insights-from-current-research.

[22] Lyman E, Schoeppner M, Von Hippel F. Nuclear safety regulation in the post-Fukushima era. Science. 2017;356:808–9.

[23] Normile D. The pacific swallows Fukushima's fallout. Science. 2013;340:547.

[24] Sanial V. Unexpected source of Fukushima-derived radiocesium to the coastal ocean of Japan. Proc Natl Acad Sci. 2017;114:11092–6.

[25] For a comprehensive summary on multidisciplinary research articles, s., e.g.: http://www.nature.com/news/specials/japanquake/index.html.

[26] Sovacool BK. A critical evaluation of nuclear power and renewable electricity in Asia. J Contemp Asia. 2010;40:369–400.

[27] Chen H. Progress in electrical energy storage system: a critical review. Prog Nat Sci. 2009;19:291–312.

[28] Cook TR. Solar energy supply and storage for the legacy and nonlegacy worlds. Chem Rev. 2010;110:6474–502.

[29] http://energystorage.org/energy-storage/technologies/pumped-hydroelectric-storage.

[30] Liu C. Advanced materials for energy storage. Adv Mater. 2010;22:E28–62.

[31] http://www.energystorageexchange.org.

[32] Jacobson MZ. Review of solutions to global warming, air pollution, and energy security. Energy Environ Sci. 2009;2:148–73.

[33] https://permaculturenews.org/2015/10/01/storing-energy-by-gravity/.

[34] Denholm P. Improving the technical, environmental and social performance of wind energy systems using biomass-based energy storage. Renew Energy. 2006;31:1355–70.

[35] Xue XD, Cheng KW, Sutanto D. A study of the status and future of superconducting magnetic energy storage in power systems. Supercond Sci Technol. 2006;19:R31.

[36] Hassenzahl WV. Electric power applications of superconductivity. Proc of the IEEE. 2004;92:1655–74.

[37] Dunn B, Kamath H, Tarascon JM. Electrical energy storage for the grid: a battery of choices. Science. 2011;334:928–35.

[38] Thackeray MM, Wolverton C, Isaacs ED. Electrical energy storage for transportation-approaching the limits of, and going beyond, lithium-ion batteries. Energy Environ Sci. 2012;5:7854–63.

[39] Deng D. Green energy storage materials: nanostructured TiO_2 and Sn-based anodes for lithium-ion batteries. Energy Environ Sci. 2009;2:818–37.

[40] Palacin MR. Recent advances in rechargeable battery materials: a chemist's perspective. Chem Soc Rev. 2009;38:2565–75.

[41] Yang Z. Electrochemical energy storage for green grid. Chem Rev. 2011;111:3577–613.

[42] Yin Y-X. Lithium–Sulfur batteries: electrochemistry, materials, and prospects. Angew Chem Inter Ed. 2013;52:13186–200.

[43] Larcher D, Tarascon JM. Towards greener and more sustainable batteries for electrical energy storage. Nat Chem. 2014;7:19.

[44] https://www.eaglepicher.com/technology/battery-chemistries/lithium-carbon-monofluoride-cfx-and-licfx-mno2-hybrid/.

[45] Simon P, Gogotsi Y. Materials for electrochemical capacitors. Nat Mater. 2008;7:845.

[46] Simon P, Gogotsi Y. Capacitive energy storage in nanostructured carbon–electrolyte systems. Acc Chem Res. 2013;46:1094–103.

[47] Hall PJ. Energy storage in electrochemical capacitors: designing functional materials to improve performance. Energy Environ Sci. 2010;3:1238–51.

[48] Frackowiak E, Béguin F. Carbon materials for the electrochemical storage of energy in capacitors. Carbon. 2001;39:937–50.

[49] Burke A. R&D considerations for the performance and application of electrochemical capacitors. Electrochim Acta. 2007;53:1083–91.

[50] http://www.gravitybattery.info/.

[51] http://www.economist.com/node/21548495.

[52] http://sinkfloatsolutions.com/?page_id=1005.

[53] http://www.stratosolar.com/gravity-energy-storage.html.

[54] https://gravitylight.org/.

[55] Regin AF, Solanki SC, Saini JS. Heat transfer characteristics of thermal energy storage system using PCM capsules: a review. Renew Sustainable Energy Rev. 2008;12:2438–58.

[56] Zhou Z. Phase change materials for solar thermal energy storage in residential buildings in cold climate. Renew Sustainable Energy Rev. 2015;48:692–703.

[57] Agyenim F. A review of materials, heat transfer and phase change problem formulation for latent heat thermal energy storage systems (LHTESS). Renew Sustain Energy Rev. 2010;14:615–28.

[58] Zalba B. Review on thermal energy storage with phase change: materials, heat transfer analysis and applications. Appl Ther Eng. 2003;23:251–83.

[59] Sharma A. Review on thermal energy storage with phase change materials and applications. Renew Sustainable Energy Rev. 2009;13:318–45.

[60] Kenisarin M, Mahkamov K. Solar energy storage using phase change materials. Renew Sustainable Energy Rev. 2007;11:1913–65.

[61] Farid MM. A review on phase change energy storage: materials and applications. Energy Convers Manage. 2004;45:1597–615.

[62] Fopah Lele A. A thermochemical heat storage system for households. Switzerland: Springer International Publishing, 2016.

[63] Hui L. Evaluation of a seasonal storage system of solar energy for house heating using different absorption couples. Energy Convers Manage. 2011;52:2427–36.

[64] Katulić S, Čehil M, Bogdan Ž. A novel method for finding the optimal heat storage tank capacity for a cogeneration power plant. Appl Therm Eng. 2014;65:530–8.

[65] Prieto C. Review of technology: thermochemical energy storage for concentrated solar power plants. Renew Sustainable Energy Rev. 2016;60:909–29.

[66] Fopah-Lele A, Tamba JG. A review on the use of $SrBr_2 \cdot 6H_2O$ as a potential material for low temperature energy storage systems and building applications. Sol Energy Mater Sol Cells. 2017;164:175–87.

[67] Ward PA. Technical challenges and future direction for high-efficiency metal hydride thermal energy storage systems. App Phys A. 2016;122:462.

[68] Chacartegui R. Thermochemical energy storage of concentrated solar power by integration of the calcium looping process and a CO_2 power cycle. Appl Energy. 2016;173:589–605.

[69] Cot-Gores J, Castell A, Cabeza LF. Thermochemical energy storage and conversion: a-state-of-the-art review of the experimental research under practical conditions. Renew Sustainable Energy Rev. 2012;16:5207–24.

[70] Pardo P. A review on high temperature thermochemical heat energy storage. Renew Sustainable Energy Rev. 2014;32:591–610.

[71] Cabeza LF. Lithium in thermal energy storage: a state-of-the-art review. Renew Sustainable Energy Rev. 2015;42:1106–12.

[72] Solé A, Martorell I, Cabeza LF. State of the art on gas–Solid thermochemical energy storage systems and reactors for building applications. Renew Sustainable Energy Rev. 2015;47:386–98.

[73] Kucharski TJ. Chemical solutions for the closed-cycle storage of solar energy. Energy Environ Sci. 2011;4:4449–72.

[74] Aydin D, Casey SP, Riffat S. The latest advancements on thermochemical heat storage systems. Renew Sustainable Energy Rev. 2015;41:356–67.

[75] Tatsidjodoung P, Le Pierrès N, Luo L. A review of potential materials for thermal energy storage in building applications. Renew Sustainable Energy Rev. 2013;18:327–49.

[76] Yu N, Wang RZ, Wang LW. Sorption thermal storage for solar energy. Prog Energy Combust Sci. 2013;39:489–514.

[77] http://www.desertec.org/.

[78] https://www.wired.com/2017/05/electric-airplanes-2/.

[79] http://www.theenergycollective.com/robertwilson190/351596/flying-without-fossil-fuels-need-high-energy-density.

[80] http://airbus-xo.com/electrification-powering-the-future-of-flight/.

[81] Züttel A, Borgschulte A, Schlapbach L. Hydrogen as a future energy carrier. Weinheim: Wiley-VCH, 2008.

[82] Lunsford JH. Catalytic conversion of methane to more useful chemicals and fuels: a challenge for the twenty-first century. Catalysis Today. 2000;63:165–74.

[83] Holladay JD. An overview of hydrogen production technologies. Catal Today. 2009;139:244–60.

[84] Farnell P. Engineering aspects of hydrocarbon steam reforming catalysts. Top Catal. 2016;59:802–8.

[85] Kubacka A, Fernández-García M, Martínez-Arias A. Catalytic hydrogen production through WGS or steam reforming of alcohols over Cu, Ni and Co catalysts. Appl Catal A: Gen. 2016;518:2–17.

[86] Sengodan S. Advances in reforming and partial oxidation of hydrocarbons for hydrogen production and fuel cell applications. Renew Sustainable Energy Rev. 2018;82:761–80.

[87] Lavoie J-M. Review on dry reforming of methane, a potentially more environmentally-friendly approach to the increasing natural gas exploitation. Front Chem. 2014;2:1–17

[88] Bradford MC, Vannice MA. CO_2 reforming of CH_4. Catal Rev. 1999;41:1–42.

[89] Pakhare D, Spivey J. A review of dry (CO_2) reforming of methane over noble metal catalysts. Chem Soc Rev. 2014;43:7813–37.

[90] Fidalgo B, Menendez JÁ. Carbon materials as catalysts for decomposition and CO_2 reforming of methane: a review. Chin J Catal. 2011;32:207–16.

[91] Arora S, Prasad R. An overview on dry reforming of methane: strategies to reduce carbonaceous deactivation of catalysts. RSC Adv. 2016;6:108668–88.

[92] Fan M-S, Abdullah AZ, Bhatia S. Catalytic technology for carbon dioxide reforming of methane to synthesis gas. Chem Cat Chem. 2009;1:192–208.

[93] Kawi S. Progress in synthesis of highly active and stable nickel-based catalysts for carbon dioxide reforming of methane. Chem Sus Chem. 2015;8:3556–75.

[94] Bharadwaj SS, Schmidt LD. Catalytic partial oxidation of natural gas to syngas. Fuel Process Technol. 1995;42:109–27.

[95] Uddin MN, Daud WM. Technological diversity and economics: coupling effects on hydrogen production from biomass. Energy Fuels. 2014;28:4300–20.

[96] Kumar A, Chakraborty JP, Singh R. Bio-oil: the future of hydrogen generation. Biofuels. 2017;8:663–74.

[97] Chen J, Sun J, Wang Y. Catalysts for steam reforming of bio-oil: a review. Ind Eng Chem Res. 2017;56:4627–37.

[98]   Guan G. Catalytic steam reforming of biomass tar: prospects and challenges. Renew Sustainable Energy Rev. 2016;58:450–61.

[99]   Demirbas A. Comparison of thermochemical conversion processes of biomass to hydrogen-rich gas mixtures. Energy Sources Part A. 2016;38:2971–6.

[100] Wang D, Czernik S, Chornet E. Production of hydrogen from biomass by catalytic steam reforming of fast pyrolysis oils. Energy Fuels. 1998;12:19–24.

[101] Armaroli N, Balzani V. The hydrogen issue. Chem Sus Chem. 2011;4:21–36.

[102] Machhammer O, Bode A, Hormuth W. Financial and ecological evaluation of hydrogen production processes on large scale. Chem Eng Technol. 2016;39:1185–93.

[103] http://www.npc.org/reports/FTF-report-080112/Chapter_15-Hydrogen.pdf, s.e.g.

[104] https://www.nrel.gov/docs/fy07osti/41134.pdf, s.e.g.

[105] Kalamaras CM, Efstathiou AM. Hydrogen production technologies: current state and future developments. Conf Pap Energy. 2013;2013:9.

[106] Bockris JO. A hydrogen economy. Science. 1972;176:1323.

[107] Schüth F. Chemical compounds for energy storage. Chem Ingenieur Technik. 2011;83:1984–93.

[108] https://www.nrel.gov/docs/fy09osti/44103.pdf.

[109] http://www.hydrogenics.com/wp-content/uploads/2-2-1-power-to-gas-4pg-brochure-2012. pdf?utm_campaign=Power-to-Gas%20Brochure&utm_source=hs_automation&utm_medium= email&utm_content=49677686&_hsenc=p2ANqtz-9IGGF9k6tTQamKXK2Ee56zKCTeVixHDOB 3P6VuKqD0Zgk7o_TBtO4SeltDmo5ai0NKyvOYZGUv3o4gBeXlsRplN9g53g&_hsmi=49677686.

[110] https://energy.gov/sites/prod/files/2014/03/f12/fcm01r0.pdf.

[111] Eberle U, Felderhoff M, Schüth F. Chemische und physikalische Lösungen für die Speicherung von Wasserstoff. Angew Chem. 2009;121:6732–57.

[112] https://www.forbes.com/sites/greatspeculations/2017/12/01/why-toyota-is-focusing-on-hydrogen-fuel-cells/#6bd6e949a888.

[113] http://world.honda.com/FuelCell/.

[114] http://www.toyota-global.com/innovation/environmental_technology/fuelcell_vehicle/.

[115] https://energy.gov/eere/articles/5-things-know-when-filling-your-fuel-cell-electric-vehicle.

[116] http://www.scandinavianhydrogen.org/shhp/vehicles/.

[117] http://media.daimler.com/marsMediaSite/en/instance/ko/Fuel-Cells.xhtml?oid=9265782.

[118] http://www.fuelcellbuses.eu/.

[119] http://www.hydrogenics.com/buses.

[120] https://nikolamotor.com/one.

[121] https://www.theverge.com/2017/10/12/16461412/toyota-hydrogen-fuel-cell-truck-port-la.

[122] https://edition.cnn.com/travel/article/hy4-fuel-cell-plane/index.html.

[123] https://www.theregister.co.uk/2010/07/13/phantom_eye_rollout/.

[124] http://juser.fz-juelich.de/record/135790/files/Energie%26Umwelt_78-04.pdf.

[125] https://energy.gov/eere/fuelcells/fuel-cell-technologies-office.

[126] http://www.uscar.org/guest/partnership/1/us-drive.

[127] https://energy.gov/sites/prod/files/2017/05/f34/fcto_targets_onboard_hydro_storage_explanation.pdf.

[128] Wang L, Yang RT. New sorbents for hydrogen storage by hydrogen spillover - a review. Energy Environ Sci. 2008;1:268–79.

[129] https://energy.gov/sites/prod/files/2015/05/f22/fcto_myrdd_storage.pdf.

[130] https://energy.gov/eere/fuelcells/hydrogen-storage.

[131] Makridis SS. Hydrogen storage and compression. In: Ting David S-K., Carriveau Rupp, editor(s). Methane and hydrogen for energy storage. Institution of Engineering and Technology, 2016:1–28.

[132] Von Helmolt R, U Eberle. Fuel cell vehicles: Status 2007. J Power Sources. 2007;165:833–43.

[133] Felderhoff M. Hydrogen storage: the remaining scientific and technological challenges. Phys Chem Chem Phys. 2007;9:2643–53.

[134] Schlapbach L, Zuttel A. Hydrogen-storage materials for mobile applications. Nature. 2001;414:353–8.

[135] https://www.h2tools.org/hyarc/data/hydrogen-properties.

[136] Zhang J. A review of heat transfer issues in hydrogen storage technologies. J Heat Transfer. 2005;127:1391–9.

[137] https://www.nasa.gov/mission_pages/shuttle/launch/LOX-LH2-storage.html.

[138] https://www.nasa.gov/topics/technology/hydrogen/hydrogen_fuel_of_choice.html.

[139] Züttel A. Materials for hydrogen storage. Mater Today. 2003;6:24–33.

[140] McQuarrie DA. Physical chemistry: a molecular approach. Sausalito, Calif.: University Science Books, 1997. [1997] ©1997.

[141] Suh MP. Hydrogen storage in metal–Organic frameworks. Chem Rev. 2012;112:782–835.

[142] Furukawa H. Ultrahigh porosity in metal-organic frameworks. Science. 2010;329:424–8.

[143] Farha OK. De novo synthesis of a metal–organic framework material featuring ultrahigh surface area and gas storage capacities. Nat Chem. 2010;2:944.

[144] Rowsell JL, Yaghi OM. Strategies for hydrogen storage in metal–organic frameworks. Angew Chem Int Ed. 2005;44:4670–9.

[145] Dincă, M, Long JR. Hydrogen storage in microporous metal–organic frameworks with exposed metal sites. Angew Chem Int Ed. 2008;47:6766–79.

[146] Getman RB. Review and analysis of molecular simulations of methane, hydrogen, and acetylene storage in metal–organic frameworks. Chem Rev. 2012;112:703–23.

[147] Mueller U. Metal-organic frameworks-prospective industrial applications. J Mater Chem. 2006;16:626–36.

[148] Langmi HW. Hydrogen storage in metal-organic frameworks: a review. Electrochim Acta. 2014;128:368–92.

[149] Hirscher M, Panella B. Hydrogen storage in metal–organic frameworks. Scr Mater. 2007;56:809–12.

[150] Kitagawa S, Uemura K. Dynamic porous properties of coordination polymers inspired by hydrogen bonds. Chem Soc Rev. 2005;34:109–19.

[151] Rosi NL. Hydrogen storage in microporous metal-organic frameworks. Science. 2003;300:1127–9.

[152] Ding S-Y, Wang W. Covalent organic frameworks (COFs): from design to applications. Chem Soc Rev. 2013;42:548–68.

[153] Furukawa H, Yaghi OM. Storage of hydrogen, methane, and carbon dioxide in highly porous covalent organic frameworks for clean energy applications. J Am Chem Soc. 2009;131:8875–83.

[154] Han SS, Mendoza-Cortes JL, Goddard WA, Iii. Recent advances on simulation and theory of hydrogen storage in metal-organic frameworks and covalent organic frameworks. Chem Soc Rev. 2009;38:1460–76.

[155] Kalidindi SB, Fischer RA. Covalent organic frameworks and their metal nanoparticle composites: prospects for hydrogen storage. Phys Stat Solidi (B). 2013;250:1119–27.

[156] Feng X, Ding X, Jiang D. Covalent organic frameworks. Chem Soc Rev. 2012;41:6010–22.

[157] Sevilla M, Mokaya R. Energy storage applications of activated carbons: supercapacitors and hydrogen storage. Energy Environ Sci. 2014;7:1250–80.

[158] Candelaria SL. Nanostructured carbon for energy storage and conversion. Nano Energy. 2012;1:195–220.

[159] Darkrim FL, Malbrunot P, Tartaglia GP. Review of hydrogen storage by adsorption in carbon nanotubes. Int J Hydrogen Energy. 2002;27:193–202.

[160] Froudakis GE. Hydrogen storage in nanotubes & nanostructures. Mater Today. 2011;14:324–8.

[161] Schimmel HG. Hydrogen adsorption in carbon nanostructures: comparison of nanotubes, fibers, and coals. Chem – Eur J. 2003;9:4764–70.

[162] Wood CD. Hydrogen storage in microporous hypercrosslinked organic polymer networks. Chem Mater. 2007;19:2034–48.

[163] Kato R, Nishide H. Polymers for carrying and storing hydrogen. Polym J. 2017;50:77.

[164] Lu W. Strategies for hydrogen storage in porous organic polymers. In Chen Y-P, Bashir S, Liu JL, editors. Nanostructured materials for next-generation energy storage and conversion: hydrogen production, storage, and utilization. Berlin, Heidelberg: Springer Berlin Heidelberg, 2017:203–23.

[165] Budd PM. The potential of organic polymer-based hydrogen storage materials. Phys Chem Chem Phys. 2007;9:1802–8.

[166] Xu Y. Conjugated microporous polymers: Design, synthesis and application. Chem Soc Rev. 2013;42:8012–31.

[167] Weitkamp J, Fritz M, Ernst S. Zeolites as media for hydrogen storage. Int J Hydrogen Energy. 1995;20:967–70.

[168] Dong J. Hydrogen storage in several microporous zeolites. Int J Hydrogen Energy. 2007;32:4998–5004.

[169] Li Y, Yang RT. Hydrogen storage in low silica type X zeolites. J Phys Chem B. 2006;110:17175–81.

[170] Veluswamy HP, Kumar R, Linga P. Hydrogen storage in clathrate hydrates: current state of the art and future directions. Appl Energy. 2014;122:112–32.

[171] Struzhkin VV. Hydrogen storage in molecular clathrates. Chem Rev. 2007;107:4133–51.

[172] Schüth F. Hydrogen and hydrates. Nature. 2005;434:712.

[173] He T. Hydrogen carriers. Nature Rev Mater. 2016;1:16059.

[174] Jena P. Materials for hydrogen storage: past, present, and future. J Phys Chem Lett. 2011;2:206–11.

[175] Yang J. High capacity hydrogen storage materials: attributes for automotive applications and techniques for materials discovery. Chem Soc Rev. 2010;39:656–75.

[176] Sakintuna B, Lamari-Darkrim F, Hirscher M. Metal hydride materials for solid hydrogen storage: a review. Int J Hydrogen Energy. 2007;32:1121–40.

[177] Seayad AM, Antonelli DM. Recent advances in hydrogen storage in metal-containing inorganic nanostructures and related materials. Adv Mater. 2004;16:765–77.

[178] Orimo Si. Complex hydrides for hydrogen storage. Chem Rev. 2007;107:4111–32.

[179] Zhu Y, Gao S, Hosmane NS. Boron-enriched advanced energy materials. Inorg Chim Acta. 2018;471:577–86.

[180] Graetz J. New approaches to hydrogen storage. Chem Soc Rev. 2009;38:73–82.

[181] Bérubé V. Size effects on the hydrogen storage properties of nanostructured metal hydrides: a review. Int J Energy Res. 2007;31:637–63.

[182] Orimo S, Fujii H. Materials science of Mg-Ni-based new hydrides. Appl Phys A. 2001;72:167–86.

[183] Zaluska A, Zaluski L, Ström-Olsen JO. Structure, catalysis and atomic reactions on the nano-scale: a systematic approach to metal hydrides for hydrogen storage. Appl Phys A. 2001;72:157–65.

[184] Jain IP, Lal C, Jain A. Hydrogen storage in Mg: A most promising material. Int J Hydrogen Energy. 2010;35:5133–44.

[185] Rusman NA, Dahari M. A review on the current progress of metal hydrides material for solid-state hydrogen storage applications. Int J Hydrogen Energy. 2016;41:12108–26.

[186] Dornheim M. Hydrogen storage in magnesium-based hydrides and hydride composites. Scr Mater. 2007;56:841–6.

[187] Vajo JJ, Olson GL. Hydrogen storage in destabilized chemical systems. Scr Mater. 2007;56:829–34.

[188] Yvon K. Metal hydrides: Transition metal hydride complexes A2. In Buschow KH, Cahn RW, et al., editors. Encyclopedia of materials: science and technology, 2nd ed. Oxford: Elsevier, 2004:1–9.

[189] Adams BD, Chen A. The role of palladium in a hydrogen economy. Mater Today. 2011;14:282–9.

[190] Flanagan TB, Oates WA. The palladium-hydrogen system. Annu Rev Mater Sci. 1991;21:269–304.

[191] Nakatsuji H, Hada M. Interaction of a hydrogen molecule with palladium. J Am Chem Soc. 1985;107:8264–6.

[192] Bogdanović B, Schwickardi M. Ti-doped alkali metal aluminium hydrides as potential novel reversible hydrogen storage materials 1 invited paper presented at the International Symposium on Metal–Hydrogen Systems, Les Diablerets, August 25–30, 1996, Switzerland.1. J Alloys Compd. 1997;253–254:1–9.

[193] Li L. Sodium alanate system for efficient hydrogen storage. Int J Hydrogen Energy. 2013;38:8798–812.

[194] Graetz J. Aluminum hydride as a hydrogen and energy storage material: past, present and future. J Alloys Compd. 2011;509:S517–28.

[195] Suttisawat Y. A reality check on using NaAlH4 as a hydrogen storage material. J Solid State Electrochem. 2010;14:1813–9.

[196] Marder TB. Will we soon be fueling our automobiles with ammonia–borane? Angew Chem Int Ed. 2007;46:8116–8.

[197] Staubitz A, Robertson AP, Manners I. Ammonia-borane and related compounds as dihydrogen sources. Chem Rev. 2010;110:4079–124.

[198] Hamilton CW. B-N compounds for chemical hydrogen storage. Chem Soc Rev. 2009;38:279–93.

[199] Stephens FH, Pons V, Tom Baker R. Ammonia-borane: the hydrogen source par excellence? Dalton Transactions. 2007;25:2613–26.

[200] Yadav M, Xu Q. Liquid-phase chemical hydrogen storage materials. Energy Environ Sci. 2012;5:9698–725.

[201] Umegaki T. Boron- and nitrogen-based chemical hydrogen storage materials. Int J Hydrogen Energy. 2009;34:2303–11.

[202] Fakioğlu E, Yürüm Y, Nejat Veziroğlu T. A review of hydrogen storage systems based on boron and its compounds. Int J Hydrogen Energy. 2004;29:1371–6.

[203] Züttel A. LiBH4 a new hydrogen storage material. J Power Sources. 2003;118:1–7.

[204] Hansen BR. Metal boranes: progress and applications. Coord Chem Rev. 2016;323:60–70.

[205] Moussa G. Boron-based hydrides for chemical hydrogen storage. Int J Energy Res. 2013;37:825–42.

[206] Li HW. Recent progress in metal borohydrides for hydrogen storage. Energies. 2011;4:185.

Thomas Schaub

2 CO₂-based hydrogen storage: CO₂ hydrogenation to formic acid, formaldehyde and methanol

Abstract: The storage of hydrogen via hydrogenation of CO_2 to small organic molecules can be attractive for mobile applications. In this article, the state of the art regarding hydrogen storage in Methanol, Formic Acid as well as Formaldehyde and derivates based on CO_2 hydrogenation is summarized. The reverse reaction, the release of hydrogen from these molecules is also crucial and described in the articles together with possible concepts for the use of hydrogen storage by CO_2 hydrogenation.

Keywords: CO_2, hydrogen, formic acid, methanol, formaldehyde, reformation

2.1 Introduction

One of the possibilities to store hydrogen, which is ideally generated from renewable resources, is via hydrogenation of CO_2 to simple C1-compounds like methane, methanol, formic acid or formaldehyde. Out of these molecules, methanol, formic acid and aqueous formaldehyde or its acetals are liquids at ambient conditions and can therefore be stored and shipped without the need for pressure or cryogenic equipment. In principle these compounds are providing a high hydrogen content (see Figure 2.1) as well as energy density and are relatively easy to handle [1–3].
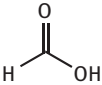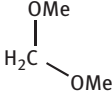
C1-Compund:	Methanol	Formic Acid	Formaldehyde	Dimethoxymethane
Hydrogen Content:	12.6 wt%	4.4 wt%	6.6 wt%	10.5 wt%

Figure 2.1: Hydrogen content of the C1 compounds discussed in this article.

Therefore, over the last years different concepts were developed to use methanol, formic acid and formaldehyde to store hydrogen based on CO_2 hydrogenation. Mainly the storage of hydrogen in methanol, formic acid or formaldehyde is discussed

for mobile applications where a high energy density is desirable. In all these cases, catalysts are playing a crucial role to allow the hydrogenation of CO$_2$ and also the release of hydrogen from the resulting organic molecule [4–10].

To store hydrogen via CO$_2$ hydrogenation it has to be distinguished between two different concepts (see Figure 2.2):

A. Decoupled: The CO$_2$ hydrogenation takes place in a stationary unit; the organic molecule is isolated and can be shipped to the desired application where its energy is used. During the dehydrogenation reaction the CO$_2$ is then liberated to the atmosphere.

B. Integrated: The CO$_2$ hydrogenation is carried out in the same system from which hydrogen is later released by the reverse reaction ("hydrogen battery"). This type of storage does in principle not release CO$_2$ to the atmosphere and is therefore carbon neutral.
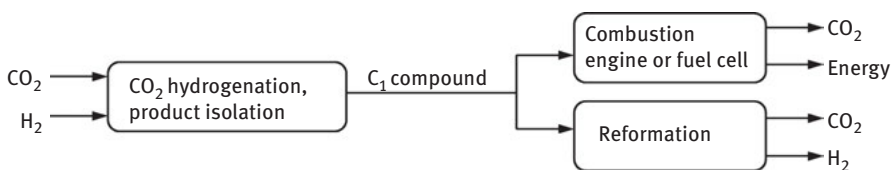
A) Decoupled Concept
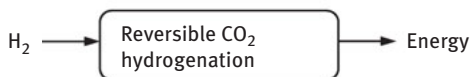
B) Integrated Concept

Figure 2.2: Main concepts for H$_2$ storage via CO$_2$ hydrogenation to MeOH, HCOOH and H$_2$CO.

Notably, also decoupled systems can be overall (on a global scale) be considered carbon neutral, as long as the hydrogen storage material is produced from atmospheric CO$_2$. Both concepts have advantages and drawbacks, but are also at a different level of maturity.

The decoupled approach A allows the CO$_2$ hydrogenation in dedicated plants providing a proper economy of scale and heat integration. One is also more flexible to choose optimal reaction conditions in the CO$_2$-hydrogenation, when this step does not have to be compatible with the requirements of a small-scale mobile device. In other words, the reaction setup can be tailored to the requirements of the hydrogenation step, which are different from the requirements of the dehydrogenation step. The liquid organic compound, which is obtained, can then be stored, shipped and distributed with the existing infrastructure of the gasoline industry. This would, for example,

also allow for fast energy refilling of mobile devices such as cars, busses and trucks. The energy density of the pure organic compounds is relatively high compared to currently available batteries, but lower than gasoline [11]. The main drawback is that the CO_2 will be released to the atmosphere when the energy is used from the organic carrier either by direct use in a combustion engine/fuel cell or reforming to generate the hydrogen for the use in a hydrogen fuel cell. Nowadays, this concept is the most mature and currently in the pilot-phase for CO_2 hydrogenation to methanol [12].

The integrated approach B requires a catalyst system, which is capable to hydrogenate CO_2 reversibly. A hydrogen infrastructure to refill the device is required, and also the hydrogenation of the CO_2 should proceed fast, in order to avoid long refilling times. The main advantage is that the CO_2 could be kept in the system during H_2 generation without being released to the atmosphere. This would be relevant in a future scenario, where no more fossil fuels will be burned as the main anthropogenic source for relatively easy available CO_2. On the other hand, a proper heat integration is difficult in mobile devices and in most concepts a solvent is necessary in the device, lowering the specific energy density.

For the use of methanol, formic acid and formaldehyde to store hydrogen via CO_2 hydrogenation, the most crucial parameters are the hydrogen densities of the systems and the thermodynamics of the corresponding hydrogenation/dehydrogenation reactions [5].

2.2 Methanol

Methanol provides with 12.6 wt% the highest hydrogen as well as energy density out of the three compounds, which makes it also viable for direct use in fuel cells or combustion engines. Methanol has also the benefit of a relatively clean burning process in combustion engines, forming less pollutants like soot compared to gasoline or diesel. Even if methanol is still used in mobile applications as a fuel or to blend gasoline [13, 14], it has to be considered that its energy density is with 5.6 kWh/kg only less than a half compared to diesel fuel (12 kWh/kg) and also lower than ethanol with 7.5 kWh/kg [11].

2.2.1 Heterogeneous catalyzed hydrogenation to methanol and reforming

The technology for the hydrogenation of CO_2 to methanol is the most mature out of the compounds discussed in this article. In conventional methanol plants, syngas containing up to 10 % CO_2 is currently used, as the conventional heterogeneous methanol catalysts can deal to a certain extent with CO_2 and it was shown that some CO_2 in the syngas mixture is even beneficial for the catalyst activity [13, 14].

But, nevertheless, for the synthesis of methanol only from CO_2 and H_2 new catalysts and a modified process design had to be developed. Notably, such hydrogenation

reactions are currently performed in the pilot phase showing the technical feasibility of the CO$_2$ hydrogenation to methanol [12, 14].

The hydrogenation of CO$_2$ to methanol is an exothermic and exergonic reaction at ambient conditions:

$$CO_2(g) + 3H_2(g) \rightleftharpoons CH_3OH(I) + H_2O(I)$$
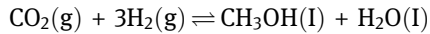
$$\Delta G^0 = -9.5 \text{ kJ/mol}, \Delta H^0 = -131 \text{ kJ/mol}$$

[5]

The currently most sophisticated catalysts for this hydrogenation are heterogeneous and based on modified Cu-ZnO-Al$_2$O$_3$ systems and are usually operated between 30–400 bar and 230–280 °C in order to achieve acceptable space time yields [13, 15–17]. A significant amount of alternative heterogeneous catalysts based on Pd or bimetallic system like Ni-Ga, Co-Cu or Pd-Cu were developed over the last years and the research is ongoing to identify catalysts combining a high activity and long catalyst lifetimes [15–17].

For a decoupled concept A to store hydrogen in MeOH, these systems can be well used in stationary plants to produce CO$_2$-based methanol. As mentioned above, this was recently applied in a 5000 t/a pilot plant in Iceland ("George Olah Plant"). This site has the strategic economic advantage that renewable and cheap geothermal energy is used to produce the electric energy, which is used for the hydrogen generation via electrolysis of water. The methanol is utilized as fuel ("Vulcanol^{TM}") for combustion engines in transportation, which means that the CO$_2$ will be released to the atmosphere after the use of the methanol [12].

If only the hydrogen from the methanol is required, it can be generated by methanol reforming. This technology is for example commercialized for the production of pure H$_2$ on sites, where no other hydrogen infrastructure like steam reforming of methane or connection to a H$_2$ pipeline grid is available [18]. The reformation of methanol is endothermic and is carried out with the conventional heterogeneous CuO/ZnO/Al$_2$O$_3$ catalysts at pressures of about 20 bar in a temperature range of 200–300 °C [19, 20].

$$MeOH(g) + H_2O(g) \rightleftharpoons CO_2(g) + 3H_2(g)$$
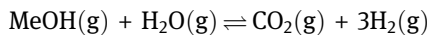
$$\Delta G^0 = +0.6 \text{ kJ/mol}, \Delta H^0 = 53.3 \text{ kJ/mol}$$

[21]

Due to the one equivalent water, the amount of hydrogen which can be generated out of the mixture by the reforming is with 18.9 wt% even higher than in pure methanol (12.6 %) [19]. But it has to be taken into account that the reformation is endothermic and MeOH and water has to be brought in the gas phase when the current catalysts

are used. Therefore, an additional amount of energy has to be provided for the reforming process.

Also concepts for the mobile use of methanol reforming were developed [22, 23]. The generated hydrogen can be used in a fuel cell, combining the advantages of an effective hydrogen fuel cell with the easy storage and handling of methanol. A prototype of a car utilizing the combination of MeOH reforming and an hydrogen fuel cell was presented by Daimler-Chrysler in the year 2000 (NECAR 5) and successfully tested, but the concept was never commercialized [24].

For the design of an integrated concept for the hydrogen storage with CO_2 (see Figure 2.3), a combination of the above described systems for methanol synthesis and reformation is hard to realize and could so far not be achieved.
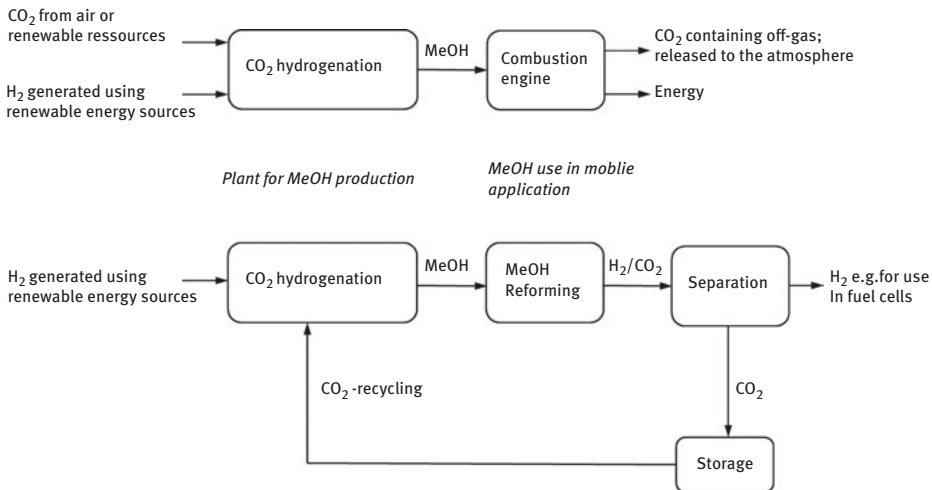
Figure 2.3: CO_2-neutral concepts for hydrogen storage using methanol and established heterogeneous catalysts.

If a combustion engine is used, separation and storage of the formed CO_2 from the off-gas stream is difficult in mobile applications. In case of methanol reforming and the use of H_2 in a fuel cell, the CO_2 has anyway to be separated prior use in the fuel cell by membranes. One can think about to store the separated CO_2 in a pressure tank and to bring it back to the CO_2 hydrogenation site, where it can be recycled. For sure, this will reduce the overall energy efficiency of the system, as the additional weight of the CO_2 storage system has to be transported. On the other hand, storage of compressed CO_2 in the liquid form is much simpler than for pressurized H_2. In a future scenario, where the CO_2 for the methanol formation could be obtained via efficient separation from air and the hydrogen could be produced from renewable resources, the release of CO_2 to the atmosphere after the dehydrogenation of methanol would lead to a

neutral CO_2 balance. First small-scale commercial units for CO_2 separation from air are available, but also this CO_2 capture is energy demanding and has low space time yields, which has to be taken into account in the overall energy efficiency of this hydrogen storage approach [25]. Another CO_2 neutral scenario would be, if the CO_2 is obtained from more concentrated CO_2 containing streams produced via renewable resources, for example from biogas plants.

2.2.2 Homogeneous catalyzed hydrogenation to methanol and reforming

In order to achieve the CO_2-hydrogenation as well as the MeOH-reformation at milder conditions and to develop integrated systems, different homogeneous catalysts were investigated in the CO_2 hydrogenation to methanol in the last years [9, 26]. The homogeneous catalyzed CO_2 hydrogenation to methanol proceeds usually via formic acid [27, 28], formates [27–29] or formamides [30, 31] as intermediates (see Figure 2.4), albeit direct hydrogenation reactions were reported [32].
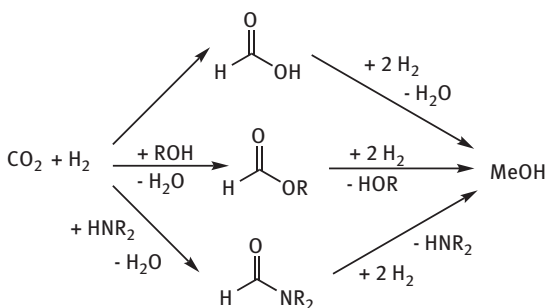
Figure 2.4: Homogeneous catalyzed CO_2-hydrogenation to methanol via formic acid derivate as intermediates.

The hydrogenation can be carried out in a cascade reaction using two different hydrogenation catalysts (one for CO_2 reduction to formates and the other for the formate hydrogenation) [27] or with a single catalyst which is able to carry out both reductions [28–31]. So far, most catalysts are based on ruthenium in combination with multidentate phosphine ligands and the catalytic reaction usually require co-catalysts such as K_3PO_4 [30, 31], KOtBu or acids [29]. Quite recently, the homogeneous catalyzed hydrogenation of CO_2 to methanol could be achieved with a non-precious cobalt-based catalyst. However, compared to the Ru catalysts the Co catalyst showed a significantly lower activity [28]. In contrast to the heterogeneous systems, the reaction conditions of the homogeneous catalysts are milder and are in the range of 100–160 °C at pressures of 40–90 bar. The catalyst activities in the homogenous approaches are currently relatively low and still far away from a technical use. For

example, the so far highest reported TON (turnover number) in a single run of 1200 could only be achieved after a reaction time of 200 h [27]. But it also has to be taken into account, that this is a relatively new field and more active catalysts will probably be identified with ongoing research efforts.

A first step for a more applied approach was developed with a biphasic reaction system, where the catalyst could be easily separated from the product and recycled [32]. In this approach, 2-methyl-tetrahydrofuran and water were used as the solvent mixture. After the reaction, the methanol is dissolved in the aqueous phase and the ruthenium catalyst in the 2-methyl-tetrahydrofuran-phase. After phase separation, the catalyst was recycled in the hydrogenation, and the methanol separated from the water via distillation. The catalyst was reused four times, resulting in an overall TON of 769.

Another interesting initial concept addressing the above-mentioned drawbacks on the use of atmospheric CO_2 was developed by carrying out the CO_2 hydrogenation to methanol with CO_2 captured from air with polyamines using ruthenium pincer complexes as catalysts (see Figure 2.5) [31].
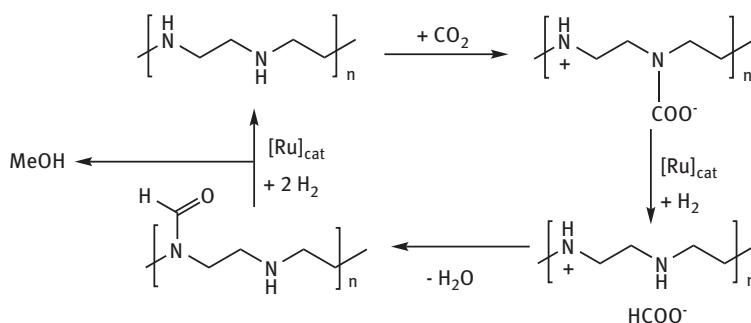
Figure 2.5: Hydrogenation of CO_2 from air to Methanol [31].

This hydrogenation proceeds via formylated polyamines as intermediates. TON of 765 could be achieved at 155 °C and 75 bar after 40 h. Here, the slow loading of the amine with CO_2 from the air represents the bottle neck of the process resulting in a not attractive space-time-yield of the overall system. Further optimization of this technology may lead in the future to a more promising catalytic system.

In contrast to the hydrogenation, for the reformation of methanol with water remarkable active homogeneous catalyst systems at mild conditions were reported [21, 33–37]. For example, a TON of 350 000 at a TOF (turn over frequency) of 4700 h^{-1} was achieved with a ruthenium pincer complex as catalyst in neat methanol containing 8.0 M KOH at 95 °C [33]. The high activity under the mild reaction conditions was obtained due to the presence of a base, which captures the CO_2 and therefore drives the reaction. In a base-free reformation reaction sequence, using two different ruthenium catalysts (one for the dehydrogenation of methanol and the other one for the

decomposition of intermediate formed formic acid), high boiling triglyme was used as solvent to obtain a TON of 4200 at a H$_2$ yield of 26 % [37]. Iron catalysts can also be applied in the reformation, providing excellent activities [35, 36]. Thus so far most active iron catalyst, an iron pincer complex, can provide TONs of up to 51,000 when the reaction is carried out under reflux with ethyl acetate as the solvent and 10 mol% LiBF$_4$ as additive [35]. This system works base-free, but a relatively diluted solution of methanol/water in ethyl acetate has to be used and the fate of the LiBF$_4$ additive in a long-term use has to be investigated, as it is known, that BF$_4$- can hydrolyze forming HF. Due to the low operational temperature, the homogenous catalyzed methanol reforming has the potential to be applied in a new generation of low temperature and liquid phase methanol reforming units.

Despite a significant progress, which has been achieved in the field of homogeneous CO$_2$ hydrogenation and methanol reforming, an integrated system for hydrogen storage utilizing the maximum H$_2$ density of 18.9 wt% for a MeOH/H$_2$O mixture could not yet be developed [38].

2.3 Formic acid

Pure formic acid contains 4.4 wt% considerably less hydrogen than methanol. Despite the fact that FA is a flammable liquid in air and it is not applied as fuel in combustion engines, due to its lower energy content of 2.1 kW/L [39] as compared to MeOH and its corrosivity. However, fuel cells for the direct electricity generation from formic acid were developed over the last years [40]. As the CO$_2$ hydrogenation to formic acid and certain formates can be performed reversibly under relatively mild conditions, this topic was thoroughly investigated over the last years in the context of hydrogen storage, especially for the development of integrated H$_2$ storage systems ("hydrogen batteries").

2.3.1 CO$_2$ hydrogenation to formic acid

The hydrogenation of CO$_2$ to formic acid was first reported in 1935 using Raney nickel as a heterogeneous catalyst [41] and the first homogenous approach was published in 1976 by using a ruthenium phosphine complex as catalyst [42]. Since then, a numerous amount of homogenous as well as heterogeneous catalysts with different active metals were utilized in this reaction, which is very well summarized in a series of excellent reviews [3, 5, 10, 15, 27, 43, 44, 45].

The hydrogenation of CO$_2$ to formic acid is an exothermic but endergonic reaction and therefore not favored under ambient conditions:

$$CO_2(g) + H_2(g) \rightleftharpoons HCOOH(I)$$
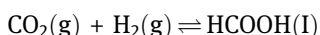
$$\Delta G^0 = 32.9 \text{ kJ/mol}, \Delta H^0 = -31.2 \text{ kJ/mol}$$

[46]

A common and broadly used approach is to carry out the CO_2 hydrogenation in the presence of a base, whereby the formation of salts or adducts is driving the reaction:

$$CO_2(g) + H_2(g) + NH_3(aq) \rightleftharpoons HCO_2 - (aq) + NH_4 + (aq)$$

$$\Delta G^0 = -9.5 \text{ kJ/mol}, \Delta H^0 = -84.3 \text{ kJ/mol}$$

[46]

Therefore, the use of amine bases, hydroxides or bicarbonates is a common approach to foster the CO_2 hydrogenation to formic acid or formates/amine adducts respectively. For example, the so far most active reported system uses this approach, where a combination of a ruthenium pincer complex wit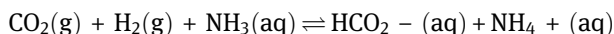h the base 1,8-diazabicylo[5,4,0]undec-7-ene (DBU) in dimethylformamide as solvent resulted in a TOF of 1 100 000 h^{-1} at 120 °C and 40 bar [47]. Even if the addition of bases is beneficial to achieve good activities with a lot of different catalysts, there are also significant drawbacks. If one wants to make pure formic acid, the acid has to be separated from the base, which requires significant amounts of energy or an additional acid resulting in salt formation as a by-product. One possibility to isolate formic acid is by taking appropriate high boiling amines like trihexylamine [46] or a basic ionic liquid [48, 49] from which the formic acid can be separated directly via distillation and also the catalyst can be separated. Even high activities were achieved with the frequently used NEt$_3$ as a base, the formic acid cannot be isolated directly by distillation, as it forms a stable azeotrope. In this case, another energy consuming base exchanging step with a higher boiling base like N-butylimidazole [50–53] or NHex$_3$ [54] is required from which free formic acid can be distilled off, leading to a less efficient overall process. When heterogeneous catalysts are used, in most cases also bases are used as additives to shift the unfavorable equilibrium and as a result to obtain reasonable catalyst activities [15]. In contrast to the previous mentioned systems, which uses homogeneous catalysts, for sure catalyst separation and recycling is much more straightforward, but the issues with the separation of the formic acid from the base still have to be tackled. Also, the very high catalysts activities of homogenous systems could not be achieved so far using heterogeneous catalysts.

To overcome the drawbacks from the use of a base in the CO_2 hydrogenation if one wants to isolate formic acid after the reaction, solvation of the formic acid in a suitable solvent can also help. For example, by using water, the reaction becomes exergonic:

$$CO_2(aq) + H_2(aq) \rightleftharpoons HCOOH(aq)$$
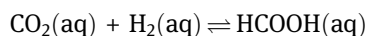
$$\Delta G^0 = -4 \text{ kJ/mol}$$

[15]

Although the CO_2 hydrogenation in water is exergonic, only low formic acid concentrations of currently max. 0.55 wt% could be obtained so far. Additionally, the catalyst activities for these reactions are much lower compared to the systems containing bases [55, 56]. A much more appropriate solvent for the base-free CO_2 hydrogenation to formic acid seems to be dimethylsulfoxide (DMSO) or mixtures of DMSO/H_2O. The solvation enthalpy of formic acid in DMSO is with 11.6 kJ/mol^{-1} significant higher than in pure water with 0.8 kJ/mol^{-1}, which was shown by calorimetric measurements [57]. By using homogeneous ruthenium catalysts, concentrations of formic acid up to 9.6 wt% were obtained in pure DMSO at pressures of 100 bar at 60 °C after a relatively long reaction time of 120 h [58]. Significant higher activities can be observed in DMSO-H_2O mixtures using ruthenium pincer catalysts at 120 bar and 60 °C, whereby a TOF of 260 h^{-1} was the highest reported in a 95 % DMSO mixture at a final HCOOH concentration of 1.53 wt% [59]. By adding an acetate buffer, the TOF could be increased to 1019 h^{-1} at a final HCOOH concentration of 5.8 wt% which is a significant achievement, but still some orders of magnitude away from the most active systems containing a base (see above). These base-free systems, in principle, have the advantage of a simpler and less energy consuming formic acid isolation compared to the base containing systems. Here, however, it is necessary to further improve the catalyst activities in order to increase the space-time-yield of the systems. Also, proper process concepts have to be designed with an efficient catalysts recycling and separation of the FA from the solvent.

The overall energy efficiency of the formic acid based hydrogen storage using isolated formic acid, based on the hydrogenation of CO_2 has to be carefully compared with other options like batteries of energy storage, such as compressed H_2 or MeOH. For example, it was recently shown in a study addressing the overall energy efficiency of the concept of formic acid production based on CO_2 hydrogenation, that a water gas shift of CO_2/H_2 to CO and then producing formic acid using the conventional route via CO [60] can be more efficient in terms of the energy use of the overall process [61]. This is mainly caused by the energy consuming formic acid isolation and low space time yield in the hydrogenation. So, there is still room for further investigations to develop more efficient CO_2 hydrogenation systems for energy storage.

2.3.2 Hydrogen generation from formic acid

The major advantages for the use of formic acids or its derivates in H_2 storage are that hydrogen can be generated efficiently under moderate conditions from neat formic acid, formic acid amine adducts or aqueous formate salt solution (see Figure 2.6).
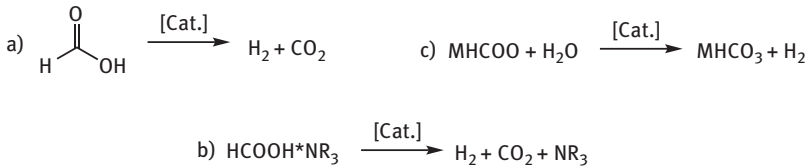
a)
$$\text{HCOOH} \xrightarrow{\text{[Cat.]}} H_2 + CO_2$$

c)
$$\text{MHCOO} + H_2O \xrightarrow{\text{[Cat.]}} \text{MHCO}_3 + H_2$$

b)
$$\text{HCOOH*NR}_3 \xrightarrow{\text{[Cat.]}} H_2 + CO_2 + NR_3$$

Figure 2.6: H_2 generation from (a) formic acid, (b) formic acid amine adducts or (c) aqueous formate salts.

If the amine adducts or formates are used as the H_2 storage compounds, the isolation of formic acid from the reaction mixture of a CO_2 hydrogenation reaction is no longer necessary.

Like in the CO_2 hydrogenation, numerous homogeneous and heterogeneous catalysts for the formic acid decomposition were reported and the systems are well and comprehensively reviewed [1, 5, 62–67]. Catalysts are necessary for the decomposition to H_2/CO_2 by lowering the activation barrier and for selectivity reasons, as at higher temperatures, formic acid can thermally also be decomposed to CO and H_2O. For the use of the H_2 in fuel cells, CO should be avoided due to poisoning of the electrodes. The activity and robustness of, which are achieved by state-of-the-art systems are quite remarkable and in an advanced technological state. For example, different continuous concepts were developed using ruthenium phosphine catalysts for the H_2-generation from formic acid/amine-adducts with TON over 1 000 000 during 45 days [68] or from an aqueous sodium formate solution in an integrated system with an power output of 1 KW electrical energy (see Figure 2.7) [69].
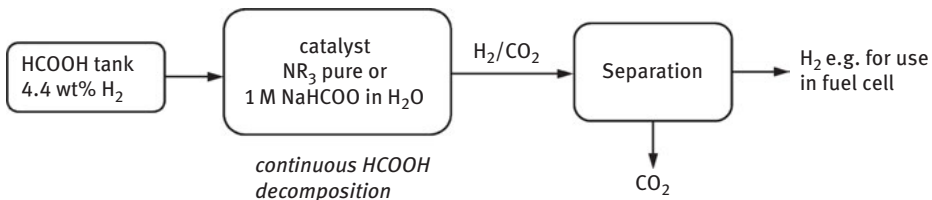
Figure 2.7: Pilot concepts for the continuous H_2 generation from formic acid.

In this case the catalysts were shown to be stable in the continuous mode for more than a year [69].

The hydrogen density in the actual hydrogen generating units is lower than the 4.4 wt% in the free formic acid due to the dilution effect of the base. But as the base remains in this unit and pure FA is fed continuously in both cases, in the FA tank the hydrogen density is 4.4 wt%. H_2 pressures of more than 40 bar H_2 at temperatures below 100 °C can easily be achieved using this systems for the formic acid decomposition [68, 69].

Currently, significant research progress was reported in using non-precious metals as catalysts for the CO_2 decomposition, in order to replace expensive metals in the H_2 generation [65].

For decoupled CO_2 neutral concepts using formic acid in the hydrogen storage, the above-mentioned systems can be combined. As formic acid is not used in combustion engines, the CO_2 can relatively simple be separated from a formic acid decomposition unit or the off-gas from a fuel cell and be recycled as described for the methanol concept (see Figure 2.8).
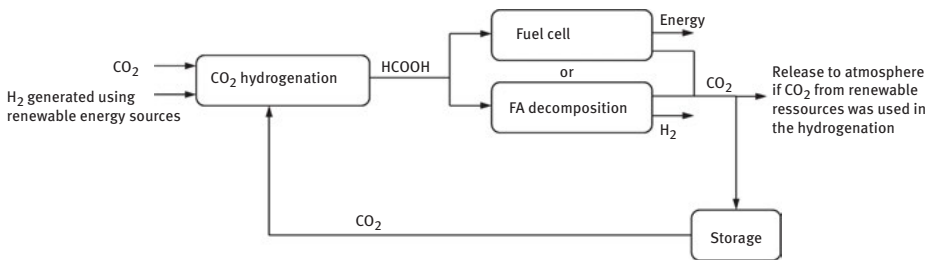
Figure 2.8: Decoupled CO_2-neutral concepts for hydrogen storage using formic acid.

If CO_2 from renewable sources is used in the hydrogenation, CO_2 can be released to the atmosphere after formic acid use for a CO_2 neutral concept. But in contrast to the hydrogen storage using methanol, it is much easier to perform the H_2 storage in an integrated system based on formic acid/formates.

2.3.3 H_2 storage in integrated systems via formic acid/formates

As many catalysts for the CO_2 hydrogenation to formic acid (or formates) are also catalyzing the decomposition using similar solvents and additives like in the hydrogenation and due to the favorable thermodynamics, the realization of integrated systems for H_2 storage could be achieved during the last years (see Figure 2.9) [4, 43, 47, 64, 65, 70–75].

Within these approaches, it has to be distinguished between two main concepts, the CO_2 is bound as a carbonate and stays in the reaction mixture, whereas in the other, CO_2 has to be fed to the hydrogenation and is released after the dehydrogenation respectively.

For the first case, the CO_2 is bound in an aqueous alkali bicarbonate or carbonate solution and hydrogenated to the corresponding aqueous formate solution under H_2 pressure using homogenous [70, 76] or heterogeneous catalysts [75]. The reaction is reversible and therefore H_2 is generated when decreasing the pressure. The CO_2 stays in the solution as a bicarbonate or carbonate. The system has the advantage that it is

Charging:
$MHCO_3 + H_2 \rightarrow 2\ MHCOO + H_2O$
typically 80-100 bar, 60-80°C

Discharging:
$MHCOO + H_2O \rightarrow MHCO_3 + H_2$
release pressure, typically 40-60°C
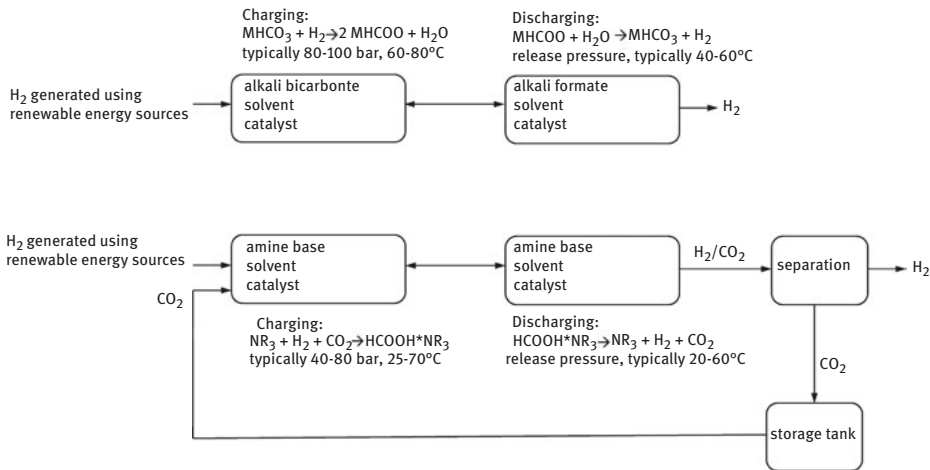
H_2 generated using renewable energy sources

alkali bicarbonte
solvent
catalyst

alkali formate
solvent
catalyst

H_2

H_2 generated using renewable energy sources

CO_2

amine base
solvent
catalyst

amine base
solvent
catalyst

H_2/CO_2

separation

H_2

Charging:
$NR_3 + H_2 + CO_2 \rightarrow HCOOH{*}NR_3$
typically 40-80 bar, 25-70°C

Discharging:
$HCOOH{*}NR_3 \rightarrow NR_3 + H_2 + CO_2$
release pressure, typically 20-60°C

CO_2

storage tank

Figure 2.9: Integrated concepts for H_2 storage via reversible CO_2 hydrogenation to formic acid/formats.

not necessary to separate CO_2 from the H_2 and stays in the reaction system. The main drawback of the available systems is, that the achieved hydrogen capacities due to the dilution effect of the required solvent are below 1wt%, reducing the efficiency of the H_2 storage system significantly. This is especially an issue for potential mobile applications. There is room for improvement, as the approach seems to be promising for the storage of H_2 but still has a too low energy density for most practical uses.

In the second case, the CO_2 is not kept in the reaction system and released along with the H_2, which also means that both CO_2 and H_2 need to be fed when charging the system [47, 71–73]. For example amine bases in combination with organic solvents can be used as reaction media for such systems. Unfortunately, the base and solvent are also "diluting" the density for available hydrogen which remains below 1 wt% in the known systems. If one would want to keep the CO_2 in the system, a H_2/CO_2 separation unit and a CO_2-storage tank is needed. The CO_2 from the storage thank then has to be recompressed for the CO_2 hydrogenation requiring additional equipment. This compression step, naturally, consumes additional energy.

2.4 Formaldehyde

Free formaldehyde is a gas at ambient conditions and contains 6.6 wt% more hydrogen than formic acid. Formaldehyde is usually produced and shipped on commercial scale as a 37 wt% solution in water, in which it forms methylene glycole ($HOCH_2OH$) along with low molecular mass poly(oxymethylene)glycols [77]. In the form of the diol, the available amount of hydrogen is with 8.4 wt% even higher than in free formaldehyde. With methanol, the stable and liquid acetale dimethoxymethane (DMM; $MeOCH_2OMe$) can be formed, which has a hydrogen content of 10.5 wt% (see Figure 2.10).
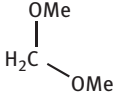
C1-Compund:	Formaldehyde	Formaldehyde-Hydrate	Dimethoxymethane
Hydrogen Content:	6.6 wt%	8.4 wt%	10.5 wt%

Figure 2.10: Hydrogen content of formaldehyde and derivates.

The relatively high hydrogen content of methylene glycol and DMM makes them attractive for the hydrogen storage based on CO_2. DMM itself is already used as fuel additive and also discussed as an alternative diesel fuel due to its combustion properties. But in contrast to methanol and formic acid the syntheses of formaldehyde or DMM via CO_2 hydrogenation is much less investigated and reports on systems for CO_2 hydrogenations to these targets are rare so far [43, 78].

2.4.1 CO_2 Hydrogenation to formaldehyde

One reason for the lack of reports on the hydrogenation of CO_2 to formaldehyde is that this reaction is thermodynamically not favored, at ambient conditions, as it is a strongly endergonic and endothermic reaction:

$$CO_2(g) + 2 H_2(g) \rightarrow H_2CO\ (g) + H_2O\ (g)$$
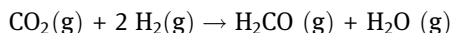
$$\Delta G^0 = 59.8\ kJ/mol,\ \Delta H^0 = 39.8\ kJ/mol,\ \Delta S^0 = -67 J/Kmol$$

[79]

In addition to the unfavorable thermodynamics, the highly reactive nature of formaldehyde causes in most cases overreduction of CO_2 to methanol or methane, which is usually thermodynamically preferred over formation of formaldehyde in reaction of CO_2 and H_2.

Despite these drawbacks, formaldehyde formation based on CO_2 hydrogenation could be observed at 150 °C and 6 bar when a heterogeneous $PtCu/SiO_2$-catalyst was used [80] and with NiCo/P-nanoparticles as catalyst at 200 °C and 6 bar [81]. But the CO_2 conversions were below \lt1 % and certain byproducts such as methanol or CO was formed. These systems are only first observations and still far away from any practical application. Apart from this two heterogeneous systems, there is also a single report, where by using a ruthenium complex in water at 34 bar and 40 °C small amounts of formaldehyde were detected along with formic acid as the major products from the CO_2 hydrogenation [82].

The thermodynamic situation changes when the hydrogenation is performed in the presence of methanol and DMM is formed:

$$CO_2(g) + 2 H_2(g) + 2 MeOH (I) \rightarrow MeOCH_2OMe (I) + 2 H_2O (I)$$
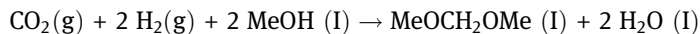
$$\Delta G^0 = 12.5 \text{ kJ/mol}, \Delta H^0 = -73.4 \text{ kJ/mol}$$

[79]

In contrast to the formaldehyde formation this reaction is exothermic and the free reaction enthalpy is only slightly positive. By increasing the pressure above 80 bar, the equilibrium can be shifted at room temperature toward the products if the reaction is conducted in the presence of an appropriate catalyst:

$$CO_2(40 \text{ bar}) + 2 H_2(40 \text{ bar}) + 2 MeOH (I) \rightarrow MeOCH_2OMe (I) + 2 H_2O (I)$$

$$\Delta G = -0.3 \text{ kJ/mol}, \Delta H = -73.4 \text{ kJ/mol}$$

[79]

The formation of the stable DMM can also help to prevent the overreduction, as the reactive carbonyl functionality of the formaldehyde is masked in this derivate. The synthesis of DMM could recently be achieved performing the CO_2 hydrogenation in methanol using ruthenium- or cobalt triphos (= 1,1,1-tris(diphenylphosphinomethyl) ethane) complexes in combination with an acidic co-catalyst like $Al(OTf)_3$ or $HNTf_2$ (Tf = trifluoromethanesulfonyl) [83, 84]. The reactions are typically performed at 80–120 °C and 80–120 bar and a max TON of 214 was observed after 18 h (see Figure 2.11).
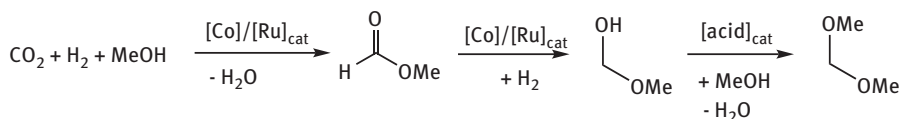
Figure 2.11: CO_2 hydrogenation in methanol to DMM via MeFo [83, 84].

The hydrogenation proceeds via methylformate (MeFo) as intermediate and therefore the product mixtures are containing MeFo as a byproduct. This would not be a significant drawback in a potential technical application, as DMM and MeFo can easily be separated by distillation and the MeFo recycled in the reaction and further hydrogenated to DMM. For this catalytic reaction the catalyst activities and yields are still low, but taking into account that only the first reports on this topic have been published, one may be optimistic and expect improvements in the future.

If the used methanol is based on a CO_2 hydrogenation, the resulting DMM will also be a fully CO_2-based hydrogen storage material.

A very elegant, but hitherto unknown method would be, if CO_2 can directly be hydrogenated to DMM without the use of MeOH produced by another process:

$$3 \text{ CO}_2 + 8 \text{ H}_2 \rightarrow \text{H}_3\text{COCH}_2\text{OCH}_3 + 4 \text{ H}_2\text{O}$$
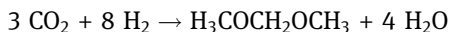
The development of this reaction may be very challenging as catalysts, which are capable of hydrogenating CO$_2$ to methanol are also able to hydrogenate the intermediate MeFo very fast to methanol or dimethylether and presumably not to DMM. Certainly, the development of an efficient process for the direct DMM synthesis represents a challenging task for the future.

2.4.2 Hydrogen generation from formaldehyde

In contrast to the CO$_2$ hydrogenation to formaldehyde, its reforming is thermodynamically strongly favored under ambient conditions (see Section 2.3.2 and Figure 2.12).
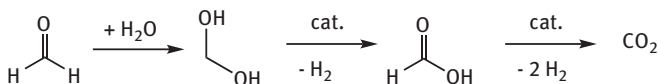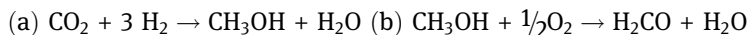

Figure 2.12: Reforming of formaldehyde [78].

In this context it is surprising that deeper investigations on the hydrogen generation from formaldehyde were only reported in the last years [85–88]. Simple homogeneous iridium and ruthenium catalysts can be used to produce hydrogen efficiently from aqueous formaldehyde solutions at temperatures typically in a range of 25–95 °C. In comparison to the MeOH reforming, an advantage of the reforming of formaldehyde is that not bases as additives are needed. The reforming proceeds via the dehydrogenation of methylene glycol to formic acid as the intermediate, which is further dehydrogenated to CO$_2$ and H$_2$.

Despite the fact that this reformation proceeds very well under mild conditions, due to the favorable thermodynamics, at the moment there is no technical process, which provides formaldehyde based on a direct CO$_2$ hydrogenation. Certainly one can think about to hydrogenating CO$_2$ to methanol using one of the above described processes (see subchapter 2.1) and then producing a CO$_2$-based formaldehyde with the state-of-the-art methanol oxidation [77]:

$$\text{(a) CO}_2 + 3 \text{ H}_2 \rightarrow \text{CH}_3\text{OH} + \text{H}_2\text{O} \quad \text{(b) CH}_3\text{OH} + \tfrac{1}{2}\text{O}_2 \rightarrow \text{H}_2\text{CO} + \text{H}_2\text{O}$$

But in terms of an efficient hydrogen storage this would be a very uneconomic approach, as one equivalent of the energy containing H$_2$ is lost as water in the methanol oxidation. In this case, it makes much more sense to utilize the CO$_2$-based methanol directly in a reforming unit or as fuel (see subchapter 2).

On the other hand, one can also think about using CO$_2$-based DMM in the reforming, which is in principle with the above described systems accessible. The

available hydrogen content of the reforming mixture DMM/H_2O is with 10.9 wt% relatively high:

$$MeOCH_2OMe + 4\ H_2O \rightarrow 8\ H_2 + 3\ CO_2$$
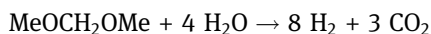
Several heterogeneous catalysts systems are reported for the DMM reformation and CuO-ZnO/Al_2O_3- [89–91] or CuO-CeO$_2$/Al_2O_3-base catalysts [92] can be used. In a temperature range of 250–350 °C at ambient pressure catalysts activities of up to 15.5 l H_2/(g_{cat}*h) were reported at full DMM conversion. In order to achieve a high selectivity in respect to a negligible CO formation, acidic co-catalysts are beneficial [89, 90].

Currently, there are no systems known for the design of an integrated concept for a formaldehyde-based hydrogen storage. Decoupled concepts would look quite similar to the ones presented for methanol (see Figure 2.13).
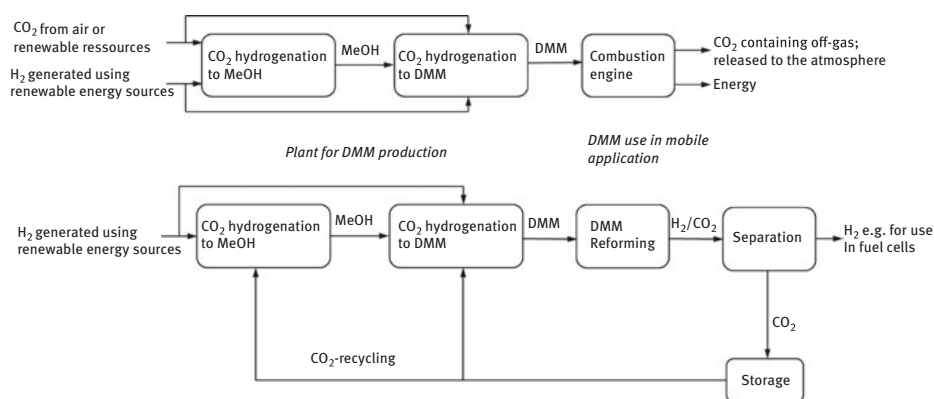
Figure 2.13: CO_2-neutral concepts for hydrogen storage using dimethoxymethane and hitherto known catalyst systems.

However, taking into account the current state the application of such systems still remains elusive. For the use of DMM as a hydrogen storage material based on CO_2 hydrogenation, according to the state of the art a decoupled concept is imaginable. In contrast to methanol as hydrogen carrier, as no catalysts is currently known to produce DMM directly from CO_2/H_2 two hydrogenation units would be required: One for the synthesis of CO_2-based methanol and another for the DMM synthesis using this methanol.

2.5 Conclusion

The hydrogenation of CO_2 to the C_1 compounds methanol, formic acid and formaldehyde offers the possibility for efficient H_2 storage, with methanol having the highest

theoretical hydrogen content of these molecules. The use of methanol in hydrogen storage is currently also the most advanced out of the three presented compound classes. But as extensive research is ongoing in the field of CO$_2$ hydrogenation, further attractive H$_2$ storage systems will probably be developed in the future.

A final remark, however, needs to be stated: Independently which C$_1$ compound is used for the CO$_2$-based hydrogen storage, one has carefully to evaluate and compare the overall energy efficiencies of different systems. Such a calculation starts with hydrogen generation and ends with the utilization of the energy/hydrogen in the final device. This has to be compared with all the possible alternatives such as hydrogen pressure tanks, batteries, reforming/fuel cell vs. direct use in combustion engine and so on. Such a comprehensive comparison is necessary to eventually choose the best and most efficient solution for the given request.

References

[1]   Aresta M. Carbon dioxide: utilization options to reduce its accumulation in the atmosphere. In: Aresta M, editor. Carbon dioxide as chemical feedstock. New York-Weinheim: Wiley-VCH, 2010.

[2]   Schlögel R, editor. Chemical energy storage. Berlin-Boston: de Gruyter, 2013.

[3]   Yadav M, Xu Q. Liquid-phase chemical hydrogen storage materials. Energy Environ Sci. 2012;5:9698–725.

[4]   Dalebrook AF, Gan W, Grasemann M, Moret S, Laurenczy G. Hydrogen storage: Beyond conventional methods. Chem Commun. 2013;49:8735–51.

[5]   Wang WH, Himeda Y, Muckerman JT, Manbeck GF, Fujita E. CO$_2$ hydrogenation to formate and methanol as an alternative to photo- and electrochemical CO$_2$ reduction. Chem Rev. 2015;115:12936–73.

[6]   Ali KA, Abdullah AZ, Mohamed AR. Recent development in catalytic technologies for methanol synthesis from renewable sources: A critical review. Renew Sustainable Energy Rev. 2015;44:508–18.

[7]   Jadhav SG, Vaidya PD, Bhanage BM, Joshi JB. Catalytic carbon dioxide hydrogenation to methanol: A review of recent studies. Chem Eng Res Des. 2014;92:2557–67.

[8]   Li YN, Ma R, He LN, Diao ZF. Homogeneous hydrogenation of carbon dioxide to methanol. Catal Sci Technol. 2014;4:1498–512.

[9]   Ma J, Sun N, Zhang X, Zhao N, Xiao F, Wei W, et al. A short review of catalysis for CO$_2$ conversion. Catal Today. 2009;148:221–31.

[10]   Jessop PG, Joó F, Tai CC. Recent advances in the homogeneous hydrogenation of carbon dioxide. Coord Chem Rev. 2004;248:2425–42.

[11]   Schüth F. Energy storage strategies. In: Schlögl R, editor. Chemical energy storage. Berlin-Boston: de Gruyter, 2013.

[12]   Information on the George Olah renewable methanol plant in Iceland Available at: http://carbonrecycling.is/george-olah/.

[13]   Kunkes E, Beherns M. Methanol chemistry. In: Schlögl R, editor. Chemical energy storage. Berlin-Boston: de Gruyter, 2013.

[14]   Ott J, Gronemann V, Pontzen F, Fiedler E, Grossmann G, Kersebohm DB, et al. Methanol. In: Ullmann´s encyclopedia of industrial chemistry. Weinheim: Wiley-VCH, 2012.

[15] Alvsrez A, Bansode A, Urakawa A, Bavykina AV, Wezendonk TA, Makkee M, et al. Challenges in the greener production of formates/formic acid, methanol and DME by heterogeneously catalyzed CO_2 hydrogenation processes. Chem Rev. 2017;117:9804–38.

[16] Ganesh I. Conversion of carbon dioxide into methanol - A poential liquid fuel: Fundamental challenges and opportunities (a review). Renew Sustainable Energy Rev. 2014;31:221–57.

[17] Beherns M. Promoting the synthesis of methanol: Understanding the requirements for an industrial catalyst for the conversion of CO_2. Angew Chem Int Ed. 2016;55:14906–08.

[18] For commercial available methanol reformer on different scales see for example: (a) http://www.altergy.com/products-2/methanol-reformer/, (b) http://www.mahler-ags.com/hydrogen/hydroform-m.htm, (c) https://www.topsoe.com/subprocess/methanol-reforming.

[19] Palo DR, Dagle RA, Holladay JD. Methanol steam reforming for hydrogen production. Chem Rev. 2007;107:3992–4021.

[20] Sá S, Silva H, Brandao L, Sousa JM, Mendes A. Catalysts for methanol steam reforming - A review. Appl Catal B. 2010;99:43–57.

[21] Alberico E, Lennox AJ, Vogt LK, Jiao H, Baumann W, Drexler HJ, et al. Unravelling the mechanism of basic aqeous methanol dehydrogenation catalyzed by Ru-PNP Pincer complexes. J Am Chem Soc. 2016;138:14890–904.

[22] Peters R, Düsterwald HG, Höhlein BJ. Investigation of a methanol reformer concept considering the particular impact of dynamics and long-term stability for use in a fuel-cell powered passenger car. Power Sources. 2000;86:507–14.

[23] Wiese W, Emonts B, Peters RJ. Methanol steam reforming in a fuel cell drive system. Power Sources. 1999;84:187–93 and Emonts B, Hansen, JB, Jorgensen SL, Höhlein B, Peters R. J. Compact methanol reformer test for fuel cell powered light duty vehicles. Power Sources 1998;71:288–93.

[24] http://www.hybrid-autos.info/Wasserstoff-Fahrzeuge/Mercedes/necar5-2000.

[25] www.climeworks.com.

[26] Alberico E, Nielsen M. Towards a methanol economy based on homogeneous catalysis: methanol to H_2 and CO_2 to methanol. Chem Commun. 2015;51:6714–25.

[27] Huff CA, Sanford MS. Cascade catalysis for the homogeneous hydrogenation of CO_2 to methanol. J Am Chem Soc. 2011;133:18122–25.

[28] Schneidewind J, Adam R, Baumann W, Jackstell R, Beller M. Low -temperature hydrogenation of carbon dioxide to methanol with a homogeneous catalyst. Angew Chem Int Ed. 2017; 56:1890–93.

[29] Wesselbaum S, vom Stein T, Klankermayer J, Leitner W. Hydrogenation of carbon dioxide to methanol by using a homogeneous ruthenium-phosphine catalyst. Angew Chem Int Ed. 2012;51:7499–502.

[30] Rezayee NM, Huff CA, Sanford MS. Tandem amine and ruthenium-catalyzed hydrogenation of CO_2 to methanol. J Am Chem Soc. 2015;137:1028–31.

[31] Kothandaraman J, Goeppert A, Czaun M, Olah GA, Prakash GK. Conversion of CO_2 from air into methanol using a polyamine and a homogeneous ruthenium catalyst. J Am Chem Soc. 2015;138:778–81.

[32] Wesselbaum S, Moha V, Meuresch M, Brosinski S, Thenert KM, Kothe J, et al. Hydrogenation of carbon dioxide to methanol using a homogeneous ruthenium-triphos catalyst: From mechanistic investigations to multiphase catalysis. Chem Sci. 2015;6:693–704.

[33] Nielsen M, Alberico E, Baumann W, Drexler HJ, Junge H, Gladiali S. Low-temperature aqueous-phase methanol dehydrogenation to hydrogen and carbon dioxide. Beller M Nat. 2013; 495:85–89.

[34] Hu P, Diskin-Posner Y, Ben-David Y, Milstein D. Reusable homogeneous catalytic system for hydrogen production from methanol and water. ACS Catal. 2014;4:2649–52.

[35] Bielinski EA, Förster M, Zhang Y, Bernskoetter WH, Hazari N, Holthausen MC. Base-free methanol dehydrogenation using a pincer-supported iron compound and lewis acid co-catalyst. ACS Catal. 2015;5:2404–15.

[36] Alberico E, Sponholz P, Cordes C, Nielsen M, Drexler HJ, Baumann W, et al. Selective hydrogen production from methanol with a defined iron pincer catalyst under mild conditions. Angew Chem Int Ed. 2013;52:14162–66.

[37] Monney A, Barsch E, Sponholz P, Junge H, Ludwig R, Beller M. Base-free hydrogenation from methanol using a bi-catalytic system. Chem Commun. 2014;50:707–09.

[38] Kothandaraman J, Kar S, Sen R, Goeppert A, Olah GA, Prakash GK. Efficient reversible hydrogen carrier system based on amine reforming of methanol. J Am Chem Soc. 2017;139:2549–52.

[39] Yu X, Pickup PG. Recent advances in direct formic acid fuel cells (DFAFC). J Power Sources. 2008;182:124–32.

[40] Aslam NM, Masdar MS, Kamarudin SK, Daud WR. Overview on direct formic acid fuel cells (DFAFCs) as an energy sources. APCBEE Procedia. 2012;3:33–39.

[41] Farlow MW, Adkins HJ. The hydrogenation of carbon dioxide and a correction of the reported synthesis of urethans. J Am Chem Soc. 1935;57:2222–23.

[42] Inoue Y, Izumida H, Sasaki Y, Hashimoto H. Catalytic fixation of carbon dioxide to formic acid by transition-metal complexes under mild conditions. Chem Let. 1976;5:863–64.

[43] Klankermayer J, Wesselbaum S, Beydoun K, Leitner W. Selective catalytic synthesis using the combination of carbon dioxide and hydrogen: Catalytic chess at the interface of energy and chemistry. Angew Int Ed. 2016;55:7296–343.

[44] Gunasekar GH, Park K, Jung KD, Yoon S. Recent developments in the catalytic hydrogenation of CO$_2$ to formic acid/formate using heterogeneous catalysts. Inorg Chem Front. 2016;3:882–95.

[45] Leitner W. Carbon dioxide as a raw material: The synthesis of formic acid and its derivatives from CO$_2$. Angew Chem Int Ed. 1995;34:2207–21.

[46] Schaub T, Paciello RA. A process for the synthesis of formic acid by CO$_2$ hydrogenation: Thermodynamic aspects and the role of CO. Angew Chem Int Ed. 2011;50:7278–82.

[47] Filonenko GA, Van Putten R, Schulpne EN, Hensen EJ, Pidko EA. Highly efficient reversible hydrogenation of carbon dioxide to formates using a ruthenium PNP-Pincer catalyst. Chem Cat Chem. 2014;6:1526–30.

[48] Zhang Z, Xie Y, Li W, Hu S, Song J, Jiang T, et al. Hydrogenation of carbon dioxide is promoted by a task-specific ionic liquid. Angew Chem Int Ed. 2008;47:1127–29.

[49] Wesselbaum S, Hintermair U, Leitner W. Continuous-flow hydrogenation of carbon dioxide to pure formic acid using an integrated scCO$_2$ process with immobilized catalyst and base. Angew Chem Int Ed. 2012;51:8585–88.

[50] Anderson JJ, Hamlin JE. EP0126524 Process for the preparation of formic acid 1984.

[51] Anderson JJ, Drury DJ, Hamlin JE, Kent AG. EP0181078 Process for the preparation of formic acid 1985.

[52] Beevor RG, Gulliver DJ, Kitson M, Sorrell RM. EP0357243 The production of formate salts of nitrogenous bases 1989.

[53] Green MJ, Lucy AR, Kitson M, Smith SJ. EP0329337 The production of formic acid from a nitrogenous base, carbon dioxide and hydrogen. 1989.

[54] Preti D, Resta C, Squarcialupi S, Fachinetti G. Carbon dioxide hydrogenation to formic acid by using a heterogeneous gold catalyst. Angew Chem Int Ed. 2011;50:12551–54.

[55] Hayashi H, Ogo S, Fukuzumi S. Aqueous hydrogenation of carbon dioxide catalysed by water-soluble ruthenium aqua complexes under acidic conditions. Chem Commun. 2004;(23):2714–15.

[56] Lu SM, Wang Z, Li J, Xiao J, Li C. Base-free hydrogenation of CO_2 to formic acid in water with an iridium complex bearing an N,N-diimine ligand. Green Chem. 2016;18:4553–58.

[57] Fink C, Katsyuba S, Laurenczy G. Calorimetric and spectroscopic studies on solvation energetics for H_2 storage in the CO_2/HCOOH system. Phys Chem Chem Phys. 2016;18:10764–73.

[58] Moret S, Dyson PJ, Laurenczy G. Direct synthesis of formic acid from carbon dioxide by hydrogenation in acidic media. Nat Commun. 2014;5(4017):23. DOI: 10.1038/ncomms5017.

[59] Rohmann K, Kothe J, Haenel MW, Englert U, Hölscher M, Leitner W. Hydrogenation of CO_2 to formic acid witrh a highly active ruthenium acriphos complex in DMSO and DMSO/water. Angew Chem Int Ed. 2016;55:8966–69.

[60] Reutemann W, Kieczka H. Formic acid. In: Ullmann´s encyclopedia of industrial chemistry. Weinheim: Wiley-VCH, 2012.

[61] Schmidt I, Müller K, Arlt W. Evaluation of formic-acid-based hydrogen storage technologies. Energy Fuels. 2014;28:6540–44.

[62] Loges B, Boddien A, Gärtner F, Junge H, Beller M. Catalytic generation of hydrogen from formic acid and its derivates: Useful hydrogen storage materials. Top Catal. 2010;53:902–14.

[63] Li J, Zhu QL, Xu Q. Dehydrogenation of formic acid by heterogeneous catalysts. Chimia. 2015;69:348–52.

[64] Singh AK, Singh S, Kumar A. Hydrogen energy future with formic acid: A renewable chemical hydrogen storage system. Cat Sci Technol. 2016;6:12–40.

[65] Mellmann D, Sponholz P, Junge H, Beller M. Formic acid as a hydrogen storage material - Development of homogeneous catalysts for selective hydrogen release. Chem Soc Rev. 2016;45:3954–88.

[66] Kawanami H, Himeda Y, Laurenczy G. Formic acid as a hydrogen carrier for fuel cells toward a sustainable energy system. Adv Inorg Chem. 2017;70:395–427.

[67] Laurenczy G, Dyson PJ. Homogeneous catalytic dehydrogenation of formic acid: Progress towards a hydrogen-based economy. J Braz Chem Soc. 2014;25:2157–63.

[68] Sponholz P, Mellmann D, Junge H, Beller M. Towards a practical setup for hydrogen production from formic acid. Chem Sus Chem. 2013;6:1172–76.

[69] Grasemann M, Laurenczy G. Formic acid as a hydrogen source - Recent developments and future trends. Energy Environ Sci. 2012;5:8171–81.

[70] Papp G, Csorba J, Laurenczy G, Joó F. A charge/discharge device for chemical hydrogen storage and generation. Angew Chem Int Ed. 2011;50:10433–35.

[71] Boddien A, Federsel C, Sponholz P, Mellmann D, Jackstell R, Junge H, et al. Towards the development of a hydrogen battery. Energy Environ Sci. 2012;5:8907–11.

[72] Hull JF, Himeda Y, Wang WH, Hashiguchi B, Periana R, Szalda DJ, et al. Reversible hydrogen storage using CO_2 and a proton-switchable iridium catalyst in aqueous media under mild temperatuers and pressures. Nat Chem. 2012;4:383–88.

[73] Wang L, Onishi N, Murata K, Hirose T, Muckerman JT, Fujita E, et al. Efficient hydrogen storage and production using a catalyst with an imidazoline-based, proton-responsive ligand. Chem Sus Chem. 2017;10:1071–75.

[74] Leitner W, Dinjus E, Gassner FJ. Activation of carbon dioxide: IV. Rhodium-catalysed hydrogenation of carbon dioxide to formic acid. Organomet Chem. 1994;475:257–66.

[75] Koh K, Jeon M, Chevrier DM, Zhang P, Yoon CW, Asefa T. Novel nanoporous N-doped carbon-supported ultrasmall Pd nanoparticles: Efficient catalysts for hydrogen storage and release. Appl Catal B. 2017;203:820–28.

[76] Boddien A, Gärtner F, Federsel C, Sponholz P, Mellmann D, Jackstell R, et al. CO_2-"Neutral" hydrogen storage based on bicarbonates and formates. Angew Chem Int Ed. 2011;50:6411–14.

[77] Reuss G, Disteldorf W, Gamer AO, Hilt A. Formaldehyde. In: Ullmann´s encyclopedia of industrial chemistry. Weinheim: Wiley-VCH; 2012.

[78] Heim LE, Konnerth H, Pretzl MH. Future perspectives for formaldehyde: Pathways for reductive synthesis and energy storage. Green Chem. 2017;19:2347–55.

[79] Thermodynamic values based on calculations performed in the authors lab: Structures with MP2/def2-TZVP, single-point energies with CCSD(T)/def2-QZVPP, solvation contributions with COSMO-RS/BP86/def-TZVP.

[80] Lee DK, Kim DS, Kim SW. Selective formation of formaldehyde from carbon dioxide and hydrogen over PtCu/SiO$_2$. Appl Organomet Chem. 2001;15:148–50.

[81] Carenco S, Wu CH, Shavorskiy A, Alayoglu S, Somorjai GA, Bluhm H, et al. Synthesis and structural evolution of nickel-cobalt nanoparticles under H$_2$ and CO$_2$. Small. 2015;11:3045–53.

[82] Kahn MM, Hallogudi SB, Shukla S. Reduction of CO$_2$ by molecular hydrogen to formic acid and formaldehyde and their decomposition to CO and H$_2$O. J Mol Catal. 1989;57:47–60.

[83] Thenert K, Beydoun K, Wiesenthal J, Leitner W, Klankermayer J. Ruthenium-catalyzed synthesis of dialkoxymethane ethers utilizing carbon dioxide and molecular hydrogen. Angew Chem Int Ed. 2016;55:12266–69.

[84] Schwieweck BG, Klankermayer J. Tailor-made molecular cobalt catalyst system for the selective transformation of carbon dioxide to dialkoxymethane ethers. Angew Chem Int Ed. 2017;56:10854–7.

[85] Heim LE, Schloerer NE, Choi JH, Prechtl MH. Selective and mild hydrogen production using water and formaldehyde. Nat Commun. 2014;5:3621. DOI: 10.1038/ncomms4621.

[86] Heim LE, Thiel D, Gedig C, Deska J, Prechtl MH. Bioinduced room-temperature methanol reforming. Angew Chem Int Ed. 2015;54:10308–12.

[87] Fujita K, Kawahara R, Aikawa T, Yamaguchi R. Hydrogen production from a methanol-water solution catalyzed by an anionic iridium complex bearing a functional bipyridonate ligand under weakly basic conditions. Angew Chem Int Ed. 2015;54:9057–60.

[88] Suenobu T, Isaka Y, Shibata S, Fukuzumi S. Catalytic hydrogen production from paraformal-dehyde and water using an organoiridium complex. Chem Commun. 2015;51:1670–72.

[89] Fu Y, Shen J. Production of hydrogen by catalytic reforming of dimethoxymethane over bifunc-tional catalysts. J Catal. 2007;248:101–10.

[90] Shen H, Fu Y, Sun Q, Zuo S, Auroux A, Shen J. High surface area carbons as acidic components with Cu-ZnO/Al$_2$Ol$_2$ for the reforming of dimethoxymethane. Catal Commun. 2008;9:801–806.

[91] Badmaev SD, Pechenkin AA, Belyaev VD, Sobyanin VA. Hydrogen production by steam reforming of dimethoxymethane over bifunctional CuO-ZnO/γ-Al2O3 catalyst. Int J Hydrogen Energy. 2015;40:14052–57.

[92] Pechenki AA, Badmaev SD, Belyaev VD, Sobyanin VA. Performance of bifunctional CuO-CeO$_2$/γ-Al$_2$Ol$_3$ catalyst in dimethoxymethane steam reforming to hydrogen-rich gas for fuel cell feeding. Appl Catal B. 2015;166–167:535–43.

Thomas Zell and Robert Langer

3 CO$_2$-based hydrogen storage – formic acid dehydrogenation

Abstract: Changing demands on the energy landscape are causing the need for sustainable approaches. The shift toward alternative, renewable energy sources is closely associated with new demands for energy storage and transportation. Besides storage of electrical energy, also storage of energy by generating and consuming hydrogen (H$_2$) is possible and highly attractive. Notably, both secondary energy vectors, electric energy and hydrogen, have practical advantages so that one should not ask "which one is better?" but "which one fits better the specific application?"

Molecular hydrogen can be stored reversibly in form of formic acid (FA, HCOOH). In the presence of suitable catalysts, FA can be selectively decomposed to hydrogen and carbon dioxide (CO$_2$). A CO$_2$-neutral hydrogen storage cycle can be achieved when carbon dioxide serves as starting material for the production of the FA. Examples of CO$_2$ hydrogenation to FA are known in the literature. Herein, the formal reverse reaction, the decomposition of FA to H$_2$ and CO$_2$ by different catalyst systems is reviewed and selected examples for reversible storage applications based on FA as hydrogen storage compound are discussed.

Keywords: hydrogen storage, formic acid, carbon dioxide, CO$_2$, hydrogenation, dehydrogenation

3.1 Introduction

Fulfilling demands of a growing and developing world population requires changes in the current global energy landscape [1, 2]. Fossil fuels (coal, oil, and natural gas) are unfortunately still the main source for the global supply of energy, but they are dwindling. In addition, their combustion generates carbon dioxide (CO$_2$) which is one of the major greenhouse gases leading to global warming. Other gases which can be emitted in such combustion processes are methane, NO$_x$ (X = 1,2), and SO$_x$ (X = 2, 3) gases. As a result, there is a demand for regenerative renewable and sustainable energy sources. The transition to a more sustainable energy landscape is a project that takes decades and the associated challenges are manifold, ranging from overcoming technical limitations up to opposing politic interests of different countries.

Besides developing and improving renewable energy sources, one of the major technical challenges is the development of new energy storage and distribution systems.

Storage of energy in form of hydrogen (H_2) is attractive. Already in 1972, Bockris has suggested a hydrogen economy, which is based on hydrogen serving as medium for energy storage and transportation rather than of electric energy [3]. It is apparent that such a hydrogen-based economy requires scientific and technological solutions for the safe, efficient, and inexpensive storage of hydrogen. Due to the disadvantages of pressure storage of hydrogen, or its liquefaction, other solutions for hydrogen storage have been developed (for selected references see [4–12]). In this context, the concept of chemical hydrogen storage is an attractive approach. It implies that H_2 is bound in a chemical compound and can be released on demand. Among different hydrogen storage platforms, liquid organic hydrogen carriers, so-called LOHCs, are especially promising. These are compounds which are liquid in their hydrogenated state under standard conditions. Although there is no uniform definition of the term LOHC in the literature, this does necessarily imply that the dehydrogenated (hydrogen-depleted form) of the LOHC needs to be liquid as well. LOHCs are easier to handle than gaseous or solid hydrogen carriers and depending on the application, existing infrastructures of petrol-based industry may be used with only minor modifications, for example for mobile applications.

3.2 The concept of formic acid (FA) as hydrogen storage compound

FA as hydrogen storage compound has been investigated over the last decade, for selected references see e.g. [5, 9, 11, 13–34]. Reversible hydrogen storage is achieved by catalytic dehydrogenation of FA resulting in hydrogen and carbon dioxide. This corresponds to the discharging step of the system with hydrogen. The hydrogen storage cycle is then closed by the corresponding reverse reaction, the catalytic hydrogenation of carbon dioxide to FA, which is equivalent to charging the system with hydrogen. This concept is systematically visualized in Figure 3.1 and is often referred to as hydrogen battery, simply due to its similarity with regular batteries. Here charging the system/battery with energy corresponds to the hydrogenation step and discharging the system/battery is equivalent to the dehydrogenation step. Instead of electric energy hydrogen is charged to the system, stored in the system, and delivered on demand. Hydrogenation reactions of CO_2 to FA have been reviewed comprehensively, see e.g. [13, 26, 35–44]. Notably, in conjunction with this work a critical overview of various CO_2 hydrogenation reactions to CO_2-derived hydrogen storage compounds was published [37].

It is important to note that this hydrogen storage cycle can be carried out in two different ways. One option is in a closed system, which means that the CO_2 formed as
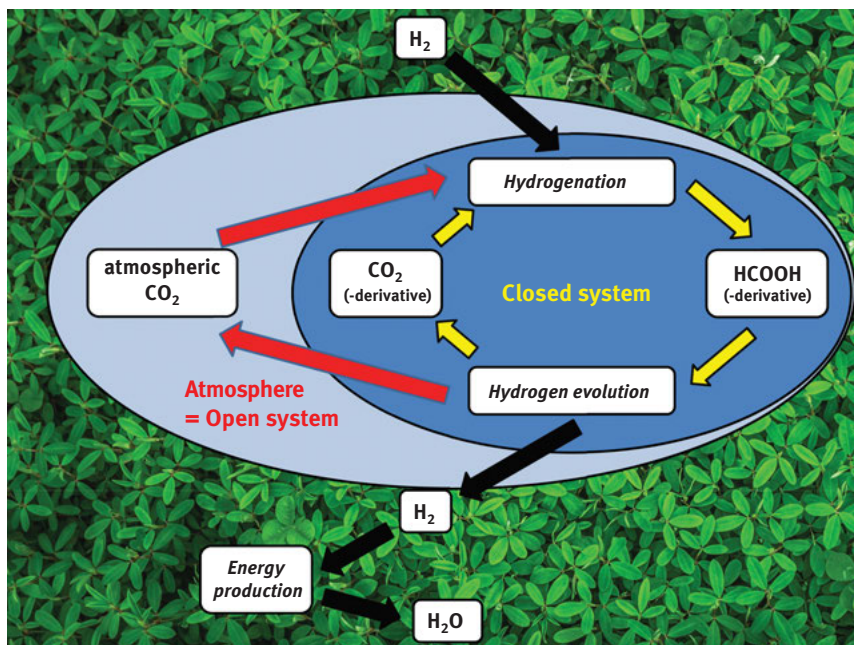
Figure 3.1: Hydrogen storage based on carbon dioxide (derivative) hydrogenation and FA (derivative) dehydrogenation.

byproduct of the hydrogen generation step is stored in the system and afterwards hydrogenated again (compare yellow cycle in Figure 3.1). Alternatively, also an open system can be envisioned. In this case, the CO_2 can be released to the atmosphere, and as long as atmospheric CO_2 serves as starting material for the FA production, the overall process can be regarded as CO_2-neutral (see red arrows in Figure 3.1). In such a system, the CO_2 balance is neutral as the emitted amount of CO_2 equals to the amount bound initially. Hydrogen obtained from the decomposition of FA can then be used to generate energy in fuel cells or by combustion engines, leading to water (=H_2O) as the sole byproduct of the energy storage cycle.

FA has a hydrogen content of 4.4 wt.% H_2. This is in comparison to other storage molecules moderate. For example, the other CO_2-based hydrogen storage molecules methanol (MeOH) and formaldehyde (CH_2O) have max. theoretical storage capacities of 12.1 and 8.4 wt.% in aqueous reforming processes, see Figure 3.2. Notably, in conjunction with our review, overviews on MeOH [45] and Formaldehyde [46] dehydrogenation have been published.

Pure FA is moderately corrosive and its low volatility and toxicity, compared to other LOHC, as well as the fact that it is non-flammable under standard conditions make it attractive for H_2 storage applications. In the presence of catalysts, FA can be decomposed via two different pathways, namely (i) the dehydrogenation/decarboxylation

Formic acid dehydrogenation:

4.4 wt.% of H_2
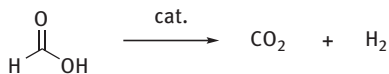
Dehydrogenation of aqueous formaldehyde:

8.4 wt.% of H_2
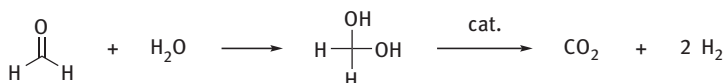
Dehydrogenation of aqueous methanol:

12.1 wt.% of H_2

$$MeOH + H_2O \xrightarrow{cat.} CO_2 + 3\ H_2$$
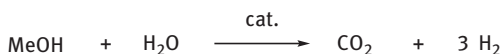
Figure 3.2: Comparison of CO_2-based hydrogen storage systems.

pathway and (ii) the dehydration/decarbonylation pathway. For hydrogen storage, the decomposition via dehydrogenation/decarboxylation to CO_2 and H_2 is of interest. However, also the decomposition of FA to carbon monoxide (=CO) and water (=H_2O) via dehydration/decarbonylation is known. Notably, both decomposition pathways are thermodynamically downhill, compare thermodynamic parameters (Figure 3.3) [20].
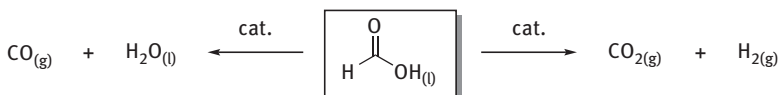
dehydration / decarbonylation:

$\Delta G° = -12.4$ kJ/mol
$\Delta H° = 28.7$ kJ/mol
$\Delta S° = 138$ J/mol K

dehydrogenation / decarboxylation:

$\Delta G° = -32.9$ kJ/mol
$\Delta H° = 31.2$ kJ/mol
$\Delta S° = 215$ J/mol K

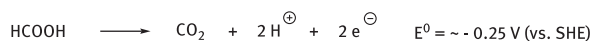**Figure 3.3:** Thermodynamic parameters of FA decomposition pathways [20].

For H_2 storage applications that are based on fuel cells, selective dehydrogenation reactions are essential. The presence of small amounts of carbon monoxide

(CO) in the CO_2/H_2 has a detrimental effect on fuel cell performances and life times, as CO acts a fuel catalyst poison [20]. Thus, minimizing the levels of CO to ppm or even ppb levels is essential for practical applications. This, in turn, requires highly selective catalysts and catalytic processes for the hydrogen generation from FA.

At the industrial scale, the production volume of FA is around 800,000 metric tons per year. This feedstock chemical is produced today mainly via the reaction of MeOH with carbon monoxide and a strong base [47]. Globally, approximately 90 % of the overall FA is produced via this so-called methyl formate hydrolysis process [48]. FA has various applications, the main ones being silage and animal feed (~27 %), leather and tanning industry (~ 22 %), pharmaceuticals and food chemicals (~ 14 %), textile industry (~ 9 %), natural rubber industry (~ 7 %), drilling fluids (~ 4 %) and ~ 17 % of the global production volume is assigned to miscellaneous applications [48]. Although today there is no cost-attractive solution for the catalytic hydrogenation of CO_2 of FA, this technology is available and with this a CO_2-neutral storage of energy by storing H_2 in FA is theoretically conceivable.

Alternatively to the catalytic dehydrogenation of FA to H_2 and CO_2, polymer electrolyte membrane-based direct formic acid fuel cells (DFAFCs) can be used to transform FA into electric energy [49]. In DFAFCs, FA can be converted directly to energy without a separate dehydrogenation step. These proton exchange membrane fuels cells use a direct feed of FA on the on anode side. For the cathode, both actively and passively breathing cathodes have been developed. The direct oxidation of FA is a two-electron process with a potential of $E_0 \sim -0.25$ V vs. SHE (standard hydrogen electrode). This reaction is usually performed over supported or unsupported palladium- or platinum-based catalyst materials. The oxygen reduction, taking place at the anode, is a four-electron process with a potential of $E_0 = 1.23$ V vs. SHE. For this reaction, usually supported Pt-based catalysts are used. The anode and cathode reactions are given in Figure 3.4. DFAFCs can at the current state of the technology not yet be regarded as robust technology, which is suitable for broad scale commercialization. Problems associated with this technology are on the one hand the

Anode reaction :

$$HCOOH \longrightarrow CO_2 + 2\,H^{\oplus} + 2\,e^{\ominus} \qquad E^0 = \sim -0.25\ \text{V (vs. SHE)}$$

Cathode reaction :

$$0.5\,O_2 + 2\,H^{\oplus} + 2\,e^{\ominus} \longrightarrow H_2O \qquad E^0 = 1.23\ \text{V (vs. SHE)}$$

Net reaction :

$$HCOOH + 0.5\,O_2 \longrightarrow CO_2 + H_2O \qquad OCV = \sim 1.48\text{V}$$

Figure 3.4: Electrochemical reactions taking place in a DFAFC.

intrinsically high sensitivity of the fuel cell catalysts to poisoning by CO and on the other hand crossover of FA through the fuel cell membrane. Both processes lead to deactivation of the fuel cell.

3.3 Selected catalytic processes for the hydrogen generation from FA

Various catalytic systems for the dehydrogenation of FA have been reported. This includes a vast number of homogeneous and heterogeneous catalysts. In here, selected examples of different catalyst systems are discussed. This includes examples of main group catalysts, noble and non-noble transition metal-based catalysts as well as examples for catalyst systems which were used for reversible storage applications. In addition, also some examples of heterogeneous catalysts will be shown. Notably, a full account on the topic is beyond the scope of this work. However, we would like to refer for further reading to comprehensive reviews on the topic, for selected recommendations see e.g. [5, 9, 11, 13–33].

3.4 Main group compounds as catalysts for FA dehydrogenation

The field of main group catalysis for FA decomposition reactions is almost unexplored. In 2014, Berben and coworkers have reported an Al pincer complex which was applied as catalyst for the selective dehydrogenation of a 5:2 mixture of FA and triethylamine (=TEA, NEt$_3$), Figure 3.5 [50]. The highest catalytic activity was found when performing the reaction in THF at 65 °C. Under these conditions a Turnover number (TON) of 2200 was reported after 1 h and an initial Turnover frequency (TOF) of 5200 h^{-1}. Based on experimental and theoretical data, an aluminum–ligand cooperation was found to play a crucial role in the catalytic system. Stoichiometric reactions have been performed with the thf-coordinated aluminum hydride complex **1**. In the absence of protons, which are capable to protonate the ligand, the insertion of CO$_2$ under formation of the formate complex **2** is favored. The β-hydride abstraction of formate is favored upon protonation of the ligand, which is essential for catalytic progress in the FA decomposition. A proposed mechanism of the catalytic reaction is shown in Figure 3.5.

Also in 2014, Maschmeyer and coworkers reported hydrogen liberation from FA through it selective disproportionation over sodium germinate [51]. Using this heterogeneous catalyst system, the authors were able to achieve hydrogen formation at 300 °C. However, when compared to homogeneous state-of-the-art catalysts, only a low selectivity toward the dehydrogenation/decarboxylation pathway was achieved. At these conditions, a quotient of the type n(H$_2$)/[n(H$_2$) + n(CO)] = 95 % was reported.

CO$_2$ insertion reaction:
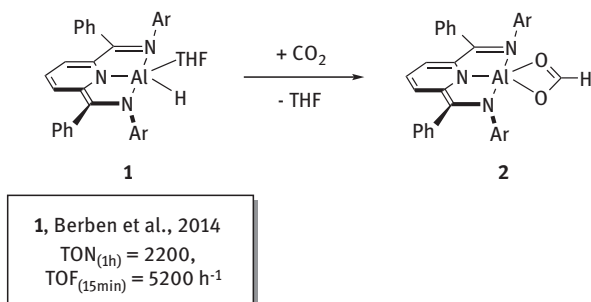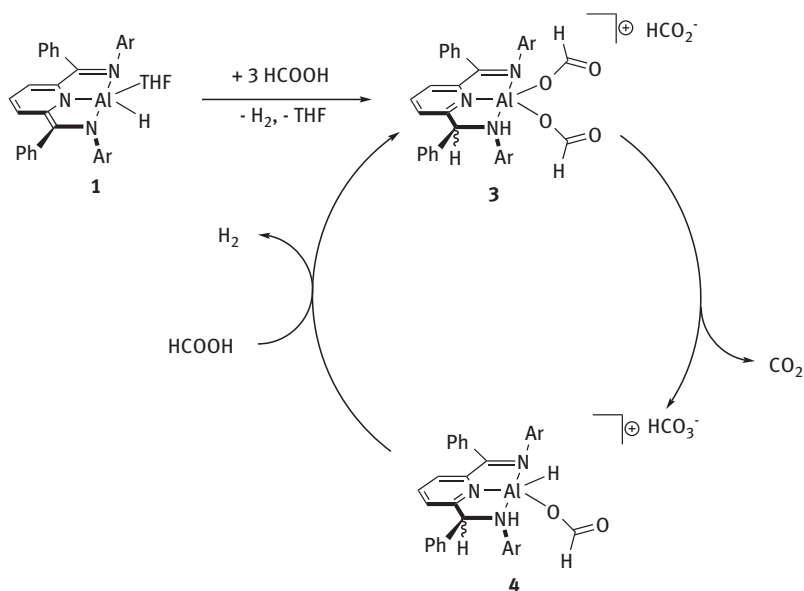
Ph ... Ar
=N
N—Al—THF
N
H
Ph Ar

1

+ CO$_2$
− THF

Ph ... Ar
=N
N—Al—O
N O—H
Ph Ar

2

1, Berben et al., 2014
TON$_{(1h)}$ = 2200,
TOF$_{(15min)}$ = 5200 h^{-1}

- -

Proposed catalytic mechanism:

Ph ... Ar
=N
N—Al—THF
N
H
Ph Ar

1

+ 3 HCOOH
− H$_2$, − THF

$\oplus$ HCO$_2^-$

3

H$_2$

HCOOH

CO$_2$

$\oplus$ HCO$_3^-$

4

Figure 3.5: Al-catalyzed dehydrogenation of FA (for Ar = 2,6-Diisopropylphenyl).

Later-on in 2015, the Cantat group reported on the use of boron-based catalysts for the metal-free dehydrogenation of FA, Figure 3.6 [52]. This is the first report on a metal-free catalyst for the dehydrogenation of FA. The authors demonstrated in their study that FA can be decomposed selectively to H$_2$ and CO$_2$ using dialkylbor-ane derivatives as catalysts in the presence of a base with high selectivity. Experiment and computational results suggested the involvement of bis

(formyloxy)borates, such as **7,** as catalytic key intermediates (see Figure 3.6). Overall, TONs of up to 100 were reported for bis(cyclohexyl)borane-based catalyst **5** (see Figure 3.6). A mechanism was suggested on the basis of experimental and computational data for the 9-BBN (=9-Borabicyclo[3.3.1]nonane) based catalyst system which is depicted in Figure 3.6.
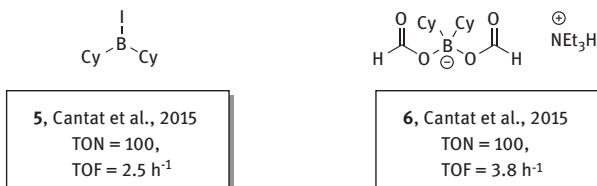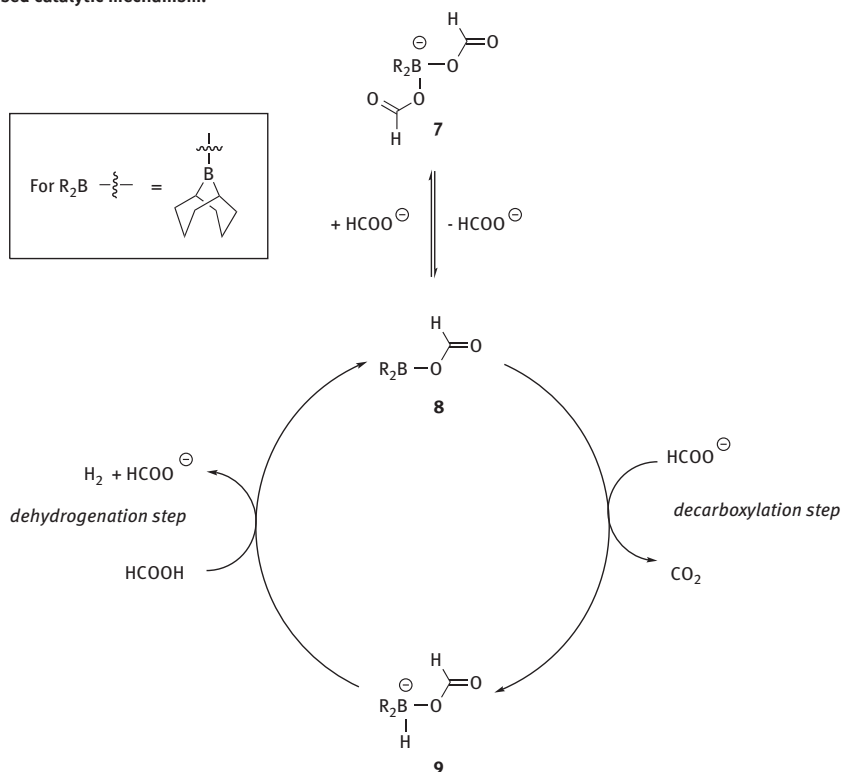

Figure 3.6: Boron-based catalysts for the dehydrogenation of FA.

3.5 Noble metal catalysts for FA dehydrogenation

In contrast to main group catalysts, a large number of noble metal complexes have been reported as catalysts for the dehydrogenation FA to CO_2 and H_2.

The first examples of homogeneous catalysts for the dehydrogenation of FA date back to 1967, when Coffey reported that many phosphine stabilized transition metal complexes, especially complexes of ruthenium and iridium, are capable of catalyzing the dehydrogenation of FA [53]. Additionally, it was mentioned that these systems can be used in transfer hydrogenation reactions. This was demonstrated by the hydrogenation of aldehydes to alcohols. The highest activity of the complexes reported for the hydrogen generation reaction, was found for iridium catalyst [Ir(PPh$_3$)$_3$(H)$_2$Cl] **10**. Using this catalyst, he was able to reach a TOF of 1187 h^{-1} in a boiling mixture of FA 0.75 M in acetic acid.

In the following decades, a variety of different noble metal complexes was reported that are capable of catalyzing the decomposition of FA to CO_2 and hydrogen. Figure 3.7 shows selected examples along with the maximum activity and productivity. These examples include mononuclear Rh complex **11** [54], dinuclear Pt complex **12** [55], dinuclear Ru complex **13** [56], heterobinuclear complexes **14** [57], Rh complex **15** [58], and Ir complex **16** [59].

Notably, it is difficult to compare the catalyst performances (which is catalyst activity and productivity) for these systems as the conditions of the hydrogen generation reactions vary for the different examples. This variations include parameters such as temperature, catalyst loading, additives (such as amine or inorganic bases), solvents, length of experiment, type of addition of the FA (batch reaction or continuous addition), which all have significant influences on the reaction.

However, besides varying metals, this selection of complexes nicely demonstrates that also a variety of ligands was used for different catalyst systems. This selection includes ligands with different donor-atoms, resulting in varying ligand-fields, and also ligands with different denticity.

Besides classical ligands, which act as spectators and do not actively participate in the catalytic turnover, also ligands capable of metal-ligand cooperation (MLC) [26, 60–70] were employed in the dehydrogenation of FA. The term MLC describes catalyst systems with cooperative ligand behavior which allow for bifunctional substrate activation during catalytic transformations. With this type of catalysts, which are also called bifunctional catalysts or cooperative catalysts or concerto catalysts, the ligand can actively participate in bond breaking and bond forming steps. This means that for example a coordinated amine ligand can act as proton source in a concerted or stepwise proton-hydride transfer mechanism from the catalyst to the substrate.

One example of a FA hydrogenation catalysts, capable of MLC was reported by Milstein and coworkers and is shown in Figure 3.8. The Re(I) Complex**17** catalyzes the dehydrogenation of FA under base-free conditions [71]. Base-free reaction conditions
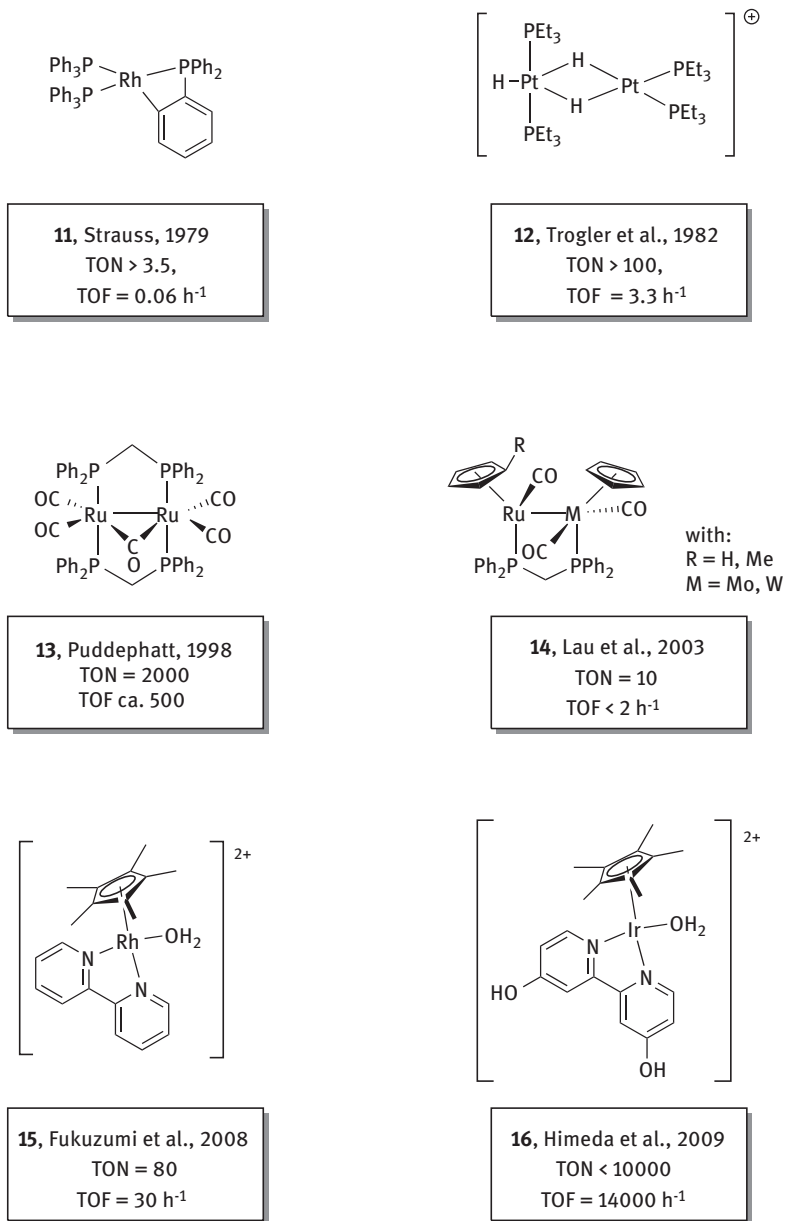
11, Strauss, 1979
TON > 3.5,
TOF = 0.06 h^{-1}

12, Trogler et al., 1982
TON > 100,
TOF = 3.3 h^{-1}

13, Puddephatt, 1998
TON = 2000
TOF ca. 500

14, Lau et al., 2003
TON = 10
TOF < 2 h^{-1}

with:
R = H, Me
M = Mo, W

15, Fukuzumi et al., 2008
TON = 80
TOF = 30 h^{-1}

16, Himeda et al., 2009
TON < 10000
TOF = 14000 h^{-1}

Figure 3.7: Selected noble metal-based FA decomposition catalysts.

are desirable, as the addition of (sub)stoichiometric amounts of any additive to the dehydrogenation reactions results in a decrease of the H$_2$ storage capacity. Complete conversion of FA was observed when heated in a Fisher Porter tube to 180 °C in the presence of 0.03 mol% **16** after 1 h. This corresponds to a TON of 30,000 and a TOF of

$30,000\,h^{-1}$. Based on stoichiometric reactions, the authors suggested that MLC is involved in the catalytic reaction. In fact, it was demonstrated that a reaction of the dearomatized dicarbonyl complex **18** with FA leads to the formation of formate complex **17**. In this reaction, the ligand arm is protonated, which is accompanied by aromatization of the ligand. CO_2 is liberated from complex **17** at elevated temperatures to result in hydride complex **19**, Figure 3.8. At lower temperatures, on the other hand, CO_2 insertion in the rhenium hydride bond of **19** under formation of the formate complex **17** can be observed. Similarly, the addition of one equivalent of FA to the hydride complex **19** result in the formation of formate complex **17** along with one
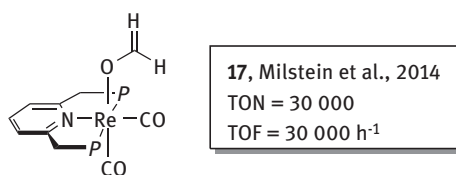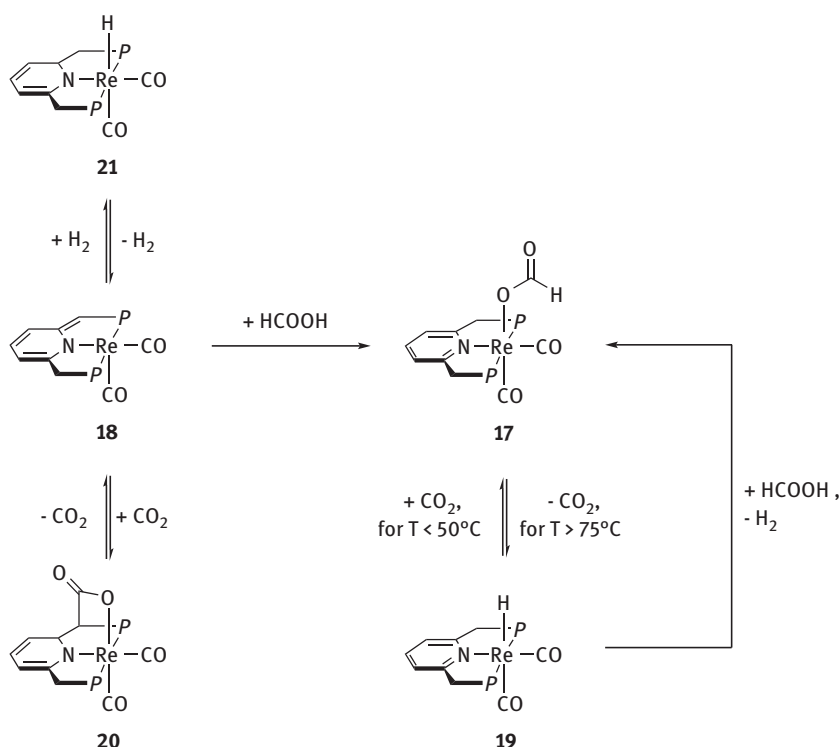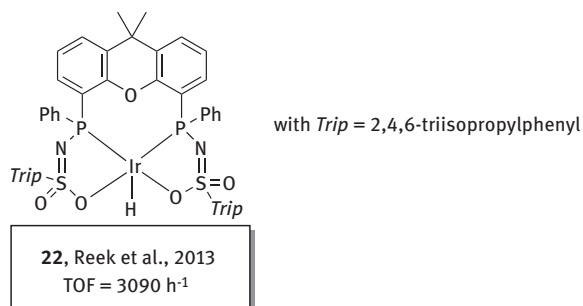

Figure 3.8: FA dehydrogenation catalyzed by a bifunctional Re catalyst.

equivalent of hydrogen. The authors also studied the reactivity of the dearomatized dicarbonyl complex **18** toward CO$_2$ and H$_2$. Complex **18** reacts with H$_2$ to the hydride complex **21**. This reaction can be regarded as bifunctional H$_2$ activation, in which the H$_2$ is cleaved heterolytically, a proton is transferred to the ligand arm and a hydride is transferred to the metal center. Similarly, the reaction of dearomatized complex **18** with CO$_2$ results in reversible binding of the CO$_2$ to the complex in a bifunctional manner under formation of complex **20**. The CO$_2$ is bound to the complex via the O atom to the metal atom and via a reversible C–C bond formation, which as a result leads to aromatization of the central pyridine unit of the pincer ligand. Notably, a similar bifunctional binding of CO$_2$ to dearomatized pyridine-based pincer complex fragments has also been observed PNP pincer complexes of ruthenium [72] and iron [73].

An additional example for a bifunctional FA dehydrogenation catalyst is iridium (III) complex **22** which is the bearing a bisMETAMORPhos ligand, Figure 3.9 [74, 75]. Also this catalyst, published by the Reek group, is capable of dehydrogentating FA without further additives. High initial rates were observed for the hydrogen liberation (TOF$_{max}$ = 3090 h^{-1}) in toluene at 85 °C. Unfortunately, however, no information was given in their publication on the long-term stability of the catalytic system. A bifunctional mechanism was proposed for the catalyst system, based on Density functional theory (DFT) calculations, Figure 3.9 [75]. The proton-responsive and hydrogen-bonding nature of the ligand allows for MLC taking place during the dehydrogenation catalysis. In the first step of the proposed mechanism, FA binds to the Ir complex, via coordination of the oxygen to the iridium center and formation of a hydrogen bond to the oxygen atom to result in complex **23**. This complex rearranges to result in the nitrogen bound species **24**. The transfer of a proton to the basic nitrogen atom of the ligand and simultaneous transfer of a hydride to the metal center is then taking place via transition state **TS26**. This results in the formation of iridium hydride complex **25**, which features a protonated ligand. Liberation of hydrogen via **TS27** is then assisted by and additional molecule of FA to regenerate the active catalyst **22**.

Besides molecularly well-defined catalysts, also a variety of *in situ* generated FA decomposition catalysts have been reported. Selected examples are shown in Figure 3.10. In 2008, for example, the Beller group reported an comprehensive study, extensively screening different combinations of ruthenium precursors, with mono- and bidentate phosphine ligands and (sub)stoichiometric amine additives as well as different reaction conditions [76]. The highest activity in this study was observed for an *in situ* catalyst **28** composed of (RuBr$_3$· H$_2$O) with three equivalents of triphenylphosphine (= PPh$_3$). This system gave an initial TOF (measured in the first 20 min of the dehydrogenation experiment) of 3,630 h^{-1} for the decomposition of a 5:2 mixture of FA and triethylamine. The highest TON (1,376, after 3 h) on the other hand was observed for *in situ* catalyst **29** composed of [{RuCl$_2$(benzene)}$_2$] and 1,2-bis (diphenylphosphino)ethane (dppe) in a three-fold excess. In addition, the authors

with *Trip* = 2,4,6-triisopropylphenyl

22, Reek et al., 2013
TOF = 3090 h^{-1}

Schematic proposed mechanism:
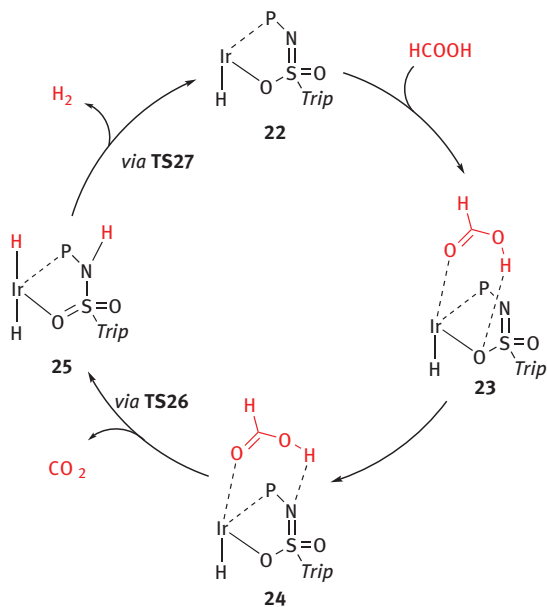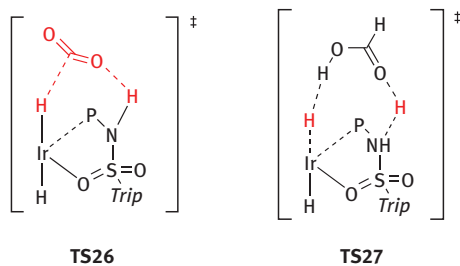

Transition states:

Figure 3.9: FA dehydrogenation catalyzed by a bifunctional Ir catalyst. Top: Catalyst, and bottom: proposed mechanism on the basis of DFT calculations.

$RuBr_3 \cdot H_2O$ + 3 PPh_3

28, Beller et al. 2008
TOF = 3630 h^{-1}

[{$RuCl_2$(benzene)}]$_2$ + 3 dppe

29, Beller et al. 2008
TON = 1376

[{$RuCl_2$(benzene)}]$_2$ + 6 PPh_3

30, Beller et al. 2008 and 2009
TON = 260 000
TOF > 900 h^{-1}

[$Ru(H_2O)_6$](tos)$_2$ + 2

$Na^+{}^-O_3S$ ... $SO_3^-Na^+$

P

$SO_3^-Na^+$

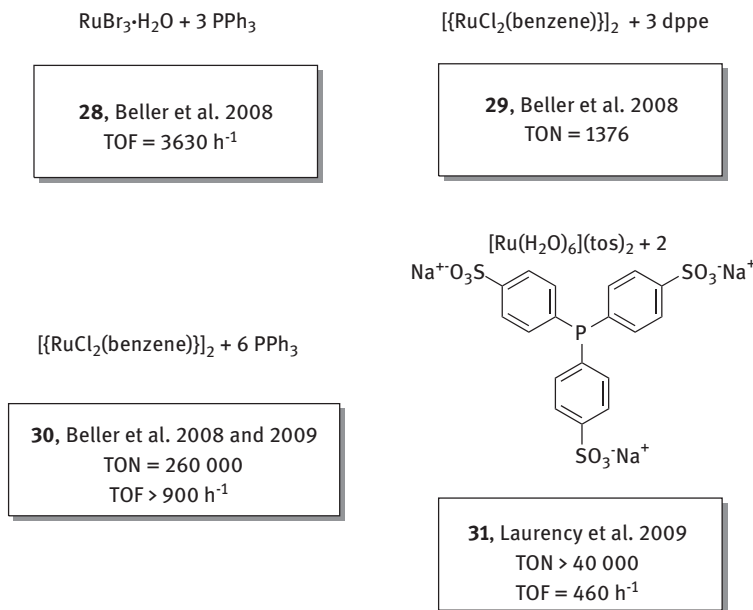| |
|---|
| **31**, Laurency et al. 2009 |
| TON > 40 000 |
| TOF = 460 h^{-1} |

Figure 3.10: Selected examples of *in situ* noble metal catalysts for FA decomposition.

also build a setup where hydrogen was generated and transformed into electric energy via a fuel cell. The hydrogen generation reaction was performed using an *in situ* catalyst **30** composed of 30 mmol [{$RuCl_2$(benzene)}]$_2$ and 180 mmol PPh_3. With this catalyst, 20 mL of a 5:4 mixture of FA with hexyldimethylamine (= $HexNMe_2$) was decomposed at 26 °C and converted to electrical energy. Although a decrease of catalyst activity was observed over time, the authors reported that this system was able to provide electrical energy for 69 h.

The same group reported in 2009 the application of the in situ catalyst **30** in batch and continuous mode, reaching TONs of up to 260,000 with an average TOF of more than 900 h^{-1} in the continuous setup at 25 °C, Figure 3.10 [77]. The impressive catalyst stability of the system allowed running the continuous dehydrogenation experiments for up to 2 months.

An additional example for an active *in situ* catalyst includes the water soluble Ru-mtppts (mtppts = meta trisulfonated triphenylphosphine) catalyst system **31** (Figure 3.10) [78]. This system is capable of hydrogen generation from 4-M HCOOH/HCOONa (9:1) in water with a TOF of 460 h^{-1} and a TON of 440,000 at 120 °C [79]. The decomposition reaction using this *in situ* catalyst was performed in an autoclave. When the initial amount of FA was decomposed to H_2 and CO_2, FA was added continuously and the product gases were release in constant pressure intervals, so that the internal pressure of the autoclave remained between 50 and 250 bar. However, this catalyst system remained active in a wide pressure range of up to 600 bar.

3.6 Base-metal catalysts for FA dehydrogenation

The development of active and durable non-noble metal catalysts for different hydrogenation and dehydrogenation reactions is highly desirable [9, 26, 69, 80–98]. During the last years, many research groups focus increasingly on the design base-metal catalysts systems. As a result, for many substrates, hydrogenation and dehydrogenation base-metal catalysts have already been developed and the catalyst performances are rising steadily. It is commonly accepted that replacing expensive and potentially toxic noble metals in catalyst, such as ruthenium, by greener, more abundant and potentially less toxic metals, such as iron, is beneficial for potential large scale and commercial applications. Whereas noble metal catalysts usually suffer from high costs, simply due costs contribution of the noble metal, for non-noble metal catalysts usually the expensive contributor to the overall costs is the ligand.

For the FA dehydrogenation, iron catalysts have been proven extraordinarily active [9, 25]. In 2010, the research groups of Beller and Ludwig reported the first FA dehydrogenation reaction catalyzed by an iron complex, Figure 3.11 [99]. In their report, the authors screened different combinations of *in situ* catalysts under irradiation with a 300 W xenon lamp. The most active catalyst system **32** was composed of a 1:1:1 mixture of 20 μmol $Fe_3(CO)_{12}$, PPh_3, and phen (= 1,10-phenanthroline). With this *in situ* catalyst a TON of 126 was achieved for the hydrogen liberation reaction from 5 mL of a FA/NEt_3 adduct (5:2) under irradiation with a 300 W Xe-lamp after 24 h at 60 °C in DMF (Figure 3.11).

Shortly after, also in 2010, the same groups reported an improved system for the iron-catalyzed FA dehydrogenation [100]. The improvement was achieved by replacing triphenylphosphine (=PPh_3) by benzyldiphenylphospine (=$PBnPh_2$) or by tribenzylphosphine (=PBn_3) ligands. With this change a more stable catalyst systems were obtained. This allowed for achieving a TON of 1266 in a decomposition reaction of 10 mL of FA and NEt_3 (5:2) mixture using an *in situ* generated catalyst **33** from a 1:1:1 mixture of 20 μmol $Fe_3(CO)_{12}$, tpy (= 2,2':6'2''-terpyridine), and tribenzylphoshine. This TON was observed at 60 °C in DMF after 51 h under irradiation with a Xe-lamp. Similarly, the authors were able to demonstrate that the well-defined isolated *trans*-bis(phosphine) tricarbonyl complexes [(PRR'_2)$Fe(CO)_3$] (**34**: PRR'_2 = PBn_3, and **35**: PRR'_2 = $PBnPh_2$, Figure 3.11) were active catalysts for the dehydrogenation reaction, initially even in the absence of tpy. For achieving a long-term stability of these catalysts tpy needed to be added. Although the full mechanistic picture of the catalyst systems was not reported, the authors suggested that, based on NMR experiments and DFT calculations, ortho-metalation of the benzyl substituents plays a crucial role in the mechanism of the catalytic reaction. Without irradiation, however, for all these catalyst systems **32–35** no hydrogen formation was observed.

One year later, in 2011, the research groups of Ludwig, Beller and Laurenczy reported on an *in situ* catalyst system which was capable of dehydrogenating FA
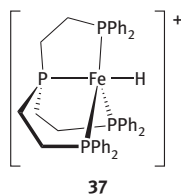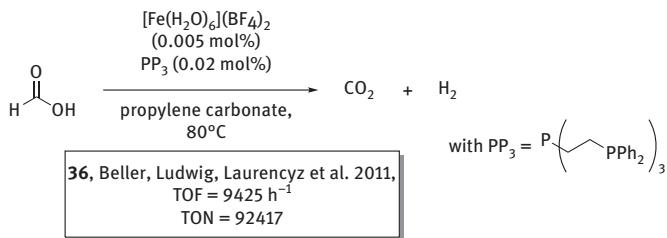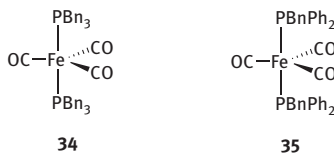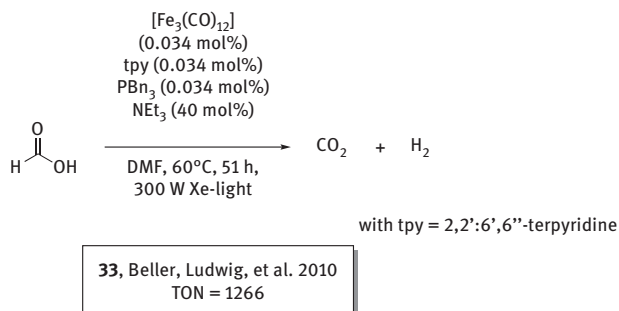
[Fe$_3$(CO)$_{12}$]
(0.034 mol%)
phen (0.034 mol%)
PPh$_3$ (0.034 mol%)
NEt$_3$ (40 mol%)

$$\text{H}-\text{C}(=\text{O})-\text{OH} \xrightarrow[\text{300 W Xe-light}]{\text{DMF, 60°C, 24 h,}} \text{CO}_2 \;+\; \text{H}_2$$

with phen = 1,10-phenanthroline

32, Beller, Ludwig, et al. 2010
TON = 126

- -

[Fe$_3$(CO)$_{12}$]
(0.034 mol%)
tpy (0.034 mol%)
PBn$_3$ (0.034 mol%)
NEt$_3$ (40 mol%)

$$\text{H}-\text{C}(=\text{O})-\text{OH} \xrightarrow[\text{300 W Xe-light}]{\text{DMF, 60°C, 51 h,}} \text{CO}_2 \;+\; \text{H}_2$$

with tpy = 2,2':6',6''-terpyridine

33, Beller, Ludwig, et al. 2010
TON = 1266

PBn$_3$ | PBnPh$_2$
OC—Fe‴CO / CO | OC—Fe‴CO / CO
PBn$_3$ | PBnPh$_2$

34 | **35**

- -

[Fe(H$_2$O)$_6$](BF$_4$)$_2$
(0.005 mol%)
PP$_3$ (0.02 mol%)

$$\text{H}-\text{C}(=\text{O})-\text{OH} \xrightarrow[\text{80°C}]{\text{propylene carbonate,}} \text{CO}_2 \;+\; \text{H}_2$$

with PP$_3$ = P$\left(\!\!\diagdown\!\!\diagdown\text{PPh}_2\right)_3$

36, Beller, Ludwig, Laurencyz et al. 2011,
TOF = 9425 h^{-1}
TON = 92417

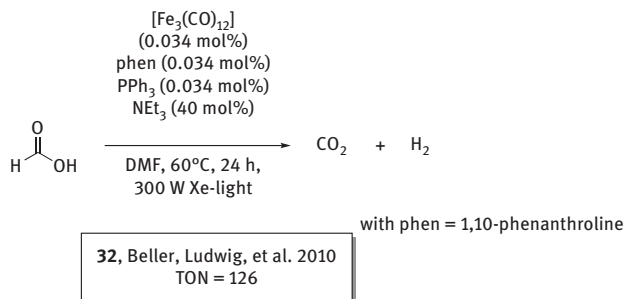$$\left[\; \text{P}-\text{Fe}-\text{H} \text{ with PPh}_2 \text{ ligands} \;\right]^{+}$$

37

Figure 3.11: *In situ* generated iron FA dehydrogenation catalysts.

without irradiation. This *in situ* catalyst systems, which is composed of $[Fe(H_2O)_6]$ $(BF_4)_2$ and tris[(2-diphenylphosphino)ethyl]phosphine (=$P(CH_2CH_2PPh_2)_3$, = PP_3), was operating with unprecedented catalyst performance in propylene carbonate (PC) without any additives and most importantly without the need for irradiation. For example an extraordinary high initial activity of TOF = $9425\,h^{-1}$ was observed in a catalytic decomposition experiment using 0.005 mol% iron precursor with a four-fold excess of PP_3 in PC as solvent at 80 °C. The high catalyst robustness of this system was demonstrated using a continuous hydrogen generation setup. After overcoming an induction period of approximately 2 h, a constant gas evolution was obtained for approximately 16 h. Afterwards a decrease in catalyst activity was observed, which was believed to be a result of water accumulation in the batch reactor. However, in this experiment the total amount of gas produced corresponds to a total TON of 92,417. Interestingly, in the catalytic reaction the protonated ligand was observed by NMR. Also lower catalytic activity was observed when 1:1 mixtures of iron precursor and PP_3 ligand were employed, suggesting that an excess of ligand is essential for this catalyst system.

Based on stoichiometric experiments and a computational study, the authors suggested a mechanism that is based on the formation of the iron hydride complex $[(PP_3)Fe(H)]^+$ (**37**, Figure 3.11). This complex was synthesized, isolated, and used as catalyst for the dehydrogenation reaction. When employed with excess ligand, **37** showed comparable catalytic activity to the *in situ* catalyst. The initially suggested mechanism was discussed controversially in the literature [101–103], until the original authors, later-on, presented a comprehensive study on the mechanism of the dehydrogenation reaction, see Figure 3.12 [103].

The detailed mechanistic study indicates that the active species formed under *in situ* conditions is the monocationic η^2-formate complex **38**. Based on DFT calculations it was suggested that this complex is possibly formed by protonation of a hydride ligand by the coordinated FA followed by subsequent liberation of hydrogen. The elimination of carbon dioxide from **38** results in the formation of monocationic monohydride complex **37**. Subsequent coordination of formate to the monocationic **37** results in the neutral formate hydride intermediate **39**. Elimination of CO_2 from **39** then yields the neutral dihydride intermediate **40**, which upon protonation by FA gives the monocationic dihydrogen hydride intermediate **41**. This step is followed by the liberation of H_2, which regenerates the monocationic monohydride complex **37**.

Interestingly, this *in situ* generated catalyst system has also been found to be capable of catalyzing the hydrogenation of CO_2 and sodium bicarbonate to sodium formate [31].

Also in case of iron, pincer complexes, which are capable of MLC, have been employed in FA dehydrogenation reactions. In 2013, Milstein and coworkers reported the catalytic FA decomposition catalyzed by the pyridine-based iron PNP pincer complex $[(^tBu\text{-}PNP)Fe(H)_2(CO)]$ (**42**, Figure 3.13, with ^tBu-PNP = 2,6-bis(di-tert-butylphosphinomethyl)pyridine) [104]. This complex has been used earlier as
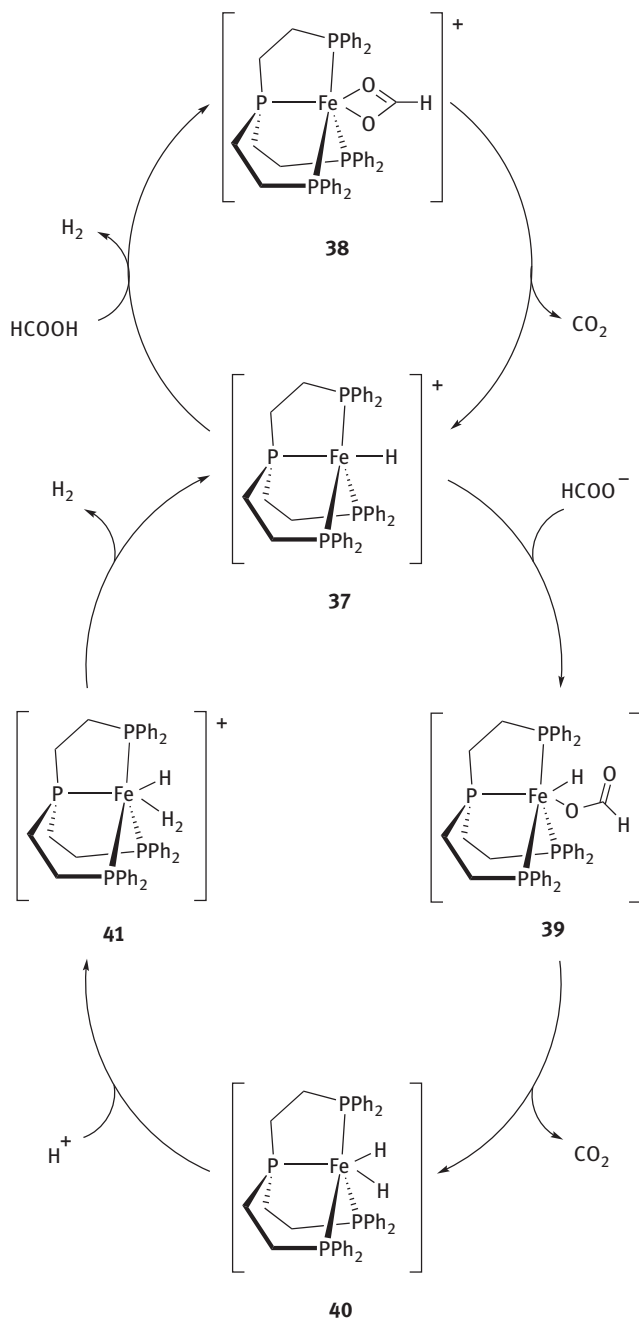
Figure 3.12: Reaction mechanism for the iron-catalyzed dehydrogenation of FA catalyzed by *in situ* catalyst 36.
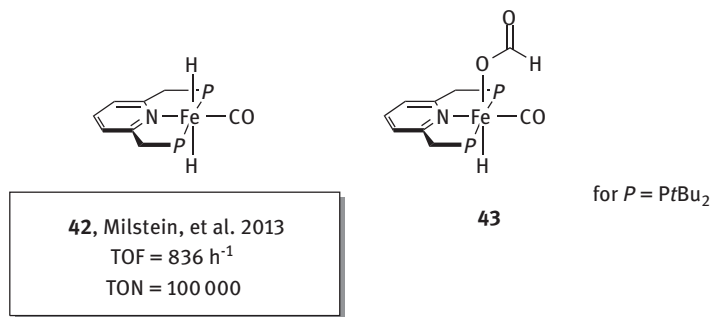
Figure 3.13: Pyridine-based Fe-PNP pincer complexes as catalysts for the FA dehydrogenation in the presence of trialkylamines.

catalyst for the hydrogenation of CO_2 in aqueous NaOH solutions to give sodium formate [105]. Whereas only a poor catalytic activity was observed for the decomposition of FA in the absence of amines additives (TOF of approximately $1\,h^{-1}$) this iron pincer complex displays significantly higher catalytic performance in the presence of trialkylamines. Using 0.05 mol% of complex **42** for the dehydrogenation of a FA/NEt$_3$ mixture (1:1) resulted in a TOF of $836\,h^{-1}$ at 40 °C. Compared to the *in situ* catalyst **36**, which is composed of PP$_3$ and $[Fe(H_2O)_6](BF_4)_2$, at the same temperature the activity is approximately 30 % higher, but in the presence of triethylamine [106]. The catalyst durability was demonstrated in a long-term experiment in which 1 mol FA was decomposed over 10 days with a catalyst loading of 0.001 mol% **42**. This corresponds to a TON of 100,000.

Although the iron pincer complex **42** features a pyridine-based PNP ligand, which is known to allow for catalysis via MLC, a mechanism was proposed on the basis of stoichiometric experiments and a computational study, which does not necessarily rely on the bifunctional nature of the ligand. The proposed mechanism is outlined in Figure 3.14. Protonation of the dihydride complex **42** with FA leads in a clean reaction to the formation of hydrido formate complex **43**. Hydrogen is detected as side product of this reaction. The authors proposed that this hydrogen liberation likely proceeds via protonation of one hydride to result in hydride dihydrogen complex **44** as intermediate which then loses dihydrogen to give the coordinatively unsaturated intermediate **45**. Formate coordination to **45** results in formate complex **43**. From this complex CO_2 is liberated to regenerate dihydride complex **42**. This step corresponds to a non-traditional β-hydride elimination, since complex does not have a vacant coordination site. This step was modeled by DFT analysis and the authors proposed a reaction sequence which is strictly intramolecular and does not involve dissociation of the formate ligand as suggested earlier by Yang [35].

FA dehydrogenation by similar iron PNP pincer complex was presented in 2014 by the groups of Hazari and Schneider. The authors have employed an aliphatic PNHP pincer ligands for the synthesis of their catalysts and were able to show that treatment
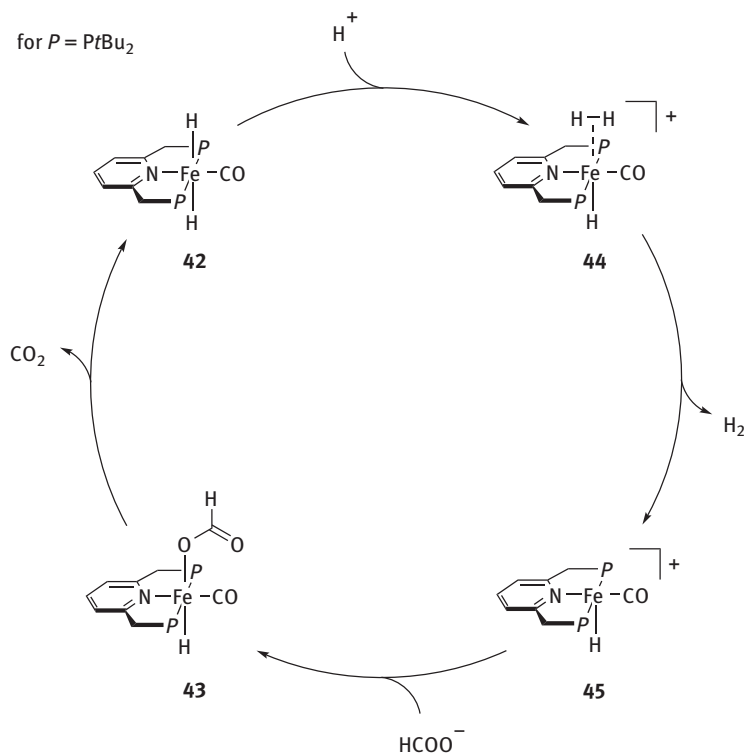
Figure 3.14: Proposed mechanism for the dehydrogenation of FA catalyzed by iron catalyst **42**.

of the five-coordinate iron amide complexes [(^{i}Pr-PN^{-H}P)Fe(H)(CO)] (**46**; ^{i}Pr-PN^{-H}P = N{CH$_2$CH$_2$(PiPr$_2$)}$_2$) and [(Cy-PN^{-H}P)Fe(H)(CO)] (**47**; Cy-PN^{-H}P = N{CH$_2$CH$_2$(PCy$_2$)$_2$}) results in the formation of the six-coordinated η^1-formate amine complexes [(^{i}Pr-PNHP)Fe(H)(CO)(η^1-OOCH)] (**48**; ^{i}Pr-PNHP = HN{CH$_2$CH$_2$(PiPr$_2$)}$_2$) and [(Cy-PNHP)Fe(H)(CO)(η^1-OOCH)] (**49**; Cy-PNHP = HN{CH$_2$CH$_2$(PCy$_2$)}$_2$), respectively (Figure 3.15). Notably, similar iron complexes with aliphatic PNHP pincer ligands have been used by the Beller group earlier as catalysts for the hydrogen liberation from aqueous methanol solutions [107].

Complexes **46–48** are catalyzing the dehydrogenation of FA in the presence of 50 mol% triethylamine. Using 0.1 mol% of catalyst loading in dioxane at 40 °C with the addition of 50 mol% NEt$_3$ gave TOFs up to 238 h^{-1} (observed when using catalyst **48**) and TONS up to 904 (observed when using catalyst **49**). Increased TOFs were observed at 80 °C under otherwise the same conditions (TOFs up to 739 h^{-1} for **49**). As expected, the catalytic performance of both iso-propyl catalysts **46** and **48** as well as the performance of both cyclohexyl-substituted catalysts **47** and **49** was found to be very similar. In analogy to Milstein's catalyst **42** almost no catalytic activity was observed in the absence of amine. Based on a computational study and stoichiometric experiments
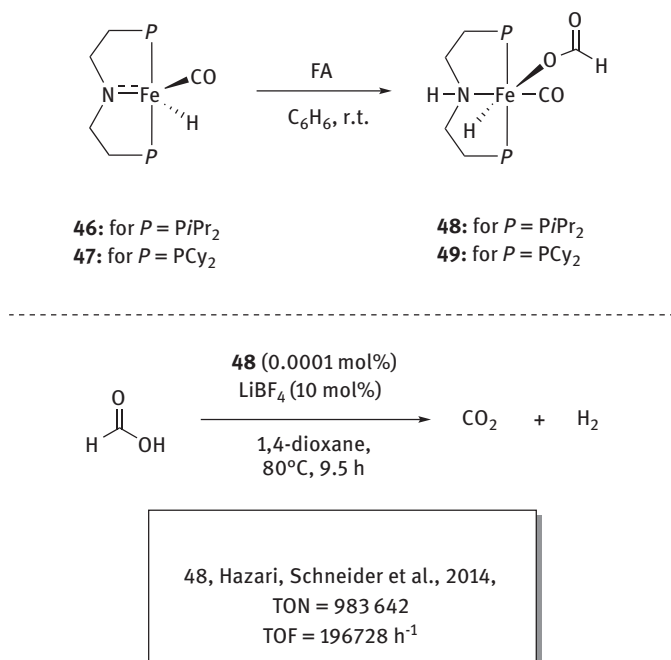
46: for $P = PiPr_2$
47: for $P = PCy_2$

48: for $P = PiPr_2$
49: for $P = PCy_2$

48 (0.0001 mol%)
LiBF$_4$ (10 mol%)

$\longrightarrow$ CO_2 + H_2

1,4-dioxane,
80°C, 9.5 h

48, Hazari, Schneider et al., 2014,
TON = 983 642
TOF = 196728 h^{-1}

Figure 3.15: Iron catalysts based on aliphatic PNP ligands for the catalytic dehydrogenation of FA.

a mechanism similar to Milstein's mechanism was proposed, Figure 3.16. The authors suggested that in the presence of NEt$_3$, HNEt$_3^+$ is formed under catalytic conditions, which is beneficial for the decarboxylation step. This beneficial effect was assigned to a stabilization of the H-bound formate intermediate by hydrogen bonds during the non-traditional β-hydride elimination step. Based on this working hypothesis, the authors have conducted a screening of different Lewis Acid (LA) and found that the addition Lewis acids is beneficial for the catalytic performance. The best results were obtained when 10 mol% LiBF$_4$ was added in the absence of triethylamine, Figure 3.15. In reactions using 0.0001 mol% of formate complex **48** as catalyst, 10 mol% LiBF$_4$ as co-catalyst, after 9.5 h a TON of 983,642 was observed in dioxane as solvent at 80 °C. An initial TOF of 196,728 h^{-1} was measured in this reaction after the first hour.

These examples illustrate that FA dehydrogenation by iron catalysts can be achieved with simple Fe(0) and Fe(II) phosphine complexes. Also *in situ* generated catalysts were found to be suitable. Interestingly, the presence of a bifunctional ligands is not necessary for this transformation. In fact, for the two catalysts systems having ligands that could operate via a MLC mechanism, no evidence was reported that such mechanisms are actually taking place. Based on the examples reported in the literature it seems that three dentate pincer type ligands as well as tripodal ligands with a coordinating atom in the bridge head seem to result in the most active catalysts.
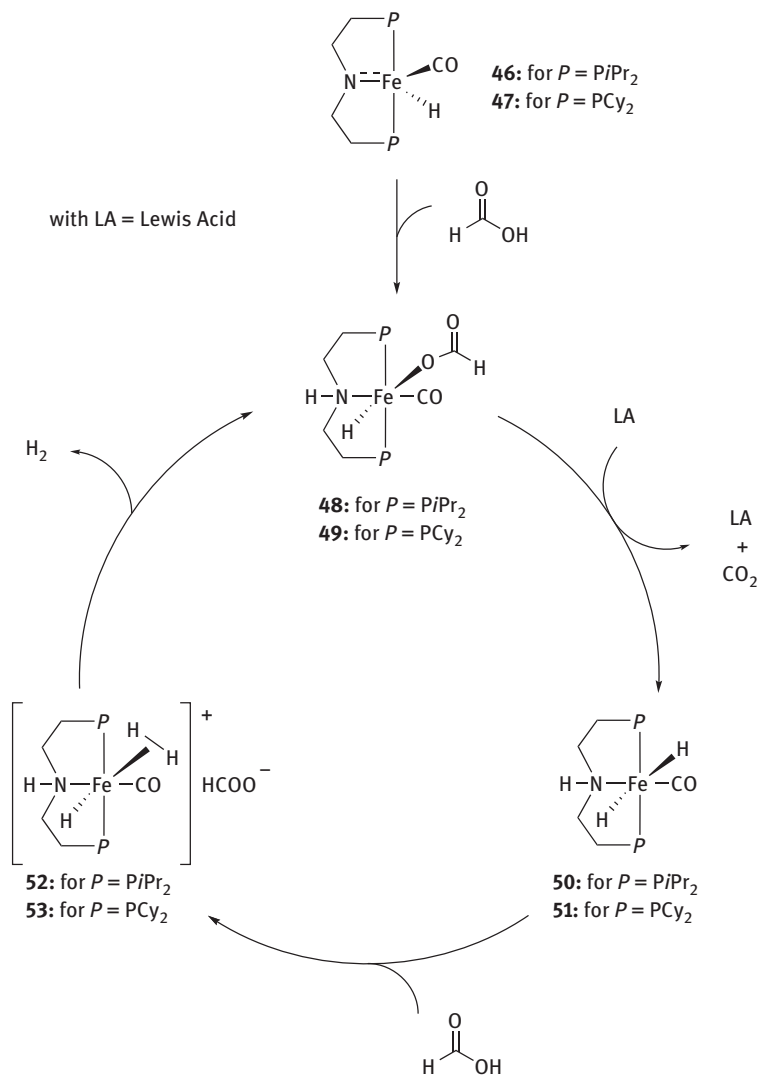
Figure 3.16: Mechanism, suggested for the Lewis acid assisted catalytic dehydrogenation of FA catalyzed by the PNHP iron pincer complexes.

Examples of base-metal catalysts for the dehydrogenation of FA other than iron are rather scarce. In 2015, Enthaler and Junge reported an example of a Ni PCP pincer complex which is active in the FA decomposition, Figure 3.17 [108]. The highest TON of 626 was measured when the nickel hydride catalyst was used to decompose FA in mixture with octyldimethylamine (=OctNMe$_2$=) in a 11:10 mixture in PC as solvent at 80 °C. In addition, this nickel hydride catalyst could also be used in the reduction of sodium bicarbonate to sodium formate [108].
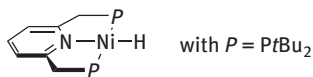
54, Enthaler, Junge, et al. 2015
$TON_{max} = 626$

$[Ni(PMe_3)_4]$

55, Parkin et al. 2016
$TON_{max} = 70$ and $TOF = 1.7 \, h^{-1}$

Figure 3.17: Ni-catalyzed FA dehydrogenation.

In 2016, another nickel (pre)catalyst for the decomposition of FA was reported by the Parkin group [109]. The complex $[Ni(PMe_3)_4]$ (**55**, Figure 3.17) catalyzes the dehydrogenation of FA with moderate activity. In a decomposition reaction conducted 80 °C in C_6D_6 a TON of 70 with an initial TOF of $1.7 \, h^{-1}$ was reported. Whereas for complex **54** amines needed to be added to the reaction mixture complex **55** catalyzes the FA decomposition in the absence of additional additives.

In 2015, the Parkin group was able to demonstrate that $[CpMo(PMe_3)_2(CO)H]$ (**56**, Figure 3.18, Cp = cyclopentadienyl) catalyzes FA dehydrogenation at a rate of $31 \, h^{-1}$ in benzene at 100 °C, also in the absence of additional additives [110]. Replacing the Cp ligand by the sterically more demanding Cp* (= 1,2,3,4,5-pentamethylcyclopentadienyl) ligand resulted in a slight increase of TOF to $54 \, h^{-1}$ observed for complex $[Cp^{\star}Mo(PMe_3)_2(CO)H]$ (**57**, Figure 3.18). For the catalytic reaction, a mechanism was proposed which is composed of three steps, namely (i) protonation of the metal center of **57**, formally a two electron oxidation, results in the formation of cationic dihydride species **58** followed by (ii) elimination of H_2 from **58** and coordination of formate to give neutral formate complex **59**, and finally (iii) decarboxylation of the formate complex **59** to regenerate hydride complex **56** or **57**.

Interestingly, although there are some cobalt complexes known, which catalyze the hydrogenation of CO_2 [111–115], the formal reverse reaction, the cobalt-catalyzed FA decomposition has not been reported yet. There is however a theoretical study by the Yang group, which predicts on the basis of DFT calculations that cobalt complexes should be capable of catalyzing the dehydrogenation of FA, too [116]. Experimental evidence for this hypothesis is to date still missing.

3.7 Heterogeneous catalysts for FA dehydrogenation

Interestingly, the first example of a dehydrogenation of FA was performed with a heterogeneous catalyst by the Noble price winner Paul Sabatier in 1912 [117]. In his Noble Lecture, held on 11 December 1912, he says:
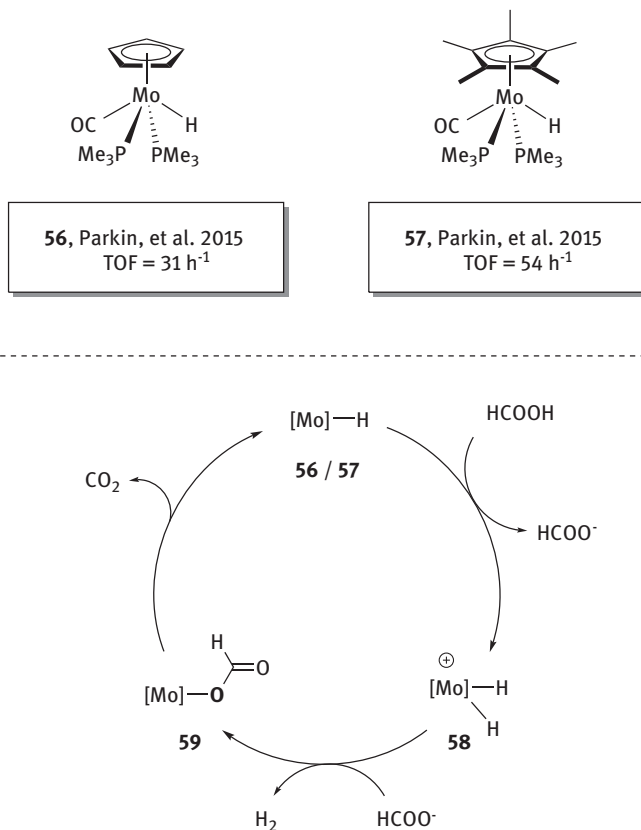
56, Parkin, et al. 2015
TOF = 31 h^{-1}

57, Parkin, et al. 2015
TOF = 54 h^{-1}

Figure 3.18: Mo-catalyzed FA decomposition.

> I have recently found, with Mailhe, that formic acid vapour breaks down at 250 °C only into carbon dioxide and hydrogen in the presence of zinc oxide, and only into water and carbon monoxide in the presence of titanium oxide. Here the two catalyst oxides have no physical dissimilarity, and such a complete reversal of the phenomenon can only be explained by the intervention of special chemical affinities operating at the surface of these catalysts. [118]

Since this seminal work in the field of hydrogen generation reactions, there has been progress in the development of various heterogeneous catalyst systems, for selected reviews see [14, 34]. Compared to homogeneous catalysis, this field however seems less developed. Table 3.1 summarizes selected examples of heterogeneous catalysts for the dehydrogenation of FA in aqueous media.

Over the last years, many studies have focused on heterogeneous FA dehydrogenation catalysts based monometallic noble metal nanoparticles (NPs) in aqueous solutions. The catalysts reported are supported on various support

Table 3.1: Selected examples for FA dehydrogenation catalysts in aqueous media [14]. [A]: initial TOF calculated for the initial H_2 evolution measured; [B]: TOF calculated for metal atoms at surface; [C]: CO gas was either not measured or not reported.

Heterogeneous catalyst	Temperature/°C	TOF/h^{-1}	CO gas detected[C]/ppm
Pd/C	25	64	–
Au/ZrO$_2$	50	1590[A]	–
Pd/MSC-30	50	2623	–
Pd-B/C	30	1184[A,B]	–
PdAu/C-CeO$_2$	92	227	<140
Pd/basic resin	75	820	<5
PdAg/basic resin	75	1900	<5
Ag@Pd/C	20	125[B]	–
Ag@Pd/C	90	626[B]	84
AuPd/ED-MIL-101	90	106	–
Pd/NH2-MIL-125	32	214	<5
AgPd/MIL-101	80	848	–
Ag$_{18}$Pd$_{82}$@ZIF-8	80	580	–
Ag$_{0.1}$Pd$_{0.9}$/rGO	25	105[A]	–
Au@Pd/N-mrGO	25	89[A]	–
(Co6)Ag$_{0.1}$Pd$_{0.9}$/RGO	50	2739	–
PtRuBiOx	80	312	–
PdAuEu/C	92	387	<100
Co$_{0.30}$Au$_{0.35}$Pd$_{0.35}$/C	25	80[A]	–
CoAuPd/DNA-rGO	25	85[A]	–
Ni$_{0.40}$Au$_{0.15}$Pd$_{0.45}$/C	25	12[A]	–
PdNi@Pd/GNs-CB	25	150[A]	–
MCM41-Si-(CH$_2$)$_2$PPh$_2$/Ru-mtppts	110	2780	<3
Pd-S-SiO$_2$	80	719	–

materials, such as metal–organic frameworks, silica, graphene, and porous carbons. When adding a second metal usually the electronic structure of the active phase and the adsorption behavior is altered. In addition also the metal dispersion on the support/particle size can be affected by this change. This can have a beneficial effect on the catalytic performance. For example, it has been found that the addition of Au or Ag affect the stability of Pd NPs in aqueous media which results in an enhancement of the catalytic activity [119–128]. This introduction of additional elements can either take place in the bulk phase, by formation of NPs composed of alloys or by so-called core-shell NPs. Whereas in alloy NPs all metals are equally distributed within the particle for core-shell particles this is not the case. These particles consist of an inner core of one or two metal elements and an external shell of other metal elements (e.g. PdAu@Au core-shell NPs). This composition has led in many cases to unique chemical and physical properties. As for the FA dehydrogenation, for example it

has been demonstrated that PdAu@Au core-shell NPs supported on activated carbon are superior over Au/C and Pd/C NP catalysts for the liquid phase dehydrogenation of FA at 92 °C [124].

The immobilization of highly active homogeneous catalysts is an interesting alternative to deposited metal NPs as catalysts. Ideally, this allows the combination of the excellent performance of the homogeneous catalysts with the advantage of reusability of the heterogeneous catalysts. This however is only the case if decomposition of the catalyst is not a dominant factor. However, in case of FA dehydrogenation, the Laurenczy group has developed in 2009 immobilized versions of their highly active Ru-mtppts (mtppts = meta trisulfonated triphenyl phosphine) catalyst system **31** (Figure 3.10)[78, 79] on various supports [129]. These immobilization efforts resulted in catalyst systems with high initial activities although gradual deactivation could be observed [129]. In 2013, the Laurenczy group has presented an improved catalytic system, which allowed achieving a TOF$_{max}$ 2780 h^{-1} [130].

3.8 Catalytic systems for the reversible storage of H$_2$ in FA

Compared to many other hydrogen storage systems, for the FA-amine adducts/CO$_2$ couple, reversible hydrogen storage has been demonstrated. In 2012, the Beller group has shown that *in situ* Ru catalyst **60** is an efficient catalyst for the dehydrogenation of FA, Figure 3.19 [131]. This catalyst is composed of the dimeric ruthenium precursor [{RuCl$_2$(benzene)}$_2$] combined with an six-fold excess of the bis-chelating diphosphine ligand dppe (=1,2-bis(diphenylphosphino)ethane). The catalytic FA decomposition reaction, achieving high catalyst activity (TOF$_{max}$ = 47,970 h^{-1}) and high catalyst stability (TON$_{max}$ = 800,000), was performed in *N,N*-dimethylhexylamine (= HexNMe$_2$) as solvent and the FA was added by a dosing pump at 80 °C. Notably, at the time, this was the highest TON observed for the hydrogen production from FA.

Possibly more important, however, is that this work has demonstrated the feasibility of reversible hydrogen storage. Along the lines the authors have also coined the expression "hydrogen battery" in this publication. In addition to FA decomposition, also CO$_2$ hydrogenation in amines as solvents was studied. Along with this study, the authors applied their catalytic system for reversible storage experiments. They were able to run up to eight consecutive hydrogenation/dehydrogenation cycles using [Ru(H)$_2$(dppm)$_2$] (**61**, dppm = bis(diphenylphosphino)methane, Figure 3.19) as catalyst in DMF (20 mL) in the presence of NEt$_3$ (2 mL, 14.3 mmol). The hydrogenation reaction to give FA in form of triethylammonium formate was performed in a commercial 100 mL autoclave using a 1:1 mixture of H$_2$ and CO$_2$ at overall 60 bar pressure. The reaction was allowed to progress until a pressure to ca. 45 bar was observed. At ambient temperature, this was reached overnight. The dehydrogenation of the FA-triethylamine adduct, which was formed in the hydrogenation
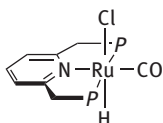
[{RuCl$_2$(benzene)}]$_2$ + 6 dppe

[Ru(H)$_2$(dppm)$_2$]

60, Beller et al. 2012
TOF = 47 970 h^{-1}
TON = 800 000
for FA - HexNMe$_2$
dehydrogenation
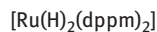
61, Beller et al. 2012
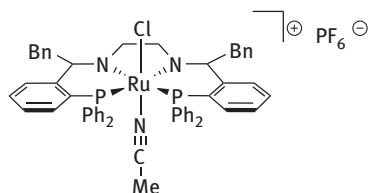
Used for reversible H$_2$
storage for FA - NEt$_3$

dppe = Bis(diphenylphosphino)ethane; dppm = Bis(diphenylphosphino)methane

Used for reversible H$_2$
storage for FA - DBU

with *P* = P(*t*Bu)$_2$

62, Pidko et al. 2014
TOF = 256000 h^{-1}
TON = 706 500
for FA - NHex$_3$
dehydrogenation

Used for reversible H$_2$
storage for FA - DBU

63, Plietker et al. 2014
TOF = 1142 h^{-1}
TON = 1333
for FA - DBU
dehydrogenation

Figure 3.19: Reversible hydrogen storage based on CO_2/FA-amine adducts.

step, was then observed when the pressure was released from the autoclave. During the FA dehydrogenation, the amount of gas formed was measured over ca. 5 h. In the first seven cycles between 1620 to 2170 mL of gas mixture were released. In comparison, when performing a blank experiment, where 1.67 mL of liquid FA (44.3 mmol) were decomposed under identical conditions 2105 mL of H$_2$/CO$_2$ gas mixture were received. In order to compensate the small amounts of NEt$_3$ lost due to evaporation from the reaction setup, each cycle a small amount of NEt$_3$ (0.1 mL, 0.73 mmol) were added. As the authors did not give the exact catalyst loading for this series of reversible hydrogenation/dehydrogenation series, it is not possible to extract TOFs or TONs for these experiments. However, it needs to be emphasized that the reversible storage experiments reached a volumetric ratios of 1: 0.835 (vol NEt$_3$: vol FA), which corresponds to molar ratio of FA: NEt$_3$ of 3.1. Although the system can store more FA than triethylamine is added (in moles), the overall storage capacity is significantly lowered by the addition of the solvent. The system as described reaches a hydrogen storage capacity of 1.0 wt.%, which is significantly lower than the max. theoretical storage capacity of 4.4 wt.% for pure FA

Later-on, in 2014 a similar study was reported by the Pidko group using a molecular defined catalyst, Milstein-type catalyst **62**, Figure 3.19. For the reversible hydrogenation of CO$_2$, DBU (=1,8-diazabicyclo[5.4.0]undec-7-ene) was used as amine base to obtain the corresponding FA-amine adduct. In the reversible storage experiments, this adduct was subsequently dehydrogenated. Initially, however, catalytic reactions necessary for the hydrogen storage were optimized. These are (i) the hydrogenation reaction of CO$_2$ in the presence of amine to get the amine-formate adduct and (ii) the dehydrogenation reactions of amine-formate adduct. The best catalyst performance for the hydrogenation reaction of CO$_2$ using catalyst **62** was obtained when 0.178 μmol of **62** were dissolved in 30 mL DMF and the reaction was conducted at 120 °C in the presence of 33.4 mmol DBU at 30 bar H$_2$ pressure and 10 bar CO$_2$ pressure. In this experiment, an impressive initial catalyst activity characterized by TOF$_{max}$ = 1,100,000 was achieved. A maximum turnover number was unfortunately not reported. The highest catalyst activity (TOF$_{max}$ = 256,000 h^{-1}) and catalytic productivity (TON$_{max}$ = 706,500) for the FA-adduct decomposition was observed using 1.42 μmol catalyst **62** in the presence of 33.5 mmol trihexylamine (=NHex$_3$) in DMF at 90 °C. The reversible storage experiments were then conducted using DBU (=1,8-diazabicyclo[5.4.0]undec-7-ene) as amine additive instead of NHex$_3$. In these hydrogen storage applications, the hydrogenation reactions were performed at different pressures, ranging from 5 to 40 bar, of 1:1 mixtures of CO$_2$ and H$_2$ at 65 °C. This series of experiments demonstrated that the Milstein-type catalyst **62** is efficiently hydrogenating CO$_2$, even at pressures as low as 5 bar total, which is a prerequisite for low pressure hydrogen storage applications. Molar ratios of acid/amine of 1.6 were obtained in the high pressure experiments, whereas the low pressure experiments were resulting in slightly lower ratio of 1.1. This phenomena is simply a result of the chemical

equilibrium shift according to Le Chatelier's principle. Similar to Beller's initial system, vide supra, dehydrogenation of the mixtures was observed upon releasing the pressure from the system. In comparison to Beller's initial system the molar acid amine ratios were significantly lower. The hydrogen generation step was performed at 90 °C. Under these conditions, both the hydrogenation and the dehydrogenation step proceed in a relatively short time of 3 and 1 h, respectively.

An additional example for reversible H$_2$ storage by hydrogenation of CO$_2$ in the presence of amine and its subsequent decomposition was reported by Plietker and coworkers also in 2014 [132]. The authors used for their reversible storage experiments 0.075 mol% of the ruthenium complex **63** (Figure 3.19), which is based on a tetradentate PNNP ligand, and DBU as additive. Both reactions, the hydrogenation and dehydrogenation reactions were performed at 100 °C. The hydrogenation was conducted using dry ice (as CO$_2$ source) under 70 bar of H$_2$ pressure. When heating this mixture a total pressure of 140 bar was observed initially. The hydrogenation stage was then stopped after a pressure drop to 100 bar was observed. Subsequently, the dehydrogenation step was initiated by releasing the pressure from the system, and running the reaction at ambient pressure. Up to five storage cycles were performed with this hydrogen battery, without observing a significant drop of activity.

In 2015, following the initial reports of hydrogen storage by dehydrogenation and re-hydrogenation of FA-amine adducts and CO$_2$, Olah and coworkers reported on a system which operates without the addition of amines [133]. For this amine-free system, the authors employed ruthenium PNP pincer complex **64** (Figure 3.20) as precatalyst and presented a system of a H$_2$ based charge discharge device operated

64, Olah et al., 2014,
TON$_{max}$ = 100
TOF$_{max}$ = 663 h^{-1}
for sodium formate dehydrogenation

65, Olah et al., 2014,
TON$_{max}$ = 5000
TOF$_{max}$ = 250 h^{-1}
for sodium formate dehydrogenation

Used for reversible H$_2$ storage for sodium formate
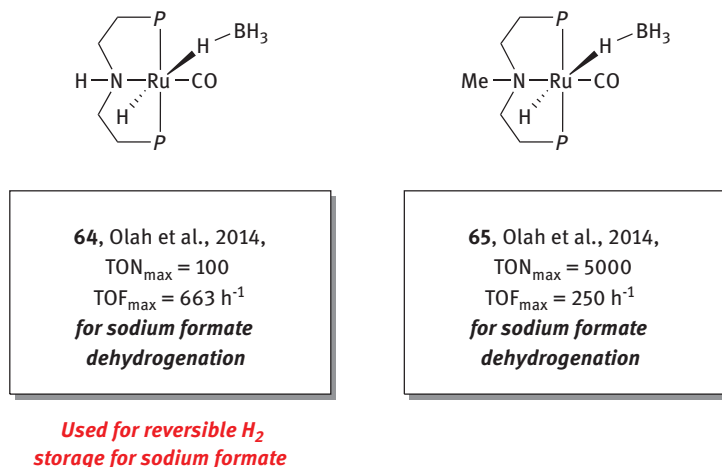
Figure 3.20: Amine-free catalyst system for reversible hydrogen storage based on the CO$_2$/FA couple *P* = PPh$_2$.

by pressure swing. This complex is very similar to the Fe-PNP catalyst system **46** and **47** (Figure 3.15). It is worth mentioning that the potential bifunctional catalyst possibly does not operate via a MLC mechanism. The fact that the NH moiety of precatalyst **64** is not crucial for the catalysis is underlined by the observation that the corresponding N-methylated complex **65** (Figure 3.20) shows similar performance to precatalyst **64** in catalytic hydrogenation and dehydrogenation reactions under identical conditions, Table 3.2.

Table 3.2: Comparison of catalytic performance of **64** and **65** under identical conditions [14].

(Pre)catalyst	Substrate	t/min	T/°C	Initial TOF/h^{-1}	TOF/h^{-1}	TON
Dehydrogenation reactions[A]						
64	HCOONa	270	69	286	222	1,000
65	HCOONa	240	68	430	250	1,000
(Pre)catalyst	**Base**	**t/min**	**T/°C**	**Initial TOF/h^{-1}**	**TOF/h^{-1}**	**TON**
Hydrogenation reactions[B]						
64	NaHCO$_3$	120	70	–	588	1175
65	NaHCO$_3$	76	73	–	760	963

Initially the authors have studied the performance of the catalytic systems in dehydrogenation reaction of different formate salts (sodium, lithium, potassium, and cesium formate) as well as the hydrogenation reaction in the presence of different bases (NaOH, KOH, LiOH, Na$_2$CO$_3$, K$_2$CO$_3$, Ca CO$_3$, NaHCO$_3$, and KHCO$_3$).

Notably, when potassium or sodium bicarbonate were employed as bases in hydrogenation reactions, no CO$_2$ was added to the system. This is due to the carbon dioxide (=CO$_2$) carbonic acid (H$_2$CO$_3$) equilibrium in water. The maximum TON for the hydrogenation reactions was achieved when using precatalyst **65**, in combination with NaOH at 70 degrees. After preforming the reaction for 590 min at a pressure of 61 bar/20 bar partial pressure of H$_2$ and CO$_2$, respectively, 84 % of formate yield were observed. This corresponds to a TON of 10,775, with a TOF 1096 h^{-1}. The highest TOF of >2000 was observed for the hydrogenation reaction of KHCO$_3$ with 40 bar H$_2$. In this experiment, full conversion was observed before the autoclave had reached the target temperature of 70 °C; overall the reaction was finished in less than 30 min.

The dehydrogenation reactions were studied with formate salts (Li, Na, K, Cs formate). The highest TON of 5000 was observed for precatalyst **65** at 70 °C in a dioxane water mixture. The experiment was performed over 1440 minutes using 2

µmol catalyst loading and 20 mmol substrate. After this time 50 % yield was achieved. The highest TOF (663 h^{-1}) in the series of experiments was observed for precatalyst **64** at 84 °C. Ninety-nine percent conversion was observed in this experiment after 90 min using 20 µmol catalyst loading and 20 mmol HCOONa as substrate.

[A] Reaction conditions dehydrogenation reaction: Catalyst loading = 20 mmol, sodium formate = 20 mmol, total volume of the solvent = 30 mL (20 mL 1,4-dioxane + 10 mL water). Initial TOF = TOF in first 2 h of the reaction. The error in the yield calculation is <10 %. [B] Reaction conditions hydrogenation reaction: 10 mmol catalyst, 12.5 mmol base, THF (5 mL), and H_2O (10 mL) were used. $p(H_2)$ = 40 bar given at ambient temperature. Time t, chosen so that no change in pressure is observed anymore. Yields calculated by NMR after evaporation of solvents by internal standards method. TOF is calculated by using time t.

Reversible hydrogen storage cycles were performed at 70 °C with NaOH as base and **64** as precatalyst using a H_2/CO_2 mixture (3:1) at an overall pressure of 75 bar. The subsequent dehydrogenation reactions were initiated by releasing the pressure so that the reaction mixture was allowed to equilibrate at 70 °C. Overall, the authors demonstrated that after six consecutive cycles, no significant loss in activity of the catalyst system was observed. In this six cycles, an overall TON of 11,500 was achieved.

This approach of amine-free hydrogen storage by a formate/CO_2 cycle is possibly a superior approach to amine-based systems. The inorganic bases used (ideally LiOH) have commonly lower molecular weights compared to typical amines (e.g. MW(LiOH) = 23.95 g/mol, MW(NaOH) = 40.00 g/mol vs. MW (NEt$_3$) = 101.19 g/mol, MW(NHex$_3$) = 269.51 g/mol). Although for amines it was demonstrated that FA/amine ratios of ~3 [131] can be achieved, whereas here stoichiometric amounts of base were employed, in case of light bases, such as NaOH or LiOH the systems may be more weight efficient. In addition the costs of the inorganic bases are lower and there are no problems associated with loss of amines by evaporation.

3.9 Conclusions and outlook

We have reviewed catalytic reactions for the FA dehydrogenation. This reaction has a max. theoretical H_2 storage capacity of 4.4 wt.%, which is undoubtfully lower than for MeOH and formaldehyde (12.1 and 8.4 wt.%) in aqueous reforming processes. However in case of FA, it has been demonstrated that reversible H_2 storage is feasible. Different systems which allow performing consecutive hydrogenation and dehydrogenation sequences in a one-pot systems without the addition of any additives between the reactions have been reported. More specifically, the storage systems are based either on amines, resulting in FA- amine adducts as storage intermediates

or based on inorganic bases, such as NaOH, resulting in formate salts as storage compounds.

The dehydrogenation of FA, in the presence of various additives (amines, other bases, Lewis acid, etc.) can in principle be catalyzed by various catalysts both of homogeneous and heterogeneous nature. In case of homogeneous catalysis, noble metal catalysts are the most common, but there are also a series of iron complexes known, which efficiently catalyze this reaction. Examples of other base metals used as catalyst are rather rare, as is the use of main group compounds.

References

[1]   Schüth F. Chemical compounds for energy storage. Chemie Ingenieur Technik. 2011;83: 1984–93.
[2]   Schüth F. Guest editorial: paving the way to new energy systems: the key role of the chemical sciences. ChemSusChem. 2010;3:6–8.
[3]   Bockris JOM. A hydrogen economy. Science. 1972;176:1323.
[4]   Eberle U, Felderhoff M, Schüth F. Chemical and physical solutions for hydrogen storage. Angew Chem Int Ed. 2009;48:6608–30.
[5]   Dalebrook AF, et al. Hydrogen storage: beyond conventional methods. Chem Commun (Camb). 2013;49:8735–51.
[6]   Schlapbach L, Zuttel A. Hydrogen-storage materials for mobile applications. Nature. 2001;414:353–8.
[7]   Jessop P. Hydrogen storage: reactions with a reverse gear. Nat Chem. 2009;1:350–1.
[8]   Teichmann D, et al. A future energy supply based on liquid organic hydrogen carriers (LOHC). Energy Environ Sci. 2011;4:2767–73.
[9]   Zell T, Langer R. Iron-catalyzed hydrogenation and dehydrogenation reactions with relevance to reversible hydrogen storage applications. Recycl Catal. 2015;2:87–109.
[10] Makowski, P, et al. Organic materials for hydrogen storage applications: from physisorption on organic solids to chemisorption in organic molecules. Energy Environ Sci. 2009;2:480–90.
[11] Boddien A, Junge H, Beller M. Katalyse für die chemische Wasserstoffspeicherung. Nachr Chem. 2011;59:1142–6.
[12] Geburtig D, et al. Chemical utilization of hydrogen from fluctuating energy sources – catalytic transfer hydrogenation from charged liquid organic hydrogen carrier systems. Int J Hydrogen Energy. 2016;41:1010–7.
[13] Himeda Y, Wang W-H. Chapter 6 – application of carbon dioxide in hydrogen storage: homogeneous hydrogenation of carbon dioxide and dehydrogenation of formic acid A2. In: Suib SL, editor. New and future developments in catalysis. Amsterdam: Elsevier, 2013:171–88.
[14] Li J, Zhu Q-L, Xu Q. Dehydrogenation of formic acid by heterogeneous catalysts. CHIMIA Int J Chem. 2015;69:348–52.
[15] Fink C, Montandon-Clerc M, Laurenczy G. Hydrogen storage in the carbon dioxide – formic acid cycle. CHIMIA Int J Chem. 2015;69:746–52.
[16] Joó F. Breakthroughs in hydrogen storage – formic acid as a sustainable storage material for hydrogen. ChemSusChem. 2008;1:805–8.
[17] Grasemann M, Laurenczy G. Formic acid as a hydrogen source – recent developments and future trends. Energy Environ Sci. 2012;5:8171–81.
[18] Laurenczy G, Dyson PJ. Homogeneous catalytic dehydrogenation of formic acid: progress towards a hydrogen-based economy. J Braz Chem Soc. 2014;25:2157–63.

[19] Boddien A. 6.20 – hydrogen generation from formic acid and alcohols. In: Poeppelmeier JR, et al., editor. Comprehensive inorganic chemistry II. 2nd ed. Amsterdam: Elsevier, 2013:587–603.

[20] Loges B, et al. Catalytic generation of hydrogen from formic acid and its derivatives: useful hydrogen storage materials. Top Catal. 2010;53:902–14.

[21] Fukuzumi, S, et al. Catalytic mechanisms of hydrogen evolution with homogeneous and heterogeneous catalysts. Energy Environ Sci. 2011;4:2754–66.

[22] Fukuzumi S. Bioinspired energy conversion systems for hydrogen production and storage. Eur J Inorg Chem. 2008;2008:1351–62.

[23] Johnson TC, Morris DJ, Wills M. Hydrogen generation from formic acid and alcohols using homogeneous catalysts. Chem Soc Rev. 2010;39:81–8.

[24] Czaun M, et al. Hydrogen generation from formic acid decomposition by ruthenium carbonyl complexes. tetraruthenium dodecacarbonyl tetrahydride as an active intermediate. ChemSusChem. 2011;4:1241–8.

[25] Enthaler S, Loges B. The rise of the iron age in hydrogen evolution?. ChemCatChem. 2012;4:323–5.

[26] Zell T, Milstein D. Hydrogenation and dehydrogenation iron pincer catalysts capable of metal-ligand cooperation by aromatization/dearomatization. Acc Chem Res. 2015;48:1979–94.

[27] Singh AK, Singh S, Kumar A. Hydrogen energy future with formic acid: a renewable chemical hydrogen storage system. Catal Sci Technol. 2016;6:12–40.

[28] Mellmann, D, et al. Formic acid as a hydrogen storage material – development of homogeneous catalysts for selective hydrogen release. Chem Soc Rev. 2016;45:3954–88.

[29] Enthaler S, Von Langermann J, Schmidt T. Carbon dioxide and formic acid-the couple for environmental-friendly hydrogen storage?. Energy Environ Sci. 2010;3:1207–17.

[30] Sordakis K, et al. Homogeneous catalysis for sustainable hydrogen storage in formic acid and alcohols. Chem Rev. 2018;118:372–433.

[31] Onishi N, et al. Recent progress for reversible homogeneous catalytic hydrogen storage in formic acid and in methanol. Coord Chem Rev. 2017, DOI: https://doi.org/10.1016/j.ccr.2017.11.021.

[32] Wang X, et al. Recent progress in hydrogen production from formic acid decomposition. Int J Hydrogen Energy. 2018;43:7055–71.

[33] Boddien A, Junge H. Acidic ideas for hydrogen storage. Nat Nanotechnol. 2011;6:265.

[34] Li Z, Xu Q. Metal-nanoparticle-catalyzed hydrogen generation from formic acid. Acc Chem Res. 2017;50:1449–58.

[35] Jessop PG, Ikariya T, Noyori R. Homogeneous hydrogenation of carbon dioxide. Chem Rev. 1995;95:259–72.

[36] Wang W.-H., et al. CO_2 hydrogenation to formate and methanol as an alternative to photo- and electrochemical CO_2 reduction. Chem Rev. 2015;115:12936–73.

[37] Schaub T. CO_2-based hydrogen storage: CO_2 hydrogenation to formic acid, formaldehyde and methanol. Phys Sci Rev. 2018, doi:10.1515/psr-2017-0015.

[38] Appel AM, et al. Frontiers, opportunities, and challenges in biochemical and chemical catalysis of CO_2 fixation. Chem Rev. 2013;113:6621–58.

[39] Dibenedetto A, Angelini A, Stufano P. Use of carbon dioxide as feedstock for chemicals and fuels: homogeneous and heterogeneous catalysis. J Chem Technol Biotechnol. 2014;89:334–53.

[40] Olah GA, Prakash GKS, Goeppert A. Anthropogenic chemical carbon cycle for a sustainable future. J Am Chem Soc. 2011;133:12881–98.

[41] Álvarez A, et al. Challenges in the greener production of formates/formic acid, methanol, and DME by heterogeneously catalyzed CO_2 hydrogenation processes. Chem Rev. 2017;117:9804–38.

[42] Centi G, Perathoner S. Opportunities and prospects in the chemical recycling of carbon dioxide to fuels. Catal Today. 2009;148:191–205.

[43] Wang W, et al. Recent advances in catalytic hydrogenation of carbon dioxide. Chem Soc Rev. 2011;40:3703–27.

[44] Jessop PG, Joó F, Tai -C-C. Recent advances in the homogeneous hydrogenation of carbon dioxide. Coord Chem Rev. 2004;248:2425–42.

[45] Trincado M, Vogt M. CO_2-based hydrogen storage – hydrogen liberation from methanol/water mixtures and from anhydrous methanol. Phys Sci Rev. 2018, doi:10.1515/psr-2017-0014.

[46] Trincado M, Grützmacher H, Prechtl Martin HG. CO_2-based hydrogen storage – hydrogen generation from formaldehyde/water. Phys Sci Rev. 2018, doi:10.1515/psr-2017-0013.

[47] Moret S, Dyson PJ, Laurenczy G. Direct synthesis of formic acid from carbon dioxide by hydrogenation in acidic media. Nat Commun. 2014;5:4017.

[48] Hietala J, et al. Formic acid. Ullmann's Encyclopedia Ind Chem 2016, doi:10.1002/14356007. a12_013.pub3.

[49] Yu X, Pickup PG. Recent advances in direct formic acid fuel cells (DFAFC). J Power Sour. 2008;182:124–32.

[50] Myers TW, Berben LA. Aluminium-ligand cooperation promotes selective dehydrogenation of formic acid to H_2 and CO_2. Chem Sci. 2014;5:2771–7.

[51] Amos RIJ, et al. Hydrogen from formic acid through its selective disproportionation over sodium germanate – a non-transition-metal catalysis system. Angew Chem Intl Ed. 2014;53:11275–9.

[52] Chauvier C, et al. Metal-free dehydrogenation of formic acid to H_2 and CO_2 using boron-based catalysts. Chem Sci. 2015;6:2938–42.

[53] Coffey RS. The decomposition of formic acid catalysed by soluble metal complexes. Chem Commun (London). 1967:923b–924.

[54] Strauss SH, Whitmire KH, Shriver DF. Rhodium(I) catalyzed decomposition of formic acid. J Organomet Chem. 1979;174:C59–C62.

[55] Paonessa RS, Trogler WC. Solvent-dependent reactions of carbon dioxide with a platinum(II) dihydride. Reversible formation of a platinum(II) formatohydride and a cationic platinum(II) dimer, [Pt2H3(PEt3)4][HCO2]. J Am Chem Soc. 1982;104:3529–30.

[56] Gao Y, et al. An efficient binuclear catalyst for decomposition of formic acid. Chem Commun. 1998:2365–6.

[57] Man ML, et al. Synthesis, characterization and reactivity of heterobimetallic complexes ([small eta]5-C5R5)Ru(CO)([small mu]-dppm)M(CO)2([small eta]5-C5H5) (R = H, CH3; M = Mo, W). Interconversion of hydrogen/carbon dioxide and formic acid by these complexes. Dalton Trans. 2003;3727–35.

[58] Shunichi F, Takeshi K, Tomoyoshi S. Efficient catalytic decomposition of formic acid for the selective generation of H2 and H/D exchange with a water-soluble rhodium complex in aqueous solution. ChemSusChem. 2008;1:827–34.

[59] Himeda Y. Highly efficient hydrogen evolution by decomposition of formic acid using an iridium catalyst with 4,4[prime or minute]-dihydroxy-2,2[prime or minute]-bipyridine. Green Chem. 2009;11:2018–22.

[60] Gunanathan C, Milstein D. Bond activation and catalysis by ruthenium pincer complexes. Chem Rev. 2014;114:12024–87.

[61] Milstein D. Metal-ligand cooperation by aromatization-dearomatization as a tool in single bond activation. Trans Philosoph R Soc A. 2015;373:20140189.

[62] Gunanathan C, Milstein D. Applications of acceptorless dehydrogenation and related trans-formations in chemical synthesis. Science. 2013;341:1229712.

[63] Gunanathan C, Milstein D. Metal–ligand cooperation by aromatization–dearomatization: a new paradigm in bond activation and "green" catalysis. Acc Chem Res. 2011;44:588–602.

[64] Chakraborty S, Guan H. First-row transition metal catalyzed reduction of carbonyl functional-ities: a mechanistic perspective. Dalton Trans. 2010;39:7427–36.

[65] Gunanathan C, Milstein D. Bond activation by metal-ligand cooperation: design of "green" catalytic reactions based on aromatization-dearomatization of pincer complexes. Top Organomet Chem. 2011;37:55–84.

[66] Grützmacher H. Cooperating ligands in catalysis. Angew Chem Intl Ed. 2008;47:1814–8.

[67] Khusnutdinova JR, Milstein D. Metal–ligand cooperation. Angew Chem Intl Ed. 2015;54: 12236–73.

[68] Milstein D. Discovery of environmentally benign catalytic reactions of alcohols catalyzed by pyridine-based pincer Ru complexes, based on metal–ligand cooperation. Top Catal. 2010;53:915–23.

[69] Zell T, Langer R. From ruthenium to iron and manganese-a mechanistic view on challenges and design principles of base-metal hydrogenation catalysts. ChemCatChem. 2018;10:1930–40.

[70] Ikariya T. Bifunctional Transition metal-based molecular catalysts for asymmetric syntheses. In: Ikariya T, Shibasaki M, editors. Bifunctional molecular catalysis. Berlin: Springer Berlin Heidelberg; 2011:31–53.

[71] Vogt M, et al. Reversible CO_2 binding triggered by metal-ligand cooperation in a rhenium(i) PNP pincer-type complex and the reaction with dihydrogen. Chem Sci. 2014;5:2043–51.

[72] Vogt M, et al. A new mode of activation of CO_2 by metal-ligand cooperation with reversible C-C and M-O bond formation at ambient temperature. Chemistry. 2012;18:9194–7.

[73] Rivada-Wheelaghan O, et al. Synthesis and reactivity of iron complexes with a new pyrazine-based pincer ligand, and application in catalytic low-pressure hydrogenation of carbon diox-ide. Inorg Chem. 2015;54:4526–38.

[74] Oldenhof S, et al. Base-free production of H_2 by dehydrogenation of formic acid using an iridium–bisMETAMORPhos complex. Chem. Eur. J. 2013;19:11507–11.

[75] Oldenhof S, et al. Dehydrogenation of formic acid by Ir-bisMETAMORPhos complexes: experi-mental and computational insight into the role of a cooperative ligand. Chem. Sci., 2015;6:1027–34.

[76] Boddien A, et al. Hydrogen generation at ambient conditions: application in fuel cells. ChemSusChem. 2008;1:751–8.

[77] Albert B, et al. Continuous hydrogen generation from formic acid: highly active and stable ruthenium catalysts. Adv Synth Catal. 2009;351:2517–20.

[78] Céline F, D. PJ, Gábor L. A viable hydrogen-storage system based on selective formic acid decomposition with a ruthenium catalyst. Angew Chem Intl Ed. 2008;47:3966–8.

[79] Céline F, et al. Selective formic acid decomposition for high-pressure hydrogen generation: a mechanistic study. Chem – Eur J. 2009;15:3752–60.

[80] Enthaler S, Junge K, Beller M. Sustainable metal catalysis with iron: from rust to a rising star?. Angew Chem Intl Ed. 2008;47:3317–21.

[81] Morris RH. Asymmetric hydrogenation, transfer hydrogenation and hydrosilylation of ketones catalyzed by iron complexes. Chem Soc Rev. 2009;38:2282–91.

[82] Junge K, Schröder K, Beller M. Homogeneous catalysis using iron complexes: recent develop-ments in selective reductions. Chem Commun. 2011;47:4849–59.

[83] Dupau P, et al. Iron-catalyzed hydrogenation of esters to alcohols. Angew Chem Int Ed Engl. 2014;53:13004–6.

[84] Gaillard S, Renaud J-L. Iron-catalyzed hydrogenation, hydride transfer, and hydrosilylation: an alternative to precious-metal complexes?. ChemSusChem. 2008;1:505–9.

[85] Mérel DS, et al. Iron-catalyzed reduction of carboxylic and carbonic acid derivatives. Coord Chem Rev. 2015;288:50–68.

[86] Mérel DS, et al. Bifunctional iron complexes: efficient catalysts for C=O and C=N reduction in water. ChemCatChem. 2013;5:2939–45.

[87] Darwish M, Wills M. Asymmetric catalysis using iron complexes – 'Ruthenium Lite'?. Catal Sci Technol. 2012;2:243–55.

[88] Morris RH. Exploiting metal-ligand bifunctional reactions in the design of iron asymmetric hydrogenation catalysts. Acc Chem Res. 2015;48:1494–502.

[89] Chirik PJ. Iron- and cobalt-catalyzed alkene hydrogenation: catalysis with both redox-active and strong field ligands. Acc Chem Res. 2015;48:1687–95.

[90] Bullock RM. An iron catalyst for ketone hydrogenations under mild conditions. Angew Chem Intl Ed. 2007;46:7360–63.

[91] Bullock RM. Abundant metals give precious hydrogenation performance. Science. 2013;342:1054–5.

[92] Chakraborty S, et al. Nickel and iron pincer complexes as catalysts for the reduction of carbonyl compounds. Acc Chem Res. 2015;48:1995–2003.

[93] Li Y-Y, et al. Iron-, cobalt-, and nickel-catalyzed asymmetric transfer hydrogenation and asymmetric hydrogenation of ketones. Acc Chem Res. 2015;48:2587–98.

[94] Marcel G, Kathrin J, Matthias B. Homogeneous catalysis by manganese-based pincer complexes. Eur J Org Chem. 2017;2017:4344–62.

[95] Maji B, Barman MK. Recent developments of manganese complexes for catalytic hydrogenation and dehydrogenation reactions. Synthesis. 2017;49:3377–93.

[96] Fabian K, Rhett K. Manganese complexes for (de)hydrogenation catalysis: a comparison to cobalt and iron catalysts. Angew Chem Intl Ed. 2018;57:46–60.

[97] Yoshimura M, Tanaka S, Kitamura M. Recent topics in catalytic asymmetric hydrogenation of ketones. Tetrahedron Lett. 2014;55:3635–40.

[98] Filonenko GA, et al. Catalytic (de)hydrogenation promoted by non-precious metals – Co, Fe and Mn: recent advances in an emerging field. Chem Soc Rev. 2018;47:1459–83.

[99] Boddien A, et al. Iron-catalyzed hydrogen production from formic acid. J Am Chem Soc. 2010;132:8924–34.

[100] Boddien A, et al. Ortho-metalation of iron(0) tribenzylphosphine complexes: homogeneous catalysts for the generation of hydrogen from formic acid. Angew Chem Intl Ed. 2010;49: 8993–6.

[101] Yang X. Mechanistic insights into iron catalyzed dehydrogenation of formic acid: [small beta]-hydride elimination vs. direct hydride transfer. Dalton Trans. 2013;42:11987–91.

[102] Sanchez-de-Armas R, Xue L, Ahlquist MS One site is enough: a theoretical investigation of iron-catalyzed dehydrogenation of formic acid. Chemistry. 2013;19:11869–73.

[103] Mellmann D, et al. Base-free non-noble-metal-catalyzed hydrogen generation from formic acid: scope and mechanistic insights. Chemistry. 2014;20:13589–602.

[104] Zell T, et al. Efficient hydrogen liberation from formic acid catalyzed by a well-defined iron pincer complex under mild conditions. Chem – Eur J. 2013;19:8068–72.

[105] Langer R, et al. Low-pressure hydrogenation of carbon dioxide catalyzed by an iron pincer complex exhibiting noble metal activity. Angew Chem Intl Ed. 2011;50:9948–52.

[106] Boddien A, et al. Efficient dehydrogenation of formic acid using an iron catalyst. Science. 2011;333:1733–6.

[107] Alberico E, et al. Selective hydrogen production from methanol with a defined iron pincer catalyst under mild conditions. Angew Chem Int Ed Engl. 2013;52:14162–6.

[108] Stephan E, et al. Exploring the reactivity of nickel pincer complexes in the decomposition of formic acid to CO$_2$/H$_2$ and the hydrogenation of NaHCO$_3$ to HCOONa. ChemCatChem. 2015;7:65–9.

[109] Neary MC, Parkin G. Nickel-catalyzed release of H_2 from formic acid and a new method for the synthesis of zerovalent Ni(PMe3)$_4$. Dalton Trans. 2016;45:14645–50.

[110] Neary MC, Parkin G. Dehydrogenation, disproportionation and transfer hydrogenation reactions of formic acid catalyzed by molybdenum hydride compounds. Chem Sci. 2015;6:1859–65.

[111] Inoue Y, Sasaki Y, Hashimoto H. Synthesis of formates from alcohols, carbon dioxide, and hydrogen catalysed by a combination of group VIII transition-metal complexes and tertiary amines. J Chem Soc Chem Commun. 1975:718–9.

[112] Tai C-C, et al. High-pressure combinatorial screening of homogeneous catalysts: hydrogenation of carbon dioxide. Inorg Chem. 2003;42:7340–1.

[113] Christopher F, et al. Catalytic hydrogenation of carbon dioxide and bicarbonates with a well-defined cobalt dihydrogen complex. Chem – Eur J. 2012;18:72–5.

[114] Jeletic MS, et al. A cobalt-based catalyst for the hydrogenation of CO_2 under ambient conditions. J Am Chem Soc. 2013;135:11533–6.

[115] Spentzos AZ, Barnes CL, Bernskoetter WH. Effective pincer cobalt precatalysts for Lewis acid assisted CO_2 hydrogenation. Inorg Chem. 2016;55:8225–33.

[116] Ge H, Jing Y, Yang X. Computational design of cobalt catalysts for hydrogenation of carbon dioxide and dehydrogenation of formic acid. Inorg Chem. 2016;55:12179–84.

[117] Mailhe A, Sabatier P. Catalytic decomposition of formic acid. Compt Rend. 1912;152:1212–5.

[118] https://www.nobelprize.org/nobel_prizes/chemistry/laureates/191912/sabatier-lecture.html.

[119] Zhou X, et al. High-quality hydrogen from the catalyzed decomposition of formic acid by Pd-Au/C and Pd-Ag/C. Chem Commun. 2008:3540–2.

[120] Mori K, Dojo M, Yamashita H. Pd and Pd–Ag nanoparticles within a macroreticular basic resin: an efficient catalyst for hydrogen production from formic acid decomposition. ACS Catal. 2013;3:1114–9.

[121] Gu X, et al. Synergistic catalysis of metal–organic framework-immobilized Au–Pd nanoparticles in dehydrogenation of formic acid for chemical hydrogen storage. J Am Chem Soc. 2011;133:11822–5.

[122] Martis M, et al. Amine-functionalized MIL-125 with imbedded palladium nanoparticles as an efficient catalyst for dehydrogenation of formic acid at ambient temperature. J Phys Chem C. 2013;117:22805–10.

[123] Tedsree K, et al. Hydrogen production from formic acid decomposition at room temperature using a Ag–Pd core–shell nanocatalyst. Nat Nanotechnol. 2011;6:302.

[124] Huang Y, et al. Novel PdAu@Au/C core–shell catalyst: superior activity and selectivity in formic acid decomposition for hydrogen generation. Chem Mater. 2010;22:5122–8.

[125] Wang Z-L, et al. Au@Pd core-shell nanoclusters growing on nitrogen-doped mildly reduced graphene oxide with enhanced catalytic performance for hydrogen generation from formic acid. J Mater Chem A. 2013;1:12721–5.

[126] Ping Y, et al. Ag0.1-Pd0.9/rGO: an efficient catalyst for hydrogen generation from formic acid/sodium formate. J Mater Chem A. 2013;1:12188–91.

[127] Dai H, et al. Synergistic catalysis of AgPd@ZIF-8 on dehydrogenation of formic acid. Appl Catal B: Environ. 2015;165:57–62.

[128] Dai H, et al. AgPd nanoparticles supported on MIL-101 as high performance catalysts for catalytic dehydrogenation of formic acid. J Mater Chem A. 2014;2:11060–4.

[129] Gan W, Dyson PJ, Laurenczy G. Hydrogen storage and delivery: immobilization of a highly active homogeneous catalyst for the decomposition of formic acid to hydrogen and carbon dioxide. React Kinet Catal Lett. 2009;98:205.

[130] Arnaud T, et al. Formic acid dehydrogenation catalysed by tris(TPPTS) ruthenium species: mechanism of the initial "fast" cycle. ChemCatChem. 2014;6:3146–52.

[131] Boddien A, et al. Towards the development of a hydrogen battery. Energy Environ Sci. 2012;5:8907–11.

[132] Hsu SF, et al. A rechargeable hydrogen battery based on Ru catalysis. Angew Chem Int Ed Engl. 2014;53:7074–8.

[133] Kothandaraman J, et al. Amine-free reversible hydrogen storage in formate salts catalyzed by ruthenium pincer complex without pH control or solvent change. ChemSusChem. 2015;8: 1442–51.

Monica Trincado, Hansjörg Grützmacher and Martin H. G. Prechtl

4 CO₂-based hydrogen storage – Hydrogen generation from formaldehyde/water

Abstract: Formaldehyde (CH_2O) is the simplest and most significant industrially produced aldehyde. The global demand is about 30 megatons annually. Industrially it is produced by oxidation of methanol under energy intensive conditions. More recently, new fields of application for the use of formaldehyde and its derivatives as, i.e. cross-linker for resins or disinfectant, have been suggested. Dialkoxymethane has been envisioned as a combustion fuel for conventional engines or aqueous formaldehyde and paraformaldehyde may act as a liquid organic hydrogen carrier molecule (LOHC) for hydrogen generation to be used for hydrogen fuel cells. For the realization of these processes, it requires less energy-intensive technologies for the synthesis of formaldehyde. This overview summarizes the recent developments in low-temperature reductive synthesis of formaldehyde and its derivatives and low-temperature formaldehyde reforming. These aspects are important for the future demands on modern societies' energy management, in the form of a methanol and hydrogen economy, and the required formaldehyde feedstock for the manufacture of many formaldehyde-based daily products.

Keywords: formaldehyde, methanol, carbon dioxide, reforming, hydrogen storage, hydrogen generation

4.1 Introduction

Formaldehyde (CH_2O) is the simplest and most significant industrially produced aldehyde. Since the discovery in 1855 by Butlerow and early synthesis by von Hofmann in 1867, the potential applications of this compound underwent a rapid headway. In the early twentieth century, formaldehyde became an industrially produced chemical. When combined with phenol, it formed the first successful derivative, "Bakelite", which introduced mankind to the "plastic age" [1]. The work by Haber, Bosch, and others in the 1920s marked a turning point. Synthesis gas manufactured from coal became a source of ammonia, methanol, and urea on an

industrial scale. In 1926, I.G. Farben introduced Kaurit glue to the market, a polymer based on formaldehyde and urea. The suitability of the low-cost urea–formaldehyde resins for bonding wood significantly contributed to the popularity of particle board and launched a revolution in the construction and furniture industries. Several types of formaldehyde-based resins have exhibited exceptional heat and chemical resistance, which make them particularly important in the automobile and aerospace industries. The properties as a preservative and disinfectant were also documented by Blum at the end of the nineteenth century [2]. Due to its ability to cross-link primary amino groups and other nucleophilic functional groups in proteins, formaldehyde is a common fixative used to preserve tissue for histology. Driven by new discoveries in science and technology which see formaldehyde as useful for a wide range of applications, the demand for formaldehyde has risen steadily in the past decades. Nowadays, it is one of the most important industrial organic chemicals and the worldwide production capacity surpasses 30 million tons per year [3].

Formaldehyde is ubiquitous in the atmosphere, where is released *via* photochemical oxidation and incomplete combustion of hydrocarbons. It is a well-known pollutant, since is contained in car exhaust and tobacco smoke and therefore significant concentrations have been observed in polluted urban air [4]. Moreover, formaldehyde was one of the first "complex" organic molecules detected in the interstellar medium [5]. New research shows that the organic or carbon-containing materials (including amino acids) were likely made from formaldehyde in the primitive solar system – thus formaldehyde is one of the key molecules that are relevant to the origin of life.

Formaldehyde is gaseous at ambient conditions but typically available as aqueous solutions known as formol or formalin. A saturated water solution of formaldehyde (37 wt%) is commercialized as 100 % formalin. Pure aqueous solutions contain mainly the formaldehyde hydrate, methylene glycol (HOCH$_2$OH) in equilibrium with mixtures of oligomeric poly(oxymethylene) glycols [HO-(CH$_2$O)$_n$-H, n = 1–8], where the degree of polymerization depends on the temperature, concentration and pH. The non-hydrated form (H$_2$CO) is present at room temperature, below 0.1 wt%, instead the major species is the hydrated form methanediol (K ≈ 2$\star$10^3). Paraformaldehyde is the solid polymerization product of formaldehyde (mp = 120°C) with an average degree of polymerization of 8–100 units, which is depolymerized to the monomer upon heating or under slightly acidic conditions (e. g. pH 5–6), which leads to opening of the poly-acetal. A more expensive alternative to paraformaldehyde is trioxane which is much more stable, and therefore the acetal opening requires much harsher and more acidic conditions.

The formaldehyde molecule is relatively stable, with a heat formation of –115.9 kJ mol^{-1} (see Table 4.1 for a selection of physical properties). Decomposition by direct heating occurs at temperatures above 423 K, forming methanol and carbon dioxide (CO$_2$). The selectivity in the decomposition seems to be dependent on the temperature. Higher temperatures (>623 K) provoke the formation of synthesis gas (H$_2$/CO) [7]. At

Table 4.1: Physical properties of formaldehyde [6].

Molar mass	30.026 a.u.
Vapor pressure (295 K)	470 kPa
Boiling point	254 K
Flash point	358 K
Ignition temperature	697 K
Standard heat of combustion	570.7 kJ mol^{-1}
Ionization energy	10.88 eV = 87793.3 cm^{-1}
Dipole moment	2.33 D
Heat of formation (298 K)	-115.9 ± 6.3 kJ mol^{-1}
Gibbs energy (298 K)	-109.9 kJ mol^{-1}
Heat of combustion (298 K)	-561.5 kJ mol^{-1}
Specific heat capacity (298 K)	35.425 J mol^{-1} K^{-1}

lower temperatures, transition metal catalysts (rhodium, iridium, ruthenium, or cobalt) can promote the decarbonylation of the molecule and allow the use of formaldehyde as surrogates of syngas in hydroformylation reactions [8].

Formaldehyde is becoming a promising energy carrier for on-demand hydrogen generation. Some of the most recent research focusses on hydrogen production by decomposing formalin at low temperatures by employing catalysts with only CO_2 as by-product. The latter could be recycled resulting in a carbon-neutral fuel cycle. Related liquid-phase chemical hydrogen storage C1 materials such as methanol /water mixtures and formic acid have been intensively studied in the past years. Figure 4.1 shows a comparison of the gravimetric H_2 content and corresponding thermodynamic data for the complete dehydrogenation of each of these liquid organic fuels (LOF). This data show that formaldehyde is a good compromise between hydrogen content and energy required for the hydrogen release reaction. Although the MeOH/H_2O system has a higher hydrogen content (12 wt%), the higher energy required for complete dehydrogenation makes methanediol a competitive and equally attractive C1 energy carrier.

$$\text{LOF-H}_2 \leftrightarrows \text{LOF} + \text{H}_2$$
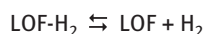
Reaction	wt% H_2	ΔH_r (kJ mol^{-1})	ΔG^0 (kJ mol^{-1})
MeOH + $H_2O \rightarrow CO_2$ + 3H_2	12.0	38.8	8.8
H_2CO + $H_2O \rightarrow CO_2$ + 2H_2	8.3	-35.8	-47.4
$HCO_2H \rightarrow CO_2 + H_2$	4.3	-14.9	-31.8

Figure 4.1: Comparison of gravimetric H_2 content of C1 liquid organic fuels (LOF) and thermodynamic data for the dehydrogenation reaction. Data obtained from http://webbook.nist.gov.
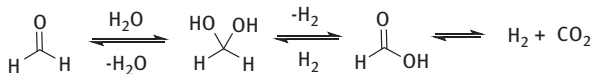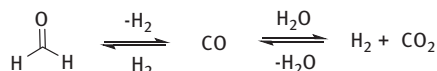
Pathway A

Pathway B

	Pathway A		Pathway B	
	Hydration/Dehydrogenation	*Decarboxylation*	*Decarbonylation*	*WGS*
ΔH_r	-20.9	-14.9	5.4	-41.2
ΔG^0	-15.5	-31.8	-27.2	-20.2
ΔE_F	-262.7	-256.7	-236.6	-243.2

Figure 4.2: Reaction pathways of formaldehyde reforming. WGS = Water gas shift. Comparison of thermodynamic data (ΔH_r) standard Gibbs free energy (ΔG^0) and overall "fuel energy" gain in the process (ΔE_F) in kJ mol^{-1}. Data obtained from webbook.nist.gov/chemistry.

Figure 4.2 summarizes the thermodynamic data for two possible dehydrogenation pathways of formaldehyde in water: Pathway (A) sequential hydration/dehydrogenation/decarboxylation and pathway (B) decarbonylation of H_2CO followed by a water gas shift reaction (WGS). The potential "fuel energy", ΔE_F, which can be gained in the overall process through the combustion of the produced H_2 with O_2, is given as $\Delta E_F = [n \, \Delta H_R(H_2 + \frac{1}{2}O_2) - \Delta Hr]$ with n = number of equivalents liberated in the dehydrogenation step. In the pathway A, the hydration of formaldehyde and the first dehydrogenative step of methanediol is an exergonic process overall (-20.9 kJ mol^{-1}), as is the second dehydrogenation step forming CO_2 (-14.9 kJ mol^{-1}). In the alternative pathway B, aldehyde decarbonylation is thermodynamically less favored than this hydration/dehydrogenation sequence because the first step is endergonic although only slightly by 5.4 kJ mol^{-1} (298 K). Depending on the individual activation barriers, which determine the kinetics of each reaction step, the formation of carbon monoxide as intermediate has to be taken into account (vide infra Section 2.2.2.).

New strategies for the catalytic reforming of H_2CO under mild conditions have raised expectations of this affordable compound as an alternative fuel. Herein, we discuss mainly catalyzed processes using heterogeneous or homogeneous systems. Most of the presented work is very much in its early stages, compared with other organic fuels (methanol or formic acid), especially the selective reversible conversion of CO_2 back to formaldehyde.

4.2 Production of formaldehyde and related technologies

4.2.1 Formaldehyde production and metabolism by biological systems

Formaldehyde (H_2CO) exists globally in the natural atmosphere as an oxidation product of CH_4. It is also a naturally occurring biological compound present in all tissues, cells, and biological fluids. Most formaldehyde is produced as the oxidation product of methanol [9]. Bacteria utilize three classic mechanisms for methanol metabolism: the Calvin cycle, the ribulose monophosphate cycle, and the serine cycle (Figure 4.3). First, the most energetically costly pathway of methanol metabolism begins with the sequential oxidation of methanol to formaldehyde, further to formate and then to carbon dioxide, which is then incorporated into the Calvin cycle as a carbon source.
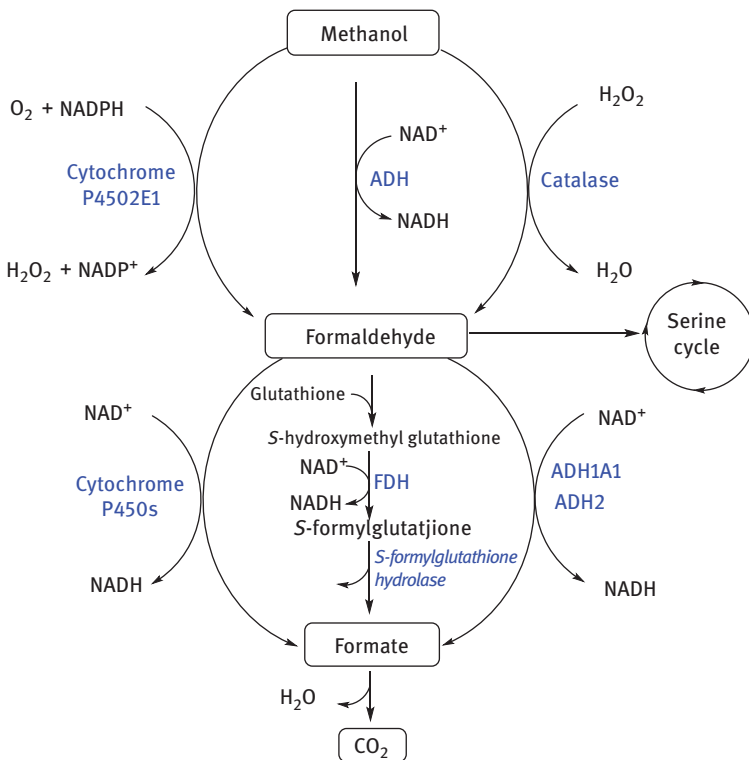
Figure 4.3: Formaldehyde production and metabolism. Overview of the pathways to convert sequentially methanol to formaldehyde and CO_2. NAD+/NADH, oxidized, and reduced form of nicotinamide adenine dinucleotide; ADH, Alcohol dehydrogenase; FDH, formaldehyde dehydrogenase; cytosolic (ALDH1A1) and a mitochondrial (ALDH2) aldehyde dehydrogenases. Figure adapted from reference [8].

This first oxidative step from methanol to formaldehyde can be executed *via* one of at least three different pathways: the catalase-H_2O_2 system, the cytochrome P450 (CYP2E1), and the zinc-based alcohol dehydrogenase I (ADH1) *via* NAD$^+$-dependent oxidation. The bulk of the formaldehyde is exported to the cytoplasm where it is further oxidized. The oxidation of formaldehyde to formate occurs by several separate pathways with the participation of P450 monooxygenases, mitochondrial aldehyde dehydrogenase 2 (ALDH2), and formaldehyde dehydrogenase (FDH). Under certain conditions, some formaldehyde may be oxidized to formate in the peroxisomes, either by methanol oxidase, which possesses dual substrate specificity, or by the reaction of hydrogen peroxide and catalase. The formate generated by formaldehyde oxidation can undergo further oxidization to carbon dioxide. These metabolic pathways involve catalase, 10-formyltetrahydrofolate dehydrogenase also known as ALDH1L1, or ALDH1L2, its mitochondrial isoform. Another endogenous source of formaldehyde is the oxidative deamination of methylamine by semicarbazide-sensitive amine oxidases (SSAOs), according to eq. (4.1).

$$CH_3NH_2 + O_2 + H_2O \overset{SSAO}{\rightarrow} HCOH + H_2O_2 + NH_3 \qquad (4.1)$$
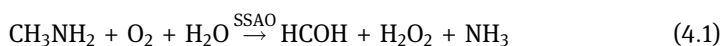
Beside the oxidation of methanol, formaldehyde is also formed by the conversion of glycine to serine in the presence of tetrahydrofolate (serine cycle) [10]. Furthermore, formaldehyde is part of the C1-carbon pool, which is utilized for the biosynthesis of purines, thymidine, and several amino acids, which are incorporated into DNA, RNA, and proteins during macromolecular synthesis.

4.2.2 Industrial production of formaldehyde

The large-scale production of formaldehyde involves a sequence of three reactions: (i) steam reforming of natural gas producing synthesis gas, a mixture of CO and H_2. (ii) Conversion of CO/H_2 to methanol, and (iii) finally partial oxidation and/or dehydrogenation of methanol to formaldehyde eqs (4.2) 4.2 (4.3) [11].

$$CH_3OH \rightleftharpoons CH_2O + H_2 \; \Delta Hr = 84 kJ\, mol^{-1} \qquad (4.2)$$

$$CH_3OH + 1/2\, O_2 \rightarrow CH_2O + H_2O \; \Delta Hr = -159 kJ\, mol^{-1} \qquad (4.3)$$
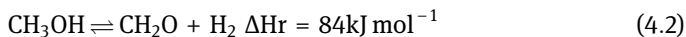
The industrial production of formaldehyde from methanol is based on two major processes: (a) The air-deficient process or silver contact process. In this process methanol air mixtures are dehydrogenated eq. (4.2) and partially oxidized by O_2 eq. (4.3) to formaldehyde at atmospheric pressure and in a temperature range of 600–

720°C. Under these conditions, the liberated H_2 is oxidized with O_2 to water (BASF, Borden, Bayer, Degussa, Imperial Chemical Industries (ICI), Celanese, DuPont, Mitsubishi, and Mitsui) [12]. This process can be further classified into two types: the methanol ballast and the water ballast process (or BASF process). In the second large-scale process, the Formox process, partial oxidation of methanol takes place in the presence of an excess of air (Lummus, Montecatini, Hiag/Lurgi, and Perstorp/ Reichold). Due to the higher stability of the catalyst (iron/molybdenum or vanadium oxide) and lower temperatures (250–400°C), the Formox process attracts more attention than silver-based catalytic process [13].

4.2.3 Related technologies for formaldehyde synthesis

Processes for converting hydrocarbons or ethers (e. g., dimethyl ether) [14] into formaldehyde are not of major industrial importance for economic reasons. Additionally, other processes that employ partial hydrogenation of CO [15] or oxidation of methane cannot compete with methanol conversion methods due to the lower yields obtained in these processes. Formaldehyde production from CO_2 itself would be advantageous due to the usage of non-fossil fuel sources and the possibility of recycling CO_2 formed in large amounts by burning fossil fuels. The chemical recycling of CO_2 may give formalin as a renewable, carbon-neutral, almost unlimited source for transportation fuels, as medium for storing and transporting energy, as well as a convenient feedstock for the production of fine chemicals. Recent studies focused on developing alternatives to the oxidative synthesis of methanol from natural gas based on reductive processes using CO_2 as raw material. Although there are many studies on the hydrogenation of CO_2 to formic acid and methanol, the selective catalytic hydrogenation to formaldehyde has been scarcely investigated although in the formation of CH_3OH from CO_2, theoretical calculations suggest the transient formation of formaldehyde as intermediate [16].

Lee et al. presented the first report on the direct formation of formaldehyde from CO_2 by a heterogeneous catalyst. An optimum atomic ratio of Pt : Cu = 0.03 : 1 supported on SiO_2 gives a catalytic system which allows the production of 0.87×10^{-4} mol min^{-1} g^{-1} catalyst and a selectivity of *ca.* 80 % with MeOH as side product. The H_2 : CO_2 ratio of 20 : 1 is essential to achieve a high selectivity (Figure 4.4a) [17].

An alternative production of formaldehyde by hydrogenation of CO or CO_2 has been reported by Tanksale and co-workers in 2015, respectively in 2017 [18, 19]. In their proof-of-concept study they demonstrated that the thermodynamically disfavored conversion of syngas to formaldehyde in the gas phase (Gibbs energy is positive) can be indeed successfully performed by simply conducting the reaction in the aqueous phase (Gibbs energy is negative). When the conversion level reached 19 %, aqueous formaldehyde is formed with 100 % selectivity at temperatures as low as 80°C in water under 100 bar with a NiRu catalysts

(Figure 4.4b). In the continuation of this research line, these authors demonstrated that under fairly similar conditions, CO can be substituted by carbon dioxide, resulting in a catalytic system which is capable to convert CO_2 into aqueous formaldehyde at temperatures below 100°C and at low pressure (70 bar) (Figure 4.4b) [19].

Heterogeneous systems

a) $CO_2 + 2\,H_2$ $\xrightarrow[\text{150°C}]{\text{PtCu/SiO}_2}$ $H_2CO + H_2O$

b) $CO + H_2$ $\xrightarrow[\substack{<100\text{°C} \\ <100\text{ bar} \\ H_2O}]{\text{NiRu}}$ H_2CO

or   100% selectivity

$CO_2 + 2\,H_2$ $\xrightarrow{\textit{idem}}$ $H_2CO + H_2O$

c) $CO_2 + 4\,H^+ + 4\,e^-$ $\xrightarrow{\text{BBD/Pt}}$ $H_2CO + H_2O$

Enzymatic systems

$CO_2 + 2\,\text{NADH} + 2\,H^+$ $\xrightleftharpoons{\text{FDH-TiO}_2/\text{FADH}}$ $H_2CO + 2\,\text{NAD}^+ + H_2O$
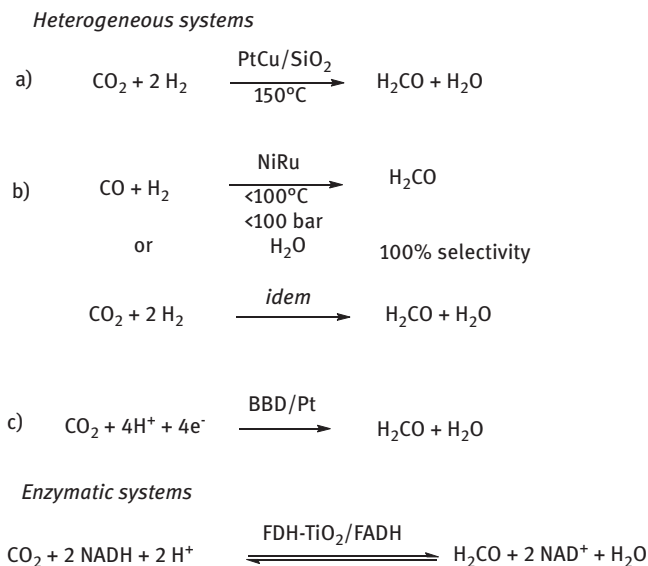
Figure 4.4: Heterogeneous or enzymatic catalytic reduction of CO_2 to formaldehyde. BDD (boron-doped diamond electrode). FDH (formate dehydrogenase) and FADH (formaldehyde hydrogenase)

The authors considered two possible mechanistic pathways through two-reaction step which involve CO or formic acid as intermediates, respectively. In the first proposed route (a), CO_2 is initially hydrogenated to formic acid ($\Delta H_{298} = -7.5$ kJ mol^{-1}), which consecutively undergoes hydrogenation to the formaldehyde hydrate ($\Delta H_{298} = -1.2$ kJ mol^{-1}). In the second pathway (b), CO is formed *via* reverse water gas shift reaction (RWGS) (endothermic by $\Delta H_{298} = 11.2$ kJ mol^{-1}) which in turn is hydrogenated to H_2CO (exothermic by $\Delta H_{298} = 19.9$ kJ mol^{-1}). The authors did not find any experimental evidence for the formation of formic acid or CO during the course of the reaction. However, in experiments with formic acid as substrate, the authors found that the molar yield of formaldehyde was lower than the corresponding consumption of formic acid, indicative of competing reactions. Hence, it is stated that route b is a more plausible pathway.

Nakata et al. described the electrocatalytic sequential reduction of CO_2 to first formic acid and then formaldehyde using a boron-doped diamond (BDD) electrode with a p-type surface and a Pt counter electrode under ambient conditions. This method overcomes the usual limitation of a narrow potential window and low electrochemical stability of other electrodes (Cu, Sn, Ag), achieving high Faradaic efficiency (74 %) for the production of formaldehyde. Either methanol, aqueous NaCl, or seawater can be used as the electrolyte. [20] Although photoreduction of CO_2 shows great potential, at present only low conversion rates are achieved. The main key factors which limit the efficiency are the low solubility of CO_2 in water, reverse reaction, the reduction of water to hydrogen as competing reaction, and poor charge carrier separation efficiency [21].

Enzymatic systems have been scarcely explored for CO_2 conversion to formaldehyde. They involve several consecutive reductions catalyzed by two different dehydrogenases, FDH (formate dehydrogenase) and FADH (formaldehyde hydrogenase). One of the few successful examples was reported by Zhang et al. who entrapped formate dehydrogenase during the formation of titania nanoparticles (NPs) through bio-inspired titanification. After *in situ* surface functionalization of NPs with pre-polymerized dopa (oligodopa, dopa = 3,4-dihydroxy-L-phenyl-alanine), formaldehyde dehydrogenase is immobilized on the surface of these NPs through an amine-catechol adduct reaction. Formaldehyde yields of up to 81 % and initial specific activity (1.87 U mg^{-1} of active enzyme) (enzyme unit (U) = 1 µmol min^{-1}) were achieved by reducing the particle size down to 75 nm. After storing for 20 days at 4°C, this multi-enzyme system was able to retain up to 70 % of its initial activity [22].

Unfortunately, a catalytic system for the selective hydrogenation of CO_2 to formaldehyde with only molecular H_2 still remains very rare. There are, however, other approaches where formaldehyde is trapped in the form of acetals by reduction with metal hydrides, boranes, silanes or H_2/alcohol mixtures. Soluble transition metal hydride complexes have emerged catalysts capable of the reduction of CO_2. The work by Floriani et al. [23]. exemplified the stepwise reduction of CO_2 to formaldehyde and methanol using the Schwartz's reagent, $[Cp_2Zr(Cl)H]_n$. This study was followed by mechanistic investigations to elucidate the CO_2 reduction pathways using metal hydrides [24]. Experimental evidence for a dinuclear complex with a bridging diolate $L_nM{-}OCH_2O{-}ML_n$ as intermediate has been initially presented by Berger et al. [25]. The authors applied successfully DOSY NMR spectroscopy to detect the extremely unstable diolate intermediate in the reaction of $[Cp_2Zr(Cl)H]$ with CO_2 (Figure 4.5a). A recent report by Cummins et al. describes the isolation and structural characterization of a tantalum methylene diolate complex. This compound could be the key to develop an efficient molecular hydrogenation catalyst if the $[H_2CO_2]^{2-}$ ligand could be liberated by heterolytic splitting of hydrogen regenerating the tantalum hydride species (Figure 4.5b) [26].

Significant progress has been made with homogeneous catalysts and boranes or silanes as reductants, where acetals (E-OCH_2-E, E = SiR_3, BR_2) are the direct product
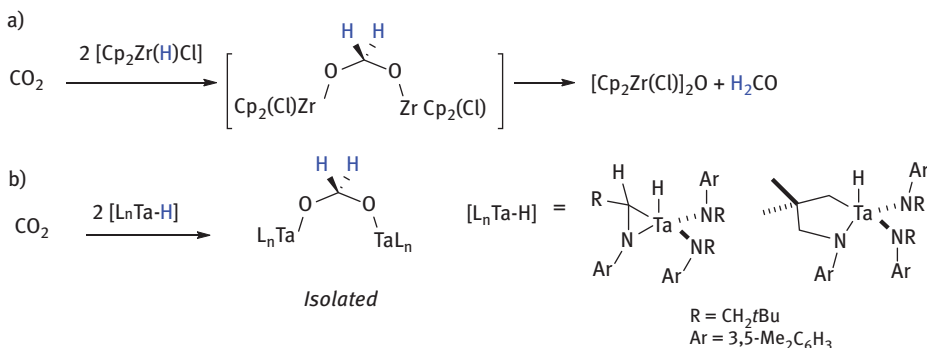
Figure 4.5: Carbon dioxide reduction by metal hydrides. Detection and isolation of bridging methylene diolate complexes [ref 24, 25].

from the reaction. Sabo-Etienne et al. achieved the hydroborylation of CO_2 (1 bar) with pinacol borane (HBPin) in a reaction catalyzed by complex $[RuH_2(H_2)_2(PCy_3)_2]$ (Cy = cyclohexyl) at ambient conditions [27]. The formation of several boryl compounds from CO_2 and pinacol borane could be observed as intermediates on the pathway to formic acid and methanol. One of the intermediates was identified as a C2-boron compound derived from formaldehyde formed *in situ* (Figure 4.6a). A slight modification of the phosphine ligand from cyclohexyl to cyclopentyl (= Cyp) gives the catalyst $[RuH_2(H_2)_2(PCyp_3)_2]$ and thereby enables the synthesis and isolation of formaldehyde. This reaction involves a reduction with borane in the presence of a sterically hindered aniline. This has the purpose of trapping $H_2C = O$ forming a formyl imine intermediate, which is then hydrolyzed to formaline or paraformaldehyde [28].

Oestreich et al. have described the ruthenium-catalyzed reduction of CO_2 to bis (silyl)acetal or methyl silyl ether by adjusting the reaction temperature [29]. The groups of Berke [30], Parvez [31], and Rodriguez [32] applied the frustrated Lewis pair (FLP) concept to the selective hydrosilylation of CO_2, employing rhenium, scandium, and nickel complexes, respectively, in combination with a Lewis acid (Figure 4.6b).

Khan et al. described the use of K[Ru(EDTA-H)Cl] (EDTA = ethylenediamine tetraacetic acid disodium salt) for the homogeneous catalytic reduction of carbon dioxide by hydrogen to give formic acid and formaldehyde as the initial reaction products, which they decompose to give CO and H_2O. The decomposition of formaldehyde was faster than its formation, thus imposing an important obstacle for the practical application of this catalytic system to the production of formaldehyde [33]. The ruthenium complex [Ru(triphos)(tmm)] (triphos = 1,1,1-tris(diphenylphosphinomethyl)ethane, tmm = trimethylenemethane) was employed successfully by Klankermayer for the first documented reduction of CO_2 to formaldehyde using H_2. The reaction achieved TON up to 200 and formaldehyde was trapped in form of dialkylmethylene ethers, which were formed in a tandem reaction in the presence of alcohols (Figure 4.7) [34].

a)

b)
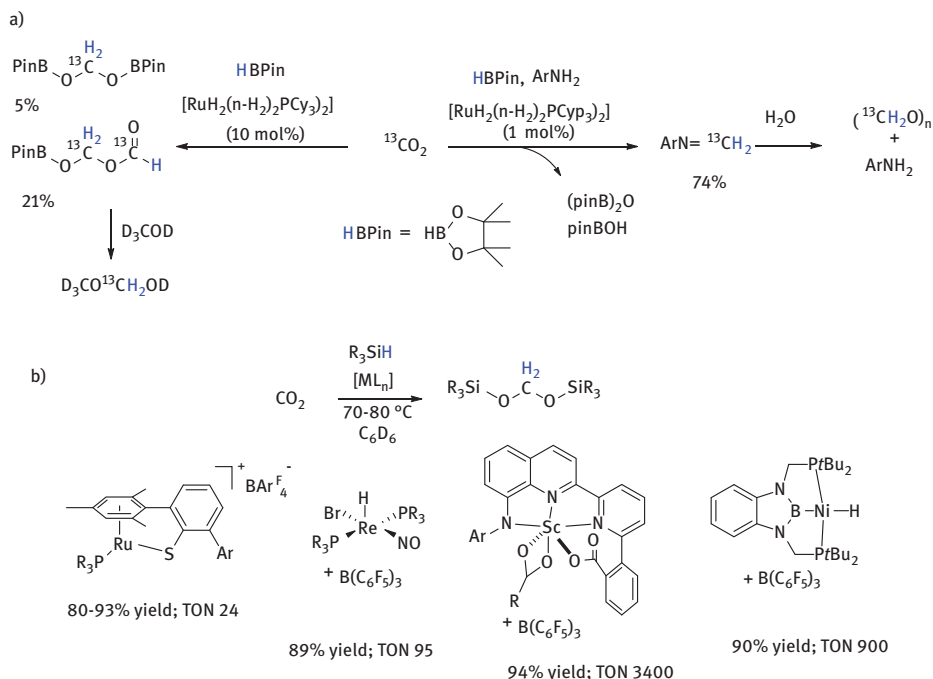
Figure 4.6: Reduction of CO_2 to acetals by boranes and silanes catalyzed by metal complexes.

$$CO_2 + 2 H_2 + 2 ROH \xrightarrow[80\ °C]{Al(OTf)_3} RO\!-\!\underset{O}{\overset{H_2}{C}}\!-\!OR$$

(20 bar)   (60 bar)

TON 214 (R = Me)
29 (R = iPr)
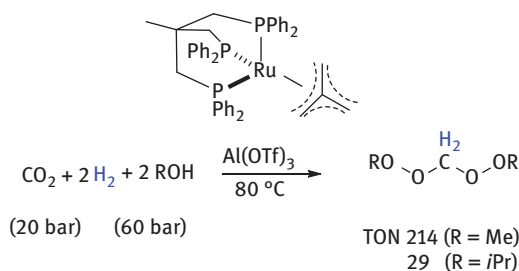
Figure 4.7: Hydrogenation of CO_2 to acetals in the presence of alcohols catalyzed by [Ru(triphos)(tmm)].

4.3 Aqueous formaldehyde as hydrogen and energy carrier

4.3.1 Base promoted dehydrogenation

Since the Cannizzaro reaction was discovered in 1853 [35], the release of very small quantities of hydrogen was noticed from aqueous solutions of formaldehyde and NaOH. In the past decades, this hydrogen evolution reaction has become of great

concern because it can cause the detonation of storage solution from nuclear waste, particularly mixtures containing ethylenediaminetetraacetic acid (EDTA) in highly basic media. Formaldehyde is one of the products formed in the photolysis, radioIysis, and thermal degradation of EDTA and therefore could be an important intermediate in the release of H$_2$ during its storage. In order to control this process, a fundamental understanding of the reaction responsible for the formation of hydrogen was carried out independently by Sauer, Ashby, and Kapoor et al. [36]. An initial explanation of hydrogen evolution is shown in the proposed mechanism in Figure 4.8 [36a]
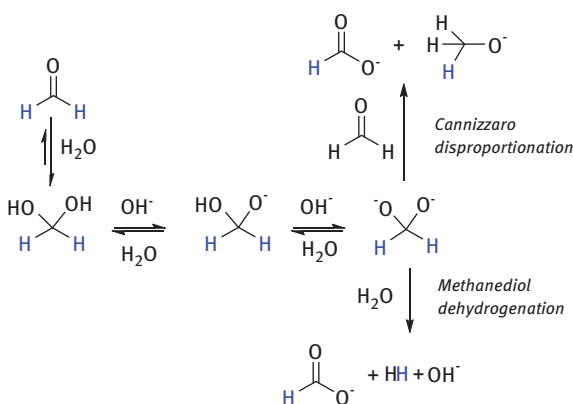
Figure 4.8: Reactivity of formaldehyde in aqueous basic solutions.

When formaldehyde reacts with an excess of base, it generates a dianionic Cannizzaro acetal, which serve as hydride donor to reduce another molecule of formaldehyde to form methoxide (CH$_3$O$^-$) and formate (HCO$_2^-$) (Cannizzaro disproportionation pathway, Figure 4.8). It was initially calculated that the same intermediate could react with water to form H$_2$ and a second molecule of formate (Methanediol dehydrogenation pathway, Figure 4.8). The authors found experimentally that high concentrations of base (16 M) and low concentrations of formaldehyde (1.5 mM) give quantitative formation of H$_2$ (98 % yield) at 60°C. No methanol was observed. The reaction is found to be first order in substrate, which implies that only one molecule of formaldehyde participates in the rate-determining step. A primary isotope effect was observed in experiments with deuterated formaldehyde (D$_2$CO) indicating that the cleavage of the C-H bond likely determines the rate of the reaction.

4.3.2 Metal catalyzed dehydrogenation

4.3.2.1 Heterogeneous catalytic processes

Several reports have shown that nanometallic catalysts, especially Cu, Ag, Au, Pd, Pt, and Zn can significantly accelerate the rate of hydrogen production from formaldehyde/water mixtures. Most of them are able to operate under thermal, electrochemical, or photochemical conditions. However, metal nanoparticles suffer from the intrinsic problem to agglomerate into larger particles over time, which greatly decreases the amount of active sites and consequently reduces the catalytic performance. Therefore, more recent investigations mainly focus on the prevention of this agglomeration by immobilizing the nanoparticles on different supports. In some cases, a synergetic interaction between the metal and support was observed and hence the type of the support and the dispersity of the metal nanoparticles play an important role in the catalytic performance of the catalysts.

4.3.2.1.1 Cu catalysts

In an early example, Bi et al. achieved the production of pure hydrogen with no detectable content of CO from aqueous formaldehyde solutions in a reaction catalyzed by various nano-sized metal particles (Pt, Au, Ni, and Cu) at room temperature and atmospheric pressure. In particular, a nano-Cu catalyst exhibited a high activity toward formate and H_2 formation at 60°C under basic conditions (140 mL $min^{-1} g^{-1}$ catalyst). In the absence of base, hydrogen could not be detected. Moreover, at higher concentrations of base (NaOH) and formaldehyde, the Cannizzaro reaction occurred, which resulted in the retardation of hydrogen generation [37]. Preti et al. reported that the aerobic oxidation of alkaline H_2CO to formate catalyzed by CuO microparticles was selective, quantitative, and accompanied by the generation of fuel cell grade hydrogen (8 mL $min^{-1} g^{-1}$ catalyst) [38]. Using MgO as a sacrificial agent, Cu_2O microcrystals can generate hydrogen from formaldehyde at room temperature. The authors explored the formation of paramagnetic oxygen deficient Cu(I) oxide and hydroxyl radicals as principal reagents for the formaldehyde degradation [39]. The anodic oxidation in alkaline media of H_2CO can be also promoted by Cu metal or Cu-based amorphous alloys (CuTi, CuZr) as electrocatalysts, especially when treated with HF. High current densities (*ca*. 40 mA cm^{-2}) were observed at a potential as low as 0.2V (NHE) [40]. CuO-Ag_2O nanowires, prepared on the surface of a ternary AgCuZn alloy, displayed an efficient electrocatalytic oxidation of formaldehyde to hydrogen and formate at room temperature [41]. The authors proposed a mechanism based on the electro-oxidation of a highly electroactive Cu_8O species as intermediate, which is produced in the reduction of CuO by formaldehyde. This complex catalyst provides a convenient gas sensor to monitor formaldehyde at the ppb level (52.40 mA $ppm^{-1} cm^{-2}$ with a detection limit of ca 21 ppb) and generates much more hydrogen (70 mL $min^{-1} g^{-1}$) than previous CuO microparticles.

4.3.2.1.2 Ag catalysts

Lu et al. demonstrated that Ag nanocrystals could catalyze the quantitative conversion at room temperature of formaldehyde in alkaline aqueous solution into hydrogen and formate, and no CO could be detected. The reaction conditions were very mild and there was a hydrogen production rate of up to 164 mL min^{-1} g^{-1} catalyst. The hydrogen can be detected immediately both in high and in low concentrations of H$_2$CO. Hence, Ag nanocrystals can be used to degrade formaldehyde on large scale and also to detect formaldehyde [42]. As mentioned above, nanoparticles as such inevitably tend to agglomerate to larger particles. To circumvent this defect, Ag nanocrystals were dispersed on the surface of γ -Al$_2$O$_3$ and indeed showed much higher catalytic activities (414 mL min^{-1} g^{-1} catalyst) and allowed the use of a lower amount of metal by weight [43]. In a recent report, Zou et al. introduced a heterogeneous catalyst based on Ag nanoparticles supported on MgO (AgNPs/MgO), which promoted the hydrogen evolution from aqueous formaldehyde with TOF up to 6000 h^{-1}. The TOF reported by the authors is an apparent TOF value considering the surface number of Ag atoms in the catalyst, calculated by the equation: TOF = $(n_{H_2}/n_{Ag}$ x $t) \times (d/1.3)$, (n_{H_2} = molar amount of evolved H$_2$, n_{Ag} = molar amount of Ag catalyst, d = average diameter of Ag NPs and 1.3/d is the empirical surface atom dispersion) [44]. In this case, molecular oxygen was used as a promoter of the reaction. The reaction kinetics depend almost linearly on the oxygen partial pressure. As the temperature increases from 0 to 50°C, the steady-state hydrogen release rate increases from 100 to 120 mmol h^{-1} g^{-1} catalyst (ca. 48 mL min^{-1} g^{-1} catalyst). The authors proposed, based on EPR spin-trapping experiments and calculations, that a surface stabilized MgO/Ag-•OOH complex is probably a catalytically active species. Bimetallic nanoparticles may exhibit advantages over their monometallic counterparts, since it is possible to tailor the electronic and geometric structures of the particles to enhance their catalytic activity and selectivity. Bimetallic AgPd particles supported on Vulcan XC-72 (AgPd@C-72) – a conducting carbon support – exhibit high catalytic activity and good stability, and the hydrogen generation rates reached up to 237 mL min^{-1} g^{-1} catalyst [45].

4.3.2.1.3 Au Catalyst

An Au-SrTiO$_3$ composite was used by Jia et al. in the H$_2$ evolution from aqueous formaldehyde solutions without any additives at low temperature. The support plays an important role in the activation of formaldehyde, which is further transformed into formate as intermediate and later decomposed into hydrogen and carbon dioxide. However, the catalyst exhibits low efficiency for H$_2$ evolution (<1 μmol min^{-1} g^{-1} catalyst) compared with Cu- and Ag-based catalysts [46]. Formaldehyde aqueous solutions (10 %v/v) were degraded to H$_2$ and CO$_2$ on supported titanium dioxide (TiO$_2$) nanotubes (NTs), which were loaded with Au or Pt nanoparticles (NPs). The TiO$_2$–NTs were produced by an oxidation process at an anode (anodization). Compared with Pt-loaded TiO$_2$-NTs, hydrogen production was superior with Au NPs. Using this catalyst, H$_2$ evolved steadily (0.06 μmol h^{-1} cm^{-2}) after many hours

of continuous UV-Vis irradiation without decrease in the photocatalytic activity. When Au NPs/TiO$_2$ NTs were used, hydrogen was also produced using only visible light irradiation (λ >400 or 450 nm) [47].

4.3.2.1.4 Pd catalysts

Hollow Pd nanotubes serve as a highly efficient and convenient catalyst for inhibiting the Cannizzaro reaction and facilitating hydrogen generation from alkaline formaldehyde solutions at room temperature. Pd nanotubes show significant higher catalytic activity (up to 170 mL min^{-1} g^{-1} catalyst) compared with Pd nanoparticles (40 mL min^{-1} g^{-1} catalyst). The kinetics of the reaction are highly dependent on the temperature, concentration of formaldehyde and base. The dehydrogenation process was successfully extended to higher aldehydes, such as acetaldehyde, propanal and benzaldehyde [48]. Ultra-thin TiO$_2$ nanosheets containing Pd quantum dots were used recently as catalyst (250 mL min^{-1} g^{-1} catalyst) for hydrogen generation from aqueous formaldehyde solutions at room temp, which is much more efficient than the previous Pd nanostructures [49]. Perovskite LaCoO$_3$ was found to be an efficient photocatalyst and displayed promising photocatalytic activity for H$_2$ production. The low efficiency to keep photogenerated electrons and holes separated and poor adsorptive performance could be improved with the p-type semiconductor PdO. Because of the resulting PdO/LaCoO$_3$ heterojunction, this photocatalysts shows an optimal activity in H$_2$ production from aqueous formaldehyde solution under irradiation with visible light which exceeds the one of LaCoO$_3$ alone (0.5 mL min^{-1} g^{-1} catalyst) by ten times [50].

4.3.2.1.5 Zinc catalysts

ZnO is well-known as a support and co-catalyst for methanol or formaldehyde steam reforming [51]. Fan et al. presented recently a Lewis acid-base combination as strategy to design a new heterogeneous catalysts for hydrogen formation (0.75 mL h^{-1}) from aqueous formaldehyde without additional additives [52]. The system is based on a core-shell structured ZnO@Bi(NO$_3$)$_3$ composite (BN-ZnO-X) with a strong electronic interaction at the interphase between both components. Several experiments were performed to correlate the catalytic activity of BN-ZnO to the interface between ZnO and Bi(NO$_3$)$_3$. First, the authors evaluated of the H$_2$ evolved as a function of the percentage of upshifted Zn 2p (Zn$^{2+\delta}$), considered as a descriptor for the number of interfacial sites in different BN-ZnO samples. In a second experiment, annealing a BN-ZnO sample at 550°C, provoked the decomposition of Bi(NO$_3$)$_3$ into Bi$_2$O$_3$. The treated sample had the same Zn 2p signal with ZnO and the 3.3 eV upshift disappeared, suggesting that the interfacial electronic interaction between ZnO and Bi(NO$_3$)$_3$ is destroyed. Destroying the interfacial electronic interaction leads to a fast deactivation while increasing interfacial sites proportionally enhances the activity, indicating that they are in fact the active sites. DFT calculations confirmed that the catalyst composites greatly lower the activation barrier for H$_2$ formation from two adsorbed H atoms and thus promote the H$_2$ production (Figure 4.9).
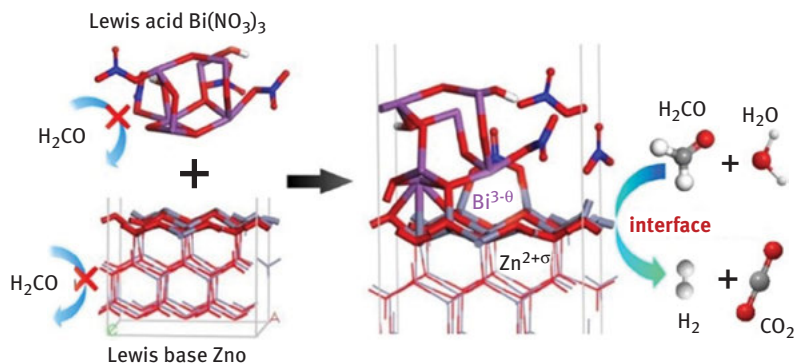
Figure 4.9: H$_2$ evolution from aqueous formaldehyde catalyzed by ZnO@Bi(NO$_3$)$_3$. Reproduced with permission of Ref. 49. Copyright 2017 ACS.

The activities and efficiency of the heterogeneous catalysts developed so far for formaldehyde reforming are shown in Table 4.2. The highest catalytic activities up to date are achieved by Ag nanocrystals dispersed on the surface of γ-Al$_2$O$_3$ (ref 43). Based on the amount of generated hydrogen (1230 mL H$_2$ g^{-1}), this system has theoretically a potential energy density of up to 13 MJ/Kg (3,700 Wh/Kg), assuming that the produced H$_2$ is completely combusted of with O$_2$ (ΔH = 242 kJ mol^{-1}) which leads potentially to a power density of 369 W/Kg. Compared to conventional Li-ion batteries (energy density 100 to 250 Wh/kg; power density 300 to 1500 W/kg), energy storage devices based on formalin may have a considerably higher energy density and acceptable power density values.

At present, the catalytic activities of heterogeneous catalyst do not compare favorably with those achieved with homogeneous systems. A strong limitation of the heterogeneous systems is the fact that most of them are only capable to liberate one equivalent of H$_2$ rather than two from a H$_2$CO/H$_2$O mixture because formic acid or formate salt, respectively, remains unconverted after the first dehydrogenation step in the reaction mixture (Table 4.2). At present, those heterogeneous systems are unsuitable for a complete formaldehyde reforming and lower the theoretically accessible hydrogen capacity of formaldehyde to the one of formic acid. Moreover, the mechanism of a catalytic reaction promoted by a heterogeneous catalyst is in general more difficult to investigate. Especially under this aspect, the application of a homogeneous catalytic system has its advantages because the core structure of a molecular complex as catalyst can be more easily modified such that electronic and steric factors, which are important for the catalytic activity become evident. Even if in the end a heterogeneous catalyst is the better choice for large-scale conversions given economic and technical constraints.

Table 4.2: Heterogeneous catalysts for the formaldehyde/water dehydrogenation reaction.

Entry	Catalyst	Additives	Conditions	Average rate of H$_2$ production (mL min^{-1} g^{-1})[a]	Products	Ref.
1	Nano-Cu	NaOH	60°C	140	HCO$_2$Na	37
2	CuO microparticles	NaOH	25°C	8	HCO$_2$Na	38
3	Cu$_2$O microcrystals	MgO	hu	<2	Mg(HCO$_2$)$_2$	39
4	CuO-Ag$_2$O nanowires	KOH	electro-catalytic	70	HCO$_2$K	41
5	Ag nanocrystals	NaOH	25°C	164	HCO$_2$Na	42
6	Ag nanocrystals/ γ-Al$_2$O$_3$	NaOH	25°C	414	HCO$_2$Na	43
7	Ag NPs/MgO	O$_2$	50°C	48	HC(OMe)$_3$ (from HCO$_2$H and MeOH), MgCO$_3$	44
8	AgPd@C-72	NaOH	25°C	237	HCO$_2$Na	45
9	Au-SrTiO$_3$	–	35°C	<0.02	CO$_2$	46
10	Pd NTs	NaOH	25°C	170	HCO$_2$Na	48
11	Pd NPs	NaOH	25°C	40	HCO$_2$Na	48
12	Pd/TiO$_2$	NaOH	25°C	250	HCO$_2$Na	49
13	Pd/LaCoO$_3$	–	hu	0.5	CO$_2$	50

[a] Activities are given in mL per minute and gram of catalyst.

4.3.2.2 Homogeneous catalysts and mechanistic insights

Very recently, the first clean low temperature dehydrogenations of aqueous methanol to H$_2$ and CO$_2$ were reported, which were catalyzed by well-defined group 8 or 9 metal complexes (**1–4**) (Figure 4.10) [53]. In these reactions, water serves as an oxygen transfer reagent and in any case no trace of CO contamination was observed. The three dehydrogenation steps, which allow complete methanol reforming are shown in Figure 4.10 and each requires a catalyst. The first H$_2$ release originates from the dehydrogenation of methanol to formaldehyde. The subsequent reaction with water gives methandiol from which a second equivalent of H$_2$ is liberated upon dehydrogenation to formic acid. Final dehydrogenation of HCOOH to CO$_2$ releases the third H$_2$ molecule.

Although in previous work on methanol reforming, formaldehyde hydrate or its oligomers were not observed, it has been repeatedly proposed as logical intermediate in the dehydrogention of methanol. A priori, it seems trivial that any of the previously studied catalysts must be considered for the reforming of formaldehyde. However, the dehydrogenation of aqueous formaldehyde and paraformaldehyde to H$_2$ and CO$_2$
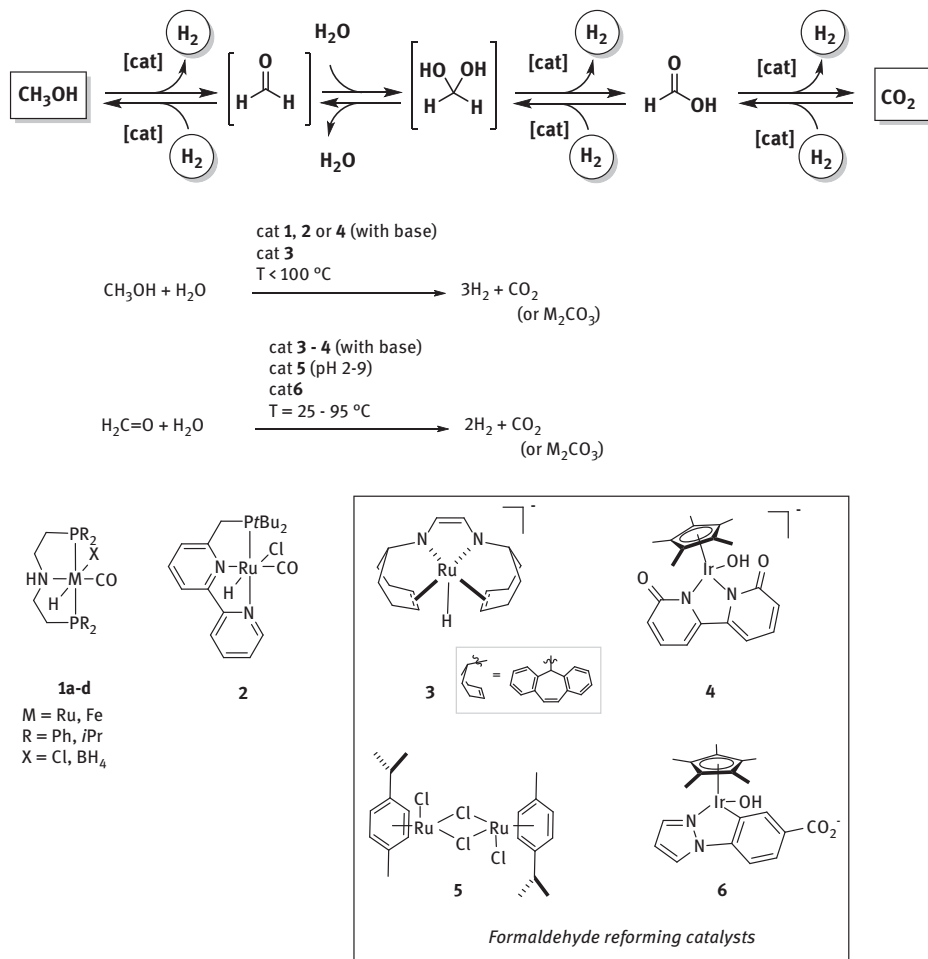
Figure 4.10: (A) Sequence of catalyzed dehydrogenation steps of methanol/water system. (B) Molecular catalyst for the dehydrogenation of methanol/water (**1**–**4**) or formaldehyde/water mixtures **3**–**6**.

catalyzed by a molecular catalyst has been scarcely investigated [54, 55, 57, 58]. In fact, few reports have described the conversion of aldehyde/water mixtures to hydrogen and carboxylate derivatives. An early study from Maitlis et al. showed that a series of half-sandwich complexes of Rh, Ir, and Ru were able to catalyze the disproportionation of aliphatic aldehydes under neutral conditions to a mixture of alcohols and acids. Because the acids were obtained as main products, substantial amounts of H$_2$ must have been produced in the reaction. In particular, the water-soluble hydroxocomplex [Ru$_2$(C$_6$Me$_6$)$_2$(OH)$_3$Cl] gave a 5:1 ratio of acetic acid/ethanol in the disproportionation of aqueous acetaldehyde with TONs of up to 2,400 at 45°C [56].

In 2014, homogeneous formaldehyde reforming was reported for the first time by Prechtl et al. [57]. The air-stable and easily accessible ruthenium catalyst [(Ru(p-cymene))$_2$(μ-Cl)$_2$Cl$_2$] (**5**) catalyzed the formation of H$_2$ from aqueous solutions at temperatures between 25°C and 95°C [54, 55, 57, 58]. The decomposition of formaldehyde (37 wt%) and paraformaldehyde proceeded preferably in the pH range of 5.5 to 7.0, with conversions up to 85 % within 60 minutes [57]. Note that the catalyst itself is active in over a rather broad pH range between 2.0 and 9.0. The best catalytic performance was observed at 95°C, where hydrogen was obtained with acceptable TONs (188) and turn over frequencies (TOFs) of up to 170 h^{-1}. This catalytic process tolerates oxygen and gives pure mixtures of CO$_2$ and H$_2$ without detectable traces of CO. Water is clearly involved in the reaction and labelling experiments with H$_2^{18}$O indicate that water acts as the oxygen donor in the formation of the methanediol intermediate and is also the proton source to form H$_2$ and final product (CO$_2$). The authors were able to identify and isolate [(Ru(p-cymene))$_2$(μ-H)(μ-HCO$_2$)(μ-Cl)]$^+$ as active species and hydroxocomplexes (i. e. [(Ru(p-cymene))$_2$(μ-OH)$_3$]$^+$) were detected as intermediates on course of the formation of the active species in this reaction [57]. In a diluted solution (5 wt%), the catalyst was able to reduce the content of formaldehyde to levels below 45 ppm. Quantitative conversion was achieved within 24 h giving a TON of up to ca. 1000 and initial TOFs of >3000 h^{-1} [55]. More recently, Prechtl, Deska et al. merged the catalytic activity of this ruthenium complex with the alcohol oxidase *Candida Boidinii*. This system allowed the sequential conversion of aqueous methanol to formaldehyde (catalyzed by the enzyme) and then the dehydrogenation of methanediol (catalyzed by the Ru complex) to H$_2$ yielding 15.3 µmol mL^{-1} and CO$_2$ at room temperature (Figure 4.11). [58] In addition, the authors demonstrated that aqueous formaldehyde undergoes dismutation in presence of an organometallic formaldehyde dismutase mimic [59], and is suitable for redox self-sufficient reductive N-methylation [60].
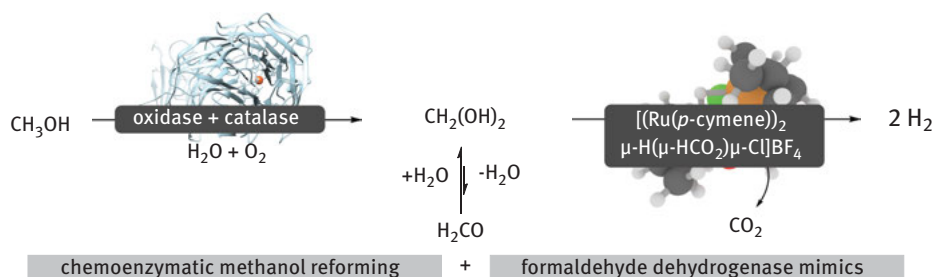
Figure 4.11: Chemoenzymatic methanol reforming [58] in presence of the formaldehyde dehydrogenase mimic [(Ru(p-cymene))$_2$(μ-H)(μ-HCO$_2$)(μ-Cl)]$^+$ [54, 55, 57, 58].

Fukuzumi et al. showed that the water-soluble aqua complex [Ir^{III}(Cp*)(4-(1H-pyrazol-1-yl-kN^2)benzoic acid-kC^3)(H$_2$O)]$_2$SO$_4$ is able to produce H$_2$ and CO$_2$ in a 2:1 ratio from paraformaldehyde solutions (Figure 4.10). Although with very low TONs (<24), the reaction proceeded at room temperature and the rate of H$_2$ production increased with increasing pH [61]. The optimal H$_2$ production is obtained at pH 11, at which the hydroxocomplex **6** is the actual catalyst that reacts with paraformaldehyde to form formate and an iridium hydride complex. The formation of metal hydride species led to the proposition of a classical mechanism in which the substrate is activated and converted at the metal center (Figure 4.12). The reaction of formalin to CO$_2$/H$_2$ mixtures was also catalyzed using a similar Ir complex **4** (Figure 4.10). In this system, the cooperative α,α'-bipyridonate ligand participates as a proton acceptor in the activation step and the intramolecular reaction of hydride on the metal with protic hydrogen on the resulting α-hydroxypyridine-based ligand leads to the formation of molecular hydrogen (Figure 4.13) [62]. The system operates using catalytic amounts of base and achieves a TON of 178. The protonated aqua complexes showed very low catalytic activities.

The catalyst [K(dme)$_2$][Ru(H)(trop2dad)] (**3**) (trop$_2$dad = 1,4-bis(5H-dibenzo[a,d]cyclohepten-5-yl)-1,4-diazabuta-1,3-diene) developed by Grützmacher, Trincado et al. was able to catalyze efficiently the dehydrogenation of both, methanol [53]f and formalin [63]. The ruthenium species was also able to promote the dehydrogenation of formic acid with one of the highest TOFs reported to date for a process without any additives (24,000 h^{-1}). In Yamaguchi's and Grützmacher's approaches, the metal center is coordinated by a cooperative ligand. The complex **3** contains a redox and chemically non-innocent diolefin diazadiene ligand which participates actively in the dehydrogenation reactions of all C1-susbtrates. Diazadiene ligands [64] behave as chemically "non-innocent" ligands, accepting up to 2 equivalents of H$_2$ forming the fully hydrogenated species **3(H4)** (Figure 4.14), which is also an active catalyst. This particular metal-ligand cooperativity is illustrated in simplified form by the equilibria between the structures **3N** and **3N'** (redox non-innocence; either as resonance forms or distinctive electronic states) and the fully hydrogenated complex **3(H4)** (chemical non-innocence) (Figure 4.14). The tetradentate, robust trop$_2$dad ligand contains no phosphanyl but two olefinic binding sites which can also behave as non-innocent ligands. Their electronic flexibility allows for the stabilization of low-valent metal centers by metal-to-ligand back donation of electron density. The most remarkable results were achieved in the reforming of aqueous solutions of paraformaldehyde (c$_0$ = 0.47 M) at low reaction temperature (60°C) achieving high conversion to carbonate and H$_2$ (up to 90 %). The catalyst was recycled up to six times without significant loss of efficiency (TOF$_{50}$ > 20,000 h^{-1}). The various reaction pathways A and B shown in Figure 4.2 for the conversion of formalin were taken into account. One of those involves the production of carbon monoxide as an intermediate from the reaction H$_2$CO → CO + H$_2$, a molecule that frequently "poisons" the metal catalysts.
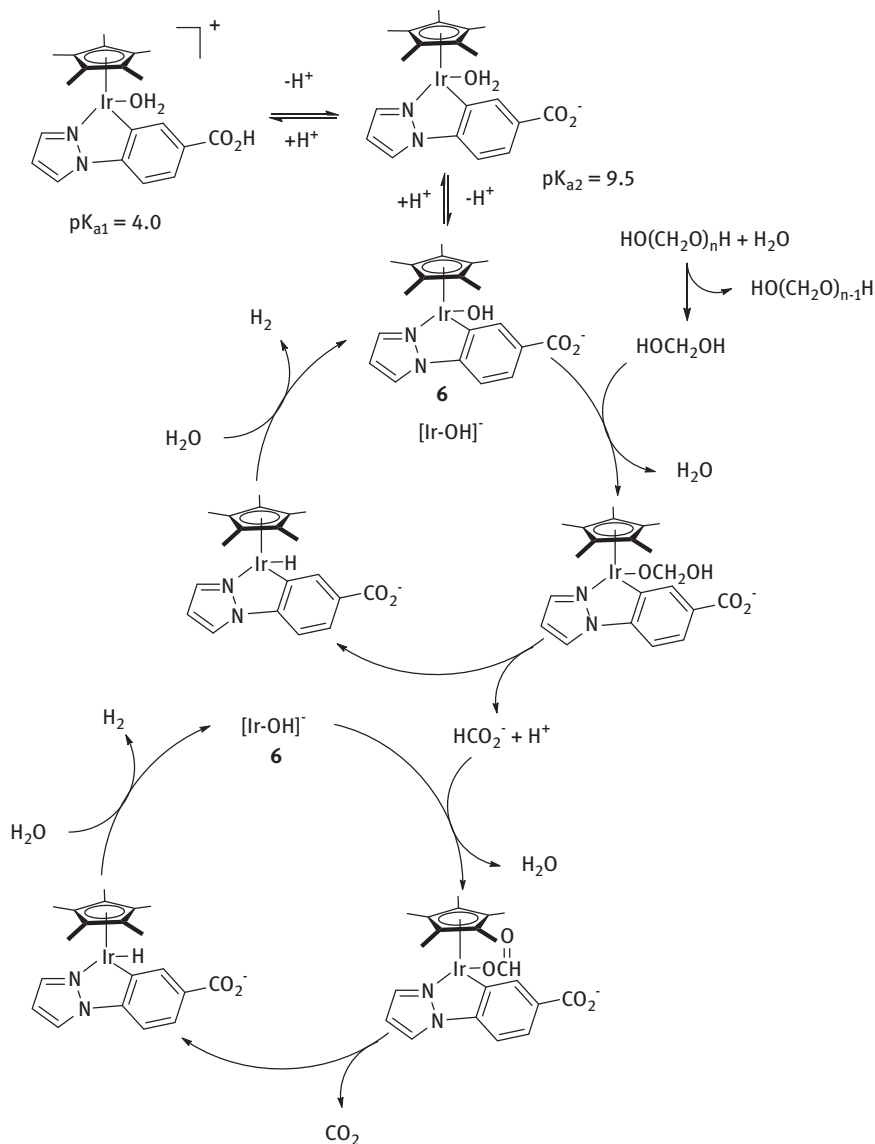
Figure 4.12: Proposed pathway for dehydrogenations of formaldehyde/water mixtures catalyzed by iridium complex **6** (classical metal-centered mechanism).

Remarkably, the ruthenium catalyst **3** is able to operate in a carbon monoxide atmosphere, although with much lower activity. This observation may be taken as indication that **3** acts as a catalytic "chameleon" and actually catalyzes the conversion of aqueous formaldehyde along different pathways (decarbonylation/WGS
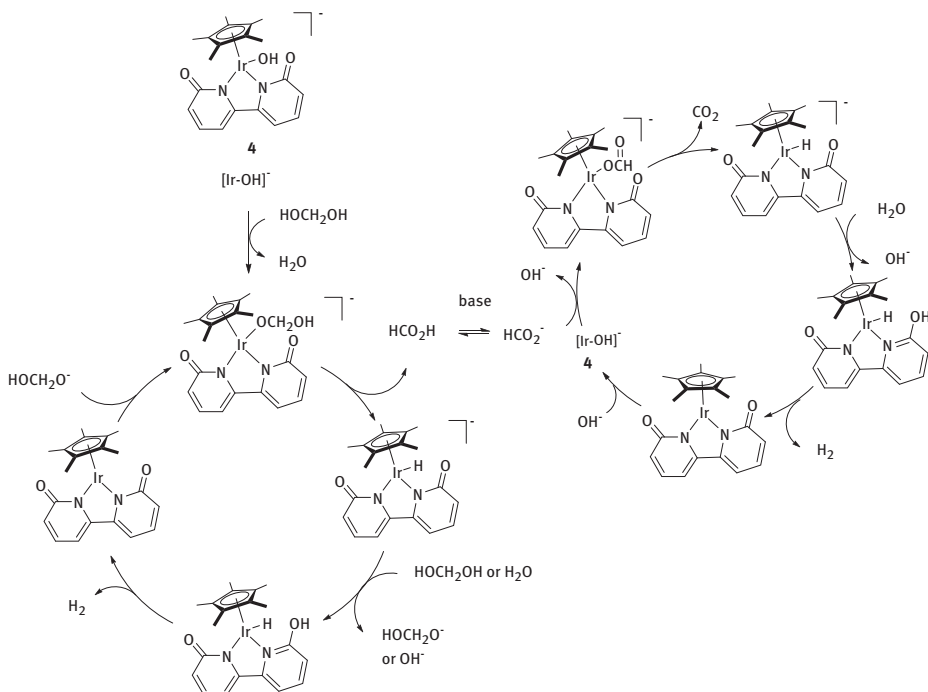
Figure 4.13: Proposed pathway for dehydrogenations of formaldehyde/water mixtures catalyzed by iridium complex **4** (metal ligand cooperative mechanism).
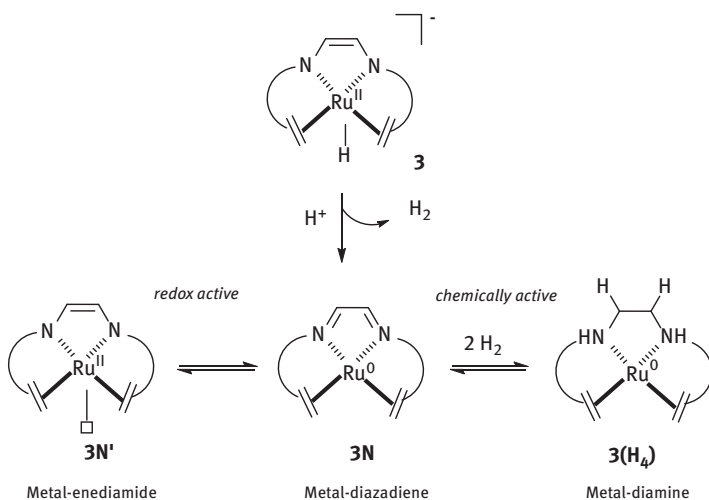
Figure 4.14: Redox- and chemically active metal–diazadiene–olefin system.

and hydration/dehydrogenation and Cannizzaro/methanol dehydrogenation; see Figure 4.2).

Because the formaldehyde hydration/methandiol dehydrogenation path is the most likely one, this reaction sequence was calculated with DFT methods. Since **3** rapidly converts to the neutral species **3N**, the latter complex was set as starting point of the catalytic cycle. The theoretical data suggest that the first step is the exergonic formation of the methanediol complex **A**, followed by proton transfer from the alcohol to one of the iminic nitrogen atoms in the ligand backbone (Figure 4.15). The initially formed complex **B'** rearranges to a hydrogen-bond stabilized complex **B**, which by β-hydride elimination subsequently converts to the Ru hydride complex **C'**.
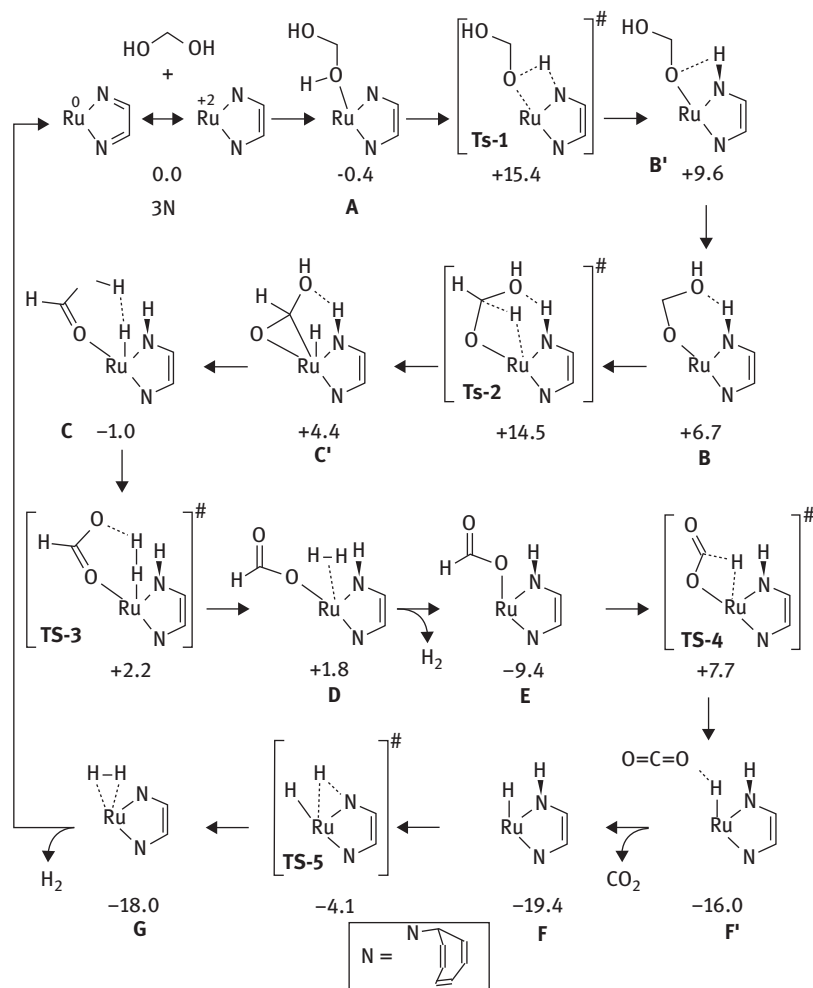
Figure 4.15: Proposed mechanism for H_2 production from formaline catalyzed by complex **3N**.

The complex **C'** rearranges further to give intermediate **C** in which the Ru-H hydride unit is interacting with the proton of the hydroxyl group of the coordinated formic acid moiety. In **C** the formation of H_2 is pre-organized and indeed only a small activation barrier (3.2 kcal mol^{-1}) separates **C** from the H_2 complex **D** which loses H_2 in an essentially barrier-less reaction to produce formate complex **E**. In a second β-hydrogen elimination the formate ligand in **E** is converted to the ruthenium hydride complex **F'** which contains loosely bound CO_2. The calculations imply that the transformation **E → F'** may be the rate determining step (**TS-4**: $E_a = 17.1$ kcal mol^{-1}). Loss of CO_2 gives the amino hydride complex **F** which rearranges via the activated complex **TS-5** at $E_a = 15.3$ kcal mol^{-1} to the diazadien hydrogen complex **G**, which readily loses H_2 to complete the catalytic cycle. It is also possible that under the experimental conditions **3N** is hydrogenated to **3(H4)** [63] which was likewise considered as catalyst for formaldehyde dehydrogenation.

Indeed, the DFT data show a comparable minimum energy reaction pathway (MERP) and indicate that it is quite likely that both, **3N** and **3(H4)**, are involved and contribute to the observed catalytic activity. In both pathways, hydride migration from the substrate to the metal are key steps in the catalytic cycle to produce H_2, and in both mechanisms metal-ligand cooperativity plays an important role.

4.4 Future perspectives

In the last decade, major progress has been made with respect to the conversion of CO_2 to formaldehyde. This makes the use of formaldehyde as liquid organic hydrogen carrier (LOHC) promising, indeed. For the first time a promising direct formaldehyde synthesis from CO_2, respectively syngas, *via* RWGS (reverse water gas shift) has been realized and the synthesis of dialkoxyl methanes *via* catalytic reduction of CO_2 has been demonstrated. The electrocatalytic conversion of CO_2 to formaldehyde in sea water as electrolyte is another highly interesting concept. Such approaches have the potential to substitute old fashioned high-temperature oxidative production of formaldehyde from methanol. These novel pathways for conversion and generation of a C_1-chemical feedstock open up new opportunities toward more cost and energy saving production chains with formaldehyde as a platform molecule. Carbon dioxide for the *in situ* generation of CO may turn the annual multi-megaton market of formaldehyde into a more sustainable chemical platform by eliminating fossil sources from the production chain. The stabilization of formaldehyde by water and alcohols will be the key to improve these syntheses due to the favorable thermodynamics in solution and the reactivity of all solute species and intermediates: Methanediol and (di)alkoxymethane, in the case of formaldehyde, or carbonic acid and carbonates in the case of CO_2 as hydrated species in solution. Moreover, the conversion of formaldehyde into bis(silyl) or bis(boryl) methylene acetals may generate further interest to use these compounds for inorganic materials with

formaldehyde as cross-linker [54]. Notably, sequential enzyme catalysis applying FDH and FADH in presence of NADH as co-factor leads also to the selective formation of formaline from CO_2. This eventually brings biotechnological processes into the play for the production of formaldehyde under very mild conditions to complement the industrial procedures which are already established in order to meet the high global demands of formaldehyde.

New applications of formaldehyde in the energy sector for renewable combustion fuels (i. e. bio-derived methylene ethers) or as LOHCs for hydrogen fuel cell technologies require an enhanced global production of formaldehyde based on renewable resources and waste rather than fossil sources. The realization of a formaldehyde-based hydrogen battery requires the immobilization of the catalyst. In terms of long-term stability, the system seems quite promising, also taking into account the usual limitations of battery life-time issues and the superior energy content of hydrogen and LOHC in comparison to conventional batteries.

Secondary batteries represent one of the biggest and most developed group of energy storage technologies. However, the research in this area is approaching the maximum energy density limits, under safe operational conditions. Electrochemical devices based on a direct or indirect formalin fuel cell could being considered as possible solutions to the limitations of conventional batteries. In terms of weight and volume, an electrochemical device with a liquid organic fuel (LOC) can offer a higher energy content. For example, the system based on formalin and a heterogeneous catalyst (Ag/Al_2O_3) [40] could store a ten-fold higher energy (3.39 KWh/Kg) than a Li-ion battery and gives a comparable power density (369 W/Kg) under the assumption that a complete oxidation occurs. On the other hand, the most efficient homogeneous system based on a ruthenium catalyst could also deliver an acceptable power density of 230.5 W/Kg. Further considerations (cost, safety, and convenience) will be also critical for the successful introduction of formaldehyde-fuel cells as replacements for batteries. The high prices for noble metal catalyst used up to now will not allow to make such a fuel cell competitive with established energy storage devices. Future research must concentrate on the development of system which contain earth-abundant and cheap metals from the fourth period of the periodic table. Recent work shows that this goal may be achieved as there are iron or manganese complexes which can be applied for the dehydrogenation of LOCs although the activities and stability are still rather low [65, 66].

References

[1]   Crespy D, Bozonnet M, Meier M. 100 years of bakelite, the material of a 1000 uses. Angew Chem
      Int Ed. 2008;47:3322.

[2]   Blum J. Der Formaldehyd als Haertungsmittel. Zool Anz. 1893;16:450.

[3]   Tang X, Bai Y, Duong A, Smith MT, Li L, Zhang L. Formaldehyde in China: production, con-
      sumption, exposure levels, and health effects. Environ Int. 2009;35:1210.

[4]   Tuazon EC, Winer AM, Pitts JN. Trace pollutant concentrations in a multiday smog episode in the
      California South Coast Air Basin by long path length Fourier transform infrared spectroscopy.
      Env Sci Tech. 1981;15:1232.

[5]   Snyder LE, Buhl D, Zuckerman B, Palmer. P. Microwave Detection of Interstellar Formaldehyde.
      Phys Rev Lett. 1969;22:679.

[6]   Reuss G, Disteldorf W, Gamer AO, Hilt A. Ullmann's encyclopedia of industrial chemistry.
      Weinheim: Wiley; 2003.

[7]   Bone WA, Smith HL. XCIV.—The thermal decomposition of formaldehyde and acetalde-
      hyde. J Chem Soc Trans. 1905;87:910.

[8]   Beck CM, Rathmill SE, Park YJ, Chen J, Crabtree RH, Liable-Sands LM, et al. (a). Aldehyde
      decarbonylation catalysis under mild conditions. Organometallics. 1999;18:5311 (b) Lenges CP,
      Brookhart M. Isomerization of Aldehydes Catalyzed by Rhodium(I) Olefin Complexes. Angew
      Chem Int Ed. 1999;38:3533.

[9]   Dorokhov YL, Shindyapina AV, Sheshukova EV, Komarova TV. Metabolic methanol: molecular
      pathways and physiological roles. Physiol Rev. 2015;95:603.

[10] Blakley RL. The biochemistry of folic acid and related pteridines. London: North Holland, 1969.

[11] Reuss G, Disteldorf W, Gamer AO, Hilt A. Ullmann's encyclopedia of industrial chemistry, 7th
      Edn ed., vol. A11. Weinheim: Wiley-VCH Verlag GmbH, 2008: 619.

[12] Brenk M. Silver catalyst for formaldehyde preparation. PCT/EP2009/006170, 2010.

[13] Adkins H, Peterson WR. The oxidation of methanol with air over iron, molybdenum, and iron-
      molybdenum oxides. J Am Chem Soc. 1931;53:1512.

[14] Tadenumar H. Hydrocarbon Process. 1966;45:195.

[15] Ipatieff VN, Monroe GS. Synthesis of Methanol from Carbon Dioxide and Hydrogen over Copper-
      Alumina Catalysts. Mechanism of Reaction. J Am Chem Soc. 1945;67:2168.

[16] Huang F, Lu G, Zhao L, Li H, Wang Z-X. (a). The catalytic role of N-heterocyclic carbene in a metal-
      free conversion of carbon dioxide into methanol: a computational mechanism study. J Am Chem
      Soc. 2010;132:12388 (b) Huang F, Zhang C, Jiang J, Wang Z-X, Guan H. How Does the Nickel
      Pincer Complex Catalyze the Conversion of CO2 to a Methanol Derivative? A Computational
      Mechanistic Study. Inorg Chem. 2011;50:3816.

[17] Lee D-K, Kim D-S, Kim S-W. Selective formation of formaldehyde from carbon dioxide and
      hydrogen over PtCu/SiO2. Appl Organomet Chem. 2001;15:148.

[18] Bahmanpour AM, Hoadleya A, Tanksale A. Formaldehyde production via hydrogenation of
      carbon monoxide in the aqueous phase. Green Chem. 2015;17:3500.

[19] Chan Fan Liang, Altinkaya Garen, Fung Nicholas, Tanksale Akshat. Low temperature hydro-
      genation of carbon dioxide into formaldehyde in liquid media. Catalysis Today. 2017;6. DOI:
      10.1016/j.cattod.2017.06.012.

[20] Nakata K, Ozaki T, Terashima C, Fujishima A, Einaga Y. High-yield electrochemical production of
      formaldehyde from CO2 and seawater. Angew Chem Int Ed. 2014;53:871.

[21] Qin GH, Zhang Y, Ke XB, Tong XL, Sun Z, Liang M, et al. See, for example: (a). Photocatalytic
      reduction of carbon dioxide to formic acid, formaldehyde, and methanol using dye-sensitized
      TiO2 film. Appl Catal B. 2013;129:599 (b) Tennakone K, Jayatissa AH, Punchihewa S. Selective
      photoreduction of carbon dioxide to methanol with hydrous cuprous oxide. J Photochem

Photobiol A. 1989;49:369; (c) Matsumoto Y, Obata M, Hombo J. Photocatalytic Reduction of Carbon Dioxide on p-Type CaFe2O4 Powder. J Phys Chem. 1994;98:2950; (d) Inoue T, Fujishima A, Konishi S, Honda K. Photoelectrocatalytic reduction of carbon dioxide in aqueous suspensions of semiconductor powders. Nature. 1979;277:637; (e) Li K, An X, Park KH, Khraisheh M, Tang J. A critical review of CO2 photoconversion: Catalysts and reactors. Catal Today. 2014;224:3; (f) Aurianblajeni B, Halmann M, Manassen J. Photoreduction of carbon dioxide and water into formaldehyde and methanol on semiconductor materials. Sol Energy. 1980;25:165.

[22] Shi J, Wang X, Jiang Z, Liang Y, Zhu Y, Zhang C. Constructing spatially separated multienzyme system through bioadhesion-assisted bio-inspired mineralization for efficient carbon dioxide conversion. Bioresour Technol. 2012;118:359.

[23] Fachinetti G, Floriani C, Roselli A, Pucci S. (a). Stoichiometric reduction of CO and CO2 to methanol: evidence for carbon monoxide insertion into zirconium–hydrogen bond. J Chem Soc Chem Commun. 1978;6:269 (b) Gambarotta S, Strologo S, Floriani C, Chiesi-Villa A, Guastini C. Stepwise reduction of carbon dioxide to formaldehyde and methanol: Reactions of CO2 and CO2-like molecules with hydridochlorobis(cyclopentadienyl)zirconium(IV). J Am Chem Soc. 1985;107:6278.

[24] Aresta M, Dibenedetto A. Utilisation of CO2 as a chemical feedstock: opportunities and challenges. Dalton Trans. 2007;28:2975.

[25] Schloerer NE, Berger S. (a). First Spectroscopical Evidence of a Dioxomethylene Intermediate in the Reaction of CO2 with Cp2Zr(H)Cl: A 13C NMR Study. Organometallics. 2001;20:1703 (b) Schloerer NE, Cabrita EJ, Berger S. Characterization of Reactive Intermediates by Diffusion-Ordered NMR Spectroscopy: A Snapshot of the Reaction of 13CO2 with [Cp2Zr(Cl)H]. Angew Chem Int Ed. 2002;41:107.

[26] Rankin MA, Cummins CC. Carbon dioxide reduction by terminal tantalum hydrides: formation and isolation of bridging methylene diolate complexes. J Am Chem Soc. 2010;132:10021.

[27] Bontemps S, Vendier L, Sabo-Etienne S. Borane-Mediated Carbon Dioxide Reduction at Ruthenium: Formation of C1 and C2 Compounds. Angew Chem Int Ed. 2012;51:1671.

[28] Bontemps S, Vendier L, Sabo-Etienne S. Ruthenium-Catalyzed Reduction of Carbon Dioxide to Formaldehyde. J Am Chem Soc. 2014;136:4419.

[29] Metsaenen TT, Oestreich M. Temperature-Dependent Chemoselective Hydrosilylation of Carbon Dioxide to Formaldehyde or Methanol Oxidation State. Organometallics. 2015;34:543.

[30] Jiang Y, Blacque O, Fox T, Berke H. Catalytic CO2 Activation Assisted by Rhenium Hydride/B (C6F5)3 Frustrated Lewis Pairs—Metal Hydrides Functioning as FLP Bases. J Am Chem Soc. 2013;135:7751.

[31] LeBlanc FA, Piers WE, Parvez M. Selective hydrosilation of CO2 to a bis(silylacetal) using an anilido bipyridyl-ligated organoscandium catalyst. Angew Chem Int Ed. 2014;53:789.

[32] Rios P, Curado N, Lopez-Serrano J, Rodriguez A. Selective reduction of carbon dioxide to bis (silyl)acetal catalyzed by a PBP-supported nickel complex. Chem Comm. 2016;52:2114.

[33] Khan MMT, Halligudi SB, Shukla S. Reduction of CO2 by molecular hydrogen to formic acid and formaldehyde and their decomposition to CO and H2O. J Mol Cat. 1989;57:47.

[34] Stein T, Meuresch M, Limper D, Schmitz M, Hölscher M, Coetzee J, et al. Highly Versatile Catalytic Hydrogenation of Carboxylic and Carbonic Acid Derivatives using a Ru-Triphos Complex: Molecular Control over Selectivity and Substrate Scope. J Am Chem Soc. 2014;136:13217.

[35] Cannizzaro S. Ueber den der Benzoësäure entsprechenden Alkohol. Liebigs Ann. 1853;88:129.

[36] Ashby EC, Doctorovich F, Liotta CL, Neumann HM, Barefield EK, Konda A, et al. (a). Concerning the formation of hydrogen in nuclear waste. Quantitative generation of hydrogen via a Cannizzaro intermediate. J Am Chem Soc. 1993;1171 (b) Kapoor, S., Barnabas, F.A., Sauer Jr., M.C., Meisel, D., Jonah, C.D. Kinetics of Hydrogen Formation from Formaldehyde in Basic Aqueous Solutions. J.

Phys. Chem. 1995, 99, 6857. (c) Kapoor, S.; Naumov, S. On the origin of hydrogen in the formaldehyde reaction in alkaline solution. Chem. Phys. Lett. 2004, 387, 322.

[37]   Yingpu B, Gongxuan L. Nano-Cu catalyze hydrogen production from formaldehyde solution at room temperature. Int J Hydrogen Energy. 2008;33:2225.

[38]   Preti D, Squarcialupi S, Fachinetti G. Carbon Dioxide Hydrogenation to Formic Acid by Using a Heterogeneous Gold Catalyst. Angew Chem Int Ed. 2009;48:4763.

[39]   Gao H, Zhang J, Wang R, Wang M. Highly efficient hydrogen production and formaldehyde degradation by Cu2O microcrystals. Appl Catal B Environ. 2015;172:1.

[40]   Machida KI, Enyo M. Formaldehyde Electro-oxidation on Copper Metal and Copper-based Amorphous Alloys in Alkaline Media. Bull Chem Soc Jpn. 1985;58:2043.

[41]   Jin Z, Li P, Liu G, Zheng B, Yuan H, Xiao D. Enhancing catalytic formaldehyde oxidation on CuO−Ag2O nanowires for gas sensing and hydrogen evolution. J Mater Chem A. 2013;1:14736.

[42]   Bi Y, Hu H, Li Q, Lu G. Efficient generation of hydrogen from biomass without carbon monoxide at room temperature – Formaldehyde to hydrogen catalyzed by Ag nanocrystals. Int J Hydrogen Energy. 2010;35:7177.

[43]   Li Y, Chen T, Wang T, Zhang Y, Lu G, Bi Y. Highly efficient hydrogen production from formaldehyde over Ag/γ-Al2O3 catalyst at room temperature. Int J Hydrogen Energy. 2014;39:9114.

[44]   Li R, Zhu X, Yan X, Kobayashi H, Yoshida S, Chen W, et al. Oxygen-Controlled Hydrogen Evolution Reaction: Molecular Oxygen Promotes Hydrogen Production from Formaldehyde Solution Using Ag/MgO Nanocatalyst. ACS Catal. 2017;7:1478.

[45]   Gao S, Feng T, Wu Q, Feng C, Shang N, Wang C. Immobilizing AgPd alloy on Vulcan XC-72 carbon: a novel catalyst for highly efficient hydrogen generation from formaldehyde aqueous solution. RSC Adv. 2016;6:105638.

[46]   Pan X, Wang L, Ling F, Li Y, Han D, Pang Q, et al. A novel biomass assisted synthesis of Au−SrTiO3 as a catalyst for direct hydrogen generation from formaldehyde aqueous solution at low temperature. Int J Hydrogen Energy. 2015;40:1752.

[47]   Dalcin Fornari AM, De Araujo MB, Bergamin Duarte C, Machado G, Teixeira SR, Weibel DE. Photocatalytic reforming of aqueous formaldehyde with hydrogen generation over TiO2 nano-tubes loaded with Pt or Au nanoparticles. Int J Hydrogen Energy. 2016;41:11599.

[48]   Hu H, Jiao Z, Ye J, Lu G, Bi Y. Highly efficient hydrogen production from alkaline aldehyde solutions facilitated by palladium nanotubes. Nano Energy. 2014;8:103.

[49]   Li S, Hu H, Bi Y. Ultra-thin TiO2 nanosheets decorated with Pd quantum dots for high-efficiency hydrogen production from aldehyde solution. J Mat Chem A. 2016;4:796.

[50]   Feng L, Okonkwo A, Qiong X, Mingping L, Xinwei P, Lishan J, et al. PdO/LaCoO3 heterojunction photocatalysts for highly hydrogen production from formaldehyde aqueous solution under visible light. Int J Hydrogen Energy. 2016;41:6115.

[51]   Jeroro E, Vohs JM. Zn Modification of the Reactivity of Pd(111) Toward Methanol and Formaldehyde. J Am Chem Soc. 2008;130:10199.

[52]   Zou S, Liu J, Kobayashi H, Chen C, Qiao P, Li R, et al. Boosting Hydrogen Evolution Activities by Strong Interfacial Electronic Interaction in ZnO@Bi(NO3)3 Core−Shell Structures. J Phys Chem C. 2017;121:4343.

[53]   Nielsen M, Alberico E, Baumann W, Drexler H-J, Junge H, Gladiali S, et al. (a). Low-temperature aqueous-phase methanol dehydrogenation to hydrogen and carbon dioxide. Nature. 2013;495:85 (b) Monney A, Barsch E, Sponholz P, Junge H, Ludwig R, Beller M. Base-free hydro-gen generation from methanol using a bi-catalytic system. Chem Commun. 2014;50:707; (c) Sponholz P, Mellmann D, Cordes C, Alsabeh PG, Li B, Li Y, Nielsen M, Junge H, Dixneuf P, Beller M. Efficient and Selective Hydrogen Generation from Bioethanol using Ruthenium Pincer-type Complexes. Chem Sus Chem. 2014;7:2419; (d) Alberico E, Sponholz P, Cordes C, Nielsen M,

Drexler H-J, Baumann W, Junge H, Beller M. Selective Hydrogen Production from Methanol with a Defined Iron Pincer Catalyst under Mild Conditions. Angew Chem Int Ed. 2013;52:14162; (e) Hu P, Diskin-Posner Yl, Ben-David Y, Milstein D. Reusable Homogeneous Catalytic System for Hydrogen Production from Methanol and Water. ACS Catal. 2014;4:2649; (f) Rodríguez-Lugo RE, Trincado M, Vogt M, Tewes F, Santiso-Quinones G, Grützmacher H. A homogeneous transition metal complex for clean hydrogen production from methanol-water mixtures. Nat Chem. 2013;5:342.

[54] Heim LE., Konnerth H, Prechtl MHG. Future perspectives for formaldehyde: pathways for reductive synthesis and energy storage. Green Chemistry. 2017;19(10):2347.

[55] Heim LE, Vallazza S, Van Der Waals D, Prechtl MHG. Water decontamination with hydrogen production using microwave-formed minute-made ruthenium catalysts. Green Chem. 2016;18:1469.

[56] Cook J, Hamlin JE, Nutton A, Maitlis PM. Homogeneously catalysed disproportionation of acetaldehyde into ethanol and acetic acid. J C S Chem Soc. 1980;144.

[57] Heim LE, Schloerer NE, Choi JH, Prechtl MHG. Selective and mild hydrogen production using water and formaldehyde. Nat Commun. 2014;5:3621.

[58] Heim LE, Thiel D, Gedig C, Deska J, Prechtl MHG. Bioinduced room-temperature methanol reforming. Angew Chem Int Ed. 2015;54:10308.

[59] Van Der Waals D, Heim LE, Vallazza S, Gedig C, Deska J, Prechtl MHG. Self-Sufficient Formaldehyde-to-Methanol Conversion by Organometallic Formaldehyde Dismutase Mimic. Chem Eur J. 2016;22:11568.

[60] van der Waals D, Heim LE, Gedig C, Herbrik F, Vallazza S, Prechtl MHG. Ruthenium-Catalyzed Methylation of Amines with Paraformaldehyde in Water under Mild Conditions. ChemSusChem. 2016 8 5;9(17):2343–2347. 10.1002/cssc.201600824.

[61] Suenobu T, Isaka Y, Shibata S, Fukuzumi S. Catalytic hydrogen production from paraformaldehyde and water using an organoiridium complex. Chem Commun. 2015;51:1670.

[62] Fujita K, Kawahara R, Aikawa T, Yamaguchi R. Hydrogen production from a methanol–water solution catalyzed by an anionic iridium complex bearing a functional bipyridonate ligand under weakly basic conditions. Angew Chem Int Ed. 2015;54:9057.

[63] Trincado M, Sinha V, Rodriguez-Lugo RE, Pribanic B, De Bruin B, Grützmacher H. Homogeneously catalysed conversion of aqueous formaldehyde to H2 and carbonate. Nature Comm. 2017;8:14990.

[64] Knijnenburg Q, Gambarottab S, Budzelaar PHM. Ligand-centred reactivity in diiminepyridine complexes. Dalton Trans. 2006;5442.

[65] Bielinski EA, Forster M, Zhang Y, Bernskoetter WH, Hazari N, Holthausen MC. Base-Free Methanol Dehydrogenation Using a Pincer-Supported Iron Compound and Lewis Acid Co-catalyst. ACS Catal. 2015;5:2404.

[66] Andérez-Fernández M, Vogt LK, Fischer S, Zhou W, Jiao H, Garbe M, et al. A Stable Manganese Pincer Catalyst for the Selective Dehydrogenation of Methanol. Angew Chem Int Ed. 2017;56:559.

Monica Trincado and Matthias Vogt

5 CO$_2$-based hydrogen storage – hydrogen liberation from methanol/water mixtures and from anhydrous methanol

Abstract: New strategies for the reforming of methanol under mild conditions on the basis of heterogeneous and molecular catalysts have raised the hopes and expectations on this fuel. This contribution will focus on the progress achieved in the production of hydrogen from aqueous and anhydrous methanol with molecular and heterogeneous catalysts. The report entails thermal approaches, as well as light-triggered dehydrogenation reactions. A comparison of the efficiency and mechanistic aspects will be made and principles of catalytic pathways operating in biological systems will be also addressed.

Keywords: catalysis, coordination complexes, hydrogen storage, methanol reforming, methanol dehydrogenation, methanol production, methane oxidation, steam reforming, methanol dehydrogenase, CO$_2$ hydrogenation, CO$_2$ reduction

5.1 Introduction

The depletion of limited fossil fuel resources, the increasing energy needs and the contamination of the environment caused by consumption of these fuels make hydrogen an attractive alternative energy carrier. Hydrogen is easily converted into electricity using fuel cell technology, liberates a large amount of energy per unit mass, and does not generate pollutants. Although it is currently produced by steam reforming or partial oxidation of methane and coal gasification, in principle it could be generated from renewable resources such as alcohols or water. An industrially applicable catalytic methodology for dihydrogen formation from a proton source remains the main target to replace the present fossil fuel economy by a hydrogen economy. Still nowadays, efficient hydrogen production from water requires a high-energy input. Technologies generating hydrogen from biomass, such as enzymatic decomposition of sugars, steam reforming of bio-oils, and gasification, are often accompanied by low hydrogen yields and require complex processing procedures. The past years have witnessed important improvements in the efficiency of the production of hydrogen from stable hydrogen-rich molecules. These developments encompass the utilization of new molecular and heterogeneous catalysts, triggering

the dehydrogenation of alcohols, which can be considered as "organic" molecular storage forms of energy. The utilization of this type of compounds may solve problems related to storage and transport of large quantities of hydrogen to potential users worldwide using the existing infrastructure. Against this background methanol may serve a cheap, safe, easy-to-store and -transport hydrogen storage material [1a].

Methanol is one of the most important commodities of the chemical industry, with a global annual demand reaching 80 million metric tons in 2016. The global market of methanol has been witnessed dramatic changes in the past decade, mainly due to the fact that it has become the source of a wide range of derivatives that compete with fossil fuel derived products. These changes include the development of new end-uses and a geographical shift in capacity on demand and production. Figure 5.1 gives an overview of the value chain from methanol *via* its derivatives to a large variety of products. In 2015 the three major products produced from methanol were formaldehyde (FAld) (27%), methyl*tert*-butylether/*tert*-amyl methylether (*MTBE/TAME*; 8%) and acetic acid (9%). The remaining 56% of global methanol consumption is divided into the production of chemical intermediates (chloromethane, methylamine, methylmethacrylate and methylmercaptane), as well as the direct use of methanol in internal combustion engines. Moreover, it is a convenient starting material for the production of light olefins (ethylene and propylene) (MTO = methanol to olefin process) and in consequence any derived hydrocarbon product.
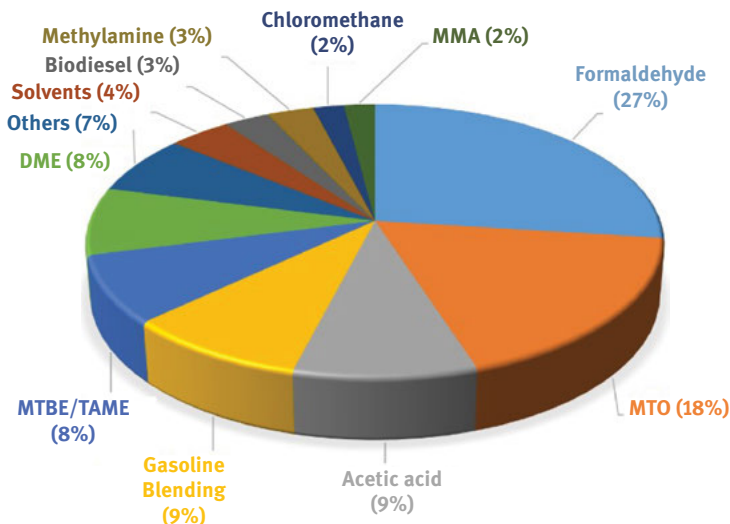
Figure 5.1: Global methanol demand by end-use in 2015. MMA: methyl methacrylate; MTO: methanol-to-olefins process; MTBE/TAME: methyl-tertiary-butyl ether/tertiary-amyl methylether; DME: dimethyl ether (Data extracted from: Annual report 2016 Johnson and Matthey. www.matthey.com/investor/reports/2015-16).

Contrary to (bio)ethanol, methanol does not interfere directly with the food chain. In contrast to methanol, ethanol is produced through fermentation of sugars and consequently made from potential food crops. An increasing demand on this biofuel may create a problematic situation of a commercial competition with food production [1a]. Nowadays, methanol is produced mainly from syn-gas, which is obtained by catalytic reforming of fossil fuels, it can also be obtained through the hydrogenation of CO_2, derived from natural or industrial sources. Ideally, methanol could be made by the reaction of atmospheric CO_2 with the hydrogen produced electrolytically from using renewable non-fossil fuel -based energy. Olah suggested in the late 90s an economy based on methanol [1a]. Methanol is a promising fuel, since it is a stable liquid under ambient conditions, and has a high content of hydrogen. The development of efficient processes for releasing hydrogen from methanol or for the direct conversion into electrical energy (in direct methanol fuel cells, DMFC) is essential for the success of this proposition.

New strategies for the reforming of methanol under mild conditions based on heterogeneous or molecular catalysts have raised the hopes and expectations in this fuel. This chapter will focus on the progress achieved in the production of hydrogen from aqueous methanol with molecular and heterogeneous catalysts. A comparison of the efficiency and mechanistic aspects will be made and some principles of catalysts operating in biological systems will be also addressed.

5.2 Production of methanol

5.2.1 Industrial bulk production

The oldest process for the industrial production of methanol is the dry distillation of wood. Other processes, such as the oxidation of hydrocarbon mixtures and conversion of oxygenated byproducts of the Fischer–Tropsch synthesis, derived from syngas according to the *Synthol* process, have no industrial relevance. In the Synthol process, the catalyzed hydrogenation of CO leads to mixtures of aliphatic hydrocarbons, with a high percentage of methane. Other byproducts include higher alcohols, aldehydes, ketones and higher fatty acids [1c,d]. Nowadays, methanol is currently produced on an industrial scale from natural gas, *via* synthetic processes operating at 50–100 atm and temperatures of 200–300°C. A very limited number of different process layouts are available (Figure 5.2). Most of the actual processes operate in the gas phase and use copper-based catalysts. The main differences between them are related to the reactor design and catalyst arrangements. The industrial production can be subdivided into three main steps; (1) production of synthesis gas; (2) synthesis of methanol and (3) processing of crude.
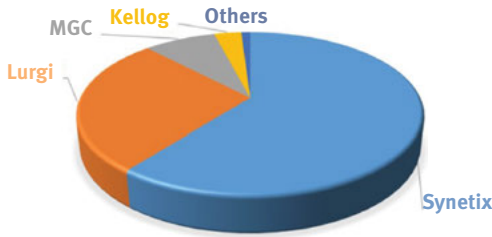
Figure 5.2: Worldwide methanol production by process in 2015 (Data extracted from: Annual report 2016 Johnson and Matthey. www.matthey.com/investor/reports/2015-16).

The most common technology used for producing syn-gas is a highly endothermic process known as methane steam reforming, whose operating temperatures and pressures are in the range of 800–1,000°C and 20–30 atm, respectively. A mixture of CO and H$_2$ is obtained along with CO$_2$, which originates from the water gas shift reaction (WGS) (eqs. (5.1) and (5.2)).

$$CH_4 + H_2O \rightleftharpoons CO + 3H_2 \ \Delta H_{298K} = 206 \text{ kJ mol}^{-1} \qquad [2] \qquad (5.1)$$

$$CO + H_2O \rightleftharpoons CO_2 + H_2 \ \Delta H_{298K} = -41 \text{ kJ mol}^{-1} \qquad [3] \qquad (5.2)$$

$$CH_4 + CO_2 \rightleftharpoons 2CO + 2H_2 \ \Delta H_{298K} = 247 \text{ kJ mol}^{-1} \qquad [2] \qquad (5.3)$$

$$CH_4 + 1/2O_2 \rightleftharpoons CH_3OH \ \Delta H_{298K} = -128 \text{ kJ mol}^{-1} \qquad [2] \qquad (5.4)$$

$$CO + 2H_2 \rightleftharpoons CH_3OH \ \Delta H_{298K} = -91 \text{ kJ mol}^{-1} \qquad [2] \qquad (5.5)$$
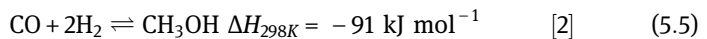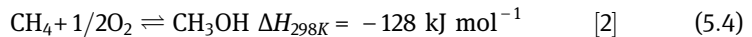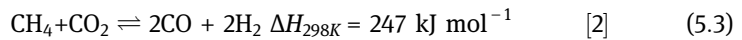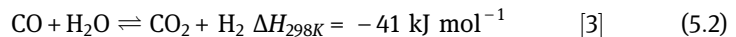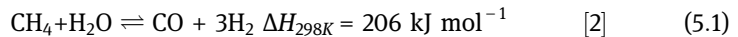
5.2.2 Experimental approaches toward the formation of methanol

5.2.2.1 The *holy grail* - direct methane oxidation

Relying on fossil hydrocarbons for the production of fuels and chemical commodities is self-evidently not sustainable. However, natural gas and shale gas, with its main component being methane, is available in vast amounts [4]. Hence, methane could potentially serve as an interim replacement for petroleum. The efficient and selective oxidation of methane to methanol would not only be an economically viable process, it would rather modernize the chemical value chain [5]. Currently, natural gas is used

as fuel in thermal combustion for heating and electrical power generation. Significant amounts of natural gas are currently just flared from fossil deposits due to the difficult and cost intensive transportation of methane. In this respect, the oxidation of methane to syn-gas and the subsequent reduction of CO to MeOH depicts an energetic detour. Naturally, the direct oxidation of methane to methanol would be an efficient and thus preferable strategy and is considered the holy grail of chemistry. Although the direct oxidation to MeOH is possible from a thermodynamic point of view (eq. (5.4)), it remains with great difficulty to prevent over-oxidation due to the relatively facile oxidation of methanol [5, 6].

The direct aerobic oxidation of methane in the gas phase has been studied for decades but remains a major challenge as the reaction still proceeds with low conversion and modest selectivity in poor yields and is thus far away from any practical applications.(For reviews see [6‒10])

Major contributions in the field of partial oxidation of methane with respect to the formation of other more stable methanol precursors were introduced by Periana and co-workers, with an initial report almost 20 years ago [11]: In this well-known example, methane is converted into methyl bisulfate using a platinum(II) complex with 2,2′-bipyrimidine ligand. This reaction occurs under homogeneous conditions and utilizes concentrated sulfuric acid as reaction media, where SO_3 functions as oxidant. Over-oxidation is hampered by the formation of the more stable methyl bisulfate (eq. (5.6)). Subsequent hydrolysis gives rise to MeOH and sulfuric acid (eq. (5.7)).

$$CH_4 + 2H_2SO_4 \rightleftharpoons CH_3OSO_3H + 2H_2O + SO_2 \qquad (5.6)$$

$$CH_3OSO_3H + H_2O \rightleftharpoons CH_3OH + H_2SO_4 \qquad (5.7)$$
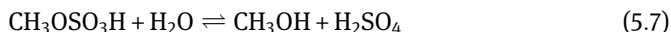
The development of a commercial process utilizing a $CH_4/SO_3/H_2SO_4$ oxidation route with subsequent hydrolysis to eventually give methanol as bulk chemical, may be economically difficult. However, recently the German company *GrilloWerke AG* announced the development of a process allowing for the production of methane-sulfonic acid (MSA) directly from methane and SO_3 [12]. The significantly higher market value of MSA, with respect to methanol, may successfully address the economic challenges of this direct methane oxidation approach. Along these lines, the stepwise oxidation of methane over copper-containing zeolites were reported over the last 12 years giving rise to a conversion of methane at lower temperatures [13‒19]. This approach outlines an overall three-step sequential reaction scheme: Firstly, the high temperature activation of the zeolite with oxygen, followed by the methane activation at lower temperatures (*ca.* 200°C) and finally the MeOH desorption step. Importantly, the second step (methane activation) occurs under the absence of

oxygen and hence prevents the formed MeOH from over-oxidation. The third step involves the extraction of the MeOH by water (off-line)[13] or steam (on-line)[20]; the latter gives rise to the realization of successive reaction cycles. This stepwise conversion of methane bears the advantage that the oxidant (oxygen) is never in direct contact with neither the substrate methane nor the formed methanol and therefore allows for higher selectivity (Figure 5.3).
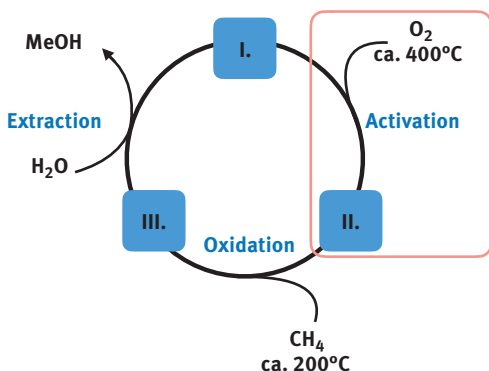
Figure 5.3: Overview of the three-step conversion of methane to methanol over copper zeolite: (I) oxidative activation of the material; (II) methane oxidation to form surface-bound methanol precursors; (III) aqueous (liquid or steam) extraction of methanol. The oxidative activation proceeds in the absence of substrate (indicated by the red box). Therefore, methane and methanol are never directly in contact with oxygen throughout the whole process.

Remarkably, a very recent report by Shushkevich, van Bokhoven and co-workers disclosed an advanced approach for the direct *anaerobic* methane oxidation, in which H_2O formally functions as an oxidant (eq. (5.8)). This aqueous approach facilitates copper sites in a zeolite and offers high selectivity toward methanol formation. The reaction does not require harsh conditions or expensive precious metal catalysts and gives H_2 as the only byproduct, which possesses additional commercial value itself [21].

$$CH_4 + H_2O \rightarrow CH_3OH + H_2 \qquad \text{selective anaerobic methane oxidation} \qquad (5.8)$$
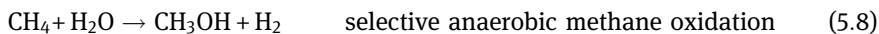
Lercher and co-workers reported very recently the utilization of Cu-oxo clusters stabilized in a metal-organic-framework (MOF; NU 100 typ) as catalytic system for methane oxidation for the first time [22]. However, the reaction reported proceeds with moderate selectivity (45–60%) with respect to methanol formation. DME and CO_2 were observed as common byproducts of the oxidation.

5.2.2.2 Environmental benign methanol formation – CO_2 reduction with dihydrogen under homogeneous conditions

The exploitation of fossil energy reserves to meet the energy demands of a constantly growing human population leads inherently to rising anthropogenic levels of CO_2 in our atmosphere, which raises concerns regarding global climate alteration, acidification of the oceans, glacial melt and rising sea levels. The intrinsically limited fossil reserves of our planet cannot feed the rising demands for energy and raw materials of our societies. It becomes obvious, that renewable sources must be sought and the carbon footprint of such must be drastically reduced to eventually enable a sustainable economic system. Along these lines, an attractive approach is the utilization of CO_2 as a renewable abundant C_1 feedstock. This section will briefly discuss the direct reduction of CO_2 to methanol under homogeneous conditions with non-sacrificial reductants. Specifically, when stemming from non-fossil sources, hydrogen would give rise to a sustainable option for the chemical reduction of CO_2 into a value-added commodity. Moreover, such a process would utilize CO_2 as a recyclable energy carrier. (For recent reviews on CO_2 reduction see [23–26]) The conversion (reduction) is kinetically difficult, yet from a thermodynamic point of view exergonic (eq. (5.9)).

$$CO_2 + 3H_2 \rightleftharpoons CH_3OH + H_2O \quad \Delta G^o{}_{298K} = -9.5 \text{ kJmol}^{-1}; \Delta H^o{}_{298K} = -131 \text{ kJmol}^{-1}$$

(5.9)
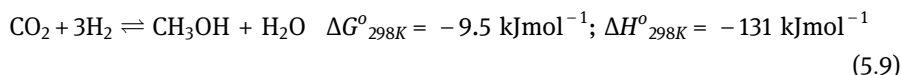
[27]

A major challenge depicts the non-polar gaseous nature of CO_2 and H_2. In contrast, the products and byproducts of the reduction are highly polar molecules (e.g. methanol and water) and often efficiently poison the catalyst. Hence the reduction of CO_2 to methanol remains very difficult and reports in the literature are still scarce and mostly involve late transition metal complexes of group 6, 7, 8, 9 and 10. The high kinetic inertness can be tackled by the pre-coordination and thus activation of CO_2 at the transition metal center. Commonly, CO_2 binds to a transition metal center *via* π bonding of the C=O double bond or more rarely *via* formation of a M−O or M−C sigma bond. However, at this point it shall be noted that alternative binding motives of CO_2 to a coordination entity utilizing, for instance, metal-ligand cooperation or second-coordination sphere approaches, attracted increased attention during the last years [28–38].

Landmarks in homogeneous hydrogenation of CO_2 to methanol

In 1993, Sasaki and co-workers described their findings regarding the homogeneous hydrogenation of CO_2 utilizing [$Ru_3(CO)_{12}$]/KI as catalytic system [39]. The formation of methane is associated with the initial formation of CO (and H_2O) *via* the reverse water gas shift reaction and the subsequent hydrogenation of CO to methanol. However, the required reaction conditions were rather harsh (*N*-methylpyrrolidone, 240°C, 90–140 bars, Figure 5.4). Interestingly, while homogeneous components trigger the reverse water gas shift reaction, the final reduction to methane is

$$CO_2 + H_2 \xrightarrow[\substack{240°C,\ 90\text{-}140bar \\ \text{N-methylpyrrolidone}}]{\textbf{[RU}_3\textbf{(CO)}_{12}\textbf{] / KI}} CO + CH_3OH + CH_4$$
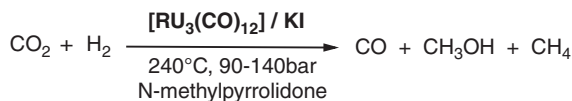
Figure 5.4: Hydrogenation of CO$_2$ reported by Sasaki and co-workers.

associated with ruthenium deposits. The utilization of KI as additive precludes the deposition, that is, the formation of a potentially heterogeneous catalyst is hampered by the additive. Hence the selectivity was shifted toward methanol formation.

The selective hydrogenation of CO$_2$ to methanol under mild conditions using a single ruthenium phosphine catalyst in homogeneous solution was reported in 2012 by Leitner, Klankermayer and co-workers (Figure 5.5(A)) [40]. The report describes the *in situ* formation of the active catalyst from [Ru(acac)$_3$] and the triphos ligand (triphos = 1,1,1-tris(diphenylphosphinomethyl)ethane). The complex [Ru(triphos)(TMM)] (**1**; TMM = trimethylenemethane) was also used as a potent pre-catalyst. Both systems perform in the presence of an acidic co-catalytic additive. As a prime
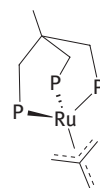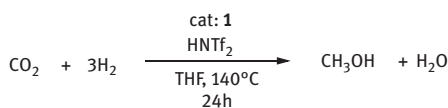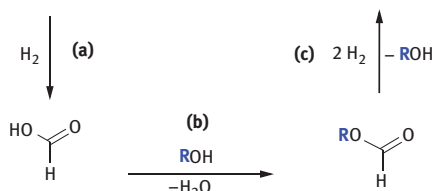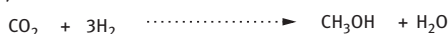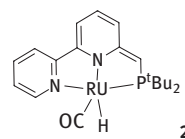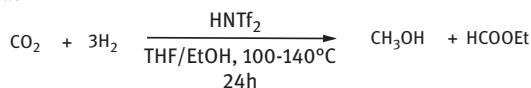
Figure 5.5: Direct hydrogenation of CO$_2$ to methanol. Approaches of *Leitner/Klankermayer* (A), *Sanford* (B) and *Beller* (C).

example, complex **1** and one equivalent of HNTf$_2$ (bis(trifluoromethane)sulfonamide) was shown to catalyze the formation of methanol with a TON of up to 221 (reaction conditions: 140°C, 20 bar CO$_2$, 60 bar of H$_2$ in THF/EtOH). Ethylformate was identified in trace amounts in the course of the reaction. When the reaction was performed in THF/MeOH media only methanol was detected as the sole product formed. Note that methyl formate and ethylformate could also be readily reduced to methanol. Later in 2015, Leitner and Klankermayer showed in a detailed mechanistic study that the multi-step reduction of CO$_2$ to methanol can directly occur at a single Ru -triphos center: A sequence of hydride transfers and protonolysis reactions gives rise to the stepwise reduction of CO$_2$*via* the subsequent formation of formate/formic acid, hydroxymethanolate/formaldehyde, and methanolate/methanol. Note that the substrate remains coordinated to the Ru center throughout the entire multi-step reaction sequence giving rise to a sort of "inner sphere mechanism." [41] Therefore, this significant work showed that the selective reduction of CO$_2$ to methanol can proceed directly at a single Ru center without formation of alkylformate intermediates. Along these lines, Beller and co-workers published very recently a catalytic system based on a non-noble metal. An *in situ* generated catalysts from [Co(acac)$_3$], triphos and HNTf$_2$ enables the reduction of CO$_2$ to methanol at remarkable low temperature (100°C). Representative reaction conditions comprise a molar ratio of 1:2:3 for Co: triphos: HNTf$_2$. The reaction is carried out in THF/EtOH under a CO$_2$ pressure of 20 bars and a H$_2$ pressure of 70 bars. Methanol is formed with a TON of 50 accompanied by small amounts of ethyl formate (Figure 5.5 (C)) [42]. Sanford and co-workers outlined in their initial publication in 2011 an interesting one-pot cascade approach, in which three different homogeneous catalysts participating synergistically in the reduction of CO$_2$. Each catalyst promotes a specific sequential step toward the eventual formation of methanol: [(PMe$_3$)$_4$Ru(Cl)(OAc)] catalyzes the reduction of CO$_2$ to formic acid (FAc) (Figure 5.5 (B, a)), [Sc(OTf)$_3$] promotes the esterification of FAc and methanol to give methyl formate (Figure 5.5 (B, b)), and the complex [Ru(PNN)(CO)(H)] (**2**, PNN = [(2,2′-Bipyridyl-6-yl)methyl]bis(*tert*-butyl)phosphine) catalyzes the hydrogenation of methylformate to methanol (Figure 5.5 (B, c)). Naturally, a significant challenge is the compatibility of all catalysts under the reaction conditions applied. It was specifically shown that the presence of CO$_2$ and [Sc(OTf)$_3$] deactivates **2** and thus hampered the last hydrogenation step c, which is reflected in a low TON of 2.5. However, by simple spatial separation of [Sc(OTf)$_3$] and **2** in combination with a higher H$_2$ pressure a TON up to 21 could be achieved.

Hydrogenation of CO$_2$ derivatives– the indirect approach toward methanol formation

CO$_2$ can be directly converted, for instance, into formates, (poly)carbonates, carbamates, formamides, urea or urea derivatives. These stable intermediates offer a pathway to the indirect hydrogenation of CO$_2$ to methanol as they have been shown to be hydrogenated under rather mild conditions. Conceptually, such a

sustainable approach is characterized by a capture-hydrogenation sequence, in which the reactant/absorber enabling CO$_2$-capture is released after the final hydrogenation step and therefore takes a role as non-sacrificial agent and can be readily recycled for consecutive capture reactions. For instance, Milstein and co-workers showed in 2011 the successful homogeneous hydrogenation of dimethyl carbonate (Figure 5.6 (b)), which can be principally captured from the reaction of CO$_2$ and two equivalents of methanol, using ruthenium PNN pincer-type complexes as catalysts. The hydrogenation results in three equivalents of methanol giving rise to the indirect sequential hydrogenation of CO$_2$ to methanol [43]. Ding and co-workers reported in 2012 the co-formation of methanol along with ethylene glycol, when ethylene carbonate, formed *via* the reaction of CO$_2$ with ethylene oxide, was hydrogenated in a reaction catalyzed by Ru(II) complexes with PNP amino-bisphosphine pincer ligands. This process is of interest since it yields efficiently methanol and ethylene glycol,
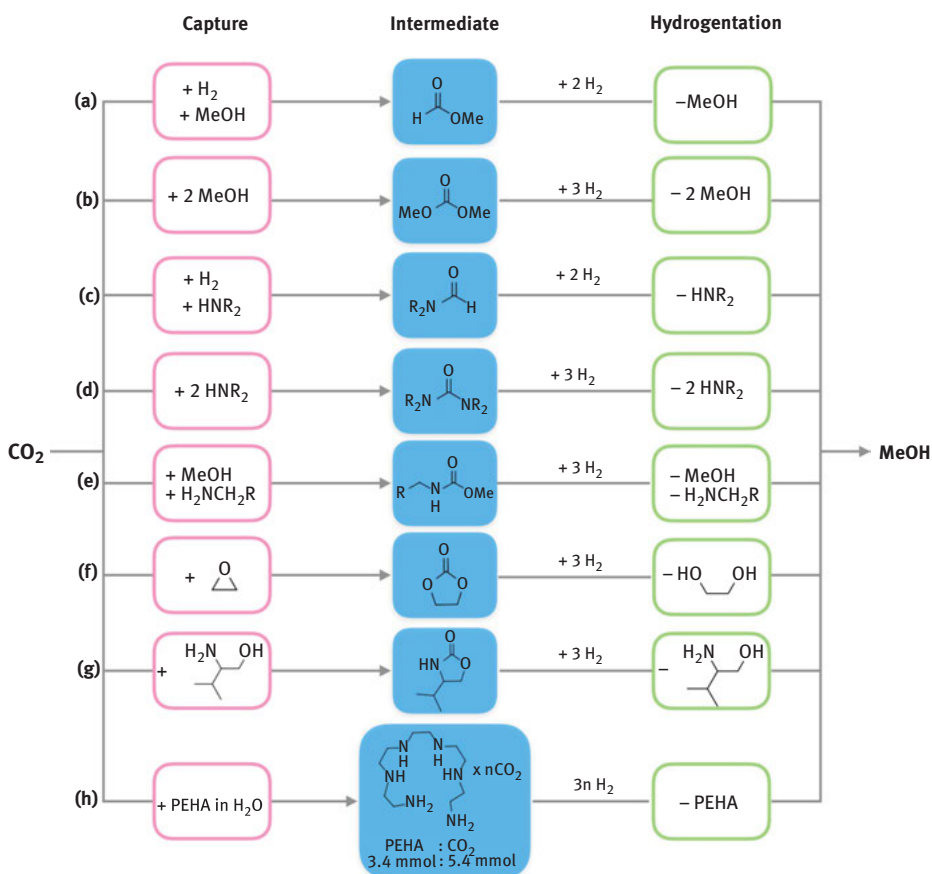
Figure 5.6: Capture of CO$_2$ stable intermediates and the sequential hydrogenation to methanol.

which represent two important commodity chemicals (Figure 5.6 (f)). Note the reaction is not limited to ethyl carbonate. Various cyclic carbonates were shown to be hydrogenated yielding methanol and the corresponding diol [44]. Likewise, alkyl formates and specifically methyl formate, represent a captured intermediate of CO_2 considering the stepwise formation *via* the hydrogenation of CO_2 to FAc and subsequent esterification with methanol (see Figure 5.5(b)). The catalytic hydrogenation of methyl formate (Figure 5.6(a)) was reported by Milstein[43] and, as mentioned above, utilized in a cascade one-pot approach by Sanford and co-workers [45].

The post-combustion CO_2 sequestration using aqueous amine solutions to remove CO_2 from the flue gases is a promising approach with an applied industrial background, as amine-scrubbing is employed for the removal of CO_2 from natural gas or hydrogen [46]. In general, amines can bind CO_2 reversibly, which is a prerequisite for an efficient CO_2 scrubbing technology. Thus, amine-based absorption technologies potentially allow for the separation of CO_2 from a variety of gaseous mixtures including air and flue gas components [47]. Along these lines, Milstein (2011, Figure 5.6(c−e)) [43,48,[49], Sanford (2015, Figure 5.6(c) with R=Me) [50] and Prakash & Olah (2016, Figure 5.6(h))[51] pushed forward the idea of the sequential indirect hydrogenation of CO_2 to methanol utilizing stable intermediates of the reaction of CO_2 and amines, that is methyl carbamates, methyl formamides and urea derivatives. The hydrogenation reactions of the various stable intermediates proceed under homogeneous catalytic conditions using ruthenium based catalysts decorated with ligand motifs entailing PNN or PNP tridentate phosphine ligands. Similarly, aminoethanol derivatives can be utilized for CO_2-capture forming cyclic oxazolidinones as stable intermediates. In 2015 Milstein and co-workers demonstrated the catalytic hydrogenation of oxazolidinones, for instance derived from the reaction of CO_2 and valinol, to methanol (Figure 5.6(g)).

5.3 Aqueous methanol as hydrogen and energy carrier

Hydrogen, when produced in a sustainable process from renewable resources, is an attractive energy carrier for the efficient generation of electricity using fuel cell technologies. However, owing to its physical properties, hydrogen storage and handling intrinsically possesses safety issues. Therefore, it appears very attractive to reversibly store hydrogen chemically in a safer and easy-to-handle carrier compound. The release of hydrogen gas can in turn be achieved on demand, e.g. directly prior usage in a fuel cell. Methanol offers great potential as hydrogen storage material, due to its high gravimetric hydrogen content of 12.6%. The dehydrogenation of an aqueous methanol solution gives rise to the release of CO_2 and three equivalents of H_2. That is, the entire hydrogen content in CH_3OH/H_2O (12.1%) can be released and CO_2 functions as carrier (eq. (5.10)). With an environmentally benign

source of hydrogen coupled with a sustainable reduction process of CO$_2$, methanol might become an attractive molecule for a practical hydrogen storage.

$$CH_3OH + H_2O \rightleftharpoons CO_2 + 3H_2$$
$$(12.1 \; wt.\% \; H_2)$$

(5.10)
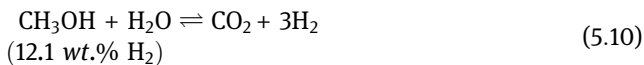
The so-called methanol reforming process (eq. (5.10)) is industrially performed at rather high temperatures and high-pressure limiting the practical application, especially for portable applications of fuel cells. In the following section an overview is given concerning methanol reforming approaches, with special focus on state of the art of catalyzed acceptorless dehydrogenation under mild conditions.

5.3.1 Biological systems

In general, alcohol dehydrogenases (ADH) are an important class of enzymes in the metabolism of alcohols in mammals (and yeasts)[52]; prominent examples are horse liver ADH or human liver ADH. These enzymes have a broader substrate spectrum being also active with respect to methanol oxidation [53]. The enzyme methanol dehydrogenase (MDH) catalyzes the oxidation of methanol to FAld *via* hydrogen transfer in methylotropic bacteria. A large number of bacteria (and also some type of yeast) are known to grow on methanol substrates as sole carbon source [54]. Three different operating classical mechanisms are identified in course of their methanol metabolism: The Calvin cycle (CaC), the ribulose monophosphate cycle (RuMPC) and the serine cycle (SerC). Common to all cycles is the initial oxidation of methanol to FAld, which is subsequently assimilated either into the RuMPC or SerC, respectively. The energetically costlier pathway oxidizes methanol to CO$_2$, which is consecutively incorporated into the CaC [55]. The latter metabolic degradation of methanol follows a sequential pathway involving three dehydrogenation steps (Figure 5.7): (1) Methanol
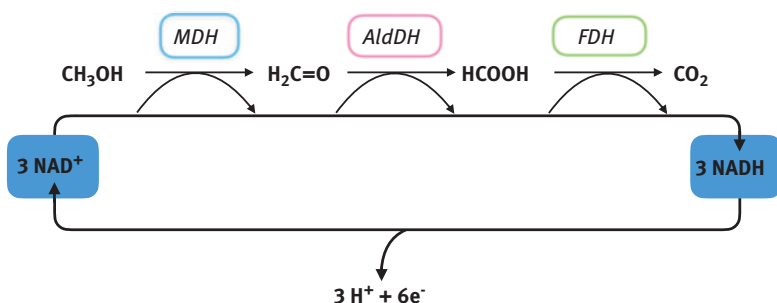
Figure 5.7: Schematic example of the sequential three-step oxidation of methanol under liberation of three equivalents of NADH (3H$^+$ + 6e$^-$): (1) methanol to FAld catalyzed by MDH; (2) FAld to FAc catalyzed by aldehyde dehydrogenase (AldDH); (3) FAc to carbon dioxide catalyzed by formic acid dehydrogenase (FDH).

to FAld, (2) FAld to FAc, and (3) FAc to CO_2 [56, 57]. Bacteria mainly facilitate for the first step MDHs, which essentially catalyze the dehydrogenation of methanol to FAld. Different types of MDHs are known, each one categorized according to its associated cofactor; for instance: cytochrome c-dependent MDH, which requires a pyrroloquinoline quinine (PQQ-MDH), NAD-dependent MDH, and NADPH-dependent MDH.

The sequential three-step oxidation of methanol occurs under liberation of three reduction equivalents 3[H⁻]; that is, for instance NADH ($3H^+ + 6e^-$). Particularly, in step 1 methanol is oxidized to FAld catalyzed by methanol dehydrogenase (e. g. NAD-MDH): A hydride is transferred to the NAD^+ cofactor, which is concomitantly reduced to NADH. Subsequent dehydrogenation of FAld to FAc (step 2) is mediated by AldDH to give another equivalent of NADH. Eventually, in step 3, FAc is dehydrogenated to give carbon dioxide catalyzed by FDH. Thus the third equivalent of NADH is formed *via* another hydride transfer. Such reaction cascades using multiple enzymes, which enable the selective oxidation of methanol to CO_2 ("deep-oxidation "), gained importance in enzymatic biofuel cells using methanol as anodic fuel [58].

Structural features of MDH. Ghosh, Blake and co-workers reported the structure of the MDH in *methylobacterium exorquens* at higher (1.94 Å) resolution [59]. The active *PQQ* prosthetic group requires a Ca^{2+} cation and utilizes *cytochrome c_L* as electron acceptor. The MDH has a $\alpha_2\beta_2$ tetrameric structure with each α unit (66 kDa) carrying one molecule of PQQ with one Ca^{2+} cation coordinated. The β unit is rather small (8.5 kDa) The α-subunit exhibits eight-fold ("propeller-like") radial symmetry forming a large barrel structure. The PQQ moiety is anchored between a co-planar tryptophan residue and a rare eight-membered ring formed by two neighboring cysteine moieties connected by a disulfide bridge (Figure 5.8, top) [60].

Methanol dehydrogenation is coupled to PQQ reduction to $PQQH_2$. A subsequent release of FAld and two single-electron transfers from $PQQH_2$ to *cytochrome c_L* regenerates the PQQ quinone *via* the radical semi-quinone intermediate. Two mechanisms are proposed: The addition/elimination mechanism is shown in Figure 5.8, bottom. Initial deprotonation of methanol *via* a base within the active site is subsequently followed by the nucleophilic attack of the methoxide at the carbonyl carbon C5 of the quinone. This step is assisted by the Lewis acidic Ca^{2+}center. The formation of a hemiacetal adduct with covalent C(5)−OMe bond is the key feature of this proposed mechanism. In the identified rate limiting step, a hydride is transferred from the CH_3 moiety of the bound methanol to the neighboring carbonyl carbon C4 giving rise to the release of FAld and the formation of the aromatic $PQQH_2$ hydroquinone. The alternative mechanistic proposal involves, after initial deprotonation of the hydroxyl group, direct hydride transfer from the CH_3 of methanol to the carbonyl carbon C5 of the quinone. After release of FAld and a subsequent tautomerization step, the hydroquinone $PQQH_2$ is formed [61, 62]. For both mechanisms, the re-oxidation of $PQQH_2$ to PQQ
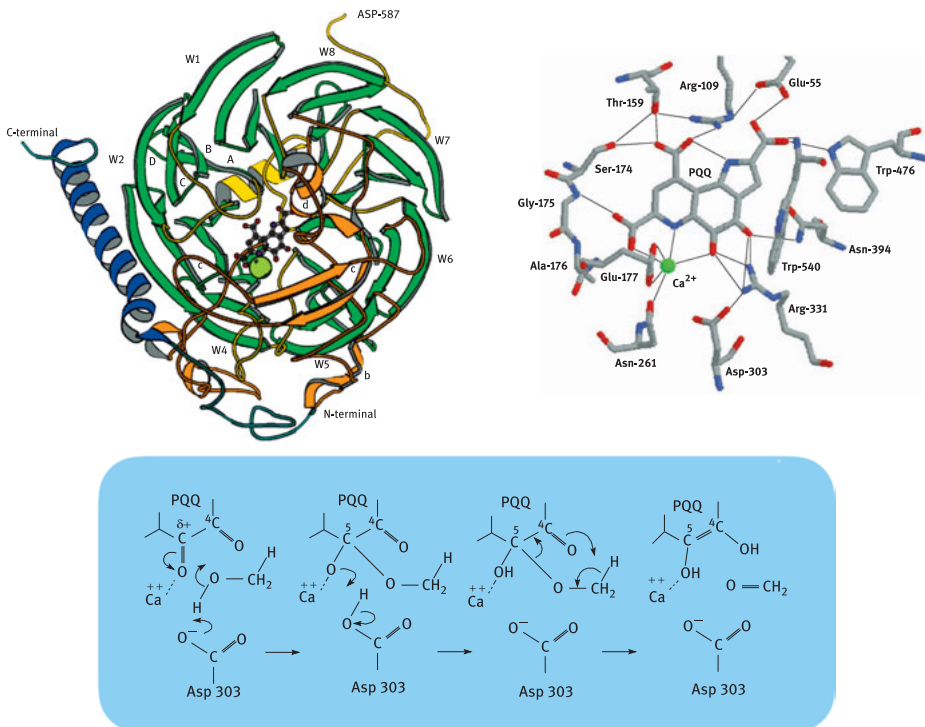
Figure 5.8: Structural and mechanistic features of the MDH found in *methylobacterium extorquens* [59, 60]. Top left: Simplified illustration of the proposed αβ unit of MDH with the PQQ prosthetic group and coordinated Ca^{2+} shown as ball-and-stick model. Top right: Section of the proposed interactions of PQQ and coordination of Ca^{2+} in the active site of MDH (eight-membered ring with disulfide bridge neglected for clarity). Bottom: Proposed mechanism for methanol dehydrogenation at the PQQ unit. Reprint with permission from Biochimica et Biophysica Acta, 1647 (2003) 18–23; Anthony et al. [60], Elsevier copyright 2003.

is required to close the catalytic cycle. A stepwise one-electron transfer to *cytochrome c_L* as electron acceptor is proposed [60].

5.3.2 Hydrogen production from aqueous methanol in artificial systems

5.3.2.1 Heterogeneous metal -based catalysis

Although proton exchange membrane fuel cells (PEMFC) can be used as suitable power sources for automotive applications, due to their low operating temperature [63], storage of hydrogen as fuel in liquid form or as gas under high pressure in a vehicle is considered to be potentially dangerous. Liquid alcohols can be used instead in the so-called "Direct Alcohol Fuel Cell (DAFC) ". In comparison, the direct methanol fuel cell (DMFC, Figure 5.9) is the most developed system. In a DMFC, methanol is electro-oxidized to carbon dioxide at the anode, which is mainly made of Pt. The anodic reaction which is proposed to occur at a Pt electrode is represented in

Anode:	$CH_3OH + H_2O$	$\longrightarrow$	$CO_2 + 6H^+ + 6e^-$	0.03 V
Cathode:	$3/2\, O_2 + 6H^+ + 6e^-$	$\longrightarrow$	$3H_2O$	1.22 V
Overall:	$CH_3OH + 3/2\, O_2$	$\longrightarrow$	$CO_2 + H_2O$	1.19 V
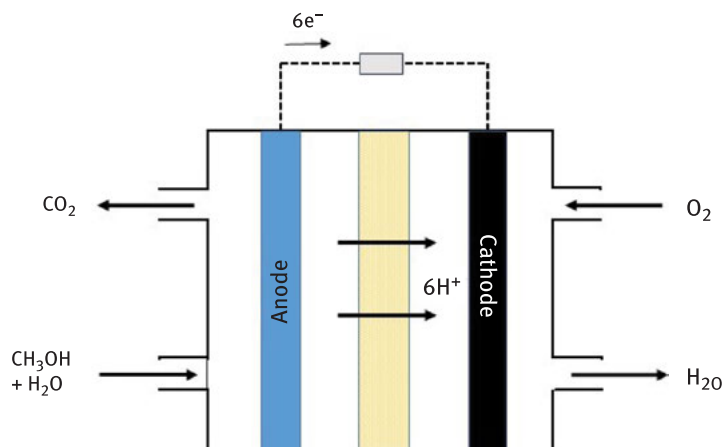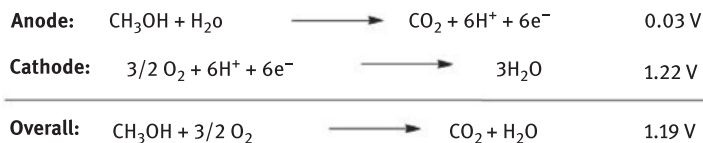
Figure 5.9: Diagram of the DMFC system.

Figure 10 [64]. The DMFC has been proposed as the most promising DAFC system for portable application due to several advantages, such as ease of transportation, storage and distribution of methanol. However, the key challenges that need to be overcome for the widespread commercialization of DMFCs include the exorbitant costs, mainly due to precious metal catalyst and membrane-electrode assembly. Moreover, low power density or low cell performance compared to the PEMFC are important drawbacks, owing the poor kinetics of the anodic methanol oxidation reaction (MOR), poor proton conductivity and methanol crossover through the polymer electrolyte membrane. To resolve the last two issues, the proton electrolyte membrane must be able to only allow protons to pass through to the cathode. Here, we mention some selected examples of heterogeneous electro-oxidation catalyst of methanol and refer to the articles dedicated to this particular topic [64–73].

$$CH_3OH + 3Pt(s) \longrightarrow Pt_3\text{-}COH + 3H^+ + 3e^-$$
$$Pt_3\text{-}COH \longrightarrow Pt\text{-}CO + 2Pt(s) + H^+ + e^-$$
$$Pt(s) + H_2O \longrightarrow Pt\text{-}OH + H^+ + e^-$$
$$Pt\text{-}CO + H_2O \longrightarrow Pt\text{-}COOH + H^+ + e^-$$
$$Pt\text{-}COOH \longrightarrow Pt(s) + CO_2H^+ + e^-$$
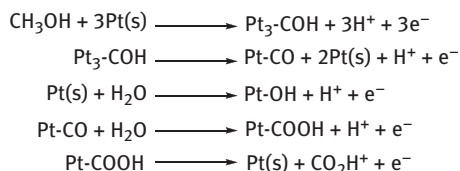
Figure 5.10: Proposed reaction steps for methanol oxidation on a Pt anode.

Although oxidation of methanol is a rapid process on a clean Pt anode, adsorption of carbon monoxide which is generated as an intermediate in this reaction, poisons the catalyst making the overall methanol oxidation sluggish. To overcome this problem, considerable efforts have been devoted to the development of suitable anode materials that achieve high reactivity, stability and durability. Furthermore, attempts have been made to reduce the costs by decreasing the amount of expensive Pt-based noble metal catalysts. In this regard, different Pt-alloys with more oxophilic metals such as Pt–Sn, Pt–Ni, Pt–Cu, Pt–Mo, Pt–Au, especially Pt–Ru-based catalysts have been thoroughly investigated [74–81]. Extensive amount of research has been dedicated for the development of DMFCs as portable low power devices and remarkable results were achieved using Pt–Ru-based catalytic systems which give power densities ranging from 45 to 207 mW cm^{-2} at 25–70°C [82]. The optimal DMFC for application in transportation was developed by Siemens AG (Germany) which reaches a maximum power density of 250 mW/cm^2 at 110°C.

Still nowadays, Pt gives the best catalytic activity concerning the MOR, both in acidic and alkaline solutions. [83].

The activity of Pd in the MOR in alkaline solution can be greatly enhanced by incorporating another metal in the alloyed form (such as Pd–Ni/C)[84, 85] or in the oxide form (such as Pd–NiO/C) [86, 87] thus explaining the reason why most reports today on this reaction media, deploy Pd-based bimetallic nano-catalysts. The promoting effect of Ni or its oxide form is not surprising, since Ni is known to oxidize primary alcohols to acids [88]. When Ni is placed in an alkaline solution, it is covered with a layer of nickel hydroxide. Consequently, the surface transformation and subsequent electro-oxidation of the alcohol to the organic acid occurs. The NiO is known to promote the anti-poisoning properties of the PdNiO/C catalyst. The last five years have seen an increase in research activities aiming at the improvement of the catalytic activity of nanostructured Pd-based bimetallic catalysts in alkaline media. Recently, some non-precious metal oxides (mainly oxides of tin, cobalt, and nickel) have been reported as viable nano-catalysts for the electrooxidation of methanol. Shi and co-workers showed that nanocomposites of tin-oxide nanocrystals (~3 nm) homogeneously supported on the surface of mesoporous zeolite (i.e. SnO$_2$/m-ZSM-5) exhibited high and stable electrocatalytic properties for the reaction, which is comparable to the Pt/C system [89]. The enhanced performance was related to the excellent resistance to CO poisoning, stemming from the interaction between SnO$_2$ and m-ZSM-5. Recently Asghari and co-workers showed that hierarchically nanostructured tin-oxide-polypyrrole on nanoporous copper (porous Cu/PPy/SnO$_x$) showed enhanced catalytic activity compared to its smooth Cu/PPy/SnO$_x$ and porous Cu/PPy counterparts [90]. The improved performance was attributed to factors such as the ability of the SnO$_x$ to accomplish the adsorption of the methanol oxidation intermediates and transformation of the products, such as CO, permitting the dehydrogenation of the alcohols. Wu and co-workers reported that a Co$_3$O$_4$/NiO core–shell nanowire array (with mesoporous nanowire core and branched nanoflake shell), obtained by combined hydrothermal and electrodeposition methods,

showed excellent electrocatalysis toward the MOR compared to its single Co_3O_4 nanowire array [91]. The enhanced performance was attributed to the synergy between the core–shell architecture, which allowed the fast kinetics and a lower overpotential. An interesting finding on the electrocatalytic properties of NiOx and MnOx was reported by Saleh and co-workers [92]. Electrodeposited nickel and manganese oxide nanocomposites on glassy carbon provided an excellent catalyst system, but to achieve the desired catalytic effects, NiOx must be sitting on the MnOx surface, which increased the adsorption of MeOH on the catalyst.

5.3.2.1.1 Photo-catalytic processes

In the pioneering studies by Fujisima and co-workers, it was demonstrated that the overall water splitting can be achieved using a photo-electrochemical device comprising a single-crystalline TiO_2 (rutile) anode and a Pt cathode under UV irradiation [93]. Since then, most recent research has been directed to the photo-catalytic production of hydrogen from water and a number of catalysts have been designed for this purpose. A large number of semiconducting metal oxides and sulfides (CdS, ZnO, ZrO_2, titanates, niobates and tantalates) have suitable properties (band gaps of *ca.* 3 eV and conduction bands in the range of –2 to –1 V for proton reduction in aqueous media) for the photo-catalytic splitting of water using UV light. Visible-light-responsive photo-catalysts are accessible by coupling a wide band gap semiconductor (TiO_2 3.2 eV) with a narrow one (CdS 2.44 eV, In_2S_3 2.1 eV) as a sensitizer [94–98]. The rate of hydrogen production from alcohol/water mixtures is considerably higher compared to that from pure water. Under irradiation, the TiO_2-promoted photo-catalytic reaction is initiated by charge-separation into electrons (e^-) and holes (h^+) with photons of energy equal or higher than the band gap. The electrons injected into the conduction band reduces water to generate H_2 while the remaining h^+ in the valence band oxidizes the hydroxide ions (HO^-), to give a highly reactive $HO^\bullet$ radical [99]. With alcohols as sacrificial electron donors, the reaction is accelerated since they are not only consumed by the photo-generated holes but they also react rapidly with the photo-generated $HO^\bullet$ radicals, thus decreasing the rate of electron-hole recombination and suppressing the "Knallgas" reaction which both lower the quantum yield of the H_2 production [100–104]. The use of water/methanol mixtures for the light-induced production of H_2 has been extensively investigated. Methanol plays a crucial role as sacrificial donor for the hydrogen production from water and its photochemistry has been extensively investigated on single-crystalline TiO_2 surfaces [105–109] and on TiO_2 powders [110–112]. Although little is known about the mechanistic details, these studies show that beside hydrogen, FAld, FAc and carbon dioxide are generated from methanol (Figure 5.11) [113, 114].

Typically, noble metal deposits including Pt [115–139] Pd [140–145] Rh [142, 146] Ru [147, 148] Au [140, 148–151] Ag [152] and less frequently, non-noble metals such as Ni [153–155] Cu [156–158] and Fe [159] have been reported to significantly enhance the
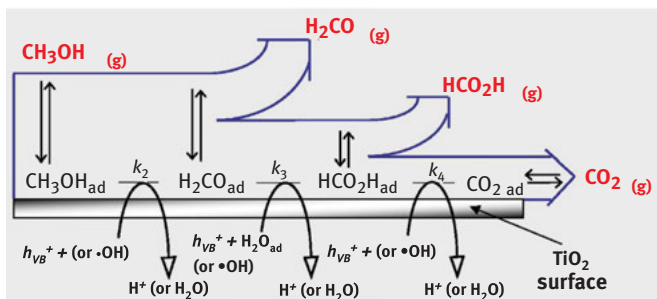
Figure 5.11: Proposed reaction mechanism for methanol photoreforming using a M/TiO$_2$ (M = noble metal) catalyst. Reproduced with permission from reference [19b]. Copyright (2011) Elsevier.

efficiency of TiO$_2$ mediated photocatalysis (Table 5.1) [160]. Comparative studies have shown a trend in the performance of different noble metal catalysts (Pt > Rh > Pd > Ru >> Ag) using TiO$_2$ as the light-harvesting semiconductor. One of the most relevant examples is the efficient H$_2$ production achieved in the photoreforming of methanol (up to 571 mmol H$_2$ g$_{cat}^{-1}$ h^{-1}, Φ_a=78%), however, observed at considerably high temperatures (280°C) on Pt/TiO$_2$ under simulated solar light [139].

The Fermi levels of these noble metals lie below that of TiO$_2$ and photo-excited electrons are efficiently injected from the TiO$_2$ conduction band to the metal particles deposited on the surface of TiO$_2$. The photo-generated holes remain in the valence band of the TiO$_2$. This modification significantly reduces electron-hole recombination, enhances the life time of the charge separated state of the photo-catalysts, and thereby raises the photo-catalytic yield in the reduction of protons to H$_2$ (Figure 5.12) [161–179].

In their pioneering experiments, Grätzel and co-workers described a hybrid system composed from hydrogenase enzymes and an inorganic light-harvesting support. Three different redox enzymes fixed to TiO$_2$ as semiconducting support were able to catalyze the H$_2$ production under excitation of the band gap in the presence of MeOH as electron donor. The H$_2$ formation was obtained by direct electron transfer from the conduction band of the TiO$_2$ particles to the active site of the enzyme at pH > 7. In addition, rhodium polypyridyl complexes were used to enhance the efficiency of the electron transfer from the TiO$_2$ particles to the adsorbed enzyme. The maximum rate of hydrogen evolution was 1.42 mmol (g^{-1} TiO$_2$) h^{-1} in the presence of [Rh(bpy)$_3$]$^+$ [180].

5.3.2.1.2 Thermal dehydrogenation of methanol (methanol reforming processes)

With the fast-emerging fuel cell technology there is a demand of high purity hydrogen gas as most efficient fuel cells (FC), e.g. PEMFC, require a hydrogen source without contaminants [181]. As already discussed before, most of the used dihydrogen gas stems from steam reforming of natural gas giving rise to a hydrogen-rich gas mixture, which is subsequently subjected to additional purification, process to meet the required quality of hydrogen gas for FC applications. The energetic and economical costs incurring thereby effect of course the economic efficiency of the FC itself. As

Table 5.1: Classes of photo-catalysts for the reforming of methanol.

Photocatalyst	Reaction medium	Light source	P/W (l/mW cm^{-2})	T (°C)	H$_2$ production rate (µmol h^{-1} g$_{cat}^{-1}$)	[Ref.]
Pt(4%)/TiO$_2$	H$_2$O/MeOH(l, 1:1)	Xe (>320 nm)	500	–	3,000	[116]
Pt(4%)/TiO$_2$	MeOH(l)	Xe (350–400 nm)	500	25	6	[117]
Pt(4.85%)/P25 TiO$_2$	MeOH(l)	Hg	125	–	4,524	[115]
Pt(4.85%)/P25 TiO$_2$	H$_2$O/MeOH(l, 1:1)	Hg	125	–	3,810	[115]
Pt(5%) + TiO$_2$ (rutile)	H$_2$O/MeOH(l, 1:1)	Hg	100	–	2,022	[118]
Pt(5%) + TiO$_2$ (rutile)	MeOH(aq, 0.1 M)	Hg	500	–	40	[119]
Pt(0.6%)/SiO$_2$/ TiO$_2$	MeOH(aq, 0.5 M)	Xe (350–420 nm)	900	–	1,072	[120]
Pt(0.5%)/P25 TiO$_2$	MeOH(l)	Hg (>366 nm)	250	20	2,267	[121]
Pt(0.5%)/P25 TiO$_2$	MeOH(aq, 0.85 mM)	Solar simulator	280	40	269	[122]
Pt(0.5%)/P25 TiO$_2$	MeOH(aq, 1 M)	LED (365 nm)	(3)	–	4,005	[123]
Pt(1%)/TiO$_2$ (anatase)	MeOH(l)	Hg	100	33	2,356	[124]
Pt(0.1%)/TiO$_2$ (74% rutile)	H$_2$O/MeOH(l, 4:1)	Xe	300	–	7,094	[125]
Pt/TiO$_2$ (black)	H$_2$O/MeOH(l, 1:1)	Solar	–	–	10,000	[126]
17% Pt + 33% graphite-silica + P25 TiO$_2$	H$_2$O/MeOH(l, 3:2)	Hg (300–400 nm)	–	–	4,800	[127]
Pt(0.6%)/TiO$_2$ (mesoporous)	H$_2$O/MeOH(l, 10:1)	Hg (>320 nm)	300	–	6,925	[128]
Pt(0.5%)/TiO$_2$ (porous)	H$_2$O/MeOH(l, 5:1)	Hg	500	30	13,000	[129]
PtO(1%)/TiO$_2$ (nanosheets)	H$_2$O/MeOH(l, 7:3)	Xe	300	–	4,400	[130]
Pt(1%) TiO$_2$ (nanofibers)	H$_2$O/MeOH(l, 9:1)	Xe	300	–	10,860	[131]
Pt(0.3%)/Gd (0.5%): TiO$_2$	H$_2$O/MeOH(l, 50:1)	Hg	300	–	13,200	[132]
Pt(0.3%)/Eu (0.5%): TiO$_2$	H$_2$O/MeOH(l, 50:1)	Hg	300	–	10,800	[132]
Pt(1%)/(CNT + TiO$_2$)	MeOH(aq, 2.5 M)	Hg	150	25	1,380	[133]

Table 5.1 (continued)

Photocatalyst	Reaction medium	Light source	P/W (l/mW cm^{-2})	T (°C)	H$_2$ production rate (µmol h^{-1} g$_{cat}^{-1}$)	[Ref.]
Pt(0.5%)/TiO$_2$/CNT(10%) (nanofibers)	H$_2$O/MeOH(l, 1:1)	Hg	200	–	40,600	[134]
Pt(3%)/Sn(1%)/TiO$_2$	H$_2$O/MeOH(l, 33:1)	Hg	125	20	80,800	[135]
Pt(0.5%)/Cu$_2$O	MeOH(aq, 2.5 M)	Halo. (> 420 nm)	(280)	–	149	[136]
Pt(0.1%)/SiO$_2$ (pillars) Ca$_2$Nb$_3$O$_{10}$	H$_2$O/MeOH(l, 9:1)	Hg	450	–	10,800	[122]
Pt(5%)/CdS	H$_2$O/MeOH(l, 100:0.17)	Xe	500	r.t.	400	[137]
Pt(0.5%)/g-C$_3$N$_4$	H$_2$O/MeOH(l, 9:1)	Xe (>420 nm)	300	–	30	[138]
Pt(1%)/P25TiO$_2$/SiO$_2$	H$_2$O/MeOH(l, 7:3)	Solar simulator	(100)	280	571,000	[139]
Pd(0.5%)/TiO$_2$	H$_2$O/MeOH(l, 1000:1)	Xe	400	–	555	[140]
Pd(1%)/TiO$_2$	H$_2$O/MeOH(l, 1000:1)	Solar	280	–	225	[141]
Pd(2%)/TiO$_2$	MeOH(l)	Xe	450	–	18,762	[142]
Pd(5%)/P25 TiO$_2$	H$_2$O/MeOH(l, 1:1)	–	–	–	2,261	[143]
Pd$_{shell}$ Aucore (1%)/P25 TiO$_2$	H$_2$O/MeOH(l, 3:1)	UV LED (365 nm)	(60)	–	20,529	[144]
Pd(0.5%)/P25 TiO$_2$	H$_2$O/MeOH(l, 1000:1)	Xe	400	–	486	[145]
Rh(2%)/TiO$_2$	MeOH(l)	Xe	450	–	19,655	[142]
Rh-Cr/N:ZnGa$_2$O$_4$	H$_2$O/MeOH(l, 9:1)	Hg	125	–	37,201	[146]
RuO^2/Pt/TiO$_2$	H$_2$O/MeOH(l, 1:1)	Xe	500	–	1,733	[148]
Ru(5%)/ZnS/CdS (Cd/Zn=4)	H$_2$O/MeOH(l, 9:1)	Xe (>420 nm)	(70)	–	4,900	[147]
Au(1%)/P25 TiO$_2$	H$_2$O/MeOH(v, 69:31)	Fe-halogen -Hg	–	–	15,000	[114]
Au(2%)/TiO$_2$	H$_2$O/MeOH(l, 100:1)	Solar simulator	(30)	–	7,200	[149]
Au(1%)/TiO$_2$	H$_2$O/MeOH(l, 1000:1)	Solar	280	–	100	[141]
Au(2%)/TiO$_2$	H$_2$O/MeOH(l, 1000:1)	Xe	400	–	169	[150]
Au(0.43%)/P25 TiO$_2$	MeOH(aq, 1 M)	Xe	300	–	383	[151]

(continued)

Table 5.1 (continued)

Photocatalyst	Reaction medium	Light source	P/W (l/mW cm^{-2})	T (°C)	H_2 production rate (µmol h^{-1} g_{cat}^{-1})	[Ref.]
Ag(0.5%)/TiO_2 (rutile)	H_2O/MeOH(l, 1:1)	UVA (352 nm)	6 × 6	–	357	[152]
Ag(0.5%)/TiO_2 (anatase)	H_2O/MeOH(l, 1:1)	UVA (352 nm)	6 × 6	–	222	[152]
NiO(1.5%)/TiO_2	H_2O/MeOH(l, 30:1)	Hg	450	–	82	[153]
NiO(0.5%)/TiO_2	MeOH (aq, 0.03 M)	UV (300–400 nm)	(60)	–	9,938	[154]
NiO(0.1%)/K4 Nb_6 O17	H_2 O/MeOH(l, 30:1)	Hg	450	–	1,593	[155]
CuO(1%) + P25 TiO_2	H_2O/MeOH(l, 9:1)	Black light	(15.1)	–	200	[156]
CuO(0.5%) + Al_2O_3 (0.3%) + P25 TiO_2	H_2O/MeOH(l, 9:1)	Black light	(15.1)	–	400	[156]
CuO(9.1%)/P25 TiO_2	H_2O/MeOH(l, 9:1)	Hg	450	25	18,500	[157]
Cu(3% mol vs. Ti)/S: TiO_2	H_2O/MeOH(l, 9:1)	Hg	125	23	18,000	[158]
Fe(20%)/TiO_2	MeOH(aq, 1 M)	Hg	–	25	2	[159]
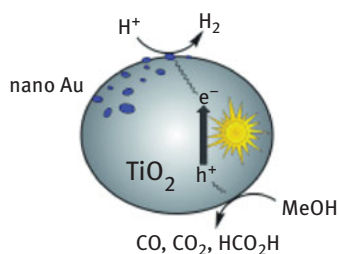
Figure 5.12: Au/TiO_2 generates hydrogen on liter scale from water/methanol mixtures and is stable for more than two days. Best activity: 8.4 µmol H_2 h^{-1} mg^{-1} catalyst (0.97 wt% Au loading); TON 1006, turnover frequency (TOF) 168 h^{-1}. Reproduced with permission of ref [179]. Wiley (2012) copyright.

discussed above, carbon monoxide present in the gas stream stemming from natural gas reforming, is particularly harmful in FC application as it acts as a strong catalyst-poison for the FC exchange-membranes. Therefore, the concentration of CO must be kept minimal in suitable hydrogen feeding gas in FCs (significantly below 20 ppm)

[182]. An increasing number of scientific reports are dealing with the aspects of production of high purity hydrogen. For instance, Basile and co-workers summarized membrane reactors that allow for the direct hydrogen production-purification process and methanol steam reforming [183]. Along these lines methanol is a very attractive hydrogen carrier and methanol reforming processes give rise to a hydrogen source with promising purity levels [184]. Advantageously, with respect to methane, the reforming processes can occur at much lower temperatures (240–260°C for methanol [185]; 800–1,000°C for methane [186]). Another striking advantage is the absence of additional C–C bonds in methanol, which allows for lower reforming temperatures. For instance, the reforming of ethanol requires temperatures around 400–450°C [187]. Although the direct use of methanol in FC is possible, note that PEMFCs have a much higher power output than DMFC. It remains promising to use heterogeneous catalysts for steam reforming to utilize methanol as vector for clean hydrogen gas in this way. Owing to the high hydrogen content of methanol and relatively low activation temperatures, steam reforming of methanol (SRM) is an option for the on-line production of hydrogen coupled directly to portable applications of FCs. Against this background, the methanol reforming processes will be discussed in this subchapter.

Commonly, four different fundamental reactions are discussed regarding the dehydrogenation of methanol: methanol decomposition (MD), SRM, the partially oxygenation of methanol (POM), and the oxidative steam reforming of methanol (OSRM). The relevant chemical reactions are summarized in eqs. (5.11)−(5.16) (Enthalpy values taken from Yong et al [188].).

Methanol Decomposition (MD)
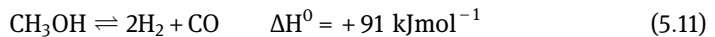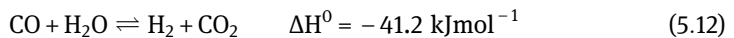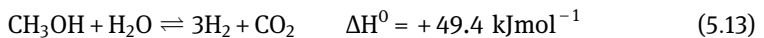
$$CH_3OH \rightleftharpoons 2H_2 + CO \qquad \Delta H^0 = +91 \text{ kJmol}^{-1} \tag{5.11}$$

Water Gas Shift Reaction (WGS)

$$CO + H_2O \rightleftharpoons H_2 + CO_2 \qquad \Delta H^0 = -41.2 \text{ kJmol}^{-1} \tag{5.12}$$

Steam Reforming of Methanol (SRM)

$$CH_3OH + H_2O \rightleftharpoons 3H_2 + CO_2 \qquad \Delta H^0 = +49.4 \text{ kJmol}^{-1} \tag{5.13}$$

Partial Oxidation of Methanol (POM)

$$CH_3OH + 0.5O_2 \rightleftharpoons 2H_2 + CO_2 \qquad \Delta H^0 = -192.2 \text{ kJmol}^{-1} \tag{5.14}$$

Oxidative Steam Reforming of Methanol (OSRM)

$$CH_3OH + (1-n)H_2O + 0.5nO_2 \rightleftharpoons (3-n)H_2 + CO_2 \qquad \Delta H^0 = +49 - 242*n \text{ kJmol}^{-1}$$
$$\tag{5.15}$$

Total Oxidation of Methanol (*TOM*)

$$CH_3OH + 1.5O_2 \rightleftharpoons 2H_2O + CO_2 \qquad \Delta H^0 = -723 \text{ kJmol}^{-1} \qquad (5.16)$$
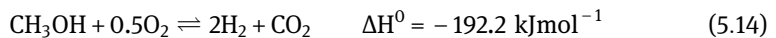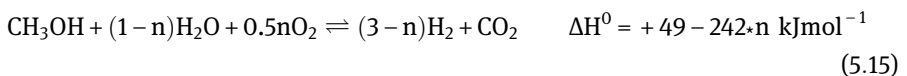
SRM is a very promising process as it generates up to 75 mol% of hydrogen and 25 mol% of CO_2 [184]. However, difficulties comprise the endothermic nature of the process and the formation of carbon monoxide in side reactions, which feeds a parallel WGS/*reverse* WGS reaction (eq. (5.12)). Nevertheless, smart catalyst application can minimize the levels of CO. Combining high yields of hydrogen and controllable low levels of CO makes SRM a promising process for the production of hydrogen from methanol suitable for FC applications.

MD can be essentially understood as the reverse reaction of CO hydrogenation to methanol (eq. (5.11)). The endothermic process gives rise to gas mixtures containing up to 67% of hydrogen [184]. Naturally, the remaining 33 mol% of CO must be removed, e.g. by reaction with H_2O in a WGS reaction, to meet the purity required for FC application. Technically this remains difficult.

POM[189] is an exothermic reaction (eq. (5.14)) that allows for a hydrogen production of up to 67 mol% and the associated formation of CO_2. However, for such high conversions pure O_2 is required as oxidant. The utilization of air causes a reduced yield of 41 mol%. Side reactions such as MD, SRM and TOM can occur along with WGS and reverse WGS giving also rise to significant levels of CO formed in course of the POM [184]. In general, POM features a fast start-up and a rapid response. Technical POM solutions are rather compact [188].

OSRM describes a combination of POM and SRM (eq. (5.15)). The process suffers from relatively high levels of produced CO; reports of catalytic systems with high selectivity still report CO levels of 500 ppm exceeding the requirements significantly [184].

Mechanistic considerations concerning *SRM*
A great deal of attention was devoted to the investigation of the reaction mechanism over Cu-based catalyst. Five principal mechanistic proposals for SRM have been mainly discussed in the literature[188]:

I. Early studies suggested a simple MD-WGS mechanism, reverse to the mechanism for methanol formation from hydrogenation of CO. Consequently, the MD reaction was proposed as initial step to give CO and H_2, followed by the WGS allowing for the conversion of CO and H_2O to CO_2 and H_2 (eq. (5.11) and (5.12)) [190–193].

II. Successively, reports were published suggesting the one-step SRM *via* direct dehydrogenation of methanol, whereby the concentration of intermediate CO gas remains small [194–196].

III. A multi-step mechanism involving in the first stage the dehydrogenation of methanol to give methyl formate (eq. (5.17)) was suggested by Takahashi

and co-workers [197]. The mechanism entails the subsequent hydrolysis of HCOOCH$_3$ to FAc (eq. (5.18)), which is selectively dehydrogenated to CO$_2$ and H$_2$ (eq. (5.19)) [198–200]. Remarkably, the observed concentration of CO was very low and thus a participation of MD-WGS seems to be unlikely. Instead, the low levels of CO gas were assumed to arise from the decomposition of methyl formate (eq. (5.20)).

$$2CH_3OH \rightleftharpoons HCOOCH_3 + 2H_2 \tag{5.17}$$

$$HCOOCH_3 + H_2O \rightleftharpoons CH_3OH + HCOOH \tag{5.18}$$

$$HCOOH \rightleftharpoons CO_2 + H_2 \tag{5.19}$$

$$HCOOCH_3 \rightleftharpoons CH_3OH + CO \tag{5.20}$$
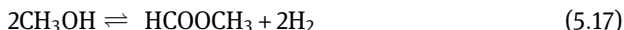
IV. A more complex description of the reforming process termed "reaction network" was given by Peppley [201, 202]. Essentially, in the studies reported, a MD side-reaction is paralleling the SRM and WGS reaction. Furthermore, a mixture of H$_2$ and CO$_2$ stemming from SRM is constantly transformed into H$_2$O and CO by the reverse WGS. Peppley and co-workers propose for the Cu system two different surface reactions centered at two distinct catalytic sites: one for SRM and reverse WGS, the other exclusively catalyzes the MD.

V. A dehydrogenation mechanism following a path *via* FAld –FAc intermediates was also proposed [203, 204]. The initial dehydrogenation of methanol gives rise to the formation of FAld and hydrogen (eq. (5.21)). The nucleophilic attack by water results most likely in the formation of methanediol, which is subsequently dehydrogenated to FAc (eq. (5.22)). The decomposition of FAc results in the release of CO$_2$ and H$_2$ (eq. (5.23)). The formation of FAld and water was also observed by Rabe and Vogel in course of a POM reaction under rich O$_2$ conditions, using a commercially available Cu/ZnO/Al$_2$O$_3$ catalyst. Remarkably, at higher oxygen/methanol ratios (>0.5), and hence more oxidized Cu centers at temperatures below 220°C FAld is formed, which is further dehydrogenated to CO$_2$[205].

$$CH_3OH \rightleftharpoons HCHO + H_2 \tag{5.21}$$

$$HCHO + H_2O \rightleftharpoons [H_2C(OH)OH] \rightleftharpoons HCOOH + H_2 \tag{5.22}$$

$$HCOOH \rightleftharpoons CO_2 + H_2 \qquad\qquad (5.23)$$
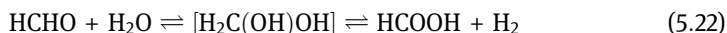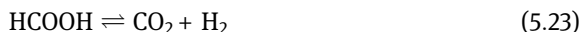
The principal proposed pathways (I-IV) may be more complex due to the existence of other secondary processes, such as, the TOM to CO_2 and H_2O, the formation of elemental carbon during the reaction, or partial oxidation of CO and H_2 to CO_2 and H_2O, respectively. The study of $Cu/ZnO/Al_2O_3$ based catalytic system for SRM revealed that, strongly depending on the concentration of O_2, POM and MD can initially occur. With a decreasing concentration of O_2, SRM started to be effective. This is also owed to the formation of H_2O in course of the initial POM and MD reaction [206]. TOM was also suspected to take place in partial oxidation reaction schemes. The combination of TOM and subsequent SRM leads formally to an overall POM-type reaction. The initial accumulation of water formed *via* methanol combustion (TOM, eq. (5.16)) gives rise to a consecutive SRM reaction (eq. (5.13)). The sum of eqs. (5.16) and (5.13) would result formally in a POM-type reaction (eq. (5.14); TOM + SRM = POM). However, depending on the catalyst preparation also a one-step POM reaction scheme was proposed, which allows for the direct formation of H_2 for systems based on Cu/ZnO [207, 208]. Similar systems using Cu/ZnO-based catalysts with Pd and zirconia promotors were described by Schuyten and co-workers additionally taking a SRM-MD-reverse WGS sequence into account.

Surface reactions in the course of SRM – detailed mechanistic proposals for Cu-based catalysts

Schomäcker and co-workers introduced a proposal for a catalytic cycle featuring several mechanisms reported in the literature, which is shown in Figure 5.13 [209]. The cycle entails two active sites S_A and S_B, whereby S_A hosts the adsorption processes involving all substrates and intermediates and S_B accommodates hydrogen adsorption processes exclusively. The catalytic conversion is entered *via* methanol adsorption (1). Dehydrogenation and subsequent hydrogen desorption gives rise to surface-bound FAld (2). Following pathway A, water addition and consecutive dehydrogenation allows for the formation of a dioxomethylene moiety (3). Hydride transfer to S_B gives formate (4). Dehydrogenation of formate to CO_2 and dissociative adsorption of methanol closes the catalytic cycle A. Alternatively, the FAld initially formed can be attacked by methoxide to form methyl formate (pathway C). A sequence of hydration and dehydrogenation gives rise to formate, which can enter pathway A for the final dehydrogenation step. Methoxide is formed as well (B), which can reenter in the pathway C.

Catalysts for SRM

Vast amounts of catalytic systems for SRM have been reported. An overview was given by Mendes and co-workers[210] and Lachowska and co-workers [184]. Cu-based catalysts are by far the most commonly used systems owing to their cost
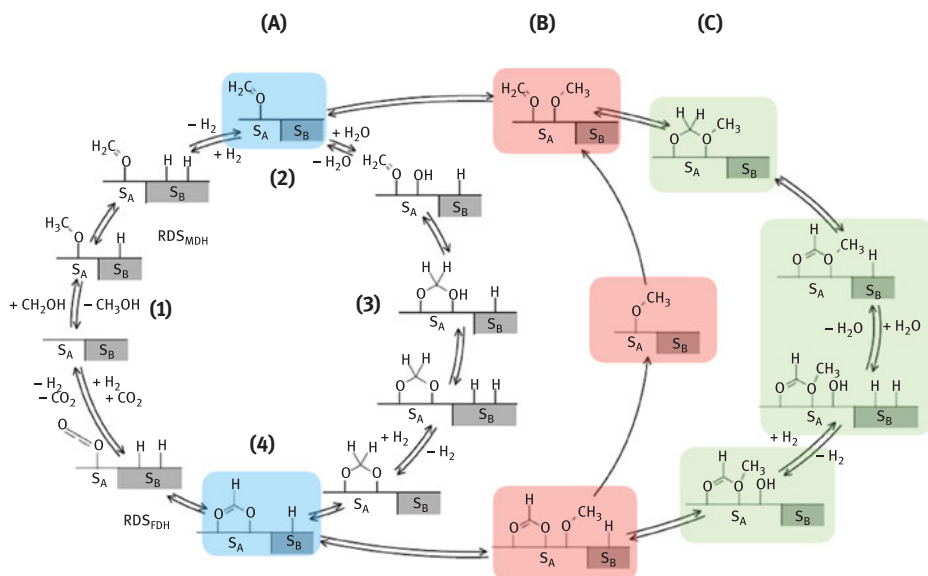
Figure 5.13: Catalytic cycle of methanol steam reforming according to Jiang, Peppley, Takezawa and Iwasa. Reprinted with permission from: Schomäcker et al. [209]. Applied Catalysis B: 2010 43–57, Elsevier (2010) copyright.

Reprinted with permission from: Schomäcker et al. [209]. Applied Catalysis B: 2010 43–57, Elsevier (2010) copyright.

efficiency, high activity and high selectivity. CuO/ZnO/Al$_2$O$_3$ serves as commercially available reference catalyst in various reports. Common reaction conditions involve atmospheric pressure at temperatures ranging from 220 to 300 °C in a stream of inert gas. The catalyst is activated *via* reduction prior to usage (e. g. heating in H$_2$/N$_2$ atmosphere) [184]. In general, the performance of such heterogeneous catalysts is enhanced by a large surface area, high copper dispersion and overall small particle sizes. The preparation of the catalyst has also a significant effect on the performance [210]. Special attention was payed to the interaction between ZnO and the Cu centers where a synergistic effect was found allowing for higher activity and selectivity. It was proposed that ZnO facilitates the reduction of the Cu centers[211] and thus allowing for lower reaction temperatures [212]. It is further suggested that ZnO acts as dispersive agent [213]. Developed Cu/ZnO-based catalytic formulations contain supplementary promotors and stabilizers comprising, for instance, alumina or other oxides (e. g. ZrO$_2$, CeO$_2$, SiO$_2$, CoO, Cr$_2$O$_3$, Mn–O). Common commercially available catalytic systems encompass Cu/ZnO/Al$_2$O$_3$. Cu-based catalysts employed in SRM were identified to suppress the formation of undesired CO much better than other transition metals of group 8–10. Transition metals such as Ni, Pt and Rh gave rise to more pronounced decarbonylation reactions[214] and hence high levels of CO, that is, the formation

of syn-gas [203]. However, Cu catalysts bear likewise technical drawbacks such as their pyrophoric nature and their tendency to become deactivated by thermal sintering. Therefore, other catalytic systems have been investigated mainly encompassing transition metals of group 8–10 seeking solutions for catalysts with higher stability and improved selectivity. Active catalysts for SRM were reported employing the latter transition metals. However, smaller hydrogen yields were observed with respect to their Cu-based congeners [210]. Along these lines, palladium supported on zinc oxide shows high activity and enhanced thermal stability, with respect to the Cu formulations. $Pd/ZnO/Al_2O_3$ systems show remarkable long-term stability [215]. Mendes and co-workers summarize a variety of catalysts based on group 8–10 metals (Pd, Pt, Ni, Co, Ir, Ru) on various supports comprising for example SiO_2, Nd_2O_3, MgO, In_2O_3, Ga_2O_3, CeO_2, HfO_2, Ta_2O_3, ZrO_2 or SiO_2 [210]. Molybdenum carbide was utilized as an alternative to oxide-based support materials. The catalysts were obtained *via in situ* carburization of $M-MoO_x$ doped with M=Pt, Fe, Co or Ni at 700°C in an atmosphere of CH_4/H_2. The obtained Pt-doped formulations were described as active catalyst allowing for quantitative methanol conversion at low temperature (200°C). Remarkably, a conversion of 60% was still observed at a reaction temperature as low as 150°C. The base metals formulations however, required higher temperatures (>300°C) to show similar activity [216, 217]. In the last decade Cu-based catalysts for several related reforming reactions were reported facilitating a spinel-type lattice support ($M_a^{2+}M_b^{3+}O_4$), such as CuM_2O_4 with M=Fe[218], Mn[219], Al, Cr and Ga [220]. Owing to the high degree of organization of neighboring divalent and trivalent metal oxides, highly dispersed active copper centers are present in such catalysts. Furthermore, the $[M_2O_4]^{2-}$ moieties hamper sintering of the Cu sites and stabilize reduced Cu centers allowing for more thermally robust and catalytically active systems [188]. Spinel-type catalysts require high initial reduction temperatures (700°C) to reduce the copper centers in the presence of H_2. A major problem with respect to the spinel-type catalysts is the relatively small surface area. It was suggested that the high initial calcination temperatures may cause the low surface area and thus a restricted availability of active Cu sites giving rise to limited activity in SRM [221]. However, other base metal catalysts with spinel lattice support have been reported by employing improved preparation methods, which allow for significantly larger surface areas. Yong and co-workers summarized various examples involving, for instance, $NiFe_2O_3$, $ZnGa_2O_4$, $MgAlsO_4$ or $ZnCr_2O_4$ [188].

Catalyst deactivationin Cu/ZnO/Al₂O₃ systems

Copper-based catalysts are relatively facilely deactivated, which is associated to a change in the oxidation state of the Cu center, sintering, or coke deposition. Poisoning can occur due to the presence of contaminants in the feed stream [222–224]. In this aspect, it was reported that an increased steam-to-carbon-ratio or the presence of oxygen (e.g. in OSRM) precludes coking and thus decreases catalyst

deactivation. Al$_2$O$_3$ can be used as structural promotor to prevent Cu crystallites to agglomerate and thus avoiding the reduction of reactive surface area. In this aspect it was also found that high levels of CO enhance the agglomeration of Cu centers [222].

5.3.2.2 Molecular catalysts for dehydrogenation of methanol/water mixtures
5.3.2.2.1 Electro-oxidation of methanol

The acceptorless electrochemical oxidation of an alcohol is closely related to the separation of protons and electrons and the reversible recombination to give molecular hydrogen. A hypothetical general setup for the electro-reforming of methanol (ERM) can be essentially understood as a modified direct methanol FC. Roduner describes such a cell as an anaerobic DMFC, that is an electrochemical approach to the acceptorless dehydrogenation of methanol in a setup reminiscent to a DMFC [225]. Theoretically, in the absence of an acceptor at the cathode, such as oxygen in the DMFC, hydrogen would be directly formed instead of water, the reaction would proceed solely at the anode, and H$_2$ would be formed spatially separated at the cathode side, where the recombination of the separated protons and electrons can occur. Alongside CO$_2$ would be formed as oxidized carbon species at the anode (see Figure 5.14). This ERM/water mixtures would offer a convenient way for a mobile approach for hydrogen delivery. The hydrogen production can be controlled by the variable size of the bias potential. Such an ERM cell may be an attractive on-demand approach for the dynamic production of H$_2$ with short response time to flexibly address short-term spikes in hydrogen-demand. Roduner outlines the compact size of such potential devices.
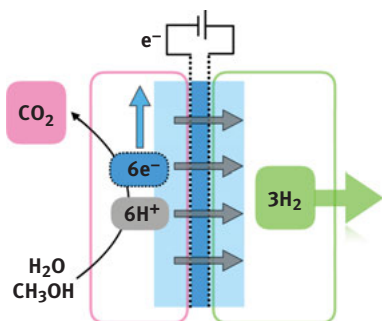
Figure 5.14: Hypothetical cell for the ERM/water mixtures outlined by Roduner.[225] The approach follows essentially a set-up of a DMFC that operates without an acceptor (oxygen). At the cathode hydrogen is formed instead of water. All reactants are solely fed to the side of the anode.

The literature reveals only a small number of studies on molecular catalyst designs for the electro-oxidation of methanol in aqueous media. Molecular systems are summarized in Figure 5.15. None of the examples allows the direct formation of hydrogen gas.

Waymouth 2013

$$CH_3OH + 5OH^- \xrightarrow[\text{catalyst immobilized on graphite electrode}]{} HCOO^- + 4H_2O + 4e^-$$ (3)

McElwee-White 2011

$$CH_3OH\ (+ H_2O)^i \xrightarrow[\substack{\text{catalyst } \mathbf{a\text{–}c} \text{ dissolved in MeOH (10mM)}\\ \text{0.1M TBAPF}_6 \text{ electrolyte in MeOH}}]{} \begin{bmatrix} HCOOH \\ H_2C{=}O \end{bmatrix} \xrightarrow{MeOH} \substack{HC(O)OMe \\ + \\ H_2C(OMe)_2}$$

Complex	M_1	M_2
4a	Ru	Pt
4b	Ru	Pd
4c	Fe	Pt

[i] dry and aqueous conditions

Bond & Zang 2016

$$CH_3OH + H_2O \xrightarrow[\substack{\text{catalyst dissolved in MeOH (0.1mM)}\\ \text{or}\\ \text{immobilized on carbon cloth-electrode}\\ \text{0.50M H}_2SO_4 \text{ electrolyte}}]{\text{cat:}[Ru_4O_4(OH_2)(H_2O)_4)(SiW_{10}O_{36})_2]^{10-}} \substack{HCOOH \\ + \\ H_2C{=}O} \xrightarrow{MeOH} \substack{HC(O)OMe \\ + \\ H_2C(OMe)_2}$$ (5)

Figure 5.15: Molecular catalysts for the electro-oxidation of methanol.

Articles concerning the electro-oxidation of alcohols other than methanol using a molecular system are more frequent, although the reactions usually do not entail the direct formation of H_2 [226]. In principle, a molecular catalyst could be utilized in such an ERM cell in two ways. Firstly, the compound is directly dissolved in the electrolyte and hence catalyzes the oxidation of methanol homogeneously. Secondly, the catalyst is immobilized in a secondary phase, i.e. embedded or attached to the electrode material [227]. In both cases, the substrate does not exchange electrons directly with the electrode. Saveant and co-workers specifically categorize electro-catalysts into two types [228]. On one hand, there are redox-catalysts functioning as electron carriers or mediators (Figure 5.16, left). On the other hand, there are catalysts with functions beyond the sole electron shuttling allowing for chemical conversion. The latter is characterized by the transient formation of catalyst-substrate complexes,
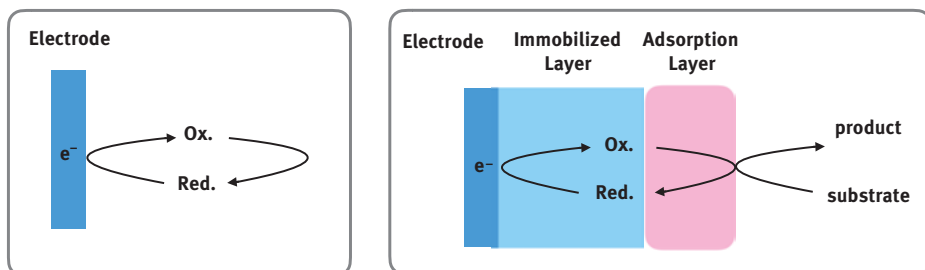
Figure 5.16: The general principle of electrocatalytic reforming utilizing a molecular catalyst. Left: Homogeneous conditions. The catalyst is dissolved within the electrolyte. Right: The catalyst is immobilized within the surface of the electrode. The substrates are adsorbed onto the electrode layer prior to the redox reaction occurs and products are subsequently released (desorption).

which is represented in the illustration on the right side in Figure 5.16. Obviously, molecular catalyst designs bear the great advantage of structural tuning of the active species resulting from the large number of available metals and ligands. But moreover, it allows for a deeper understanding of the reaction mechanisms due to the precise knowledge with respect of the structural molecular designs.

Waymouth and co-workers reported the transfer-hydrogenation catalyst [Ru (*p*-cymene)(Cl)(N,O-(1*R*,2*S*)-*cis*-1-amino-2-indanolate)] (**3**) physisorbed onto an edge-plane graphite electrode capable for the electro-oxidation of methanol (Figure 5.15, top) [229]. The four-electron oxidation of methanol (1.23 M) occurs in a buffered aqueous solution at a pH value of 11.5 with NaClO$_4$ (0.1 M) as electrolyte with a TOF of 1 s^{-1} at 0.75 V vs. NHE. The mechanistic investigation revealed formate as formed product. On the basis of a desorption electrospray ionization mass spectrometry study, the authors suggest an in situ formed ruthenium-oxo species supported on the electrode surface as active catalytic species. McElwee-White and co-workers presented heterobimetallic Ru−Pt, Ru−Pd and Fe-Pt complexes **4a**−**c** (Figure 5.15) as active homogeneous catalysts for methanol oxidation [230]. This report entails the bulk electrolysis of methanol, in which the catalysts **4a**−**c** are directly dissolved in the electrolyte/substrate giving rise to the formation of dimethoxymethane (DMM) and methylformate (MF). In this study, the catalyst is promoting both, the two- and four-electron oxidation of methanol. The products resulted from an initial formation of FAld and FAc and subsequent condensation with excess methanol. Notably, CO$_2$ was detected in course of the electrolysis tentatively suggesting a possible full oxidation (6e$^-$/ 6H$^+$) of methanol. However, thorough isotopic labeling experiments reveal a carbonyl ligand present in the catalyst, presumably due to WGS reaction. Faradaic efficiencies reported are below 50%. The Ru/Pt complex **4a** was identified as the most active catalyst with a TON of 12 for a solution in dry methanol

and TON of 10 for aqueous methanol, with respect to the formed products DMM and MF per mole catalyst, after passing 200 Coulomb.

The Ru-based polyoxometalate $[(Ru_4O_4(OH_2)(H_2O)_4)(\gamma\text{-}SiW_{10}O_{36})_2)_2]^{10-}$ (**5**) is a molecularly well-defined catalyst, which served previously as an excellent water-oxidation catalyst when linked to functionalized carbon nanotubes or grafted on graphene oxide. Bond, Zhang and co-workers utilized this system for the oxidation of methanol in aqueous and dry alcoholic media (Figure 5.15) [229]. Complex **5** can be used as homogeneous catalyst (0.1 mM) in solution (MeOH/0.5 M H_2SO_4) as well as under surface-confined conditions (carbon-cloth). After a charge of 100 Coulomb was passed at a carbon-cloth electrode with embedded **5** at a potential of 0.93 V (vs. Fc/Fc+) a product distribution of 22.4% FAld and 77.6% FAc was found by HPLC analysis. The same reaction was investigated with **5** in homogeneous solution (0.1 mM in methanol with 0.5 M H_2SO_4 electrolyte) at an applied potential of 0.86 V (vs. Fc/Fc$^+$). The found product distribution entailed 47.6% FAld and 52.4% FAc. Thus, both bulk electrolysis experiments gave rise to the formation of significant amount of FAc (4e$^-$ process) and FAld (2e$^-$ process). The faradaic efficiency obtained (95.8–98.1%) is remarkably high. Representative experiments for immobilized **5** catalyst and methanol solutions with 0.5 mM H_2SO_4 gave product-to-catalyst ratios of 1,071 for FAc and 310 for FAld. Likewise, the homogeneous approach gave rise to ratios of 165 (FAc) and 150 (FAld), respectively. The authors report difficulties determining the TOF due to experimental limitations. However, they estimate a TOF of about 0.2 s^{-1} assuming a two-electron transfer. Nevertheless, **5** is an active and robust catalyst operating at low overpotential and within a wide pH range (acidic, neutral and basic conditions). It can be operated under homogeneously and immobilized on carbon electrodes making **5** a versatile platform.

5.3.2.2.2 Photo-chemical dehydrogenation of methanol

Reports concerning the photo-induced dehydrogenation of methanol utilizing molecular catalysts are particularly rare in the literature. Early work by Saito and co-workers reach back to 1980s. In particular, Saito described the soluble complexes [PdCl(dppm)]$_2$ (**6**) and cis-[RhCl(CO)(dppm)]$_2$, (**7**) (Figure 5.17), which generate hydrogen from methanol under irradiation of light (high-pressure Hg lamp) [166]. Typical reported TOFs (hydrogen evolution) for a methanol/acetone mixture (9:1) 450 mL at 64°C and irradiation from a 400 W Hg lamp are 156 h^{-1} for **7** (0.05 mM) and 130 h^{-1} for **6** (0.05 mM), respectively. Inspection of the liquid phase allowed for the identification of the soluble reaction products: FAld, DMM, ethylene glycol, 2-propanol and 2-methyl-1,2-propandiol, signaling a process with rather low selectivity. However, preference for the formation of FAld and DMM is observed in case of the [PdCl(dppm)]$_2$ catalyzed reaction and DMM for the *cis*-[RhCl(CO)(dppm)]$_2$ catalyst, respectively. While a photo-reaction in neat methanol with complex **7** as catalyst gives selectively hydrogen as the only detectable product in the gas phase and FAld and DMM in the liquid phase, the presence of acetone gives rise to the formation of methane (90%), CO (8.8%)
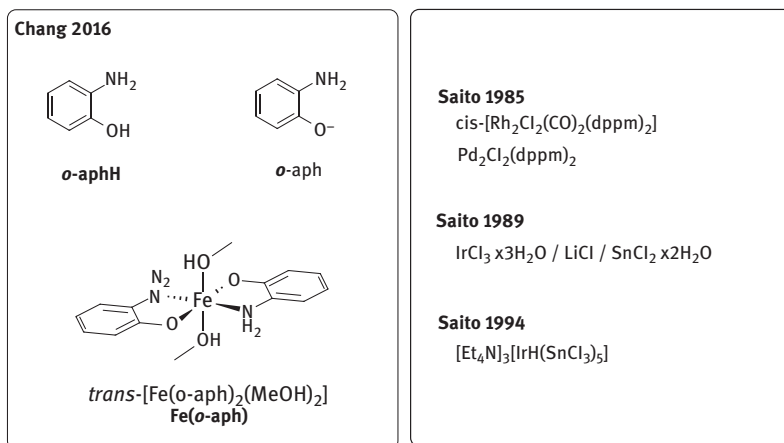
Figure 5.17: Molecular catalysts for the photo-chemically triggered dehydrogenation of methanol; dppm = bis(diphenylphosphino)methane.

and hydrogen (1.2%) in the gas phase and ethylene glycol, 2-propanol, 2-methyl-1,2-propanediol along with FAld and DMM. It was documented that acetone itself allows for a light-induced dehydrogenation of methanol. However, complex **7** enhances the formation of FAld and DMM significantly [165]. Subsequently, Saito and co-workers reported in 1989 an Ir-based soluble formulation with high catalytic activity mediating the dehydrogenation of methanol to give DMM. Boiling methanol at 65°C in the presence of a mixture of IrCl$_3$ × 3H$_2$O/ LiCl/SnCl$_2$ × 2H$_2$O (in 1:18:4 mmol ratio in 400 mL methanol) and the concomitant irradiation of light (high-pressure Hg lamp) leads to the almost exclusive formation of DMM and H$_2$ in equimolar amounts (Figure 5.17). It was speculated that the *in situ* formation of excess SnCl$_3^-$ facilitates the reaction. The TOF values vary depending on the molar ratio of the components from 0.4 to 1.82 h^{-1}. On the basis of a ^{119}Sn NMR and a UV/VIS spectroscopy study it was speculated that the iridium-hydride species [IrH(SnCl$_3$)$_5$]$^{3-}$ is formed under the conditions applied and suggested that this compound plays a key role in the catalytic conversion of methanol [231].

In this regard, Saito and co-workers revealed the photo-catalytic activity of well-defined [Et$_4$N][IrH(SnCl$_3$)$_5$] (**8**) with respect to the dehydrogenation of methanol and selective formation of DMM and hydrogen gas in stoichiometric ratio (Figure 5.17) [170]. Nevertheless, the authors kept utilizing SnCl$_2$ and LiCl as additives to enhance the catalytic performance. The influence of water and aqueous HCl was tested; while water led to a drop in the reaction rate (TOF = 0.28 h^{-1}), the acidification with HCl enhanced the reaction rate. Applying optimized reaction conditions, that is a solution of complex **9**/SnCl$_2$ × 2H$_2$O/LiCl in a 0.3:1.5:5.4 mmolar ratio in 400 mL of methanol at 65°C and concomitant irradiation of light (400 W high-pressure Hg lamp), gave rise to a TOF of

$1.06\ h^{-1}$. The addition of 0.5 mL 11.4 M HCl to the initial optimized reaction mixtures led to a significant increase in the TOF value to $2.87\ h^{-1}$. Very recently, Chang and co-workers reported the selective photo-catalytic dehydrogenation of anhydrous methanol to give FAld and hydrogen gas employing the simple organic molecules, *ortho*-aminophenol (*o*-aphH; **10**) and *ortho*-aminophenolate (*o*-aph; **11**), as well as the related iron(II) complex *trans*-[Fe(*o*-aph)$_2$(MeOH)$_2$] (**Fe(o-aph); 12**). The selective formation of FAld and dihydrogen was observed for all three species. Prolonged reaction times gave rise to small amounts of methyl formate and FAc. The reaction proceeds at room temperature under irradiation of UV light (289 ± 10 nm) with quantum yields for H_2 evolution of 2.9 to 4.8 ± 0.2%. Photo-chemically formed hydrogen radicals were suspected to drive the reaction [232]. The iron complex shows comparable catalytic activity to (*o*-aph). The authors conclude that the coordination of (*o*-aph) to the Fe(II) center gives rise to a charge transfer band allowing for the photo-chemical reactivity relevant to methanol dehydrogenation to occur at much longer wavelength than required for the light-triggered hydrogen evolution catalyzed by the organo-catalysts (*o-aphH*) and (*o-aph*). This observation is of paramount importance with respect to the development of photo-catalysts for methanol dehydrogenation driven by lower energy light sources.

5.3.2.2.3 Thermal dehydrogenation of aqueous methanol

The earliest example of an acceptorless dehydrogenation of an alcohol was reported more than 40 years ago. In this first report, Robinson and co-workers used a catalytic system based on the perfluorocarboxylate complexes [M(OCOR$_F$)$_2$(CO)(PPh$_3$)$_2$] (M=Ru, Os; R$_F$=CF$_3$, C$_2$F$_5$ or C$_6$F$_5$) and trifluoroacetic acid as proton source to accomplish the dehydrogenation of primary and secondary alcohols to aldehydes and ketones, respectively [233, 234]. While an acceptable initial TOF of $8,172\ h^{-1}$ was achieved in the conversion of benzyl alcohol to benzaldehyde, no activity was observed in the case of methanol. The authors isolated the stable adduct [Ru(OCOCF$_3$)$_2$(CH$_3$OH)(CO)(PPh$_3$)$_2$] from the reaction mixture, which is not further converted. The mechanistic proposal suggested that the coordinated ROH molecule is internally deprotonated by the carboxylate ligand under liberation of the free acid. The formed alkoxide complex would subsequently undergo a β-hydride elimination to form an aldehyde (or ketone) and the hydride species [MH(OCOR$_F$)(CO)(PPh$_3$)$_2$]. Reaction with the acid would lead to H_2 formation which closes the catalytic cycle with regeneration of [M(OCOR$_F$)$_2$(CO)(PPh$_3$)$_2$] (M=Ru, Os). The fact that methanol was not dehydrogenated is attributed to the slightly stronger α-CH bond in methyl groups when compared to alkyl groups present in higher primary or secondary alcohols. A decade later, other ruthenium-based homogeneous catalysts proved more success for the production of hydrogen from methanol, but they still showed low activity and selectivity. Most of the reactions afforded as carbon-containing byproducts: FAld , methyl formate, formate salts or acetic acid. Saito and co-workers demonstrated that the *in situ* prepared complex [Ru(OAc)(Cl)(PEtPPh$_2$)$_3$] was an acceptable catalyst for the dehydrogenation of methanol

to FAld with an initial TOF of 0.96 h^{-1} and a total TON of 34 over a period of 90 h [235, 236]. The addition of two equivalent of acetic acid relative to the catalyst was necessary for the observed reactivity, as in the case of Robinson 's system. While FAld was the only product in the early stage of the reaction, at higher conversion, both methyl formate (from Tishchenko reaction of FAld) and dimethoxymethane (FAld dimethyl acetal) were detected in the reaction mixture. Side reactions, as decarbonylation or formation of methane were excluded. Maitlis and co-workers also reported the dehydrogenation of methanol to methylformate and dimethoxymethane catalyzed by [Ru(Cl)$_2$(PPh$_3$)$_3$] at 150°C achieving a TON up to 65 for hydrogen evolution. After *ca.* 18 h, the catalytic activity decreased, likely due to the decarbonylation of the FAld intermediate and the formation of the carbonyl complexes [Ru(PPh$_3$)$_3$(H)(CO)Cl], [Ru(PPh$_3$)$_2$(CO)$_2$Cl$_2$] and [(PPh$_3$)$_2$Ru(CO)(μ-H)(μ-Cl$_2$)Ru(CO)(PPh$_3$)$_2$]$^+$, which were isolated from the reaction media and proved to be inactive in the dehydrogenation process. Cole-Hamilton and co-workers showed that simple alcohols can be dehydrogenated by performing the reaction with complex [RuH$_2$(N$_2$)(PPh$_3$)$_3$] or, alternatively, [Ru(H)$_2$(PPh$_3$)$_4$] as catalysts. The rate of hydrogen evolution from methanol at 150°C could be greatly improved by using excess of base (NaOH) relative to the ruthenium catalyst (TOF up to 7.5 h^{-1}) [163, 237–240]. As previously mentioned for the Robinson catalyst, decarbonylation of the aldehyde product can result in catalyst poisoning by the formation of stable and catalytically inactive Ru carbonyl complexes. Irradiation with light may promote the release of CO and regeneration of the active species. A mechanism in which the Ru center in various catalytically active intermediates remains coordinated to all three PPh$_3$ ligands was initially proposed [238], while later studies indicated that the active catalyst is generated in a pre-equilibrium involving PPh$_3$ dissociation [239]. Bühl and co-workers calculated four different reaction pathways for alcohol dehydrogenation promoted by the catalyst precursor [RuH$_2$(N$_2$)(PPh$_3$)$_3$], which is presumably converted to the hydrogen complex [RuH$_2$(H$_2$)(PPh$_3$)$_3$] as active species. In all of them, the rate determining step for hydrogen evolution was found to be the β-hydrogen elimination from a methanol or methoxide complex. The different reaction channels differ by various ligand dissociations (PPh$_3$ or H$_2$) prior to β-hydrogen elimination. The authors found that all pathways are competitive with respect to their energy profile [240]. The groups of Beller [241] and Grützmacher [242] described the first efficient aqueous-phase methanol dehydrogenation process that achieves a complete dehydrogenation to CO$_2$ using a homogeneous system (Figure 5.18). In both cases, the reaction was catalyzed by well-defined ruthenium complexes (**13** and **14**). The accessibility to this approach could establish the starting point for the development of methanol as hydrogen storage material since the reaction temperatures in both examples lie significantly below 100°C. At ambient pressure, three equivalents of H$_2$ were released from the H$_3$COH/H$_2$O mixtures, with almost no trace of CO contamination, allowing the direct use of methanol in PEMFC [242]. Both catalysts contain cooperative or chemically "non-innocent" multidentate ligands, which participate synergistically with the metal in the hydrogen abstraction from the

$$CH_3OH + H_2O \xrightarrow[T < 100\ °C]{cat\ \textbf{13-20}} 3H_2 + CO_2\ (or\ M_2CO_3)$$
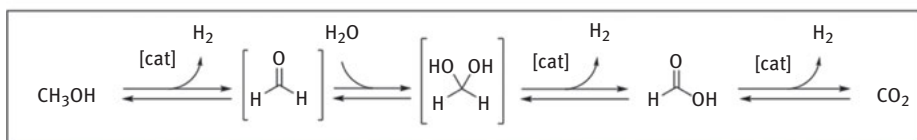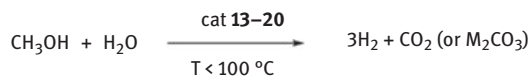
Catalyst	Beller *et al.* **13a**	Gruetzmacher *et al.* **14**	Milstein *et al.* **15**	Crabtree *et al.* **16**	Fujita *et al.* **17**
Additive	KOH	no additive	KOH	KOH	NaOH
Solvent	No solvent	THF	toluene	No solvent	No solvent
Temp.	90 °C	90 °C	100 - 105 °C	90 °C	reflux
Yield (H₂)	27%	84%	73%	81%	64%
TON	353' 400 (24d)	540 (10h)	28'700 (27d)	3'600 (24h)	10'500 (150h)

Catalyst	Holthausen *et al.* **18**	Beller *et al.* **19**	**20**
Additive	LiBF₄	KOH	KOH
Solvent	Ethyl Acetate	No solvent	Triglyme*
Temp.	reflux	92 °C	92 °C
Yield (H₂)	>99%	<5%	ca. 10%
TON	30'000 (52h)	65 (5h)	20'000 (30d)

*Addition of glyme and excess of ligand increases life time of catalyst

Figure 5.18: Catalyzed thermal reforming of MeOH by homogeneous catalysts based on noble (**13–17**) and non-noble metal complexes (**18–20**).

alcohol [243–245]. The complete dehydrogenation of methanol is assumed to proceed through three sequential steps: (a) dehydrogenation of methanol to FAld , which in aqueous solution forms methanediol and a mixture of methyleneglycol oligomers; (b) dehydrogenation of the diol to FAc and (c) final dehydrogenation of FAc to CO_2, which

releases the third H_2 molecule (Figure 5.18, top). Note, the theoretical hydrogen storage capacity of 12.6 wt% for neat MeOH and 12.1 wt% for MeOH/H_2O 1:1 mixtures may be considerably reduced due to the presence of required additives and/or solvent. Grützmacher, Trincado and co-workers found experimentally that complex **14** was able to dehydrogenate aqueous MeOH quantitatively in the absence of a base additive, achieving a TON of 540 over a period of 10 h. The same complex can decompose FAc at 90°C with a TOF of up to 24,000 h^{-1}, without the need of any additive [242]. Additionally, the ammonium derivative [NBu$_4$][RuH(trop$_2$dad)] proved to be the most efficient catalyst reported for the dehydrogenation of formalin, leading to TON = 1,800 with initial TOF of 12,000 h^{-1} at 60°C, confirming therefore the proposed mechanistic sequence [246–248]. This complex contains the chemically and redox *non-innocent* diolefin diazadiene ligand trop$_2$dad which participates actively in the alcohol dehydrogenation. The authors propose that the catalytic active species (**A**) is initially formed by reaction of the complex **14** with a proton source (H_2O). This intermediate was recently isolated and fully characterized [249]. The methanol molecule is added across the Ru–N bond and thus a methoxide group is bound to the metal center. Activation of the α-C–H bond of the coordinated methoxide occurs and a hydride (H$^-$) is transferred to the diazadiene-backbone of the ligand forming intermediate **B**. A second hydrogen transfer from a new molecule of methanol, FAld hydrate or FAc derives in the bis(amino)ethylene ligand (trop$_2$dae) coordinated to ruthenium (intermediate **C**). The later intermediate was isolated form a stoichiometric reaction with aqueous alcohol and its molecular structure confirmed as the fully hydrogenated intermediate **C**, which conversion back to complex **14** was also proved under basic conditions. This process is further accompanied by the reduction of the Ru(II) center to Ru(0). The activity of the catalyst in the dehydrogenation of aqueous methanol can be improved under slightly basic conditions which can promote the fast dehydrogenation of the isolated Ru(0) complex **C** to the hydride species **14** and can sequestrate the released CO_2 as carbonate (Figure 5.19).

The reaction catalyzed by complex **13a** proved to be favored under strongly alkaline conditions (KOH as base), temperature of *ca*. 90°C and a high MeOH/H_2O ratio (9:1). Under optimal conditions, an average TOF = 4,700 h^{-1} was achieved after 3 h leading to pure hydrogen and potassium carbonate as only products. A maximum TON of 350,000 was obtained in a 90-day experiment with an average TOF of 200 h^{-1} over the last 24 h, where the activity of the catalyst is significantly diminished. The catalytic cycle for methanol dehydrogenation shown in Figure 5.20 was proposed by Beller and co-workers based on the known behavior of complexes [RuClH(PNP^{Ph})(CO)] (PNP^{Ph} = bis[(2-diphenylphosphino)ethyl]amine) (**13b**) in the dehydrogenation of primary and secondary alcohols [246–248]. As in the reaction with higher alcohols, addition of base is essential to deprotonate the amine ligand in the pre-catalyst **13a** and generate the bifunctional [Ru(II)PNP] amido active species **A**. The authors proposed the activation of a methanol molecule which binds with the acidic OH group to the amide function of the catalyst and with the hydridic α-CH group to the Ru
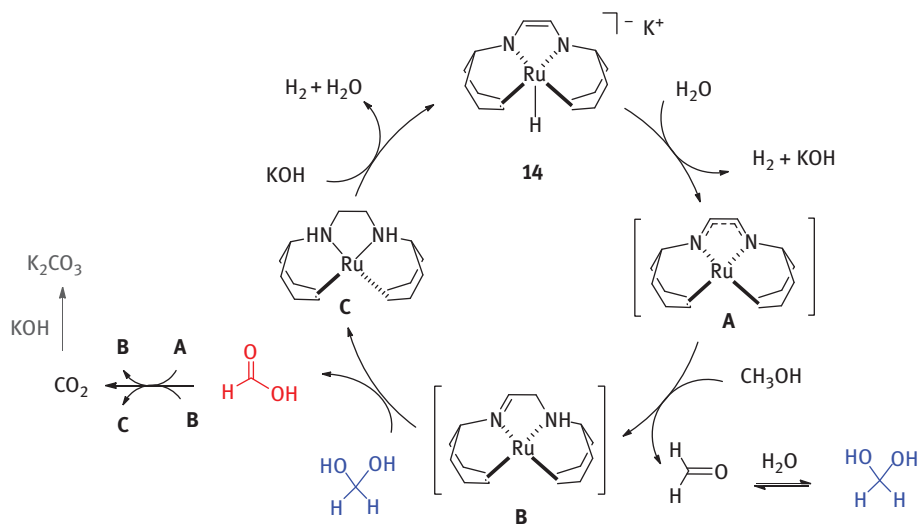
Figure 5.19: Proposed catalytic cycle for aqueous-phase methanol dehydrogenation by catalyst **14**.

center (see **TS-A**). This interaction induces the release of a hydrogen molecule and formation of FAld ($H_2C=O$) which is further converted under aqueous conditions to $H_2C(OH)_2$ and dehydrogenated to formate (HCO_2^-) under alkaline conditions. Decomposition of formate to CO_2 and a third hydrogen molecule regenerates the active form of the catalyst. In independent experiments the amido complex **A** could be converted to the dihydride intermediate **B** by reaction with dihydrogen or 2-propanol. Thus, the authors suggested that the interconversion of **A** and **B** is the key for assuring the dehydrogenation and hydrogen evolution processes. The metal–ligand cooperative mechanism proposed has been supported by DFT calculations [250, 251]. Water or methanol have a relevant role by allowing a proton shuttle from the amine ligand to the ruthenium hydride leading to the formation of a non-classical ruthenium dihydrogen complex (**B**) which releases H_2 regenerating species **A**. The base additive was used not only for the formation of the active species **A** from the precursor, but also to increase the operational temperature and to drive the reaction to the formation of carbonate from the generated CO_2. More recently, a different role of the cooperative ligand has been proposed plausible [252]. The amine ligand would be involved in the catalytic reaction stabilizing certain transition states through hydrogen-bonding interactions with the substrate rather than undergoing a reversible chemical transformation. In a following study, the system formed by the borohydride catalyst [Ru(H)(BH$_4$)(CO)(PNP^{Ph})] and [Ru(H)$_2$(dppe)$_2$] (dppe = 1,2-bis(diphenylphosphino)ethane) in the presence of triglyme promoted the dehydrogenation of aqueous methanol, without the need of base achieving a TON of 4,300 at $T < 95°C$. In this system, both catalysts operate in a synergistic
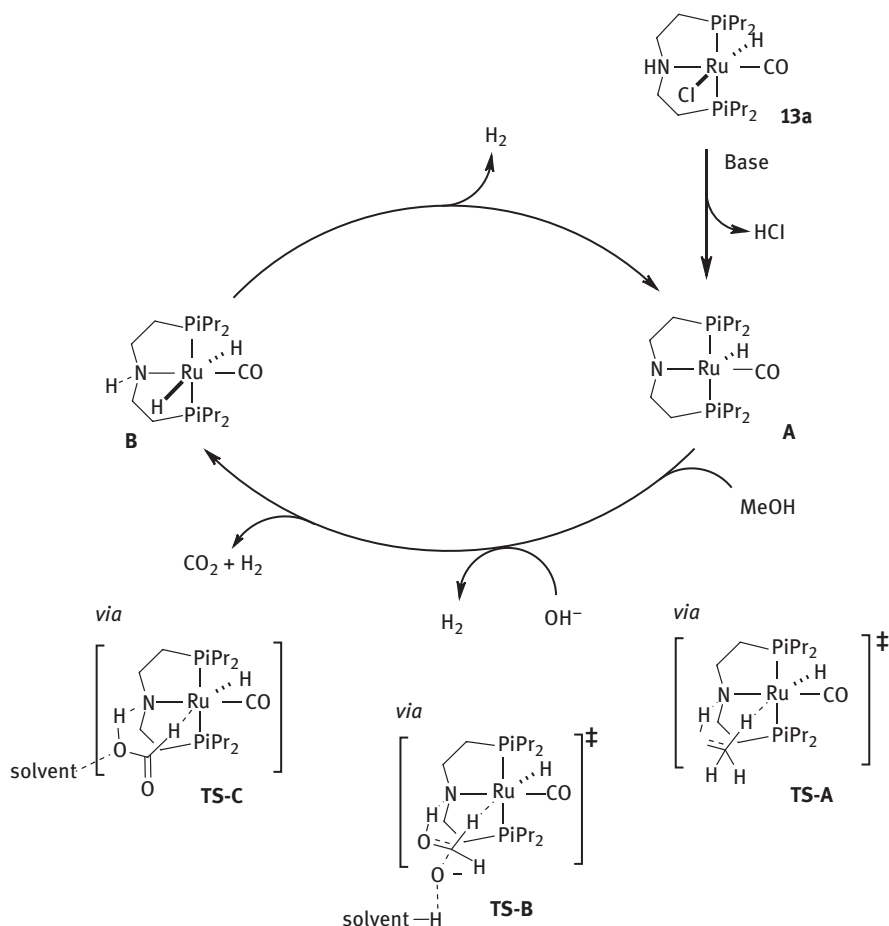
Figure 5.20: Proposed catalytic cycle for the aqueous dehydrogenation of methanol by pincer complex **13a**.

manner, since their combined activity is superior to the activities displayed by each of them separately [253].

The good performance of Milstein-type catalysts like [RuHCl(CO)(PNN)] (**15**) shows that the basic site may reside in a remote position with respect to the metal center, instead of being located in the first coordination sphere like in the previous PNP aliphatic pincer system. The reaction catalyzed by **15**, in the presence of base and at slightly higher temperatures than earlier Ru catalysts ($T = 100–105°C$), gave rise to a 73% yield of hydrogen over 27 days reaction time, which corresponds to a TON of 28,700 [254]. The base is needed in order to generate the catalytic active species **A**, as shown in the mechanism presented in Figure 5.21. The dearomatized complex **A**

dehydrogenates methanol, methanediol or FAc to give the aromatized dihydrido complex **B**, which then thermally eliminates H_2. An alternative mechanism which does not involve the interconversion of the amine/amide ligand has been proposed based on recent DFT calculations, including solvent effects [252].
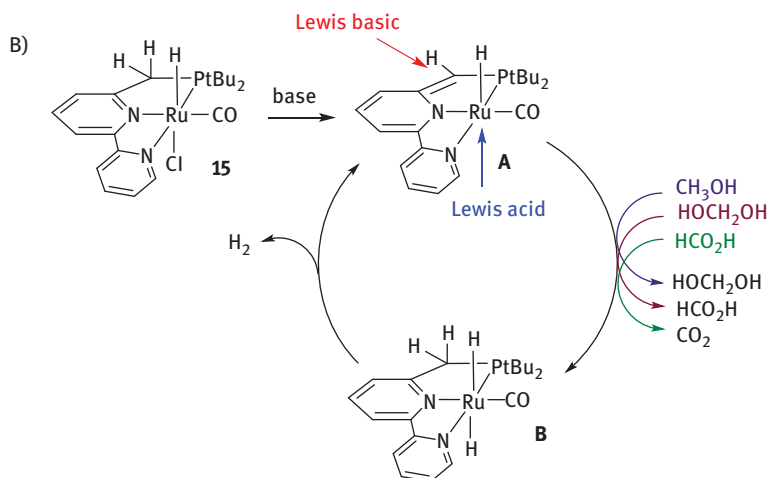
Figure 5.21: Proposed catalytic cycles for the aqueous dehydrogenation of methanol by Milstein's pincer complex **15**.

Crabtree *et al.* have also reported the acceptorless dehydrogenation of methanol using the homogeneous iridium bis(*N*-heterocyclic) carbene dicarbonyl catalysts (**16**, Figure 5.18) [255]. The reaction was highly dependent on the MeOH, the KOH concentration and on the temperature. At 90°C the system achieves TON of 8,000 after 40 h, being potassium formate the main product from the reaction. Although less active than previous systems, the catalysts are based on simple and accessible phosphine free ligands and are able to promote the reaction in the presence of air. The dehydrogenation reactions of aqueous methanol, FAld or formate to CO_2/H_2 mixtures can be catalyzed using iridium complexes bearing cooperative bipyridine and bipyridonate ligands [256]. The iridate complex **17** (Figure 5.18) can catalyze the reaction using only catalytic amounts of base, achieving good activities (TON = 10,500 after 150 h). In catalyst **17**, the cooperative α,α'-bipyridonate ligand and the metal participate simultaneously as hydrogen acceptors, leading to the formation of a α-hydroxypyridine hydride complex. Intramolecular proton hydride interaction would then occur to give the neutral bipyridonate iridium complex and H_2. In an entirely different approach, Prechtl and co-workers presented a methanol reforming process at ambient temperature or artificial methanol metabolism (Figure 5.22). The strategy was based on the
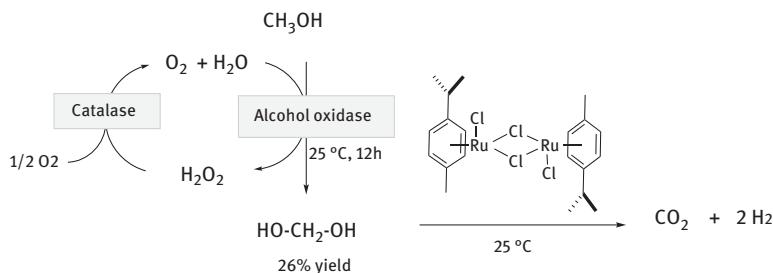
Figure 5.22: Tandem enzymatic oxidation of methanol to FAld and metal-catalyzed conversion of FAld hydrate to CO$_2$ and H$_2$.

combination of a oxidase-catalase system for the biocatalytic conversion of methanol into methanediol and the complexes [{Ru(p-$cymene$)Cl$_2$}$_2$] or alternatively [(Ru(p-$cymene$))μ-H(μ-HCO$_2$)μ-Cl]Cl, as catalysts for the conversion of the bio-generated FAld hydrate into pure hydrogen and CO$_2$. A one-pot system (enzyme-metal complex) provided a H$_2$ enriched gas phase of 3.2 μmol mL^{-1} H$_2$ at 25°C. The major drawbacks of this new method refer to the low efficiency and compatibility of the metal complex and the enzymes. A possible solution is based in the development of a system in which the biocatalyst and the metal are coupled [257].

Driven by economic and environmental considerations, recent efforts have been focused on the replacement of noble-metals by cheaper, more abundant, and non-toxic metals. Beller and co-workers used the iron complex [Fe(H)(BH$_4$)(CO)(PNP^{iPr})] as catalyst for aqueous methanol reforming [258]. Under similar conditions employed for the ruthenium system, a TON of 6,270 over a period of ca. 43 h was achieved. By adding an excess of ligand to the reaction media, it was possible to increase the active catalyst lifetime up to five days and consequently the TON was improved to 9,200. Related pentacoordinated amido compounds [Fe(H)(CO)(PNP^R)] (R=iPr, Cy) have been investigated in several dehydrogenation reactions [259–262]. It has been demonstrated that [FeH(CO)(PNP^{iPr})] can dehydrogenate primary alcohols under anhydrous conditions to the corresponding esters without a base or H$_2$ acceptor. The related formate complex [FeH(O$_2$CH)(CO)(PNPR)] (**18, Figure 18**) is also an active catalyst for FAc dehydrogenation in the presence of a Lewis acid [261]. Recently, Jones, Schneider and co-workers presented the most efficient catalyst based on a first-row transition metal complex [262]. The system employs complex **18** and LiBF$_4$, as co-catalyst, providing a TON of ca. 30,000 over a period of 52 h. This catalyst comprises several advantages compared with the reforming of methanol under alkaline conditions: (a) the reaction conditions are milder ($T < 80$°C), which would allow for the use of less stable molecular complexes; and (b) the loading of the co-catalyst (acid) required is considerably lower than the loading of base typically used. Catalysts based on manganese can also be regarded as one of the most desirable candidates due to its low price, rich chemistry and good biocompatibility [263]a–c). Very

recently, manganese pincer catalysts with the metal in low oxidation state were successfully tested in hydrogenation and dehydrogenation reactions [264–270]. Beller and co-workers reported, for the first time, the low-temperature methanol reforming in the presence of manganese complexes (**19** and **20** in Figure 5.18). Under optimized reaction conditions (ten-fold excess of free ligand, base and 90°C in triglyme), a TON of *ca*. 20,000 was reached and the catalyst was active for a period of one month. Although the iron and manganese systems are still less active than the heavier congeners, these promising results show that it would be possible to design molecularly defined non-noble metal catalysts, stable under the reforming conditions, which will be of great importance for future industrial applications.

5.4 Outlook

5.4.1 Hydrogen as sustainable energy carrier and methanol as hydrogen storage material

The intrinsically limited fossil reserves cannot feed the foreseen rising demands for energy of our societies. Renewable sources must be sought and the carbon footprint of such must be drastically reduced to enable a more sustainable economic system. Against this background, hydrogen is an attractive energy carrier for the efficient generation of electricity using e.g. fuel cell technologies. Self-explanatory, hydrogen must be produced in a sustainable process from renewable resources as a prerequisite for an attractive carbon-neutral energy carrier. Practical drawbacks in the utilization of hydrogen are caused by its physical properties. Hydrogen storage, especially for portable applications, is associated with significant costs and safety hazards. Against this background, the reversible chemical fixation of hydrogen in a carrier molecule may offer a safer and more efficient alternative for hydrogen handling. Especially liquid carrier substances offer advantages with respect to the existing infrastructure of the petrol supply chain. It appears likely that the required modifications and the associated investments are smaller compared to a utilization of gaseous or solid carrier compounds. Along these lines, methanol is a promising fuel since it is a stable liquid under ambient conditions, and has a high gravimetric hydrogen content of 12.6 wt%, whereas a 1:1 mixture of CH_3/H_2O contains a 12.1 wt% of H_2. The dehydrogenation of an aqueous methanol solution gives rise to the release of CO_2 and three equivalents of H_2. Hence, the entire hydrogen content in CH_3OH/H_2O can be released alongside with CO_2. At this point it should be mentioned that, although the above stated theoretical hydrogen storage capacity of 12.6 wt% for neat MeOH and 12.1% $MeOH/H_2O$ 1:1 mixtures, does not consider the remaining additional components of the system (e.g. catalyst, additives, and most importantly solvent). The actual specific or volumetric capacity may be in fact considerably lower and has to be individually assessed for the specific set-up.

Given an environmentally benign source of hydrogen coupled with an efficient reduction process of CO$_2$, methanol might become an attractive molecule for a practical and sustainable hydrogen storage. In this way CO$_2$ takes the role as a recyclable hydrogen carrier. Methanol is obtained mainly from syn-gas which is produced by catalytic reforming of fossil fuels, which is self-evidently not a sustainable process. However, natural gas and shale gas, with its main component being methane, is available in vast amounts. Hence, methane could potentially serve as an interim replacement for fuels based on crude oil. The selective oxidation of methane to methanol would be an economically viable process. Natural gas is used directly as fuel in thermal combustion for heating and electrical power generation. Significant amounts of natural gas are currently just flared from fossil deposits due to the difficult and cost intensive transportation of methane. The oxidation of methane to syn-gas (methane steam reforming) and the subsequent reduction of CO to MeOH is an energetically costly detour. The direct oxidation of methane to methanol would be very efficient and thus a preferable strategy to obtain methanol. However, it remains with great difficulty to prevent over-oxidation due to the relatively facile oxidation of methanol itself and practical solutions remain elusive.

5.4.2 Dehydrogenation of methanol

New strategies for the reforming of methanol under mild conditions based on heterogeneous or molecular catalysts have raised the expectations on this fuel. The DMFC addresses the immediate conversion of chemically stored hydrogen into electrical power, being a promising device for portable electrical power generation. However, their demand a significant amount of precious metals and costly membrane-electrode assembly precludes a mass commercialization. Moreover, DMFCs suffer from a lower power density and low cell performance compared to the PEMFC.

The use of water/methanol mixtures for the light-induced production of H$_2$ has been extensively investigated. Methanol plays a crucial role as sacrificial donor for the hydrogen production from water and its photochemistry with heterogeneous TiO$_2$–based systems seems very promising. In contrast, reports concerning the photo-induced dehydrogenation of methanol utilizing molecular homogeneous catalysts are scarce. Only recently well-defined homogeneous catalysts were reported entailing purely organic compounds as well as a coordination thereof to a transition metal (iron). This coordination complex gives rise to a charge transfer band allowing for the photo-chemical reactivity, relevant to methanol dehydrogenation, to occur at lower energy with respect to the free organo-catalysts.

It remains promising to use heterogeneous catalysts mediating the SRM. SRM is discussed as an option for the on-line production of hydrogen integrated directly into portable applications of FCs. Reactor designs featuring dense metal membranes can provide high purity hydrogen for such applications. A great deal

of attention has been payed to the understanding of the mechanism as well as improvement of the performance of the systems catalyzing the SRM and closely related processes such as partial oxygenation of methanol (POM), and the OSRM). However, product selectivity and catalyst deactivation remain still problematic.

Besides the initial reports in the 1980s, it was not until very recently that homogeneous metal catalysts were reported to promote methanol reforming to CO_2 and H_2 under very mild conditions (<100°C). The catalyzed reforming reactions are characterized by a high selectivity. The hydrogen gas formed is of great purity and not contaminated with CO. The number of published homogeneous catalytic systems on the basis of coordination complexes for methanol dehydrogenation are still scarce but will certainly increase in the near future, as this is an important and fruitful field of research. It still remains a long way before these catalytic systems find an industrial application. However, the chemistry of well-defined coordination complexes has important advantages with respect to a better mechanistic understanding of key-steps in the (reversible) dehydrogenation of methanol or methanol-water mixtures. The ultimate goal would be the development of catalysts, which contain non-toxic and cost-efficient metals and ligands. The compounds must be ideally characterized by a rather simple ligand structure, as well as by an overall energy and cost-efficient preparation. That is, of course, the preparation must not require more energy than the device can deliver during its life-cycle. Along these lines, important advances have been made with iron- and manganese-based homogeneous catalytic systems.

Typically, the metal center in the catalyst has a key role in the activation and conversion of the substrate. In this regard, application of alternative reaction schemes may promote the catalyst development: For instance, metal-ligand cooperativity is a relatively novel strategy and was successfully applied in catalysts triggering methanol reforming with a performance superior to classical metal center-based reactivity. Future advances related to the modification of the structure of such cooperative ligands may involve the increase in diversity of functional groups that participate in bond cleavage and bond formation. Although most of the studied cooperative systems are based on N donor- or remote carbon sites, sulfur may have great potential in metal-ligand cooperative reaction schemes, as multiple active sites in metallo-enzymes exhibit cooperative sulfur-based moieties. Other functionalities may include Lewis acidic cooperative ligands: For instance, the coordination of σ-acceptor ligands (ER_3, E=B, Al, Ga, In or ER_4, E=Si, Sn) can not only influence the geometric and electronic properties of a metal fragment, but may also actively cooperate with the metal center in the course of the substrate activation. This concept remains not reported with respect to the catalyzed reforming of methanol.

References

[1]   (a) Olah GA, Goeppert A, Prakash GK. Beyond oil and gas: the methanol economy. 2006. (b) Tenenbaum DJ. Food vs fuel: diversion of crops could cause more hunger. Environ Health Perspect. 2008;116:A254–A257. (c) Fischer F, Tropsch H. The preparation of synthetic oil mixtures (synthol) from carbon monoxide and hydrogen. Brennstoff Chem. 1923;4:276–285. (d) Schulz H. Short history and present trends of Fischer–Tropsch synthesis. Appl Catal A Gen. 1999;186:3–12.

[2]   Zhang Q, He D, Zhu Q. Recent progress in direct partial oxidation of methane to methanol. J Nat Gas Chem. 2003;309:263–268

[3]   King AD, King RB, Yang DB. Homogeneous catalysis of the water gas shift reaction using iron pentacarbonyl. J Am Chem Soc. 1980;102:1028–32.

[4]   McFarland E. Unconventional chemistry for unconventional natural gas. Science. 2012;338:340–2.

[5]   Hammond C, Conrad S, Hermans I. Oxidative methane upgrading. Chem Sus Chem. 2012;5:1668–86.

[6]   Caballero A, Pérez PJ. Methane as raw material in synthetic chemistry: the final frontier. Chem Soc Rev. 2013;42:8809–20.

[7]   Tomkins P, Ranocchiari M, Van Bokhoven JA. Direct conversion of methane to methanol under mild conditions over Cu-Zeolites and beyond. Acc Chem Res. 2017;50:418–25.

[8]   Tang P, Zhu Q, Wu Z, Ma D. Methane activation: the past and future. Energy Environ Sci. 2014;7:2580–91.

[9]   Dybkjær I, Aasberg Petersen K. Synthesis gas technology large-scale applications. Can J Chem Eng. 2016;94:607–12.

[10]   Olivos-Suarez AI, Szécsényi À, Hensen EJ, Ruiz-Martinez J, Pidko EA, Gascon J. Strategies for the direct catalytic valorization of methane using heterogeneous catalysis: challenges and opportunities. ACS Catal. 2016;6:2965–81.

[11]   Periana RA, Taube DJ, Gamble S, Taube H, Satoh T, Fujii H. Platinum catalysts for the high-yield oxidation of methane to a methanol derivative. Science. 1998;280:560–4.

[12]   McCoy M. German firm claims new route to methanesulfonic acid. Chem Eng News. 2016;94:10.

[13]   Groothaert MH, Smeets PJ, Sels BF, Jacobs PA, Schoonheydt A, Selective RA. Oxidation of methane by the Bis(μ-oxo)dicopper core stabilized on ZSM-5 and mordenite zeolites. J Am Chem Soc. 2005;127:1394–5.

[14]   Beznis NV, Weckhuysen BM, Bitter JH. Cu-ZSM-5 zeolites for the formation of methanol from methane and oxygen: probing the active sites and spectator species. Catal Lett. 2010;138:14–22.

[15]   Alayon EM, Nachtegaal M, Bodi A, Ranocchiari M, Van Bokhoven JA. Bis(μ-oxo) versus mono (μ-oxo)dicopper cores in a zeolite for converting methane to methanol: an in situ XAS and DFT investigation. Phys Chem Chem Phys. 2015;17:7681–93.

[16]   Vanelderen P, Snyder BE, Tsai M-L, Hadt RG, Vancauwenbergh J, Coussens O, et al. Spectroscopic definition of the copper active sites in mordenite: selective methane oxidation. J Am Chem Soc. 2015;137:6383–92.

[17]   Li G, Vassilev P, Sanchez-Sanchez M, Lercher JA, Hensen EJ, Pidko EA. Stability and reactivity of copper oxo-clusters in ZSM-5 zeolite for selective methane oxidation to methanol. J Catal. 2016;338:305–12.

[18]   Bozbag SE, Alayon EM, Pecháček J, Nachtegaal M, Ranocchiari M, Van Bokhoven JA. Methane to methanol over copper mordenite: yield improvement through multiple cycles and different synthesis techniques. Catal Sci Technol. 2016;6:5011–22.

[19]   Tomkins P, Mansouri A, Bozbag SE, Krumeich F, Park MB, Alayon EM, et al. Isothermal cyclic conversion of methane into methanol over copper-exchanged zeolite at low temperature. Angew Chem Int Ed. 2016;55:5467–71.

[20] Alayon EM, Nachtegaal M, Ranocchiari M, Van Bokhoven JA. Catalytic conversion of methane to methanol over Cu-mordenite. Chem Commun (Camb). 2012;48:404–6.

[21] Sushkevich VL, Palagin D, Ranocchiari M, Van Bokhoven JA. Selective anaerobic oxidation of methane enables direct synthesis of methanol. Science. 2017;356:523–7.

[22] Ikuno T, Zheng J, Vjunov A, Sanchez-Sanchez M, Ortuño MA, Pahls DR, et al. Methane oxidation to methanol catalyzed by Cu-Oxo clusters stabilized in NU-1000 metal–organic framework. J Am Chem Soc. 2017;139:10294–301.

[23] Li Y-N, Ma R, He L-N, Diao Z-F. Homogeneous hydrogenation of carbon dioxide to methanol. Catal Sci Technol. 2014;4:1498–512.

[24] Klankermayer J, Wesselbaum S, Beydoun K, Leitner W. Selective catalytic synthesis using the combination of carbon dioxide and hydrogen: catalytic chess at the interface of energy and chemistry. Angew Chem Int Ed. 2016;55:7296–343.

[25] Chauvier C, Cantat TA. Viewpoint on chemical reductions of carbon–oxygen bonds in renewable feedstocks including CO_2 and biomass. ACS Catal. 2017;7:2107–15.

[26] Dong K, Razzaq R, Hu Y, Ding K. Homogeneous reduction of carbon dioxide with hydrogen. Top Curr Chem. 2017;2:1–26.

[27] Wang W-H, Himeda Y, Muckerman JT, Manbeck GF, Fujita E. CO_2 hydrogenation to formate and methanol as an alternative to photo- and electrochemical CO_2 reduction. Chem Rev. 2015;115:12936–73.

[28] Annibale VT, Song D. Reversible formal insertion of CO_2 into a remote C-H bond of a ligand in a Ru(ii) complex at room temperature. Chem Commun (Camb). 2012;48:5416–8.

[29] Vogt M, Nerush A, Diskin-Posner Y, Ben-David Y, Milstein D. Reversible CO_2 binding triggered by metal-ligand cooperation in a rhenium(i) PNP pincer-type complex and the reaction with dihydrogen. Chem Sci. 2014;5:2043–51.

[30] Vogt M, Gargir M, Iron MA, Diskin-Posner Y, Ben-David Y, Milstein D, et al. Mode of activation of CO_2 by metal–ligand cooperation with reversible C–C and M–O bond formation at ambient temperature. Chem-Eur J. 2012;18:9194–7.

[31] Huff CA, Kampf JW, Sanford MS. Role of a noninnocent pincer ligand in the activation of CO_2 at (PNN)Ru(H)(CO). Organometallics. 2012;31:4643–5.

[32] Filonenko GA, Conley MP, Copéret C, Lutz M, Hensen EJ, Pidko EA. The impact of metal–ligand cooperation in hydrogenation of carbon dioxide catalyzed by ruthenium PNP pincer. ACS Catal. 2013;3:2522–6.

[33] Stichauer R, Helmers A, Bremer J, Rohdenburg M, Wark A, Lork E, et al. Rhenium(I) triscarbonyl complexes with redox-active amino- and iminopyridine ligands: metal–ligand cooperation as trigger for the reversible binding of CO_2 via a dearmomatization/rearomatization reaction sequence. Organometallics. 2017;36:839–48.

[34] Castro-Rodriguez I, Nakai H, Zakharov LN, Rheingold AL, Meyer K. A linear, O-coordinated eta1-CO_2 bound to uranium. Science. 2004;305:1757–9.

[35] Annibale VT, Song D. Reaction of dinuclear rhodium 4,5-diazafluorenyl-9-carboxylate complexes with H_2 and CO_2. Organometallics. 2014;33:2776–83.

[36] Annibale VT, Dalessandro DA, Song D. Tuning the reactivity of an actor ligand for tandem CO_2 and C–H activations: from spectator metals to metal-free. J Am Chem Soc. 2013;135:16175–83.

[37] Braunstein P, Matt D, Dusausoy Y, Fischer J, Mitschler A, Ricard L. Complexes of functional phosphines. 4. Coordination properties of (diphenylphosphino)acetonitrile, ethyl (diphenyl-phosphino)acetate and corresponding carbanions. Characterization of a new facile reversible carbon dioxide insertion into palladium(II) complexes. J Am Chem Soc. 1981;103:5115–25.

[38] Braunstein P, Matt D, Nobel D. Carbon dioxide activation and catalytic lactone synthesis by telomerization of butadiene and carbon dioxide. J Am Chem Soc. 1988;110:3207–12.

[39] Tominaga K-I, Sasaki Y, Kawai M, Watanabe T, Saito M. Ruthenium complex catalysed hydrogenation of carbon dioxide to carbon monoxide, methanol and methane. J Chem Soc Chem Commun. 1993;0:629–31.

[40] Wesselbaum S, Stein Vom T, Klankermayer J, Leitner W. Hydrogenation of carbon dioxide to methanol by using a homogeneous ruthenium-phosphine catalyst. Angew Chem Int Ed. 2012;51:7499–502.

[41] Wesselbaum S, Moha V, Meuresch M, Brosinski S, Thenert KM, Kothe J, et al. Hydrogenation of carbon dioxide to methanol using a homogeneous ruthenium–triphos catalyst: from mechanistic investigations to multiphase catalysis. Chem Sci. 2014;6:693–04.

[42] Schneidewind J, Adam R, Baumann W, Jackstell R, Beller M. Low-temperature hydrogenation of carbon dioxide to methanol with a homogeneous cobalt catalyst. Angew Chem. 2017;129:1916–9.

[43] Balaraman E, Gunanathan C, Zhang J, Shimon LJ, Milstein D. Efficient hydrogenation of organic carbonates, carbamates and formates indicates alternative routes to methanol based on CO₂ and CO. Nat Chem. 2011;3:609–14.

[44] Han Z, Rong L, Wu J, Zhang L, Wang Z, Ding K. Catalytic hydrogenation of cyclic carbonates: a practical approach from CO₂ and epoxides to methanol and diols. Angew Chem Int Ed. 2012;51:13041–5.

[45] Huff CA, Sanford MS. Cascade catalysis for the homogeneous hydrogenation of CO₂ to methanol. J Am Chem Soc. 2012;133:18122–5.

[46] Rochelle GT. Amine scrubbing for CO₂ capture. Science. 2009;325:1652–4.

[47] Dutcher B, Fan M, Russell AG. Amine-based CO₂ capture technology development from the beginning of 2013 – a review. ACS Appl Mater Interfaces. 2015;7:2137–48.

[48] Balaraman E, Ben-David Y, Milstein D. Unprecedented catalytic hydrogenation of urea derivatives to amines and methanol. Angew Chem Int Ed. 2011;50:11702–5.

[49] Balaraman E, Gnanaprakasam B, Shimon LJ, Milstein D. Direct hydrogenation of amides to alcohols and amines under mild conditions. J Am Chem Soc. 2010;132:16756–8.

[50] Rezayee NM, Huff CA, Sanford MS. Tandem amine and ruthenium-catalyzed hydrogenation of CO₂ to methanol. J Am Chem Soc. 2015;137:1028–31.

[51] Kothandaraman J, Goeppert A, Czaun M, Olah GA, Prakash GK. Conversion of CO₂ from air into methanol using a polyamine and a homogeneous ruthenium catalyst. J Am Chem Soc. 2016;138:778–81.

[52] Sahm H, Wagner F. Microbial assimilation of methanol. Febs J. 1973;36:250–6.

[53] Mani J-C, Pietruszko R, Theorell H. Methanol activity of alcohol dehydrogenases from human liver, horse liver, and yeast. Arch Biochem Biophys. 1970;140:52–9.

[54] Sheehan MC, Bailey CJ, Dowds BC, McConnell DJ. A new alcohol dehydrogenase, reactive towards methanol, from Bacillus stearothermophilus. Biochem J. 1988;252:661–6.

[55] Dorokhov YL, Shindyapina AV, Sheshukova EV, Komarova TV. Metabolic methanol: molecular pathways and physiological roles. Physiol Rev. 2015;95:603–44.

[56] Wagner F. Methanol: a fermentation substrate. Experientia. 1977;33:110–3.

[57] Patel RN, Bose HR, Mandy WJ, Hoare DS. Physiological studies of methane- and methanol-oxidizing bacteria: comparison of a primary alcohol dehydrogenase from Methylococcus capsulatus (Texas strain) and Pseudomonas species M27. J Bacteriol. 1972;110:570–7.

[58] Rasmussen M, Abdellaoui S, Minteer SD. Enzymatic biofuel cells: 30 years of critical advancements. Biosens Bioelectr. 2016;76:91–102.

[59] Ghosh M, Anthony C, Harlos K, Goodwin MG, Blake C. The refined structure of the quinoprotein methanol dehydrogenase from Methylobacterium extorquens at 1.94 å. Structure. 1995;3:177–87.

[60] Anthony C, Williams P. The structure and mechanism of methanol dehydrogenase. Biochim Biophys Acta (BBA) Prot Proteom. 2003;1647:18–23.

[61] Oubrie A, Dijkstra BW. Structural requirements of pyrroloquinoline quinone dependent enzymatic reactions. Prot Sci. 2000;9:1265–73.

[62] Jongejan A, Jongejan JA, Hagen WR. Direct hydride transfer in the reaction mechanism of quinoprotein alcohol dehydrogenases: a quantum mechanical investigation. J Comput Chem. 2001;22:1732–49.

[63] Dircks K. Recent advances in fuel cells for transportation applications. In: SAE international: 400 commonwealth drive. vol. 1. SAE Technical Paper, Warrendale, PA, United States, 1999:1999–01–0534.

[64] Hamnett A. Mechanism and electrocatalysis in the direct methanol fuel cell. Catal Today. 1997;38:445–57.

[65] Heinzel A, Barragan VM. A review of the state-of-the-art of the methanol crossover in direct methanol fuel cells. J Pow Sour. 1999;84:70–4.

[66] Iwasita T. Electrocatalysis of methanol oxidation. Electrochimica Acta. 2002;47:3663–74.

[67] Lamy C, Lima A, LeRhun V, Delime F, Coutanceau C, Léger J-M. Recent advances in the development of direct alcohol fuel cells (DAFC). J Pow Sour. 2002;105:283–96.

[68] Liu H, Song C, Zhang L, Zhang J, Wang H, Wilkinson DP. A review of anode catalysis in the direct methanol fuel cell. J Pow Sour. 2006;155:95–110.

[69] Neburchilov V, Martin J, Wang H, Zhang J. A review of polymer electrolyte membranes for direct methanol fuel cells. J Pow Sour. 2007;169:221–38.

[70] Lamy C, Léger JM, Srinivasan S. In: Bockris JO, Conway BE, editors. Modern aspects of electrochemistry, vol. 34. Springer US, New York, 2000.

[71] Van Den Tillaart JA, Kuster BF, Marin GB. Oxidative dehydrogenation of aqueous ethanol on a carbon supported platinum catalyst. Appl Catal A: General. 1994;120:127–45.

[72] Antolini E, Gonzalez ER. Alkaline direct alcohol fuel cells. J Pow Sour. 2010;195:3431–50.

[73] Zhou W, Zhou Z, Song S, Li W, Sun G, Tsiakaras P, et al. Pt based anode catalysts for direct ethanol fuel cells. Appl Catal B: Environmental. 2003;46:273–85.

[74] Garcia G, Baglio V, Stassi A, Pastor E, Antonucci V, Aricò AS. Investigation of Pt-Ru nanoparticle catalysts for low temperature methanol electro-oxidation. J Solid State Electrochem. 2007;11:1229–38.

[75] Mustain WE, Kim H, Narayanan V, Osborn T, Kohl PA. Electroless deposition and characterization of $PtxRu1–x$ catalysts on Pt/C nanoparticles for methanol oxidation. J Fuel Cell Sci Technol. 2010;7:041013.

[76] Jo J-N, Lee H-G, Yu Y-T. Size effect of Au nanoparticle on electrocatalytic activity of Pt-Au/C composite catalysts for methanol oxidation. Electrochem Solid-State Lett. 2011;14:B89–91.

[77] Hsu C-H, Liao H-Y, Wu Y-F, Kuo P-L. Benzylamine-assisted noncovalent exfoliation of graphite-protecting Pt nanoparticles applied as catalyst for methanol oxidation. ACS Appl Mater Interf. 2011;3:2169–72.

[78] Naidoo S, Naidoo QY, Vaivars G. Low temperature quaternary catalyst synthesis used for methanol and hydrogen oxidation on MWCNT. Integr Ferroelectrics. 2010;103:80–9.

[79] Kageyama S, Seino S, Nakagawa T, Nitani H, Ueno K, Daimon H, et al. Formation of PtRu alloy nanoparticle catalyst by radiolytic process assisted by addition of dl-tartaric acid and its enhanced methanol oxidation activity. J Nanopart Res. 2011;13:5275–87.

[80] Kashyout AB, Nassr A, Giorgi L. Electrooxidation of methanol on carbon supported Pt-Ru nanocatalysts prepared by ethanol reduction method. Int J Electrochem Sci. 2011;6:379–393

[81] Ross PN. "Electrocatalysis" in frontiers of electrochemistry. Lipkowski J, Ross PN, editors. New York: Ross PN NY: Wiley VCN, 1998.

[82] Dillon R, Srinivasan S, Aricò AS, Antonucci V. International activities in DMFC R&D: status of technologies and potential applications. J Pow Sour. 2004;127:112–26.

[83] Hamnett A. Mechanism and electrocatalysis in the direct methanol fuel cell. Catalysis Today. 1997;38:445.

[84] Liu Z, Zhang X, Hong L. Physical and electrochemical characterizations of nanostructured Pd/C and PdNi/C catalysts for methanol oxidation. Electrochem Commun. 2009;11:925–8.

[85] Kumar KS, Haridoss P, Seshadri SK. Synthesis and characterization of electrodeposited Ni–Pd alloy electrodes for methanol oxidation. Surf Coat Technol. 2008;202:1764–70.

[86] Shen PK, Xu C, Zeng R, Liu Y. Electro-oxidation of methanol on NiO-promoted Pt∕C and Pd∕C catalysts. Electrochem Solid-State Lett. 2006;9:A39–42.

[87] Wang M, Liu W, Huang C. Investigation of PdNiO/C catalyst for methanol electrooxidation. Int J Hydrogen Energy. 2009;34:2758–64.

[88] Fleischmann M, Korinek K, Pletcher D. The oxidation of organic compounds at a nickel anode in alkaline solution. J Electroanal Chem Interfacial Electrochem. 1971;31:39–49.

[89] Cui X, Zhu Y, Hua Z, Feng J, Liu Z, Chen L, et al. SnO$_2$ nanocrystal-decorated mesoporous ZSM-5 as a precious metal-free electrode catalyst for methanol oxidation. Energy Environ Sci. 2015;8:1261–6.

[90] Asghari E, Ashassi-Sorkhabi H, Vahed A, Rezaei-Moghadam B, Charmi GR. The use of a hierarchically platinum-free electrode composed of tin oxide decorated polypyrrole on nanoporous copper in catalysis of methanol electrooxidation. Thin Solid Films. 2016;598:6–15.

[91] Wu JB, Li ZG, Huang XH, Porous LY. Co$_3$O$_4$/NiO core/shell nanowire array with enhanced catalytic activity for methanol electro-oxidation. J Pow Sour. 2013;224:1–5.

[92] Tammam RH, Fekry AM, Saleh MM. Electrocatalytic oxidation of methanol on ordered binary catalyst of manganese and nickel oxide nanoparticles. Int J Hydrogen Energy. 2015;40:275–83.

[93] Fujishima A, Honda K. Electrochemical photolysis of water at a semiconductor electrode. Nature. 1972;238:37–38.

[94] Dai K, Peng T, Ke D, Wei B. Photocatalytic hydrogen generation using a nanocomposite of multi-walled carbon nanotubes and TiO$_2$ nanoparticles under visible light irradiation. Nanotechnology. 2009;20:125603.

[95] Qian S, Wang C, Liu W, Zhu Y, Yao W, Lu X. An enhanced CdS/TiO$_2$ photocatalyst with high stability and activity: effect of mesoporous substrate and bifunctional linking molecule. J Mater Chem. 2011;21:4945–52.

[96] Edri E, Rabinovich E, Niitsoo O, Cohen H, Bendikov T, Hodes G. Uniform coating of light-absorbing semiconductors by chemical bath deposition on sulfide-treated ZnO nanorods. J Phys Chem C. 2010;114:13092–7.

[97] Huang H, Li D, Lin Q, Zhang W, Shao Y, Chen Y, et al. Efficient degradation of benzene over LaVO$_4$/TiO$_2$ nanocrystalline heterojunction photocatalyst under visible light irradiation. Environ Sci Technol. 2009;43:4164–8.

[98] Park H, Choi W, Hoffmann MR. Effects of the preparation method of the ternary CdS/TiO 2/Pt hybrid photocatalysts on visible light-induced hydrogen production. J Mater Chem. 2008;18:2379–85.

[99] Galińska A, Walendziewski J. Photocatalytic water splitting over Pt–TiO$_2$ in the presence of sacrificial reagents. Energy & Fuels. 2005;19:1143–7.

[100] Bolton JR. Solar photoproduction of hydrogen: a review. Solar Energy. 1996;57:37–50.

[101] Bard AJ. Design of semiconductor photoelectrochemical systems for solar energy conversion. J Phys Chem. 1982;86:172–7.

[102] Hashimoto K, Kawai T, Sakata T. Photocatalytic reactions of hydrocarbons and fossil fuels with water. Hydrogen production and oxidation. J Phys Chem. 1984;88:4083–8.

[103] Sakata T. Photocatalysis of irradiated semiconductor surfaces: its application to water splitting and some organic reactions. J Photochem. 1985;29:205–15.

[104] Nada A, Barakat M, Hamed H, Mohamed N, Veziroglu T. Studies on the photocatalytic hydrogen production using suspended modified photocatalysts. Int J Hydrogen Energy. 2005;30:687–91.

[105] Zhang Z, Bondarchuk O, White JM, Kay BD, Dohnálek Z. Imaging adsorbate O–H bond cleavage: methanol on TiO_2(110). J Am Chem Soc. 2006;128:4198–9.

[106] Oviedo J, Sánchez-de-Armas R, San Miguel MÁ, Sanz JF. Methanol and water dissociation on TiO_2 (110): the role of surface oxygen. J Phys Chem C. 2008;112:17737–40.

[107] Zhao J, Yang J, Petek H. Theoretical study of the molecular and electronic structure of methanol on a TiO_2 (110) surface. Phys Rev B. 2009;80:235416.

[108] Zhou C, Ma Z, Ren Z, Mao X, Dai D, Yang X. Effect of defects on photocatalytic dissociation of methanol on TiO_2(110). Chem Sci. 2011;2:1980–3.

[109] Guo Q, Xu C, Ren Z, Yang W, Ma Z, Dai D, et al. Stepwise photocatalytic dissociation of methanol and water on TiO_2(110). J Am Chem Soc. 2012;134:13366–73.

[110] Awate SV, Deshpande SS, Rakesh K, Dhanasekaran P, Gupta NM. Role of micro-structure and interfacial properties in the higher photocatalytic activity of TiO_2-supported nanogold for methanol-assisted visible-light-induced splitting of water. Phys Chem Chem Phys. 2011;13:11329–39.

[111] Chiarello GL, Aguirre MH, Selli E. Hydrogen production by photocatalytic steam reforming of methanol on noble metal-modified TiO_2. J Catal. 2010;273:182–90.

[112] Kominami H, Sugahara H, Hashimoto K. Photocatalytic selective oxidation of methanol to methyl formate in gas phase over titanium(IV) oxide in a flow-type reactor. Catal Commun. 2010;11:426–9.

[113] Kudo A, Miseki Y. Heterogeneous photocatalyst materials for water splitting. Chem Soc Rev. 2009;38:253–78.

[114] Chiarello GL, Ferri D, Selli E. Effect of the CH_3OH/H_2O ratio on the mechanism of the gas-phase photocatalytic reforming of methanol on noble metal-modified TiO_2. J Catal. 2011;280:168–77.

[115] Pichat P, Herrmann JM, Disdier J, Courbon H, Mozzanega MN. Photocatalytic hydrogen-production from aliphatic-alcohols over a bifunctional platinum on titanium-dioxide catalyst. Nouv J Chim. 1981;5:627–36.

[116] Sakata T, Kawai T, Hashimoto K. Photochemical diode model of Pt/TiO_2 particle and its photocatalytic activity. Chem Phys Lett. 1982;88:50–4.

[117] Kawai M, Naito S, Tamaru K, Kawai T. The mechanism of photocatalytic hydrogen production from gaseous methanol and water: IR spectroscopic approach. Chem Phys Lett. 1983;98:377–80.

[118] Harada H, Ueda T. Photocatalytic activity of ultra-fine rutile in methanol-water solution and dependence of activity on particle size. Chem Phys Lett. 1984;106:229–31.

[119] Nishimoto S-I, Ohtani B, Kagiya T. Photocatalytic dehydrogenation of aliphatic alcohols by aqueous suspensions of platinized titanium dioxide. J Chem Soc, Faraday Trans 1: Phys Chem Cond Phases. 1985;81:2467–74.

[120] Dincer I, Acar C. Review and evaluation of hydrogen production methods for better sustainability. Int J Hydrogen Energy. 2015;40:11094–111.

[121] Hussein FH, Rudham R. Photocatalytic dehydrogenation of liquid alcohols by platinized anatase. J Chem Soc, Faraday Trans 1: Phys Chem Cond Phases. 1987;83:1631–9.

[122] Ebina Y, Tanaka A, Kondo JN, Domen K. Preparation of silica pillared Ca 2Nb 3O 10 and its photocatalytic activity. Chem Mater. 1996;8:2534–8.

[123] Patsoura A, Kondarides DI, Verykios XE. Photocatalytic degradation of organic pollutants with simultaneous production of hydrogen. Catalysis Today. 2007;124:94–102.

[124] Yang Y, Chang C, Idriss H. Photo-catalytic production of hydrogen form ethanol over M/TiO_2 catalysts (M=Pd, Pt or Rh). Appl Catal B: Environmental. 2006;67:217–22.

[125] Xu Q, Ma Y, Zhang J, Wang X, Feng Z, Li C. Enhancing hydrogen production activity and suppressing CO formation from photocatalytic biomass reforming on Pt/TiO$_2$ by optimizing anatase–rutile phase structure. J Catal. 2011;278:329–35.

[126] Chen X, Liu L, Yu PY, Mao SS. Increasing solar absorption for photocatalysis with black hydrogenated titanium dioxide nanocrystals. Science. 2011;331:746–50.

[127] Ikeda M, Kusumoto Y, Yakushijin Y, Somekawa S, Ngweniform P, Ahmmad B. Hybridized synergy effect among TiO$_2$, Pt and graphite silica on photocatalytic hydrogen production from water–methanol solution. Catal Commun. 2007;8:1943–6.

[128] Jitputti J, Pavasupree S, Suzuki Y, Yoshikawa S. Synthesis and photocatalytic activity for water-splitting reaction of nanocrystalline mesoporous titania prepared by hydrothermal method. J Solid State Chem. 2007;180:1743–9.

[129] Sun W, Zhang S, Liu Z, Wang C, Mao Z. Studies on the enhanced photocatalytic hydrogen evolution over Pt/PEG-modified TiO$_2$ photocatalysts. Int J Hydrogen Energy. 2008;33:1112–7.

[130] Hang L, Xing Y, Jia Chen J, Li Z, Tian Z, Rong Zheng F, et al. Unidirectional suppression of hydrogen oxidation on oxidized platinum clusters. Nat Commun. 2013;4:127.

[131] Wang C, Zhang X, Wei Y, Kong L, Chang F, Zheng H, et al. Correlation between band alignment and enhanced photocatalysis: a case study with anatase/TiO 2(B) nanotube heterojunction. Dalton Trans. 2015;44:13331–9.

[132] Zalas M, Laniecki M. Photocatalytic hydrogen generation over lanthanides-doped titania. Solar Energy Mater Solar Cells. 2005;89:287–96.

[133] Silva CG, Sampaio MJ, Marques RR, Ferreira LA, Tavares PB, Silva AM, et al. Photocatalytic production of hydrogen from methanol and saccharides using carbon nanotube-TiO$_2$ catalysts. Appl Catal B: Environmental. 2015;178:82–90.

[134] Moya A, Cherevan A, Marchesan S, Gebhardt P, Prato M, Eder D, et al. Oxygen vacancies and interfaces enhancing photocatalytic hydrogen production in mesoporous CNT/TiO$_2$ hybrids. Appl Catal B: Environmental. 2015;179:574–82.

[135] Gu Q, Long J, Zhuang H, Zhang C, Zhou Y, Wang X. Ternary Pt/SnOx/TiO$_2$ photocatalysts for hydrogen production: consequence of Pt sites for synergy of dual co-catalysts. Phys Chem Chem Phys. 2014;16:12521–34.

[136] Kakuta S, Abe T, Novel A. Example of molecular hydrogen generation from formic acid at visible-light-responsive photocatalyst. ACS Appl Mater Interfaces. 2009;1:2707–10.

[137] Matsumura M, Hiramoto M, Iehara T, Tsubomura H. Photocatalytic and photoelectrochemical reactions of aqueous solutions of formic acid, formaldehyde, and methanol on platinized cadmium sulfide powder and at a cadmium sulfide electrode. J Phys Chem. 1984;88:248–50.

[138] Wang X, Maeda K, Thomas A, Takanabe K, Xin G, Carlsson JM, et al. A metal-free polymeric photocatalyst for hydrogen production from water under visible light. Nat Mater. 2008;8:76–80.

[139] Han B, Hu YH. Highly efficient temperature-induced visible light photocatalytic hydrogen production from water. J Phys Chem C. 2015;119:18927–34.

[140] Bowker M, Davies PR, Al-Mazroai LS. Photocatalytic reforming of glycerol over gold and palladium as an alternative fuel source. Catal Lett. 2009;128:253–5.

[141] Greaves J, Al-Mazroai L, Nuhu A, Davies P, Bowker M. Photocatalytic methanol reforming on Au/TiO$_2$ for hydrogen production. Gold Bull. 2006;39:216–9.

[142] Borgarello E, Pelizzetti E. UV-VIS light photocatalytic dihydrogen production from aliphatic alcohols over semiconductor particles. Chim & L Industria. 1983;65:474–8.

[143] Bahruji H, Bowker M, Brookes C, Davies PR, Wawata I. The adsorption and reaction of alcohols on TiO$_2$ and Pd/TiO$_2$ catalysts. Appl Catal A: General. 2013;454:66–73.

[144] Su R, Tiruvalam R, Logsdail AJ, He Q, Downing CA, Jensen MT, et al. Designer titania-supported Au–Pd nanoparticles for efficient photocatalytic hydrogen production. ACS Nano. 2014;8:3490–7.

[145] Bowker M, Morton C, Kennedy J, Bahruji H, Greves J, Jones W, et al. Hydrogen production by photoreforming of biofuels using Au, Pd and Au–Pd/TiO$_2$ photocatalysts. J Catal. 2014;310:10–5.

[146] Parida KM, Martha S, Das DP, Biswal N. Facile fabrication of hierarchical N-doped GaZn mixed oxides for water splitting reactions. J Mater Chem. 2010;20:7144–9.

[147] Wang X, Peng W-C, Li X-Y. Photocatalytic hydrogen generation with simultaneous organic degradation by composite CdS–ZnS nanoparticles under visible light. Int J Hydrogen Energy. 2014;39:13454–61.

[148] Kawai T, Sakata T. Photocatalytic hydrogen production from liquid methanol and water. J Chem Soc, Chem Commun. 1980;0:694–5.

[149] Rosseler O, Shankar MV, Du MK, Schmidlin L, Keller N, Keller V. Solar light photocatalytic hydrogen production from water over Pt and Au/TiO$_2$(anatase/rutile) photocatalysts: influence of noble metal and porogen promotion. J Catal. 2010;269:179–90.

[150] Bowker M, Millard L, Greaves J, James D, Soares J. Photocatalysis by au nanoparticles: reforming of methanol. Gold Bull. 2004;37:170–3.

[151] Wu G, Chen T, Su W, Zhou G, Zong X, Lei Z, et al. H$_2$ production with ultra-low CO selectivity via photocatalytic reforming of methanol on Au/TiO$_2$ catalyst. Int J Hydrogen Energy. 2008;33:1243–51.

[152] Park M-S, Kang M. The preparation of the anatase and rutile forms of Ag–TiO$_2$ and hydrogen production from methanol/water decomposition. Mater Lett. 2008;62:183–7.

[153] Kudo A, Domen K, Maruya K-I, Onishi T. Photocatalytic activities of TiO$_2$ loaded with NiO. Chem Phys Lett. 1987;133:517–9.

[154] Kandiel TA, Dillert R, Robben L, Bahnemann DW. Photonic efficiency and mechanism of photocatalytic molecular hydrogen production over platinized titanium dioxide from aqueous methanol solutions. Catal Today. 2011;161:196–201.

[155] Kudo A, Tanaka A, Domen K, Maruya K-I, Aika K-I, Onishi T. Photocatalytic decomposition of water over NiOK4Nb6O17 catalyst. J Catal. 1988;111:67–76.

[156] Miwa T, Kaneco S, Katsumata H, Suzuki T, Ohta K, Chand Verma S, et al. Photocatalytic hydrogen production from aqueous methanol solution with CuO/Al$_2$O$_3$/TiO$_2$ nanocomposite. Int J Hydrogen Energy. 2010;35:6554–60.

[157] Xu S, Sun DD. Significant improvement of photocatalytic hydrogen generation rate over TiO$_2$ with deposited CuO. Int J Hydrogen Energy. 2009;34:6096–104.

[158] Valero JM, Obregón S, Active Site CG. Considerations on the photocatalytic H$_2$ evolution performance of Cu-doped TiO$_2$ obtained by different doping methods. ACS Catal. 2014;4:3320–9.

[159] Mozia S, Kułagowska A, Morawski A. Formation of combustible hydrocarbons and H$_2$ during photocatalytic decomposition of various organic compounds under aerated and deaerated conditions. Molecules. 2014;19:19633–47.

[160] Puga AV. Photocatalytic production of hydrogen from biomass-derived feedstocks. Coordin Chem Rev. 2016;315:1–66.

[161] Yamakawa T, Katsurao T, Shinoda S, Saito Y. Photocatalysis of trans-[RhCl(CO)(PPh3)2] under MLCT irradiation for 2-propanol dehydrogenation. J Mol Catal. 1987;42:183–6.

[162] Nomura K, Saito Y, Shinoda S. Photocatalytic dehydrogenation of 2-propanol with carbonyl (halogeno)phosphine-rhodium complexes. J Mol Catal. 1989;52:99–111.

[163] Morton D, Cole-Hamilton DJ, Utuk ID, Paneque-Sosa M, Lopez-Poveda M. Hydrogen production from ethanol catalysed by group 8 metal complexes. J Chem Soc, Dalton Trans. 1989;0:489–95.

[164] Yoshida T, Okano T, Otsuka S. Activation of water molecules. 4. Generation of dihydrogen from water by rhodium(I) hydrido and rhodium(0) carbonyl compounds. J Am Chem Soc. 1980;102:5966–7.

[165] Takahashi T, Shinoda S, Saito Y. The mechanisms of photocatalytic dehydrogenation of methanol in the liquid phase with cis- [Rh$_2$Cl$_2$(CO)$_2$(dpm)$_2$] complex catalyst. J Mol Catal. 1985;31:301–9.

[166] Yamamoto H, Shinoda S, Saito Y. Photocatalytic dehydrogenation of methanol in the liquid phase with cis-Rh2Cl2(CO)2(dpm)2 and Pd2Cl2(dpm)2 complex catalysts. J Mol Catal. 1985;30:259–66.

[167] Shinoda S, Moriyama H, Kise Y, Saito Y. Photo-enhanced production of hydrogen by liquid-phase catalytic dehydrogenation of propan-2-ol with rhodium–tin chloride complexes. J Chem Soc, Chem Commun. 1978;0:348–9.

[168] Moriyama H, Aoki T, Shinoda S, Saito Y. Photoenhanced catalytic dehydrogenation of propan-2-ol with homogeneous rhodium–tin complexes. J Chem Soc, Perkin Trans. 1982;2:369–74.

[169] Matsubara T, Saito Y, Yamakawa T, Shinoda S. Photocatalysis of tin(II)-coordinated iridium complexes for energy storing with quantum yield higher than unity in 2-propanol dehydrogenation. J Mol Catal. 1991;67:175–84.

[170] Makita K, Nomura K, Saito Y. Photocatalytic dehydrogenation of methanol using [IrH(SnCl3)5]$^{3-}$ complex. J Mol Catal. 1994;89:143–9.

[171] Yamakawa T, Miyake H, Moriyama H, Shinoda S, Saito Y. Energy-storing photocatalysis of transition metal complexes with high quantum efficiency. J Chem Soc, Chem Commun. 1986;0:326–7.

[172] Matsubara T, Saito Y, Yamakawa T, Shinoda S. Thermo- and photocatalytic dehydrogenation of 2-propanol with [RuL(SnCl3)5]4– (L Cl– or SnCl3–) complexes. J Mol Catal. 1993;79:29–37.

[173] Moriyama H, Pregosin PS, Saito Y, Yamakawa T. Synthesis and tin-119 nuclear magnetic resonance studies of trichlorostannate(II) complexes of ruthenium, osmium, and iridium. J Chem Soc, Dalton Trans. 1984;0:2329–32.

[174] Irie R, Li X, Saito Y. Photocatalytic dehydrogenation of secondary alcohols with rhodium porphyrin complex. J Mol Catal. 1983;18:263–5.

[175] Irie R, Li X, Saito Y. Reaction mechanism of photocatalysis for the liquid-phase dehydrogenation of 2-propanol with rhodium porphyrin complex. J Mol Catal. 1984;23:17–22.

[176] Irie R, Li X, Saito Y. Quantum chemical interpretation of the dihydrogen formation process in photocatalytic 2-propanol dehydrogenation with rhodium porphyrin complex. J Mol Catal. 1984;23:23–7.

[177] Li X, Shinoda S, Saito Y. Photocatalytic liquid-phase dehydrogenation of cyclohexanol with rhodium porphyrin complex. J Mol Catal. 1989;49:113–9.

[178] Ligthart GB, Meijer RH, Donners MP, Meuldijk J, Vekemans JA, Hulshof LA. Highly sustainable catalytic dehydrogenation of alcohols with evolution of hydrogen gas. Tetrah Lett. 2003;44:1507–9.

[179] Gärtner F, Losse S, Boddien A, Pohl M-M, Denurra S, Junge H, et al. Hydrogen evolution from water/alcohol mixtures: effective in situ generation of an active Au/TiO$_2$ catalyst. Chem Sus Chem. 2011;5:530–3.

[180] Cuendet P, Rao KK, Grätzel M, Hall DO. Light induced H$_2$ evolution in a hydrogenase-TiO$_2$ particle system by direct electron transfer or via rhodium complexes. Biochimie. 1986;68:217–21.

[181] Wee J-H. Applications of proton exchange membrane fuel cell systems. Renew Sus Energy Rev. 2007;11:1720–38.

[182] Pettersson LJ, Westerholm R. State of the art of multi-fuel reformers for fuel cell vehicles: problem identification and research needs. Int J Hydrogen Energy. 2001;26:243–64.

[183] Iulianelli A, Ribeirinha P, Mendes A, Basile A. Methanol steam reforming for hydrogen generation via conventional and membrane reactors: a review. Renew Sus Energy Rev. 2014;29:355–68.

[184] Madej-Lachowska M, Kulawska M, Słoczyński J. Methanol as a high purity hydrogen source for fuel cells: a brief review of catalysts and rate expressions. Chem Process Eng. 2017;38:147–62.

[185] Chein RY, Chen YC, Lin YS, Chung JN. Hydrogen production using integrated methanol-steam reforming reactor with various reformer designs for PEM fuel cells. Int J Energy Res. 2012;36:466–76.

[186] Basile A, Iulianelli A, Longo T, Liguori S, De Falco M. Pd-based selective membrane state-of-the-art. In: De De Falco M., Marrelli L., Iaquaniello G. (eds) Membrane Reactors for Hydrogen Production Processes. Springer, London, 2011:21–55.

[187] Tosti S, Basile A, Borgognoni F, Capaldo V, Cordiner S, Di Cave S, et al. Low temperature ethanol steam reforming in a Pd-Ag membrane reactor Part 1: Ru-based catalyst. J Membr Sci. 2008;308:250–7.

[188] Yong ST, Ooi CW, Chai SP, Wu XS. Review of methanol reforming-Cu-based catalysts, surface reaction mechanisms, and reaction schemes. Int J Hydrogen Energy. 2013;38:9541–52.

[189] Hohn KL, Lin YC. Catalytic partial oxidation of methanol and ethanol for hydrogen generation. Chem Sus Chem. 2009;2:927–40.

[190] Amphlett JC, Evans MJ, Mann RF, Weir RD. Hydrogen production by the catalytic steam reforming of methanol: part 2: kinetics of methanol decomposition using girdler G66B catalyst. Can J Chem Engineering. 1985;63:605–11.

[191] Bartoň J, Pour V. Kinetics of catalytic conversion of methanol at higher pressures. Collect Czechoslov Chem Commun. 1980;45:3402–7.

[192] Pour V, Bartoň J, Benda A. Kinetics of catalyzed reaction of methanol with water vapour. Collect Czechoslov Chem Commun. 1975;40:2923–34.

[193] Santacesaria E, Carrá S. Kinetics of catalytic steam reforming of methanol in a CSTR reactor. Appl Catal. 1983;5:345–58.

[194] Geissler K, Newson E, Vogel F, Truong T-B, Hottinger P, Wokaun A. Autothermal methanol reforming for hydrogen production in fuel cell applications. Phys Chem Chem Phys. 2001;3:289–93.

[195] Turco M, Bagnasco G, Costantino U, Marmottini F, Montanari T, Ramis G, et al. Production of hydrogen from oxidative steam reforming of methanol. Catalytic activity and reaction mechanism on $Cu/ZnO/Al_2O_3$ hydrotalcite-derived catalysts. J Catal. 2004;228:56–65.

[196] Agrell J, Birgersson H, Boutonnet M. Steam reforming of methanol over a $Cu/ZnO/Al_2O_3$ catalyst: a kinetic analysis and strategies for suppression of CO formation. J Pow Sour. 2002;106:249–57.

[197] Takahashi K, Takezawa N, Kobayashi H. The mechanism of steam reforming of methanol over a copper-silica catalyst. Appl Catal. 1982;2:363–6.

[198] Jiang CJ, Trimm DL, Wainwright MS, Cant NW. Kinetic mechanism for the reaction between methanol and water over a Cu-ZnO-Al₂O₃ catalyst. Appl Catal A: General. 1993;97:145–58.

[199] Jiang CJ, Trimm DL, Wainwright MS, Cant NW. Kinetic study of steam reforming of methanol over copper-based catalysts. Appl Catal A: General. 1993;93:245–55.

[200] Breen JP, Ross JR. Methanol reforming for fuel-cell applications: development of zirconia-containing Cu–Zn–Al catalysts. Catal Today. 1999;51:521–33.

[201] Peppley BA, Amphlett JC, Kearns LM, Mann RF. Methanol–steam reforming on $Cu/ZnO/Al_2O_3$ catalysts. Part 2. A comprehensive kinetic model. Appl Catal A: General. 1999;179:31–49.

[202] Peppley BA, Amphlett JC, Kearns LM, Mann RF. Methanol–steam reforming on $Cu/ZnO/Al_2O_3$. Part 1: the reaction network. Appl Catal A: General. 1999;179:21–9.

[203] Takezawa N, Iwasa N. Steam reforming and dehydrogenation of methanol: difference in the catalytic functions of copper and group VIII metals. Catal Today. 1997;36:45–56.

[204] Shishido T, Yamamoto Y, Morioka H, Takehira K. Production of hydrogen from methanol over Cu/ZnO and Cu/ZnO/Al$_2$O$_3$ catalysts prepared by homogeneous precipitation: steam reforming and oxidative steam reforming. J Mol Catal A: Chemical. 2007;268:185–94.

[205] Rabe S, Vogel F. A thermogravimetric study of the partial oxidation of methanol for hydrogen production over a Cu/ZnO/Al$_2$O$_3$ catalyst. Appl Catal B: Environmental. 2008;84:827–34.

[206] Murcia-Mascaros S, Navarro RM, Gomez-Sainero L, Costantino U, Nocchetti M, Fierro JL. Oxidative methanol reforming reactions on CuZnAl catalysts derived from hydrotalcite-like precursors. J Catal. 2001;198:338–47.

[207] Agrell J, Boutonnet M, Fierro JL. Production of hydrogen from methanol over binary Cu/ZnO catalysts. Appl Catal A: General. 2003;253:213–23.

[208] Agrell J. Production of hydrogen from methanol over Cu/ZnO catalysts promoted by ZrO$_2$ and Al$_2$O$_3$. J Catal. 2003;219:389–403.

[209] Frank B, Jentoft F, Soerijanto H, Kröhnert J, Schlögl R, Schomäcker R. Steam reforming of methanol over copper-containing catalysts: influence of support material on microkinetics. J Catal. 2007;246:177–92.

[210] Sá S, Silva H, Brandão L, Sousa JM, Mendes A. Catalysts for methanol steam reforming – a review. Appl Catal B: Environmental. 2010;99:43–57.

[211] Matsumura Y, Ishibe H. Suppression of CO by-production in steam reforming of methanol by addition of zinc oxide to silica-supported copper catalyst. J Catal. 2009;268:282–9.

[212] Matter P. Steam reforming of methanol to H$_2$ over nonreduced Zr-containing CuO/ZnO catalysts. J Catal. 2004;223:340–51.

[213] Chen C-C, Jeng M-S, Leu C-H, Yang C-C, Lin Y-L, King S-C, et al. Low-level CO in hydrogen-rich gas supplied by a methanol processor for PEMFCs. Chem Eng Sci. 2011;66:5095–106.

[214] Ayalur Chattanathan S, Adhikari S, Abdoulmoumine N. A review on current status of hydrogen production from bio-oil. Renew Sus Energy Rev. 2012;16:2366–72.

[215] Conant T, Karim A, Lebarbier V, Wang Y, Girgsdies F, Schlögl R, et al. Stability of bimetallic Pd–Zn catalysts for the steam reforming of methanol. J Catal. 2008;257:64–70.

[216] Ma Y, Guan G, Shi C, Zhu A, Hao X, Wang Z, et al. Low-temperature steam reforming of methanol to produce hydrogen over various metal-doped molybdenum carbide catalysts. Int J Hydrogen Energy. 2014;39:258–66.

[217] Cao J, Ma Y, Guan G, Hao X, Ma X, Wang Z, et al. Reaction intermediate species during the steam reforming of methanol over metal modified molybdenum carbide catalysts. Appl Catal B: Environmental. 2016;189:12–8.

[218] Kameoka S, Tanabe T, Tsai AP. Spinel CuFe$_2$O$_4$: a precursor for copper catalyst with high thermal stability and activity. Catal Lett. 2005;100:89–93.

[219] Tanaka Y, Kikuchi R, Takeguchi T, Eguchi K. Steam reforming of dimethyl ether over composite catalysts of γ-Al$_2$O$_3$ and Cu-based spinel. Appl Catal B: Environmental. 2005;57:211–22.

[220] Faungnawakij K, Shimoda N, Fukunaga T, Kikuchi R, Eguchi K. Cu-based spinel catalysts CuB$_2$O$_4$ (B=Fe, Mn, Cr, Ga, Al, Fe0.75Mn0.25) for steam reforming of dimethyl ether. Appl Catal A: General. 2008;341:139–45.

[221] Faungnawakij K, Kikuchi R, Shimoda N, Fukunaga T, Eguchi K. Effect of thermal treatment on activity and durability of CuFe$_2$O$_4$–Al$_2$O$_3$ composite catalysts for steam reforming of dimethyl ether. Angew Chem Int Ed. 2008;47:9314–7.

[222] Kurtz M, Wilmer H, Genger T, Hinrichsen O, Muhler M. Deactivation of supported copper catalysts for methanol synthesis. Catal Lett. 2003;86:77–80.

[223] Cao W, Chen G, Li S, Yuan Q. Methanol-steam reforming over a ZnO–Cr$_2$O$_3$/CeO$_2$–ZrO$_2$/Al$_2$O$_3$ catalyst. Chem Eng J. 2006;119:93–8.

[224] Valdés-Solís T, Marbán G, Fuertes AB. Nanosized catalysts for the production of hydrogen by methanol steam reforming. Catal Today. 2006;116:354–60.

[225] Roduner E. Selected fundamentals of catalysis and electrocatalysis in energy conversion reactions – a tutorial. Catal Today. 2017;309:263–268

[226] Trincado M, Banerjee D, Grützmacher H. Molecular catalysts for hydrogen production from alcohols. Energy Environ Sci. 2014;7:2464–503.

[227] Cheung K, Wong W, Ma D, Lai T, Wong K. Transition metal complexes as electrocatalysts – development and applications in electro-oxidation reactions. Coordin Chem Rev. 2007;251:2367–85.

[228] Andrieux CP, Dumas-Bouchiat JM, Savéant JM. Homogeneous redox catalysis of electrochemical reactions. J Electroanal Chem Interfacial Electrochem. 1978;87:39–53.

[229] Liu Y, Zhao S-F, Guo S-X, Bond AM, Zhang J, Zhu G, et al. Electrooxidation of ethanol and methanol using the molecular catalyst [{Ru $4O_4$(OH) 2(H_2O) 4}(γ-SiW 10O 36) 2] 10⁻. J Am Chem Soc. 2016;138:2617–28.

[230] Serra D, Correia MC, McElwee-White L. Iron and ruthenium heterobimetallic carbonyl complexes as electrocatalysts for alcohol oxidation: electrochemical and mechanistic studies. Organometallics. 2011;30:5568–77.

[231] Nomura K, Saito Y, Shinda S. Photoenhanced catalytic dehydrogenation of methanol with tin (II)-coordinated iridium complexes. J Mol Catal. 1989;50:303–13.

[232] Wakizaka M, Matsumoto T, Tanaka R, Chang H-C. Dehydrogenation of anhydrous methanol at room temperature by o-aminophenol-based photocatalysts. Nat Commun. 2016;7:12333.

[233] Dobscn A, Robinson SD. Catalytic dehydrogenation of primary and secondary alcohols by Ru(OCOCF$_3$)$_2$(CO)(PPh$_3$)$_2$. J Organomet Chem. 1975;87:C52–3.

[234] Dobson A, Robinson SD. Complexes of the platinum metals. 7. Homogeneous ruthenium and osmium catalysts for the dehydrogenation of primary and secondary alcohols. Inorg Chem. 1977;16:137–42.

[235] Shinoda S, Itagaki H, Saito Y. Dehydrogenation of methanol in the liquid phase with a homogeneous ruthenium complex catalyst. J Chem Soc, Chem Commun. 1985;0:860–1.

[236] Itagaki H, Saito Y, Shinoda S. Transition metal homogeneous catalysis for liquidphase dehydrogenation of methanol. J Mol Catal. 1987;41:209–20.

[237] Morton D, Cole-Hamilton DJ. Rapid thermal hydrogen production from alcohols catalysed by [Rh(2,2′-bipyridyl)$_2$]Cl. J Chem Soc, Chem Commun. 1987;0:248–9.

[238] Morton D, Cole-Hamilton DJ. Molecular hydrogen complexes in catalysis: highly efficient hydrogen production from alcoholic substrates catalysed by ruthenium complexes. J Chem Soc, Chem Commun. 1988;0:1154–6.

[239] Yang L-C, Ishida T, Yamakawa T, Shinoda S. Mechanistic study on dehydrogenation of methanol with [RuCl$_2$(PR$_3$)$_3$]-type catalyst in homogeneous solutions. J Mol Catalysis A: Chem. 1996;108:87–93.

[240] Sieffert N, Hydrogen BM. Generation from alcohols catalyzed by ruthenium–triphenylphosphine complexes: multiple reaction pathways. J Am Chem Soc. 2010;132:8056–70.

[241] Nielsen MM, Alberico EE, Baumann WW, Drexler H-J, Junge HH, Gladiali SS, et al. Low-temperature aqueous-phase methanol dehydrogenation to hydrogen and carbon dioxide. Nature. 2013;495:85–9.

[242] Rodríguez-Lugo RE, Trincado M, Vogt M, Tewes F, Santiso-Quinones G, Grützmacher H. A homogeneous transition metal complex for clean hydrogen production from methanol-water mixtures. Nat Chem. 2013;5:342–7.

[243] Grützmacher H. Cooperating ligands in catalysis. Angew Chem Int Ed Engl. 2008;47:1814–8.

[244] Khusnutdinova JR, Milstein D. Metal-Ligand Cooperation. Angew Chem Int Ed. 2015;54:12236–73.

[245] Crabtree RH. Multifunctional ligands in transition metal catalysis. New J Chem. 2011;35:18–23.

[246] Bertoli M, Choualeb A, Lough AJ, Moore B, Spasyuk D, Gusev DG. Osmium and ruthenium catalysts for dehydrogenation of alcohols. Organometallics. 2011;30:3479–82.

[247] Spasyuk D, Smith S, Gusev DG. From esters to alcohols and back with ruthenium and osmium catalysts. Angew Chem Int Ed. 2012;51:2772–5.

[248] Nielsen M, Junge H, Kammer A, Beller M. Towards a green process for bulk-scale synthesis of ethyl acetate: efficient acceptorless dehydrogenation of ethanol. Angew Chem Int Ed. 2012;51:5711–3.

[249] Sinha V, Pribanic B, Trincado M, De Bruin B, Gruetzmacher H. Ligand- and metal-based reactivity of a neutral ruthenium diolefin diazadiene complex; the innocent, the guilty, and the suspicious. Chem Eur J. 2018. in press. DOI: 10.1002/chem.201705957.

[250] Yang X. Mechanistic insights into ruthenium-catalyzed production of H$_2$ and CO$_2$ from methanol and water: a DFT study. ACS Catalysis. 2014;4:1129–33.

[251] Lei M, Pan Y, Ma X. The nature of hydrogen production from aqueous-phase methanol dehydrogenation with ruthenium pincer complexes under mild conditions. Eur J Inorg Chem. 2015;2015:794–803.

[252] Dub PA, Gordon JC. Metal–ligand bifunctional catalysis: the "Accepted" mechanism, the issue of concertedness, and the function of the ligand in catalytic cycles involving hydrogen atoms. ACS Catal. 2017;7:6635–55.

[253] Monney A, Barsch E, Sponholz P, Junge H, Ludwig R, Beller M. Base-free hydrogen generation from methanol using a bi-catalytic system. Chem Commun (Camb). 2014;50:707–9.

[254] Hu P, Diskin-Posner Y, Ben-David Y, Milstein D. Reusable homogeneous catalytic system for hydrogen production from methanol and water. ACS Catal. 2014;4:2649–52.

[255] Campos J, Sharninghausen LS, Manas MG, Crabtree RH. Methanol dehydrogenation by Iridium N-heterocyclic carbene complexes. Inorg Chem. 2015;54:5079–84.

[256] Fujita K-I, Kawahara R, Aikawa T, Yamaguchi R. Hydrogen production from a methanol-water solution catalyzed by an anionic iridium complex bearing a functional bipyridonate ligand under weakly basic conditions. Angew Chem Int Ed. 2015;54:9057–60.

[257] Heim LE, Thiel D, Gedig C, Deska J, Prechtl MH. Bioinduced room-temperature methanol reforming. Angew Chem Int Ed. 2015;54:10308–12.

[258] Alberico E, Sponholz P, Cordes C, Nielsen M, Drexler H-J, Baumann W, et al. Selective hydrogen production from methanol with a defined iron pincer catalyst under mild conditions. Angew Chem. 2013;125:14412–6.

[259] Chakraborty S, Brennessel WW, Jones WD. A molecular iron catalyst for the acceptorless dehydrogenation and hydrogenation of N-heterocycles. J Am Chem Soc. 2014;136:8564–7.

[260] Bornschein C, Werkmeister S, Wendt B, Jiao H, Alberico E, Baumann W, et al. Mild and selective hydrogenation of aromatic and aliphatic (di)nitriles with a well-defined iron pincer complex. Nat Commun. 2014;5:1193.

[261] Bielinski EA, Lagaditis PO, Zhang Y, Mercado BQ, Würtele C, Bernskoetter WH, et al. Lewis acid-assisted formic acid dehydrogenation using a pincer-supported iron catalyst. J Am Chem Soc. 2014;136:10234–7.

[262] Chakraborty S, Lagaditis PO, Förster M, Bielinski EA, Hazari N, Holthausen MC, et al. Well-defined iron catalysts for the acceptorless reversible dehydrogenation-hydrogenation of alcohols and ketones. ACS Catal. 2014;4:3994–4003.

[263] (a) Valyaev DA, Lavigne G, Lugan N. Manganese organometallic compounds in homogeneous catalysis: past, present, and prospects. Coordin Chem Rev. 2016;308:191–235. (b) Zell T, Langer R. From ruthenium to iron and manganese – a mechanistic view on challenges and design principles of base metal hydrogenation catalysts. Chem Cat Chem. 2017. DOI: 10.1002/cctc.201701722.

[264] Elangovan S, Topf C, Fischer S, Jiao H, Spannenberg A, Baumann W, et al. Selective catalytic hydrogenations of nitriles, ketones, and aldehydes by well-defined manganese pincer complexes. J Am Chem Soc. 2016;138:8809–14.

[265] Mastalir M, Glatz M, Gorgas N, Stöger B, Pittenauer E, Allmaier G, et al. Divergent coupling of alcohols and amines catalyzed by isoelectronic hydride Mn Iand Fe IIPNP pincer complexes. Chem-Eur J. 2016;22:12316–20.

[266] Mukherjee A, Nerush A, Leitus G, Shimon LJ, Ben-David Y, Jalapa NA, et al. Manganese-catalyzed environmentally benign dehydrogenative coupling of alcohols and amines to form aldimines and H$_2$: a catalytic and mechanistic study. J Am Chem Soc. 2016;138:4298–301.

[267] Tondreau AM, Boncella JM. 1,2-addition of formic or oxalic acid to −N{CH$_2$CH$_2$(PiPr$_2$)}$_2$-supported Mn(I) dicarbonyl complexes and the manganese-mediated decomposition of formic acid. Organometallics. 2016;35:2049–52.

[268] Vijjamarri S, Chidara VK, Rousova J, Du G. Dehydrogenative coupling of alcohols and carboxylic acids with hydrosilanes catalyzed by a salen−Mn(V) complex. Catal Sci Technol. 2016;6:3886–92.

[269] Kallmeier F, Irrgang T, Dietel T, Kempe R. Highly active and selective manganese C=O bond hydrogenation catalysts: the importance of the multidentate ligand, the ancillary ligands, and the oxidation state. Angew Chem Int Ed. 2016;55:11806–9.

[270] Elangovan S, Neumann J, Sortais J-B, Junge K, Darcel C, Beller M. Efficient and selective N-alkylation of amines with alcohols catalysed by manganese pincer complexes. Nat Commun. 2016;7:12641.

Andrés Suárez

6 Hydrogenation of carbonyl compounds of relevance to hydrogen storage in alcohols

Abstract: Alcohols are a promising source for the sustainable production of hydrogen that may also serve as rechargeable liquid organic hydrogen carriers (LOHCs). Metal-catalyzed acceptorless dehydrogenation of alcohols produces carbonyl derivatives as H_2-depleted by-products, which by means of a hydrogenation reaction can be reconverted to the initial alcohols. Hence, reversible H_2-storage systems based on pairs of secondary alcohols/ketones and primary alcohols/carboxylic acid derivatives may be envisaged. In this contribution, the hydrogenation of carbonyl derivatives, including ketones, esters, amides and carboxylic acids, is reviewed from the perspective of the hydrogen storage in alcohols.

Keywords: hydrogen storage, homogeneous catalysis, hydrogenation, carbonyl compounds, dehydrogenation

6.1 Introduction

The search for solutions to the issue of hydrogen storage is a pivotal aspect for the full implementation of a global economy based on hydrogen as an energy carrier, the so-called Hydrogen Economy [1]. In this respect, the incorporation of hydrogen into small organic molecules through the formation of covalent bonds has been proposed as a potential method for chemical energy storage [2, 3]. Since ideal H_2-storage systems require low molecular weights, wide availability of the hydrogen carrier, and high gravimetric and volumetric hydrogen contents, liquid organic hydrogen carriers (LOHCs) are of considerable interest due to their physical and chemical properties. Among other hydrogen sources, alcohols are an interesting alternative due to their wide availability from both human and natural sources. As described in detail in the previous chapter of this book [4] and elsewhere [5–7], depending on the catalyst employed and reaction conditions, acceptorless alcohol dehydrogenation produces different carbonyl derivatives, which can be regarded as the H_2-depleted carrier counterparts. Since reversibility is one of the central questions to hydrogen storage [8], development of H_2-storage systems based on alcohols/carbonyl derivatives pairs is of practical interest. Chemically bonded hydrogen can be incorporated into an organic molecule by means of a hydrogenation reaction assisted by a catalyst. This procedure

coupled with the reverse dehydrogenation process may serve as an efficient method for the storage (hydrogenation) and release of hydrogen (dehydrogenation). Particularly appealing is the full realization of a hydrogen storage cycle when the dehydrogenation of the carrier and hydrogenation of H_2-depleted derivative is accomplished by the same catalyst by just adjusting the reaction conditions, mainly pressure and temperature. Storage systems of this sort may find applications for on-board generation of H_2 [9].

Considered as the back side of the previous chapter of this book, in this contribution we will focus on the particular aspect of the hydrogenation of small organic molecules containing carbonyl functionalities to produce alcohols as a way of regenerating the carrier of a H_2-storage system. However, when reported, the reverse dehydrogenation process will also be briefly described. As can be deduced, all the dehydrogenation reactions mentioned in this contribution have been performed in the absence of hydrogen acceptors.

Hydrogenation reactions are widely employed processes for the synthesis of organic molecules both in industry and in academia laboratories [10]. From a purely chemical point of view, hydrogenation of some classes of carbonyl derivatives, such as ketones, is a well-established field, although progress toward the development of more active, cheap catalysts is still an important topic. Alternatively, development of hydrogenation catalysts for other types of carbonyl derivatives, including esters, amides and carboxylic acids, is almost in its infancy, although significant efforts have been carried out in the last 10 years for the development of efficient homogeneous catalysts. This difference can be traced to the lower reactivity of the carboxylic acid derivatives, such esters and amides, in comparison to ketones that makes the search for efficient catalysts more challenging [11]. Furthermore, hydrogenation of carboxylic acids poses a significant difficulty since in addition to the reduced electrophilicity of the carbonyl group, the substrate may interact with the metal center leading to catalyst deactivation.

Although from the principle of microscopic reversibility it can be expected that catalysts that promote the hydrogenation of a carbonyl compound should also be active for the reverse alcohol dehydrogenation, the reaction rates and conditions for both processes may differ significantly. In fact, as demonstrated by their limited number, development of reversible H_2-storage systems is a difficult task, and in many cases the hydrogenation and dehydrogenation reactions are frequently carried out under conditions involving different solvents and/or additives. Moreover, for a widespread implementation of these H_2-storage systems, catalysts should fulfil cost and sustainability requirements. In this respect the development of catalysts based on earth-abundant, non-toxic metals is an important issue, although to develop hydrogenation catalysts based on non-precious metals is a particularly difficult task due to the lower hydricity of first-row metal hydrides in comparison to their second- and third-row congeners. Furthermore, the cost of ligands is a frequently neglected aspect, and in this regard use of non-phosphorous ligands may offer advantages in terms of expense, availability and easiness of preparation.

A particularly successful approach to the development of hydrogenation and dehydrogenation catalysts consists on the use of ligands containing an acidic group susceptible to getting involved in protonation/deprotonation reactions and cooperating with the metal center in the activation of H-X (X = H, C, O) bonds [12]. Significant examples of these catalysts are metal complexes based on ligands that contain acid/base responsive M-NH functionalities that may participate in metal-amine/metal-amido transformations [13], and those containing lutidine-derived moieties in which pyridine aromatization/dearomatization may take place upon deprotonation of the methylene group [14]. Furthermore, by avoiding the requirement for oxidative addition through metal–ligand cooperation, metals do not change their formal oxidation state, what is particularly appropriate for the development of catalysts based on first-row transition metals since these complexes are prone to get involved in one-electron redox and radical processes.

6.2 Hydrogenation of ketones

6.2.1 General considerations

The hydrogenation of ketones to the corresponding secondary alcohols is a fundamental process in synthetic chemistry, and a large number of homogeneous catalysts for this reaction, including noble and base metal complexes, have been reported. Since the acceptorless dehydrogenation of secondary alcohols mediated by a metal complex yield a molecule of H_2 and the corresponding ketone [5–7], systems based on secondary alcohol/ketone pairs can be envisaged for the reversible storage of hydrogen (Figure 6.1). A particularly appealing H_2-storage system involving ketone/alcohol pairs is that based on 2-propanol/acetone since both partners are widely available and offers the highest H_2 content (3.3%wt H_2) among the secondary alcohol/ketone systems. Moreover, the easiness of the dehydrogenation of 2-propanol, at least in the presence of a hydrogen acceptor, has been demonstrated by its use as a hydrogen source in transfer hydrogenation reactions of synthetic utility [15]. However, unfortunately, reversible hydrogen storage in 2-propanol/acetone mixtures has only been reported in one case by using an iridium catalyst [16].
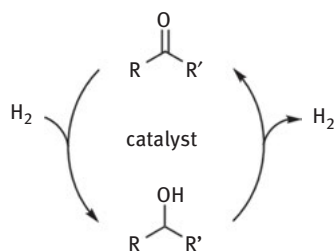
Figure 6.1: H_2-storage based on secondary alcohol/ketone systems.

Because significant advances have been made for the development of efficient catalysts for the release of H_2 from secondary alcohols [5–7], as well as for the hydrogenation of ketones [10], due to space constraints, this section will focus on examples of catalysts that have been shown, or are expected, to efficiently catalyze both types of processes. It should be noted that apart from the above-mentioned 2-propanol/acetone based H_2-storage system [16], no other reversible dehydrogenation of secondary alcohols has been reported so far.

6.2.2 Ruthenium and osmium catalysts

A considerable number of ruthenium catalytic systems have been reported for the dehydrogenation of secondary alcohols. Many of these catalysts are formed *in situ* from available ruthenium precursors in combination with phosphine and amine ligands [17, 18], although catalysts with well-defined structures have also been described [5–7]. However, for most of these complexes the catalytic activity in the hydrogenation of ketones has not been reported.

The first ruthenium complexes that have been shown to be catalytically active in both the hydrogenation of ketones and the dehydrogenation of secondary alcohols are Shvo-type catalysts (Figure 6.2). In addition to catalyze the hydrogenation of ketones with relatively low catalyst loadings (S/C = 200–2000) in the absence of solvents (34.5 bar H_2, 100–145 °C) [19], Shvo-type complexes catalyze numerous
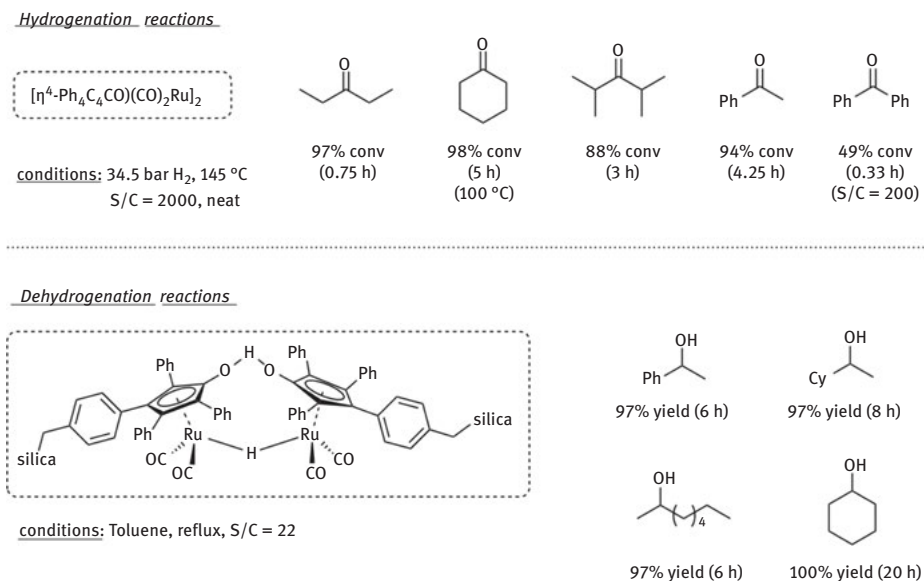
Figure 6.2: Hydrogenation of ketones and dehydrogenation of secondary alcohols with Shvo-type complexes.

reactions involving alcohol oxidation [20]. In a significant example, Park and co-workers demonstrated the efficiency of complex $[(\eta^5\text{-Ph}_4\text{C}_4\text{CO})_2\text{H}]\text{Ru}_2(\text{CO})_4(\mu\text{-H})]$ in the dehydrogenation of 1-phenylethanol and subsequently prepared a recyclable silica-immobilized complex that catalyzes the dehydrogenation of secondary alcohols in refluxing toluene [21].

Based on the unprecedented efficiency in the hydrogenation of ketones demonstrated by the ruthenium catalysts of the type $[\text{RuCl}_2(\text{diphosphine})(\text{diamine})]$ developed by Noyori et al. [22, 23], Baratta and co-workers have studied ruthenium and osmium catalysts based on ligands containing N-H functionalities in the hydrogenation of ketones and in the oxidation of secondary alcohols. Although osmium is a costly, third-row metal, the higher thermal and oxidative stability of the complexes may facilitate their use at higher temperatures and allow for lower catalyst loadings. Initially, Baratta and co-workers synthetized osmium complexes $[\text{OsCl}_2(\text{dppf})(\text{diamine})]$ incorporating the flexible diphosphine 1,1´-bis(diphenylphosphino)ferrocene (dppf). These derivatives were extremely active in the hydrogenation of ketones (Figure 6.3) [24]. Reduction of aromatic and aliphatic ketones in basic ethanol at low H_2 pressures with S/C ratios of 10,000–200,000 was accomplished with turnover frequencies of up to 3.0×10^5 h^{-1} (at 50 % conversion). As expected from the principle of microscopic reversibility, the osmium complex $[\text{OsCl}_2(\text{dppf})(\text{NH}_2\text{CH}_2\text{CH}_2\text{NH}_2)]$ and its ruthenium congener were efficient alcohol oxidation catalysts through dehydrogenation [25]. Secondary alcohols were converted to the corresponding ketones at 130 °C in the presence of KO^{t}Bu, providing TOF values up to 300 h^{-1} (at 50 % conversion). Comparison of the dehydrogenation activity of the ruthenium and osmium catalysts shows that the former generally provided faster reactions (Figure 6.3, bottom).

Furthermore, following previous contributions from the Noyori group reporting that the substitution of chiral C_2-symmetrical diamines by 2-aminomethylpyridine (ampy) allowed for higher activities and enantioselectivities in the hydrogenation of sterically demanding ketones [26], Baratta and co-workers prepared new osmium catalysts incorporating the ampy and dppb $(\text{PPh}_2(\text{CH}_2)_4\text{PPh}_2)$ ligands (Figure 6.4) [27]. A mixture of *cis*- and *trans*-$[\text{OsCl}_2(\text{dppb})(\text{ampy})]$ complexes was proven to be a highly active catalyst for the hydrogenation of ketones (TOF up to 1.5×10^4 h^{-1} at 50 % conversion), including bulky substrates such as *tert*-butyl substituted derivatives, under low H_2 pressures (5.0 bar) in basic ethanol (KO^{t}Bu) at 70 °C. Moreover, analogous ruthenium and osmium catalysts based on the dppf ligand were examined in the hydrogenation of ketones to secondary alcohols [28]. By using the complexes $[\text{MCl}_2(\text{dppf})(\text{ampy})]$ (M = Ru, Os) (S/C = 1000–5000), the reduction of ketones in basic ethanol or MeOH/EtOH solutions under mild conditions (30–90 °C, 5 bar H_2) was achieved with TOFs up to 7.5×10^4 h^{-1}. Comparison of the catalytic performance of the diphosphine/diamine complexes demonstrated that osmium catalysts give comparable reaction rates to the ruthenium derivatives provided higher temperatures are employed.

Interestingly, the acceptorless dehydrogenation of alcohols to ketones in refluxing ^{t}BuOH in the presence of KO^{t}Bu could also be carried out using low catalyst loadings
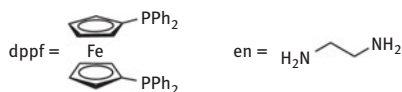
Hydrogenation reactions

cis-[OsCl$_2$(dppf)(en)]

conditions: 5 bar H$_2$, 60-70 °C
1.0 mol% NaOEt, EtOH

98% conv
(2 h)
S/C = 200000

>99% conv
(0.5 h)
S/C = 10000

95% conv
(1 h)
S/C = 50000

97% conv
(1 h)
S/C = 50000
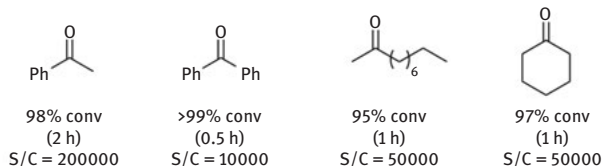
Dehydrogenation reactions

cis-[MCl$_2$(dppf)(en)]

conditions: 130 °C, ^{t}BuOH
2.0 mol% KO^{t}Bu
S/C = 250

[Ru]: 97% conv (4 h)
[Os]: 96% conv (20 h)

[Ru]: 57% conv (20 h)
[Os]: 68% conv (20 h)

[Ru]: 5% conv (20 h)
[Os]: 41% conv (30 h)

[Ru]: 73% conv (20 h)
[Os]: 40% conv (30 h)

[Ru]: 98% conv (3 h)
[Os]: 98% conv (6 h)

[Ru]: 95% conv (7 h)
[Os]: 98% conv (6 h)
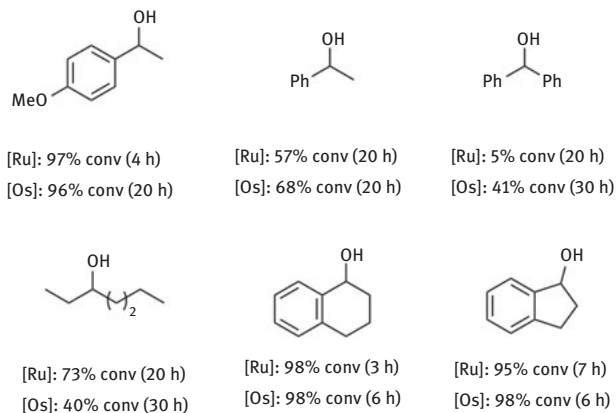
Figure 6.3: Hydrogenation of ketones and dehydrogenation of secondary alcohols by [MCl$_2$(dppf)(en)] (M = Ru, Os) complexes.

(S/C = 250) of the [MCl$_2$(dppf)(ampy)] (M = Ru, Os) complexes. The efficiency of these catalysts was attributed to the flexible ferrocenyldiphosphine ligand that allows the formation of thermally more stable active species with respect to the analogous derivatives having diphosphines with an alkyl backbone. Contrary to the hydrogenation reactions, significantly higher reaction rates were observed with ruthenium-based catalysts than with osmium complexes. In addition, the ampy-containing complexes provided a 10-fold increase in reaction rate with respect to the analogous ethylenediamine derivatives in the dehydrogenation of a cholesterol derivative.

Another type of osmium and ruthenium derivatives for the hydrogenation of ketones developed by the Baratta group is based on orthometalated CNN pincer ligands containing a primary amine donor (Figure 6.5) [29–31]. The [MCl(CNN)(PP)] (M = Os, Ru; PP = dppf, dppb, Josiphos) complexes are highly active catalysts for the
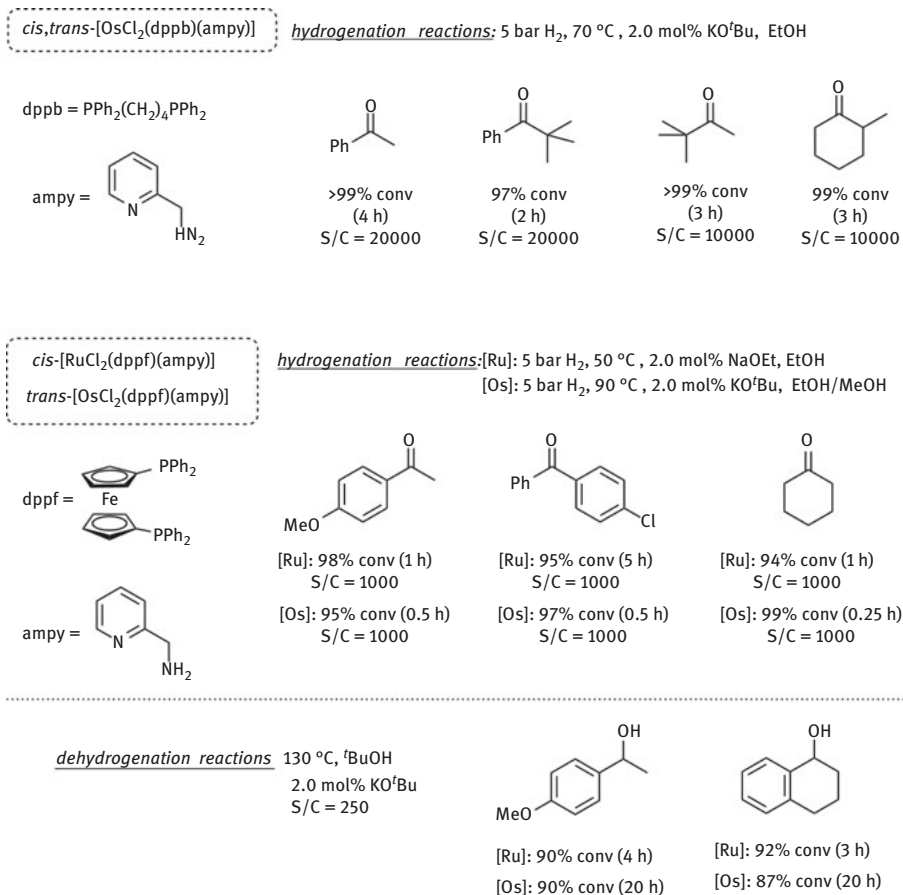
Figure 6.4: Hydrogenation of ketones and dehydrogenation of secondary alcohols by [MCl$_2$(PP)(ampy)] (M = Ru, Os; PP = dppf, dppb) complexes.

hydrogenation of aromatic and aliphatic ketones under 5 bar of H$_2$ at 40–70 °C using high catalyst-to-substrate ratios of 5000–50,000 in basic alcohol solutions. The osmium catalysts required slightly higher temperatures (60–70 °C) in comparison to the ruthenium complexes (40–60 °C) for achieving similar catalytic activities. Furthermore, the pincer [MCl(CNN)(diphosphine)] (M = Ru, Os) complexes were also tested in the dehydrogenation of α-tetralol (Figure 6.6). The ruthenium complexes were found to be significantly more active than the osmium derivatives, giving >90 % conversion to α-tetralone after 24 h [25].

Although the hydrogenation of ketones with some ruthenium catalysts that efficiently catalyze the dehydrogenation of secondary alcohols have not been reported, their catalytic activity in the hydrogenation of esters and other carbonyl compounds make them potential candidates for the development of secondary alcohol/ketone H$_2$-
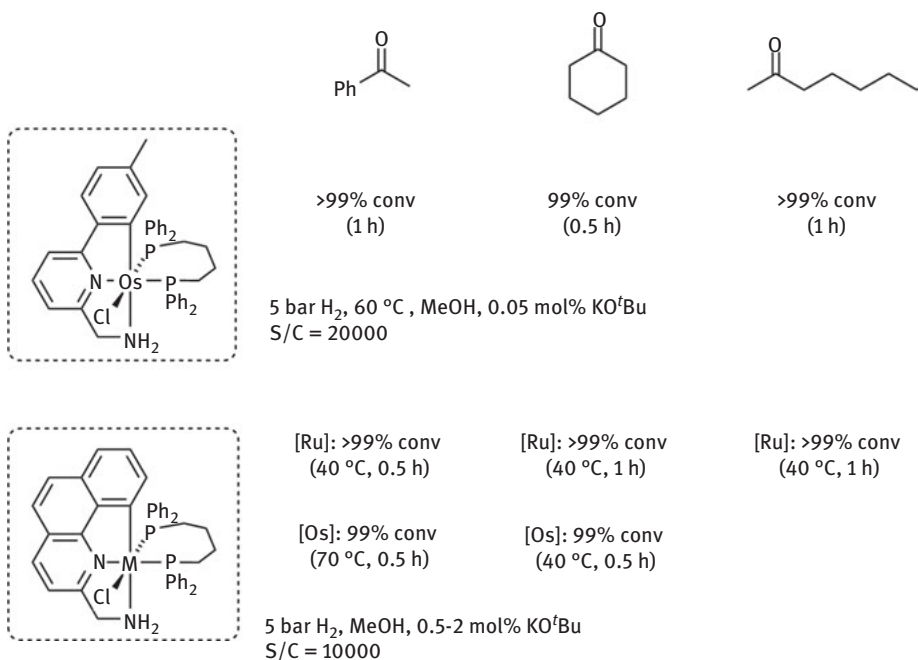
Figure 6.5: Hydrogenation of ketones by [MCl(CNN)(dppb)] (M = Ru, Os) complexes.
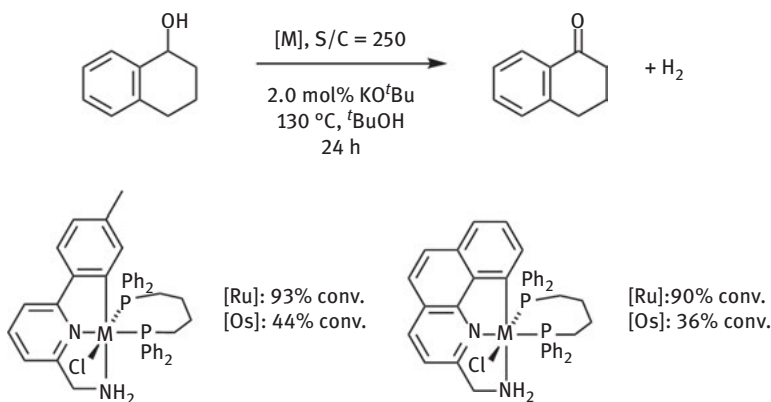
Figure 6.6: Dehydrogenation of α-tetralol by [MCl(CNN)(dppb)] (M = Ru, Os) complexes.

storage systems. One such an example is due to Beller and co-workers that screened a series of ruthenium complexes and proton-responsive aliphatic pincer ligands (PN^{H}P = HN(CH$_2$CH$_2$PR$_2$)$_2$) and proved their efficiency in the dehydrogenation of 2-propanol to acetone and ethanol to ethyl acetate [32]. These catalysts, which likely operate through metal-amide/metal-amine interconversion, were found superior to analogous

complexes containing lutidine-derived pincer PN^{Py}P ligands and Baratta-type CNN-ruthenium complexes. Particularly, by combining the metal precursor [RuH$_2$(CO)(PPh$_3$)$_3$] and the ^{i}Pr-PN^{H}P ligand, dehydrogenation of 2-propanol to acetone under neutral conditions at moderately low temperature (90 ^{o}C) was achieved with TOF values of 8382 h^{-1} at 6.7 % conversion and 4835 h^{-1} at 11.6 % conversion by using a high S/C ratio of 250,000. In addition, a TON higher than 40,000 was observed after 12 h reaction time. It is interesting to note that Ru-PN^{H}P complexes have been demonstrated to efficiently catalyze the hydrogenation of esters [33].

Similarly, the hydrogenation of ketones with ruthenium complexes based on lutidine-derived pincer ligands has not been reported, although their catalytic activity in the hydrogenation of esters and amides makes them potentially good catalysts for secondary alcohol/ketone H$_2$-storage systems [12]. With respect to the H$_2$ release process, in 2004, Milstein and coworkers reported the dehydrogenation of primary and secondary alcohols with ruthenium complexes incorporating lutidine-derived PN^{Py}P ligands (Figure 6.7) [34]. By using the dimeric complex [(RuCl$_2$(^{t}Bu-PN^{Py}P))$_2$(μ-N$_2$)] or the monomer [(^{t}BuPN^{Py}P)RuClH(N$_2$)] (S/Ru = 250) in the presence of sodium isopropoxide at 100 °C, secondary alcohols were dehydrogenated to the corresponding ketones in high yields and selectivity. Furthermore, neat 2-propanol was dehydrogenated by mixtures of [(^{t}BuPN^{Py}P)RuClH(N$_2$)] and NaO^{i}Pr with a TON of 924.

In addition, the catalytic activity in the dehydrogenation of secondary alcohols to ketones using PN^{Py}N-Ru complexes having a hemilabile amino group was studied by the same group (Figure 6.7) [35]. The dimer [(RuCl$_2$(^{t}Bu-PN^{Py}N))$_2$(μ-N$_2$)] exhibited a somewhat higher catalytic activity (TON = 304) than the analogous complex based on the ^{t}Bu-PN^{Py}P ligand (TON = 220) in the dehydrogenation of 2-propanol under solventless conditions in the presence of NaO^{i}Pr, whereas the carbonyl derivative [RuCl$_2$(^{t}Bu-PN^{Py}N)(CO)] provided a TON of 230. The dimer [(RuCl$_2$(^{t}Bu-PN^{Py}N))$_2$(μ-N$_2$)] also dehydrogenated other secondary alcohols in dioxane at 100 ^{o}C with TONs between 240 and 470.

Analogous PN^{Py}P- and PN^{Py}N-Ru complexes with a η^2-coordinated BH$_4$$^-$ ligand, [RuH(BH$_4$)(^{t}Bu-PN^{Py}P)] and [RuH(BH$_4$)(^{t}Bu-PN^{Py}N)], were also tested by the Milstein group in the dehydrogenation of alcohols under base-free conditions (Figure 6.7) [36]. The borohydride complex [RuH(BH$_4$)(^{t}Bu-PN^{Py}N)] provided higher conversions than the [RuH(BH$_4$)(^{t}Bu-PN^{Py}P)] derivative in the dehydrogenation of 1-phenylethanol and was also found to efficiently catalyze the dehydrogenation of primary alcohols and the hydrogenation of esters.

6.2.3 Iridium catalysts

Fujita, Yamaguchi et al. and the Rauchfuss group have reported a series of penta-methylcyclopentadienyl–iridium (Cp*Ir) complexes incorporating 2-hydroxypyridine-
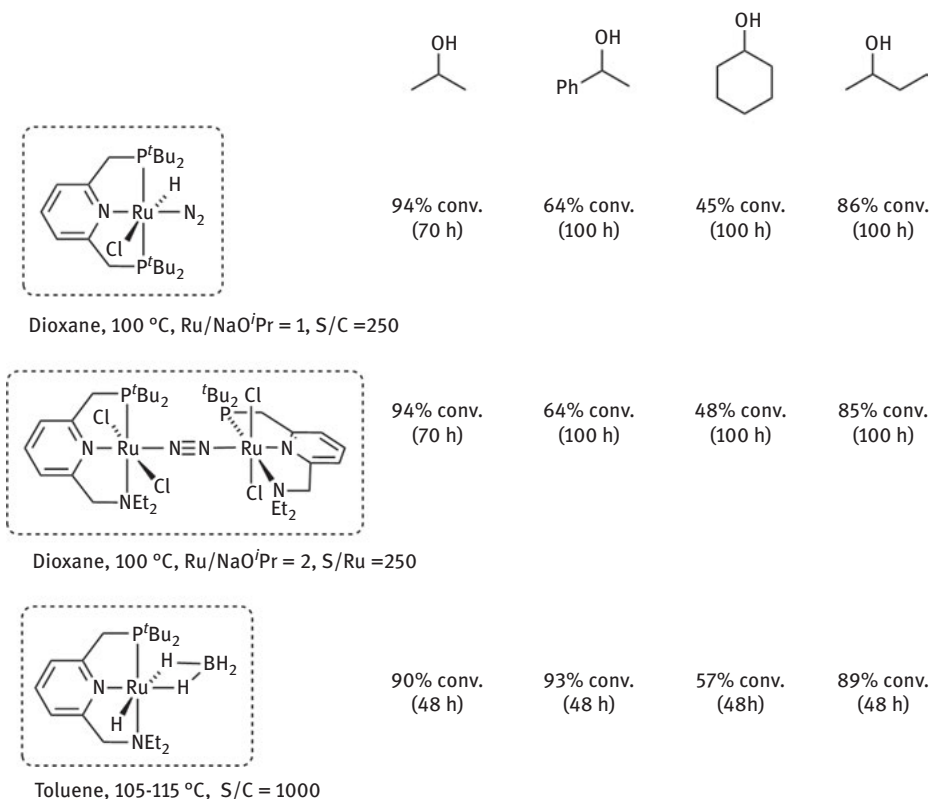
Figure 6.7: Dehydrogenation of secondary alcohols with PN^{Py}P- and PN^{Py}N-Ru complexes.

derived ligands that promote the oxidization of primary and secondary alcohols with liberation of molecular hydrogen [37–40]. Particularly, dehydrogenation of aliphatic and aromatic secondary alcohols under solventless conditions at moderately low temperatures (>90 °C) was accomplished by using an aquo Cp*Ir complex with a bipyridonate ligand (Figure 6.8) [16]. Furthermore, hydrogen release and storage based on the reversible transformation between 2-propanol and acetone were accomplished. By using the bipyridonate complex (S/C = 67, neat conditions), 2-propanol was transformed quantitatively under reflux to acetone with evolution of H$_2$. Interestingly, the H$_2$-storage step based on the quantitative hydrogenation of acetone to 2-propanol was carried out using 1 bar of H$_2$ at 40 °C. Overall, eight cycles were performed without a significant loss of the catalytic activity and in 95–100 % yield for each separated step, what represents a H$_2$ storage capacity of 2.8–2.9 %wt of a maximum theoretical value of 3.35% wt expected for 2-propanol.
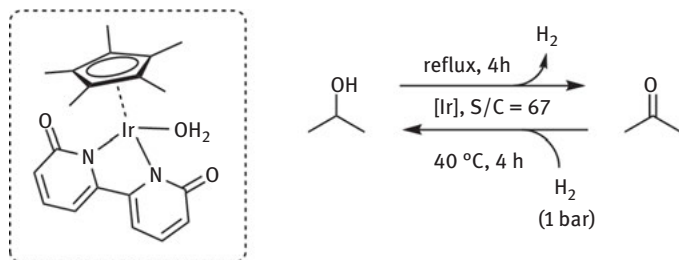
Figure 6.8: Reversible hydrogen storage in 2-propanol/acetone catalyzed by a Cp*Ir catalyst.

6.2.4 Non-noble metal catalysts

In 2014, Jones, Schneider and co-workers reported the use of pincer PN^HP-supported iron complexes that promote both the dehydrogenation of primary and secondary alcohols and the hydrogenation of acetophenones under mild, base-free conditions (Figure 6.9) [41, 42]. Dehydrogenation of benzylic and aliphatic alcohols was performed with notable efficiency with TONs of up to 790. Moreover, dehydrogenation of substrates containing primary and secondary hydroxyl groups, such as 1-phenyl-1,2-ethanediol and 1,3-butanediol, occurred selectively at the secondary alcohol moiety. Notably, the potential of this iron-based catalytic system for the reversible storage of H_2 was demonstrated with the hydrogenation of acetophenone and 4′-methoxyacetophenone under mild conditions (1–5 bar H_2, 20–50 °C) using substrate-to-catalyst ratios of up to 2000. Unfortunately, however, hydrogen release/recharge cycles were not performed.
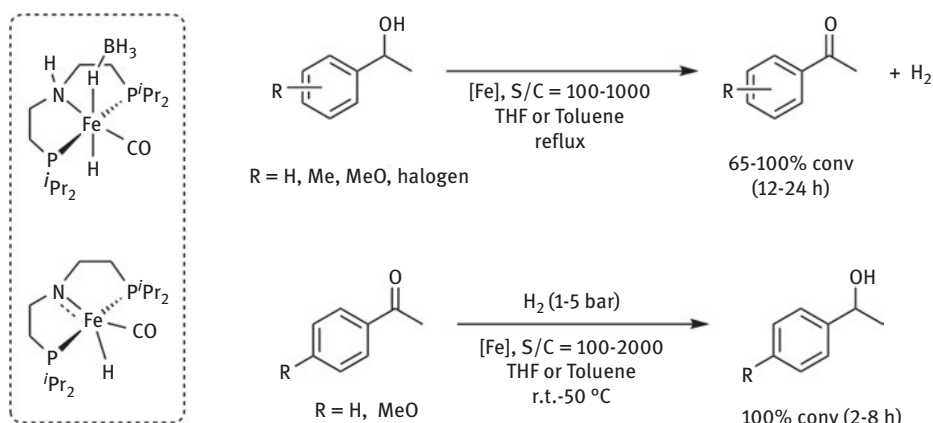
Figure 6.9: Dehydrogenation of secondary alcohols and hydrogenation of acetophenones by PN^HP-Fe complexes.

The catalytic activity in the hydrogenation of ketones to secondary alcohols of cobalt (II) complexes incorporating a bis(phosphinoethyl)amine (PN^{H}P) pincer ligand was reported by Hanson and co-workers (Figure 6.10) [43]. These derivatives hydrogenate aliphatic and aromatic ketones under mild conditions (1 bar H$_2$, 25–60 °C) with S/C ratios of 50. Furthermore, ketones, including aliphatic and aromatic derivatives, were produced by the dehydrogenation of secondary alcohols in toluene at 120 °C [44]. While the same catalytic system promotes both the hydrogenation and dehydrogenation processes, based on experimental evidences different mechanisms were proposed for each transformation [45]. An investigation of the mechanism of the dehydrogenation reaction revealed a Co(I)/Co(III) catalytic cycle, involving the formation of cobalt hydride/alkoxide species, β-elimination of the alkoxide ligand and reductive elimination to give H$_2$. Moreover, an analogous complex based on a NMe-containing pincer (PN^{Me}P) provided similar activity in the dehydrogenation reaction to the original complex, suggesting that the NH functionality is not directly involved in the catalyst reactivity. On the contrary, metal–ligand cooperativity was proposed for the hydrogenation of ketones since the analogous PN^{Me}P–Co complex was found inactive.
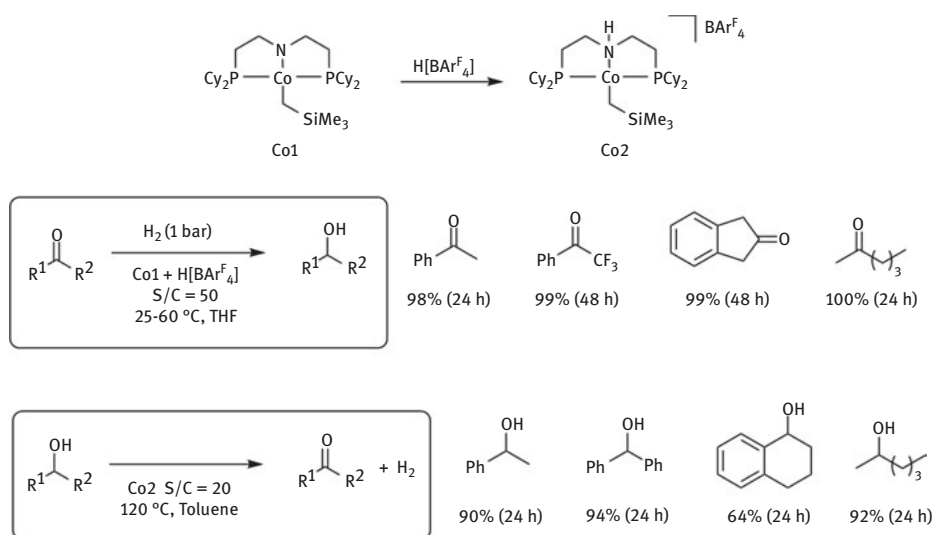
Figure 6.10: Hydrogenation of ketones and dehydrogenation of secondary alcohols by the cobalt complexes reported by Hanson and co-workers.

Inspired by the performance of the iridium–hydroxypyridinate complexes reported by Fujita, Yamaguchi et al. in the reversible dehydrogenation of alcohols [16], Jones and co-workers prepared nickel(II) complexes incorporating tris(3,5-dimethylpyrazolyl)borate (Tp´) and 2-hydroxyquinolinate ligands that are active catalysts for the reversible hydrogenation of ketones (Figure 6.11) [46]. Under neutral conditions, the
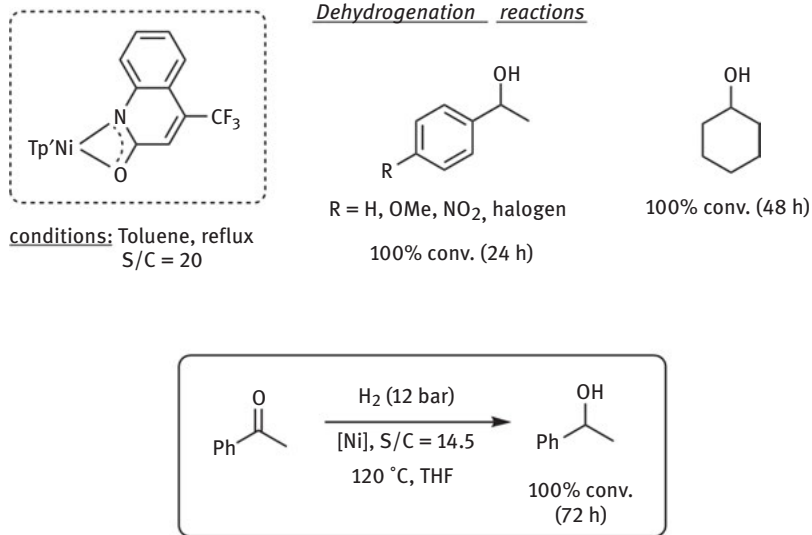
Figure 6.11: Dehydrogenation of secondary alcohols and hydrogenation of acetophenone with a Tp′Ni (2-hydroxiquinolinate) complex.

nickel catalysts (S/C = 20) performed the quantitative release of H_2 from a series of secondary alcohols in toluene in 24–48 h. Lower conversions were observed in the oxidation of 1-phenylethanol to acetophenone in THF, what was attributed to the lower boiling point of the solvent. The hydrogenation of ketones was also investigated in THF under 12 bar of H_2 at 120 °C, and quantitative conversion was observed after 72 h using a S/C = 14.5. Comparison of the catalytic activity of the catalyst with other Tp′Ni complexes ([Tp′Ni(μ-OH)]$_2$, Tp′Ni(OAc) and Tp′Ni(8-hydroxyquinolinate)) and DFT calculations indicated that the 2-hydroxyquinolinate ligand, and particularly the presence of a OH group at the ortho position, plays a fundamental role in the catalytic activity.

6.3 Hydrogenation of esters

6.3.1 General considerations

Similarly to the dehydrogenation of secondary alcohols to provide ketones, the dehydrogenation of a primary alcohol may yield the corresponding aldehyde and a molecule of H_2. However, the acceptorless dehydrogenation of primary alcohols to aldehydes is a challenging transformation since inhibition of the catalyst by coordination of CO resulting from aldehyde decarbonylation may occur. In addition, the high reactivity of aldehydes in the presence of bases makes these derivatives a poor hydrogen storage medium since many alcohol dehydrogenation catalysts operate

under basic conditions. Alternatively, a considerable number of catalysts have been shown to mediate the dehydrogenative coupling of primary alcohols to the corresponding esters following a Tishchenko-type process [4, 5, 7]. Hence, the interest in ester hydrogenation for hydrogen storage purposes resides in the development of cycles based on the dehydrogenative coupling of primary alcohols to yield two molecules of H_2 and the addition of hydrogen to the resulting symmetrical esters (Figure 6.12). Although in principle, any primary aliphatic alcohol may serve as a hydrogen carrier, the use of widely available molecules is particularly appealing. At this respect, ethanol (4.37%wt available H_2) is the most interesting carrier since it can be conveniently produced in large quantities from renewable bio-sources. In addition, ethanol dehydrogenation produces ethyl acetate, a commodity chemical widely used as solvent. However, although the hydrogenation of ethyl acetate and the dehydrogenation of ethanol have been studied with different catalytic systems, the realization of hydrogen charge/release reversible cycles in ethanol/ethyl acetate storage systems has not been reported.
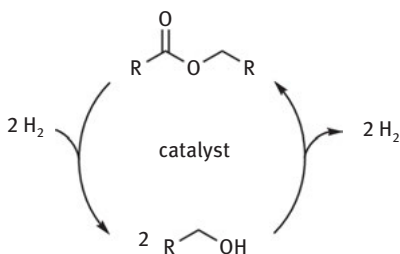
Figure 6.12: Hydrogenation of esters in connection with hydrogen storage in alcohols.

As a consequence of the lower electrophilicity of the carbonyl carbon of esters in comparison to ketones, the hydrogenation of this class of substrates is considerably more difficult. However, a remarkable progress in the hydrogenation of esters has been achieved in the last decade. While most catalysts have been developed bearing in mind their applications for the synthesis of intermediates needed for the production of fragrances, flavors, pharmaceuticals and detergents or the upgrading of bio-based feedstocks, the lessons learned with these catalytic systems can be directly translated to the field of hydrogen storage. Industrially, hydrogenation of esters has been accomplished by the use of heterogeneous catalysts, which require high temperatures (200–300 °C) and pressures (200–300 bar H_2) that cause the formation of undesired by-products resulting from competing reactions such as transesterification and reduction of C = C/aromatic groups [47]. These harsh conditions however are not adequate for hydrogen storage purposes, where state-of-the-art homogeneous catalysts that operate under milder conditions providing improved selectivities are of advantage.

6.3.2 Ruthenium and osmium catalysts

The first examples of the hydrogenation of simple esters involved the ruthenium catalyzed reduction of highly activated substrates such as trifluoroacetate esters [48]. A major improvement came from Teunissen and Elsevier, who reported a catalytic system composed of [Ru(acac)$_3$] and the Triphos (MeC(CH$_2$PPh$_2$)$_3$) ligand that was effective in the hydrogenation of unactivated aromatic and aliphatic esters (benzyl benzoate and methyl palmitate) under somewhat forcing conditions (85 bar H$_2$, 100–120 °C) [49]. Similarly, Nomura et al. used [Ru(acac)$_3$] with an excess of P(n-C$_8$H$_{17}$)$_3$ in the hydrogenation of methyl phenylacetate employing higher temperatures and lower pressures of H$_2$ (200 °C, 10 bar H$_2$) [50]. The catalytic activity of these systems is significantly modified by the use of additives, and in addition to the hydrogenation of the esters, formation of transesterification products was also observed.

A major breakthrough in ester hydrogenation was disclosed by the Milstein group in 2006. By using well-defined ruthenium catalysts based on dearomatized lutidine-derived PN^{Py}N pincer ligands, the hydrogenation of unactivated esters was achieved under base-free, mild conditions (S/C = 100, 5.4 bar H$_2$, 115 °C) (Figure 6.13) [51]. It is worth mentioning that this catalyst precursor also catalyzes efficiently the acceptorless
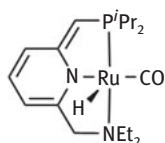
Milstein, 2006
5.3 bar H$_2$, 115 °C
TON up to 100
TOF up to 25 h^{-1}
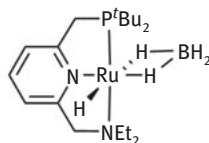
Milstein, 2011
10 bar H$_2$, 110 °C
TON up to 198
TOF up to 16.5 h^{-1}
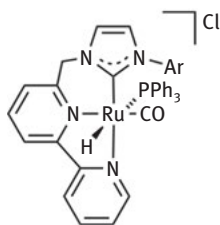
Milstein, 2011
5.4 bar H$_2$, 135 °C
1 mol% KO^{t}Bu
TON up to 98
TOF up to 49 h^{-1}
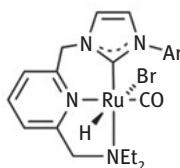
Song, 2011
5.3 bar H$_2$, 105 °C
8 mol% KO^{t}Bu
TON up to 100
TOF up to 50 h^{-1}
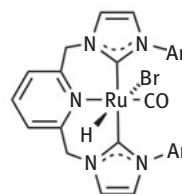
Pidko, 2014
50 bar H$_2$, 70 °C
5 mol% KOMe
TON up to 1000
TOF up to 62.5 h^{-1}

Figure 6.13: Ru-based catalysts incorporating tridentate lutidine-derived ligands for ester hydrogenation.

dehydrogenation of primary alcohols to esters [52]. The same group has also reported an analogous PN^{Py}N-Ru complex with a η^2-coordinated BH$_4^-$ ligand, [RuH(BH$_4$)(PN^{Py}N)], that was found active in both the hydrogenation of esters and the dehydrogenation of alcohols under base-free conditions [36]. Based on these results, this group and others have developed a number of ruthenium catalysts incorporating lutidine-derived pincers based on N-heterocyclic carbene donors [53, 54]. Although the presence in the ligand of a hemilabile N-donor group seems an important requisite for catalyst activity, Pidko and coworkers have reported an active complex with a CN^{Py}C ligand that converts, for example, methyl benzoate quantitatively to methanol and benzyl alcohol within 16 h using low catalyst loadings (S/C = 1000) under relatively mild conditions (70 °C, 50 bar H$_2$) [55].

In 2016, Chianese and co-workers reported related ruthenium catalysts based on a picoline-based CN^{Py}N scaffold that were tested in the hydrogenation of esters under mild conditions (105 °C, 6 bar H$_2$) (Figure 6.14) [56]. Catalyst activity was found to depend strongly on the NR$_2$ substituents since a dimethylamino-substituted ligand gave a poorly active catalyst (maximum TON of 30), while the analogous diethylamino-substituted derivative provided TONs of up to 980 in the hydrogenation of benzyl benzoate. This catalytic system efficiently catalyzes the hydrogenation of aryl- and alkyl-substituted esters with the notable exception of methyl esters. The low reactivity of the latter substrates was ascribed to an intrinsically reduced reactivity of the methyl esters with the catalyst. However, since base-catalyzed transesterification was found rapid under the reaction conditions, methyl esters could be effectively hydrogenated when benzyl alcohol was added to the reaction mixture. Interestingly, the reverse reaction, dehydrogenative homocoupling of primary alcohols to give esters, was tested with 1-hexanol to yield hexyl hexanoate with relatively high TONs of up to 920.
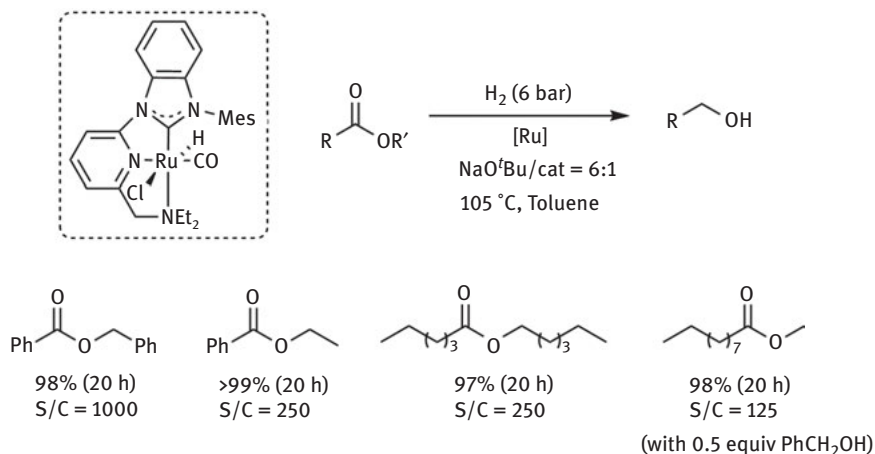
Figure 6.14: Ruthenium catalyst based on a picoline-derived CN^{Py}N ligand for ester hydrogenation reported by Chianese and co-workers.

A highly active ruthenium catalyst for ester hydrogenation featuring a tetradentate bipyridine ligand has been reported by Zhou and co-workers. In the presence of base, this complex efficiently hydrogenates bio-mass derived aromatic and aliphatic esters and lactones with low catalyst loadings (S/C up to 10^5) (Figure 6.15) [57]. The catalyst has several similarities with the Milstein system including the possibility of the pyridine central ligand fragment in getting involved in aromatization/dearomatization processes and the presence of a hemilabile amino group. Moreover, catalyst recycling was demonstrated in the hydrogenation of ethyl acetate. After removal of the produced EtOH under reduced pressure, only a minor decrease in catalyst activity was observed.
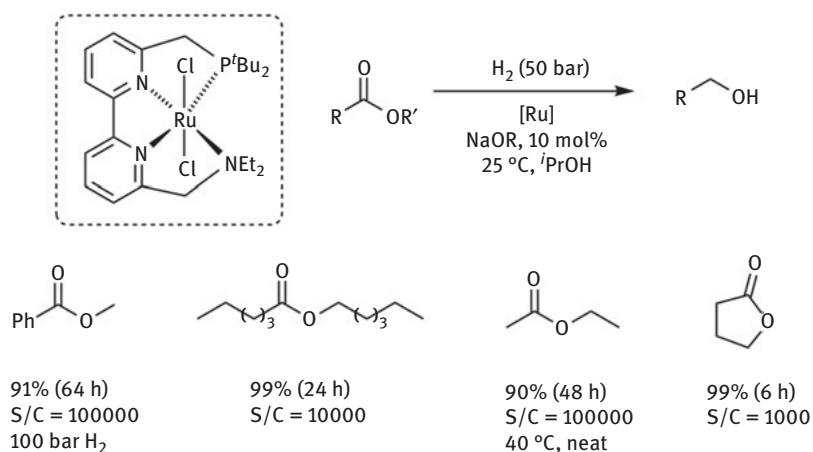
Figure 6.15: Ruthenium catalyst based on a tetradentate bipyridine $PN^{Py}N^{Py}N$ ligand for ester hydrogenation reported by Zhou and co-workers.

As expected, catalytic systems based on ligands exhibiting reversible metal–amine/metal-amido transformation have also been examined in the hydrogenation of esters. The first example of this type of catalysts was disclosed along with ruthenium complexes incorporating imine-phosphine PNNP ligands by researchers at Firmenich shortly after the Milstein group reported their results with the $PN^{Py}N$-Ru system (Figure 6.16) [58]. A ruthenium complex incorporating amino-phosphine ligands promoted the hydrogenation of aromatic and aliphatic esters operating at 100 °C under 50 bar of H_2 with low catalysts loading (S/C = 2000) in the presence of NaOMe. Under these conditions, alkyl benzoates were hydrogenated quantitatively in 1 h, whereas alkyl esters and lactones required longer reaction times (2.5 and 4 h, respectively) to produce the corresponding alcohols with >80 % yield.

Researchers at Takasago reported a ruthenium catalyst based on an aliphatic tridentate $PN^H P$ ligand having a central secondary amino group that was specifically

Conditions: 50 bar H$_2$, 100 °C, THF, 5 mol% NaOMe. S/C = 2000.
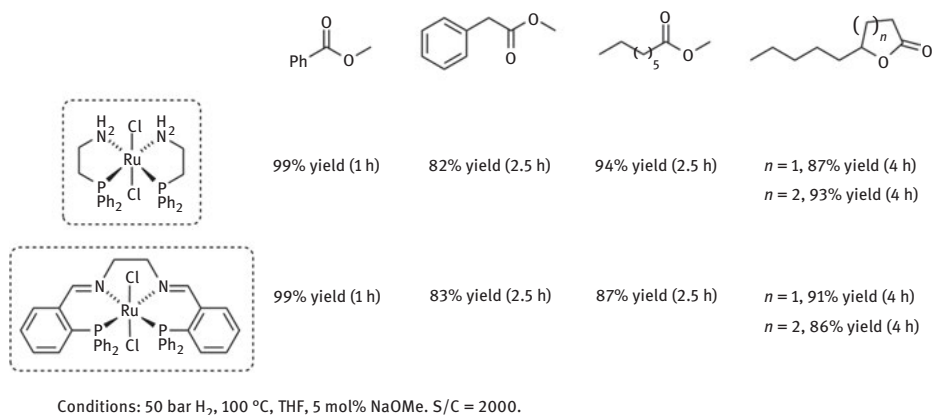
Figure 6.16: Ruthenium catalysts based on amino- and imino-phosphine ligands for ester hydrogenation.

designed for industrial applications, and particularly to operate in basic methanol solutions where solvent decarbonylation may poison the catalyst (Figure 6.17) [33]. The ruthenium-PN^{H}P complex (termed Ru-MACHO) hydrogenated a series of unactivated esters in MeOH at 100 °C under 50 bar H$_2$ in the presence of NaOMe with up to 1000 turnovers in 16 h. Interestingly, the catalytic activity of this complex to dehydrogenate ethanol to ethyl acetate under acceptorless conditions has also been demonstrated [59].
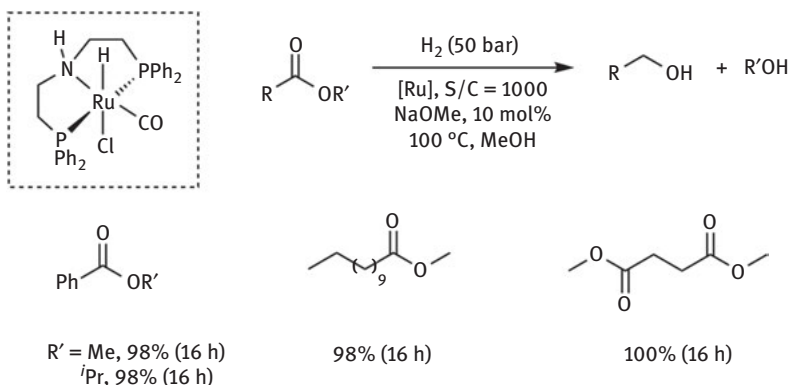
Figure 6.17: PN^{H}P-Ru catalyst for ester hydrogenation reported by researchers at Takasago.

An interesting modification of the previous catalyst consists in substituting a phosphine group by a hemilabile *N*-donor fragment. For example, Gusev and co-workers examined a compendium of ruthenium and osmium catalysts based on tridentate

PN^{H}N ligands, having a central amino group and a hemilabile pyridine arm, in the hydrogenation of methyl benzoate (Figure 6.18) [60]. A ruthenium dimer was a particularly efficient catalyst in the absence of additional base providing 18,000 turnovers in 17 hours under 50 bar of H$_2$ at 100 °C. In contrast, ruthenium and osmium monomeric complexes were active only in the presence of base (1 mol% KO^{t}Bu). The hydrogenation of other alkyl- and aryl-substituted esters was accomplished with the dimeric catalysts with TONs of up to 7100. In addition, the ruthenium monomer and the osmium dimer complexes were efficient in the dehydrogenation of alcohols, although the realization of H$_2$ release/recharge cycles was not reported.
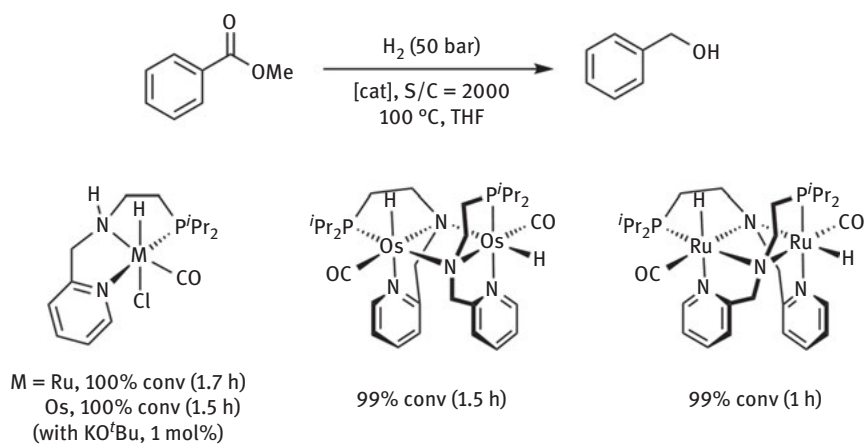
Figure 6.18: Ruthenium and osmium catalysts based on aliphatic PN^{H}N ligands for ester hydrogenation reported by Gusev and co-workers.

Further screening by the same group of related ruthenium and osmium catalysts based on PN^{H}N, NN^{H}N and PN^{H}P ligands in alcohol dehydrogenation and ester hydrogenation yielded the discovery of a highly active ruthenium catalyst able to perform the hydrogenation of esters with low catalyst loadings (S/C = 4000–20,000) (Figure 6.19) [61]. For example, under 50 bar of H$_2$ at 40 °C, the PN^{H}N–Ru complex promotes the hydrogenation of ethyl acetate to ethanol with an initial TOF of 1250 h^{-1}. Moreover, although this complex is also an efficient catalyst in the acceptorless dehydrogenation of ethanol to ethyl acetate (reflux solventless conditions, TOF up to 425 h^{-1}), reversible H$_2$-storage was not demonstrated.

In a subsequent study, osmium complexes based on PN^{H}N ligands containing phosphine, aminophosphine or phosphinite donors were evaluated in the selective hydrogenation of esters containing olefinic bonds (Figure 6.20) [62]. Particularly, the osmium complex based on an aminophosphine fragment was an efficient hydrogenation catalyst providing excellent carbonyl selectivity. It is worth noting that these
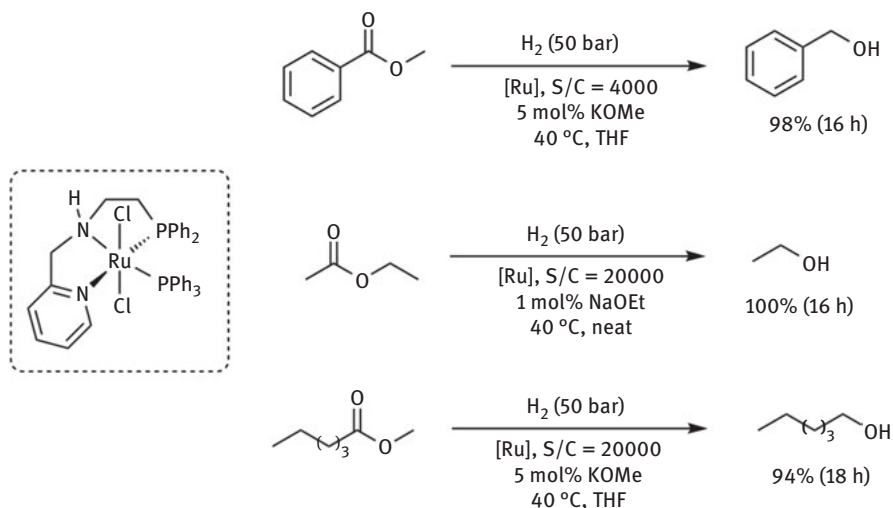
Figure 6.19: Hydrogenation of esters catalyzed by a PN^{H}N-Ru catalyst reported by Gusev and co-workers.
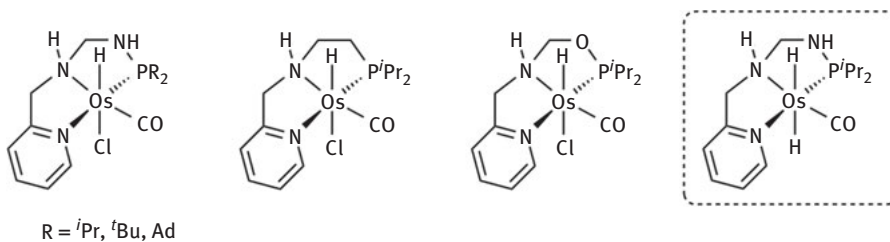
Figure 6.20: PN^{H}N-Os catalysts developed by Gusev et al. for ester hydrogenation and alcohol dehydrogenation.

catalysts also exhibit a high activity for acceptorless dehydrogenative homocoupling of alcohols to esters and coupling of amine and alcohols to amides. Finally, the analogous dihydrido complex was prepared and demonstrated to hydrogenate esters under neat conditions and 50 bar H_2 at room temperature. For example, methyl acetate, ethyl acetate, and ethyl butyrate were reduced using low catalyst loadings (S/C = 2000) with useful TONs of 730, 715, and 530, respectively, after 1 h. A marginal increase in the catalytic activity was observed in the reduction of ethyl acetate upon addition of 1 mol% NaOMe (TON = 740, 1 h), whereas the reaction without base carried out at 40 °C was effected with 1315 turnovers in 1 h.

Liu, Yang, Sun and coworkers used a ruthenium complex incorporating the 8-(2 diphenylphosphinoethyl) amidotrihydroquinoline ligand that operates with

low catalyst loadings in combination with $NaBH_4$ in the hydrogenation of esters (Figure 6.21) [63]. Both aromatic and aliphatic esters could be converted to their corresponding alcohols with high TONs of up to 50,000 and TOFs up to 2000 h^{-1}. In previous studies this ruthenium complex was shown to be a competent catalyst for alcohol dehydrogenation in the coupling cyclizations of γ-aminoalcohols with secondary alcohols [64].
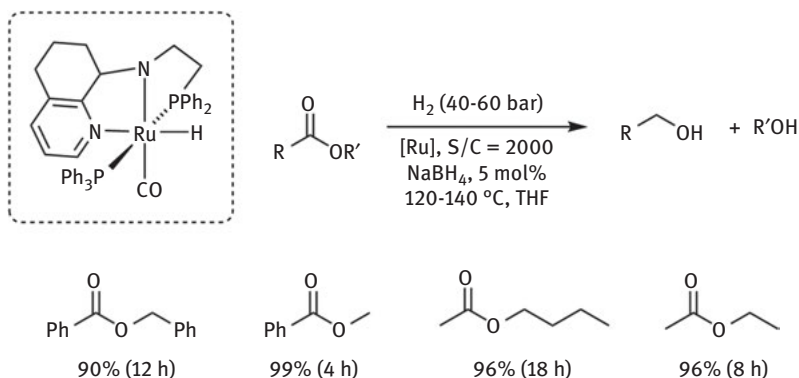
Figure 6.21: Ruthenium catalyst based on a tridentate PNN ligand for ester hydrogenation reported by Liu, Yang, Sun and coworkers.

An interesting approach for the development of competent hydrogenation catalysts consists of the use of ligands containing two proton-responsive functionalities, as explored by Milstein and co-workers by studying ruthenium complexes incorporating lutidine-based tridentate $PN^{Py}N^H$ ligands containing secondary amine donor fragments (Figure 6.22) [65]. These derivatives that can get involved in both metal-amine/metal-amide and pyridine aromatization/dearomatization processes are active ester hydrogenation catalysts under very mild conditions (room temperature, 5 bar of H_2) and catalyze the dehydrogenative coupling of alcohols to esters at low temperatures (35 °C).

Similarly, ruthenium complexes based on tetradentate lutidine-derived amino-containing $PN^HN^{Py}P$ and $PN^HN^{Py}N$ ligands have been investigated by Zhang and co-workers (Figure 6.23) [66, 67]. Particularly, the $PN^HN^{Py}P$-Ru catalyst operates at very low metal loadings (S/C = 10^4–10^5) in the presence of an alkoxide base providing very high catalytic activities. For example, up to 80,000 turnovers and a TOF of 2600 h^{-1} were achieved at 80 °C and under 50 bar of H_2 in the solventless hydrogenation of ethyl acetate.

The synthesis of phosphorous-containing ligands requires the use of expensive and difficult-to-handle organophosphorus reagents, what might represent a serious limitation to the widespread implementation of a H_2 storage system. Aiming to
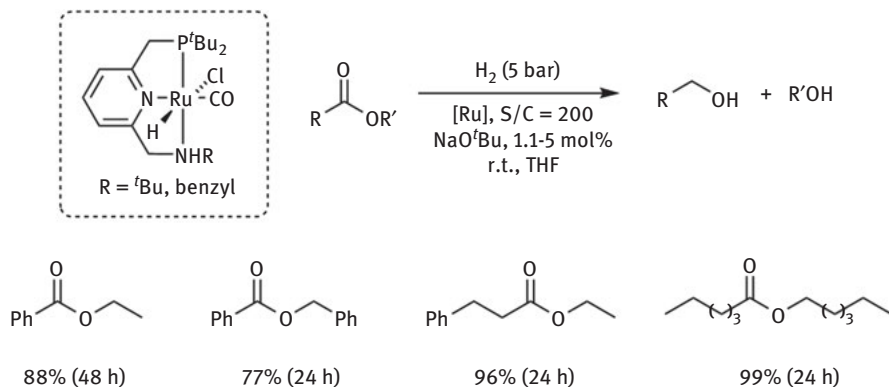
Figure 6.22: Ester hydrogenation catalyzed by PN^{Py}N^H-Ru complexes reported by Milstein and co-workers.
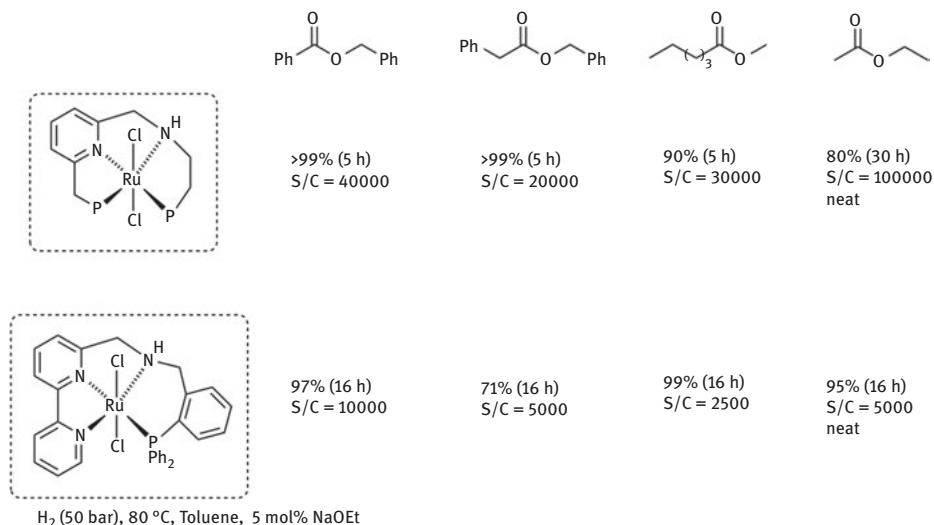
Figure 6.23: Catalytic systems for ester hydrogenation reported by Zhang and co-workers.

replace phosphine ligands by cheaper counterparts having sulfur donor groups, Gusev et al. have assessed the hydrogenation of esters mediated by SN^{H}S–Ru complexes (Figure 6.24) [68]. In addition to its high efficiency in the hydrogenation of esters to alcohols and transesterification products (TONs up to 58,400 and TOF of 2781 h^{-1} at 40 °C), this complex is also a highly active catalyst in the reverse reaction of alcohol homocoupling to afford symmetrical esters.

Another example of phosphine-free ruthenium catalysts for ester hydrogenation was disclosed by Pidko et al. and involves the use of bis-(N-heterocyclic carbene)-amino
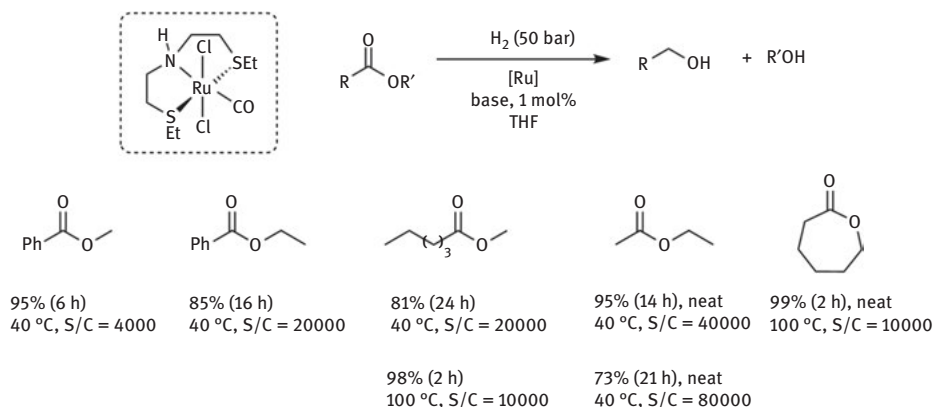
Figure 6.24: Ester hydrogenation catalyzed by the SN^{H}S–Ru complex reported by Gusev and co-workers.

ligands (Figure 6.25) [69]. Initial catalyst screening was performed by the *in situ* formation of the active species from the corresponding bis-imidazolium salts, LiHMDS and the ruthenium precursor [Ru(PPh$_3$)$_4$Cl$_2$]. The most active catalyst was isolated and tested in the hydrogenation of a range of aliphatic and aromatic esters at 70 °C under 50 bar of H$_2$ using low catalyst loadings (S/C up to 15,000).

In addition, a phosphine-free Cp*Ru catalyst bearing a *N*-heterocyclic carbene tethered to a NH$_2$ group has been reported by Morris et al. (Figure 6.26) [70]. This complex catalyzes the hydrogenation of esters to alcohols under 25 bar of H$_2$ at 50 °C in the presence of KO^{t}Bu using S/C ratios of 1500 with TOFs up to 585 h^{-1}.

The Beller group has studied the application of ruthenium-based catalytic systems containing bidentate ligands lacking proton-responsive functionalities. For example, by testing different combinations of ruthenium precursors and hemilabile
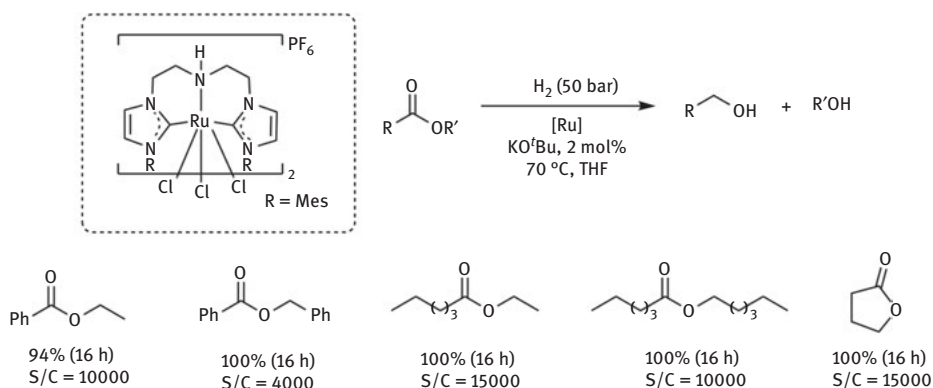
Figure 6.25: Ester hydrogenation catalyzed by a CN^{H}C–Ru complex reported by Pidko and co-workers.
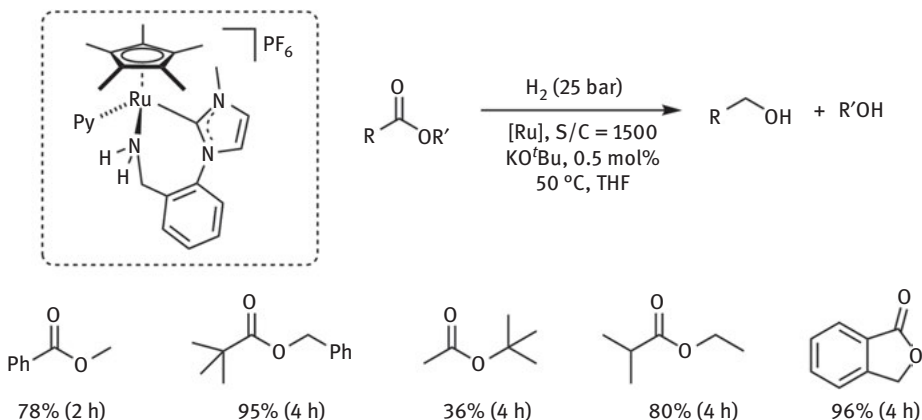
Figure 6.26: Ester hydrogenation catalyzed by the Cp*Ru complex reported by Morris and co-workers.

imidazolylphosphine ligands in the hydrogenation of methyl benzoate, efficient catalytic systems were developed for the hydrogenation of alkyl benzoates and aliphatic esters (Figure 6.27) [71]. Moreover, a phosphorous-free catalytic system composed of a ruthenium complex and a bis(imidazolium) salt precursor of a bis (*N*-heterocyclic carbene) ligand has been developed [72].
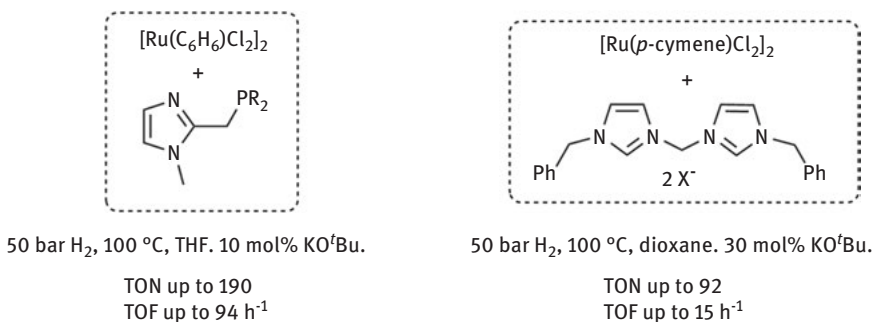
Figure 6.27: Ester hydrogenation catalyzed by the Ru/imidazolylphosphine and Ru/bis(imidazolium) salt systems reported by Beller and co-workers.

6.3.3 Iridium catalysts

In addition to ruthenium and osmium catalysts, a few examples of iridium complexes active in the hydrogenation of esters have also been reported (Figure 6.28). Beller et al. have employed iridium complexes based on aliphatic PN^{H}P ligands, [IrH$_2$X(PN^{H}P)] (X = H, Cl) [73]. While the dihydridochloro derivative was an efficient catalyst in the presence of base (50 bar H$_2$, 130 °C), the analogous trihydrido

complex was able to catalyze the hydrogenation of esters in the absence of an external base, although significantly better conversions (up to 98 turnovers) were observed in reactions carried out in basic solutions.

Moreover, Sanford, Goldberg and co-workers screened a series of cyclopentadienyl–bipyridine iridium complexes in the base-free hydrogenation of ethyl acetate (60 bar H_2, 120 °C, neat conditions) (Figure 6.28) [74]. Turnover numbers between 116 and 363 were achieved from a maximum theoretical TON of 5100, and an acceleration of the reaction rates was observed in the presence of catalytic amounts of the Lewis acid $Sc(OTf)_3$. With the best catalyst, poor conversions were observed in the reduction of acetates and benzoates, while formates were hydrogenated in good yields with significant TONs of up to 173 (S/C = 200, 30 bar H_2, 100 °C).
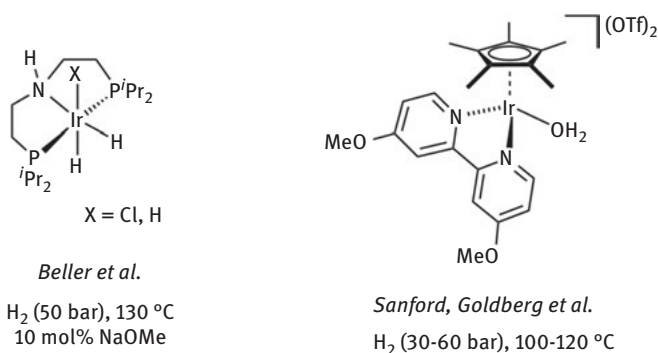
Figure 6.28: Iridium catalysts for the hydrogenation of esters.

6.3.4 Non-noble metal catalysts

In the search of cost-efficient catalysts, complexes based on first-row metals have been examined in the hydrogenation of esters. In 2014, three independent reports of iron catalysts based on PNP ligands were made by the groups of Milstein [75], Fairweather and Guan [76] and Beller [77] (Figure 6.29). While the iron complex based on a lutidine-derived PN^{Py}P ligand reported by Milstein et al. was only effective in the hydrogenation of activated esters (trifluoroacetates), the NH-containing PN^{H}P–iron complexes of Guan and Beller were able to produce the hydrogenation of non-activated esters. Interestingly, a mechanism based on metal-ligand cooperation was proposed on the basis that an analogous iron complex incorporating a PN^{Me}P ligand was not active in the hydrogenation of esters under similar reaction conditions. Furthermore, use of a second generation catalyst with a PN^{H}P ligand containing less sterically demanding ethyl groups improved the catalytic activity allowing for lower catalyst loadings and temperatures [78]. Also, addition of NEt_3 as a BH_3 scavenger was found to favor increased reaction rates [79].
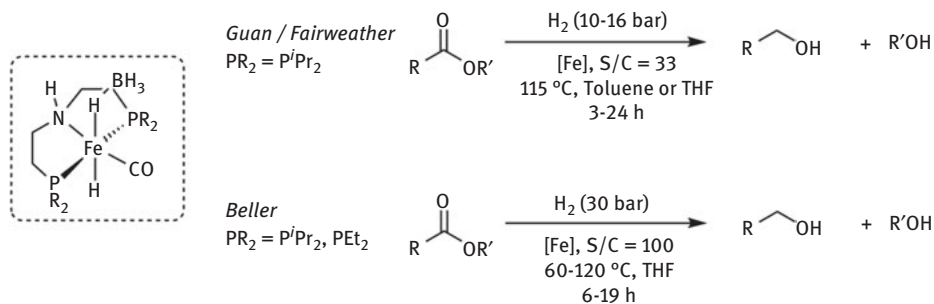
Figure 6.29: Iron catalysts incorporating aliphatic PN^{H}P ligands for ester hydrogenation.

Elsevier, de Bruin and coworkers employed a catalytic system formed from $Co(BF_4)_2 \cdot 6\,H_2O$ and the Triphos ligand in the hydrogenation of esters and carboxylic acids (Figure 6.30) [80]. The reduction of esters with this catalyst requires high catalyst loadings (S/C = 10–20) and relatively high H_2 pressures (80 bar).
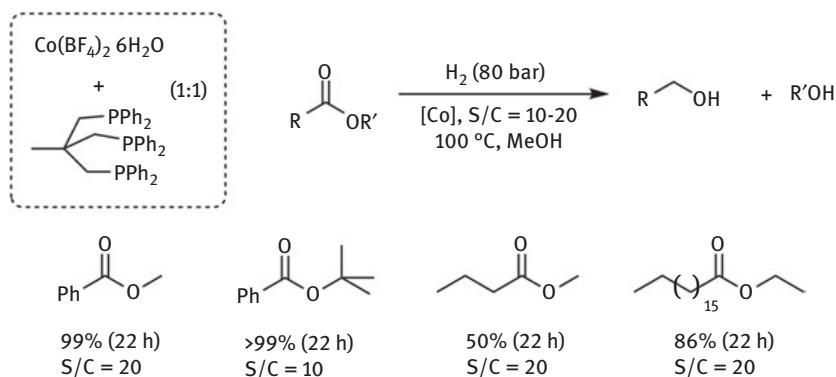
Figure 6.30: Triphos-Co catalytic system in the hydrogenation of esters.

In addition, cobalt catalysts based on proton-responsive PNP ligands have also been employed in ester hydrogenation. For example, Milstein and co-workers studied the application of lutidine-derived PN^{Py}P and PN^{Py}N ligands containing phosphine and amine donors in the cobalt-catalyzed hydrogenation of esters (Figure 6.31) [81]. While all the catalysts tested promoted the reduction of esters with H_2, a complex incorporating a secondary amino group was found the most active in the presence of sub-stoichiometric amounts of $NaHBEt_3$ and KO^{t}Bu. Interestingly, activated esters such as trifluoroacetates and aryl esters could not be reduced with this catalytic system and only the hydrogenation of enolizable derivatives was accomplished. Hence, based on the observed relative reactivity of the esters, a likely mechanism involving an ester enolate intermediate was proposed.
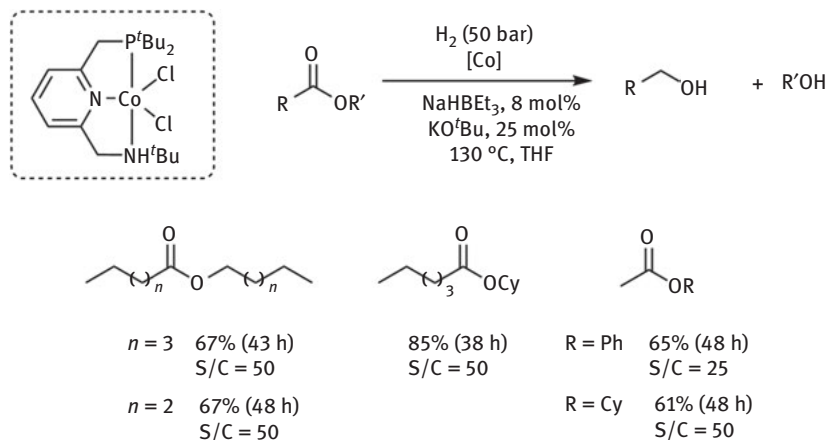
Figure 6.31: Hydrogenation of esters by a cobalt catalyst based on a PN^{Py}N^H ligand.

Alternatively, Jones and co-workers have reported the hydrogenation of esters catalyzed by a cobalt complex incorporating an amino-based PN^{H}P ligand (Figure 6.32) [82]. A serious drawback of this catalytic system is the lack of reactivity of methyl esters that have been attributed to catalyst deactivation resulting from the decarbonylation of methanol. Interestingly, an analogous cobalt complex incorporating a non-proton-responsive ligand PN^{Me}P provided a comparable activity to that obtained with the PN^{H}P-Co catalyst in the hydrogenation of benzyl benzoate and γ-valerolactone, suggesting that the reaction mechanism does not involve metal–ligand cooperation.
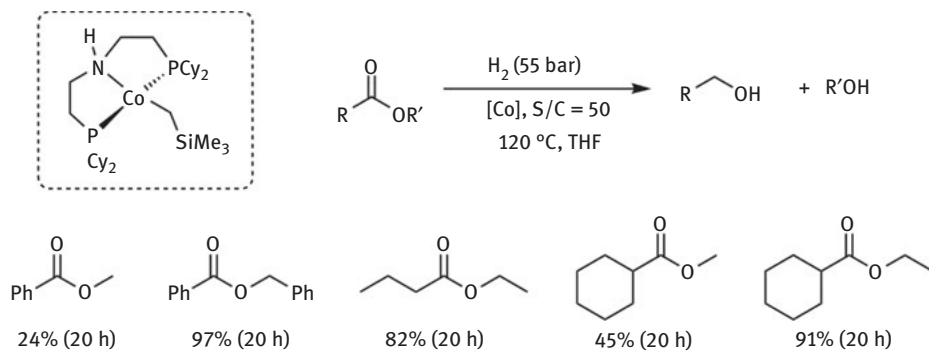
Figure 6.32: Hydrogenation of esters by a cobalt catalyst based on a PN^{H}P ligand.

In 2016, manganese catalysts containing pincer-type PN^{H}P ligands for the hydrogenation of esters were reported by the Beller group (Figure 6.33) [83]. Reaction of
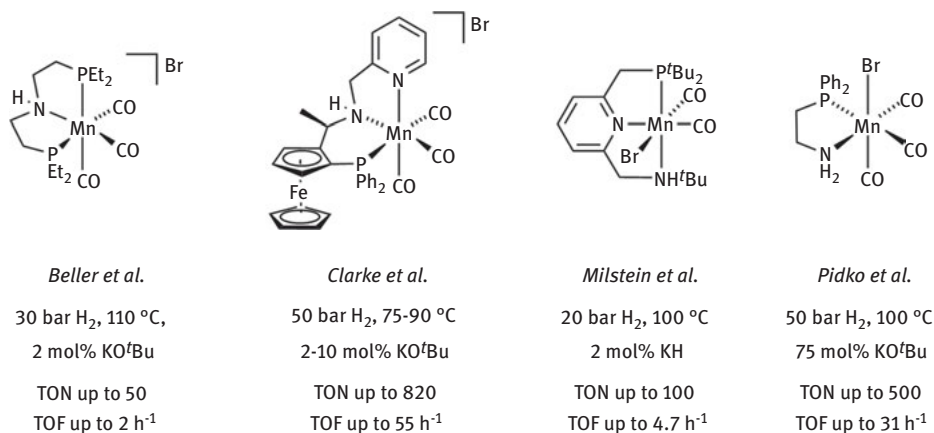
Figure 6.33: Manganese catalysts for the hydrogenation of esters.

[Mn(CO)$_5$Br] with HN(CH$_2$CH$_2$P(Et)$_2$)$_2$ yields a mixture of neutral and cationic complexes that hydrogenates aromatic and aliphatic esters, as well as lactones, in good yields using substrate-to-catalyst ratios of 50 (110 °C, 30 bar H$_2$). More sterically demanding ligands, such as those based on P^{i}Pr$_2$ and PCy$_2$ fragments provided less reactive catalysts.

Similarly, Clarke and co-workers have employed a manganese complex with a facially coordinated chiral tridentate PN^{H}N ligand that accomplished the hydrogenation of aryl- and alkyl-substituted esters in good yields using typical S/C ratios of 100 (Figure 6.33) [84], although the reduction of butyl butyrate to butanol was achieved with a S/C ratio of 1000 in 82% yield. This manganese derivative is also an efficient catalyst in the enantioselective hydrogenation of ketones.

Milstein and co-workers reported a manganese complex based on a lutidine-derived PN^{Py}N^H ligand that operates at 100 °C under 20 bar of H$_2$ in the presence of KH, providing in most cases quantitative conversions to the corresponding alcohols (Figure 6.33) [85]. Interestingly, although the ligand incorporates two proton-responsive functionalities, preliminary mechanistic studies support an outer-sphere mechanism only involving amine deprotonation.

In another recent example of manganese-catalyzed hydrogenation of esters, Pidko and co-workers examined the catalytic activity of a series of manganese complexes incorporating the 2-(aminoethyl)diphenylphosphine ligand. A particularly simple manganese-based catalyst was found to efficiently catalyze the transformation of unactivated esters to alcohols in good yields by using S/C = 500 (Figure 6.33) [86]. A significant influence of the concentration of base on the catalytic activity was evidenced, particularly in the case of methyl and ethyl esters, that was ascribed to catalyst inhibition by the formation of metal-alkoxide species from the resulting alcohols.

6.4 Hydrogenation of amides

6.4.1 General considerations

Amides can be readily obtained by the dehydrogenative coupling of primary alcohols with amines with the concomitant release of two molecules of H_2 [4, 5, 7]. Moreover, the reverse reaction, the hydrogenation of amides to yield mixtures of alcohols and amines, is also known. Hence, use of alcohol+amine/amide partners is a potential method for the development of reversible hydrogen storage systems, and several reports have demonstrated the feasibility of this approach (Figure 6.34) [87, 88]. As in the case of hydrogen storage in alcohol/ester systems, ethanol (4.37 %wt available H_2) is the most appealing alcohol carrier; however, the maximum theoretical H_2 capacity significantly depends on the amine partner.
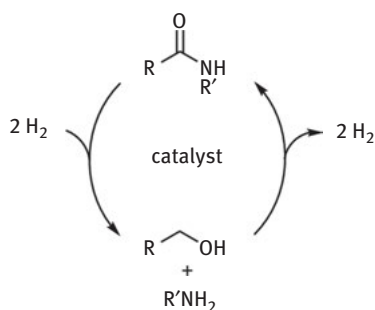
Figure 6.34: H_2-storage based on alcohol+amine/amide systems.

The hydrogenation of amides has been proven to be a more challenging reaction than that of esters due to the reduced electrophilicity of the amido group. Moreover, the reduction of amides using hydrogen gas may proceed by two different routes involving the reductive cleavage of either the C-N or C-O bonds (Figure 6.35). Addition of hydrogen to the carbonyl group of an amide gives initially the formation of the corresponding hemiaminal. Elimination of an amine molecule from this intermediate
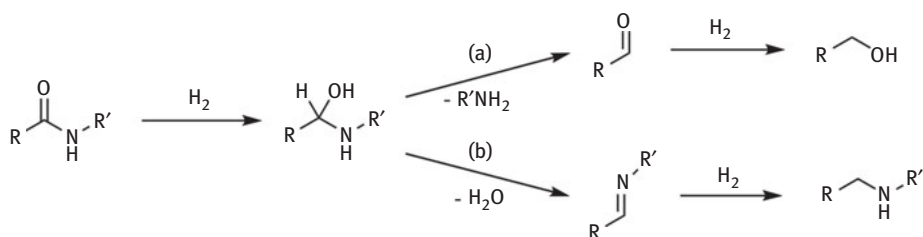
Figure 6.35: Hydrogenation of amides to: (a) alcohols and amines, and (b) imines/amines.

yields the corresponding aldehyde, which in a subsequent step can be hydrogenated to alcohol (route a). Alternatively, dehydration of the hemiaminal gives an imine (route b), which hydrogenation leads to the corresponding amine. While both processes are of significant synthetic interest, only the reduction of amides involving reductive C-N cleavage is relevant to the storage of H_2 in alcohols by the performance of cycles as shown in Figure 6.34.

6.4.2 Ruthenium catalysts

While pioneering work by Ikariya and co-workers accomplished the hydrogenation of cyclic *N*-acylcarbamates and *N*-acylsulfonamides, these substrates have a low interest for applications in H_2 storage [89]. However, shortly afterwards, in 2010 a major breakthrough in the field was made by the Milstein group. By the use of ruthenium complexes based on dearomatized lutidine-derived ligands, aliphatic and aromatic amides were selectively hydrogenated to mixtures of the corresponding alcohols and amines under mild, base-free conditions (110 °C, 10 bar H_2) (Figure 6.36) [90]. Further attempts to improve the structure of the catalysts by introducing different tethers in the pyridine-pyridine linkage were unsuccessful due to catalyst deactivation resulting from intramolecular C-H activation [91].
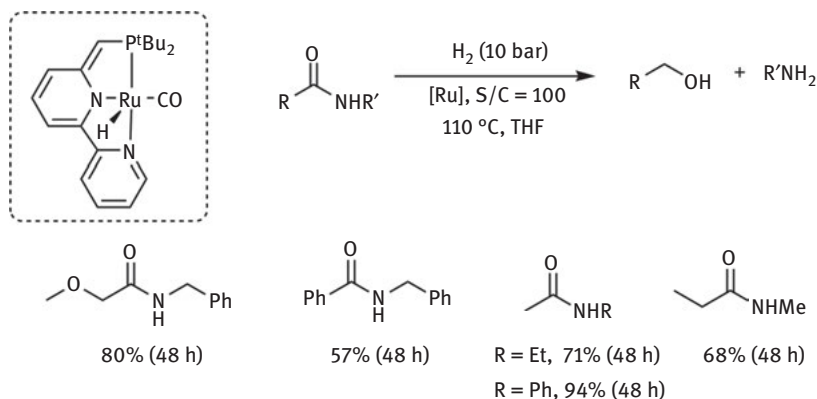
Figure 6.36: Hydrogenation of amides by a ruthenium catalyst based on a dearomatized lutidine-derived PN^{Py}N ligand.

Interestingly, PN^{Py}N-Ru complexes are also effective catalysts in the dehydrogenation of alcohols in the presence of amines to form amides [92], and consequently the development of H_2 storage systems based on alcohol+amine/amide pairs was envisaged. In 2015, Milstein and co-workers reported the reversible dehydrogenation of 2-aminoethanol (AE), an abundant and inexpensive molecule, to a cyclic dipeptide

(glycine anhydride, GA) and linear polypeptides (Figure 6.37) [87]. The maximum theoretical hydrogen content of the system is 6.56 %wt, although the formation of the polypeptides lowers the hydrogen storage capacity. Hydrogenation of glycine anhydride, and mixtures with the linear polypeptides, was performed in the presence of base with ruthenium catalysts containing lutidine-derived PN^{Py}N ligands, in which the N arm is either a hemilabile diethylamino group or a proton-responsive NH^{t}Bu functionality. Both glycine anhydride and the polypeptides were hydrogenated to yield 2-aminoethanol and 2-amino-N-(2-hydroxyethyl)acetamide (AA). More importantly, repetitive cycles of H$_2$ release/recharge were conducted in dioxane without adding new catalyst (S/C = 100), although catalytic amounts of KO^{t}Bu were added after each reaction to prevent catalyst deactivation by adventitious traces of water. The real maximum initial hydrogen storage capacity under these conditions was 0.085 %wt, which it is quite far from the maximum theoretical value of 6.56 %wt.

The same group has also developed a rechargeable H$_2$-storage system with a maximum hydrogen storage capacity of 5.3 %wt based on the dehydrogenation of ethanol in the presence of ethylenediamine (ED) to form diacetylethylenediamine (DAE) (Figure 6.37) [88]. Separated hydrogenation reactions were performed at 115 °C under 50 bar of H$_2$ using a PN^{Py}N–Ru complex (S/C = 500) to yield ethanol and ethylenediamine along with N-(2-aminoethyl)acetamide (AEA) resulting from the partial reduction of DAE. Three repetitive dehydrogenation/hydrogenation cycles were carried out using a substrate-to-catalyst ratio of 250 and dioxane as reaction medium with conversions between 92 and 100 %. Under the employed reaction conditions the actual maximum hydrogen storage capacity was 1.65 %wt.
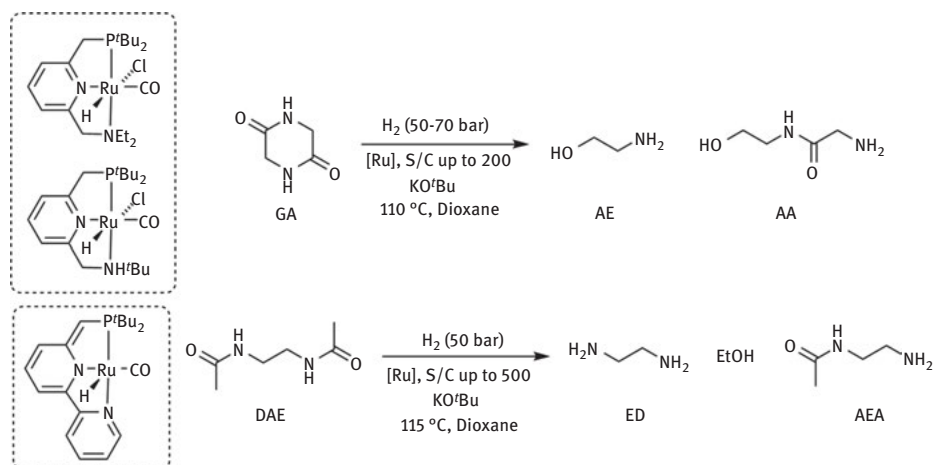
Figure 6.37: Hydrogenation of GA and DAE for reversible hydrogen storage.

Catalysts incorporating proton-responsive ligands capable of metal-amine/metal-amide interconversion have also been examined in the hydrogenation of amides. Initial work was reported in 2011 by the group of Ikariya that used Cp*Ru catalysts with a protic amine ligand in the hydrogenation of lactams and benzamides (Figure 6.38) [93]. This catalytic system, however, required the use of high catalyst loadings and is limited to substrates with *N*-aryl substituents.
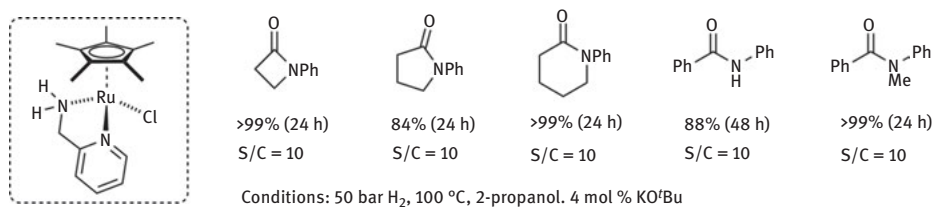
Figure 6.38: Hydrogenation of lactams and amides by the Cp*Ru catalyst reported by Ikariya and co-workers.

Ruthenium complexes based on amino-phosphine ligands have been profusely examined in the hydrogenation of amides. For example, Bergens and co-workers have reported a η^3-allyl–ruthenium complex containing the 1-amino-2-diphenylphosphinoethane ligand that was a competent catalyst in the hydrogenation of amides and lactams (Figure 6.39) [94]. High turnover numbers up to 1000 were reached for several amides, and a TON of 7120 was achieved in the hydrogenation of *N*-phenyl-pyrrolidin-2-one. In a subsequent study, the same group developed a catalytic system derived from the reaction of the cationic allyl precursor [Ru(η^3-C$_3$H$_5$)(Ph$_2$P
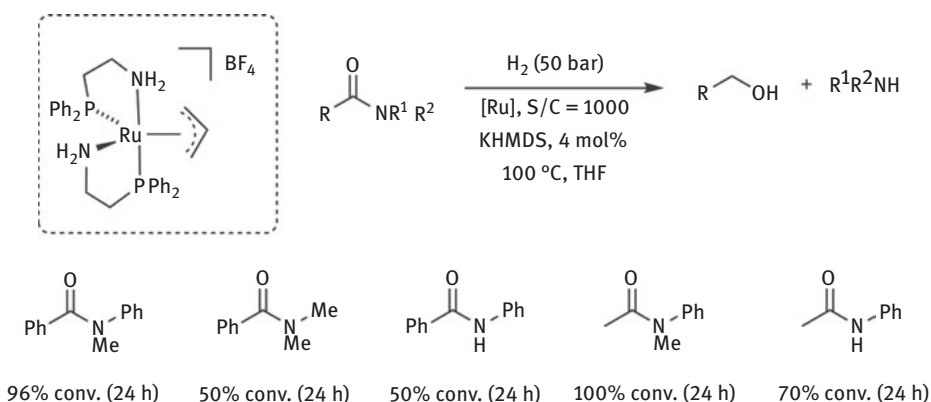
Figure 6.39: Hydrogenation of amides using the [Ru(η^3-C$_3$H$_5$)(Ph$_2$P(CH$_2$)$_2$NH$_2$)$_2$]BF$_4$ complex reported by Bergens and co-workers.

$(CH_2)_2NH_2)_2]BF_4$ and $NaBH_4$ under H_2, which under 50 bar of H_2 at 100 °C hydrogenates under base-free conditions secondary and tertiary amides with TONs between 270 and 1000 [95]. This base-free protocol is tolerant to many functional groups, and it is particularly suitable for the hydrogenation of secondary amides that may inhibit the catalytic activity by forming amidate ligands upon deprotonation. However, in the hydrogenation of a series of benzamides and secondary *N*-heterocyclic-substituted amides, the base-free reactions were less effective than those assisted by base.

Furthermore, an influence of zinc additives in the catalytic activity of the ruthenium complex $[RuCl_2(Ph_2P(CH_2)_2NH_2)_2]$ in the hydrogenation of amides was evidenced by Mashima and coworkers [96]. A combination of the ruthenium complex and $Zn(OCOCF_3)_2$ was found to efficiently hydrogenate benzamides and acetamides by using substrate-to-metal ratios of 500 under 30 bar of H_2. Other zinc additives also showed an increase in the hydrogenation rate. The beneficial role of $Zn(OCOCF_3)_2$ was ascribed to its function as a source of trifluoroacetate ligands and as a Lewis-acid promoter for amide activation.

Saito et al. have reported the hydrogenation of non-activated amides by using a phosphino-pyridine ruthenium catalyst in combination with sterically demanding alkoxide bases. Mechanistic studies demonstrated that hydrogenation of the pyridine fragment of the ligand enables catalytic activity by forming a catalytic species with a HRu-NH functionality (Figure 6.40) [97].
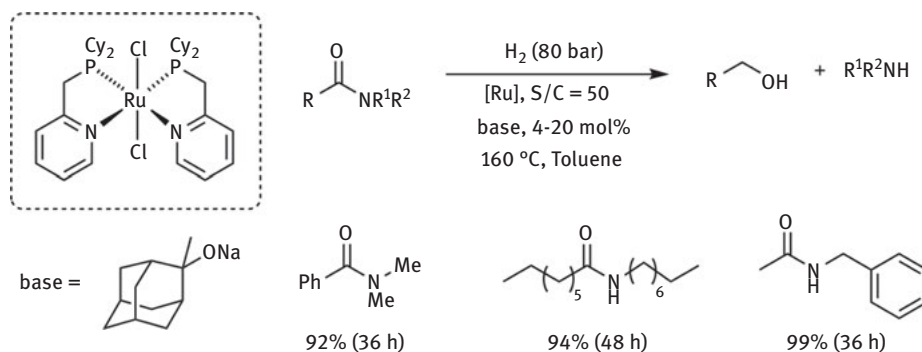
Figure 6.40: Hydrogenation of amides by the ruthenium catalyst reported by Saito and co-workers.

In 2016, Beller and co-workers reported a ruthenium complex containing an imidazolylaminophosphine ligand that affords the hydrogenation of primary and secondary amides under base-free conditions (TONs up to 200) (Figure 6.41) [98]. Moreover, this catalyst is also able to promote under basic conditions the hydrogenolysis of primary amides (150 °C, 50 bar of H_2), a class of substrates that has been scarcely investigated.
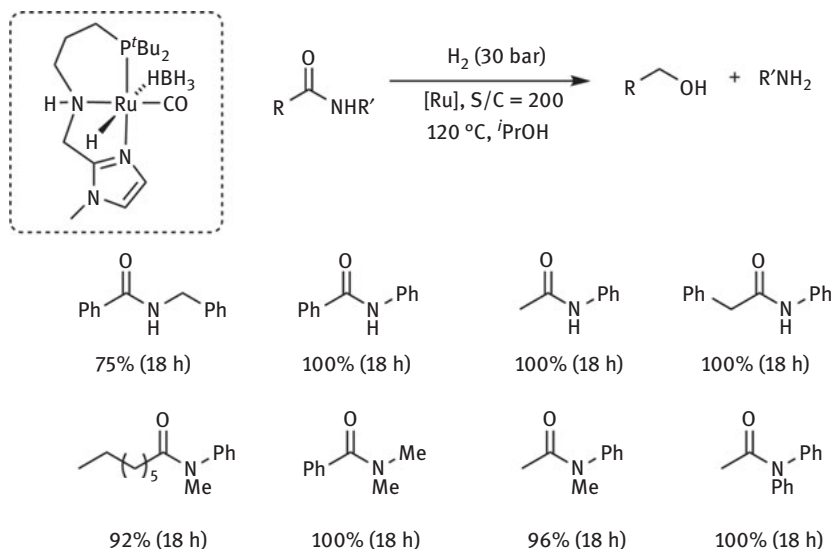
Figure 6.41: Hydrogenation of amides by the ruthenium catalyst reported by Beller and co-workers.

Recently, Zhang and coworkers disclosed a ruthenium catalyst based on a tetradentate lutidine-amino PN^{Py}N^{H}P ligand that exhibits an unprecedented catalytic activity in the hydrogenation of amides (Figure 6.42) [99]. Under 50 bar of H$_2$ at 100 °C in the presence of 1–2 mol% of KO^{t}Bu, this catalyst operates with high TONs of up to 19,600 and exhibits a wide functional group tolerance in the hydrogenation of secondary and tertiary amides.

6.4.3 Non-noble metal catalysts

Development of amide hydrogenation catalysts based on non-precious metals is a particularly difficult task due to the lower hydricity of first-row metal hydrides in comparison to their second- and third-row congeners. However, a few examples of catalysts based on earth-abundant metals have been reported. For example, the first iron-based catalytic system for the hydrogenation of amides was released by the Milstein group in 2016 and involves the use of a lutidine-based PN^{Py}P-Fe complex. This catalyst is active in the hydrogenation of activated secondary and tertiary 2,2,2-trifluoroacetamides under relatively forcing conditions (60 bar H$_2$, 140 °C) [100].

Alternatively, unactivated amides were hydrogenated by iron catalysts incorporating aliphatic amino-based PN^{H}P ligands (Figure 6.43). Langer and co-workers studied the influence on the stability and catalytic activity of the phosphino group PR$_2$ substituents of PN^{H}P–Fe complexes in the hydrogenation of methyl benzoate, and the most active catalyst (R = Et) was employed in the hydrogenation of secondary

Figure 6.42: Hydrogenation of amides by the PN^{Py}N^{H}P-Ru catalyst reported by Zhang and co-workers.

and tertiary amides under base-free conditions [101]. In a related study, Sanford et al. investigated the catalytic performance of a series of PN^{H}P-Fe complexes in the hydrogenation of *N,N*-dimethylformamide and found that the complex based on a PCy$_2$ fragment was a better catalyst than those incorporating less bulky substituents (R = Et or ^{i}Pr) [102]. TON values in the range 288–300 were obtained using S/C = 300 and K$_3$PO$_4$ as base (20–50 bar H$_2$, 110–130 °C). Moreover, the use of more enforcing reaction conditions provided 1080 turnovers at S/C = 3000. Furthermore, this catalyst was found to give an initial reaction rate only 1.7-fold slower than the analogous ruthenium catalyst. Hydrogenation of other amides, such as formamides and alkyl- and aryl-substituted amides, was accomplished with this catalytic system with TONs ranging from 25 to 300.

A related deprotonated pentacoordinated PN^{Py}P–Fe complex that operates under base-free conditions was reported by Bernskoetter and co-workers (Figure 6.43) [103]. With this catalyst, reaction rates enhancements were observed by the addition of Lewis acids (LiOTf) and secondary amides (formanilide).

In 2017, the Beller group employed a manganese catalyst based on a facially coordinated imidazolylaminophosphine PN^{H}N ligand incorporating a NH functionality in the hydrogenation of secondary and tertiary amides, including formamides. Under relatively mild, basic conditions a series of amides were reduced to alcohols and amines with high conversions using S/C ratios between 20 and 50 (Figure 6.44) [104].

Figure 6.43: Iron catalysts incorporating PN^{H}P-derived ligands for amide hydrogenation.
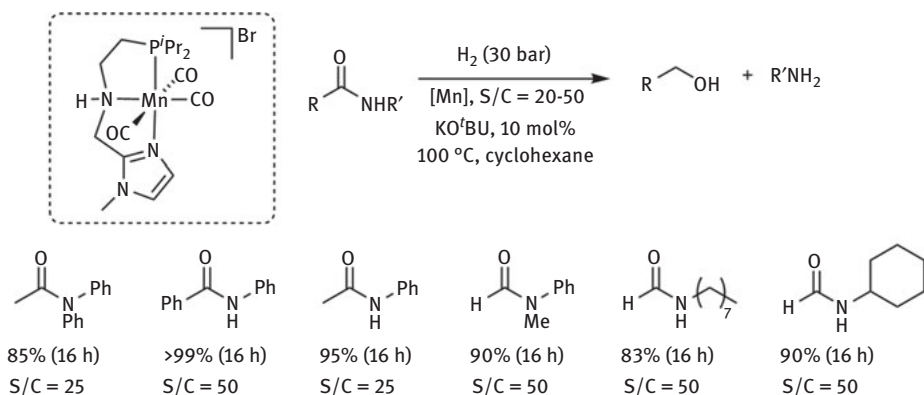
Figure 6.44: Manganese catalyst reported by Beller et al. for amide hydrogenation.

Moreover, difficult-to-hydrogenate primary benzamides were reduced to the corresponding alcohols and ammonia in moderate yields (30–65 %) by using substrate-to-catalyst ratios of 14–20 under 50 bar H$_2$ at 140 °C.

6.5 Hydrogenation of carboxylic acids

6.5.1 General considerations

A large number of carboxylic acids are available from both the petrochemical industry and biomass. Hence, since hydrogen production from the transformation of alcohols to the corresponding carboxylates using water as oxidant has been reported [105, 106], the use of carboxylic acids may result of interest in the field of hydrogen storage, although this approach remains to be tested (Figure 6.45).
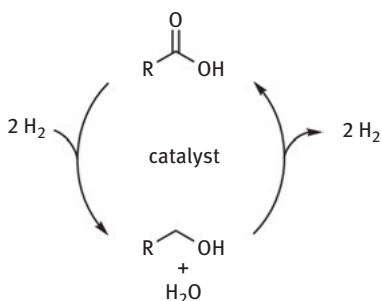
Figure 6.45: Hydrogenation of carboxylic acids in connection with H_2-storage in alcohols.

Hydrogenation of carboxylic acids involves the transfer of two H_2 molecules and the cleavage of a C-O bond, and it is significantly more difficult than the hydrogenation of esters and amides since the substrate may interact with the metal center leading to catalyst deactivation. Heterogeneous catalysts have been reported for the hydrogenation of carboxylic acids; however, the harsh reaction conditions required make them poorly adequate for the development of hydrogen storage systems since in addition to alcohols, other derivatives such as esters and ethers are formed [47]. Alternatively, homogeneous catalysts can be regarded as more appropriate for carboxylic acid hydrogenations provided that coordination of carboxylate ligands at the vacant sites leading to catalyst deactivation does not take place. Unlike the hydrogenation of esters and amides that is performed under basic or neutral conditions, catalysts for carboxylic acid hydrogenations need to operate under acidic conditions. Hence, the use of catalysts based on proton-responsive ligands seems poorly promising, and development of catalytic systems for the dehydrogenation of alcohols to carboxylic acids under neutral or acidic conditions is a prerequisite for the obtention of efficient H_2-storage systems based on alcohol+H_2O/carboxylic acid pairs. Furthermore, most research involving the hydrogenation of carboxylic acids has been carried out for biogenic substrates that serve as chemical platforms, and only few examples of the reduction of carboxylic acids leading to alcohols with high available hydrogen content, such as formic and acetic acids, have been reported.

6.5.2 Noble metal catalysts

Seminal studies involving the use of homogeneous catalysts for the hydrogenation of carboxylic acids were made under elevated hydrogen pressures (>100 bar) [47]. However, in 2013, Goldberg et al. screened a series of half-sandwich rhodium and iridium complexes in the hydrogenation of glacial acetic acid solutions under relatively mild conditions (2 mM catalyst, 30 bar H_2, 120 °C) (Figure 6.46(a)) [107]. In the reactions with the iridium complexes, conversion to ethyl acetate was accomplished with the formation of minor amounts of ethanol and diethyl ether with TONs up to 777. Moreover, catalytic activity could be increased reaching TONs of 1637 by the used of protic and Lewis acids as additives. Under the same reaction conditions rhodium complexes operate with lower TONs of up to 125. Furthermore, hydrogenation of other short-chain carboxylic acids was also tested with the Cp*-iridium catalysts. Significantly slower reactions were observed as the chain length increases, as well as changes in the alcohol/ester selectivity that increases from a 1:2.5 ratio in the hydrogenation of acetic acid to 2:1 for the propionic and butyric acids. Some of these catalysts were also applied in the hydrogenation of esters [74].
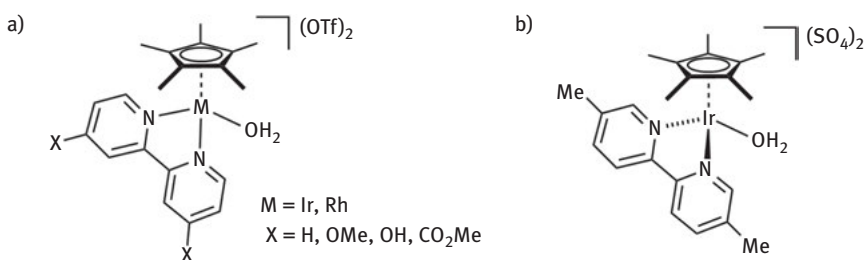
Figure 6.46: a) Cp*M (M = Rh, Ir) complexes screened by Goldberg et al. for the hydrogenation of carboxylic acids; and b) Cp*Ir catalyst for formic acid hydrogenation reported by Laurenczy, Himeda and co-workers.

Hydrogenation of formic acid has been investigated by Laurenczy, Himeda et al. using also Cp* iridium catalysts containing substituted 2,2′-bipyridine ligands (Figure 6.46(b)) [108]. With an iridium complex bearing 5,5′-dimethyl-2,2′-bipyridine in the presence of 10 mol% H_2SO_4, a TON of 1314 was achieved when formic acid aqueous solutions at 60 °C were exposed to 52 bar of H_2. In addition to MeOH, which was obtained with 47 % selectivity, methyl formate is formed because of the equilibrium under acidic aqueous conditions between formic acid/MeOH and methyl formate/water. In the absence of an external hydrogen pressure, formic acid disproportionation produced MeOH with 15 % selectivity.

Ruthenium complexes containing the Triphos ligand have shown a high efficiency in the hydrogenation of carboxylic acids (Figure 6.47). For example, Leitner
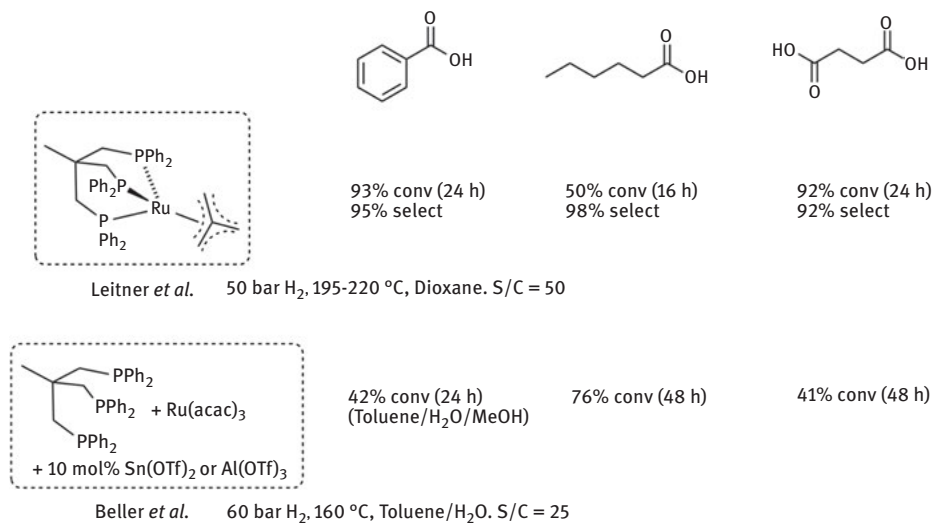
Figure 6.47: Triphos-Ru catalytic systems for the hydrogenation of carboxylic acids (selectivity toward the alcohol product).

et al. demonstrated the ability of the complex [Ru(Triphos)(TMM)] (Triphos = 1,1,1-tris (diphenylphosphinomethyl)ethane, TMM = trimethylene methane), which also promotes the hydrogenation of esters, amides, carbonates and urea derivatives, to catalyze the hydrogenation of carboxylic acids [109]. This system operates under neutral conditions thus avoiding formation of undesired by-products and giving the alcohols in high selectivity. Similarly, Beller et al. employed a catalytic system composed by [Ru(acac)$_3$] (acac = acetylacetonate), the Triphos ligand and a Lewis acid such as Sn(OTf)$_2$ for the hydrogenation of alkyl-substituted carboxylic acids, or Al(OTf)$_3$ in the reduction of benzoic acid [110]. The reduction of medium to long chain renewable carboxylic acids such as propionic, butyric, hexanoic and octanoic acids were effected with TONs from 16 to 20, and the formation of esterification products was prevented by addition of water. Interestingly, while other phosphine ligands were also screened in the hydrogenation of carboxylic acids, only the use of the Triphos ligand provided an active catalyst. Moreover, by applying the same catalyst precursor and closely related reaction conditions but in the presence of an excess of an alcohol, the hydrogenation of the carboxylic acids yielded unsymmetrical ether derivatives [111]. Based on the results reported by the Leitner and Beller groups, Deng, Palkovits et al. examined other Ru-based catalytic systems incorporating Triphos-like PPP and PPN ligands [112]. These catalysts were tested in the reduction of bio-based carboxylic acids, although shorter chain lengths carboxylic acids could also be reduced giving as the major products the corresponding esters.

Naruto and Saito determined that phosphine monocarboxylate ruthenium $[Ru(OCOR)(phosphine)_2]^+$ complexes are highly active catalysts for the hydrogenation of carboxylic acids to alcohols (Figure 6.48) [113]. These catalytically active species were generated *in situ* from a combination of $[Ru_2Cl_2(\mu\text{-Cl})_2(\mu\text{-OH}_2)(P(3,5\text{-xylyl})_3)_4]$ and NaOAc, or $[Ru_2Cl_2(\mu\text{-Cl})_2(\mu\text{-OH}_2)(dppb)_2]$ (dppb = $Ph_2P(CH_2)_4PPh_2$) and Na(acac) (acac = acetylacetonate). Interestingly, unlike other catalysts for the hydrogenation of carboxylic acids, this catalytic system cannot promote the reduction of esters.
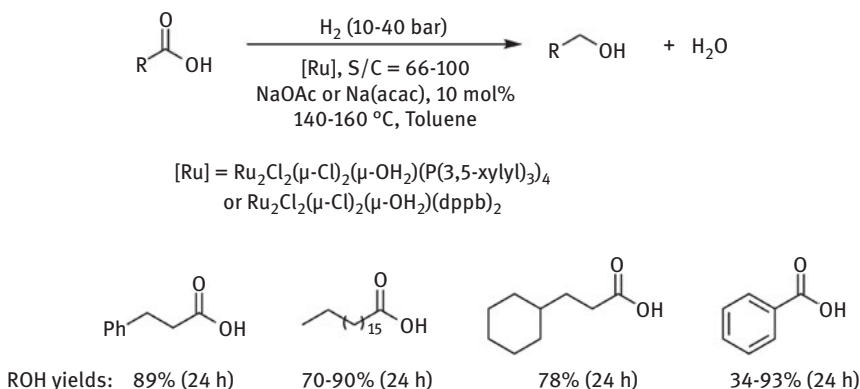
Figure 6.48: Hydrogenation of carboxylic acids by the ruthenium catalytic system reported by Naruto and Saito.

6.5.3 Non-noble metal catalysts

The only example of first-row metal-based catalyst for carboxylic acid hydrogenation has been reported by Elsevier, de Bruin and coworkers [80]. The catalytic system is formed from $Co(BF_4)_2$ and the tripodal Triphos ligand and operates under relatively mild conditions (80 bar H_2, 100 °C) providing TONs of up to 8000 in the hydrogenation of aromatic and aliphatic (long and short-chain) carboxylic acids. As shown above this catalytic system is also active in ester hydrogenation, although faster reactions were observed for the reduction of the carboxylic acids. With this catalyst, acetic acid was hydrogenated to ethanol in 94 % conversion after 22 h by using a substrate-to-catalyst ratio of 400, while reduction of formic acid to a mixture of methanol and methyl formate was accomplished with moderate to high conversions (56–99 %, 22 h) using S/C ratios between 200 and 400. Notably, the Triphos-Co catalyst is more efficient in the hydrogenation of carboxylic acids than the previously reported ruthenium and iridium catalysts.

6.6 Conclusions and outlook

Hydrogenation of carbonyl derivatives serves as a method for the regeneration of alcohols employed as liquid organic hydrogen carriers (LOHCs). While significant progresses have been achieved in the last decade in the hydrogenation of ketones as well as in the reduction of low reactive esters and amides, development of more highly active, long-lived first-row metal based catalysts is required for a widespread implementation of alcohol/carbonyl derivative systems in H_2 storage.

Furthermore, by considering the principle of microscopic reversibility, catalysts that promote the hydrogenation of a carbonyl derivative to alcohol should also catalyze the reverse dehydrogenation process. However, there are still a limited number of fully reversible H_2-storage systems based on alcohol/carbonyl derivative pairs, and all of them involve the use of costly catalysts that operate at relatively high catalyst loadings [16, 87, 88]. Among these systems, the highest hydrogen storage capacity achieved has been 2.8–2.9 %wt, obtained by the use of a 2-isopropanol/acetone system (maximum capacity of 3.35 %wt H_2) in which the hydrogenation and dehydrogenation processes are catalyzed by an iridium complex (S/C = 67) under solventless conditions [16]. On the other hand, the two other reversible systems reported are based on alcohol+amine/ amide pairs and made use of ruthenium catalysts (S/C = 100–250) [87, 88]. Since the latter systems were tested using solutions in dioxane of the hydrogen carrier, significantly lower hydrogen capacities (0.085 %wt and 1.65 %wt) with respect to the maximum theoretical values (6.56 %wt and 5.3 %wt, respectively) were obtained.

In summary, it can be expected that research in this field will continue with a focus in the development of reversible H_2-storage systems based on widely available, stable and low-toxic alcohol/carbonyl derivative pairs in which the loading and release of hydrogen can easily be performed by the participation of the same catalyst by just adjusting the reaction conditions, mainly temperature and hydrogen pressure. Regarding catalysts, as mention above, an emphasis in the development of cost-effective and productive catalytic systems that can function both in the hydrogen release (dehydrogenation) and recharge (hydrogenation) processes can be foreseen.

References

[1] Dalebrook AF, Gan W, Grasemann M, Moret S, Laurenczy G. Hydrogen storage: beyond conventional methods. Chem Commun. 2013;49:8735.

[2] Zhu QL, Xu Q. Liquid organic and inorganic chemical hydrides for high-capacity hydrogen storage. Energy Environ Sci. 2015;8:478.

[3] Preuster P, Papp C, Wasserscheid P. Liquid organic hydrogen carriers (LOHCs): toward a hydrogen-free hydrogen economy. Acc Chem Res. 2017;50:74.

[4]   Campos J. Dehydrogenation of alcohols and polyols from a hydrogen production perspective. In: Zell T, Langer R, editors. Hydrogen Storage. Berlin, Germany and Boston, MA, USA: De Gruyter, forthcoming 2018.

[5]   Trincado M, Banerjeea D, Grützmacher H. Molecular catalysts for hydrogen production from alcohols. Energy Environ Sci. 2014;7:2464.

[6]   Johnson TC, Morris DJ, Wills M. Hydrogen generation from formic acid and alcohols using homogeneous catalysts. Chem Soc Rev. 2010;39:81.

[7]   Crabtree RH. Homogeneous transition metal catalysis of acceptorless dehydrogenative alcohol oxidation: applications in hydrogen storage and to heterocycle synthesis. Chem Rev. 2017;117:9228.

[8]   Chamoun R, Demirci UB, Miele P. Cyclic dehydrogenation-(re)hydrogenation with hydrogen-storage materials: an overview. Energy Technol. 2015;3:100.

[9]   Teichmann D, Arlt W, Wasserscheid P, Freymann R. A future energy supply based on liquid organic hydrogen carriers (LOHC). Energy Environ Sci. 2011;4:2767.

[10] De Vries JG, Elsevier CJ, Eds. Handbook of homogeneous hydrogenation. Weinheim: Wiley-VCH; 2007.

[11] Dub PA, Ikariya T. Catalytic reductive transformations of carboxylic and carbonic acid derivatives using molecular hydrogen. ACS Catal. 2012;2:1718.

[12] Khusnutdinova JR, Milstein D. Metal–ligand cooperation. Angew Chem Int Ed. 2015;54:12236.

[13] Zhao B, Han Z, Ding K. The N–H functional group in organometallic catalysis. Angew Chem Int Ed. 2013;52:4744.

[14] Gunanathan C, Milstein D. Bond activation by metal–ligand cooperation: Design of "green" catalytic reactions based on aromatization–dearomatization of pincer complexes. Top Organomet Chem. 2011;37:55.

[15] Wang D, Astruc D. The golden age of transfer hydrogenation. Chem Rev. 2015;115:6621.

[16] Kawahara R, Fujita K, Yamaguchi R. Cooperative catalysis by iridium complexes with a bipyridonate ligand: versatile dehydrogenative oxidation of alcohols and reversible dehydrogenation–hydrogenation between 2-propanol and acetone. Angew Chem Int Ed. 2012;51:12790.

[17] Adair GRA, Williams JMJ. Oxidant-free oxidation: ruthenium catalysed dehydrogenation of alcohols. Tetrahedron Lett. 2005;46:8233.

[18] Junge H, Beller M. Ruthenium-catalyzed generation of hydrogen from iso-propanol. Tetrahedron Lett. 2005;46:1031.

[19] Blum Y, Czarkle D, Rahamlm Y, Shvo Y. (Cyclopentadienone)ruthenium carbonyl complexes – A new class of homogeneous hydrogenation catalysts. Organometallics. 1985;4:1459.

[20] Conley BL, Pennington-Boggio MK, Boz E, Williams TJ. Discovery, applications, and catalytic mechanisms of Shvo's catalyst. Chem Rev. 2010;110:2294.

[21] Choi JH, Kim N, Shin YJ, Park JH, Park J. Heterogeneous Shvo-type ruthenium catalyst: dehydrogenation of alcohols without hydrogen acceptors. Tetrahedron Lett. 2004;45:4607.

[22] Doucet H, Ohkuma T, Murata K, Yokozawa T, Kozawa M, Katayama E, et al. *trans*-[RuCl$_2$(phosphane)$_2$(1,2-diamine)] and chiral *trans*-[RuCl$_2$(diphosphane)(1,2-diamine)]: shelf-stable precatalysts for the rapid, productive, and stereoselective hydrogenation of ketones. Angew Chem Int Ed. 1998;37:1703.

[23] Noyori R, Ohkuma T. Asymmetric catalysis by architectural and functional molecular engineering: practical chemo- and stereoselective hydrogenation of ketones. Angew Chem Int Ed. 2001;40:40.

[24] Baratta W, Barbato C, Magnolia S, Siega K, Rigo P. Chiral and nonchiral [OsX$_2$(diphosphane)(diamine)] (X: Cl, OCH$_2$CF$_3$). Complexes for fast hydrogenation of carbonyl compounds. Chem Eur J. 2010;16:3201.

[25] Baratta W, Bossi G, Putignano E, Rigo P. Pincer and diamine Ru and Os diphosphane complexes as efficient catalysts for the dehydrogenation of alcohols to ketones. Chem Eur J. 2011;17:3474.

[26] Ohkuma T, Sandoval CA, Srinivasan R, Lin Q, Wei Y, Muñiz K, et al. Asymmetric hydrogenation of *tert*-alkyl ketones. J Am Chem Soc. 2005;127:8288.

[27] Baratta W, Ballico M, Del Zotto A, Siega K, Magnolia S, Rigo P. Osmium pyme complexes for fast hydrogenation and asymmetric transfer hydrogenation of ketones. Chem Eur J. 2008;14:2557.

[28] Putignano E, Bossi G, Rigo P, Baratta W. MCl$_2$(ampy)(dppf) (M = Ru, Os): multitasking catalysts for carbonyl compound/alcohol interconversion reactions. Organometallics. 2012;31:1133.

[29] Baratta W, Ballico M, Chelucci G, Siega K, Rigo P. Osmium(II) CNN pincer complexes as efficient catalysts for both asymmetric transfer and H$_2$ hydrogenation of ketones. Angew Chem Int Ed. 2008;47:4362.

[30] Baratta W, Chelucci G, Magnolia S, Siega K, Rigo P. Highly productive CNN pincer ruthenium catalysts for the asymmetric reduction of alkyl aryl ketones. Chem Eur J. 2009;15:726.

[31] Baratta W, Fanfoni L, Magnolia S, Siega K, Rigo P. Benzo[*h*]quinoline pincer ruthenium and osmium catalysts for hydrogenation of ketones. Eur J Inorg Chem. 2010;1419.

[32] Nielsen M, Kammer A, Cozzula D, Junge H, Gladiali S, Beller M. Efficient hydrogen production from alcohols under mild reaction conditions. Angew Chem Int Ed. 2011;50:9593.

[33] Kuriyama W, Matsumoto T, Ogata O, Ino Y, Aoki K, Tanaka S, et al. Catalytic hydrogenation of esters. Development of an efficient catalyst and processes for synthetising (*R*)-1,2-propanediol and 2-(*L*-menthoxy)ethanol. Org Process Res Dev. 2012;16:166.

[34] Zhang J, Gandelman M, Shimon LJW, Rozenberg H, Milstein D. Electron-rich, bulky ruthenium PNP-type complexes. Acceptorless catalytic alcohol dehydrogenation. Organometallics. 2004;23:4026.

[35] Zhang J, Gandelman M, Shimon LJW, Milstein D. Electron-rich, bulky PNN-type ruthenium complexes: synthesis, characterization and catalysis of alcohol dehydrogenation. Dalton Trans. 2007;107.

[36] Zhang J, Balaraman E, Leitus G, Milstein D. Electron-rich PNP- and PNN-type ruthenium(II) hydrido borohydride pincer complexes. Synthesis, structure, and catalytic dehydrogenation of alcohols and hydrogenation of esters. Organometallics. 2011;30:5716.

[37] Fujita K, Tanino N, Yamaguchi R. Ligand-promoted dehydrogenation of alcohols catalyzed by Cp*Ir complexes. A new catalytic system for oxidant-free oxidation of alcohols. Org Lett. 2007;9:109.

[38] Fujita K, Yoshida T, Imori Y, Yamaguchi R. Dehydrogenative oxidation of primary and secondary alcohols catalyzed by a Cp*Ir complex having a functional C,N-chelate ligand. Org Lett. 2011;13:2278.

[39] Kawahara R, Fujita K, Yamaguchi R. Dehydrogenative oxidation of alcohols in aqueous media using water-soluble and reusable Cp*Ir catalysts bearing a functional bipyridine ligand. J Am Chem Soc. 2012;134:3643.

[40] Royer AM, Rauchfuss TB, Gray DL. Organoiridium pyridonates and their role in the dehydrogenation of alcohols. Organometallics. 2010;29:6763.

[41] Chakraborty S, Lagaditis PO, Förster M, Bielinski EA, Hazari N, Holthausen MC, et al. Well-defined iron catalysts for the acceptorless reversible dehydrogenation-hydrogenation of alcohols and ketones. ACS Catal. 2014;4:3994.

[42] Bonitatibus PJ, Chakraborty S, Doherty MD, Siclovan O, Jones WD, Soloveichik GL. Reversible catalytic dehydrogenation of alcohols for energy storage. Proc Natl Acad Sci USA. 2015;112:1687.

[43] Zhang G, Scott BL, Hanson SK. Mild and homogeneous cobalt-catalyzed hydrogenation of C=C, C=O, and C=N bonds. Angew Chem Int Ed. 2012;51:12102.

[44] Zhang G, Hanson SK. Cobalt-catalyzed acceptorless alcohol dehydrogenation. Org Lett. 2013;15:650.

[45] Zhang G, Vasudevan KV, Scott BL, Hanson SK. Understanding the mechanisms of cobalt-catalyzed hydrogenation and dehydrogenation reactions. J Am Chem Soc. 2013;135:8668.

[46] Chakraborty S, Piszel PE, Brennessel WW, Jones WD. A single nickel catalyst for the acceptor-less dehydrogenation of alcohols and hydrogenation of carbonyl compounds. Organometallics. 2015;34:5203.

[47] Pritchard J, Filonenko GA, Van Putten R, Hensen EJM, Pidko EA. Heterogeneous and homoge-neous catalysis for the hydrogenation of carboxylic acid derivatives: history, advances and future directions. Chem Soc Rev. 2015;44:3808.

[48] Grey RA, Pez GP, Wallo A. Anionic metal hydride catalysts. 2. Application to the hydrogenation of ketones, aldehydes, carboxylic acid esters, and nitriles. J Am Chem Soc. 1981;103:7536.

[49] Teunissen HT, Elsevier CJ. Homogeneous ruthenium catalyzed hydrogenation of esters to alcohols. Chem Commun. 1998;1367.

[50] Nomura K, Ogura H, Imanishi Y. Ruthenium catalyzed hydrogenation of methyl phenylacetate under low hydrogen pressure. J Mol Catal A. 2002;178:105.

[51] Zhang J, Leitus G, Ben-David Y, Milstein D. Efficient homogeneous catalytic hydrogenation of esters to alcohols. Angew Chem Int Ed. 2006;45:1113.

[52] Zhang J, Leitus G, Ben-David Y, Milstein D. Facile conversion of alcohols into esters and dihydrogen catalyzed by new ruthenium complexes. J Am Chem Soc. 2005;127:10840.

[53] Fogler E, Balaraman E, Ben-David Y, Leitus G, Shimon LJW, Milstein D. New CNN-type ruthenium pincer NHC complexes. Mild, efficient catalytic hydrogenation of esters. Organometallics. 2011;30:3826.

[54] Sun Y, Koehler C, Tan R, Annibale VT, Song D. Ester hydrogenation catalyzed by Ru-CNN pincer complexes. Chem Commun. 2011;47:8349.

[55] Filonenko GA, Cosimi E, Lefort L, Conley MP, Coperet C, Lutz M, et al. Lutidine-derived Ru-CNC hydrogenation pincer catalysts with versatile coordination properties. ACS Catal. 2014;4:2667.

[56] Kim D, Le L, Drance MJ, Jensen KH, Bogdanovski K, Cervarich TN, et al. Ester hydrogenation catalyzed by CNN-pincer complexes of ruthenium. Organometallics. 2016;35:982.

[57] Li W, Xie J-H, Yuan M-L, Zhou Q-L. Ruthenium complexes of tetradentate bipyridine ligands: highly efficient catalysts for the hydrogenation of carboxylic esters and lactones. Green Chem. 2014;16:4081.

[58] Saudan LA, Saudan CM, Debieux C, Wyss P. Dihydrogen reduction of carboxylic esters to alcohols under the catalysis of homogeneous ruthenium complexes: high efficiency and unprecedented chemoselectivity. Angew Chem Int Ed. 2007;46:7473.

[59] Nielsen M, Junge H, Kammer A, Beller M. Towards a green process for bulk-scale synthesis of ethyl acetate: efficient acceptorless dehydrogenation of ethanol. Angew Chem Int Ed. 2012;51:5711.

[60] Spasyuk D, Smith S, Gusev DG. From esters to alcohols and back with ruthenium and osmium catalysts. Angew Chem Int Ed. 2012;51:2772.

[61] Spasyuk D, Gusev DG. Acceptorless dehydrogenative coupling of ethanol and hydrogenation of esters and imines. Organometallics. 2012;31:5239.

[62] Spasyuk D, Vicent C, Gusev DG. Chemoselective hydrogenation of carbonyl compounds and acceptorless dehydrogenative coupling of alcohols. J Am Chem Soc. 2015;137:3743.

[63] Wang Z, Chen X, Liu B, Liu Q, Solan GA, Yang X, et al. Cooperative interplay between a flexible PNN-Ru(II) complex and a $NaBH_4$ additive in the efficient catalytic hydrogenation of esters. Catal Sci Technol. 2017;7:1297.

[64] Pan B, Liu B, Yue E, Liu Q, Yang X, Wang Z, et al. A ruthenium catalyst with unprecedented effectiveness for the coupling cyclization of γ-amino alcohols and secondary alcohols. ACS Catal. 2016;6:1247.

[65] Fogler E, Garg JA, Hu P, Leitus G, Shimon LJW, Milstein D. System with potential dual modes of metal–ligand cooperation: highly catalytically active pyridine-based PNNH–Ru pincer complexes. Chem Eur J. 2014;20:15727.

[66] Tan X, Wang Y, Liu Y, Wang F, Shi L, Lee K-H, et al. Highly efficient tetradentate ruthenium catalyst for ester reduction: especially for hydrogenation of fatty acid esters. Org Lett. 2015;17:454.

[67] Wang F, Tan X, Lv H, Zhang X. New ruthenium complexes based on tetradentate bipyridine ligands for catalytic hydrogenation of esters. Chem Asian J. 2016;11:2103.

[68] Spasyuk D, Smith S, Gusev DG. Replacing phosphorus with sulfur for the efficient hydrogenation of esters. Angew Chem Int Ed. 2013;52:2538.

[69] Filonenko GA, Aguila MJB, Schulpen EN, Van Putten R, Wiecko J, Müller C, et al. Bis-*N*-heterocyclic carbene aminopincer ligands enable high activity in Ru-catalyzed ester hydrogenation. J Am Chem Soc. 2015;137:7620.

[70] Wylie WN, Morris RH. Ester hydrogenation catalyzed by a ruthenium(II) complex bearing an N-heterocyclic carbene tethered with an "NH_2" group and a DFT study of the proposed bifunctional mechanism. ACS Catal. 2013;3:32.

[71] Junge K, Wendt B, Westerhaus FA, Spannenberg A, Jiao H, Beller M. Phosphine–imidazolyl ligands for the efficient ruthenium-catalyzed hydrogenation of carboxylic esters. Chem Eur J. 2012;18:9011.

[72] Westerhaus FA, Wendt B, Dumrath A, Wienhöfer G, Junge K, Beller M. Ruthenium catalysts for hydrogenation of aromatic and aliphatic esters: make use of bidentate carbene ligands. ChemSusChem. 2013;6:1001.

[73] Junge K, Wendt B, Jiao H, Beller M. Iridium-catalyzed hydrogenation of carboxylic acid esters. ChemCatChem. 2014;6:2810.

[74] Brewster TP, Rezayee NM, Culakova Z, Sanford MS, Goldberg KI. Base-free iridium-catalyzed hydrogenation of esters and lactones. ACS Catal. 2016;6:3113.

[75] Zell T, Ben-David Y, Milstein D. Unprecedented iron-catalyzed ester hydrogenation. Mild, selective, and efficient hydrogenation of trifluoroacetic esters to alcohols catalyzed by an iron pincer complex. Angew Chem Int Ed. 2014;53:4685.

[76] Chakraborty S, Dai H, Bhattacharya P, Fairweather NT, Gibson MS, Krause JA, et al. Iron-based catalysts for the hydrogenation of esters to alcohols. J Am Chem Soc. 2014;136:7869.

[77] Werkmeister S, Junge K, Wendt B, Alberico E, Jiao H, Baumann W, et al. Hydrogenation of esters to alcohols with a well-defined iron complex. Angew Chem Int Ed. 2014;53:8722.

[78] Elangovan S, Wendt B, Topf C, Bachmann S, Scalone M, Spannenberg A, et al. Improved second generation iron pincer complexes for effective ester hydrogenation. Adv Synth Catal. 2016;358:820.

[79] Qu S, Dai H, Dang Y, Song C, Wang Z-X, Guan H. Computational mechanistic study of Fe-catalyzed hydrogenation of esters to alcohols: improving catalysis by accelerating precatalyst activation with a Lewis base. ACS Catal. 2014;4:4377.

[80] Korstanje TJ, Van Der Vlugt JI, Elsevier CJ, De Bruin B. Hydrogenation of carboxylic acids with a homogeneous cobalt catalyst. Science. 2015;350:298.

[81] Srimani D, Mukherjee A, Goldberg AFG, Leitus G, Diskin-Posner Y, Shimon LJW, et al. Cobalt-catalyzed hydrogenation of esters to alcohols: unexpected reactivity trend indicates ester enolate intermediacy. Angew Chem Int Ed. 2015;54:12357.

[82] Yuwen J, Chakraborty S, Brennessel WW, Jones WD. Additive-free cobalt-catalyzed hydrogenation of esters to alcohols. ACS Catal. 2017;7:3735.

[83] Elangovan S, Garbe M, Jiao H, Spannenberg A, Junge K, Beller M. Hydrogenation of esters to alcohols catalyzed by defined manganese pincer complexes. Angew Chem Int Ed. 2016;55:15364.

[84] Widegren MB, Harkness GJ, Slawin AMZ, Cordes DB, Clarke ML. A highly active manganese catalyst for enantioselective ketone and ester hydrogenation. Angew Chem Int Ed. 2017;56:5825.

[85] Espinosa-Jalapa NA, Nerush A, Shimon LJW, Leitus G, Avram L, Ben-David Y, et al. Manganese-catalyzed hydrogenation of esters to alcohols. Chem Eur J. 2017;23:5934.

[86] Van Putten R, Uslamin EA, Garbe M, Liu C, Gonzalez-de-Castro A, Lutz M, et al. Non-pincer-type manganese complexes as efficient catalysts for the hydrogenation of esters. Angew Chem Int Ed. 2017;56:7531.

[87] Hu P, Fogler E, Diskin-Posner Y, Iron MA, Milstein D. A novel liquid organic hydrogen carrier system based on catalytic peptide formation and hydrogenation. Nat Commun. 2015;6:6859.

[88] Hu P, Ben-David Y, Milstein D. Rechargeable hydrogen storage system based on the dehydrogenative coupling of ethylenediamine with ethanol. Angew Chem Int Ed. 2016;55:1061.

[89] Ito M, Koo LW, Himizu A, Kobayashi C, Sakaguchi A, Ikariya T. Hydrogenation of *N*-acylcarbamates and *N*-acylsulfonamides catalyzed by a bifunctional [Cp*Ru(PN)] complex. Angew Chem Int Ed. 2009;48:1324.

[90] Balaraman E, Gnanaprakasam B, Shimon LJW, Milstein D. Direct hydrogenation of amides to alcohols and amines under mild conditions. J Am Chem Soc. 2010;132:16756.

[91] Barrios-Francisco R, Balaraman E, Diskin-Posner Y, Leitus G, Shimon LJW, Milstein D. PNN ruthenium pincer complexes based on phosphinated 2,2′-dipyridinemethane and 2,2′-oxobis-pyridine. Metal–ligand cooperation in cyclometalation and catalysis. Organometallics. 2013;32:2973.

[92] Gnanaprakasam B, Milstein D. Synthesis of amides from esters and amines with liberation of H_2 under neutral conditions. J Am Chem Soc. 2011;133:1682.

[93] Ito M, Ootsuka T, Watari R, Shiibashi A, Himizu A, Ikariya T. Catalytic hydrogenation of carboxamides and esters by well-defined Cp*Ru complexes bearing a protic amine ligand. J Am Chem Soc. 2011;133:4240.

[94] John JM, Bergens SH. A highly active catalyst for the hydrogenation of amides to alcohols and amines. Angew Chem Int Ed. 2011;50:10377.

[95] John JM, Loorthuraja R, Antoniuk E, Bergens SH. Catalytic hydrogenation of functionalized amides under basic and neutral conditions. Catal Sci Technol. 2015;5:1181.

[96] Kita Y, Higuchi T, Mashima K. Hydrogenation of amides catalyzed by a combined catalytic system of a Ru complex with a zinc salt. Chem Commun. 2014;50:11211.

[97] Miura T, Held IE, Oishi S, Naruto M, Saito S. Catalytic hydrogenation of unactivated amides enabled by hydrogenation of catalyst precursor. Tetrahedron Lett. 2013;54:2674.

[98] Cabrero-Antonino JR, Alberico E, Drexler H-J, Baumann W, Junge K, Junge H, et al. Efficient base free hydrogenation of amides to alcohols and amines catalyzed by well-defined pincer imidazolyl–ruthenium complexes. ACS Catal. 2016;6:47.

[99] Shi L, Tan X, Long J, Xiong X, Yang S, Xue P, et al. Direct catalytic hydrogenation of simple amides: A highly efficient approach from amides to amines and alcohols. Chem Eur J. 2017;23:546.

[100] Garg JA, Chakraborty S, Ben-David Y, Milstein D. Unprecedented iron-catalyzed selective hydrogenation of activated amides to amines and alcohols. Chem Commun. 2016;52:5285.

[101] Schneck F, Assmann M, Balmer M, Harms K, Langer R. Selective hydrogenation of amides to amines and alcohols catalyzed by improved iron pincer complexes. Organometallics. 2016;35:1931.

[102] Rezayee NM, Samblanet DC, Sanford MS. Iron-catalyzed hydrogenation of amides to alcohols and amines. ACS Catal. 2016;6:6377.

[103] Jayarathne U, Zhang Y, Hazari N, Bernskoetter WH. Selective iron-catalyzed deaminative hydrogenation of amides. Organometallics. 2017;36:409.

[104] Papa V, Cabrero-Antonino JR, Alberico E, Spanneberg A, Junge K, Junge H, et al. Efficient and selective hydrogenation of amides to alcohols and amines using a well-defined manganese–PNN pincer complex. Chem Sci. 2017;8:3576.

[105] Balaraman E, Khaskin E, Leitus G, Milstein D. Catalytic transformation of alcohols to carboxylic acid salts and H_2 using water as the oxygen atom source. Nat Chem. 2013;5:122.

[106] Zhang L, Nguyen DH, Raffa G, Trivelli X, Capet F, Desset S, et al. Catalytic conversion of alcohols into carboxylic acid salts in water: scope, recycling, and mechanistic insights. ChemSusChem. 2016;9:1413.

[107] Brewster TP, Miller AJM, Heinekey DM, Goldberg KI. Hydrogenation of carboxylic acids catalyzed by half-sandwich complexes of iridium and rhodium. J Am Chem Soc. 2013;135:16022.

[108] Tsurusaki A, Murata K, Onishi N, Sordakis K, Laurenczy G, Himeda Y. Investigation of hydrogenation of formic acid to methanol using H_2 or formic acid as a hydrogen source. ACS Catal. 2017;7:1123.

[109] Vom Stein T, Meuresch M, Limper D, Schmitz M, Hölscher M, Coetzee J, et al. Highly versatile catalytic hydrogenation of carboxylic and carbonic acid derivatives using a Ru-Triphos complex: molecular control over selectivity and substrate scope. J Am Chem Soc. 2014;136:13217.

[110] Cui X, Li Y, Topf C, Junge K, Beller M. Direct ruthenium-catalyzed hydrogenation of carboxylic acids to alcohols. Angew Chem Int Ed. 2015;54:10596.

[111] Li Y, Topf C, Cui X, Junge K, Beller M. Lewis acid promoted ruthenium(II)-catalyzed etherifications by selective hydrogenation of carboxylic acids/esters. Angew Chem Int Ed. 2015;54:5196.

[112] Deng L, Kang B, Englert U, Klankermayer J, Palkovits R. Direct hydrogenation of biobased carboxylic acids mediated by a nitrogen-centered tridentate phosphine ligand. ChemSusChem. 2016;9:177.

[113] Naruto M, Saito S. Cationic mononuclear ruthenium carboxylates as catalyst prototypes for self-induced hydrogenation of carboxylic acids. Nat Commun. 2015;6:8140.This article has previously been published in the journal Physical Sciences Reviews. Please cite as: Suárez, A. Hydrogenation of carbonyl compounds of relevance to hydrogen storage in alcohols. Physical Sciences Reviews [Online] **2018**, 3 (5). DOI: 10.1515/psr-2017-0028

Jesús Campos

7 Dehydrogenation of alcohols and polyols from a hydrogen production perspective

Abstract: The production of hydrogen from renewable resources is still a major challenge in our way to reach a foreseen hydrogen economy. Abstracting the hydrogen contained in alcohols by means of acceptorless dehydrogenation reactions has emerged as a viable method with high potential. This is particularly true when applied to bio-based alcohols such as ethanol, glycerol or sugars, whose hydrogen extrusion is covered in this contribution. A general overview of the development of aceptorless alcohol dehydrogenation reactions and its potential implementation into future biorefineries are discussed.

Keywords: acceptorless dehydrogenation, ethanol, glycerol, homogeneous catalysis, sugar alcohols

7.1 Introduction

Transfer hydrogenation reactions mediated by homogeneous catalysts have been known for a long time and serve as powerful and versatile synthetic strategies that fit well with many principles of green chemistry [1]. Alcohols are among the most investigated substrates in these transformations. In a typical process, an alcohol is dehydrogenated by a molecular transition metal catalyst to form a more reactive unsaturated intermediate that can further react with a variety of nucleophiles to yield a diversity of compounds (Figure 7.1a). Those can subsequently be hydrogenated in the same reaction flask with the hydrogen abstracted from the starting alcohol, thus expanding the synthetic applications of these hydrogen borrowing strategies to the point that even C-C forming reactions have been shown to proceed through transfer hydrogenation mechanisms [2]. Attractive attributes of these transformations are the mild conditions required, the high versatility and capacity to account for multicomponent and cascade reactions and the high atom economy. Recent examples provide convenient access to complex pharmaceuticals [3], implementation at industrial level [4] and even intriguing bioorganometallic applications as transfer-hydrogenation drugs [5] or in the development of artificial transfer hydrogenase enzymes [6].

An interesting variation in this scheme is known as acceptorless alcohol dehydrogenation (AAD), arising when the hydrogen molecule borrowed from the alcoholic

(A)

(B)
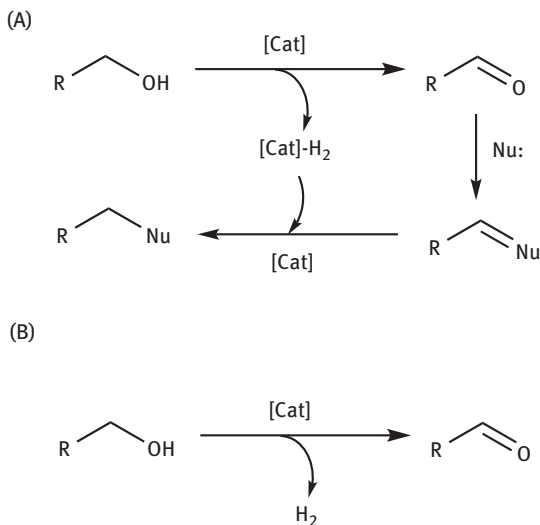
Figure 7.1: General reaction schemes for hydrogen borrowing methodologies (A) and acceptorless dehydrogenation (B) of alcohols.

precursor escapes from the catalytic cycle and evolves as H_2 (Figure 7.1b). Since the opposite transformation, that is, hydrogenation of ketones and aldehydes, is among the most widely studied catalytic processes, it becomes evident that reversible acceptorless dehydrogenation (AD)/hydrogenation reactions could be exploited as potential hydrogen storage systems, as it has been reviewed before [7] and is also analysed in more detail in another chapter. In terms of practicality, such an approach should be based on alcohols containing a high hydrogen storage capacity, a feature almost exclusively found in the simplest methanol, as well as in longer polyols (Table 7.1). While methanol dehydrogenation holds great promise for a future "methanol economy" [8] and is thus treated in a separate chapter, the complete dehydrogenation of longer polyols has not yet been achieved and does not seem truly plausible in the short term given the increased reactivity expected after each dehydrogenation event and, as a consequence, the increased likelihood of catalyst deactivation. Considering this, most efforts on AAD reactions have instead focused on their synthetic applications [9], including the one-step production of carboxylic acids, esters, amides, imines or N-containing heterocycles (Figure 7.2). Among these studies is the work carried out by the group of Milstein.

In the context of alternative energy production, the release of hydrogen gas generation from AAD processes, previously covered in several recent reviews, [9b, 10, 11] can find real uses in cases where alcohols are directly obtained from renewable sources. Moreover, dehydrogenation of renewable alcohols, besides releasing H_2 as a valuable green fuel, could in principle produce added-value unsaturated compounds with synthetic potential to monetize the entire process. This offers
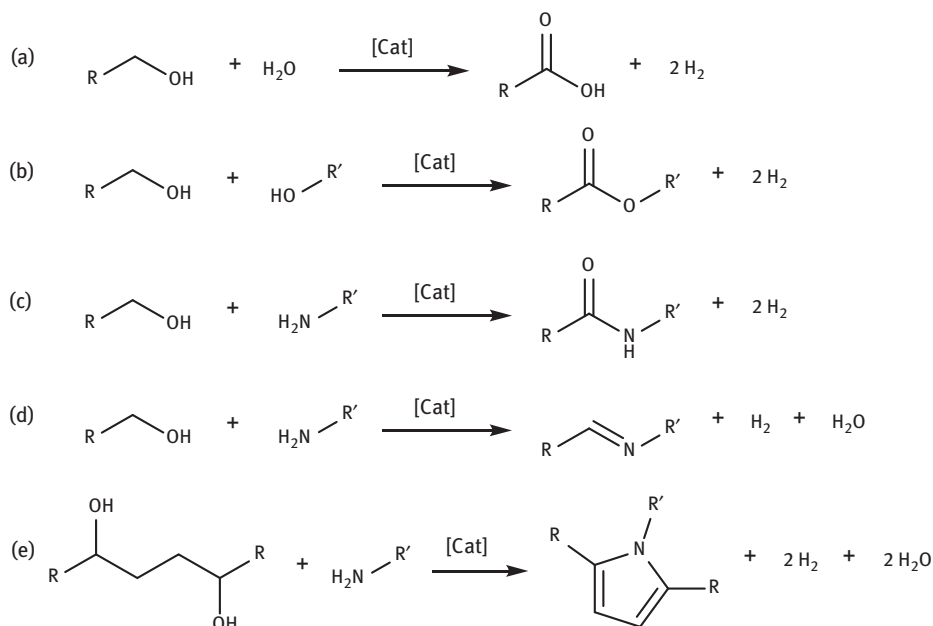
Figure 7.2: Relevant examples of synthetic applications based on AAD reactions.

a promising scenario with clear-cut advantages for implementation into biorefineries, with AAD strategies allowing for the atom economic one-pot production of energy and platform chemicals. In line with this, Table 7.1 collects a summary of relevant alcohols that fulfil the requirements discussed above and whose dehydrogenation, with the exception of methanol, will be covered in the present contribution.

Table 7.1: Summary of selected alcohols relevant for hydrogen production by AAD reactions.

Entry	Alcohol	Reaction	H$_2$ wt%	Reversibility[a]	Added value[b]
1	CH$_3$OH	CH$_3$OH + H$_2$O → CO$_2$ + 3H$_2$	12.0	✓	–
2	CH$_3$CH$_2$OH	CH$_3$CH$_2$OH → CH$_3$COH + H$_2$	4.3	✓	–
3		2 CH$_3$CH$_2$OH → CH$_3$C(O)OEt + 2H$_2$	4.3	✓	✓
4		CH$_3$CH$_2$OH + H$_2$O → CH$_3$COOH + 2H$_2$	6.2	✓	✓
5		CH$_3$CH$_2$OH + 3H$_2$O → 2CO$_2$ + 6H$_2$	12.0	–	–
6	Glycerol	C$_3$H$_g$O$_3$ → C$_3$H$_6$O$_3$ + H$_2$	2.1	✓	✓
7		C$_3$H$_g$O$_3$ + 3H$_2$O → 3 CO$_2$ + 7 H$_2$	9.6	–	–
8	Sugar alcohols	C$_n$H$_{2n + 2}$O$_n$ + n H$_2$O → n CO$_2$ + (2n + 1)H$_2$	8.9 – 9.3	–	–

[a] Transformations for which the reversible reaction (hydrogenation) has been described.
[b] Processes that involve the production of added-value chemicals.

Another general aspect of AAD reactions to bear in mind deals with its thermodynamics. They are endothermic and thermodynamically unfavoured under ambient conditions. A traditional strategy to circumvent this issue and drive the oxidation of alcohols to completion involves the use of sacrificial hydrogen acceptors such as acetone [12] or $^tBuCH=CH_2$ [13], an approach that, although being scholarly valuable, is evidently impractical from the perspective of hydrogen production and will not be covered herein. Alternatively, the thermodynamic aspect can be compensated at higher temperatures, often at the boiling point of the neat alcohol or the solvent employed, by the positive entropic factor ($-T\Delta S$) derived from releasing hydrogen gas. At the same time, working in open systems under boiling conditions favour the gas to escape from the reaction mixture driving the equilibrium to the unsaturated products.

With all this in mind, the present contribution will mainly cover homogeneously catalysed AAD reactions of biomass-derived alcohols, namely ethanol, glycerol, sugars and related substrates. A non-comprehensive perspective on the evolution and state-of-the-art AAD transformations is also presented.

7.2 General perspective on acceptorless alcohol dehydrogenation reactions

The reviews already noted constitute excellent deep surveys covering the development of AAD reactions from its infancy in the 1960s to their current sophisticated applications [9, 10]. Herein, a brief discussion about some highlights of this development and its connection with the general aspects of AAD reactions will be presented.

In the 1960s, Charman reported that Rh(III) salts are capable of catalysing the AD of isopropanol to acetone [14]. He made this interesting observation while trying to develop a catalytic version of Vaska's α-CH hydrogen abstraction reaction from alcohols [15]. Mainly based on kinetic investigations, the author proposed, for the first time, a homogeneously catalysed mechanism for AAD reactions. It is worth mentioning that the appearance of black precipitate and rhodium mirror was observed during the course of these reactions. The catalytic role of these species, as well as of other heterogeneous forms of rhodium such as nanoparticles or colloids, could not be completely ruled out, particularly since these materials have been shown to be active in AAD reactions [16].

In the next decade, Robinson described the use of ruthenium and osmium complexes of the type $[M(OCOR_F)_2(CO)(PPh_3)_2]$ ($R_F = CF_3$, C_2F_5, or C_6F_5) (**1** in Figure 7.3) as catalysts for the dehydrogenation of primary and secondary alcohols [17]. Catalysts based on ruthenium exhibited better performance than their osmium analogues, with ruthenium still today being one of the most widely applied transition metals in transfer hydrogenation chemistry. Another recurrent feature common to traditional and more sophisticated modern catalysts for AAD reactions is the non-innocent character of the
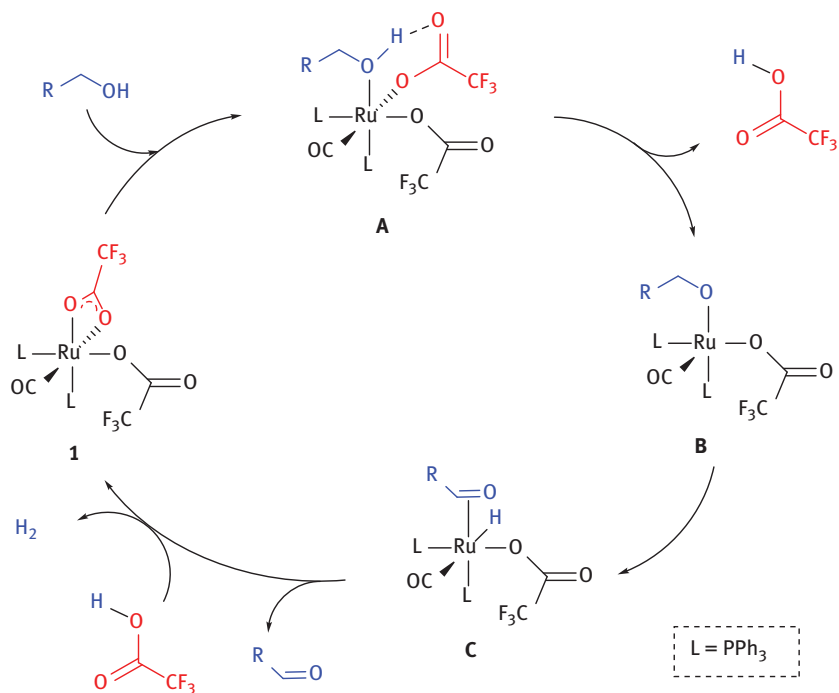
Figure 7.3: Proposed AAD mechanism mediated by [Ru(OCOCF$_3$)$_2$(CO)(PPh$_3$)$_2$] (**1**) involving metal–ligand cooperation. L = triphenylphosphine, PPh$_3$.

ligands bound to the transition metal. Metal–ligand cooperation [18] has become a fundamental aspect in modern transition metal catalysis, and this is particularly true in transfer hydrogenation chemistry [19]. In fact, even in Robinson´s early report, a fluoride-containing carboxylate ligand seems to play a pivotal role in the proposed mechanism. It was suggested that the ligand acts as an internal base to facilitate the formation of the metal–ligated alkoxide **B** (Figure 7.3). The lability of these ligands proved to be essential for catalysis and the catalytic performance followed the trend CF$_3$ ≈ C$_2$F$_5$ > C$_6$F$_6$ >> CH$_3$, in good agreement with the necessity of ligand dissociation. Thus, coordination of the alcohol substrate to catalyst **1** requires the rearrangement of a carboxylate ligand from a κ^2 to a κ^1 coordination mode in structures **1** and **A**, respectively. As stated above, the dissociated carbonyl group behaves as a non-innocent ligand to abstract a proton, being subsequently released as the parent carboxylic acid. This step provides the vacant coordination site required for β-hydrogen elimination from alkoxide **B** to take place. Subsequent aldehyde or ketone dissociation in **C**, followed by the protonation of the metal hydride by external acid, produces molecular hydrogen and regenerates the catalyst. In principle, the released carboxylic acid from **A** could be sufficient to complete the cycle. Nevertheless, the catalytic performance is greatly enhanced by the addition of an excess of trifluoroacetic acid. This mechanism

was supported by kinetic studies and by the catalytic competence of independently isolated ruthenium hydride intermediates related to structure **C**.

This system reached turnover frequencies (TOFs) over 8,000 h^{-1} for the conversion of benzyl alcohol to benzaldehyde, although dehydrogenation of secondary alcohols proved considerably less effective. A few years later, the same catalytic system was tested by Rybak and Ziólkowski to compare its activity against a polystyrene-supported version of the same ruthenium complex [20]. The catalytic performances of the homogeneous catalyst and the heterogeneized material were comparable, although the values were inconsistent with Robinson's report. Thus, the authors found catalytic activities that were six times lower than those reported previously under the same conditions. This was further examined by Garrou a year after when studying ruthenium(II) diphosphine hydride complexes of the type [RuH$_2$(CO)(PPh$_3$)(L-L)] (L-L = chelating diphosphine ligands) as catalysts for AAD reactions [21]. In that case, the activity of Robinson's system appeared to be even lower than in the two previous reports.

The evaluation of the AAD catalytic activity of [Ru(OCOCF$_3$)$_2$(CO)(PPh$_3$)$_2$] in these three studies is based on initial rates of hydrogen production. This is a good example of the inherent difficulties for precise catalytic activity comparison in AAD reactions. As pointed out by Crabtree, AAD reactions are not kinetically well behaved and several factors can significantly alter the observed efficiency of a catalyst 9b. As stated above, the dehydrogenation of alcohols competes with its reverse transformation, namely the hydrogenation of carbonyl compounds. Thus, the observed reaction rates depend in many cases on the velocity at which hydrogen is released from the reaction mixture, which in turn will be dependent on the reaction temperature and on the precise experimental set-up used. In a recent study, it was demonstrated that the initial TOFs measured for AD of primary alcohols to esters was highly dependent on stirring rates due to variations in H$_2$ liquid–gas mass transfer [22].

The above pioneering studies based on rhodium and ruthenium catalysts laid the foundations for a rapidly increasing area of research in the following decades. The other main transition metal used for dehydrogenation reactions is iridium, whose first report on AAD reactions dates back to 1987, when Lu and co-workers employed the iridium polyhydride complex [Ir(H)$_5$(P^{i}Pr$_3$)$_2$] as catalyst [23]. In contrast to previous reports based on rhodium and ruthenium, the system was active for the conversion of secondary alcohols to ketones without the need of an acid as hydride acceptor.

Instead of using strong acids as hydride acceptors, Cole-Hamilton demonstrated that AAD reactions could be performed under basic conditions. Several alcohols, including ethylene glycol, were dehydrogenated at high temperatures using [Rh(2,2′-bipyridyl)$_2$]Cl [24] or [RuH$_2$(N$_2$)(PPh$_3$)$_2$] as catalysts [25]. The catalytic performance was improved under irradiation conditions, likely due to catalyst reactivation by carbon monoxide release. It is known that aldehyde decarbonylation can take place

during AAD reactions leading to catalyst poisoning by formation of inactive carbonyl compounds [26]. In fact, this is one of the reasons for choosing *iso*-propanol, instead of ethanol, as a model substrate for AAD catalyst testing.

As in any field of catalysis, the choice of ligand is crucial. As mentioned above, AAD reactions are often carried out at relatively high temperatures, or using low boiling point solvents [27], to promote the release of molecular hydrogen from the reaction mixture. This drives the equilibrium to the desired outcome and helps overcoming the thermodynamic request of dehydrogenation, thanks to the positive entropic factor. However, this temperature requirement hampers catalyst stability. The use of chelating ligands appeared as a highly successful approach to improve this aspect. For instance, the group of Beller employed ruthenium precursor [RuCl$_2$(*p*-cymene)]$_2$ in the presence of simple tetramethylethylenediamine (TMEDA), as well as other polyamines, as stabilizing chelating ligands. The catalytic mixture exhibited TOFs higher than 500 h^{-1} for TMEDA, and the catalyst was active for more than 11 days without apparent decomposition [28].

The use of pincer-type ligands has also been widely applied. In many cases, these systems permit the incorporation of additional functional groups as integrating components of the ligand framework and thus facilitate metal–ligand cooperation mechanisms. The groups of Milstein [9] and Beller 1e have extensively exploited the non-innocent character of PNP and PNN pincer ligands in AAD reactions. In 2011, Beller reported one of the most active catalysts for the AD of *iso*-propanol to acetone by mixing [RuH$_2$(CO)(PPh$_3$)$_3$] with simple PNP ligands [29]. A maximum TOF of around 14,000 h^{-1} was measured after 20 min of reaction and up to 40,000 turnovers were reached after only 12 h. These catalysts operate through outer-sphere mechanisms in which the central amine of the pincer ligand acts as an internal base (Figure 7.4). Moreover, this system does not require external base, whose addition has indeed a detrimental effect.
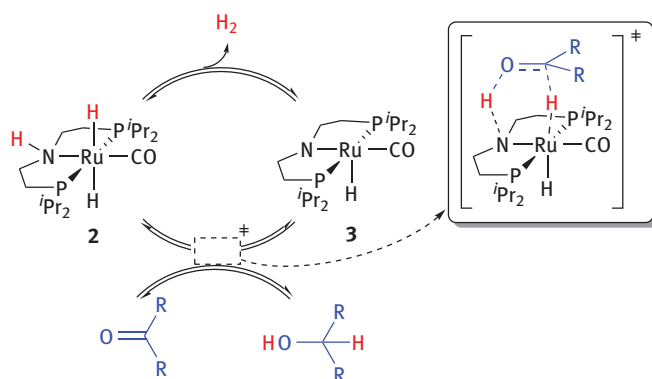
Figure 7.4: AAD reactions catalysed by **2** via an outer-sphere mechanism.

Some of the ruthenium catalysts reported by Beller exhibit an outstanding activity in the dehydrogenation of methanol, formic acid, and other related C1 substrates. It is necessary to highlight a recent example on the complete dehydrogenation of methanol to hydrogen and carbon dioxide catalysed by [RuHCl(CO)(HN($C_2H_4P^iPr_2$)$_2$)] (**4**) under basic conditions and using water as the solvent [30]. TOFs up to 4,700 h^{-1}, much higher than previously reported, were measured. The catalyst was active after 3 weeks and, once more, the proposed mechanism involves the active participation of the ligand through its amide functionality. The main drawback to consider is the need of strong basic conditions (KOH, 8 M) that limit the applicability of the method into real devices. Simultaneously, Grützmacher described another ruthenium system, **5** in Figure 7.5, capable of extracting hydrogen from methanol under base-free conditions [31]. The catalyst is constructed around a hybrid non-innocent diolefin diazadiene ligand that is directly involved in the dehydrogenation of methanol and formic acid. Although it exhibits a high activity (TOF 24,000 h^{-1}) for the dehydrogenation of the latter to CO_2 and H_2, this activity is considerably diminished when methanol is used (TOF 48 h^{-1}). Despite the paramount importance of this and related transformations based on C1 species for energy applications, they will not be further discussed here since they constitute the crux of another chapter.
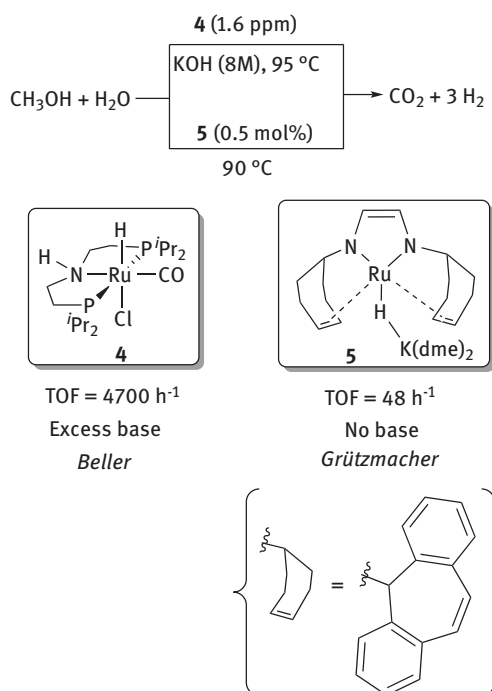
Figure 7.5: Pioneering ruthenium systems for methanol dehydrogenation.

Milstein and co-workers have also reported a number of ruthenium PNP and PNN pincer complexes for AAD reactions. In general, the activity of those for the oxidation of alcohols to ketones or aldehydes is not as high as the ones already discussed. They found, however, an outstanding potential for their application in chemical synthesis through related AAD transformations to access carboxylic acids, esters, amides, imines and other nitrogen-containing compounds (see Figure 7.2) 9a. Although that chemistry will not be specifically covered here, the non-innocent pivotal role of Milstein's pincer ligands in AAD reactions deserves an additional comment. As depicted in Figure 7.6, one of the arms of the pincer ligand readily participates in dehydrogenation and hydrogenation reactions by means of aromatization–dearomatization rearrangements. Some of these systems participate in AAD reactions that directly involve biorelevant alcohols, examples that will be addressed in their corresponding sections below, since those do offer potential specific applications for the production of both raw materials and hydrogen as a fuel.
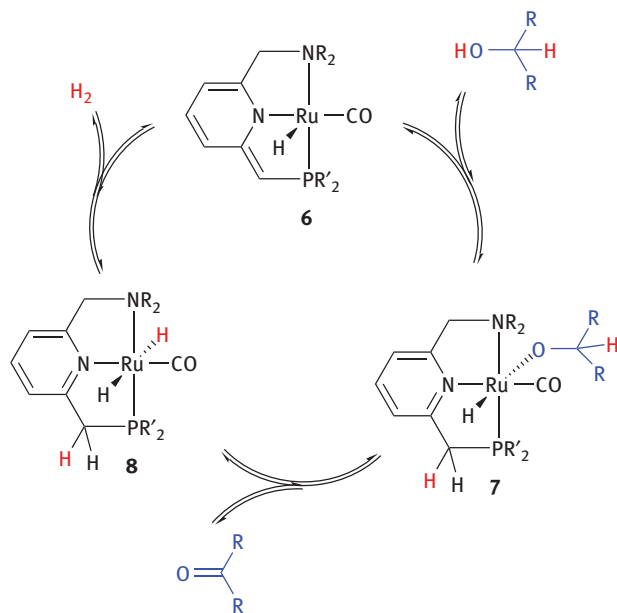
Figure 7.6: General AAD mechanism through ligand aromatization/dearomatization.

Iridium complexes stabilized by pincer ligands have additionally proved successful in AAD reactions. Koridze demonstrated that an iridium pincer complex bearing a POCOP ligand (**9** in Figure 7.7), first prepared by Brookhart [32] and highly active in alkane dehydrogenation [33], was also effective in the AD of secondary alcohols (TONs (turnover numbers) up to 3,420) [34]. The system was, however, unable to
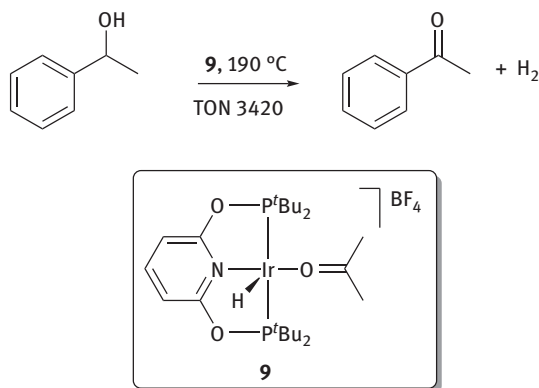
Figure 7.7: AD of 1-phenylethanol using iridium pincer complex **9**.

produce hydrogen from primary alcohols due to decarbonylation and subsequent formation of catalytically inactive species. At variance with the aforementioned ruthenium pincer systems, the POCOP ligand of complex **9** does not actively participate in the catalytic cycle.

On the contrary, in another related example based on iridium catalyst **10**, Gelman proposed the active participation of a dibenzobarrelene-based pincer ligand through an outer-sphere dehydrogenation mechanism (Figure 7.8) [35]. This system was efficient for the AD of both primary and secondary alcohols to produce aldehydes and ketones, respectively. TONs of up to 3,600 were reached and the catalyst stability was later improved by heterogeneization into a sol–gel matrix [36].

In a remarkable example reported by Kempe in 2013, the iridium triazine–pincer complex **13** enables an environmentally attractive synthesis of pyrroles [37] and pyridines [38] by condensation of secondary alcohols and aminoalcohols with concomitant production of two or three molecules of H_2, respectively (Figure 7.9). The proposed mechanism involves the participation of an iridium trihydride intermediate, **D**, whose presence during catalytic reactions was experimentally confirmed. The formation of this intermediate involves protonation of the amide arm of the pincer ligand in **D**, which evinces its non-innocent character.

Other types of non-innocent ligands have been successfully employed in several AAD reactions. In an early and pioneering example, Shvo demonstrated that its renowned dimeric ruthenium precatalyst **14** was capable of converting benzyl alcohol into benzyl benzoate with liberation of two molecules of hydrogen (Figure 7.10) [39]. The same catalyst was capable of dehydrogenating secondary alcohols to ketones and hydrogen with similar TONs (ca. 500). Shvo's precatalyst is typically used in its dimeric form and dissociates into monomeric reduced (**15**) and oxidized (**16**) structures in solution, which are formally Ru(II) and Ru(0) complexes, respectively. Its precise mechanism during hydrogenation/dehydrogenation reactions has
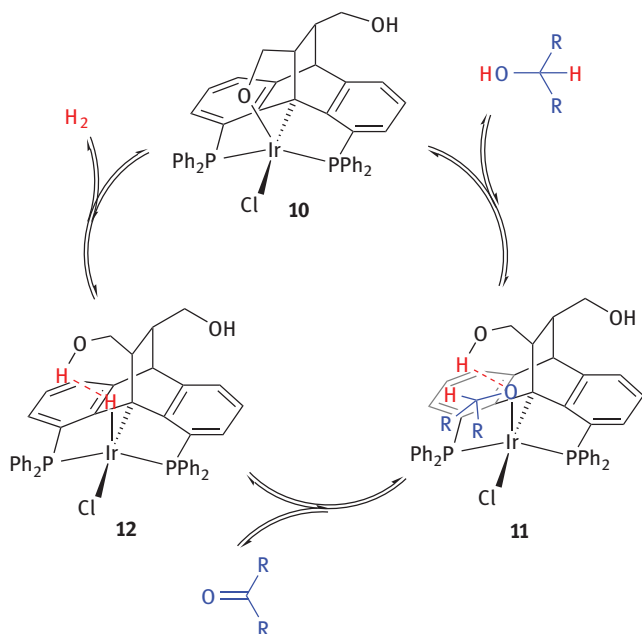
Figure 7.8: Proposed outer-sphere mechanism for AAD mediated by **10**.
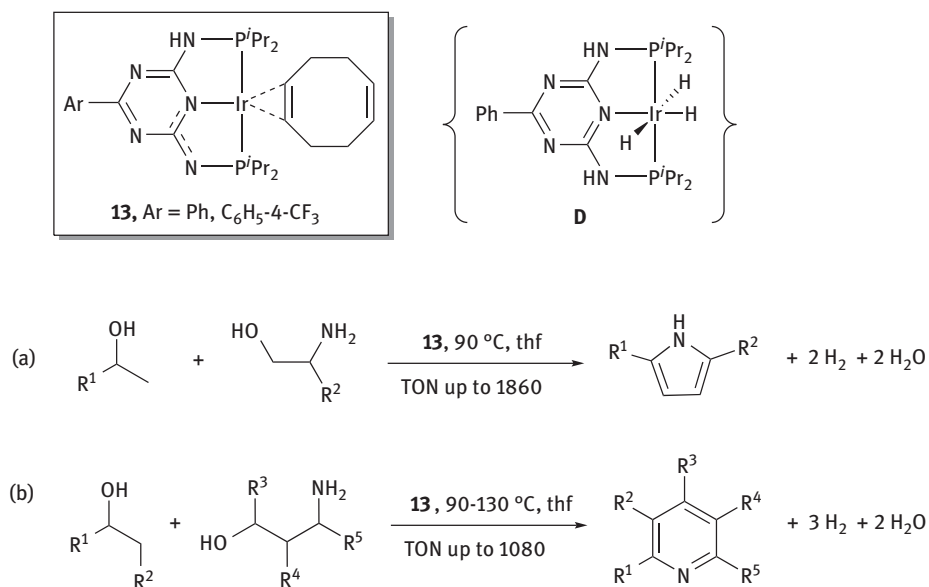
Figure 7.9: Synthesis of pyrroles (a) and pyridines (b) via AAD methods catalysed by **13** and involving the formation of intermediate **D**.
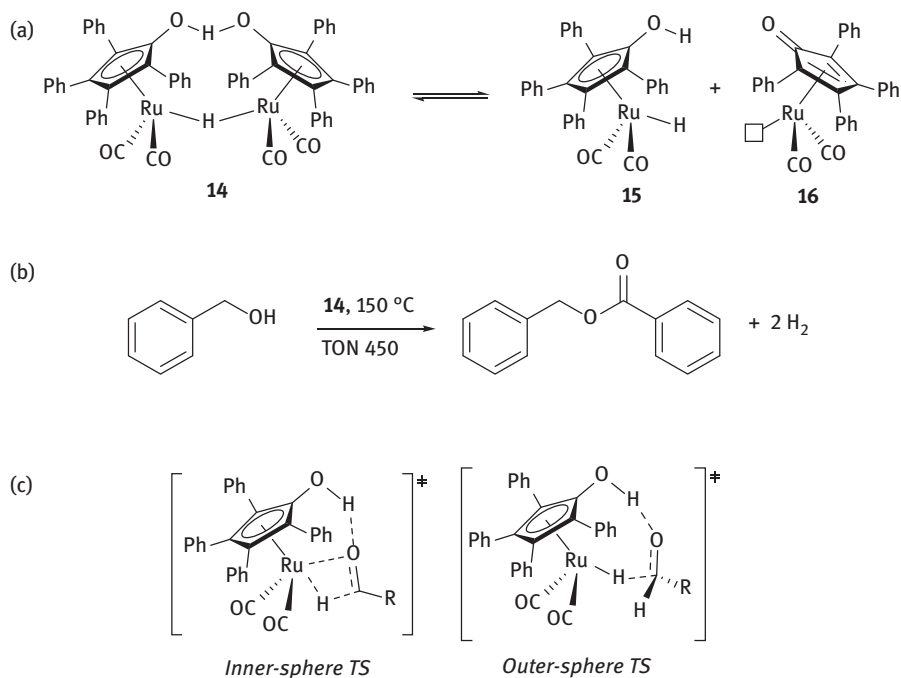
Figure 7.10: (a) Solution dynamic equilibrium of Shvo's dimer **14** and (b) its catalytic application in the AD of benzylic alcohol, including (c) key transition states of the two generally proposed mechanisms (inner and outer spheres).

been extensively investigated [40]. A comprehensive series of kinetic experiments, isotopic labelling, structural characterization of intermediates and computational studies have confirmed the cooperative nature of the system, which was first suggested by Shvo in his original reports [41]. Two main pathways, namely inner- and outer-sphere mechanisms, compete and their prevalence depends on the precise transformation [42]. Key transition states identified for both pathways are depicted in Figure 7.10. Interestingly, the ligand is directly involved both in O-H bond cleavage and H-H bond formation.

Another creative work in the field of AAD cooperative catalysts was developed by Fujita and Yamaguchi, who used a series of cyclopentadienyl Ir(III) complexes bearing non-innocent pyridine ligands (Figure 7.11) [43]. Thus, compound **17** employed 2-hydroxypyridine as a cooperating framework that permits, for instance, the intramolecular protonolysis of iridium hydrides with release of H$_2$. An inner-sphere mechanism was suggested involving the formation of an Ir(III) alkoxide (**18**) from which the carbonylic compound is released by β-hydrogen elimination. The resulting metal hydride **19** couples with the proton provided by the 2-hydroxo group (metal–ligand cooperation) to generate a four-membered Ir(III) cyclometalated
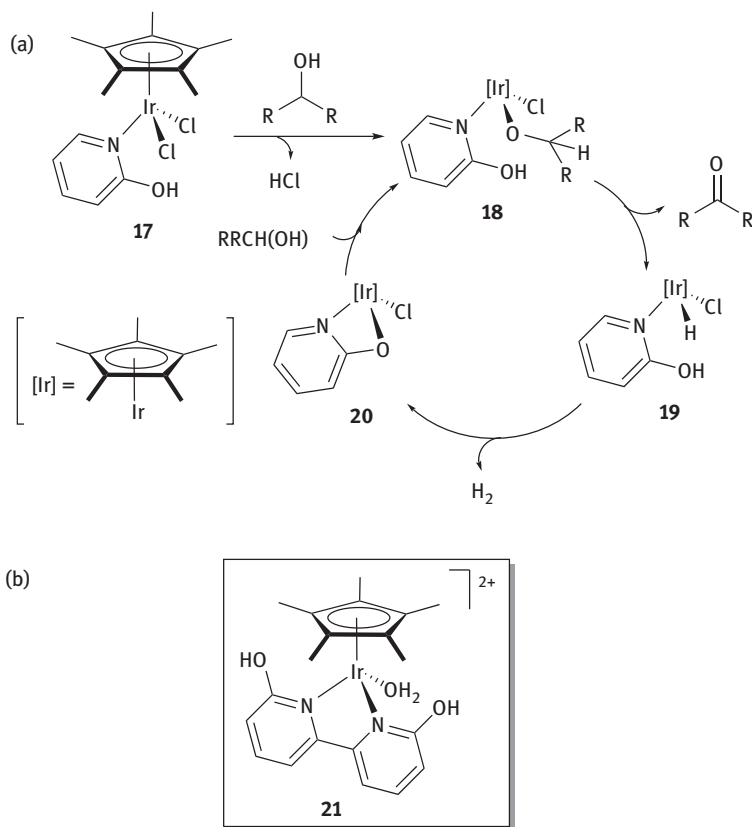
Figure 7.11: (a) General proposed mechanism for AAD reactions mediated by cyclopentadienyl Ir(III) complexes developed by Fujita and Yamaguchi. (b) Representative molecular structure of their second generation of catalysts based on bipyridonate ligands.

alkoxide, **20**. The strained four-membered cyclometallated alkoxide complex **20** is then opened. This proceeds along with the coordination of an alcohol to regenerate catalyst **18**. Compound **17** was tested in the dehydrogenation of secondary alcohols with a maximum TON of 2,120. A bipyridyl chelating version of this ligand (Figure 7.11b) allowed the same authors to extend the scope to primary alcohols, including methanol [44]. Additionally, compound **21** is highly robust and water soluble and thus exhibit good activity for the dehydrogenation of primary and secondary alcohols under organic water biphasic conditions. The catalyst could be recycled up to eight times without significant loss of activity.

In a recent study, a proposed cooperative AAD mechanism relies on the synergistic effect of two metals in close proximity (Figure 7.12) [45]. Using bimetallic diruthenium compound **22** stabilized by a sterically demanding naphthyridine–diimine ligand, the authors demonstrated the selective conversion of a wide range
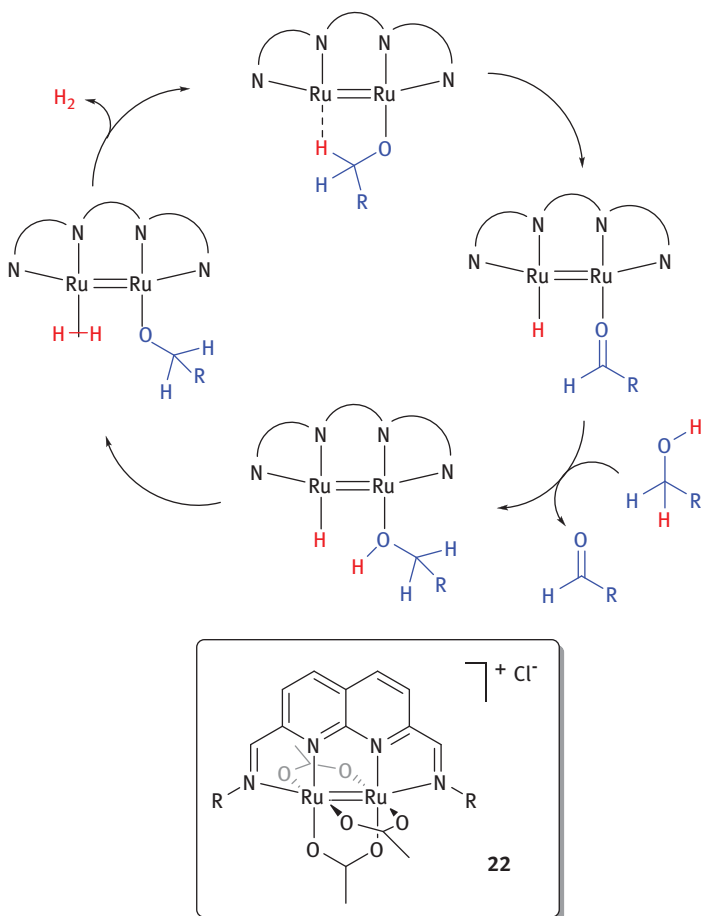
Figure 7.12: Proposed AAD mechanism by **22** based on metal–metal cooperation.

of primary alcohols into their corresponding aldehydes plus hydrogen at low temperature (70 °C). Both metals seem to play an active role in several key steps of the mechanism, such as β-hydride elimination from a diruthenium alkoxide and H-H bond formation.

Examples for the use of other transition metals as catalysts for AAD reactions are less common. However, it was shown that transition metal complexes based on osmium [46], platinum [47] or rhenium [48] are also capable of catalysing these reactions. More environmentally attractive is the recent attention paid to cheap and abundant first-row transition metals. The mechanisms already discussed for most AAD reactions described above rely on cooperative pathways with explicit ligand participation. In most cases, the oxidation state of the transition metal remains unaltered during catalysis. This is a fundamental aspect that offers opportunities

for developing environmentally sound versions of these transformations based on earth abundant metals. Usually base metal catalysts tend to undergo one electron redox reactions more easily in comparison to precious metal complexes. This may lead to undesired catalyst deactivation pathways that could be circumvented by processes that are redox neutral at the transition metal, i. e. AAD reactions employing redox non-innocent ligands.

A representative example of this rationale comes from the group of Beller, who reported an iron version (**23**) of his highly active ruthenium PNP complexes, which in turn exhibited a high activity for the base-free dehydrogenation of methanol [49]. Using the same system, Hazari and co-workers described the use of LiBF$_4$ as a Lewis acid cocatalyst which impressively boost up catalytic performance [50]. In parallel, Jones and co-workers applied the same catalyst for the dehydrogenation of alcohols [51] and heterocycles [52]. In all cases, the oxidation state of the iron centre was suggested to remain as +2 in every catalytic cycle in virtue of the cooperative action of the pincer ligand. In addition, the latter author described the use of nickel complexes alike **24** based on 2-hydroxyquinolines as ligands, that is, non-innocent analogues of the 2-hydroxypyridines developed by Fujita and Yamaguchi [42]. Compound **24** is further stabilized by a trispyrazolyl borate ligand and revealed good activity in the dehydrogenation of primary and secondary alcohols to esters and ketones, respectively [53]. Milstein recently demonstrated the activity of manganese pincer compound **25** for the dehydrogenative coupling of alcohols and amines leading to imines [54]. The same and related manganese systems were also effective catalysts for the deoxygenation of primary alcohols to alkanes in the presence of hydrazine [55]. More recently, Gauvin described the related biscarbonyl manganese(I) PNP system **26** for the AD of primary alcohols to esters under base-free conditions [56]. Simultaneously, Lang and co-workers reported on several copper clusters like **27** constructed around non-innocent N-heterocycle thiolate ligands for the dehydrogenation of primary and secondary alcohols, as well as their coupling with amines [57]. Despite these examples, a more limited number of complexes seem to operate through traditional redox mechanisms in which the oxidation state of the metal does change over the catalytic cycle. This was suggested by Hanson and co-workers when investigating the dehydrogenation of secondary alcohols to ketones catalysed by cobalt complex **28** [58]. Overall, these are only a few recent examples that clearly reflect the great potential of catalysts based on earth abundant metals for AAD reactions towards synthetic applications and hydrogen production.

7.3 Ethanol dehydrogenation

Bioethanol market has grown exponentially in the last two decades. Its worldwide production has currently surpassed 90 billion litres per year [59], which accounts for 90 % of the overall biofuel manufacture. Besides the extended use of sugars and

starch as renewable raw materials for bioethanol production, more sophisticated emerging methods rely on cellulose and other vegetable waste. This approach does not compete with food resources and permits the valorization of waste materials. In this context, the production of hydrogen from bio-based ethanol has clear environmental significance.

There are several AAD reactions that can be envisaged for hydrogen production from ethanol (Figure 7.14). In the simplest approach, ethanol dehydrogenation leads to acetaldehyde with concomitant release of one molecule of hydrogen gas (Figure 7.14a). Such a process reveals, however, a low energy gain per mass unit, as reflected by its relatively low hydrogen content (4.3 % wt). Acetaldehyde is more reactive than its alcohol precursor and can further react with a second molecule of ethanol to yield ethyl acetate and overall two molecules of hydrogen (one H_2 per EtOH molecule, Figure 7.14b). The hydrogen content is equivalent to the former reaction, but ethyl acetate is produced, which is in turn an important platform chemical in current industry. Thus, this equation implies a remarkable added value to the overall process. Alternatively, a higher hydrogen content (6.2 % wt) can be reached when reacting the intermediate aldehyde with water (Figure 7.14c) instead of ethanol. Once more, although the hydrogen percentage is still relatively low when compared to methanol reforming (12 % wt), this transformation allows access to acetic acid, which is in turn another major bulk industrial chemical. The amount of hydrogen per mass unit could be considerably increased (12 % wt) via C-C bond cleavage and formation of CO_2 (Figure 7.14d). This is however a difficult transformation for which there is very little precedent in the scientific literature when considering homogeneous systems.
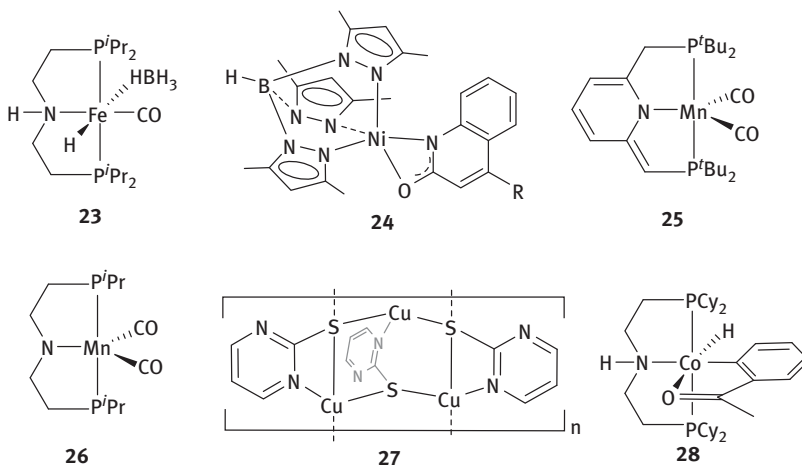
Figure 7.13: Representative examples of recent catalysts based on first-row transition metals active in AAD reactions.
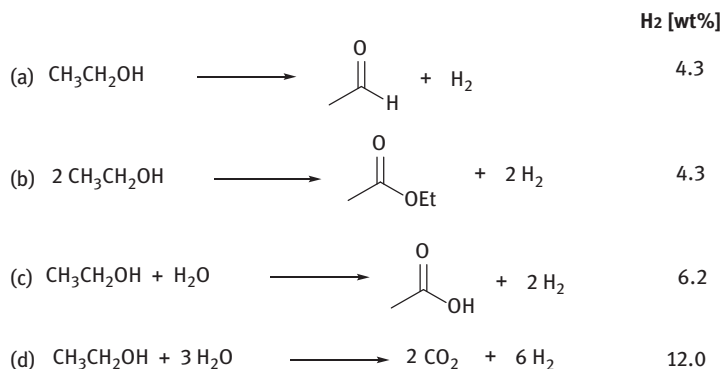
Figure 7.14: Selected AAD reactions for hydrogen generation from ethanol including their corresponding percentage of hydrogen liberated.

The first examples of ethanol dehydrogenation date back to the early work of Robinson and co-workers in the 1970s using ruthenium and osmium complexes (see Figure 7.3) [17]. Best results were obtained by using catalyst $[Ru(OCOCF_3)(CO)(PPh_3)_2]$ (**1**) in the presence of 12 equivalent of trifluoroacetic acid in boiling ethanol. Under these conditions, the maximum TOF measured was 27 h^{-1}. This activity was appreciably lower when compared to other primary alcohols such as 1-propanol (82 h^{-1}), 1-butanol (245 h^{-1}) or 1-pentanol (612 h^{-1}), a fact that the authors attributed to the increasing boiling point in the series. In addition, the authors observed a reduced activity over the course of the reaction due to product inhibition by acetaldehyde, but this could be overcome by extracting this product by continuous fractional distillation.

In the next decade, Cole-Hamilton and co-workers reported an activity for ethanol dehydrogenation that was one order of magnitude higher than previous reports [24, 25, 60]. They screened a small library of rhodium and ruthenium catalysts. In contrast to Robinson's system, catalysis was carried out under basic conditions (NaOH, 1 M). Best results in terms of activity correspond to catalysts $[Rh(bipy)_2]Cl$ (96 h^{-1}, 120 °C) (bipy = 2,2´-bipyridyl) and $[RuH_2(N_2)(PPh_3)_3]$ (148 h^{-1}, 150 °C). Besides acetaldehyde, the authors identified, in accordance with equation 1, the formation of carbon monoxide and methane in equimolar amounts. The added base has a dual effect, namely removing acetaldehyde from the reaction medium by aldol condensation, thus avoiding reversibility by hydrogenation, and also reactivating the catalyst by converting carbon monoxide into formate. Besides, aldol condensation reduces the extent of decarbonylation which, in the case of the rhodium catalyst, accounts for around 10 % of the overall dehydrogenated alcohol. Notably, carbon monoxide can act as catalyst poison by irreversible coordination to the metal centre blocking potential vacant coordination sites which are necessary for catalytic activity. With this in mind, the authors analysed the effect of irradiation with UV light and the use of

several additives to avoid catalyst poisoning by carbon monoxide. While the effect of UV light was negligible in the rhodium system, the activity of $[RuH_2(N_2)(PPh_3)_3]$ increased to TOFs over 200 h^{-1}. Ethanol dehydrogenation driven by visible light and mediated by a rhodium photocatalyst has also been investigated more recently, although with very limited activity [61].

$$CH_3CH_2OH \rightarrow CH_4 + CO + H_2 \tag{7.1}$$
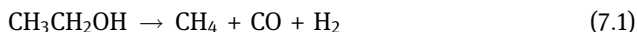
Despite the evident interest on hydrogen production from renewable alcohols, the next example of ethanol AD after Cole-Hamilton's work did not appear until 2007 [27]. In this study, the group of Beller explored the use of the widely employed ruthenium precursor $[RuCl_2(p\text{-cymene})]_2$ in the presence of easily available amine ligands for the dehydrogenation of *iso*-propanol under mild conditions (<100 °C). TOFs up to 519 h^{-1} were measured when using TMEDA as ligand (TMEDA/[Ru] = 1/1). In addition, ethanol could be dehydrogenated under analogous conditions, although the activity was considerably lower (7.6 h^{-1}). The resulting acetaldehyde was partly converted into longer chain (C4, C6, C8) alcohols by aldol condensation and Guerbet reactions [62], as detected by gas chromatography mas spectrometry (GC/MS). The dramatic decrease in activity when moving from *iso*-propanol to ethanol has become a common feature in AAD reactions. It can be attributed to the easiness of dehydrogenating secondary alcohols in comparison to primary alcohols, but also to the lower boiling point of ethanol with respect to *iso*-propanol and even to more accessible decarbonylation as a source of catalyst poisoning. Other cases include, for instance, a ruthenium catalyst stabilized by an acridine-based PNP ligand that exhibits good selectivity for the conversion of primary alcohols into acetals with liberation of one molecule of hydrogen. Thus, while 1-hexanol or 1-pentanol can be converted into their corresponding aldehydes in high yields (>90 %), the catalyst is completely inactive towards ethanol [63]. Related to this, iridium compound **9** in Figure 7.7 containing a POCOP pincer ligand exhibits moderate activity for the dehydrogenation of secondary alcohols but proved completely inactive towards ethanol [33].

Only a few years later, the group of Beller reported a landmark discovery in the field using ruthenium precursor $[RuH_2(CO)(PPh_3)_3]$ and a non-innocent PNP pincer ligand as a catalytic mixture for ethanol AD (Figure 7.15) [28]. The structure of the proposed active species and the outer-sphere mechanism by which it was suggested to operate have already been discussed (see Figure 7.4). It consists in the first example demonstrating the efficient dehydrogenation of ethanol at temperatures below 100 °C. In fact, it is still among the most active systems reported to date, yielding a TOF of 1,483 h^{-1} with catalyst loadings as low as 3.1 ppm ([Ru]/PNP: 1/1). Moreover, in contrast to previous systems, it did not need the addition of any base or acid additive, that being possible due to the active role taken by the ligand during the catalytic cycle (Figure 7.4). The authors stated that ethanol was converted into

Figure 7.15: AD of ethanol mediated by [RuH$_2$(CO)(PPh$_3$)$_3$]/PNP (1:1).

mixtures of acetaldehyde and ethyl acetate, both in substantial amounts, although without indicating specific ratios.

The conversion of two molecules of ethanol into ethyl acetate and molecular hydrogen is a reaction of great industrial and environmental interest. In fact, this transformation is currently exploited at industrial level using heterogeneous catalysts [64]. Ethyl acetate is one of the most important derivatives from acetic acid, in turn one of the top bulk industrial chemicals worldwide. Acetic acid is mainly produced by methanol carbonylation using raw materials of petrochemical origin. However, the use of bio-based ethanol circumvents the deleterious environmental effects of its current production. Ethyl acetate production exceeds 3.5 millions tons per year for its use as a general organic solvent and in other applications such as food, textile or cosmetic industries [65]. It is important to notice that this alternative approach for the synthesis of ethyl acetate results in the liberation of one molecule of hydrogen per ethyl acetate that could be used as an in-house green fuel in future biorefineries.

This transformation was independently targeted by the groups of Beller [66] and Gusev [67] showing comparable results. Beller screened several ruthenium and iridium catalysts based on PNP and PNN pincer ligands (Figure 7.16). He found that the commercially available complex **29**, also known as Ru-MACHO [68], exhibited the highest activity (TOF = 1,134 h^{-1}), though very close to the 1:1 catalytic mixture [RuH$_2$(CO)(PPh$_3$)$_3$]/PNP^{iPr} (TOF = 1,107 h^{-1}) that the same authors reported a year before [28]. A significant but reduced activity was measured for Baratta's Ru-CNN system **33** (TOF = 898 h^{-1}) [69], while the related Milstein's compound **31** [70], as well as the iridium catalysts previously synthesized by Gusev [71] (**30**) and Nozaki [72] (**32**), revealed much limited catalytic performance (TOF < 100 h^{-1}).

Under optimized conditions, catalyst **29** revealed steady activity for around 10 h, time after which conversions of up to 90 % were reached. Decreasing the catalyst loading to 50 ppm resulted in a remarkable TON of 15,400. The addition of a base is needed for efficient turnover, with best results obtained by using NaOEt (0.3–3.2 mol%). The base seems to play a dual role for both precatalyst activation and fast acetaldehyde trapping. The authors observed a strong product inhibition due to the presence of added acetaldehyde, which along with ^{1}H NMR studies of product distributions indicates that no acetaldehyde is accumulated during the course of

Figure 7.16: AD of ethanol towards ethyl acetate and hydrogen using ruthenium and iridium pincer catalysts as screened by Beller [66].

the reaction. The reaction mechanism seems to proceed through an outer-sphere pathway analogous to the one already analysed for related catalyst **2** (see Figure 7.4).

Simultaneously, the group of Gusev investigated the same transformation using a related osmium dimer catalyst (**34**) stabilized by the hemilabile PNN pincer ligand PyCH$_2$NCH$_2$CH$_2$P^{i}Pr$_2$ (Py = 2 -pyridyl) (Table 7.1) [67].[a] This and other related catalysts included in the study were active for both hydrogenation of esters to alcohols and its reverse transformation, that is, AD of primary alcohols to produce esters. Dimer **34** showed superior activity than its related ruthenium monomer **35**, reaching 61 % conversion of ethanol into ethyl acetate using 0.1 mol% of catalyst in toluene as a solvent. At variance with Beller's system, the reaction proceeds even under neutral conditions, although adding ^{t}BuOK (0.5 mol%) improved the catalyst efficacy and led to almost full conversion to ethyl acetate (96 %). These results, along with the studies simultaneously carried out by Beller [66], consist in the first reports of conversion of ethanol into ethyl acetate at temperatures below 100 °C.

In an extension of this work, Gusev and co-workers screened a small library of ruthenium and osmium catalysts based on PNP and PNN pincer ligands for the homocoupling of ethanol to ethyl acetate and hydrogen [67].[b] The general structures of the 11 catalysts screened are shown in Figure 7.17. The most effective catalyst, **36**, exhibited a maximum TON of 17,000, which is even slightly higher than Beller's report on Ru-MACHO under similar conditions (refluxing ethanol, 1 mol% NaOEt).
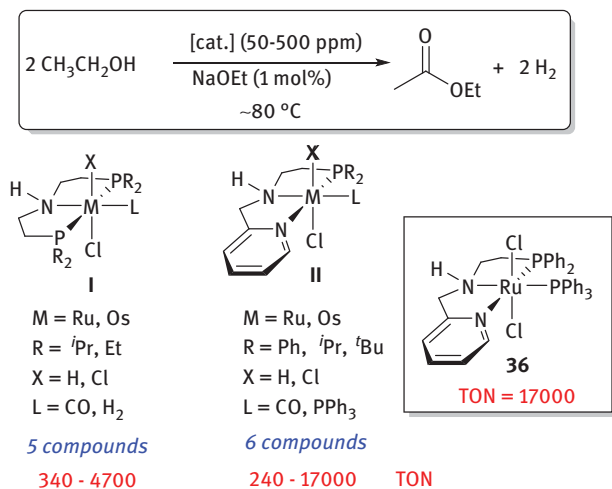
Figure 7.17: AD of ethanol towards ethyl acetate and hydrogen using ruthenium and osmium pincer catalysts as reported by Gusev.

In another important contribution, Gusev demonstrated that dihydride osmium compound **38** containing a mixed five- and six-membered chelating PNN ligand is an excellent catalyst for ethanol dehydrogenation (Table 7.2) [73]. The complex is prepared either from hydrogenation of its parent precursor **37** under basic conditions or by its reaction with Li[HBEt$_3$]. Compound **38** exists in solution as a mixture of isomers (*trans*/*cis* = 4/1) (Figure 7.18). This catalyst is active for the base-free reductive homocoupling of ethanol to ethyl acetate (TON 9,000). It also has the important advantage that is does not require the addition of NaOEt additive, such as **37** and

Table 7.2: Catalytic AD of ethanol to ethyl acetate and hydrogen using **34** and **35**.
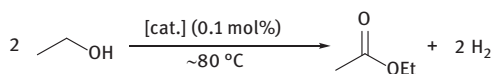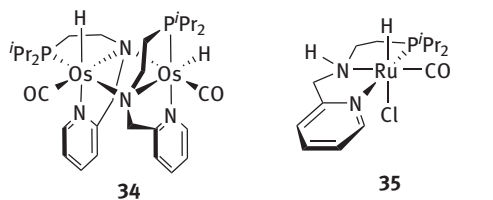
Entry	Catalyst	Solvent	Additive	t (h)	Conversion (%)	TON
1	**34**	Neat	–	24	7	70
2	**34**	Toluene	–	8	61	600
3	**34**	Toluene	^{t}BuOK	8	96	960
4	**35**	Neat	^{t}BuOK	7.5	30	300
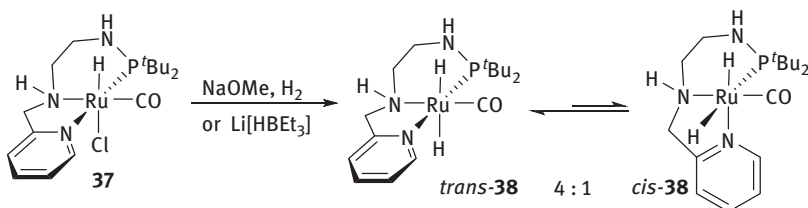
Figure 7.18: Synthesis and solution dynamic equilibrium of compound **38**.

other previously discussed systems. Additionally, compound **37** also mediates the dehydrogenative coupling of ethanol and amines to produce acetamides (Table 7.3). The method is complementary to Milstein´s catalyst for amide synthesis [74], which requires a continuous flow of argon and high temperatures (>110 °C), being not suitable for alcohols with low boiling points, such as ethanol. In contrast, complex **37** permits accessing acetamides in neat ethanol and without the need of an argon flow (Table 7.2, entries 3 and 4). Several relevant reaction intermediates, including a key species containing a ethoxyethoxide ligand, were characterized by *in situ* ESI-MS under catalytically relevant conditions [75]. These results, along with accompanying DFT studies, offer fundamental information on mechanistic aspects and on the role of the non-innocent ligand framework. Shortly after, the same research group disclosed a more comprehensive study on the precise mechanism of this type of catalyst [76]. In a joint experimental/computational approach, the authors analysed the influence of the donor group in different PNY (Y = O, S, N) pincer ligands that include other functionalities different from their original 2-pyridyl moiety.

Table 7.3: Catalytic dehydrocoupling of ethanol towards ethyl acetate or amides mediated by **37** and **38**.
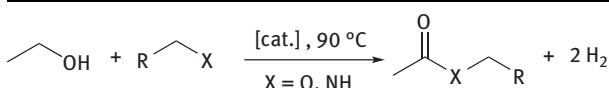
Entry	Substrate	[cat.] (mol%)	t (h)	Base (mol%)	Conv.	TON
1	R = Me, X = OH	**37** (0.01)	24	NaOEt (1)	82	8,200
2	R = Me, X = OH	**38** (0.01)	24	none	90	9,000
3	R = Pr, X = NH$_2$	**37** (0.05)	17	NaOEt (1)	90	1,800
4	R = Ph, X = NH$_2$	**37** (0.05)	17	NaOEt (1)	96	1,920

An important aspect when considering AAD reactions for hydrogen production is the reversibility of the system, that is, the possibility of regenerating the starting materials by hydrogenation. The group of Milstein focused on this aspect during the dehydrogenative coupling of ethanol and ethylenediamina catalysed by

ruthenium PNN–pincer complexes (Figure 7.19) [77]. Full conversion of ethylene-diamine and ethanol into N,N′-diacetylethylenediamine was achieved when using catalyst **39** (0.01 mol%) in the presence of KO^{t}Bu (1.2 equivalent relative to **1**) under relatively mild conditions (105 °C), reaching a maximum TON of 9,300. Most importantly, the same catalyst was capable of performing the hydrogenation of the aforementioned diacetamide under hydrogen pressure (50 bar). These findings allowed the authors to perform up to three dehydrogenation/hydrogenation cycles without decay in the activity of the catalyst. Similar results were disclosed by the same group using 2-aminoethanol for its reductive coupling towards glycine anhydride and related peptides [78].

As stated above (see Figure 7.14c), aqueous reforming of ethanol to produce acetic acid and hydrogen possess a slightly more favourable balance in terms of hydrogen storage capacity (6.2% H$_2$ wt) than the already discussed conversion to acetaldehyde or ethyl acetate (4.2% H$_2$ wt). Moreover, bioethanol is produced by fermentation of vegetable material and as such contains variable amounts of water. The direct use of aqueous bioethanol without the need of further purification presents obvious eco-
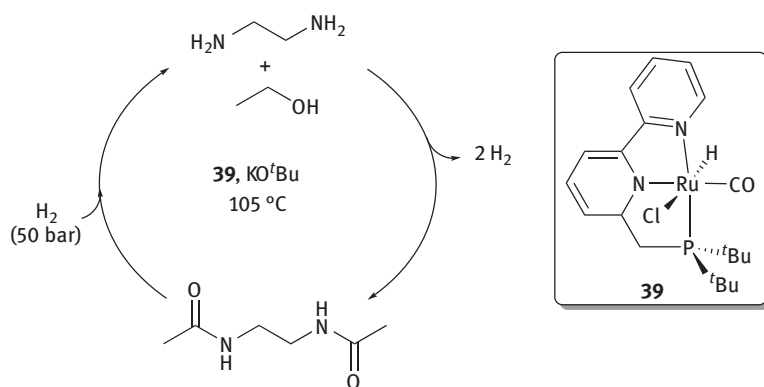
Figure 7.19: Reversible dehydrogenative coupling of ethylenediamine and ethanol catalysed by **39**.

nomic advantages, while the production of acetic acid is of interest due to the enormous amount of applications of this molecule in current chemical industry.

Once more, the group of Beller investigated aqueous ethanol reforming to acetates using a number of ruthenium pincer catalysts [79]. An impressive maximum TON of 80,000 was reached under optimized conditions using Ru–PNP complex **40** (Figure 7.20). The catalyst is active under different EtOH/H$_2$O ratios and no drop in catalytic performance was detected upon using samples of unpurified crude bioethanol obtained from biomass fermentation. A mechanistic proposal, as well as the extension of these results to other primary alcohols, was later provided by Gauvin and co-workers [80]. More recently, the latter authors described the use of these and
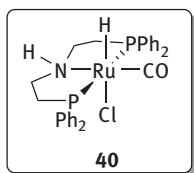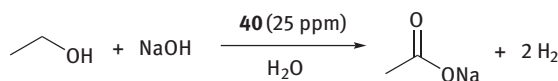
Figure 7.20: Aqueous dehydrogenation of ethanol to sodium acetate catalysed by **40**.

related catalysts based on iron and manganese for the AD of biosourced alcohols such as fatty and terpenoic derivative alcohols [81].

7.4 Glycerol dehydrogenation

Glycerol is a cheap, non-toxic and renewable feedstock whose upgrading has attracted much attention in the last two decades. This is because it is the main side product of the biodiesel production. It contributes ca. 10 wt% of the molecular weight of fatty esters. Globally, there is an overproduction of this compound, and currently there is a high demand for new technologies which aim to transfer it to higher value chemicals [82]. Moreover, glycerol worldwide production is expected to keep growing in the next future given that biodiesel is still a rising alternative to fossil fuels. This scenario offers tremendous opportunities for the implementation of glycerol upgrading methods in future biorefineries.

From a synthetic chemistry perspective, glycerol has already been successfully converted into a wide variety of added-value platform chemicals [83]. In addition, the use of glycerol as an environmentally attractive source of energy has been investigated. In fact, aqueous glycerol reforming for the production of syngas ($CO + H_2$) is arguably the most successful available technology for the utilization of this bio-based molecule. Syngas can be later employed, for instance, to access hydrocarbon fuels by means of Fischer–Tropsch processes. Aqueous glycerol reforming is mediated by heterogeneous catalysts that operate under harsh conditions (225–300 °C) [84].

On the contrary, the hydrogen contained in glycerol can be released under mild conditions using homogeneous catalysts capable of mediating AAD reactions. Glycerol is, however, a considerably more challenging substrate than ethanol to dehydrogenate. It contains three reactive hydroxyl groups whose successive dehydrogenation can lead to a variety of C3 products sufficiently functionalized and thus being capable to cause catalyst deactivation by irreversible coordination to the metal centre. The first

example of glycerol AD was reported in 1988 by Cole-Hamilton and co-workers using ruthenium and rhodium catalysts under basic conditions (NaOH, 1 M) [25]. Using compound $[RuH_2(N_2)(PPh_3)_3]$, a maximum TOF of 12.4 h^{-1}, measured from H_2 evolution, was reached when performing the reaction at 150 °C, but its activity could be enhanced three times by exposing the reaction mixture to UV light (TOF = 37.6 h^{-1}). Alternatively, rhodium complex $[Rh(bipy)_2]Cl$ (bipy = 2,2´-bipyridine) exhibited a higher activity at lower temperature (120 °C) and without the need of UV irradiation (TOF = 21.3 h^{-1}), which barely affected catalyst performance. The nature of the dehydrogenated product was not address by the authors.

Twenty years later, Farneti and co-workers reported the ability of several iridium catalysts to accomplish transfer hydrogenation reactions from glycerol to different carbonylic compounds under base-free conditions. Remarkably, they demonstrated for the first time the possibility of AD of glycerol without the need of a base [85]. From a synthetic point of view, this result is of high importance since the products derived from glycerol dehydrogenation, namely, glyceraldehyde (Gly) and dihydroxyacetone (DHA), are known to be base sensitive. Using iridium catalyst **41**, glycerol could be selectively converted into DHA and H_2 at 100 °C without the need of external base or solvent (Figure 7.21), although with a TON as low as 2. This value could be increased to 11 by using polar solvents such as 1,3-dimethoxybenzene or 2-methyl-1-phenyl-2-propanol.

More recently, Campos, Crabtree and co-workers described the first catalysts to promote the conversion of glycerol into lactic acid (LA) by AAD reaction [86]. Several iridium precatalysts containing two minimally substituted N-heterocyclic carbene (NHC) ligands proved to be highly active in the dehydrogenation of glycerol at low temperature (115 °C, Figure 7.22). It was demonstrated that under catalytic conditions these catalysts release their ancillary ligands to form bis-NHC Ir hydrides as the active species. It is interesting to note that in compound **42**, the
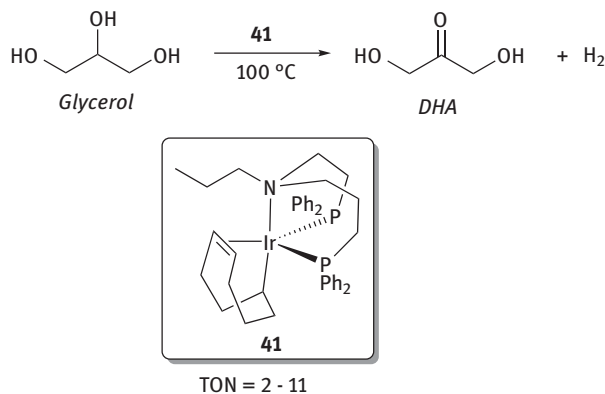
Figure 7.21: Catalytic dehydrogenation of glycerol to dihydroxyacetone (DHA) by **41**.
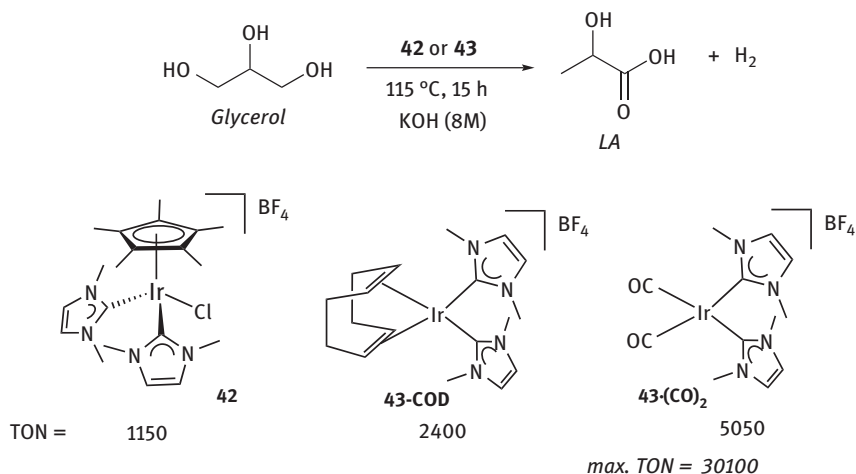
Figure 7.22: Catalytic conversion of glycerol into lactic acid (LA) and hydrogen mediated by bis-NHC iridium catalysts **42** and **43**.

pentamethylcyclopentadienyl (η^5-C_5Me_5) ligand, which is assumed to be a robust spectator ligand that remains stable during most catalytic cycles, is released even under slightly basic conditions and mild heating [87]. Having that in mind, it is not surprising that the authors identified the related Ir(I) compound **43·(CO)₂** containing two carbonyl ligands as the most active catalyst for glycerol dehydrogenation. It was proposed that these carbonyl groups can be converted into formate [88] under the strongly basic conditions at which catalysis takes place (KOH, 8 M) and thus provide highly active low-coordinate bis-NHC iridium species. When reducing the catalyst loading of **43·(CO)₂** to 20 ppm, a TON of over 30,000 could be reached. This represented the highest TON for the dehydrogenation of glycerol to LA reported at the time. Moreover, besides producing hydrogen, the selectivity for converting glycerol to LA was remarkable (up to 97 %), with propanediol, ethylene glycol and formic acid being the main side products. These side products together accounted for less than 5 % under the reaction conditions which were reported.

The high selectivity towards LA is attributed by the authors to the slow formation of dihydroxyacetone or glyceraldehyde in basic media. The importance of these results lies on the numerous applications of LA in both traditional industry and also in more modern applications such as the polymerization of lactide to produce polylactic acid, which in turn is a biodegradable polyester that offers the opportunity of substituting fossil derived plastics in a variety of applications [89]. A practical problem associated with this approach is that glycerol stemming from biodiesel refineries contains a variety of impurities. This makes direct valorization impractical while glycerol purification is too costly. Importantly, compound **43·(CO)₂** revealed a

high activity for the conversion of industrial crude glycerol into LA and hydrogen with excellent results (90 % conversion; 97 % selectivity towards LA).

Several iridium-containing decomposition products were isolated and fully characterized from reaction mixtures derived from dehydrogenation of glycerol and other alcohols. Their molecular structures were ascertained by X-ray diffraction techniques [90]. To increase catalyst activity and robustness, the formation of these inactive polynuclear species was successfully blocked by Tu and co-workers. Inspired by the proved efficiency of bis-NHC iridium homogeneous systems, the authors prepared a series of coordination polymers alike **44** in Figure 7.23. The polymers were based on rigid bisbenzimidazolium and acted as self-supported heterogeneous catalysts that could be recycled up to 31 times without loss of activity [91]. A remarkable TON of up 1.24 × 10^5 for the conversion of glycerol into LA and hydrogen was recorded under conditions otherwise analogous to those employed with their homogeneous counterparts.

Only 1 year later, the group of Williams described the related Ir(I) compound **45** stabilized by a chelating (pyridyl)carbene ligand that enables the conversion of neat glycerol into LA under basic conditions with an impressive TON of 4.56 × 10^6, the highest reported to date [92]. Compound **45** was equally active with samples of crude glycerol stemming from a biodiesel refinery with selectivity as high as 99 %.
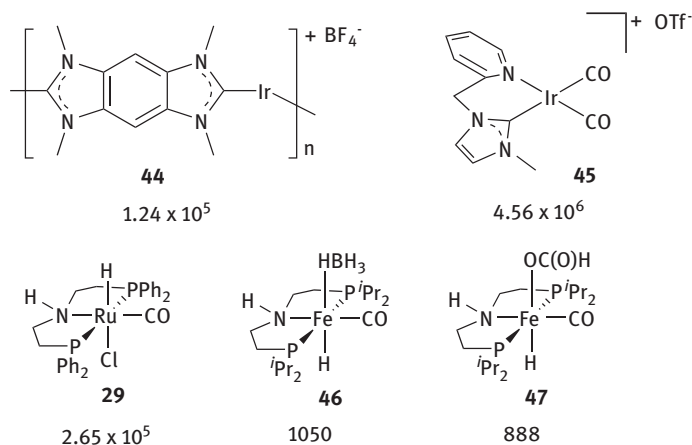
Figure 7.23: Representative examples of efficient AAD catalysts for the conversion of glycerol into lactic acid and hydrogen with reported TONs.

Moreover, the produced lactate salts could be conveniently converted into *rac-* and *meso-*lactides, basic precursors of polylactic acid.

Regarding ruthenium catalysts, the group of Beller explored the use of PNP and PNN pincer ligands. Best results were obtained using Ru-MACHO (**29**) and carrying out the reaction at 140 °C in N-methylpyrrolidine with 1.08 equivalent of NaOH, reaching TONs of up to 265,000 [93]. A moderate selectivity of 67 % towards LA was observed, considerably diminished when compared to the aforementioned iridium catalysts. Surprisingly, Ru-MACHO revealed improved TOF for the production of hydrogen when applied to crude glycerol samples instead of when using pure glycerol, a fact that could be attributed to methanol contained in crude glycerol, which in turn is known to be dehydrogenated at high rate by this and related catalysts [29].

In the same year, Crabtree and Hazari described the only example of a homogeneous first-row transition metal that catalyses conversion of glycerol into LA and H_2 [94]. In doing so, they explored the use of several iron catalysts bearing PNP pincer ligands under basic conditions at relatively low temperature (140 °C). The pincer borohydride and formate complexes **46** and **47**, respectively, emerged as the most efficient catalysts reaching up to 1,050 TONs under optimized conditions. As in previous examples, these compounds seem to mediate glycerol AD, while the rest of rearrangements towards LA are base promoted.

7.5 Sugars and sugar alcohol dehydrogenation

The primary products formed during photosynthesis are C5 and C6 sugars, which are in turn the main components of cellulose and hemicellulose after their polymerization. Out of the 170 billion metric tons of biomass produced every year by photosynthetic organisms, three quarters are carbohydrates. It seems surprising that being the most abundant renewable feedstock on earth, humans only utilize 3–4 % of those for food supply and other purposes [95]. It becomes evident that there is a growing interest on pursuing the production of hydrogen from sugars and other biomass components, which may offer a clean and sustainable energy supply in the future [96].

Current methods for releasing the hydrogen contained in sugars and related bio-based feedstocks rely on fermentative processes [97], gasification [98] and traditional reforming [99]. Leaving apart biological production of hydrogen, the aforementioned chemical processes are highly energy-intensive methods that operate under harsh conditions (500–1,300 °C; up to 300 bar). Moreover, the composition of the gas produced by these methods enforces the implementation of downstream processes, mainly due to its high content in methane. As a result, the cost efficiency of these technologies greatly diminishes. An alternative approach to these high-temperature protocols is sugars and bio-based aqueous phase reforming. This can be considered as a complex set of transformations that ultimately lead to gaseous mixtures whose main components are H_2 and CO_2, as well as variable amounts of CO, methane and other light alkanes (see equations (2)–(5)) [100]. The overall process incorporates a

complex set of reaction mechanisms that include AAD reactions and related transformations, fully justifying a brief discussion of the topic herein.

$$C_nH_{2n+2}O_n + n\,H_2O \rightarrow n\,CO + (2n+1) + H_2 \tag{7.2}$$

$$CO + H_2O \rightarrow CO_2 + H_2 \tag{7.3}$$

$$CO + 3H_2 \rightarrow CH_4 + H_2O \tag{7.4}$$

$$CO_2 + 4H_2 \rightarrow CH_4 + 2H_2O \tag{7.5}$$
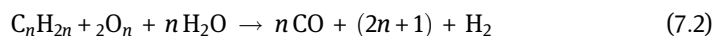
The complete reforming of biomass components to hydrogen and carbon dioxide requires catalysts and conditions that enable C-C cleavage reactions. It is noteworthy to mention, however, early examples on selective sugar dehydrogenation towards their corresponding carboxylic acids. Kieboom and Bekkum reported almost 40 years ago the conversion of a number of aldoses, including glucose, mannose and galactose, into their corresponding aldonic acids with concomitant liberation of hydrogen gas [101]. Several common heterogeneous catalysts were employed, with best results derived from the use of Pt/C and Rh/C. Complete conversion of bio-based aldehydes into carboxylates was achieved under alkaline conditions at temperatures as low as 0 °C after short reaction times.

Complete catalytic reforming of sugars to hydrogen and carbon dioxide as the major products was accomplished by Dumesic using heterogeneous Pt-based catalysts under somehow milder conditions (225–265 °C, 29–56 bar) than those offered by gasification or traditional reforming. It is worth mentioning that under similar conditions sorbitol, glycerol, ethylene glycol and methanol were also dehydrogenated [102].

As often observed, turning towards homogeneous systems results in milder reaction conditions. The group of Wasserscheid described the use of $[RuCl_2(p\text{-cymene})]_2$ in conjunction with TMEDA for sugar dehydrogenation in several methylphosphonate ionic liquids (Figure 7.24) [103]. Hydrogen production from glucose, and even cellulose, was achieved at temperatures between 150 and 180 °C and atmospheric pressure, conditions significantly milder than previously reported. The catalytic system permitted successive additions of fresh sugar up to six times, although it exhibited an overall limited activity of only around 200 turnovers. Mechanistic investigations indicate that under experimental conditions glucose experiences sequential dehydration and rehydration events to yield levulinic and formic acids. In fact, formic acid dehydrogenation seemed to be the sole responsible for hydrogen generation. This fact largely limits the applicability of the method in terms of hydrogen production since a single hydrogen molecule can be extruded for each sugar molecule. The same
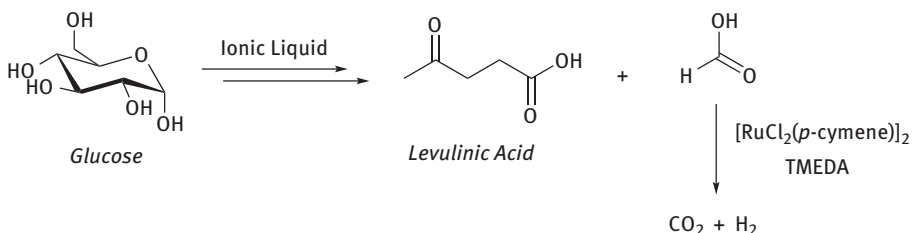
Figure 7.24: Hydrogen production from glucose using [RuCl$_2$(p-cymene)]$_2$/TMEDA system in ionic liquids.

limitation was observed in a more recent study where [(p-cymene)Ru(NH$_3$)Cl$_2$] revealed a maximum TOF of 719 h^{-1} for hydrogen production from acidic (pH = 0.5) aqueous solutions of glucose [104].

Shortly after, Beller investigated the use of ruthenium and iridium complexes based on PNP and PNN pincer ligands for aqueous reforming of sugars [105]. Under optimized conditions (95 °C, diglyme, 1.5 equivalent NaOH) iridium(I) complex **48** outperformed the other ruthenium catalysts screened in the study by enabling hydrogen production from fructose, glucose and cellobiose with up to 6,923, 4,116 and 10,269 turnovers per hour, respectively (Figure 7.25). Despite this remarkable activity, the amount of hydrogen produced is always less than one molecule per sugar, which makes the overall process still highly inefficient when compared to heterogeneous systems. The considerably more challenging cellulose and lignocellulose were subjected to the same
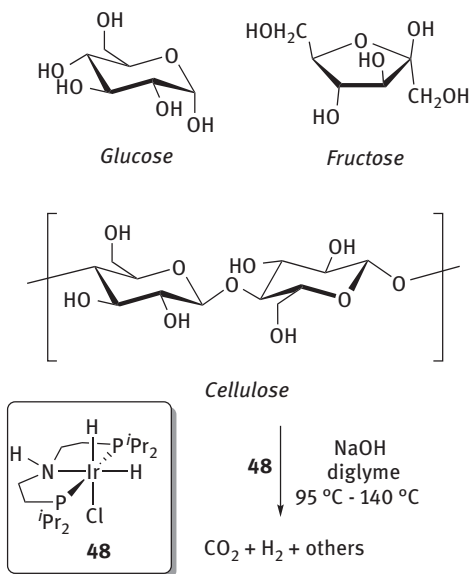
Figure 7.25: Hydrogen production from sugars and cellulose mediated by **48**.

transformation by following a one-pot three-step procedure consisting in prior hydrolysis of the biopolymer followed neutralization and subsequent incorporation of the iridium catalyst at 140 °C. This results in maximum TONs of around 6,000 and 2,000 for cellulose and lignocellulose, respectively.

Sugar alcohols (Figure 7.26) are the polyols derived from hydrogenation of sugars, whose AD also holds great interest. For instance, sorbitol (C6), xyliltol (C5) and erythritol (C4) have been identified by the US Department of Energy among the most promising renewable carbon feedstocks for the future [106]. They can be conveniently obtained on large scale from tandem hydrolysis/hydrogenation of biomass components [107].

An early report deals with the dehydrogenation of a variety of sugar alcohols using catalytic heterogeneous platinum oxide and carrying out reactions at tempera-
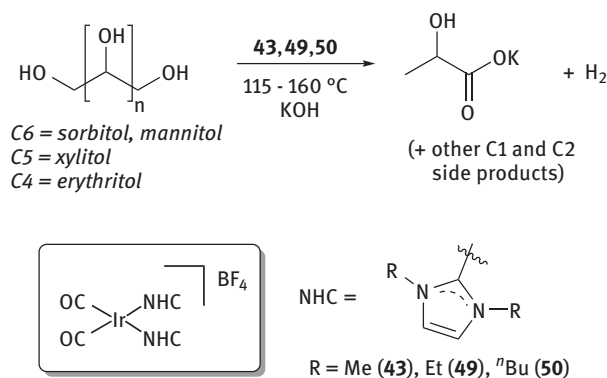
Figure 7.26: Dehydrogenation of sugar alcohols mediated by bis−NHC complexes.

tures below 100 °C [108]. Although selectivity towards the formation of aldoses was excellent, the method required the use of oxygen as a hydrogen acceptor. Long after those early studies, Crabtree and co-workers described in 2015 the use of iridium(I) bis−NHC complexes for the AD of several sugar alcohols to yield not only hydrogen gas, but also LA as a valuable platform chemical (Figure 7.26). Reactions were carried out in neat sugar alcohols at temperatures between 115 and 160 °C and under basic conditions (1.1 equivalent KOH) [109]. Sorbitol, mannitol, xylitol and erythritol were dehydrogenated with moderate efficiency. Mechanistic investigations indicate the role of iridium catalysts in converting sugar alcohols into their corresponding ketones or aldehydes which, under alkaline conditions, experience a complex scheme of reactions that ultimately lead to lactate as the major organic component (13−49 %).

7.6 Conclusion

AAD reactions have been known for decades, but its enormous potential has been mostly exploited from the beginning of the current century. From a synthetic point of view, AAD reactions are among the most versatile synthetic tools available and enable the efficient conversion of alcohols and other substrates into a variety of organic molecules with a high atom economy. AAD methods have been implemented at industrial level and their potential in medicinal chemistry has been recently investigated. Although most systems are based on ruthenium and iridium, as well as rhodium and other precious metals, a growing number of current catalysts rely on metal–ligand cooperation strategies to employ earth abundant first-row metals for a variety of AAD transformations.

The common product derived from every AAD reaction is molecular hydrogen. This gas has been proposed as the clean fuel of the future in the so-called hydrogen economy. However, one of the bottlenecks of a foreseen hydrogen economy lies on the fact that this gas is mainly produced from fossil hydrocarbon feedstocks by steam reforming. When considering environmentally sound alternatives, AAD reactions have recently emerged as a promising viable technology for the production of hydrogen. Alcohols with a high percentage of releasable hydrogen, such as methanol, could serve as hydrogen storage materials. This is not, however, a requisite for connecting AAD reactions with a future hydrogen economy. A complementary approach relies on the use of bio-based alcohols for the production of hydrogen gas, a line of thinking that is directly connected to the future of biorefineries. In this context, the dehydrogenation of ethanol, glycerol and sugar alcohols has been recently investigated and holds great promise for future implementations at industrial level. Importantly, besides extruding some of the hydrogen contained within these bioderived alcohols, AAD reactions discussed in this contribution enable the production of other added-value molecules. A prominent example is the conversion of crude glycerol, the main side product of biodiesel industry, into hydrogen gas and LA, the latter being the fundamental building block of polylactic acid, in turn a biodegradable polyester with plenty of applications.

None of the transformations discussed herein represent stand-alone operations for hydrogen production; however, they may become important processes in future biorefineries. Many important landmark discoveries in this growing field are yet to come, and there is no doubt that a number of forthcoming industrial transformations will be based on AAD methods of environmental significance.

References

[1]   For recent reviews see: (a) Dobereiner GE, Crabtree RH. Dehydrogenation as a substrate-activating strategy in homogeneous transition-metal catalysis. Chem Rev. 2010;110:681–703. (b) Nandakumar A, Midya SP, Landge VG, Balaraman E. Transition-metal-catalyzed hydrogen- transfer annulations: access to heterocyclic scaffolds. Angew Chem Int Ed. 2015;54:11022–34. (c) Wang D, Astruc D. The golden age of transfer hydrogenation. Chem Rev. 2015;115:6621–86. (d) Nixon TD, Whittlesey MK, Williams JM. Transition metal catalysed reactions of alcohols using borrowing hydrogen methodology. Dalton Trans. 2009:753–62. (e) Werkmeister S, Neumann J, Junge K, Beller M. Pincer-type complexes for catalytic (De) Hydrogenation and Transfer (De)- Hydrogenation reactions: recent progress. Chem Eur J. 2015;21:12226–50.

[2]   Huang F, Liu Z, Yu Z. C-Alkylation of ketones and related compounds by alcohols: transition-Metal-Catalyzed Dehydrogenation. Angew Chem Int Ed. 2016;55:862–75.

[3]   (a) Jumde VR, Cini E, Porcheddu A, Taddei M. Metal-catalyzed tandem 1,4-benzodiazepine synthesis based on two hydrogen-transfer reactions. Eur J Org Chem. 2015;2015:1068–74. (b) Yan T, Feringa BL, Barta K. Benzylamines via iron-catalyzed direct amination of benzyl alcohols. ACS Catal. 2016;6:381–8. (c) Luo Z, Qin F, Yan S, Li X. An efficient and promising method to prepare Ladostigil (TV3326) via asymmetric transfer hydrogenation catalyzed by Ru-Cs-DPEN in an HCOONa-H2O-surfactant system. Tetrahedron Assymetry. 2012;23:333–8. (d) Leonard J, Blacker AJ, Marsden SP, Jones MF, Mulholland KR, Newton R. A survey of the borrowing hydrogen approach to the synthesis of some pharmaceutically relevant intermediates. Org Process Res Dev. 2015;19:1400–10.

[4]   (a) Gerfaud T, Martin C, Bouquet K, Talano S, Millois-Barbuis C, Musicki B, et al. Process development and good manufacturing practice production of a tyrosinase inhibitor via titanium-mediated coupling between unprotected resorcinols and ketones. Org Process Res Dev. 2017;21:631–40. (b) Berliner MA, Dubant SP, Makowski T, Ng K, Sitter B, Wager C, et al. Org Process Res Dev. 2011;15:1052–62. (c) Frederick MO, Frank SA, Vicenzi JT, LeTourneau ME, Berglund KD, Edward AW, et al. Development of a hydrogenative reductive amination for the synthesis of evacetrapib: unexpected benefits of water. Org Process Res Dev. 2014;18:546–51.

[5]   (a) Soldevila-Barreda JJ, Romero-Canelon I, Habtemariam A, Sadler PJ. Transfer hydrogenation catalysis in cells as a new approach to anticancer drug design. Nat Commun. 2015;6:6582. (b) Bose S, Ngo AH, Do LH. Intracellular transfer hydrogenation mediated by unprotected organoiridium catalysts. J Am Chem Soc. 2017;139:8792–5. (c) Fu Y, Sanchez-Cano C, Soni R, Romero-Canelon I, Hearn JM, Liu Z, et al. The contrasting catalytic efficiency and cancer cell antiproliferative activity of stereoselective organoruthenium transfer hydrogenation catalysts. Dalton Trans. 2016;45:8367–78.

[6]   (a) Okamoto Y, Kohler V, Paul CE, Hollmann F, Ward TR. Efficient in situ regeneration of NADH mimics by an artificial metalloenzyme. ACS Catal. 2016;6:3553–7. (b) Okamoto Y, Kohler V, Ward TR. An NAD(P)H-dependent artificial transfer hydrogenase for multienzymatic cascades. J Am Chem Soc. 2016;138:5781–4.

[7]   (a) Alberico E, Nielsen M. Towards a methanol economy based on homogeneous catalysis: methanol to H2 and CO2 to methanol. Chem Commun. 2015;51:6714–25. (b) Crabtree RH. Hydrogen storage in liquid organic heterocycles. Energy Environ Sci. 2008;1:134–8. (c) Chamoun R, Demirci UB, Miele P. Cyclic dehydrogenation–(re)hydrogenation with hydrogen-storage materials. Energy Technol. 2015;3:100–17.

[8]   Olah GA, Goeppert A, Prakash GK. Beyond oil and gas: the methanol economy. Weinheim: Wiley-VCH, 2006.

[9]   (a) Gunanathan C, Milstein D. Applications of acceptorless dehydrogenation and related transformations in chemical synthesis. Science 2013;341:1229712. (b) Crabtree RH. Homogeneous transition metal catalysis of acceptorless dehydrogenative alcohol oxidation: applications in hydrogen storage and to heterocycle synthesis. Chem Rev. 2017;117:9228–46. (c) Balaraman E, Khaskin E, Leitus G, Milstein D. Catalytic transformation of alcohols to carboxylic acid salts and H2 using water as the oxygen atom source. Nat Chem. 2013;5:122–5.

[10]   Nielsen M. Hydrogen production by homogeneous catalysis: alcohol acceptorless dehydrogenation. In: Lichtfouse E, Schwarzbauer J, Robert D, editors. Hydrogen production and remediation of carbon and pollutants. Heidelberg: Springer, 2015.

[11]   (a) Johnson TC, Morris DJ, Wills M. Hydrogen generation from formic acid and alcohols using homogeneous catalysts. Chem Soc Rev. 2010;39:81–8. (b) Trincado M, Banerjee D, Grützmacher H. Molecular catalysts for hydrogen production from alcohols. Energy Environ Sci. 2014;7:2464–503.

[12]   (a) Yamamoto N, Obora Y, Ishii Y. Iridium-Catalyzed oxidative methyl esterification of primary alcohols and diols with methanol. J Org Chem. 2011;76:2937–41. (b) Hanasaka F, Fujita K, Yamaguchi R. Synthesis of new cationic Cp*Ir N-heterocyclic carbene complexes and their high catalytic activities in the Oppenauer-type oxidation of primary and secondary alcohols. Organometallics. 2005;24:3422–33. (c) Wang GZ., Baeckvall JE. Ruthenium-catalyzed oxidation of alcohols by acetone. J Chem Soc Chem Commun. 1992;4:337–9.

[13]   Choi J, MacArthur AH, Brookhart M, Goldman AS. Dehydrogenation and related reactions catalyzed by iridium pincer complexes. Chem Rev. 2011;111:1761–79. (b) Crabtree RH. The organometallic chemistry of alkanes. Chem Rev. 1985;85:245–69.

[14]   Charman HB. Hydride transfer reactions catalyzed metal complexes. Nature. 1966;212:278–9. (b) Charman HB. Hydride transfer reactions catalysed by metal complexes. J Chem Soc. 1967;6:629–32. (c) Charman HB. Hydride transfer reactions catalyzed by rhodium-tin complexes. J Chem Soc. 1970;4:584–7.

[15]   Vaska L, Diluzio JW. On the origin of hydrogen in metal hydride complexes formed by reaction with alcohols. J Am Chem Soc. 1962;84:4989–90.

[16]   Sawama Y, Morita K, Yamada T, Nagata S, Yabe Y, Monguchi Y, et al. Rhodium-on-carbon catalyzed hydrogen scavenger- and oxidant-free dehydrogenation of alcohols in aqueous media. Green Chem. 2014;16:3439–43.

[17]   (a) Dobson A, Robinson SD. Complexes of the platinum metals. 7. Homogeneous ruthenium and osmium catalysts for the dehydrogenation of primary and secondary alcohols. Inorg Chem. 1977;16:137–42. (b) Dobson A, Robinson SD. Catalytic dehydrogenation of primary and secondary alcohols by Ru(OCOCF3)2(CO)(PPh3)2. J Organomet Chem. 1975;87:C52–3.

[18]   Khusnutdinova JR, Milstein D. Metal–ligand cooperation. Angew Chem Int Ed. 2015;54:12236–73.

[19]   (a) Li HX, Wang HX. Computational mechanistic studies of acceptorless dehydrogenation reactions catalyzed by transition metal complexes. Sci China Chem. 2012;55:1991–2008. (b) Hou C, Zhang ZH, Zhao CY, Ke ZF. DFT study of acceptorless alcohol dehydrogenation mediated by ruthenium pincer complexes: ligand tautomerization governing metal ligand cooperation. Inorg Chem. 2016;55:6539–51. (c) Musa S, Shaposhnikov I, Cohen S, Gelman D. Ligand–metal cooperation in PCP pincer complexes: rational design and catalytic activity in acceptorless dehydrogenation of alcohols. Angew Chem Int Ed. 2011;50:3533–7.

[20]   Rybak WK, Ziółkowski JJ. Dehydrogenation of alcohols catalysed by polystyrene- supported ruthenium complexes. J Mol Catal. 1981;11:365–70.

[21]   Jung CW, Garrou PE. Dehydrogenation of alcohols and hydrogenation of aldehydes using homogeneous ruthenium catalysts. Organometallics. 1982;1:658–66.

[22] Zhang L, Raffa G, Nguyen DH, Swesi Y, Corbel-Demailly L, Capet F, et al. Acceptorless dehydrogenative coupling of alcohols catalysed by ruthenium PNP complexes: influence of catalyst structure and of hydrogen mass transfer. J Catal. 2016;340:331–43.

[23] Lin Y, Ma D, Lu X. Iridium pentahydride complex catalyzed dehydrogenation of alcohols in the absence of a hydrogen acceptor. Tetrahedron Lett. 1987;28:3115–8.

[24] (a) Morton D, Cole-Hamilton DJ. Rapid thermal hydrogen production from alcohols catalyzed by [Rh(2,2′-bipyridyl) 2]Cl. J Chem Soc Chem Commun. 1987; 248–9. (b) Morton D, Cole-Hamilton DJ, Schofield JA, Pryce RJ. Rapid thermal hydrogen production from 2,3-butanediol catalyzed by homogeneous rhodium catalysis. Polyhedron. 1987;6:2187–9.

[25] Morton D, Cole-Hamilton DJ. Molecular hydrogen complexes in catalysis: highly efficient hydrogen production from alcoholic substrates catalysed by ruthenium complexes. J Chem Soc Chem Commun. 1988;1154–6.

[26] See for example: (a) Van der Sluys LS, Kubas GJ, Caulton KG. Reactivity of (dihydrogen) dihydridotris(triphenylphosphine)ruthenium. Dimerization to form (PPh3)2(H)Ru(.mu.-H)3Ru (PPh3)3 and decarbonylation of ethanol under mild conditions. Organometallics. 1991;10:1033–8. (e) Kloek SM, Heynekey DM, Goldberg KI. Stereoselective decarbonylation of methanol to form a stable Iridium(III) trans-Dihydride Complex. Organometallics. 2006;25:3007–11. (g) Melnick JG, Radosevich AT, Villagran D, Nocera DG. Decarbonylation of ethanol to methane, carbon monoxide and hydrogen by a [PNP]Ir complex. Chem Commun. 2010;46:79–81.

[27] Hu P, Fogler E, Diskin-Posner Y, Iron MA, Milstein D. A novel liquid organic hydrogen carrier system based on catalytic peptide formation and hydrogenation. Nat Commun. 2015;6:6859.

[28] Junge H, Loges B, Beller M. Novel improved ruthenium catalysts for the generation of hydrogen from alcohols. Chem Commun. 2007:522–4.

[29] Nielsen M, Kammer A, Cozzula D, Junge H, Gladiali S, Beller M. Efficient hydrogen production from alcohols under mild reaction conditions. Angew Chem Int Ed. 2011;50:9593–7.

[30] Nielsen M, Alberico E, Baumann W, Drexler HJ, Junge H, Gladiali S, et al. Low-temperature aqueous-phase methanol dehydrogenation to hydrogen and carbon dioxide. Nature. 2013;495:85–90.

[31] Rodriguez-Lugo RE, Trincado M, Vogt M, Tewes F, Santiso-Quinones G, Grützmacher H. A homogeneous transition metal complex for clean hydrogen production from methanol–water mixtures. Nat Chem. 2013;5:342.

[32] (a) Göttker-Schnetmann I, White P, Brookhart M. J Am Chem Soc. 2004;126:1804. (b) Göttker-Schnetmann I, Brookhart M. Mechanistic studies of the transfer dehydrogenation of cyclooctane catalyzed by Iridium Bis(phosphinite) p-XPCP pincer complexes. J Am Chem Soc. 2004;126:9330–8.

[33] Choi J, MacArthur AH, Brookhart M, Goldman AS. Dehydrogenation and related reactions catalyzed by iridium pincer complexes. Chem Rec. 2011;111:1761–79.

[34] Polukeev AV, Petrovskii PV, Peregudov AS, Ezernitskaya MG, Koridze AA. Dehydrogenation of alcohols by Bis(phosphinite) benzene based and Bis(phosphine) ruthenocene based iridium pincer complexes. Organometallics. 2013;32:1000–15.

[35] Musa S, Shaposhnikov I, Cohen S, Gelman D. Ligand–metal cooperation in PCP pincer complexes: rational design and catalytic activity in acceptorless dehydrogenation of alcohols. Angew Chem Int Ed. 2011;50:3533–7.

[36] Oded K, Musa S, Gelman D, Blum J. Dehydrogenation of alcohols under ambient atmosphere by a recyclable sol–gel encaged iridium pincer catalyst. Catal Commun. 2012;20:68–70.

[37] Michlik S, Kempe R. A sustainable catalytic pyrrole synthesis. Nat Chem. 2013;5:140.

[38] Michlik S, Kempe R. Regioselectively functionalized pyridines from sustainable resources. Angew Chem Int Ed. 2013;52:6326–9.

[39] Blum Y, Shvo Y. Catalytically reactive (4-tetracyclone)(CO)(H)₂Ru and related complexes in dehydrogenation of alcohols to esters. J Organomet Chem. 1985;282:C7–10.

[40] Conley BL, Pennington-Boggio MK, Boz E, Williams TJ. Discovery, applications, and catalytic mechanisms of Shvo's catalyst. Chem Rev. 2010;110:2294–312.

[41] Blum Y, Shvo Y. Catalytically reactive ruthenium intermediates in the homogeneous oxidation of alcohols to esters. Isr J Chem. 1984;24:144–8.

[42] (a) Casey CP, Singer S, Powell DR, Hayashi RK, Kavana M. Hydrogen transfer to carbonyls and imines from a hydroxycyclopentadienyl ruthenium hydride: evidence for concerted hydride and proton transfer. J Am Chem Soc. 2001;123:1090. (b) Johnson JB, Bäckvall JE. Mechanism of ruthenium-catalyzed hydrogen transfer reactions. Concerted transfer of OH and CH hydrogens from an alcohol to a (cyclopentadienone)ruthenium complex. J Org Chem. 2003;68:7681. (c) Comas-Vives A, Ujaque G, Lledós A. Hydrogen transfer to ketones catalyzed by Shvo's ruthenium hydride complex: a mechanistic insight. Organometallics. 2007;26:4135.

[43] Fujita K, Tanino N, Yamaguchi R. Ligand-promoted dehydrogenation of alcohols catalyzed by Cp*Ir complexes. A new catalytic system for oxidant-free oxidation of alcohols. Org Lett. 2007;9:109–111.

[44] (a) Fujita K, Kawahara R, Aikawa T, Yamaguchi R. Hydrogen production from a methanol–water solution catalyzed by an anionic iridium complex bearing a functional bipyridonate ligand under weakly basic conditions. Angew Chem Int Ed. 2015;54:9057–60. (b) Zeng G, Sakaki S, Fujita K, Sano H, Yamaguchi R. Efficient catalyst for acceptorless alcohol dehydrogenation. ACS Catal. 2014;4:1010–20. (c) Kawahara R, Fujita K, Yamaguchi R. Cooperative catalysis by iridium complexes with a bipyridonate ligand. Angew Chem Int Ed. 2012;51:12790–4.

[45] Dutta I, Sarbajna A, Pandey P, Rahaman SM, Singh K, Bera JK. Acceptorless dehydrogenation of alcohols on a diruthenium(II,II) platform. Organometallics. 2016;35:1505–13.

[46] (a) Baratta W, Bossi G, Putignano E, Rigo P. Pincer and Diamine Ru and Os Diphosphane complexes as efficient catalysts for the dehydrogenation of alcohols to ketones. Chem Eur J. 2011;17:3474–81. (b) Esteruelas MA, Honczek N, Oliván M, Oñate E, Valencia M. Direct access to POP-Type Osmium(II) and Osmium(IV) complexes: Osmium a promising alternative to ruthenium for the synthesis of imines from alcohols and amines. Organometallics. 2011;30:2468–71.

[47] Roundhill DM. Excited-state chemistry of tetrakis(.mu.-pyrophosphito)diplatinum(II). Photoinduced addition of aryl bromides and iodides to the binuclear complex and the photo-induced catalytic conversion of isopropyl alcohol into acetone and hydrogen. J Am Chem Soc. 1985;107:4354–6.

[48] Jin H, Xie J, Pan C, Zhu Z, Cheng Y, Zhu C. Rhenium-catalyzed acceptorless dehydrogenative coupling via dual activation of alcohols and carbonyl compounds. ACS Catal. 2013;3:2195–8.

[49] Alberico E, Sponholz P, Cordes C, Nielsen M, Drexler HJ, Baumann W, et al. Selective hydrogen production from methanol with a defined iron pincer catalyst under mild conditions. Angew Chem Int Ed. 2013;52:14162–6.

[50] (a) Bielinski EA, Lagaditis PO, Zhang Y, Mercado BQ, WüRtele C, Bernskoetter WH, et al. Lewis acid-assisted formic acid dehydrogenation using a pincer-supported iron catalyst. J Am Chem Soc. 2014;136:10234–7. (b) Bielinski EA, Förster M, Zhang Y, Bernskoetter WH, Hazari N, Holthausen MC. Base-free methanol dehydrogenation using a pincer-supported iron compound and lewis acid co-catalyst. ACS Catal. 2015;5:2404–15.

[51] Chakraborty S, Lagaditis PO, FöRster M, Bielinski EA, Hazari N, Holthausen MC, et al. Well-defined iron catalysts for the acceptorless reversible dehydrogenation- hydrogenation of alcohols and ketones. ACS Catal. 2014;4:3994–4003.

[52] Chakraborty S, Brennessel WW, Jones WD. A molecular iron catalyst for the acceptorless dehydrogenation and hydrogenation of N-Heterocycles. J Am Chem Soc. 2014;136:8564–7.

[53] Chakraborty S, Piszel PE, Brennessel WW, Jones WD. A single nickel catalyst for the acceptor-less dehydrogenation of alcohols and hydrogenation of carbonyl compounds. Organometallics. 2015;34:5203–6.

[54] Mukherjee A, Nerush A, Leitus G, Shimon LJ, Ben David Y, Espinosa Jalapa NA, et al. Manganese-catalyzed environmentally benign dehydrogenative coupling of alcohols and amines to form aldimines and H_2: a catalytic and mechanistic study. J Am Chem Soc. 2016;138:4298–301.

[55] O Bauer J, Chakraborty S, Milstein D. Manganese-catalyzed direct deoxygenation of primary alcohols. ACS Catal. 2017;7:4462–6.

[56] Nguyen DH, Trivelli X, Capet F, Paul JF, Dumeignil F, Gauvin RM. Manganese pincer complexes for the base-free, acceptorless dehydrogenative coupling of alcohols to esters: development, scope, and understanding. ACS Catal. 2017;7:2022–32.

[57] Tan DW, Li HX, Zhang MJ, Yao JL, Lang JP. Acceptorless dehydrogenation of alcohols catalyzed by CuI N-Heterocycle thiolate complexes. ChemCatChem. 2017;9:1113–8.

[58] Zhang G, Hanson SK. Cobalt-catalyzed alcohol hydrogenation and dehydrogenation reactions. Org Lett. 2013;15:650–3.

[59] Data from Renewal Fuels Association (RFA). Available at: http://www.ethanolrfa.org/. Accessed: 10 Aug 2017.

[60] Morton D, Cole-Hamilton DJ, Utuk ID, Paneque-Sosa M, Lopez-Poveda M. Hydrogen production from ethanol catalysed by group 8 metal complexes. J Chem Soc Dalton Trans. 1989:489–95.

[61] Kagalwala HN, Maurer AB, Mills IN, Bernhard S. Visible-light-driven alcohol dehydrogenation with a rhodium catalyst. ChemCatChem. 2014;6:3018–26.

[62] O'Lenick AJ. Guerbet chemistry. J Surfact Det. 2001;4:311–5.

[63] Gunanathan C, Shimon LJ, Milstein D. Direct conversion of alcohols to acetals and H_2 catalyzed by an acridine-based ruthenium pincer complex. J Am Chem Soc. 2009;131:3146–7.

[64] Zonetti PC, Celnik J, Letichevsky S, Gaspar AB, Appel LG. Chemicals from ethanol – the dehydrogenative route of the ethyl acetate one-pot synthesis. J Mol Catal A: Chemical. 2011;334:29–34.

[65] Ethyl Acetate (ETAC): 2017 World Market Outlook and Forecast up to 2021. Merchant Research & Consulting ltd. Available at: https://mcgroup.co.uk. Accessed: 1 Aug 2017.

[66] Nielsen M, Junge H, Kammer A, Beller M. Towards a green process for bulk-scale synthesis of ethyl acetate: efficient acceptorless dehydrogenation of ethanol. Angew Chem Int Ed. 2012;51:5711–3.

[67] (a) Spasyuk D, Smith S, Gusev DG from esters to alcohols and back with ruthenium and osmium catalysts. Angew Chem Int Ed. 2012;51:2772–5. (b) Spasyuk D, Gusev DG. Acceptorless dehydrogenative coupling of ethanol and hydrogenation of esters and imines. Organometallics. 2012;31:5239–42.

[68] Kuriyama W, Matsumoto T, Ogata O, Ino Y, Aoki K, Tanaka S, et al. Catalytic hydrogenation of esters. Development of an efficient catalyst and processes for synthesising (R)-1,2-Propanediol and 2-(l-Menthoxy)etanol. Org Process Res Dev. 2012;16:166–71.

[69] Baratta W, Chelucci G, Gladiali S, Siega K, Toniutti M, Zanette M, et al. Ruthenium(II) terdentate CNN complexes: superlative catalysts for the hydrogen-transfer reduction of ketones by reversible insertion of a carbonyl group into the Ru[BOND]H bond. Angew Chem Int Ed. 2005;44:6214.

[70] Zhang J, Leitus G, Ben-David Y, Milstein D. Facile conversion of alcohols into esters and dihydrogen catalyzed by new ruthenium complexes. J Am Chem Soc. 2005;127:10840.

[71] Clarke ZE, Maragh PT, Dasgupta TP, Gusev DG, Lough AJ, Abdur-Rashid K. A family of active iridium catalysts for transfer hydrogenation of ketones. Organometallics. 2006;25:4113.

[72] Tanaka R, Yamashita M, Nozaki K. Catalytic hydrogenation of carbon dioxide using Ir(III)–pincer complexes. J Am Chem Soc. 2009;131:14168.

[73] Spasyuk D, Vicent C, Gusev DG. Chemoselective hydrogenation of carbonyl compounds and acceptorless dehydrogenative coupling of alcohols. J Am Chem Soc. 2015;137:3743–6.

[74] Gunanathan C, Ben-David Y, Milstein D. Direct synthesis of amides from alcohols and amines with liberation of H2. Science. 2007;317:790–2.

[75] Vicent C, Gusev DG. ESI-MS insights into acceptorless dehydrogenative coupling of alcohols. ACS Catal. 2016;6:3301–9.

[76] Gusev DG. Dehydrogenative coupling of ethanol and ester hydrogenation catalyzed by pincer-type YNP complexes. ACS Catal. 2016;6:6967–81.

[77] Hu P, Ben-David Y, Milstein D. Rechargeable hydrogen storage system based on the dehydrogenative coupling of ethylenediamine with ethanol. Angew Chem Int Ed. 2016;55:1061 −4.

[78] Hu P, Fogler E, Diskin-Posner Y, Iron MA, Milstein D. A novel liquid organic hydrogen carrier system based on catalytic peptide formation and hydrogenation. Nat Commun. 2015;6:6859.

[79] Sponholz P, Mellmann D, Cordes C, Alsabeh PG, Li B, Li Y, et al. Efficient and selective hydrogen generation from bioethanol using ruthenium pincer-type complexes. ChemSusChem. 2014;7:2419–22.

[80] Zhang L, Nguyen DH, Raffa G, Trivelli X, Capet F, Desset S, et al. Catalytic conversion of alcohols into carboxylic acid salts in water: scope, recycling, and mechanistic insights. ChemSusChem. 2016;9:1413–23.

[81] Nguyen DH, Morin Y, Zhang L, Trivelli X, Capet F, Paul S, et al. Oxidative transformations of biosourced alcohols catalyzed by earth-abundant transition metals. ChemCatChem. 2017;9:2652–60.

[82] McCoy M. Glycerin surplus. Plants are closing, and new uses for the chemical are being found. Chem Eng News. 2006;84:7.

[83] (a) Tan HW, Abdul Aziz AR, Aroua MK. Glycerol production and its applications as a raw material: a review. Renew Sustainable Energy Rev. 2013;27:118–27. (b) Pagliaro M, Ciriminna R, Kimura H, Rossi M, Pina CD. From glycerol to value-added products. 2007;46:4434–40. (c) Katryniok B, Kimura H, Skrzyńska E, Girardon JS, Fongarland P, Capron M, et al. Selective catalytic oxidation of glycerol: perspectives for high value chemicals. Green Chem. 2011;13:1960–79.

[84] (a) Soares RR, Simonetti DA, Dumesic JA. Glycerol as a source for fuels and chemicals by low-temperature catalytic processing. Angew Chem Int Ed. 2006;45:3982. (b) Huber GW, Shabaker JW, Dumesic JA. Raney Ni-Sn catalyst for H$_2$ production from biomass-derived hydrocarbons. Science. 2003;300:2075–7.

[85] Crotti C, Kasparb J, Farnetti E. Dehydrogenation of glycerol to dihydroxyacetone catalyzed by iridium complexes with P–N ligands. Green Chem. 2010;12:1295–300.

[86] Sharninghausen LS, Campos J, Manas MG, Crabtree RH. Efficient selective and atom economic catalytic conversion of glycerol to lactic acid. Nat Commun. 2014;5:5084.

[87] (a) Hintermair U, Campos J, Brewster TP, Pratt LM, Schley ND, Crabtree RH. Hydrogen-transfer catalysis with Cp*IrIII complexes: the influence of the ancillary ligands. ACS Catal 2014;4:99–108. (b) Campos J, Hintermair U, Brewster TP, Takase MK, Crabtree RH. Catalyst activation by loss of cyclopentadienyl ligands in hydrogen transfer catalysis with Cp*IrIII complexes. ACS Catal. 2014;4:973–85.

[88] Campos J, Sharninghausen LS, Manas MG, Crabtree RH. Methanol dehydrogenation by iridium N-Heterocyclic carbene complexes. Inorg Chem. 2015;54:5079–84.

[89] Dusselier M, van Wouwe P, Dewaele A, Makshina E, Sels BF. Lactic acid as a platform chemical in the biobased economy: the role of chemocatalysis. Energy Environ Sci. 2013;6:1415–42.

[90] (a) Sharninghausen LS, Mercado BQ, Crabtree RH, Balcells D, Campos J. Gel matrices for the crystallization of [Ir$_4$(IMe)$_7$(CO)H$_{10}$]$^{2+}$ and [Ir$_4$(IMe)$_8$H$_9$]$^{3+}$ clusters derived from catalytic glycerol dehydrogenation. Dalton Trans. 2015;44:18403–10. (b) Campos J, Sharninghausen LS, Crabtree RH, Balcells D. A carbene-rich but carbonyl-poor [Ir$_6$(IMe)$_8$(CO)$_2$H$_{14}$]$^{2+}$ polyhydride cluster as a deactivation product from catalytic glycerol dehydrogenation. Angew Chem Int Ed. 2014;53:12808–11.

[91] Sun Z, Liu Y, Chen J, Huang C, Tu T. Robust iridium coordination polymers: highly selective, efficient, and recyclable catalysts for oxidative conversion of glycerol to potassium lactate with dihydrogen liberation. ACS Catal. 2015;5:6573–8.

[92] Lu Z, Demianets I, Hamze R, Terrile NJ, Williams TJ. A prolific catalyst for selective conversion of neat glycerol to lactic acid. ACS Catal. 2016;6:2014–7.

[93] Li Y, Nielsen M, Li B, Dixneuf PH, Junge H, Beller M. Ruthenium-catalyzed hydrogen generation from glycerol and selective synthesis of lactic acid. Green Chem. 2015;17:193–8.

[94] Sharninghausen LS, Mercado BQ, Crabtree RH, Hazari N. Selective conversion of glycerol to lactic acid with iron pincer precatalysts. Chem Commun. 2015;51:16201–4.

[95] Starch-Stärke RH. Renewable raw materials in Europe – Industrial utilisation of starch and sugar. 2002;54:89–99.

[96] Huber GW, Dumesic JA. An overview of aqueous-phase catalytic processes for production of hydrogen and alkanes in a biorefinery. Catal Today. 2006;111:119–32.

[97] (a) Ren N, Wang A, Cao G, Xu J, Gao L. Bioconversion of lignocellulosic biomass to hydrogen: potential and challenges. Biotechnol Adv. 2009;27:1051–60. (b) Zeikus JG. Chemical and fuel production by anaerobic bacteria. Annu Rev Microbiol. 1980;34:423. (c) Li J, Ren N, Li B, Qin Z, He J. Anaerobic biohydrogen production from monosaccharides by a mixed microbial community culture. Bioresour Technol. 2008;99:6528–37.

[98] Toonssen R, Woudstra N, Verkooijen AH. Int J Hydrogen Energy. 2008;33:4074–82.

[99] (a) Garcia L, French R, Czernik S, Chornet E. Catalytic steam reforming of bio-oils for the production of hydrogen: effects of catalyst composition. Appl Catal A. 2000;201:225–39. (b) Marquevich M, Czernik S, Chornet E, Montane D. Hydrogen from biomass: steam reforming of model compounds of fast-pyrolysis oil. Energy Fuels. 1999;13:1160–6.

[100] Coronado I, Stekrova M, Reinikainen M, Simell P, Lefferts L, Lehtonen J. A review of catalytic aqueous-phase reforming of oxygenated hydrocarbons derived from biorefinery water fractions. Int J Hydrogen Energy. 2016;4:11003–32.

[101] (a) de Wit G, de Vlieger JJ, Kock-van Dalen AC, Kieboom AP, van Bekkum H. Catalytic dehydrogenation of reducing sugars in alkaline solution at ambient conditions. Transfer hydrogenation of fructose. Tetrahedron Lett. 1978;15:1327–30. (b) de Wit G, Devlieger JJ, van Dalen AC, Heus R, Laroy R, van Hengstum AJ, Kieboom AP, van Bekkum H. Catalytic dehydrogenation of reducing sugars in alkaline solution. Carbohydrate Res. 1981;91:125–38.

[102] Cortright RD, Davda RR, Dumesic JA. Hydrogen from catalytic reforming of biomass-derived hydrocarbons in liquid water. Nature. 2002;418:964–7.

[103] Taccardi N, Assenbaum D, Berger ME, Bçsmann A, Enzenberger F, Wçlfel R, et al. Catalytic production of hydrogen from glucose and other carbohydrates under exceptionally mild reaction conditions. Green Chem. 2010;12:1150–6.

[104] Zhan Y, Shen Y, Li S, Yueb B, Zhou X. Hydrogen generation from glucose catalyzed by organoruthenium catalysts under mild conditions Chem Commun. 2017;53:4230–3.

[105] Li Y, Sponholz P, Nielsen M, Junge H, Beller M. Iridium-catalyzed hydrogen production from monosaccharides, disaccharide, cellulose, and lignocellulose. ChemSusChem. 2015;8:804–8.

[106] Bozell JJ, Petersen GR. Technology development for the production of biobased products from biorefinery carbohydrates—the US Department of Energy's "Top 10" revisited. Green Chem. 2010;12:539–54.

[107] (a) Ding LN, Wang AQ, Zheng MY, Zhang T. Selective transformation of cellulose into sorbitol by using a bifunctional nickel phosphide catalyst. ChemSusChem 2010;3:818–21. (b) Fukuoka A, Dhepe PL. Catalytic conversion of cellulose into sugar alcohols. Angew Chem Int Ed. 2006;31:5161–3.

[108] Glattfeld E, Gershon S. The catalytic dehydrogenation of sugar alcohols. J Am Chem Soc. 1938;60:2013–23.

[109] Manas MG, Campos J, Sharninghausen LS, Lin E, Crabtree RH. Selective catalytic oxidation of sugar alcohols to lactic acid. Green Chem. 2015;17:594–600.

Moran Feller

8 Hydrogenation of nitriles and imines for hydrogen storage

Abstract: This review focuses on the selective catalytic hydrogenation of nitriles to primary amines both homogeneously and heterogeneously with transition metal-based catalysts in the view of nitriles as hydrogen carriers. Nitriles can be reduced with two equivalents of H_2 to primary amines, thus having a great potential to serve as liquid organic hydrogen carriers (LOHCs) for hydrogen storage. Imines are intermediates in the hydrogenation of nitriles to amines, thus they can also serve as potential LOHCs, however with a lower hydrogen storage capacity (HSC).

Keywords: hydrogen storage, imine hydrogenation, LOHCs, metal-ligand cooperativity, nitrile hydrogenation

8.1 Introduction

Reduction of nitriles produces amines and imines, which are widely used as intermediates and precursors in the synthesis of various natural products, agrochemicals, dyes, pigments, polymers, and pharmaceuticals [1–4]. Thus, the reduction of nitrile has been intensively investigated both stoichometrically and catalytically [5–12]. Conventionally, nitriles are reduced stoichiometrically by metal hydrides [13–16], however this method suffers from low functional groups tolerance and low reaction selectivity, in practice these compounds are difficult to handle due to their high reactivity, and above all it produces copious waste. Hydrosilanes [17–21] and hydroboranes [22–28] can also serve as stoichiometric reducing agents in nitrile reduction, catalyzed by transition metals or Lewis acids. These methods exhibit high selectivity at relatively moderate reaction conditions, however as stoichiometric methods, these cannot be considered as environmentally benign, and moreover, they do not produce primary amines directly. The catalytic hydrogenation of nitriles to amines represents the most environmentally benign method with the highest atom efficiency. Thus, it is a highly desirable transformation for organic synthesis applications but also in the aspect of dihydrogen storage.

Dihydrogen, which holds the highest energy density by weight, is a promising energy source and the leading candidate in replacing fossil fuel [29–33]. In the course of "Hydrogen Energy Economy" cycle, dihydrogen storage remains a major challenge due to its extremely low density (0.0898 g/L at 0 °C and 1 bar) [10]. Compressed dihydrogen or liquid dihydrogen require high pressure technology or harsh cryogenic conditions. Hydrogen storage in materials such as main-group hydrides, metal organic frameworks, metal clusters and nanostructured materials were offered as solutions for hydrogen storage, however they all suffer from significant limitations [31–33]. In recent years, liquid organic hydrogen carriers (LOHCs) are discussed as possible systems for hydrogen storage. LOHCs are consisting of materials which can bind dihydrogen reversibly. The ideal LOHC has to release pure H_2 in catalytic dehydrogenation reaction, yielding quantitatively a hydrogen-lean product, which binds hydrogen in catalytic hydrogenation reaction [34–36]. The ideal LOHC system should be based on inexpensive and abundant organic compounds with high hydrogen storage capacity (HSC), which could be hydrogenated and dehydrogenated under mild conditions (temperature and hydrogen pressure) in quantitative yields, preferably by the same catalyst. Systems which will be consist of heterogeneous catalysts and liquid organic substrates that could be used neat (solvent free) and allow catalyst recycling are preferred. Examples of LOHCs are cycloalkane derivatives such as methylcyclohexane or decalin, which exhibit relatively high HSC of 6.2 and 7.3 wt% respectively, however their dehydrogenation is highly endothermic and requires elevated temperatures (over 200 °C) [37–39]. It was found that LOHC systems containing nitrogen atoms are more efficient, probably due to lower endothermicity of dehydrogenation [40–49].

In the scope of developing new LOHCs, primary nitriles/amines couples have a great potential, as they can store up to two equivalents of H_2 per R-CH$_2$-NH$_2$ unit. Acetonitrile/methyl amine couple has a HSC of 8.9 wt%, however methyl amine is a gas under ambient conditions, thus substituted nitriles/amines couples with lower HSC should be considered. This review covers the recent publications on nitriles hydrogenation with respect to their potential utilization in a potential hydrogen storage cycle, thus only selective catalytic hydrogenation of nitriles to their corresponding primary amines are covered. Since the hydrogenation of benzonitrile is often used as a benchmark reaction, the catalytic reactions mentioned in this review are evaluated and compared by this reaction, although benzonitrile/benzylamine couple exhibit lower HSC as compared to short aliphatic nitriles. Nitriles can be considered as LOHCs only if their hydrogenation products can be dehydrogenated efficiently to nitriles. The revers dehydrogenation of amines and imines to nitriles is covered in a separate review in this book [50]. Nitriles hydrogenation produces imines as intermediates or by-products, which can be farther hydrogenated to their corresponding amines. A short chapter on imines hydrogenation in the viewpoint of LOHCs is included.

8.2 Catalytic hydrogenation of nitriles

8.2.1 Nitrile hydrogenation – selectivity issues and homogeneous Ru-based catalysts

Catalytic hydrogenation of nitriles has been intensively studied and it is known to take place both homogeneously and heterogeneously. Nitrile hydrogenation is practiced industrially on a large scale in the heterogeneous hydrogenation of adiponitrile to hexamethylenediamine, a substrate for the synthesis of Nylon 6,6 [51]. Other industrial catalytic hydrogenations of nitriles are performed heterogeneously with cobalt [52], nickel [53, 54] and palladium catalysts [55, 56], but suffer from low selectivity and low functional group tolerance. Early patents on catalytic nitrile hydrogenation describes the use of $[Fe(CO)_5]$ and $[Ni(CO)_4]$ under harsh conditions (200 °C, 140 bar H_2)[57] or $[Ru(PPh_3)_3Cl_2]$ and $[Ru(CO)HCl]$ under milder conditions (130 °C, 40 bar H_2) [58]. In 1979 Otsuka, Okano and Yoshida reported on the first example of catalytic homogenous nitrile hydrogenation to primary amines under relatively mild conditions with $[(P^iPr_3)RhH]$. While benzonitrile was hydrogenated to benzylamine with 45% yield using 1 mol% catalyst loading under only one bar of H_2 at 20 °C after 20 h, the aliphatic nitriles were hydrogenated to their corresponding primary amines under similar conditions in quantitative yields [59].

The selectivity of the nitrile reduction is a major issue, since mixtures of primary, secondary, and tertiary amines can be obtained by different reaction pathways of imine intermediates (Figure 8.1). The imine intermediate **I** undergoes nucleophilic attack by the amine product **II** to give the geminal diamine (**III**), which leads to the formation of secondary amine via a secondary imine (**IV**) by elimination of ammonia. Tertiary amines are formed by the same mechanism upon nucleophilic attack of free
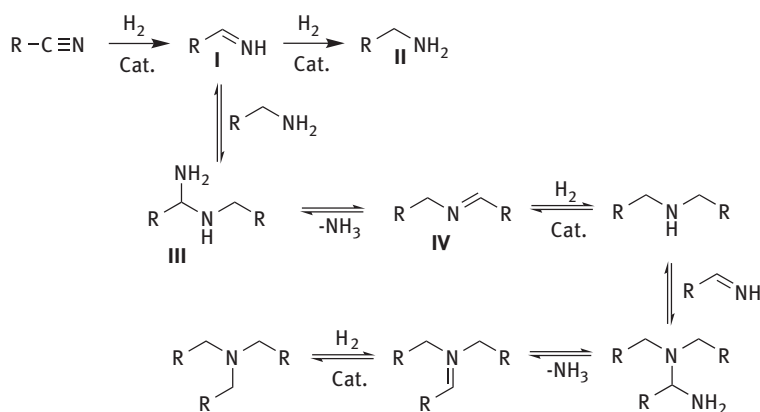
Figure 8.1: Mechanism of the hydrogenation of nitriles to primary, secondary and tertiary amines via imine intermediates.

amine (**II**) on the secondary imine (**IV**) [6, 9]. According to kinetic studies the first hydrogenation to primary imine by the catalyst is the rate determining step [6].

Selective nitrile hydrogenation toward primary amines is desirable both for synthetic applications and in light of possible hydrogen storage applications. It was found that addition of base or ammonia [60] shifts the equilibria between **III** and **IV** and **III** and **II** (Figure 8.1) toward **II**. For example, Hidai and coworkers reported on the hydrogenation of benzonitrile with a Ru based catalyst [(η^6-C_6H_6)Ru[Xy$_2$NSN] (Xy$_2$NSN = (3,5-Me$_2$C$_6$H$_3$)NH-*o*-C$_6$H$_4$)$_2$S) (**1**, Table 8.1) resulting in 72% benzylamine and 27% benzylidenebenzylamine at 80 °C and 30 bar H$_2$. Interestingly, the addition of ^{t}BuONa (10 mol %) resulted in 92% yield of benzylamine under similar catalytic conditions [61]. Beller and co-workers showed that the simple precursor [RuCl$_2$(PPh$_3$)$_3$] could give 99% yield of benzylamine from benzonitrile when 10 mol% of ^{t}BuOK were added to the catalytic reaction under 50 bar H$_2$ at 80 °C [68]. Later-on, Beller and co-workers showed that the *in situ* catalyst composed of [Ru(cod)(methylallyl)$_2$] and DPPF ligand (DPPE = 1,1-bis(diphenylphosphino)ferrocene) or the carbene ligand SIMesBF$_4$ (SIMesBF$_4$ = 1,3-bis(2,4,6-trimethylphenyl)-4,5-dihydroimidazolium tetrafluoroborate) are efficient catalysts for the selective reduction of nitriles to primary amines, too.

Table 8.1: Homogeneous Ru-based catalyst for the hydrogenation of benzonitrile to bnzylamine.
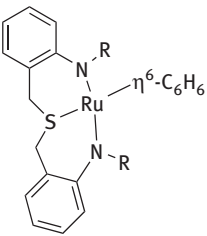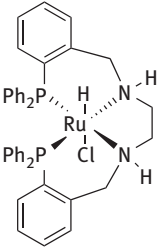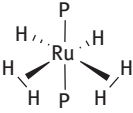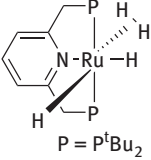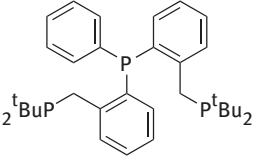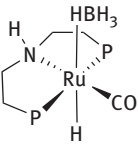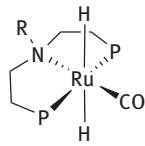
Catalyst	Reaction conditions	Conversion (%)	Yield (%)
1[61] R = 3,5-Me$_2$C$_6$H$_3$	Catalyst loading 1 mol% 30 bar H$_2$, 80 °C, 18 h Additives: ^{t}BuONa (10 mol%)	98	92
2[62] 	Catalyst loading 0.55 mol% 14 bar H$_2$, 20 °C, 3 h Additives: ^{t}BuOK (5 mol%), KH (8.3 mol%)	100	100

Table 8.1 (continued)

Catalyst	Reaction conditions	Conversion (%)	Yield (%)
3[63] P = PCyp$_3$	Catalyst loading 0.5 mol% 3 bar H$_2$, 22 °C, 24 h	97	99
6[64] P = P^{t}Bu$_2$	Catalyst loading 0.4 mol% 75 bar H$_2$, 135 °C, 24 h Additives: water 2 mol%	> 99	95% yield for p-chloroben- zonitrile 95 %
7[65] [Ru(COD)(methylallyl)$_2$]/L $_2^t$BuP P^{t}Bu$_2$ **L, 7**	Catalyst loading 0.5 mol% 15 bar, 50 °C, 17 hrs	> 99	99
8[66] P = PPh$_2$	Catalyst loading 0.5% 30 bar H$_2$, 100 °C, 3 h	> 99	97
9[67] P = P^{t}Bu$_2$ **9** R = H; **9-Me** R = Me	Catalyst loading 1 mol% 4 bar H$_2$, 90 °C, 3 h	**9** > 99 **9-Me** = 0	88

Both substituted aliphatic and aromatic nitriles could be selectively hydrogenated to their corresponding primary amines under basic conditions (10 mol% of ^{t}BuOK), 50 bar H$_2$ and 80–140 °C [69, 70].

Highly selective hydrogenation of benzonitrile to benzyl amine with a Ru-hydride complex trans-[RuHCl{ethP$_2$(NH)$_2$}] (ethP$_2$(NH)$_2$ = [PPh$_2$((o-C$_6$H$_4$) CH$_2$NHCH$_2$)]$_2$ (**2**, Table 8.1) was reported by Morris and co-workers. The reaction takes place under mild conditions (20 °C, 14 bar H$_2$) and resulted in full conversion of benzonitrile to benzylamine. The catalyst needs to be activated with ^{t}BuOK, and its reactivity is retarded in the presence of traces of water. Addition of KH to the catalytic reaction removes traces of water and increases the catalyst reactivity [62]. Other hydride Ru catalysts such as [RuH$_2$(CO)$_2$(P^{n}Bu$_3$)$_2$], [RuH$_2$(CO)$_2$(PPh$_3$)$_2$] and [RuH$_2$ (PPh$_3$)$_4$] were reported by Frediani and co-workers in 2004 to hydrogenate benzonitrile to benzylamine in maximum 76% conversion, however only mixtures of benzylamine and dibenzylamine were obtained, with the secondary amine as the major product [71].

Although selective catalytic hydrogenation of nitriles to primary amines was demonstrated by using basic additives or ammonia, developing catalytic systems for selective nitrile hydrogenation in the absence of additives is highly desirable.

In 2010, Sabo-Etienne, Grellier and co-workers reported the first example of "base free" Ru catalyst for the selective hydrogenation of nitriles. The nonclassical Ru hydride complex [RuH$_2$(H$_2$)$_2$(PCyp$_3$)$_2$] (PCyp$_3$ = tricyclopentylphosphine) (**3**, Figure 8.2, Table 8.1) catalyzes the hydrogenation of benzonitrile in 97% conversion and a product ratio of 99:1 for benzylamine and dibenzyimine respectively under three bar H$_2$ at ambient temperature (Table 8.1). Mechanistic studies allowed the isolation of two similar cyclometalated complexes (**4** and **5**, Figure 8.2), which are the catalyst resting states and exhibit similar catalytic reactivity as complex **3** [63].
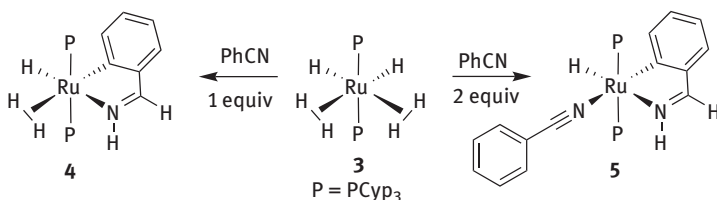
Figure 8.2: Isolated resting states in the catalytic hydrogenation of benzonitrile by complex **3** [63].

The nonclassical ruthenium hydride PNP complex **6** (PNP = 2,6-bis(di-tert-butyl-phosphanylmethyl)pyridine (Table 8.1), reported by Leitner and co-workers is also active in nitrile hydrogenation in the absence of basic additives. Interestingly, the use of water as an additive (2 mol%) was reported to increase the selectivity and the reactivity of the catalyst. For example, under 75 bar H$_2$ and 135 °C, *p*-chlorobenzonitrile was hydrogenated to the corresponding primary amine in only 36% along with secondary amines and imines after 45 h under dry conditions. When adding water productivity and selectivity of the system could be improved. Upon addition of 2 mol% of water 95%

yield were achieved after only 24 h. Similar reactivity was reported also for aliphatic nitriles. Surprisingly, for benzonitrile the addition of water resulted in lower selectivity [64]. Leitner proposed for the PNP-Ru catalyst an inner-sphere hydrogenation mechanism based on DFT calculations (Figure 8.3). Pre-coordination of the nitrile to the metal center (complex **6′a**, Figure 8.3) followed by hydride transfer from the metal center to the carbon atom of the nitrile gives complex **6′b**. H_2 coordination to complex **6′b** followed by σ-bond metathesis of the H_2 molecule and hydride transfer to the nitrogen atom of the imide in **6′c** yields complex **6′d**. The second hydride is transferred to the carbon atom of the imine, followed by a second H_2 coordination and σ-bond metathesis to give the free amine and the active catalyst **6′**.
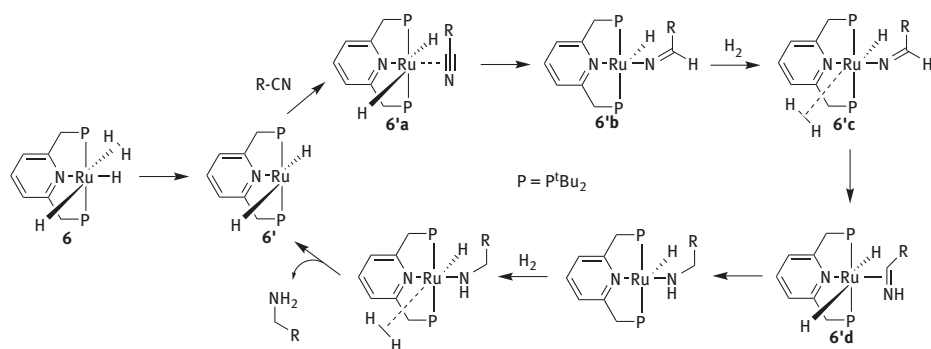
Figure 8.3: Postulated catalytic cycle for the inner-sphere hydrogenation of nitriles by [(PNP)RuH₂(H₂)] (**6**) based on DFT calculations [64].

Beller and co-workers demonstrated the selective base free hydrogenation of aliphatic and aromatic nitriles by a catalytic system based on the previously reported complex [Ru(cod)(methylallyl)₂] and the phosphine tridentate ligand **7** (Table 8.1). While using bis(diphenylphosphino)ferrocene or carbene ligands, selectivity toward primary amines was obtained under basic conditions [69, 70]. Ligand **7** allows excellent selectivity and high yields for aromatic nitriles with a variety of functional groups and for short aliphatic nitriles under 15 bar H_2 at 50 °C under neutral conditions [65]. Beller and co-workers reported also on the catalyst Ru-Macho-BH (**8**, Table 8.1), which hydrogenates benzonitrile to benzyl amine in the absence of base in 97% yield. This catalyst is also active in the selective hydrogenation of aliphatic nitriles, including adiponitrile in 96% yield [66]. DFT studies suggest an outer-sphere hydrogenation mechanism, in which metal-ligand cooperation takes place (Figure 8.4). The complex Ru-MACHO-BH **8** gives the Ru dihydrido active species (**8a**), which hydrogenates the nitrile to imide resulting in an imido complex (**8b**). The latter activates H_2 to regenerate complex **8a**, which hydrogenates the imine intermediate to the corresponding amine. Complex **8c** represents the calculated transition state for the outer-sphere acetonitrile
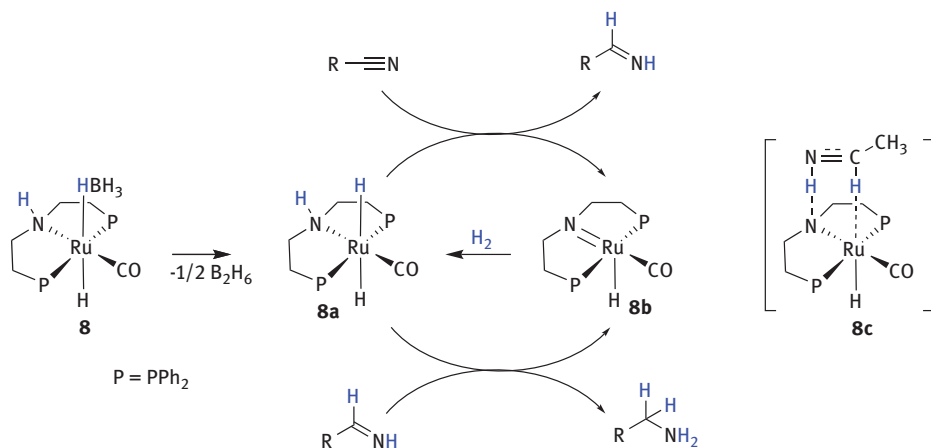
Figure 8.4: Postulated catalytic cycle for the outer-sphere hydrogenation of nitriles by [Ru-Macho-BH] (**8**) precatalyst and the calculated transition state for the outer sphere hydrogenation of acetonitrile (**8c**)[66].

hydrogenation [66]. Surprisingly, replacing the phenyl groups of the phosphinic ligands of the Ru-MACHO complex **8** with ^tBu (complex **9**, Table 8.1), a tunable hydrogenation of benzonitrile to either benzylamine or dibenzylimine was reported by Prechtl and Choi [67]. The selectivity toward imines or amines is controlled by changing the reaction conditions; benzonitrile hydrogenation with catalyst loading of 0.5 mol% and 50 °C under four bar H₂ gave dibenzylimine in 98% yield, while increasing the reaction temperature to 90 °C and the catalyst loading to 1 mol% resulted in 88% yield of benzylamine. Prechtl *et al.* also reported that the Ru analogous complex with N-methylated ligand (complex **9-Me**, Table 8.1) is inactive in nitrile hydrogenation, and by that demonstrated the importance of metal-ligand cooperativity in nitrile hydrogenation [67]. While Beller and co-workers suggested an outer-sphere mechanism for nitrile hydrogenation by Ru-Macho catalyst **8** based on DFT calculations (Figure 8.4), Prechtl *et al.* suggested an inner-sphere mechanism for Ru-Macho catalyst **9**, in which the nitrile is directly coordinated to the metal center, based on experimental evidences which suggests a Ru-nitrile complex **9a** (Figure 8.5).

8.2.2 Homogeneous earth-abundant metals-based catalysts

Earth-abundant, low-toxicity, first-row base metals present a promising alternative to the precious-metal-based catalysts [72–74]. However, low-valent late first-row transition metal complexes face a significant limitation from their greater sensitivity to air and moisture compared to their platinum group congeners. To overcome this limitation, air stable pre-catalysts, usually in a higher oxidation state, are reduced *in situ* to give the active catalysts. Common reducing agents, which are used in catalytic
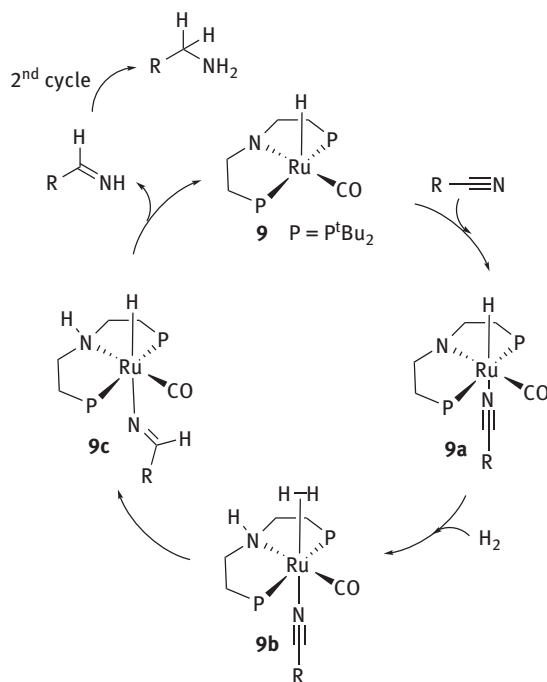
Figure 8.5: Postulated catalytic cycle for the inner-sphere hydrogenation of nitriles by [Ru-Macho] (**9**) [67].
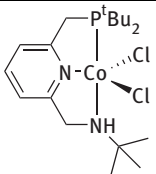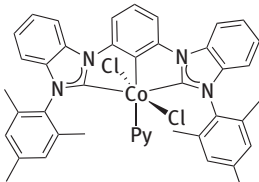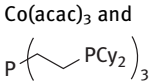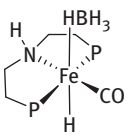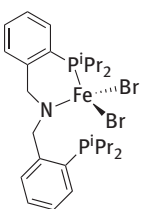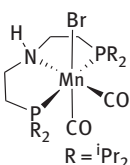
amounts are Grignard or metal hydride reagents [75–79] as well as metal alkoxides [80, 81].

In 2015 Milstein and co-workers reported on several pincer Co precatalysts which upon *in situ* reduction with NaBHEt$_3$ hydrogenated nitriles to their corresponding primary amines. The pyridine based PNNH Co pincer complex **10** (Table 8.2) was found to be the best precatalyst, with a broad applicability of different functional groups of aromatic and aliphatic nitriles in good to excellent yields under mild conditions [82].

Fout and co-workers reported in 2017 the selective hydrogenation of aromatic and aliphatic nitrile to primary amines by a pincer Co complex [83]. The active catalyst is a Co(I) complex, which is obtained *in situ* by the reduction of the air-stable precatalyst [(mesCCC) CoCl$_2$py] (**11,** Table 8.2) (py = pyridine, mesCCC = bis(mesityl-benzimidazol-2-ylidene) phenyl)) with NaBHEt$_3$. The Lewis acid by product of the reduction (BEt$_3$) plays a crucial role in the catalytic nitrile hydrogenation. Mechanistic studies showed that the Lewis acid facilitates a side-on coordination of the nitrile to the cobalt center, allowing the nitrile hydrogenation by a pairwise transfer of H$_2$ through a Co(I/III) redox process.

Beller and co-workers reported on a catalytic system comprised of [Co(acac)$_3$] and a tetradentate phosphine ligand tris[2-(dicyclohexylphosphino)ethyl]phosphine (**12,** Table 8.2). Both aromatic and aliphatic nitriles are reduced to the corresponding

Table 8.2: Homogeneous Earth-abundant-based catalyst for the hydrogenation of benzonitrile to benzylamine.

Catalyst		Reaction conditions	Conversion (%)	Yield (%)
10[82]		Catalyst loading 2 mol% 50 bar H_2, 135 °C, 36 h Additives: NaOEt (4.4 mol%), NaHBEt$_3$ (2 mol%)	93	92
11[83]		Catalyst loading 2 mol% 4 bar H_2, 115 °C, 8 h Additives: KO^{t}Bu (6 mol%), NaHBEt$_3$ (4 mol%)	> 99	97
12[84]	Co(acac)$_3$ and	Catalyst loading 4 mol% 30 bar H_2, 80 °C, 18 h Additives: KO^{t}Bu (15 mol%)	100	98
13[85] **14**[86]	**13**; P = P^{i}Pr$_2$ **14**; P = PCy$_2$	Catalyst loading: **13** – 1 mol%, **14** – 0.5 mol%. 30 bar H_2, 70 °C, 3 h (For **13** the product was isolated as HCl salt.)	> 99	**13** – 97 **14** – 90
15[87]		Catalyst loading 1 mol% 60 bar H_2, 140 °C, 16 h Additives: NaHBEt$_3$ (1 mol%), KHMDS (3 mol%)	99	99
16[88]	R = ^{i}Pr$_2$	Catalyst loading 3 mol% 50 bar H_2, 120 °C, 24 h Additives: ^{t}BuONa (10 mol%),	99	98

primary amines under moderate conditions and in high yields. The reaction is highly depended on the solvent, and takes place only with alcohols as solvents. Lower selectivity was obtained with primary and secondary alcohols as solvents as compared to ᵗBuOH. In addition, the selectivity depends on the base loading, and 10 mol % or higher prevented the formation of secondary imines and amines. Mechanistic investigations indicate a strong dependence on temperature for the formation of the active catalyst [84].

Beller and co-workers reported on iron complexes **13, 14** (Table 8.2), analogous to the MACHO-Ru complex **8**, which allow for the hydrogenation of aryl, alkyl, heterocyclic nitriles and dinitriles such as adipodinitrile [85, 86]. The catalysts exhibit tolerance toward variety of functional groups such as ester, ether, acetamido and amino substituents. DFT calculations on the actual catalyst support the outer sphere hydrogenation, as was suggested also for the analogous Ru complex [66]. The importance of metal-ligand cooperativity in nitrile hydrogenation by the MACHO-Fe complexes is supported by the observation that the N-methylated complex (bis[(2-diisopropylphosphino)ethyl] methyl amine) was not active.

Milstein and co-workers reported on the hydrogenation of nitriles by an iron complex with a novel PNP pincer ligand bis(2-diisopropylphosphinobenzyl)amine (**15**) [87]. This new PNP ligand which could form a flexible 6-membered chelate, while in the precatalyst **15** exhibits hemilability. Precatalyst **15** is activated *in situ* with NaBHEt₃ and KHMDS, hydrogenated aromatic and aliphatic nitriles to the corresponding primary amines selectively in good to excellent yields.

A rare example of a Manganese pincer complex **16** (Table 8.2) was reported by Beller and co-workers to serve as a precatalyst in the hydrogenation of aromatic and aliphatic nitriles to their corresponding primary amines [88]. Complex **16** is air stable, and requires a base (ᵗBuONa, 10 mol%) for its activation. DFT calculations supported by mechanistic studies, show that under basic conditions an imido intermediate is obtained. The imido intermediate readily activates hydrogen to give a Mn-hydride complex, which is the active catalyst in the nitriles hydrogenation. As in the hydrogenation of nitriles by the analogous Ru and Fe complexes (**8, 13** and **14**), DFT calculations support an outer-sphere mechanism involving a simultaneous transfer of the hydride from the Mn center (Mn–H) and the proton from the nitrogen (N–H) to the nitrile to give the corresponding imine. The formed imine can undergo a second reaction cycle and is finally reduced to the corresponding amine.

8.2.3 Heterogeneous metals-based catalysts

Reports on selective heterogeneous hydrogenation of nitriles to primary amines are less common, and high selectivity was reported with Raney nickel [89–91] or rhodium catalysts [92] while over supported palladium or platinum catalysts secondary amines are the main products [90, 91, 93].

Among the few examples of selective heterogeneous nitrile hydrogenation with palladium, supported Pd/C catalyst (**17**, Table 8.3) was reported to hydrogenate benzonitrile to benzylamine in high yield and selectivity (95%) under mild conditions of six bar H_2 and 30 ℃, however the high selectivity was gained by addition of two equiv. of NaH_2PO_4 (respectively to the nitrile) [94]. Supported Pd on alumina (**18**, Table 8.3) was reported to reduces benzonitrile to benzlyamine under 70 ℃ and 15 bar H_2 without additives [95]. High production rate of benzylamine with 100% selectivity was reported for gas phase hydrogenation of benzonitrile over Pd/Al_2O_3, while over Pd/C under the same conditions, toluene was obtained. The large difference in the selectivity was attributed to the partial positive charge on the Pd particles over carbon and the partial negative charge on the Pd particles over Al_2O_3, as was assigned by XPS analysis. The differences in the electron density on the metal, leads to a side-on activation of benzonitrile on Pd/Al_2O_3 and desorption of benzylamine as exclusive product, while Pd/C favors a perpendicular adsorption of benzonitrile through the nitrogen lone pair,

Table 8.3: Heterogeneous catalysts for the hydrogenation of benzonitrile to benzylamine.

Catalyst		Reaction conditions	Conversion (%)	Yield (%)
17[94]	10 % Pd/C (Selcat Q)	Catalyst loading 3 % (wt) 6 bar H_2, 30 ℃, 4.4 h Additives: NaH_2PO_4 (2 equiv. respectively to the nitrile)	100	95
18[95]	Pd/γ-Al_2O_3 or Pd/η-Al_2O_3	Catalyst loading 12.5% (wt) 15 bar H_2, 70 ℃, 4 h	100	90
19[96]	Pd/Al_2O_3	Catalyst loading 0.02% (wt) 2 bar H_2, 50 ℃, 4 h Additives: 70 bar CO_2, 5 ml H_2O	99.6	98.4
20[97]	([Co(OAc)$_2$/Phen@α-Al_2O_3]-800	Catalyst loading 4 mol% 5 bar H_2, 80 ℃, 2 h Additives: KO^{t}Bu (15 mol%) ammonia (aqueous solution, 0.1 mL)		98
21[98]	Zr$_{12}$-TPDC-Co	Catalyst loading 0.5 Co mol% 40 bar H_2, 110 ℃, 42 h	100	100
22[99]	B12@CeO$_2$-8	Catalyst loading 1.6 mol% 30 bar H_2, 120 ℃, 15 h Additives: ammonia (aqueous solution, 0.2 mL)	99	96

and under hydrogen gives imine, amine and toluene as the main product [100]. It was found that deactivation of Pd/Al$_2$O$_3$ catalysts take place due to the formation of carbonaceous compounds on the surface of the metal catalyst [101].

Arai and co-workers reported on the selective hydrogenation of benzonitrile to benzylamine by commercially available 5 wt% Pd/Al$_2$O$_3$ (**19**, Table 8.3), which was treated with H$_2$ and heated to 200 °C to give defined Pd particles. High selectivity was gained by using water and CO$_2$. The formed amine is transferred into the water phase, which prevented the primary amine from reacting with an intermediate of imine into the secondary amine in the organic phase (benzonitrile). Addition of CO$_2$ also increased the selectivity probably by its interaction with the primary amine [96].

Selective gas-phase hydrogenation of benzonitrile to benzylamine under atmospheric pressure of H$_2$ was reported for Cu–MgO. This reaction was performed in a continuous reactor. In this setup it was found that the conversion and selectivity are highly influenced by the residence time. Conversion of 98% with 70% selectivity toward the primary amine was obtained with a residence time of 4.44 s, while shorter residence time of 2.29 s resulted in 50–60% conversion and 100% selectivity [102].

Beller and co-workers reported on efficient heterogeneous cobalt catalyst supported on α-Al$_2$O$_3$ (**20**, Table 8.3). The catalyst hydrogenates selectively aliphatic and aromatic nitriles to primary amines in the presence of ammonia (25% aqueous solution, 0.1 mL), which is crucial for the selectivity. For example, benzonitrile was hydrogenated to benzyl amine in 98% yield under only five bar H$_2$ at 85 °C (Table 8.3). Heptanenitrile was hydrogenated to heptylamine in 99% yield under 40 bar H$_2$ at 135 °C [97]. Another example of heterogeneous catalytic hydrogenation of nitrile to primary amines based on Co was demonstrated by Lin *et al.* with a MOF (Metal–organic frameworks) based on triphenyldicarboxylic acid and [Zr$_{12}$(μ^3-O)$_8$(μ^3-OH)$_8$(μ^2-OH)$_6$] (**21**, Table 8.3). Metalation of the MOF with CoCl$_2$ and activation with NaBHEt$_3$ afforded the active catalyst, which hydrogenates benzonitrile to benzyl amine in 100% yield under 40 bar H$_2$ at 110 °C for 42 h. Recycle experiments showed quantitative formation of benzylamine also after eight runs with a Co loading of 1 mol% [98].

Vitamin B12 (cyanocobalamin) was used as a Co source for the formation of heterogeneous catalyst by its immobilization on ceria (**22**, Table 8.3), which was pyrolyzed under inert conditions to give a composite material with a carbonaceous cobalt phase and cobalt oxide nanoparticles. The active catalyst hydrogenates benzonitrile to benzylamine in 99% conversion and 96% yield under 30 bar H$_2$ at 120 °C for 15 h with 1.6 mol% of the catalyst. The high selectivity of the reaction was achieved by addition of aqueous NH$_3$. Hydrogenation of aliphatic nitriles was also demonstrated, and the catalyst exhibits similar yields up to five recycles [99].

8.3 Imine hydrogenation

Secondary imines are common by-products in the hydrogenation of nitriles (**III**, Figure 8.1) and their hydrogenation leads to the secondary amines. Thus, imine/amine couples can also be considered as optional liquid organic hydrogen carriers (LOHCs), however with a lower hydrogen storage capacity (HSC) as compared to nitrile/amine couples.

Catalytic imine hydrogenation with molecular hydrogen is well known with many metal-based catalysts [103, 104] such as Mo and W [105], Ti [106], Zn [107, 108], Zr [109], lanthanides [110], Fe [111–114], Ni [115], Pd [116–118], Ru [119–123], Co [124], Rh [125–127] and Ir, the latter is the most efficient metal-based catalysts for asymmetric nitrile hydrogenation [103, 128–137]. Alkaline Earth metal catalysts were also found to efficiently hydrogenate imines to amine [138], such as LiAlH$_4$ [139]. Imines can be hydrogenated catalytically also by metal-free frustrated Lewis pairs (FLPs), usually under milder conditions as compared to transition metal catalysts, at temperatures between 80 and 120 °C and H$_2$ pressures of 1–5 bar [140–145]. Although the FLPs are efficient catalysts in imine hydrogenation, their reactivity is limited to sterically demanding substituents on N, since reduction of a less hindered imine affords an amine that binds tightly to the borane center of the phosphino–borane, precluding further H$_2$ activation. Bulky imines, which do not form an adduct with B(C$_6$F$_5$)$_3$ can act as the basic pair of the Lewis acid, and cleave H$_2$, which leads to the hydrogenation of the imine to amine. Thus, the Lewis acid B(C$_6$F$_5$)$_3$ and its derivatives act as catalysts for imines hydrogenation, and were reported to hydrogenate aldimines and ketimines catalytically under mild conditions of 5–15 bar of H$_2$ at 120 °C with 5–10 mol% catalyst [146–148]. Mechanistic studies conducted by Stephan and co-workers [146] and supported by DFT calculations [149], showed that the first step involves heterolytic H$_2$ splitting by the imine/borane FLP to generate an iminium hydridoborate ion pair (**23**, Figure 8.6). The ion pair **23** rearranges to an amine-borane adduct (**24**), and dissociation of the B−N
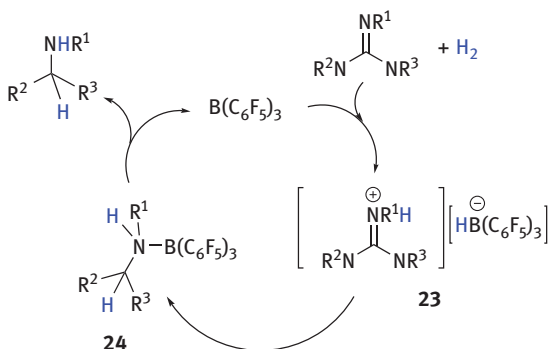
Figure 8.6: Postulated catalytic hydrogenation of imines by Lewis acid [146].

bond releases the amine and regenerates the free borane as the active catalyst. The latter step of amine dissociation is assumed to be rate-determining [146].

Diimines are good candidates as LOHCs with a higher value of HSC as compared to mono-imines. While hydrogenation of vicinal diimines by metal-based catalysts is rare, probably due to the bulky steric hindrance and the possibility of the diamine product to coordinate as a chalet ligand to the metal and detriment its reactivity, $B(C_6F_5)$ was reported as an efficient catalyst for the hydrogenation of diiamines under mild conditions (Figure 8.7) [150, 151].

ArHNNHAr   ← 5 - 10 mo% $B(C_6F_5)_3$ ArNNAr   → 5 mo% $B(C_6F_5)_3$ ArHNNHAr

Ph   Ph   20 bar H_2, 20 °C, 0.5 - 4 hrs   R   R   4 bar H_2, 120 °C, 24 hrs

R = Ph,   R = H,
Ar = C_6H_5X (X = F, Br, Me, OMe)   Ar = $C_6H_2Me_3$, $C_6H_3{}^iPr_2$
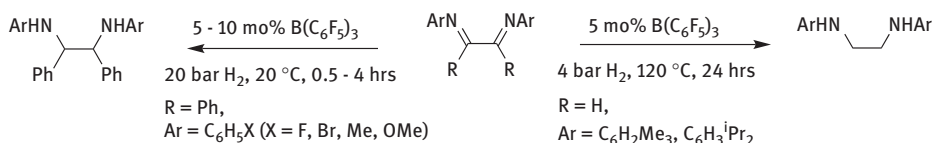
Figure 8.7: Catalytic hydrogenation of diimines by $B(C_6F_5)_3$ [150, 151].

It is important to note that FLPs are able to hydrogenate also protected nitriles such as $RC{\equiv}N(BC_6F_5)_3$ (R = Me, Ph) to give the corresponding primary amine–borane adducts, while unprotected nitriles intervene in the catalytic cycle by binding strongly to the borane center of the catalyst [144].

8.4 Conclusions

Nitrile/amine couples are promising liquid organic hydrogen carriers (LOHCs) with two equiv. of H_2 stored/released in the carbon-nitrogen bond. In the past, nitrile hydrogenation was obtained under harsh conditions of high temperatures and H_2 pressure with excess of basic additives or ammonia for selectivity control, using precious metals as catalysts. Recent examples of highly selective hydrogenation of nitriles under mild conditions, free of additives, with earth-abundant metals both homogeneously and heterogeneously catalysts systems, demonstrated the high potential of nitrile/amine couples as hydrogen carriers.

Imine/amine couples can also be considered as LOHCs. Although only one equiv. of H_2 is stored/released in the carbon-nitrogen bond, secondary imines are reduced more selectively and under milder conditions as compared to nitriles, with vast range of metal catalysts, earth-abundant metal and non-metal catalysts.

References

[1] Müller TE, Hultzsch KC, Yus M, Foubelo F, Tada M. Hydroamination: direct addition of amines to alkenes and alkynes. Chem Rev. 2008;108:3795–892

[2] Weissermel K, Arpe H-J. Industrial organic chemistry. Weinheim, Germany: 2003 WILEY-VCH Verlag GmbH & Co. KGaA, 2008.

[3] Hartwig JF. Palladium-catalyzed amination of aryl halides and related reactions. In: Negishi Ei-ichi, editor(s). Handbook of organopalladium chemistry for organic synthesis. John Wiley & Sons, Inc, 2003:1051–1096.

[4] Martin Stephen F. Recent applications of imines as key intermediates in the synthesis of alkaloids and novel nitrogen heterocycles. Pure Appl Chem. 2009;81:195

[5] Bagal DB, Bhanage BM. Recent advances in transition metal-catalyzed hydrogenation of nitriles. Adv Synth Catal. 2015;357:883–900.

[6] De Bellefon C, Fouilloux P. Homogeneous and heterogeneous hydrogenation of nitriles in a liquid phase: chemical, mechanistic, and catalytic aspects. Catalysis Rev. 1994; 36:459–506.

[7] Werkmeister S, Junge K, Beller M. Catalytic hydrogenation of carboxylic acid esters, amides, and nitriles with homogeneous catalysts. Org Process Res Dev. 2014;18:289–302.

[8] Das S, Zhou S, Addis D, Enthaler S, Junge K, Beller M. Selective catalytic reductions of amides and nitriles to amines. Top Catalysis. 2010;53:979–84

[9] Gomez S, Peters JA, Maschmeyer T. The reductive amination of aldehydes and ketones and the hydrogenation of nitriles: mechanistic aspects and selectivity control. Adv Synth Catal. 2002;344:1037–57.

[10] Bohnet M, Ullmann F. Ullmann's encyclopedia of industrial chemistry. Encyclopedia of industrial chemistry. Place of publication not identified: Wiley VCH, 2003.

[11] Wittcoff H. Industrial organic chemicals, 3rd ed. Reuben BG, Plotkin JS editors. Hoboken, N.J.: Wiley, 2013.

[12] Ricci A. Modern amination methods. Ricci A, editor. Weinheim; Cambridge: Wiley-VCH, 2000.

[13] Fleming I, Trost BM. Comprehensive organic synthesis: selectivity, strategy & efficiency in modern organic chemistry. 1st ed. Oxford: Pergamon Press, 1991.

[14] Amundsen LH, Nelson LS. Reduction of nitriles to primary amines with lithium aluminum hydride1. J Am Chem Soc. 1951;73:242–4.

[15] Liu S, Yang Y, Zhen X, He H, Feng J, Whiting A. Enhanced reduction of C-N multiple bonds using sodium borohydride and an amorphous nickel catalyst. Org Biomol Chem. 2012; 10:663–70

[16] Abdel-Magid AF C. American Chemical Society, Division of Organic, I. American Chemical Society, Meeting: Chicago. Reductions in organic synthesis: recent advances and practical applications, Vol. 641. Advances in Chemistry. Washington, DC: American Chemical Society, 1996.

[17] Laval S, Dayoub W, Favre-Reguillon A, Berthod M, Demonchaux P, Mignani G et al. A mild and efficient method for the reduction of nitriles. Tetrahedron Lett. 2009;50:7005–7

[18] Cabrita I, Fernandes AC. A novel efficient and chemoselective method for the reduction of nitriles using the system silane/oxo-rhenium complexes. Tetrahedron. 2011;67:8183–6.

[19] Gandhamsetty N, Park J, Jeong J, Park S-W, Park S, Chang S. Chemoselective silylative reduction of conjugated nitriles under metal-free catalytic conditions: β-silyl amines and enamines. Angew. Chem. Int Ed. 2015;54:6832–6

[20] Hamdaoui M, Desrousseaux C, Habbita H, Djukic J-P. Iridacycles as catalysts for the autotandem conversion of nitriles into amines by hydrosilylation: experimental investigation and scope. Organometallics. 2017;36:4864–82

[21] Murai T, Sakane T, Kato S. Cobalt carbonyl catalyzed reduction of aromatic nitriles with a hydrosilane leading to N,N-disilylamines. Tetrahedron Lett. 1985;26:5145–8.

[22] Haddenham D, Pasumansky L, DeSoto J, Eagon S, Singaram B. Reductions of aliphatic and aromatic nitriles to primary amines with diisopropylaminoborane. J Org Chem. 2009;74:1964–70

[23] Nakamura G, Nakajima Y, Matsumoto K, Srinivas V, Shimada S. Nitrile hydroboration reactions catalysed by simple nickel salts, bis(acetylacetonato)nickel(ii) and its derivatives. Catalysis Sci Technol. 2017;7:3196–9

[24] Kaithal A, Chatterjee B, Gunanathan C. Ruthenium-catalyzed selective hydroboration of nitriles and imines. J Org Chem. 2016;81:11153–61.

[25] Geri JB, Szymczak NK. A proton-switchable bifunctional ruthenium complex that catalyzes nitrile hydroboration. J Am Chem Soc. 2015;137:12808–14.

[26] Lu Z, Williams TJ. A dual site catalyst for mild, selective nitrile reduction. Chem Commun. 2014;50:5391–3.

[27] Khalimon AY, Farha PM, Nikonov GI. Imido-hydrido complexes of Mo(iv): catalysis and mechanistic aspects of hydroboration reactions. Dalton Trans. 2015;44:18945–56.

[28] Weetman C, Anker MD, Arrowsmith M, Hill MS, Kociok-Kohn G, Liptrot DJ et al. Magnesium-catalysed nitrile hydroboration. Chem Sci. 2016;7:628–41

[29] Ball M., Weeda M. The hydrogen economy – vision or reality?. International Journal of Hydrogen Energy. 2015;40(25):7903–19.

[30] Singh S, Jain S, Ps V, Jain AK, Nouni MR, Pandey JK et al. Hydrogen: a sustainable fuel for future of the transport sector. Renew Sustainable Energy Rev. 2015;51:623–33

[31] Armaroli N. Energy for a sustainable world from the oil age to a sun-powered future, 2nd ed. Balzani V editor. Weinheim, Germany: Wiley-VCH, 2011.

[32] Satyapal S, Petrovic J, Read C, Thomas G, Ordaz G. The U.S. department of energy's national hydrogen storage project: progress towards meeting hydrogen-powered vehicle requirements. Catalysis Today. 2007;120:246–56

[33] Dalebrook AF, Gan W, Grasemann M, Moret S, Laurenczy G. Hydrogen storage: beyond conventional methods. Chem Commun. 2013;49:8735–51

[34] Preuster P, Papp C, Wasserscheid P. Liquid organic hydrogen carriers (LOHCs): toward a hydrogen-free hydrogen economy. Acc Chem Res. 2017;50:74–85.

[35] Teichmann D, Stark K, Muller K, Zottl G, Wasserscheid, P, Arlt W. Energy storage in residential and commercial buildings via liquid organic hydrogen carriers (LOHC). Energy & Environmental Science. 2012;5:9044–54

[36] Teichmann D, Arlt W, Wasserscheid P, Freymann R. A future energy supply based on liquid organic hydrogen carriers (LOHC). Energy & Environmental Science. 2011;4:2767–73

[37] Kariya N, Fukuoka A, Ichikawa M. Efficient evolution of hydrogen from liquid cycloalkanes over Pt-containing catalysts supported on active carbons under "wet–dry multiphase conditions". Appl Catalysis A: Gen. 2002;233:91–102.

[38] Hodoshima S, Takaiwa S, Shono A, Satoh K, Saito Y. Hydrogen storage by decalin/naphthalene pair and hydrogen supply to fuel cells by use of superheated liquid-film-type catalysis. Appl Catalysis A: Gen. 2005;283:235–42

[39] Biniwale RB, Rayalu S, Devotta S, Ichikawa M. Chemical hydrides: a solution to high capacity hydrogen storage and supply. Int J Hydrogen Energy. 2008;33:360–5

[40] Crabtree RH. Hydrogen storage in liquid organic heterocycles. Energy & Environmental Science. 2008;1:134–8.

[41] Wechsler D, Cui Y, Dean D, Davis B, Davis PG. Production of H2 from combined endothermic and exothermic hydrogen carriers. J Am Chem Soc. 2008;130:17195–203

[42] Cui Y, Kwok S, Bucholtz A, Davis B, Whitney RA, Jessop PG. The effect of substitution on the utility of piperidines and octahydroindoles for reversible hydrogen storage. New J Chem. 2008;32:1027–37

[43] Wechsler D, Davis B, Jessop PG. The dehydrogenation of combined organic and inorganic hydrogen-storage carriers. Can J Chem. 2010;88:548–55.

[44] Fujita K, Wada T, Shiraishi T. Reversible interconversion between 2,5-dimethylpyrazine and 2, 5-dimethylpiperazine by iridium-catalyzed hydrogenation/dehydrogenation for efficient hydrogen storage. Angew. Chem. Int Ed. 2017;56:10886–9.

[45] Fujita K-I, Tanaka Y, Kobayashi M, Yamaguchi R. Homogeneous perdehydrogenation and perhydrogenation of fused bicyclic N-heterocycles catalyzed by iridium complexes bearing a functional bipyridonate ligand. J Am Chem Soc. 2014;136:4829–32

[46] Forberg D, Schwob T, Zaheer M, Friedrich M, Miyajima N, Kempe R. Single-catalyst high-weight% hydrogen storage in an N-heterocycle synthesized from lignin hydrogenolysis products and ammonia. Nat Commun. 2016;7:13201

[47] Hu P, Fogler E, Diskin-Posner Y, Iron MA, Milstein D. A novel liquid organic hydrogen carrier system based on catalytic peptide formation and hydrogenation. Nat Commun. 2015;6:6859

[48] Amende M, Gleichweit C, Werner K, Schernich S, Zhao W, Lorenz MPA et al. Model catalytic studies of liquid organic hydrogen carriers: dehydrogenation and decomposition mechanisms of dodecahydro-n-ethylcarbazole on Pt(111). ACS Catal. 2014;4:657–65

[49] Sobota M, Nikiforidis I, Amende M, Zanón BS, Staudt T, Höfert O et al. Dehydrogenation of dodecahydro-N-ethylcarbazole on Pd/Al2O3 model catalysts. Chem – Eur J. 2011;17:11542–52

[50] DOI: https://doi.org/10.1515/psr-2017-0029.

[51] Beatty RP, Paciello RA. WO 96/23802–23804, 1996.

[52] Heinzman SW, Ganem B. Mechanism of sodium borohydride-cobaltous chloride reductions. J Am Chem Soc. 1982;104:6801–2.

[53] Rode CV, Arai M, Shirai M, Nishiyama Y. Gas-phase hydrogenation of nitriles by nickel on various supports. Appl Catalysis A: Gen. 1997;148:405–13

[54] Caddick S, de K. Haynes AK, Judd DB, Judd MRV. Convenient synthesis of protected primary amines from nitriles. Tetrahedron Lett. 2000;41:3513–6

[55] Klenke B, Gilbert IH. Nitrile reduction in the presence of boc-protected amino groups by catalytic hydrogenation over palladium-activated raney-nickel. J Org Chem. 2001;66:2480–3.

[56] López-De Jesús YM, Johnson CE, Monnier JR, Williams CT. Selective hydrogenation of benzonitrile by alumina-supported Ir–pd catalysts. Top Catalysis. 2010;53:1132–7

[57] Levering DR. U.S. Patent 3,152,184, 1964 (assigned to Hercules Power Co.).

[58] Dewhirst KC. U.S. Patent 3,454,644, 1969 (assigned to Shell Oil Co.).

[59] Yoshida T, Okano T, Otsuka S. Catalytic hydrogenation of nitriles and dehydrogenation of amines with the rhodium(I) hydrido compounds [RhH(PPri3)3] and [Rh2H2([small micro]-N2) {P(cyclohexyl)3}4]. J Chem Society, Chem Commus. 1979;19:870–1.

[60] Kukula P, Studer M, Blaser H-U. Chemoselective hydrogenation of α,β-unsaturated nitriles. Adv Synth Catal. 2004;346:1487–93.

[61] Takemoto S, Kawamura H, Yamada Y, Okada T, Ono A, Yoshikawa E et al. Ruthenium complexes containing bis(diarylamido)/thioether ligands: synthesis and their catalysis for the hydroge-nation of benzonitrile. Organometallics. 2002;21:3897–904

[62] Li T, Bergner I, Haque FN, Zimmer-De Iuliis M, Song D, Morris RH. Hydrogenation of benzonitrile to benzylamine catalyzed by ruthenium hydride complexes with P–NH–NH–P tetradentate ligands: evidence for a hydridic–protonic outer sphere mechanism. Organometallics. 2007;26:5940–9

[63] Reguillo R, Grellier M, Vautravers N, Vendier L, Sabo-Etienne S. Ruthenium-catalyzed hydro-genation of nitriles: insights into the mechanism. J Am Chem Soc. 2010;132:7854–5

[64] Gunanathan C, Hölscher M, Leitner W. Reduction of nitriles to amines with H2 catalyzed by nonclassical ruthenium hydrides – water-promoted selectivity for primary amines and mechanistic investigations. Eur J Inorg Chem. 2011;2011:3381–6.

[65] Adam R, Bheeter CB, Jackstell R, Beller M. A mild and base-free protocol for the ruthenium-catalyzed hydrogenation of aliphatic and aromatic nitriles with tridentate phosphine ligands. Chem Cat Chem. 2016;8:1329–34

[66] Neumann J, Bornschein C, Jiao H, Junge K, Beller M. Hydrogenation of aliphatic and aromatic nitriles using a defined ruthenium PNP pincer catalyst. European J Org Chem. 2015;2015:5944–8

[67] Choi J-H, Prechtl MH. Tuneable hydrogenation of nitriles into imines or amines with a ruthenium pincer complex under mild conditions. Chem Cat Chem. 2015;7:1023–8.

[68] Enthaler S, Junge K, Addis D, Erre G, Beller M. A practical and benign synthesis of primary amines through ruthenium-catalyzed reduction of nitriles. Chem Sus Chem. 2008;1:1006–10

[69] Enthaler S, Addis D, Junge K, Erre G, Beller M. A general and environmentally benign catalytic reduction of nitriles to primary amines. Chem – Eur J. 2008;14:9491–4

[70] Addis D, Enthaler S, Junge K, Wendt B, Beller M. Ruthenium N-heterocyclic carbene catalysts for selective reduction of nitriles to primary amines. Tetrahedron Lett. 2009;50:3654–6

[71] Toti A, Frediani P, Salvini A, Rosi L, Giolli C, Giannelli C. Activation of single and multiple C–N bonds by Ru(II) catalysts in homogeneous phase. Comptes Rendus Chimie. 2004;7:769–78

[72] Albrecht M, Bedford R, Plietker B. Catalytic and organometallic chemistry of earth-abundant metals. Organometallics. 2014;33:5619–21.

[73] Bullock RM. Abundant metals give precious hydrogenation performance. Science. 2013;342:1054–5.

[74] Bullock RM. Catalysis without precious metals. Bullock RM, editor. Weinheim: Wiley-VCH, 2010.

[75] Friedfeld MR, Shevlin M, Hoyt JM, Krska SW, Tudge MT, Chirik PJ. Cobalt precursors for high-throughput discovery of base metal asymmetric alkene hydrogenation catalysts. Science. 2013;342:1076–80

[76] Greenhalgh MD, Thomas SP. Chemo-, regio-, and stereoselective iron-catalysed hydroboration of alkenes and alkynes. Chem Commun. 2013;49:11230–2.

[77] Chen C, Hecht MB, Kavara A, Brennessel WW, Mercado BQ, Weix DJ et al. Rapid, regioconvergent, solvent-free alkene hydrosilylation with a cobalt catalyst. J Am Chem Soc. 2015;137:13244–7

[78] Léonard NG, Bezdek MJ, Chirik PJ. Cobalt-catalyzed C(sp2)–H borylation with an air-stable, readily prepared terpyridine cobalt(II) Bis(acetate) precatalyst. Organometallics. 2017;36:142–50.

[79] Obligacion JV, Bezdek MJ, Chirik PJ. C(sp2)–H borylation of fluorinated arenes using an air-stable cobalt precatalyst: electronically enhanced site selectivity enables synthetic opportunities. J Am Chem Soc. 2017;139:2825–32.

[80] Docherty JH, Peng J, Dominey AP, Thomas SP. Activation and discovery of earth-abundant metal catalysts using sodium tert-butoxide. Nat Chem. 2017;9:595

[81] Cheng B, Lu P, Zhang H, Cheng X, Lu Z. Highly enantioselective cobalt-catalyzed hydrosilylation of alkenes. J Am Chem Soc. 2017;139:9439–42

[82] Mukherjee A, Srimani D, Chakraborty S, Ben-David Y, Milstein D. Selective hydrogenation of nitriles to primary amines catalyzed by a cobalt pincer complex. J Am Chem Soc. 2015;137:8888–91

[83] Tokmic K, Jackson BJ, Salazar A, Woods TJ, Fout AR. Cobalt-catalyzed and lewis acid-assisted nitrile hydrogenation to primary amines: a combined effort. J Am Chem Soc. 2017;139:13554–61

[84] Adam R, Bheeter CB, Cabrero-Antonino JR, Junge K, Jackstell R, Beller M. Selective hydrogenation of nitriles to primary amines by using a cobalt phosphine catalyst. Chem Sus Chem. 2017;10:842–6

[85] Bornschein C, Werkmeister S, Wendt B, Jiao H, Alberico E, Baumann W et al. Mild and selective hydrogenation of aromatic and aliphatic (di)nitriles with a well-defined iron pincer complex. Nat Commun. 2014;5:4111

[86] Lange S, Elangovan S, Cordes C, Spannenberg A, Jiao H, Junge H et al. Selective catalytic hydrogenation of nitriles to primary amines using iron pincer complexes. Catalysis Sci Technol. 2016;6:4768–72

[87] Chakraborty S, Leitus G, Milstein D. Selective hydrogenation of nitriles to primary amines catalyzed by a novel iron complex. Chem Commun. 2016;52:1812–5.

[88] Elangovan S, Topf C, Fischer S, Jiao H, Spannenberg A, Baumann W et al. Selective catalytic hydrogenations of nitriles, ketones, and aldehydes by well-defined manganese pincer complexes. J Am Chem Soc. 2016;138:8809–14

[89] Huber W. Hydrogenation of basic nitriles with Raney Nickel. J Am Chem Soc. 1944;66:876–9.

[90] Greenfield H. Catalytic hydrogenation of butyronitrile. I&EC Prod Res Dev. 1967;6:142–4.

[91] Bawane SP, Sawant SB. Reaction kinetics of the liquid-phase hydrogenation of benzonitrile to benzylamine using Raney nickel catalyst. Chem Eng J. 2004;103:13–9.

[92] Freifelder M. A low pressure process for the reduction of nitriles. Use of rhodium catalyst. J Am Chem Soc. 1960;82:2386–9.

[93] Rylander PN. 12 - nitriles, in catalytic hydrogenation over platinum metals. Academic Press, 1967:203–26.

[94] Hegedűs L, Máthé T. Selective heterogeneous catalytic hydrogenation of nitriles to primary amines in liquid phase: part I. Hydrogenation of benzonitrile over palladium. Appl Catalysis A: Gen. 2005;296:209–15.

[95] Dai C, Li Y, Ning C, Zhang W, Wang X, Zhang C. The influence of alumina phases on the performance of Pd/Al2O3 catalyst in selective hydrogenation of benzonitrile to benzylamine. Appl Catalysis A: Gen. 2017;545:97–103

[96] Yoshida H, Wang Y, Narisawa S, Fujita S-I, Liu R, Arai M. A multiphase reaction medium including pressurized carbon dioxide and water for selective hydrogenation of benzonitrile with a Pd/Al2O3 catalyst. Appl Catalysis A: Gen. 2013;456:215–22

[97] Chen F, Topf C, Radnik J, Kreyenschulte C, Lund H, Schneider M et al. Stable and inert cobalt catalysts for highly selective and practical hydrogenation of C≡N and C=O bonds. J Am Chem Soc. 2016;138:8781–8

[98] Ji P, Manna K, Lin Z, Feng X, Urban A, Song Y et al. Single-site cobalt catalysts at new Zr12(μ3-O)8(μ3-OH)8(μ2-OH)6 metal–organic framework nodes for highly active hydrogenation of nitroarenes, nitriles, and isocyanides. J Am Chem Soc. 2017;139:7004–11

[99] Ferraccioli R, Borovika D, Surkus A-E, Kreyenschulte C, Topf C, Beller M. Synthesis of cobalt nanoparticles by pyrolysis of vitamin B12: a non-noble-metal catalyst for efficient hydrogenation of nitriles. Catalysis Sci Technol. 2018;8:499–507

[100] Hao Y, Li M, Cárdenas-Lizana F, Keane MA. Selective production of benzylamine via gas phase hydrogenation of benzonitrile over supported Pd catalysts. Catal Letters. 2016; 146:109–16

[101] Dai C, Liu F, Zhang W, Li Y, Ning C, Wang X et al. Deactivation study of Pd/Al2O3 catalyst for hydrogenation of benzonitrile in fixed-bed reactor. Appl Catalysis A: Gen. 2017; 538:199–206

[102] Marella RK, Koppadi KS, Jyothi Y, Rama Rao KS, Burri DR. Selective gas-phase hydrogenation of benzonitrile into benzylamine over Cu-MgO catalysts without any additives. New J Chem. 2013;37:3229–35

[103] Xie J-H, Zhu S-F, Zhou Q-L. Transition metal-catalyzed enantioselective hydrogenation of enamines and imines. Chem Rev. 2011;111:1713–60.

[104] Zhang Z, Butt NA, Zhang W. Asymmetric hydrogenation of nonaromatic cyclic substrates. Chem Rev. 2016;116:14769–827.

[105] Chakraborty S, Blacque O, Fox T, Berke H. Highly active, low-valence molybdenum- and tungsten-amide catalysts for bifunctional imine-hydrogenation reactions. Chem – Asian J. 2014;9:328–37

[106] Willoughby CA, Buchwald SL. Catalytic asymmetric hydrogenation of imines with a chiral titanocene catalyst: kinetic and mechanistic investigations. J Am Chem Soc. 1994;116:11703–14.

[107] Jochmann P, Stephan DW. H₂cleavage, hydride formation, and catalytic hydrogenation of imines with zinc complexes of C5Me5 and N-heterocyclic carbenes. Angew. Chem. Int Ed. 2013;52:9831–5.

[108] Werkmeister S, Fleischer S, Zhou S, Junge K, Beller M. Development of new hydrogenations of imines and benign reductive hydroaminations: zinc triflate as a catalyst. Chem Sus Chem. 2012;5:777–82

[109] Flynn SR, Metters OJ, Manners I, Wass DF. Zirconium-catalyzed imine hydrogenation via a frustrated Lewis pair mechanism. Organometallics. 2016;35:847–50

[110] Obora Y, Ohta T, Stern CL, Marks TJ. Organolanthanide-catalyzed imine hydrogenation. scope, selectivity, mechanistic observations, and unusual byproducts. J Am Chem Soc. 1997;119:3745–55

[111] Lagaditis PO, Sues PE, Sonnenberg JF, Wan KY, Lough AJ, Morris RH. Iron(II) complexes containing unsymmetrical P–N–P′ pincer ligands for the catalytic asymmetric hydrogenation of ketones and imines. J Am Chem Soc. 2014;136:1367–80

[112] Zhou S, Fleischer S, Junge K, Beller M. Cooperative transition-metal and chiral brønsted acid catalysis: enantioselective hydrogenation of imines to form amines. Angew. Chem. Int Ed. 2011;50:5120–4

[113] Morris RH. Mechanisms of the H2- and transfer hydrogenation of polar bonds catalyzed by iron group hydrides. Dalton Trans. 2018;47:10809–26.

[114] Brenna D, Rossi S, Cozzi F, Benaglia M. Iron catalyzed diastereoselective hydrogenation of chiral imines. Org Biomol Chem. 2017;15:5685–8

[115] Iglesias AL, García JJ. Homogeneous hydrogenation of fluoroaromatic imines with Ni compounds, evidence for η2-CN intermediate in the catalytic cycle. J Mol Catalysis A: Chem. 2009;298:51–9.

[116] Chen Q-A, Ye Z-S, Duan Y, Zhou Y-G. Homogeneous palladium-catalyzed asymmetric hydrogenation. Chem Soc Rev. 2013;42:497–511

[117] Wang Y-Q, Lu S-M, Zhou Y-G. Highly enantioselective Pd-catalyzed asymmetric hydrogenation of activated imines. J Org Chem. 2007;72:3729–34.

[118] Qin Y, Shang G, Gao W, Deng J, Zhang X. A highly enantioselective, Pd–tangphos-catalyzed hydrogenation of N-tosylimines. Angew. Chem. Int Ed. 2006;45:3832–5

[119] Clapham SE, Hadzovic A, Morris RH. Mechanisms of the H2-hydrogenation and transfer hydrogenation of polar bonds catalyzed by ruthenium hydride complexes. Coord Chem Rev. 2004;248:2201–37.

[120] Cobley CJ, Henschke JP. Enantioselective hydrogenation of imines using a diverse library of ruthenium dichloride(diphosphine)(diamine) precatalysts. Adv Synth Catal. 2003;345:195–201.

[121] Vaquero M, Suárez A, Vargas S, Bottari G, Álvarez E, Pizzano A. Highly enantioselective imine hydrogenation catalyzed by ruthenium phosphane–phosphite diamine complexes. Chem – Eur J. 2012;18:15586–91

[122] De Julián E, Menéndez-Pedregal E, Claros M, Vaquero M, Díez J, Lastra E et al. Practical synthesis of enantiopure benzylamines by catalytic hydrogenation or transfer hydrogenation reactions in isopropanol using a Ru-pybox catalyst. Org Chem Front. 2018;5:841–9

[123] Hernández-Juárez M, López-Serrano J, Lara P, Morales-Cerón JP, Vaquero M, Álvarez E et al. Ruthenium(II) complexes containing lutidine-derived pincer CNC ligands: synthesis, structure, and catalytic hydrogenation of CN bonds. Chem Eur J. 2015;21:7540–55

[124] Amézquita-Valencia M, Cabrera A. The first example of asymmetric hydrogenation of imines with Co2(CO)8/(R)-BINAP as catalytic precursor. J Mol Catalysis A: Chem. 2013;366:17–21.

[125] Etayo P, Vidal-Ferran A. Rhodium-catalysed asymmetric hydrogenation as a valuable synthetic tool for the preparation of chiral drugs. Chem Soc Rev. 2013;42:728–54.

[126] Gao S, Qin Y, Xumu Z. Rh-catalyzed asymmetric hydrogenation of α-aryl imino esters: an efficient enantioselective synthesis of aryl glycine derivatives. Angew. Chem. Int Ed. 2006;45:6360–2.

[127] Burk MJ, Feaster JE. Enantioselective hydrogenation of the C:N group: a catalytic asymmetric reductive amination procedure. J Am Chem Soc. 1992;114:6266–7.

[128] Hopmann KH, Bayer A. Enantioselective imine hydrogenation with iridium-catalysts: reactions, mechanisms and stereocontrol. Coord Chem Rev. 2014;268:59–82.

[129] Salomó E, Rojo P, Hernández-Lladó P, Riera A, Verdaguer X. P-stereogenic and non-P-Stereogenic Ir–maxPHOX in the asymmetric hydrogenation of N-aryl imines. isolation and x-ray analysis of imine iridacycles. J Org Chem. 2018;83:4618–27

[130] Nicolas F-B, de la Fuente V, Castillón S, Claver C. Highlights of transition metal-catalyzed asymmetric hydrogenation of imines. Chem Cat Chem. 2010;2:1346–71

[131] Christian M, Carsten B. Diphenylphosphanylsulfoximines as ligands in iridium-catalyzed asymmetric imine hydrogenations. Angew. Chem. Int Ed. 2005;44:7564–7.

[132] Trifonova A, Diesen JS, Chapman CJ, Andersson PG. Application of phosphine–oxazoline ligands in ir-catalyzed asymmetric hydrogenation of acyclic aromatic N-arylimines. Org Lett. 2004;6:3825–7

[133] Tutkowski B, Kerdphon S, Limé E, Helquist P, Andersson PG, Wiest O et al. Revisiting the stereodetermining step in enantioselective iridium-catalyzed imine hydrogenation. ACS Catal. 2018;8:615–23

[134] Balakrishna B, Bauzá A, Frontera A, Vidal-Ferran A. Asymmetric hydrogenation of seven-membered C=N-containing heterocycles and rationalization of the enantioselectivity. Chem – Eur J. 2016;22:10607–13

[135] Zhang Y, Kong D, Wang R, Hou G. Synthesis of chiral cyclic amines via Ir-catalyzed enantiose-lective hydrogenation of cyclic imines. Org Biomol Chem. 2017;15:3006–12

[136] Hou G, Tao R, Sun Y, Zhang X, Gosselin F. Iridium–monodentate phosphoramidite-catalyzed asymmetric hydrogenation of substituted benzophenone N–H imines. J Am Chem Soc. 2010;132:2124–5

[137] Tang W, Xiao J. Asymmetric hydrogenation of imines via metal–organo cooperative catalysis. Synthesis. 2014;46:1297–302.

[138] Bauer H, Alonso M, Färber C, Elsen H, Pahl J, Causero A et al. Imine hydrogenation with simple alkaline earth metal catalysts. Nat Catalysis. 2018;1:40–7

[139] Holger E, Färber C, Ballmann G, Harder S. LiAlH4: from stoichiometric reduction to imine hydrogenation catalysis. Angew. Chem. Int Ed. 2018;57:7156–60

[140] Stephan DW. "Frustrated Lewis pairs": a concept for new reactivity and catalysis. Org Biomol Chem. 2008;6:1535–9.

[141] Farrell JM, Hatnean JA, Stephan DW. Activation of hydrogen and hydrogenation catalysis by a borenium cation. J Am Chem Soc. 2012;134:15728–31.

[142] Stephan DW. Frustrated Lewis Pairs: from concept to catalysis. Acc Chem Res. 2015;48:306–16.

[143] Stephan DW, Erker G. Frustrated Lewis Pair chemistry: development and perspectives. Angew. Chem. Int Ed. 2015;54:6400–41.

[144] Chase PA, Welch GC, Jurca T, Stephan DW. Metal-free catalytic hydrogenation. Angew. Chem. Int Ed. 2007;46:8050–3

[145] Paradies J. Frustrated Lewis Pair catalyzed hydrogenations. Synlett. 2013;24:777–80.

[146] Chase PA, Jurca T, Stephan DW. Lewis acid-catalyzed hydrogenation: B(C6F5)3-mediated reduction of imines and nitriles with H2. Chem Commun. 2008;14:1701–3.

[147] Jiang C, Blacque O, Berke H. Metal-free hydrogen activation and hydrogenation of imines by 1,8-bis(dipentafluorophenylboryl)naphthalene. Chem Commun. 2009;37:5518–20.

[148] Chen D, Klankermayer J. Metal-free catalytic hydrogenation of imines with tris(perfluorophenyl) borane. Chem Commun. 2008;18:2130–1.

[149] Rokob TA, Hamza A, Stirling A, Pápai I. On the mechanism of B(C6F5)3-catalyzed direct hydrogenation of imines: inherent and thermally induced frustration. J Am Chem Soc. 2009;131:2029–36

[150] Stephan DW, Greenberg S, Graham TW, Chase P, Hastie JJ, Geier SJ et al. Metal-free catalytic hydrogenation of polar substrates by frustrated Lewis Pairs. Inorg Chem. 2011;50:12338–48

[151] Zhu X, Du H. A highly stereoselective metal-free hydrogenation of diimines for the synthesis of cis-vicinal diamines. Org Lett. 2015;17:3106–9.

Daniël L. J. Broere

9 Transition metal-catalyzed dehydrogenation of amines

Abstract: This review focuses on the use of homogeneous transition metal complexes for the catalytic dehydrogenation of amines for synthetic purposes, and for hydrogen storage applications. The catalytic dehydrogenation of primary, secondary and cyclic amines is reviewed looking at reaction conditions, different catalysts and common side reactions. Recent developments in this active field of research showcase how cooperative ligands and photocatalysts can overcome the need for noble metals or harsh reaction conditions.

Keywords: amine dehydrogenation, LOHCs, hydrogen storage, ligand cooperativity, photocatalysis

9.1 Introduction

Unsaturated moieties containing carbon-nitrogen multiple bonds, e. g. imines, nitriles or pyridines play key roles in pharmaceutically active compounds [1], dyes [2], (organo)catalysts [3] or as reactive intermediates for synthetic applications [4]. As a result, a plethora of synthetic methods have been developed to convert readily accessible amines into more oxidized molecules [5]. Although many of these methods are robust and well developed, they often require the use of stoichiometric or excess reagents that are highly toxic, poorly compatible with functional groups or create waste byproducts [6]. An alternative strategy involves the use of transition metal complexes for the homogenous catalytic dehydrogenation of amines to imines or nitriles with hydrogen (H_2) gas as the sole side product (Figure 9.1) [7]. This more atom economical approach avoids hazardous reagents and can be driven to completion by removal of H_2 gas from the reaction mixture.

H_2 is a promising candidate to replace fossil fuels for transportation [8], and to store energy that is produced from renewable resources [9]. One of the main challenges toward a future hydrogen economy [10] is the storage and transportation of large amounts of H_2 [11]. Although H_2 has an excellent gravimetric energy density of 33.3 kWh/kg, it has an extremely low volumetric energy density of 3 Wh/L under normal conditions due to its low density (0.0898 g/L at 0 °C and one bar) [12]. Moreover, the facile combustion of H_2 with air in broad concentration ranges, high
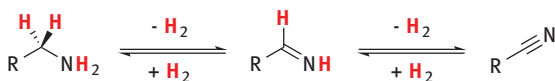
Figure 9.1: General scheme for dehydrogenation of amines to form aldimines or nitriles with release of dihydrogen.

diffusion in gases, liquids and solids, and lack of dedicated infrastructure for H_2 storage and transport, has sparked research into various technologies for hydrogen storage [8–10]. Organic liquids that allow for fully reversible acceptorless dehydrogenation and rehydrogenation are promising candidates as liquid organic hydrogen carriers (LOHCs). An attractive feature of LOHCs is that they can utilize the existing infrastructure for transportation of liquid fuels. In addition, high purity H_2 can be released upon demand from LOHCs, which is essential for proton exchange membrane fuel cells that are easily poisoned by impurities [13]. Transition metal-catalysts play an essential role in facilitating the liberation of H_2 gas from LOHCs through acceptorless dehydrogenation reactions.

Although conceptually similar to transition metal-catalyzed alcohol dehydrogenation – a well-established transformation that has been studied in great detail [7, 14] – detailed mechanistic studies and reports of highly selective transition metal-catalyzed dehydrogenation of amines are rare. Potential reasons for this disparity are the slower β-hydrogen elimination from amido complexes compared to alkoxides [7b] and the inherently more complicated nature of this reaction that often results in the formation of a mixture of products as a result of transamination reactions (Section 9.2.1). For synthetic purposes, addition of an excess of H_2 acceptor can lead to more selective transformations but is concomitant with the generation of waste. Very recent developments that employ cleverly designed cooperative ligands or photocatalysts avoid these problems demonstrating exciting new possibilities in this old but re-emerging field of research.

The focus of this review is homogeneous transition metal-catalyzed dehydrogenative reactions of amines to form H_2 and oxidized N-containing molecules. Chemical transformation of amines involving external oxidants (e. g. O_2 or alkenes) or heterogeneous catalysts will not be discussed unless they provide additional insight. This review is not intended as an exhaustive overview but is meant to provide an impression of the recent literature on transition metal-catalyzed acceptorless amine dehydrogenation for the synthesis of small molecules, and hydrogen storage. Although exciting, the recent work by Milstein and coworkers involving the reversible dehydrogenative coupling of alcohols and amines to give amides, will not be discussed as it based on alcohol dehydrogenation combined with nucleophilic attack by the amine [15]. This work is discussed elsewhere in the book. The focus of Section 9.2.1 is on the conversion of primary amines into imines, and the side reactions that occur as a result of dehydrogenative coupling. In the subsequent Section (2.2) catalyst systems that

enable the selective conversion of primary amines into nitriles through transition metal catalyzed acceptorless dehydrogenation will be analyzed. In Section 9.2.3 the various approaches for the dehydrogenation of cyclic amines will be discussed. Finally, Section 9.3 will provide a brief overview, conclusion and discussion with a focus on the current status of the field and the challenges that still remain.

9.2 Catalytic dehydrogenation of amines

9.2.1 Primary amines to imines and secondary amines

Imines are versatile synthetic handles for the introduction of various functional groups in organic chemistry [4]. In addition, imines commonly play an essential role in cooperative [16] and redox-active [17] ligands employed in homogeneous catalysis. Imine synthesis is typically achieved through condensation of amines with aldehydes or ketones to give the corresponding imine and an equivalent of water. These reactions are often acid catalyzed or driven to completion by azeotropic removal of water [18]. Because not all functional groups are compatible with such conditions a broad variety of alternative methodologies has been developed that do not require acid or prolonged heating [4]. However, these commonly require the use of (super)stoichiometric reagents that can be toxic and create significant waste. Imine synthesis through transition metal-catalyzed acceptorless dehydrogenation of amines is a more atom economic alternative, and of interest for LOHCs. However, these reactions have their challenges, especially when terminal alkyl amines are used (Figure 9.2). After dehydrogenation of the alkylamine (step A) the resulting electrophilic aldimine can react with the starting amine to form a secondary imine and NH_3 (step B). This step can either go through a direct reaction of the aldimine and amine or by in situ hydrolysis of the aldimine due to traces of water to form an intermediate aldehyde. If the hydrogen generated from the initial reaction is not fully removed
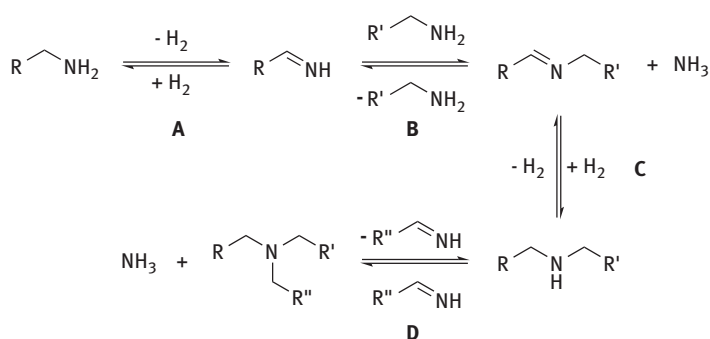
Figure 9.2: The series of reversible reactions that can lead to a complicated mixture of products during imine synthesis by acceptorless dehydrogenation of amines.

from the system, the secondary imine can be hydrogenated to form a secondary amine (step C), which in some cases can react in a similar fashion to give a tertiary amine and NH_3 (step D). As a result of the reversible nature of these reactions a mixture of products is often observed.

Various metal complexes can catalyze the racemization of amines through dehydrogenation followed by rapid rehydrogenation of the corresponding imine, showing the reversible nature of these transformations [19]. In a mechanistic study on imine hydrogenation using Shvo's complex [20] Casey and coworkers showed through isotopic labeling that there is rapid reversible hydrogen transfer between the catalyst and bound imine (Figure 9.3), which results in imine isomerization and deuterium scrambling [21]. To prevent rehydrogenation, external reagents can be employed that irreversibly react with the hydride intermediate, driving the reaction to completion. For example, Bäckvall and coworkers demonstrated the conversion of secondary amines into imines using Shvo's complex (Figure 9.3) and a co-catalyst that effectively oxidizes the equivalent of H_2 into H_2O, preventing rehydrogenation [22].
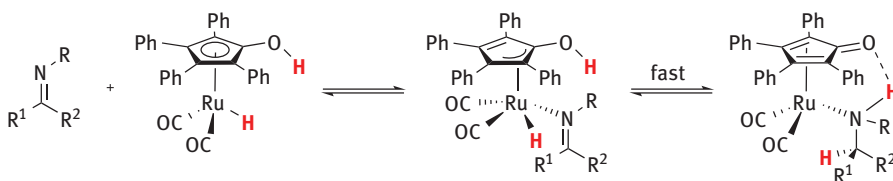
Figure 9.3: Rapid reversible hydrogen transfer between Shvo's complex and the bound imine substrate.

An early example reported by Jensen and coworkers uses a hydrogen acceptor and an Ir catalyst bearing a PCP pincer ligand (Figure 9.4), previously reported as a catalyst for the alkane dehydrogenation [23], to perform the transfer dehydrogenation of secondary amines to imines [24]. The catalytic transfer dehydrogenations of various secondary amines were performed in sealed tubes at 200 °C to give the corresponding
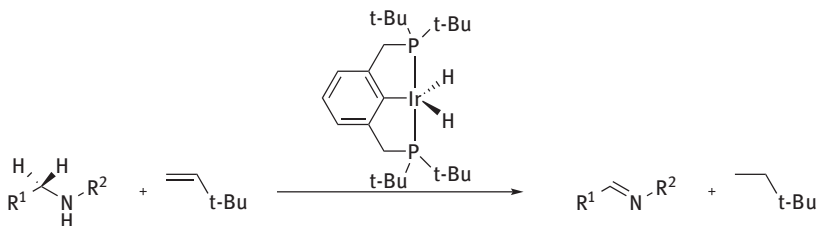
Figure 9.4: Transfer dehydrogenation of secondary amines using an Ir complex. R^1 = Pr, *i*-Pr, Me, Ph; R^2 = Pr, *i*-But, *c*-Hex, Bn, Me.

imines with high selectivity in good yields. Limited conversion (~10 %) was observed when the reaction was performed in neat amine as a result of product inhibition. Dilution of the reaction mixture with toluene was found to resolve this issue. However, high catalyst loadings (14 mol %), long reaction times (3 days), high temperatures and the requirement of a hydrogen acceptor limit the practicality of the system. Jensen and coworkers argued that the mechanism proceeds through direct C-N bond dehydrogenation rather than a C-C bond dehydrogenation followed by isomerization, based on a reaction with a substrate unable to isomerize, and the observation that tertiary amines were found to be unreactive. In contrast, Goldman and coworkers later reported the dehydrogenation of tertiary amines to form enamines using both the same catalyst and acceptor alkene under milder conditions [25], showing that the exact mechanism of these transformations is not fully understood.

Yi and Lee reported a tetranuclear Ru-μ-oxo-μ-hydroxo-hydride complex as an highly active catalyst for the transfer dehydrogenation of amines, achieving turnover numbers up to 20,000 within 2 h at 200 °C. Dehydrogenation of primary amines gave mixtures of imine and secondary amine products as a result of the side reactions depicted in Figure 9.2. The formation of NH_3 was confirmed by ^{1}H Nuclear Magnetic Resonance (NMR) spectroscopy. Notably, benzylic amines were found to exclusively give the corresponding secondary imine. Isotopic labeling at various positions of indoline, a cyclic amine, showed scrambling at various positions, suggesting rapid reversible N-H and C-H bond activation steps are occurring under catalytic conditions [26].

As described above, the many reversible reactions that are encountered in amine dehydrogenation (Figure 9.2) can result in mixtures of compounds. However, it also allows one to start at different stages, pushing reactions in different directions through the right choice of reagents, substrates and conditions. Beller and coworkers demonstrated this by converting secondary and tertiary amines to primary amines using Shvo's catalyst and NH_3 [27]. Through so-called "borrowing hydrogen" methodology [7, 28], (Figure 9.5) a secondary amine can be dehydrogenated to the corresponding imine, and subsequently react with NH_3 to give the corresponding primary amine and primary imine. Finally, the "borrowed" hydrogen is used to rehydrogenate the imine to give another equivalent of primary amine. According Le Chatelier's principle, more primary amine should be generated by performing in the presence of an excess of NH_3. However, an excess of NH_3 was found to inhibit catalyst activity by forming an inactive NH_3 complex. This inhibition could be resolved by performing the reaction at higher temperatures. Vogt et al. recently reported a similar reactivity using Ru-based half sandwich complexes [29]. Similar to Beller et al., full conversion was never observed as a result of catalyst deactivation. The authors propose this is mainly caused by nucleophilic attack of the primary amine product on a carbonyl ligand on the catalyst, which was observed by NMR, and *in situ* FTIR spectroscopies as well as mass spectrometry.

Albrecht and coworkers recently reported a catalytic system for the dehydrogenation of amines based on a Cp*Ir complex bearing a pyridyl-triazolylidene ligand
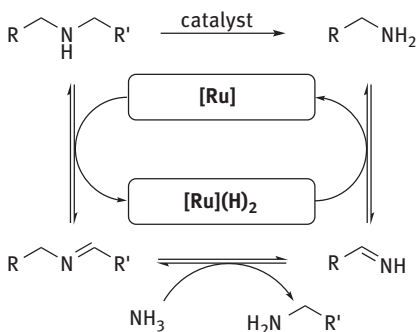
Figure 9.5: "Borrowing hydrogen" catalysis in the conversion of primary amines into secondary amines and *vice versa*.

(Figure 9.6) [30]. With a 5 mol % catalyst loading in 1,2-dichlorobenzene (1,2-DCB) at 150 °C a range of benzylamines can be converted into a mixture of secondary imines, secondary amines and tertiary amines in the absence of an external oxidant or base. Two complexes were investigated that differ in their pendant substitution, exhibiting a non-coordinating pyridyl unit or a phenyl group. The former was found to exhibit higher catalytic activity and better selectivity toward the secondary imine versus the secondary amine. Notably, this system also produces notable quantities of tertiary amines, which are formed in higher ratios when electron rich benzylamines are used. Through a set of stoichiometric reactions, X-ray diffraction, and IR and ^{1}H NMR spectroscopies, it was shown that the non-coordinated pyridyl unit has a hydrogen bonding interaction with the amine substrate, suggesting substrate activation involving cooperativity of the triazolyidene ligand. Although this work exhibits an interesting approach using metal-ligand cooperativity in a hydrogen borrowing mechanism, the reported catalytic transformations still lead to mixtures, limiting their applicability for synthetic purposes and their potential as LOHCs.
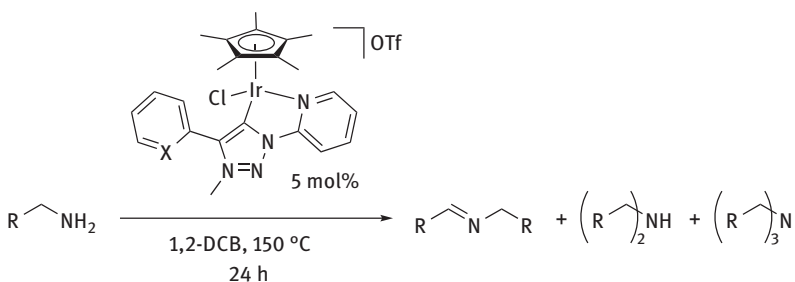
Figure 9.6: Catalytic dehydrogenation of amines using a Cp*Ir catalyst bearing a pyridyl-triazolylidene ligand. X = N or CH; R = Ph, 4-methoxyphenyl, tol, 4-chlorophenyl or 3-chlorophenyl.

Blaquiere and coworkers recently reported a Ru-based catalyst bearing a potentially cooperative ligand for the dehydrogenation of primary amines (Figure 9.7) [31]. With a 3 mol % catalyst loading in anisole at 110 °C, benzylamine can be converted into mixtures of coupled imines, secondary amines and nitriles. In the presence of an equivalent of aniline a heterocoupled imine is formed, albeit with poor selectivity.
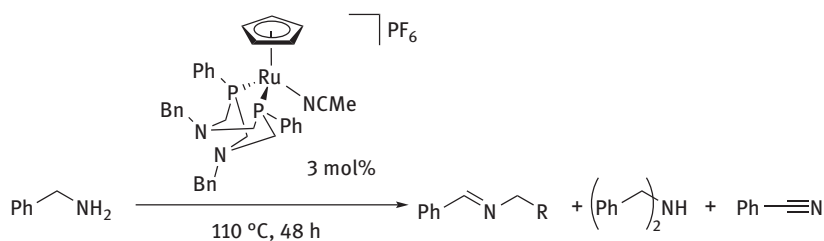
Figure 9.7: Dehydrogenation of benzylamine to form a mixture of products with using a CpRu-based catalyst bearing a bisphosphine ligand with pendent amines.

The ability of the pendent amine in the bisphosphine ligand to shuttle protons to and from the metal center has been well established in electrocatalytic proton reduction and H_2 oxidation [32]. Although a benzylamine adduct displaying an intramolecular H-bonding interaction with the pendent amine was isolated, it was found to be an off-cycle species that displays lower catalytic acitivity. In addition, a comparable Ru complex lacking pendent amines showed comparably activity but with slightly more secondary amine formation.

When secondary imines are targeted, the use of catalyst systems that are both capable of hydrogenation and dehydrogenation inevitably leads to mixtures of secondary amines and imines. However, employing a catalyst that is ineffective for imine hydrogenation can provide access to imines and H_2. Sadow et al. reported a Rh complex bearing a scorpionate ligand as an active catalyst for acceptorless photocatalytic dehydrogenation of amines to form the corresponding coupled imines (Figure 9.8) [33]. A notable feature of this transformation, besides the imine selectivity, is that the photocatalytic reaction is performed at room temperature, whereas these reactions commonly require heating at temperatures >100 °C. Unfortunately, the authors did not propose a mechanism for this transformation. It seems reasonable that it proceeds through a similar to what the authors propose for the alcohol dehydrogenation-decarbonylation that is also described. This reaction involves photodissociation of CO ligands to generate a coordinatively unsaturated species that dehydrogenates an alcohol to form an aldehyde and a Rh dihydride, which can subsequently release H_2.

When it comes to robustness and catalyst recycling it is difficult for homogeneous catalysts to compete with heterogeneous systems. Yamaguchi and Mizuno recently
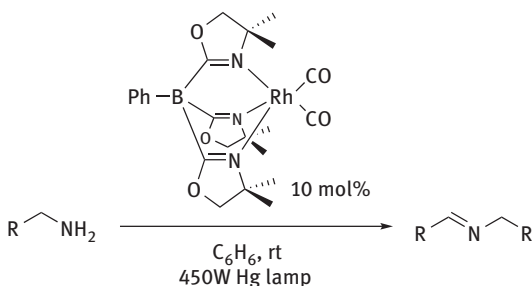
Figure 9.8: Photocatalytic dehydrogenation of amines to form the corresponding coupled imines.
R = n-C_6H_{13}, n-C_5H_{11}, c-Hex, iPr, phenyl, 4-methylphenyl, 2-methylphenyl, 4-methoxyphenyl, 2-methoxyphenyl or Bn.

reported catalytic conversion of cyclohexylamines to diarylamines through acceptor-less dehydrogenative aromatization using Au-Pd alloy nanoparticles supported on TiO_2 (Figure 9.9) [34]. A broad variety of substrates were tested giving the diarylamines in moderate to high yield in the absence of an external oxidant or hydrogen acceptor. Notably, combinations of anilines with cyclohexanones, cyclohexylamines with cyclohexanones, and nitrobenzenes with phenols could also be employed, allowing for the synthesis of non-symmetrically substituted diarylamines. The authors propose a complex catalytic pathway involving amine dehydrogenation, imine disproportionation, and condensation reactions. Pd was found to be the active metal but the activity was enhanced significantly by alloying with Au. The authors speculate that the electronegative character of Au results in more electron deficient Pd sites, facilitating the rate limiting β-hydrogen elimination. Although these
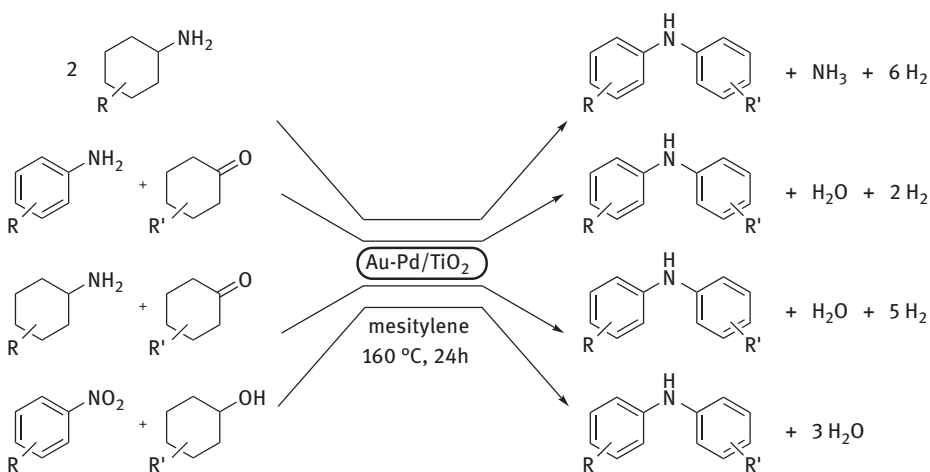
Figure 9.9: Acceptorless dehydrogenative aromatization using a heterogeneous Au-Pd alloy catalyst.

reactions are synthetically interesting, the generation of NH_3 and the irreversibility of these reactions make them unsuitable for a LOHC system.

As seen in the examples described above, transition metal catalyzed acceptorless dehydrogenation of primary amines can give rise to a mixture of products including imines, secondary and tertiary amines, and NH_3. The presence of an external oxidant in the form of a quinone or acceptor alkene can aid selectivity for synthetic purposes. An additional problem is the high temperatures and high catalyst loadings that are employed in the majority of these reactions. The use of irradiation to create coordinately unsaturated metal centers allows for lower reaction temperatures but can also give rise to photoinduced side-reactions. Transition metal-catalyzed dehydrogenation of primary amines as a strategy in LOHCs is hampered by the various side reactions, release of other gases such as NH_3, and low wt% H_2. However, catalysts capable of reversibly dehydrogenating and rehydrogenating primary amines to nitriles and back with great selectivity hold promise, which will be discussed in the next section.

9.2.2 Selective catalytic dehydrogenation of primary amines to nitriles

Nitriles are found in a variety of materials such as natural products [35], active pharmaceutical ingredients [36], glues and polymers [37]. Common synthetic procedures to install nitrile (CN) moieties involve the use of stoichiometric, toxic reagents or harsh reaction conditions [38]. The selective oxidation of primary alkylamines to nitriles, which can be achieved using stoichiometric iodine based oxidants [39], avoids the introduction of a new CN moiety. Alternatively, the oxidative dehydrogenation of alkylamines into imines or nitriles can be facilitated by a variety of heterogeneous catalysts based on Au [40], Ru [41] or Ir [42]. Notably, Au based systems, unlike the Ru and Ir based systems, are unable to dehydrogenate primary amines into nitriles, and solely give imines [43]. Homogeneous catalyst systems based on Ru [44] and Ni [45] that facilitates the dehydrogenation of amines to nitriles can operate at room temperature but require $K_2S_2O_8$ as an external oxidant. Bernskoetter and Brookhart reported the use of a well-defined iridium dihydride complex bearing a POCOP pincer ligand for the catalytic dehydrogenation of primary amines to nitriles using *tert*-butylethylene as a hydrogen acceptor [46]. A mechanistic study revealed a slow initial β-hydrogen elimination step followed by a fast second dehydrogenation to give the nitrile, which was found to have an inverse first order on the turnover frequency, indicative of product inhibition. However, because these catalysts rely on the presence of a hydrogen acceptor, they are beyond the scope of this review.

Nitriles are the most oxidized form of the carbon nitrogen bond and can store two equivalents of H_2 for each C-N fragment. Consequently, each CH_2NH_2 fragment holds 13.3 wt% H_2, which makes nitriles interesting functional groups for LOHCs [47]. Acetonitrile is the simplest nitrile but the corresponding amine, ethylamine (8.9 wt% H_2), is a gas at ambient temperature, complicating its use as an LOHC. The

incorporation of multiple nitriles into a single molecule could give rise to a material that has better physical properties without losing too much gravimetric H_2 content. Although the hydrogenation of nitriles to amines is well established [48, 49], examples of selective acceptorless dehydrogenations of primary amines to nitriles are rare. Often the formation of secondary imines and amines are observed due to the highly reactive partially dehydrogenated aldimine product (see Section 9.2.1). Jensen et al. showed that the presence of a strong base can give higher selectivity [50], similar to what is observed for the reverse hydrogenation reaction [51]. A unique system that is not troubled by these common issues was reported in 2013 by Szymczak and coworkers, who reported the dehydrogenation of primary and secondary amines to the corresponding nitriles, imines and H_2 using a RuH complex bearing an NNN pincer ligand as the catalyst (Figure 9.10). With a 1 mol% catalyst loading, a variety of amines in toluene solution were converted to the corresponding nitriles and H_2 in moderate to good yield over the course of 24 h at 110 °C [52]. Notably, solely amine and nitrile were observed upon *in situ* analysis of the reaction mixture by GC-MS and ^1H NMR spectroscopy. Because no imine nor imine-derived products were observed, the authors proposed a fast second dehydrogenation step similar to the mechanism proposed by Bernskoetter and Brookhart [46]. The authors also demonstrated the reverse hydrogenation of nitriles using a different homogeneous Ru-based catalyst at room temperature using three bars of H_2.
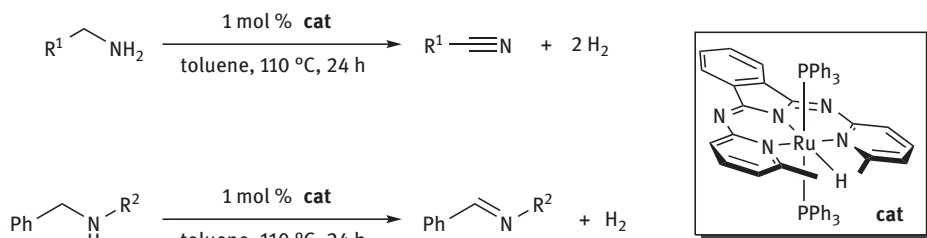
Figure 9.10: Dehydrogenation of amines catalyzed by a RuH complex bearing an NNN pincer ligand.

Recently, Scymczak and coworkers reported a detailed mechanistic study on the acceptorless double dehydrogenation of primary amines to form nitriles using the RuH complex [53]. Their objectives were to discover whether an inner or outer-sphere mechanism was operational, and why their ligand framework enabled selective double dehydrogenation while other Ru-based systems give mainly transamination products (see above) [54]. Outer-sphere, inner-sphere and alternative pathways involving ligand hemilability were investigated by ligand substitutions, kinetic studies, steric catalyst modifications and computational investigations. The latter supported an inner sphere mechanism (Figure 9.11) starting with reversible substitution
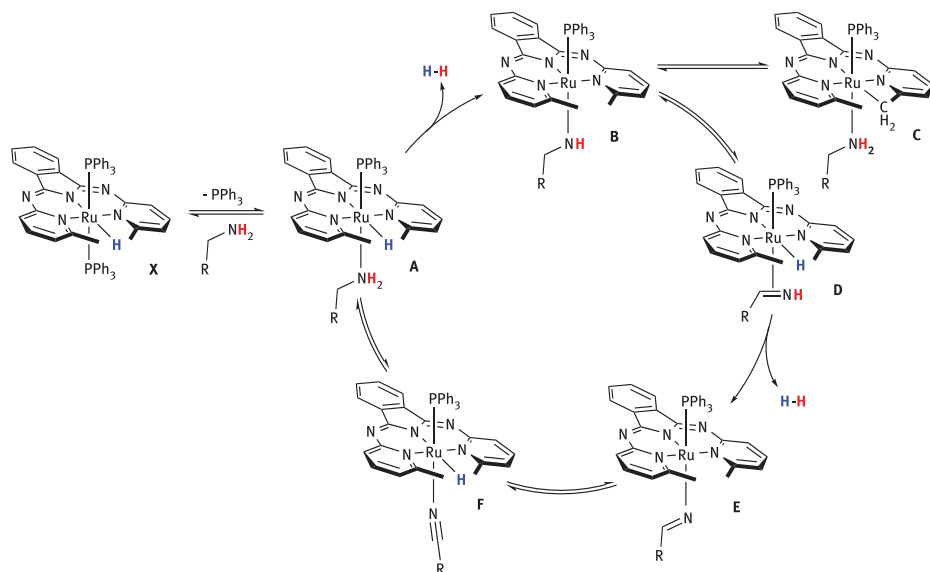
Figure 9.11: Proposed mechanism for the double dehydrogenation of primary amines to nitriles.

of one of the PPh$_3$ ligands on **X** by the amine substrate to generate amine complex **A**. A rate-determining proton transfer from the amine to the hydride results in irreversible loss of H$_2$ and the formation of amido complex **B**, which is in equilibrium with off-cycle species **C**. Complex **C** was isolated through the addition of a strong base in the absence of additional amine. It was found to be a kinetic product that is thermodynamically disfavored by 6.7 kcal/mol, and has to undergo protonation and deprotonation to reform **B** to be catalytically competent. A subsequent β-hydrogen elimination from the bound amide gives intermediate **D** in which the imine remains coordinated. A rapid second dehydrogenation proceeds through a similar irreversible deprotonation to give **E**, followed by another β-hydrogen elimination resulting in the formation of the nitrile bound species **F**. The highly selectivity toward nitriles is explained by the high binding affinity for imine intermediates, and the lower activation barrier for the second dehydrogenation step, which prevents imine dissociation and subsequent transamination steps. A notable finding was that the *ortho*-substituents on the pyridines in the pincer ligand play an essential role beyond steric hindrance. Noncovalent interactions between these methyl groups and the amido nitrogen atom were found to stabilize the Ru amido species to the extent that a modified catalyst without these methyl groups was found to be catalytically inactive, whereas an isopropyl substituted ligand showed comparable activity.

After the initial publication by Scymczak and coworkers, Grellier and Sabo-Etienne suggested the use of CN/CH$_2$NH$_2$ couples as a promising candidate for LOHCs [47]. Mata and coworkers recently reported on the use of Ru complexes with

NHC ligands for the acceptorless dehydrogenation of amines to nitriles and H_2 (Figure 9.12) [55]. The catalytic reaction was found to proceed with a 2% catalyst loading at 110 °C over the course of 24 h but suffers from moderate selectivity as a result of side reactions involving the partially dehydrogenated imine intermediate. A modified catalyst, bearing a pyrene group on one of the wingtip substituents of the NHC ligand (R^3), was immobilized on graphene and showed limited loss of activity over 10 catalytic runs. Full selectivity was achieved when long chain aliphatic amines were employed, which unfortunately have significantly lower gravimetric H_2 content.
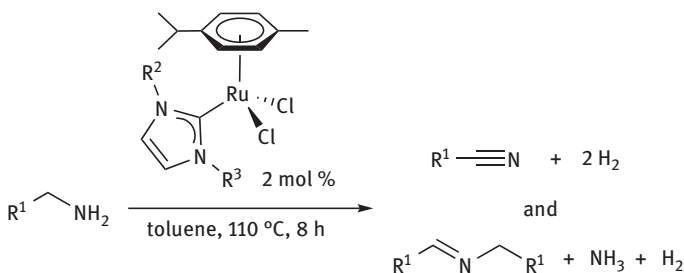
Figure 9.12: Acceptorless dehydrogenation of primary amines to form nitriles and a secondary imine side product. R^1 = Ph, 4-Chlorophenyl, tolyl, 4-methoxyphenyl, 4-trifluoromethylphenyl, naphtyl. R^2 = nBu or Me; R^3 = nBu or pyrene.

Obtaining two equivalents of H_2 from a single C-N bond makes the acceptorless dehydrogenation of primary amines to nitriles an interesting strategy for LOHCs. However, there are few examples of homogeneous transition metal-catalyzed acceptorless dehydrogenation of primary amines to nitriles. The Ru catalyst reported by Scymczak (Figure 9.10 and Figure 9.11) is the only system that does not form side products, as it holds the imine intermediate bound to the metal center, preventing undesired transamination reactions. The design and study of stable and selective catalysts that operate in a similar fashion for the acceptorless dehydrogenation of substrates featuring multiple primary amine groups could yield a LOHC system with high gravimetric H_2 content.

9.2.3 Catalytic dehydrogenation of N-heterocycles

Unsaturated nitrogen containing heterocycles are prevalent in natural products, dyes, active pharmaceutical ingredients, and ligand systems for homogeneous catalysis [1–4, 16, 17]. Catalytic oxidative dehydrogenations from saturated analogues are of interest for both synthetic and hydrogen storage applications [56–58]. Acceptorless dehydrogenation of N-heterocycles is endothermic by nature but can be driven to completion by removal of H_2 from the reaction system. In addition, computational

and experimental studies show that the presence of one or more N atoms decreases the ΔH^o of the reaction (Figure 9.13) [59]. Side reactions observed for primary amines (see Figure 9.2) are uncommon due to the cyclic nature of the substrate. Combined, these features make N-heterocycles interesting core structures for LOHCs. Several homogeneous and heterogeneous transition metal catalysts are capable of acceptor-less dehydrogenation of N-heterocycles and the reverse hydrogenation process. Liu et al. [56], He et al. [57], and Crabtree [58] recently reviewed the conversion between aromatic and saturated N-heterocycles for synthetic purposes and LOHCs, respectively. Hence, only highlights, overall conclusions, and more recent work will be described.

The first report of the use of heterocyclic compounds as LOHCs was published by Air Products And Chemicals, Inc. who investigated a broad variety of pi-conjugated substrates for the storage of H_2 through reversible catalytic hydrogenation and
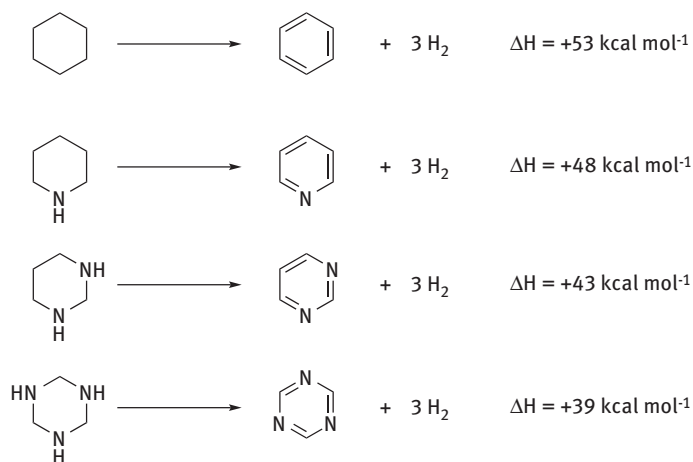
Figure 9.13: Calculated enthalpies of dehydrogenation for cyclohexane and structurally similar N-heterocycles [59].

dehydrogenation [60]. N-perhydroethylcarbazole (NEC-H_{12}, Figure 9.14) was identified as the most promising candidate with a 5.8 wt% of H_2 and energy density of 1.9 kWh/kg. Although the N-ethyl group decreases the gravimetric H_2 content, it lowers the melting point by ca. 180 °C to 68 °C easing the liquefaction of the LOHC. Hydrogenation was performed using a heterogeneous Ru on alumina catalyst at 130–160 °C under 70 bar of H_2. High purity H_2 can be released using a supported Pd or Pt catalyst at 200–230 °C and ambient pressure. The reversible uptake and release of six equivalents of H_2 per molecule of NEC was demonstrated for several cycles. Libuda et al. investigated the mechanism on Pd(111) [61] and Pt(111) [62] under
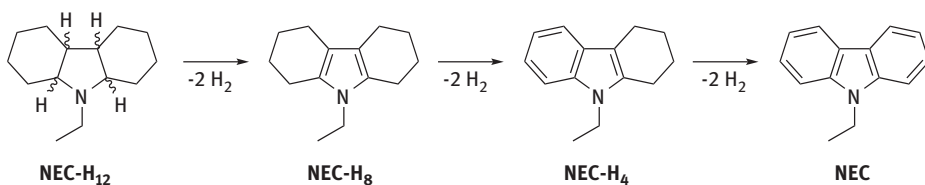
Figure 9.14: NEC-H12 and the corresponding dehydrogenation products.

ultrahigh vacuum conditions, and found that loss of the first two molecules of H_2 to form NEC-H_8 already occurs at -50–0 °C. The remaining H_2 equivalents were found to be released stepwise upon heating to 107 °C. The only significant difference between the Pd and Pt catalyst systems was that the decomposition pathway of the LOHC, which involves C-N bond scission of the ethyl group, was observed around 57 °C on Pd(111), whereas this only occurs above 117 °C on Pt(111).

Kempe and coworkers reported a single bimetallic nanocomposite containing Pd and Ru for the hydrogenation and dehydrogenation of NEC and NEC-H_{12}, respectively [63]. The catalyst system, Pd_2Ru on silicon carbonitride, was prepared by mixing well-defined Ru and Pd complexes with a polysilazane, followed by crosslinking and pyrolysis. Using a 0.5 mol% catalyst loading (mol Pd_2Ru per mol of substrate), NEC hydrogenation was achieved at 110 °C and 20 bar of H_2 pressure without solvent over the course of 7 h. The dehydrogenation of NEC-H_{12} was performed at 180 °C using the same catalyst loading over 20 h. The procedures were repeated for three cycles with little loss of activity. In addition, the authors reported the use of the octohydrophenazine (7.2 wt% H_2) as a new N-heterocyclic LOHC (Figure 9.15). This N-heterocycle can be synthesized from cyclohexane1,2-diol, which is readily accessible from lignocellulosic biomass [64]. The Pd_2Ru catalyst enabled reversible extraction and incorporation of seven equivalents of H_2 per molecule of the octohydrophenazine LOHC for seven consecutive cycles without any loss of activity, albeit with slightly more forcing conditions and the need for solvents.
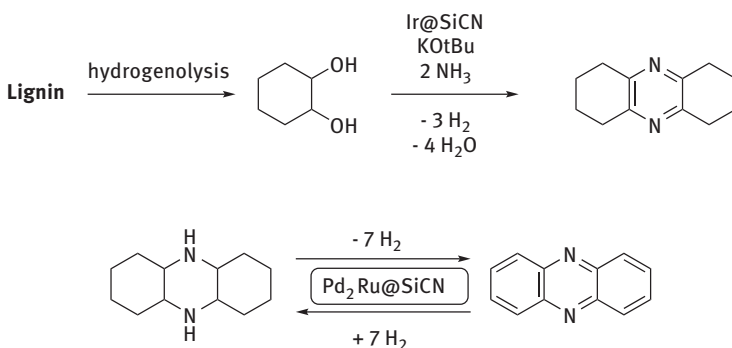
Figure 9.15: Synthesis of octahydrophenazine from lignin, and its use as a LOHC enabled by a Pd_2Ru on silicon carbonitride catalyst.

NEC has been extensively studied as a LOHC in combination with heterogeneous catalyst systems [58]. In contrast, most efforts toward the use homogeneous catalysts for the dehydrogenation and hydrogenation of N-heterocycles have focused on smaller heteroaromatic substrates.

A pioneering system capable of reversible hydrogenation and dehydrogenation of N-heterocycles using a single Cp*Ir-based catalyst was reported by Yamaguchi and Fujita in 2009 (Figure 9.16) [65]. With a 5 mol% catalyst loading in refluxing *p*-xylene (bp = 138 °C), quinolines are dehydrogenated to the corresponding 1,2,3,4-tetrahydroquinolines in 20 h in varying yields with excellent selectivity. Hydrogenation of the quinolines using the same catalyst could be achieved at 110 °C under 1 atmosphere of H_2 with varying yields. Increasing the H_2 pressure enabled shorter reaction times at lower temperature. Using the above-mentioned conditions, 2-methylquinoline (2.7 wt% H_2) can be dehydrogenated and rehydrogenated in quantitative yield, which was repeated five times with only 2 % loss in efficiency. Stoichometric reactivity studies show that the 2-hydroxy pyridine derived ligand is readily displaced to form a Ir-hydride dimer under hydrogenation conditions. However, the authors found that a reaction of the hydride dimer with the 2-hydroxypyridine in the absence of H_2 rapidly reformed the initial Cp*Ir complex under the dehydrogenation conditions, suggesting that the hydroxypyridine plays an active role during catalysis.
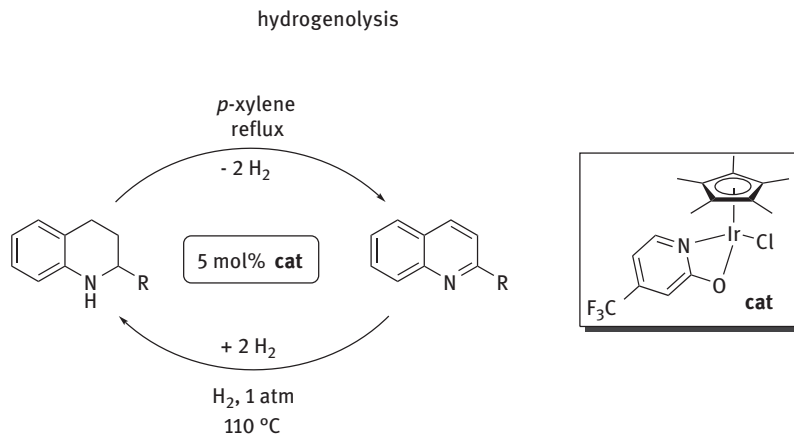
Figure 9.16: Reversible hydrogenation and dehydrogenation of 2-methylquinoline using a Cp*Ir-based catalyst.

Zhang and Xi reported a computational mechanistic investigation on this system, which is consistent with the experimental observations [66]. The proposed mechanism for the dehydrogenation involves two separate cycles (Figure 9.17) starting with a tautomerization of the hydroxypyridine (step A) followed by substrate pre-
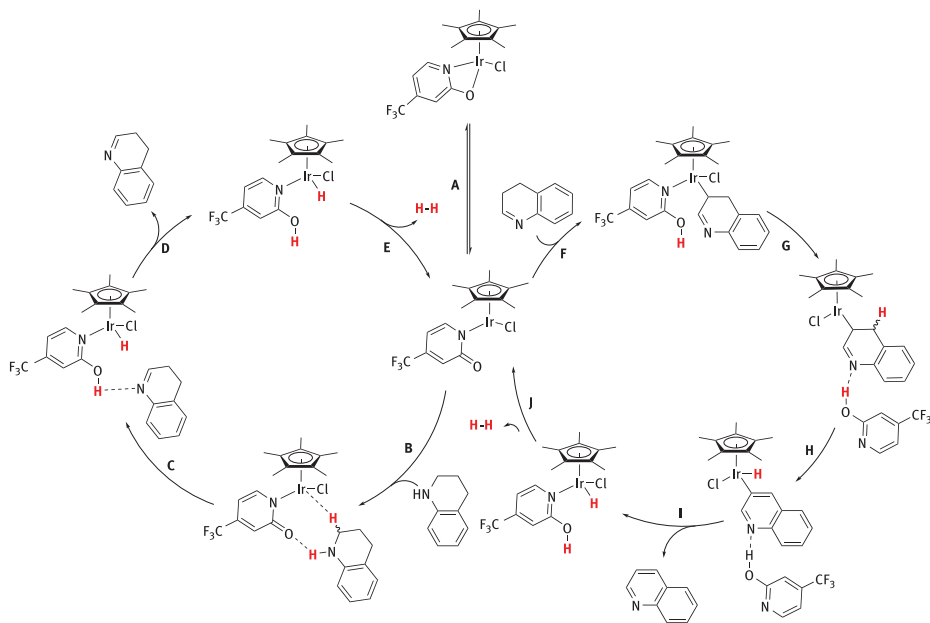
Figure 9.17: The proposed cooperative mechanism for the dehydrogenation of tetrahydroquinolines by a Cp*Ir catalyst with a 2-hydroxypyridionate ligand.

organization wherein the 1,2,3,4-tetrahydroquinoline has a hydrogen bonding interaction with the ligand, which places the C2-H in close proximity to the metal center (step B). Simultaneous transfer of a proton to the ligand and a hydride to the metal center forms a 3,4-dihydroquinoline and an iridium hydride (step C). From this species the dihydroquinoline dissociates (step D) and subsequent liberation of H_2 reforms the active catalyst (step E). This H_2 liberation is based on the bifunctional nature of the intermediate and is formed by the combination of the ligand proton with the metal hydride. Subsequently, the 3,4-dihydroquinoline undergoes a ligand-assisted C-H activation on the three-position whereby the proton ends up on the ligand (step F). Ligand dissociation enables a hydrogen-bonding interaction with the imine nitrogen (step G), which facilitates β-hydrogen elimination thereby forming the quinoline (step H). Dissociation of the product and re-coordination of the hydroxypyridine (step I) enables cooperative reductive elimination of H_2 to form the active species (step J), completing the catalytic cycle.

More recently, Yamaguchi and Fujita reported a similar Cp*Ir-based catalyst bearing a bipyridonate ligand (Figure 9.18, top) for the dehydrogenation of 2,6-dimethyldecahydro-1,5-naphthyridine and dehydrogenation of the corresponding 1,5-naphthyridines [67]. Notably, this transformation involves reversible loss and uptake of five equivalents of H_2 (5.9 wt%), albeit under more forcing conditions for the rehydrogenation in comparison to the quinoline system. Crabtree and coworkers showed that previously reported Ir-based hydrogenation catalysts are also capable of the

Fujita, Yamaguchi *et al.*[67]

Xiao *et al.*[69]

Fujita *et al.*[70]
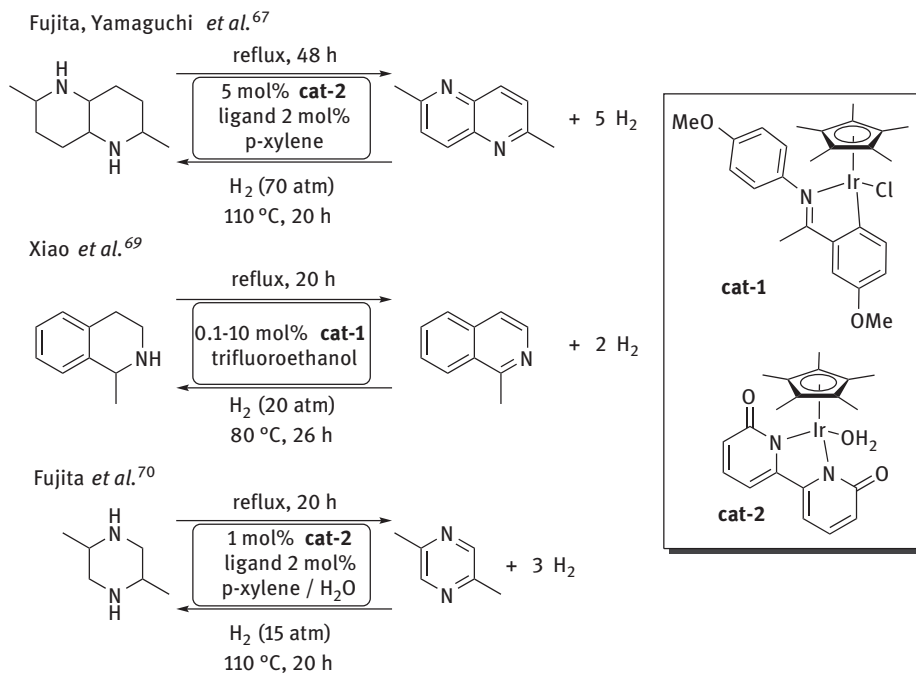
Figure 9.18: N-heterocycles that can undergo reversible hydrogenation and dehydrogenation with a single catalyst Cp*Ir derived catalyst.

reverse dehydrogenation for tetrahydroquinolines at 135 °C with 5 mol% catalyst loading over the course of 24 h [68]. Xiao et al. reported highly active Cp*Ir catalyst systems with cyclometalated aryl ketamine ligands that catalyze quinoline dehydrogenation at 80 °C with only 0.1 mol% catalyst loading (Figure 9.18, middle) [69]. Rehydrogenation could be achieved at ambient temperature and pressure with 10 mol% catalyst loading [70]. Unlike the other Cp*Ir systems described, Xiao's system has a lower H_2 content (2.7 wt%) required the use of trifluoroethanol, showing no or very limited catalytic activity in aprotic solvents. The authors suggest that the ligand plays no cooperative role during catalysis and that the hydride intermediate is likely protonated in an intermolecular fashion by trifluoroethanol to produce H_2. Schafer and Love very recently reported the isolation of a rare example of a cyclic imine bound Cp*Ir hydride complex formed by ligand-metal cooperative dehydrogenation of an N-heterocycle [71]. Although the reported complex is not catalytically competent, it provides experimental support for the proposed metal-ligand cooperativity in catalytic systems from computational studies. Very recently, Fujita and coworkers reported a new hydrogen storage system based on the hydrogenation and dehydrogenation of 2,5-dimethylpyrazine and the corresponding piperazine, respectively (Figure 9.18, bottom) [72]. Using a 1 mol% loading of a Cp*Ir-based complex with a dipyridonate ligand and 2 mol% extra

ligand, reversible release and uptake of three equivalents of H_2 (5.3 wt%) was repeated four times without loss of efficiency and near quantitative yield of substrate and hydrogen. The quantitative hydrogenation can be achieved at 110 °C under 15 atm of H_2 pressure over the course of 20 h. The quantitative dehydrogenation was performed under reflux over the same length of time. A notable feature of the reported system is the very low amount of solvent that is required compared to previously reported systems. The reversibly hydrogenation and dehydrogenation was demonstrated without solvent in slightly decreased yield, providing 1144 mL of H_2 per 2.18 mL pyrazine. In 2012, Muthaiah and Hong reported acceptorless and base-free dehydrogenation of alcohols and N-heterocyclic compounds catalyzed by Ru-hydride complexes [73]. With a 2.5 mol% catalyst loading at 165 °C a small set of tetrahydroisoquinolines and indolines were dehydrogenated in good yields over the course of 24 h. Although Shvo's catalyst gave the best yields, $RuH_2(CO)PPh_3)_3$ showed to be not far behind, which makes the proposed cooperative mechanism questionable.

Catalysts systems for reversible hydrogenation and dehydrogenation of N-heterocycles that are based on more earth abundant metals were reported by the groups of Crabtree and Jones. In 2013, Crabtree and coworkers reported the electrocatalytic dehydrogenation of a tetrahydroquinoline using CpNi-based catalysts with N-heterocyclic carbene (NHC) ligands (Figure 9.19) [74]. At room temperature electrocatalytic dehydrogenation was observed with moderate to good chemical and faradaic yield in acetonitrile solution (0.2 M NBu_4BF_4 electrolyte) using 0.5 mol% of the nickel complex. The presence of a quinone – covalently linked to the NHC ligand or in solution (5 mol%) – was found to be essential for conversion, which is in line with a previous report from the group showing that 2,3-dichloro-5,6-dicyanobenzoquinone itself is an electrochemical catalyst for amine dehydrogenation [75]. Control experiments showed that Ni powder or NiO were also active, albeit with reduced yield, questioning the homogeneous nature of this catalyst system.
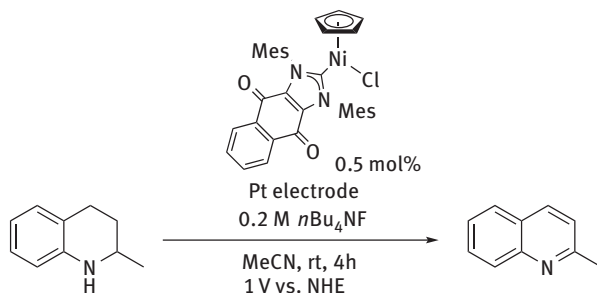
Figure 9.19: Electrocatalytic dehydrogenation catalyzed by a quinone-fused NHC-NiCp complex.

A year later, Jones and coworkers reported catalytic hydrogenation and dehydrogenation of N-heterocycles [76] using Fe complexes bearing PNP pincer ligands that were previously reported by Beller [77], Schneider and Hazari [78], and Guan (Figure 9.20) [79]. Several substituted quinolines and other N-heterocycles can be dehydrogenated with varying yields by refluxing a xylene solution with 3 mol% catalyst for 30 h. Rehydrogenation can be achieved with moderate to high yields with the same
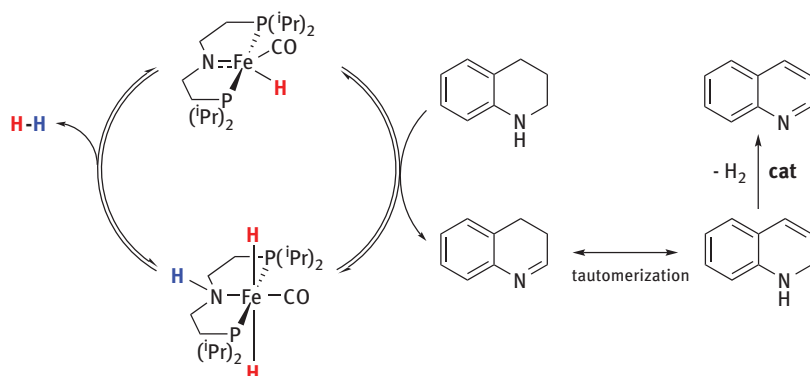
Figure 9.20: Catalytic hydrogenation and dehydrogenation of N-heterocycles by an Fe catalyst bearing a PNP pincer ligand.

catalyst loading in THF at 80 °C in the presence of 10 mol % potassium tertbutoxide. A pentacoordinated Fe-hydride was identified as the active intermediate for dehydrogenation catalysis, which was independently synthesized and found to be catalytic competent. The authors propose a trans-dihydride species Fe species to be the active catalyst for the hydrogenation catalysis based on NMR studies and trapping experiments. A recent mechanistic study showed that methylation of the nitrogen atom in the PNP ligand disables the catalytic activity for both hydrogenation and dehydrogenation, which is in agreement with the computational study that suggest a mechanism involving metal-ligand-cooperativity [80]. The computational study also showed that direct C-C bond dehydrogenation is not feasible, and thus dehydrogenation only occurs at the C-N bond with subsequent tautomerization. Substrates with relatively unpolarized C-N bonds were calculated to proceed through a concerted proton/hydride transfer transition state involving protonation at the N-atom of the PNP ligand. However, substrates with more polarized C-N bonds were found to proceed through a stepwise proton and then hydride transfer. These findings are in agreement with a computational study published at the same time by Sawatlon and Surawatanawong on both the hydrogenation and dehydrogenation of N-heterocycles by these Fe PNP pincer complexes [81].

A year later Jones et al. reported a structurally similar Co catalyst with a PNP pincer ligand (Figure 9.21) [82]. Dehydrogenation of the same N-heterocycles was
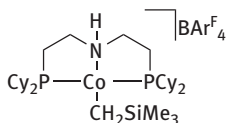
Figure 9.21: A Co catalyst bearing a PNP pincer ligand for the dehydrogenation of N-heterocycles.

observed with higher catalyst loading (10 mol%) and longer reaction times, although in better yields. Similarly, the rehydrogenation required higher temperature and catalyst loadings. Mechanistic studies indicate an initial amine dehydrogenation over alkane dehydrogenation. Interestingly, methylation at the N-atom of the PNP ligand inhibited the dehydrogenation but not the hydrogenation activity, suggesting a non-cooperative pathway for the latter.

Methods for the dehydrogenation of N-heterocycles without the need for metals were recently reported back to back by Kanai et al. [83]. and Grimme & Paradies et al. (Figure 9.22) [84]. Kanai et al. showed that showed that tris(pentafluorophenyl)borane could catalyze the acceptorless dehydrogenation of various N-heterocycles in p-xylene at 150 °C over 22 h. Grimme & Paradies et al. showed that the same Lewis acid could catalyze the acceptorless dehydrogenation of *N*-protected indoles in toluene at 120 °C. Mechanistic studies showed that the rate-determining step of the reaction was hydrogen liberation from the ammonium hydridoborate intermediate, which was also crystallographically characterized. Although these Lewis acids can facilitate the acceptorless dehydrogenation of N-heterocycles under similar conditions and catalyst loadings as the transition metal catalysts that are described above, they are unable to perform the reverse hydrogenation, and dehydrogenation of more challenging substrates with higher H_2 wt%.
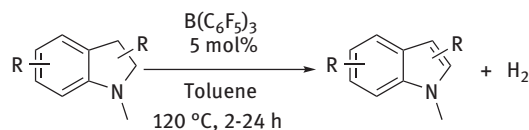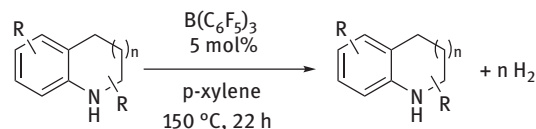
Figure 9.22: Catalytic acceptorless dehydrogenation of N-heterocycles by tris(pentafluorophenyl) borane.

The aforementioned systems based on noble and earth abundant metals all require high reaction temperatures and reaction times to facilitate the endothermic dehydrogenative reactions. Very recent studies show that the use of photocatalysts enables the catalytic dehydrogenation of N-heterocycles at ambient temperature [85]. An example – technically beyond the scope of this review as it relies on an external oxidant (O_2) – that set the stage for subsequent photocatalytic acceptorless dehydrogenation of N-heterocycles was reported by Badu-Tawiah et al. in 2016 (Figure 9.23). The authors build a picomole-scale, real-time photoreaction screening platform that couples a handheld laser source to a nano-electrospray ionization mass spectrometer, and found that photocatalysts can accelerate the dehydrogenation of tetrahydroquinolines [86]. They showed that a very common light harvesting complex, $Ru(bpy)_3Cl_2$ can perform this transformation in air at ambient temperature under direct sunlight or a common energy-saving lightbulb. In addition, the developed screening platform enabled the authors to follow the reaction in real time observing several intermediates. The proposed mechanism starts with excitation of $Ru(bpy)_3^{2+}$, which subsequently oxidizes the tetrahydroquinoline to the corresponding radical cation. The reduced $Ru(bpy)_3^+$ species is oxidized by O_2 to give to reform $Ru(bpy)_3^{2+}$, and the superoxide radical cation $O_2^{\bullet-}$. The latter is responsible for further oxidation of the tetrahydroquinoline radical cation to form the quinoline and two equivalents of H_2O_2.
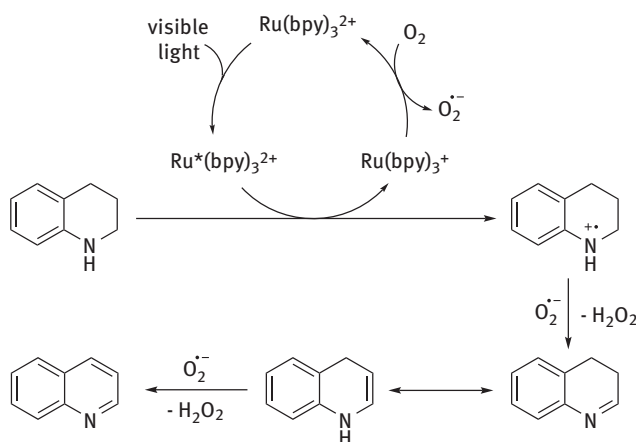
Figure 9.23: Proposed mechanism for the photocatalytic dehydrogenation of quinolines with oxygen as the oxidant.

Early in 2017, Li et al. reported the first acceptorless photocatalytic dehydrogenation of N-heterocycles through combining photoredox catalysis with a Co-based H_2 evolution catalyst (Figure 9.24) [87]. Over 40 different N-heterocyclic substrates were dehydrogenated in good to excellent yields by irradiation of ethanol solutions with
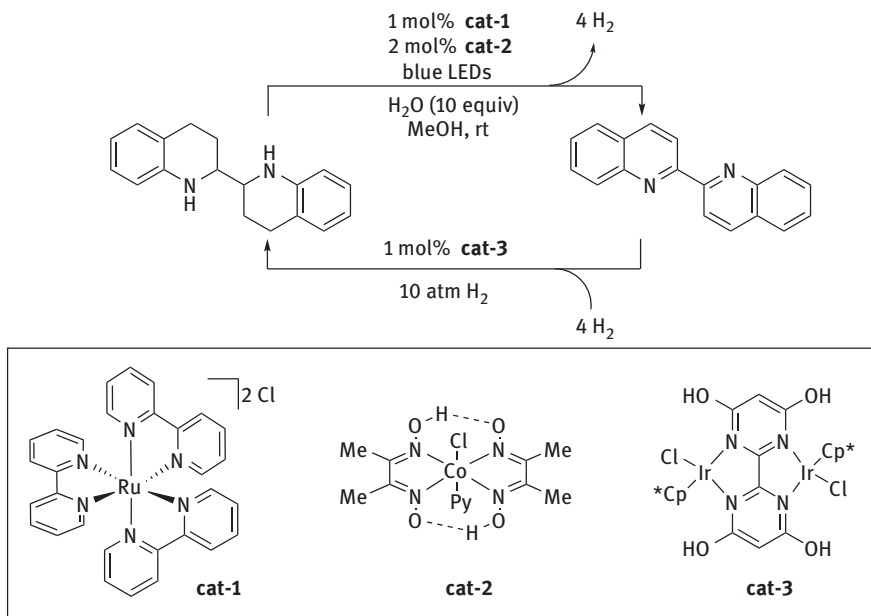
Figure 9.24: Acceptorless photocatalytic dehydrogenation of N-heterocycles through combining photoredox catalysis with a Co-based H_2 evolution catalyst, and the reverse hydrogenation using a dinuclear Cp*Ir catalyst.

blue LEDs for 6–24 h at ambient temperature in the presence of 1 mol% Ru(bpy)$_3$Cl$_2$× 6 H$_2$O and 2 mol% of a Co co-catalyst. No significant conversion was observed in the absence of either the photosensitizer, co-catalyst or irradiation. In contrast to most studies, the authors also quantified the yields of formed H$_2$, which were in line with the yields of the organic products. A substrate containing two tetrahydroquinolines was also dehydrogenated in 80 % yield under the same conditions, releasing four equivalents of H$_2$. Rehydrogenation of the corresponding quinolines was demonstrated using a 1 mol% of a dinuclear Ir catalyst under 10 atm of H$_2$ at room temperature in 85 % yield. Based on preliminary mechanistic investigations, a complicated mechanism is proposed involving several stepwise single-electron and proton transfer steps induced by excitation of the Ru(bpy)$_3$ photosensitizer. The Co-based catalyst is proposed to be responsible for the formation of H$_2$.

Around the same time Kanai et al. reported a different hybrid catalyst system for the photocatalytic dehydrogenation of benzofused saturated ring systems at ambient temperature (Figure 9.25) [88]. The combination of a acridinium photoredox catalyst with Pd (MeCN)$_4$(BF$_4$)$_2$ allowed for the acceptorless dehydrogenation of N-heterocycles at room temperature upon irradiation with visible light in moderate to excellent yield. The proposed mechanism starts with one-electron oxidation of the N-heterocycle followed by deprotonation to generate an aminyl radical species. The aminyl radical is intercepted
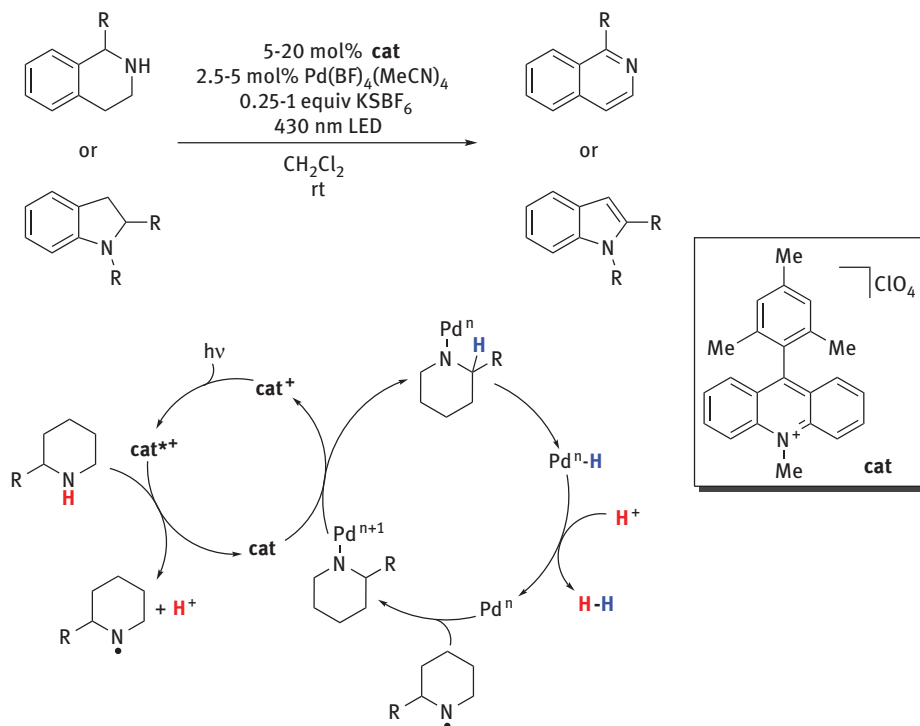
Figure 9.25: Photocatalytic dehydrogenation using an acridinium photoredox catalyst with a Pd (MeCN)$_4$(BF$_4$)$_2$ cocatalyst, and the proposed mechanism.

by a Pd complex to form a one-electron oxidized Pd amide complex. One-electron reduction of the metal amide, and β-hydrogen elimination gives the partially dehydrogenated N-heterocycle and a metal hydride species, which produces H$_2$ upon protonation. The presence of KSbF$_6$ as an additive was found to significantly accelerate the reaction but no explanation was proposed. An extraordinary feature is that upon the addition of an additional thiophosphoric imide organocatalyst tetrahydronaphtalenes could also be dehydrogenated. The proposed mechanism for this transformation, which proceeds at unusually low temperatures, involves single-electron transfer from the photoredox catalyst to the organocatalyst to generate a sulfur-centered radical that abstracts an H-atom from the benzylic position. This benzylic radical is subsequently trapped by a Pd complex and proceeds analogously as proposed for the N-heterocyclic substrates.

The examples described above show that acceptorless dehydrogenation of N-heterocycles has received significant attention in the last decade. Homogeneous catalysts enable the extraction of multiple molecules of H$_2$ from N-heterocyclic substrates with high selectivity and vice versa. Efforts toward using more abundant metals have been made but fall short in activity in comparison to their noble metal

counterparts. In addition, the need for high temperatures, solvents, additives and long reaction times are an issue that need to be resolved. The very recent efforts that use photocatalysts show promise for LOHCs that can operate at lower temperatures.

9.3 Conclusions

A great amount of progress in the development of transition metal-catalyzed acceptorless dehydrogenation of amines has been made in the last few decades. An overview of substrates, corresponding dehydrogenated products and relevant information discussed in this review is summarized in Figure 9.26. The selective dehydrogenation of primary amines is still challenging due to the many side reactions that occur due to the generation of highly electrophilic aldimines.
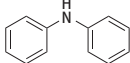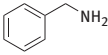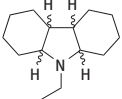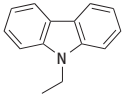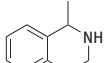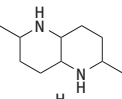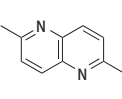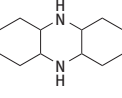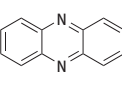
Substrate	Product	H₂ wt%	Reversibility	Notes	Reference
		6.1	✗	NH₃ also formed	34
		3.7	✓	homogeneous and immobilized examples	53-55
		5.8	✓	Robust heterogeneous catalyst	60-63
		3.0	✓	single catalyst for both directions	65,66,76, 80-83, 85,87
		2.7	✓	single catalyst for both directions	69,88
		5.9	✓	single catalyst for both directions	67
		5.3	✓	single catalyst for both directions	70
		1.5	✓	-	84,88
		7.2	✓	single catalyst for both directions	63

Figure 9.26: Overview of the substrates and corresponding dehydrogenated products with relevant information.

However, careful design of catalysts through ligand design can enable high selectivity as demonstrated by Scymczak and coworkers, which is interesting for both synthetic purposes as well as for the design of new LOHCs. The ability to selectively store and remove two equivalents of H_2 in a single C-N bond holds promise for achieving high gravimetric hydrogen content in LOHCs. To this end well-defined homogenous catalyst systems that use metal ligand cooperativity can make an impact. For synthetic purposes, selectivity is less of problem for N-heterocyclic systems, but overcoming the requirement of high reaction temperatures is still a challenge in acceptorless systems. The same challenge applies to hydrogen storage wherein long reaction times are also an issue. Perhaps, future approaches will take a bioinspired approach where amines are dehydrogenated through pathways that involve H-atom abstractions [89]. Recent studies that use hybrid catalyst systems and photocatalysis are promising in that respect. Efforts toward using catalysts systems based on base metals are being made but still fall short in activity and selectivity. However, the ever increasing interest in base metal catalysis will undoubtedly result in better systems based on these metals. Something that is rare to find in older work but more frequently investigated in recent studies is the quantification and analysis of the H_2 that is obtained from the LOHCs. Similarly, studies toward recyclability, necessity for solvents, and practicality of the LOHCs and catalyst systems are more common. The investigation and analysis of these aspects are of paramount importance toward the development of applicable systems for a future hydrogen economy.

References

[1]   (a) Liu ZY, Wang YM, Li ZR, Jiang JD, Boykin DW. Synthesis and anticancer activity of novel 3,4-diarylthiazol-2(3H)-ones (imines). Bioorg Med Chem Lett. 2009;19:5661–64; (b) Goetz AE, Garg NK. Regioselective reactions of 3,4-pyridynes enabled by the aryne distortion model. Nat Chem. 2013;5:54–60; (c) Fleming FF, Yao L, Ravikumar PC, Funk L, Shook BC. Nitrile-containing pharmaceuticals: efficacious roles of the nitrile pharmacophore. J Med Chem. 2010;53:7902–17.

[2]   (a) Luo S, Zhang E, Su Y, Cheng T, Shi C. A review of NIR dyes in cancer targeting and imaging. Biomaterials. 2011;32:7127–38; (b) Argazzi R, Iha NY, Zabri H, Odobel F, Bignozzi CA. Design of molecular dyes for application in photoelectrochemical and electrochromic devices based on nanocrystalline metal oxide semiconductors. Coord Chem Rev. 2004;248:1299–316;
(c) Forgacs E, Cserháti T, Oros G. Removal of synthetic dyes from wastewaters: a review. Environ Int 2004;30:953–71.

[3]   (a) Erkkilä A, Majander I, Pihko PM. Iminium catalysis. Chem Rev. 2007;107:5416–70;
(b) Mukherjee S, Yang JW, Hoffmann S, List B. Asymmetric enamine catalysis. Chem Rev. 2007;107:5471–5569.

[4]   (a) Layer RW. The chemistry of imines. Chem Rev. 1963;63:489–510; (b) Kobayashi S, Ishitani H. Catalytic enantioselective addition to imines. Chem. Rev. 1999;99:1069–94; (c) Kobayashi S, Mori Y, Fossey JS, Salter MM. Catalytic enantioselective addition to imines. Chem Rev. 2011;111:2626–2704; (d) Smith MB, March J. Advanced organic chemistry, 5th ed. New York: Wiley, 2001;1509–14.

[5]   (a) Chen B, Wang L, Gao S. Recent advances in aerobic oxidation of alcohols and amines to imines. ACS Catal. 2015;5:5851–76; (b) Murahashi SI, Zhang D. Ruthenium catalyzed biomimetic oxidation in organic synthesis inspired by cytochrome P-450. Chem Soc Rev. 2008;37:1490–501; (c) Modern oxidation methods. In: Backvall JE, editor, Weinheim: Wiley-VCH, 2004.

[6]   (a) Murahashi SI, Imada Y. In: Beller M, Bolm C, editors. Transition metals for organic synthesis. Weinheim: Wiley-VCH Verlag GmbH, 2008:497–507. Chapter 2.15; (b) Pinnick HW. In: Trost BM, Fleming I, Ley SV, editors. Oxidation: selectivity, strategy & efficiency in modern organic chemistry. Pergamon Press, 1992:218–32. Chapter 2.5; (c) Green G, Griffith WP, Hollinshead DM, Ley SV, Schroder M. Oxo complexes of ruthenium(VI) and (VII) as organic oxidants. J Chem Soc Perkin Trans. 1984;1:681–6.

[7]   (a) Gunanathan C, Milstein D. Applications of acceptorless dehydrogenation and related transformations in chemical synthesis. Science. 2013;341:1229712; (b) Dobereiner GE, Crabtree RH. Dehydrogenation as a substrate-activating strategy in homogeneous transition-metal catalysis. Chem Rev. 2010;110:681–703.

[8]   Sing S, Jain S, Venkateswaran PS, Tiwari AK, Nouni MR, Pandey JK, et al. Hydrogen: A sustainable fuel for future of the transport sector. Renew Sustain Energy Rev. 2015;51:623–33.

[9]   Ellabban O, Abur-Rub H, Blaabjerg F. Renewable energy resources: current status, future prospects and their enabling technology. Renew Sustain Energy Rev. 2014;39:748–64; (b) Balat M, Balat M. Political, economic and environmental impacts of biomass-based hydrogen. Int J Hydrog Energy. 2009;34:3589–603.

[10]   Ball M, Weeda M. The hydrogen economy – vision or reality? Int J Hydrog Energy. 2015;25:7903–19.

[11]   Preuster P, Papp C, Wasserscheid P. Liquid organic hydrogen carriers (LOHCs): toward a hydrogen-free hydrogen economy. Acc Chem Res. 2017;50:74–85.

[12]   Häussinger P, Lohmüller R, Watson AM. Hydrogen. Ullmann's encyclopedia of industrial chemistry. Weinheim, Germany: Wiley-VCH Verlag GmbH & Co. KGaA, 2000.

[13]   Cheng X, Shi Z, Glass N, Zhang L, Zhang J, Song D, et al. A review of PEM hydrogen fuel cell contamination: impacts, mechanisms, and mitigation J Power Sources. 2007;165:739–56.

[14]   (a) Crabtree RH. Homogeneous transition metal catalysis of acceptorless dehydrogenative alcohol oxidation: applications in hydrogen storage and to heterocycle synthesis. Chem Rev. 2017;117:9228–46; (b) Bonitatibus PJ, Jr., Chakraborty S, Doherty MD, Siclovan O, Jones WD, Soloveichik GL. Reversible catalytic dehydrogenation of alcohols for energy storage. Proc Natl Acad Sci USA. 2015;112:1687–92; (c) Johnson TC, Morris DJ, Wills M. Hydrogen generation from formic acid and alcohols using homogeneous catalysts. Chem Soc Rev. 2010;39:81–8.

[15]   (a) Hu P, Fogler E, Diskin-Posner Y, Iron MA, Milstein D. A novel liquid organic hydrogen carrier system based on catalytic peptide formation and hydrogenation. Nat Commun. 2015;6:6859–6859; (b) Hu P, Ben-David Y, Milstein D. Rechargeable hydrogen storage system based on the dehydrogenative coupling of ethylenediamine with ethanol. Angew Chem Int Ed. 2016;55:1061–4.

[16]   (a) Kim D, Park W, Jun C. Metal–organic cooperative catalysis in C–H and C–C bond activation. Chem Rev. 2017;117:8977–9015; (b) Khusnutdinova JR, Milstein D. Metal–ligand cooperation. Angew Chem Int Ed. 2015;54:12236–73; (c) van der Vlugt JI. Cooperative catalysis with first-row late transition metals. Eur J Inorg Chem. 2012;363–75.

[17] (a) Broere DL, Plessius R, van der Vlugt JI. New avenues for ligand-mediated processes – expanding metal reactivity by the use of redox-active catechol, o-aminophenol and o-phenylenediamine ligands. Chem Soc Rev. 2015;44:6886–915; (b) Luca OR, Crabtree RH. Redox-active ligands in catalysis. Chem Soc Rev. 2013;42:1440–1459; (c) Praneeth VK, Ringenberg MR, Ward TR. Redox-active ligands in catalysis. Angew Chem Int Ed. 2012;51:10228–10234; (d) Lyaskovskyy V, de Bruin B. Redox non-innocent ligands: versatile new tools to control catalytic reactions. ACS Catal. 2012;2:270–279; (e) Kaim W. Manifestations of noninnocent ligand behavior. Inorg Chem. 2011;50:9752–9765; (f) Chirik PJ, Wieghardt K. Radical ligands confer nobility on base-metal catalysts. Science 2010;327:794–795.

[18] (a) Schiff H. Mittheilungen aus dem Universitäts-laboratorium in Pisa: 2. Eine neue Reihe organischer Basen. Annals. 1864;131:118–19; (b) Moffett RB. In: N. Rabjohn, editor. Organic syntheses, Coll. Vol. 4, New York: Wiley, 1963:605–8.

[19] (a) Hateley MJ, Schidl DA, Kreuzfeld HJ, Beller M. Rhodium-catalysed racemisation of N-acyl α-amino acids. Tetrahedron Lett. 2000;41:3821–24; (b) Hateley MJ, Schichl DA, Fischer C, Beller M. An improved procedure for the mild racemization of N-Acyl α-amino acids. Synlett. 2001;1:25–8; (c) Pàmies O, Éll AH, Samec JMS, Hermanns N, Bäckvall JE. An efficient and mild ruthenium-catalyzed racemization of amines: application to the synthesis of enantiomerically pure amines. Tetrahedron Lett. 2002;43:4699–702.

[20] Blum Y, Czarkie D, Rahamim Y, Shvo Y. (Cyclopentadienone) ruthenium carbonyl complexes-a new class of homogeneous hydrogenation catalysts. Organometallics. 1985;4:1459–61.

[21] Casey CP, Johnson JB. Isomerization and deuterium scrambling evidence for a change in the rate-limiting step during imine hydrogenation by Shvo's hydroxycyclopentadienyl ruthenium hydride. J Am Chem Soc. 2005;127:1883–94.

[22] Samec JS, Ell AH, Backvall JE. Efficient ruthenium-catalyzed aerobic oxidation of amines by using a biomimetic coupled catalytic system. Chem Eur J. 2005;11:2327–34.

[23] a) Gupta M, Hagen C, Kaska WC, Flesher R, Jensen CM. A highly active alkane dehydrogenation catalyst: stabilization of dihydrido rhodium and iridium complexes by a P–C–P pincer ligand. J Chem Soc Chem Commun. 1996:2083–84; b) Xu W, Rosini GP, Gupta M, Jensen CM, Kaska WC, Krough-Jespersen K, Goldman AS. Thermochemical alkane dehydrogenation catalyzed in solution without the use of a hydrogen acceptor. J Chem Soc, Chem Commun. 1997:2273–4; c) Gupta M, Hagen C, Kaska WC, Cramer R, Jensen CM. Catalytic dehydrogenation of cycloalkanes to arenes by a dihydrido iridium P– C– P pincer complex. J Am Chem Soc. 1997;119:840–1; d) Liu F, Pak EB, Singh B, Jensen CM, Goldman AS. Dehydrogenation of n-Alkanes Catalyzed by Iridium "Pincer" Complexes: Regioselective Formation of α-Olefins. J Am Chem Soc 1999;121:4086–7.

[24] Gu XQ, Chen W, Morales-Morales D, Jensen CM. Dehydrogenation of secondary amines to imines catalyzed by an iridium PCP pincer complex: initial aliphatic or direct amino dehydrogenation? J Mol Catal A Chem. 2002;189:119–24.

[25] Zhang X, Fried A, Knapp S, Goldman AS. Novel synthesis of enamines by iridium-catalyzed dehydrogenation of tertiary amines. Chem Commun. 2003;2060–61.

[26] Yi CS, Lee DW. Efficient dehydrogenation of amines and carbonyl compounds catalyzed by a tetranuclear ruthenium-μ-oxo-μ-hydroxo-hydride complex. Organometallics. 2009;28:947–49.

[27] Bähn S, Imm S, Neubert L, Zhang M, Neumann H, Beller M. Synthesis of primary amines from secondary and tertiary amines: ruthenium-catalyzed amination using ammonia. Chem Eur J. 2011;17:4705–08.

[28] For reviews about borrowing hydrogen methodology, see: a) Dobereiner GE, Crabtree RH. Dehydrogenation as a substrate-activating strategy in homogeneous transition-metal catalysis. Chem Rev. 2010;110:681–703; b) Nixon TD, Whittlesey MK, Williams JMJ. Transition metal

catalysed reactions of alcohols using borrowing hydrogen methodology. Dalton Trans. 2009:753–62; c) Lamb GW, Williams JMJ. Borrowing hydrogen-CN bond formation from alcohols. Chim Oggi. 2008;26:17–19; d) Hamid MHSA, Slatford PA, Williams JMJ. Borrowing hydrogen in the activation of alcohols. Adv Synth Catal. 2007;349:1555–75.

[29] Pingen D, Altıntas C, Schaller MR, Vogt D. A ruthenium racemisation catalyst for the synthesis of primary amines from secondary amines. Dalton Trans. 2016;45:11765–71.

[30] Valencia M, Pereira A, Müller-Bunz H, Belderraín TR, Pérez PJ, Albrecht M. Triazolylidene-iridium complexes with a pendant pyridyl group for cooperative metal–ligand induced catalytic dehydrogenation of amines. Chem Eur J. 2017;23:8901–11.

[31] Stubbs JM, Hazlehurst RJ, Boyle PD, Blacquiere JM. Catalytic acceptorless dehydrogenation of amines with Ru(PR2NR′2) and Ru(dppp) complexes. Organometallics. 2017;36:1692–98.

[32] a) Bullock RM, Helm ML. Molecular electrocatalysts for oxidation of hydrogen using earth-abundant metals: shoving protons around with proton relays. Acc Chem Res. 2015;48:2017–26; b) Bullock RM, Appel AM, Helm ML. Production of hydrogen by electrocatalysis: making the H–H bond by combining protons and hydrides. Chem Commun. 2014;50:3125–43; c) Liu T, DuBois MR, DuBois DL, Bullock RM. Electrochemical oxidation of H_2 catalyzed by ruthenium hydride complexes bearing P2N2 ligands with pendant amines as proton relays. Energy Environ Sci. 2014;7:3630–9.

[33] Ho HA, Manna K, Sadow AD. Acceptorless photocatalytic dehydrogenation for alcohol decarbonylation and imine synthesis. Angew Chem Int Ed. 2012;51:8607–10.

[34] Taniguchi K, Jin X, Yamaguchi K, Nozaki K, Mizuno N. Versatile routes for synthesis of diarylamines through acceptorless dehydrogenative aromatization catalysis over supported gold–palladium bimetallic nanoparticles. Chem Sci. 2017;8:2131–42.

[35] Fleming FF. Nitrile-containing natural products. Nat Prod Rep. 1999;16:597–606.

[36] Fleming FF, Yao L, Ravikumar PC, Funk L, Shook BC. Nitrile-containing pharmaceuticals: efficacious roles of the nitrile pharmacophore. J Med Chem. 2010;53:7902–17.

[37] Pollak P, Romeder G, Hagedorn F, Gelbke HP. Nitriles. In: Elvers B, Hawkins S, Schulz G, editors. Ullmann's encyclopedia of industrial chemistry. Weinheim, Germany: Wiley-VCH; 2012.

[38] Mowry DT. The preparation of nitriles. Chem Rev. 1948;42:189–283.

[39] a) Nicolaou KC, Mathison CJ. Synthesis of imides, N-Acyl vinylogous carbamates and ureas, and nitriles by oxidation of amides and amines with dess-martin periodinane. Angew Chem Int Ed. 2005;44:5992–97; b) Müller P, Gilabert DM. Oxidation of amines to imines with hypervalent iodine. Tetrahedron 1988;44:7171–5.

[40] Aschwanden L, Mallat T, Maciejewski M, Krumeich F, Baiker A. Development of a new generation of gold catalysts for amine oxidation. Chem Cat Chem. 2010;2:666–73.

[41] a) Tang R, Diamond SE, Neary N, Mares F. Homogeneous catalytic oxidation of amines and secondary alcohols by molecular oxygen. J Chem Soc Chem Commun. 1978;13:562–562; b) Yamaguchi K, Mizuno N. Efficient heterogeneous aerobic oxidation of amines by a supported ruthenium catalyst. Angew Chem Int Ed. 2003;42:1480–83.

[42] Hammond C, SchüMperli MT, Hermans I. Insights into the oxidative dehydrogenation of amines with nanoparticulate iridium oxide. Chem Eur J. 2013;19:13193–98.

[43] Schü Mperli MT, Hammond C, Hermans I. Developments in the aerobic oxidation of amines. ACS Catal. 2012;2:1108–17.

[44] Griffth WP, Reddy B, Shoair AG, Suriaatmaja M, White AJ, Williams DJ. Ruthenate(VI)-catalysed dehydrogenation of primary amines to nitriles, and crystal structures of cis-[Ru(bipy)$_2$(NH$_2$CH$_2$Ph)$_2$][PF$_6$]$_2$·0.5MeOH and cis-[Ru(bipy)$_2$(NCPh)$_2$][PF$_6$]$_2$·CH$_2$Cl$_2$. Dalton Trans. 1998;2819–25.

[45] Yamazaki S, Yamazaki Y. Nickel-catalyzed dehydrogenation of amines to nitriles. Bull Chem Soc Jpn. 1990;63:301–03.

[46] Bernskoetter WH, Brookhart M. Kinetics and mechanism of iridium-catalyzed dehydrogenation of primary amines to nitriles. Organometallics. 2008;27:2036–45.

[47] Grellier M, Sabo-Etienne S. New perspectives in hydrogen storage based on RCH 2 NH 2/RCN couples. Dalton Trans. 2014;43:6283–86.

[48] Bagal DB, Bhanage BM. Recent advances in transition metal-catalyzed hydrogenation of nitriles. Adv Synth Catal. 2015;357:883–900.

[49] Recent examples using base metal catalysts: a) Bornschein C, Werkmeister S, Wendt B, Jiao H, Alberico E, Baumann W, et al. Mild and selective hydrogenation of aromatic and aliphatic (di) nitriles with a well-defined iron pincer complex. Nat Commun. 2014;5:4111; b) Mukherjee A, Srimani D, Chakraborty S, Ben-David Y, Milstein D. Selective hydrogenation of nitriles to primary amines catalyzed by a cobalt pincer complex. J Am Chem Soc. 2015;137:8888–91; c) Elangovan S, Topf C, Fischer S, Jiao H, Spannenberg A, Baumann W, Ludwig R, Junge K, Beller M. Selective Catalytic Hydrogenations of Nitriles, Ketones, and Aldehydes by Well-Defined Manganese Pincer Complexes. J Am Chem Soc. 2016;138:8809–14.

[50] Wang Z, Belli J, Jensen CM. Homogeneous dehydrogenation of liquid organic hydrogen carriers catalyzed by an iridium PCP complex. Faraday Discuss. 2011;151:297–305.

[51] Li T, Bergner I, Haque FN, Zimmer-De Luliis M, Song D, Morris RH. Hydrogenation of benzonitrile to benzylamine catalyzed by ruthenium hydride complexes with P–NH–NH–P tetradentate ligands: evidence for a hydridic–protonic outer sphere mechanism. Organometallics. 2007;26:5940–49.

[52] Tseng KN, Rizzi AM, Szymczak NK. Oxidant-free conversion of primary amines to nitriles. J Am Chem Soc. 2013;135:16352–55.

[53] Hale LV, Malakar T, Tseng KN, Zimmerman PM, Paul A, Szymczak NK. The mechanism of acceptorless amine double dehydrogenation by N,N,N-amide ruthenium(II) hydrides: a combined experimental and computational study. ACS Catal. 2016;6:4799–813.

[54] Conley BL, Pennington-Boggio MK, Boz E, Williams TJ. Discovery, applications, and catalytic mechanisms of Shvo's catalyst. Chem Rev. 2010;110:2294–312.

[55] Ventura-Espinosa D, Marzá-Beltrán A, Mata JA. Catalytic hydrogen production by ruthenium complexes from the conversion of primary amines to nitriles: potential application as a liquid organic hydrogen carrier. Chem Eur J. 2016;22:17758–66.

[56] Giustra ZX, Ishibashi JS, Liu SY. Homogeneous metal catalysis for conversion between aromatic and saturated compounds. Coord Chem Rev. 2016;314:134–81.

[57] He T, Pei Q, Chen P. Liquid organic hydrogen carriers. J Energ Chem. 2015;24:587–94.

[58] Crabtree RH. Nitrogen-containing liquid organic hydrogen carriers: progress and prospects. ACS Sustainable Chem Eng. 2017;5:4491–98.

[59] Clot E, Eisenstein O, Crabtree RH. Computational structure–activity relationships in H 2 storage: how placement of N atoms affects release temperatures in organic liquid storage materials. Chem Commun. 2007;2231–33.

[60] Pez GP, Scott AR, Cooper AC, Cheng H, Wilhelm FC, Abdourazak AH Hydrogen storage by reversible hydrogenation of piconjugated substrates. U.S. Patent 7351395B1, April 1, 2008; Pez GP, Scott AR, Cooper AC, Cheng H, Bagzis L, Appleby J. Hydrogen storage. Reversible hydrogenated of π-conjugated substrates. International patent WO 2005/000457, 2005; Pez GP, Scott AR, Cooper AC, Cheng H. Hydrogen storage by reversible hydrogenation of pi-conjugated substrates. European Patent 1475349A2, 2004.

[61] Amende M, Schernich S, Sobota M, Nikiforidis I, Hieringer W, Assenbaum D, et al. Dehydrogenation mechanism of liquid organic hydrogen carriers: dodecahydro-N-ethylcarbazole on Pd (111). Chem Eur J. 2013;19:10854–65.

[62] Amende M, Gleichweit C, Werner K, Schernich S, Zhao W, Lorenz MP, et al. Model catalytic studies of liquid organic hydrogen carriers: dehydrogenation and decomposition mechanisms of dodecahydro-N-ethylcarbazole on Pt(111). ACS Catal. 2014;4:657–65.

[63] Forberg D, Schwob T, Zaheer M, Friedrich M, Miyajima N, Kempe R. Single-catalyst high-weight% hydrogen storage in an N-heterocycle synthesized from lignin hydrogenolysis products and ammonia. Nat Commun. 2016;7:13201–13201.

[64] Vispute TP, Zhang H, Sanna A, Xiao R, Huber GW. Renewable chemical commodity feedstocks from integrated catalytic processing of pyrolysis oils. Science. 2010;330:1222–27.

[65] Yamaguchi R, Ikeda C, Takahashi Y, Fujita K. Homogeneous catalytic system for reversible dehydrogenation– hydrogenation reactions of nitrogen heterocycles with reversible intercon-version of catalytic species. J Am Chem Soc. 2009;131:8410–12.

[66] Zhang XB, Xi Z. A theoretical study of the mechanism for the homogeneous catalytic reversible dehydrogenation – hydrogenation of nitrogen heterocycles. Phys Chem Chem Phys. 2011;13:3997–4004.

[67] Fujita K, Tanaka Y, Kobayashi M, Yamaguchi R. Homogeneous perdehydrogenation and per-hydrogenation of fused bicyclic N-heterocycles catalyzed by iridium complexes bearing a functional bipyridonate ligand. J Am Chem Soc. 2014;136:4829–32.

[68] Manas MG, Sharninghausen LS, Lin E, Crabtree RH. Iridium catalyzed reversible dehydro-genation–hydrogenation of quinoline derivatives under mild conditions. J Organomet Chem. 2015;792:184–89.

[69] Wu J, Talwar D, Johnston S, Yan M, Xiao J. Acceptorless dehydrogenation of nitrogen heterocycles with a versatile iridium catalyst. Angew Chem Int Ed. 2013;52:6983–87.

[70] Wu J, Barnard JH, Zhang Y, Talwar D, Robertson CM, Xiao J. Robust cyclometallated Ir (III) catalysts for the homogeneous hydrogenation of N-heterocycles under mild conditions. Chem Commun. 2013;49:7052–54.

[71] Drover MW, Schafer LL, Love JA. Dehydrogenation of cyclic amines by a coordinatively unsaturated Cp* Ir (III) phosphoramidate complex. Dalton Trans. 2017;46:8621–25.

[72] Fujita K, Wada T, Shiraishi T. Reversible interconversion between 2,5-dimethylpyrazine and 2,5-dimethylpiperazine by iridium-catalyzed hydrogenation/dehydrogenation for efficient hydro-gen storage. Angew Chem Int Ed. 2017;56:10886–89.

[73] Muthaiah S, Hong SH. Acceptorless and base-free dehydrogenation of alcohols and amines using ruthenium-hydride complexes. Adv Synth Catal. 2012;354:3045–53.

[74] Luca OR, Huang DL, Takase MK, Crabtree RH. Redox-active cyclopentadienyl Ni complexes with quinoid N-heterocyclic carbene ligands for the electrocatalytic hydrogen release from chemical fuels. New J Chem. 2013;37:3402–05.

[75] Luca OR, Want T, Konezny SJ, Batista VS, Crabtree RH. DDQ as an electrocatalyst for amine dehydrogenation, a model system for virtual hydrogen storage. New J Chem. 2011;35:998–99.

[76] Chakraborty S, Brennessel WW, Jones WD. A molecular iron catalyst for the acceptorless dehydrogenation and hydrogenation of N-heterocycles. J Am Chem Soc. 2014;136:8564–67.

[77] Alberico E, Sponholz P, Cordes C, Nielsen M, Drexler HJ, Baumann W, et al. Selective hydrogen production from methanol with a defined iron pincer catalyst under mild conditions. Angew Chem Int Ed. 2013;52:14162–66.

[78] Koehne I, Schmeier TJ, Bielinski EA, Pan JC, Lagaditis PO, Bernskoetter WH, et al. Synthesis and structure of six-coordinate iron borohydride complexes supported by PNP ligands. Inorg Chem. 2014;53:2133–43.

[79] Chakraborty S, Dai H, Bhattacharya P, Fairweather NT, Gibson MS, Krause JA, et al. Iron-based catalysts for the hydrogenation of esters to alcohols. J Am Chem Soc. 2014;136:7869–72.

[80] Bellows SM, Chakraborty S, Gary JB, Jones WD, Cundari TR. An uncanny dehydrogenation mechanism: polar bond control over stepwise or concerted transition states. Inorg Chem. 2017;56:5519–24.

[81] Sawatlon B, Surawatanawong P. Mechanisms for dehydrogenation and hydrogenation of N-heterocycles using PNP-pincer-supported iron catalysts: a density functional study. Dalton Trans. 2016;45:14965–78.

[82] Xu R, Chakraborty S, Yuan H, Jones WD. Acceptorless, reversible dehydrogenation and hydrogenation of N-heterocycles with a cobalt pincer catalyst. ACS Catal. 2015;5:6350–54.

[83] Kojima M, Kanai M. Tris (pentafluorophenyl) borane-catalyzed acceptorless dehydrogenation of N-heterocycles. Angew Chem Int Ed. 2016;55:12224–27.

[84] Maier AF, Tussing S, Schneider T, Flörke U, Qu ZW, Grimme S, et al. Frustrated lewis pair catalyzed dehydrogenative oxidation of indolines and other heterocycles. Angew Chem Int Ed. 2016;55:12219–23.

[85] Yin Q, Oestreich M. Photocatalysis enabling acceptorless dehydrogenation of benzofused saturated rings at room temperature. Angew Chem Int Ed. 2017;56:7716–18.

[86] Chen S, Wan Q, Badu-Tawiah AK. Picomole-scale real-time photoreaction screening: discovery of the visible-light-promoted dehydrogenation of tetrahydroquinolines under ambient conditions. Angew Chem. 2016;128:9491–95.

[87] He KH, Tan FF, Zhou CZ, Zhou GJ, Yang XL, Li Y. Acceptorless dehydrogenation of n-heterocycles by merging visible-light photoredox catalysis and cobalt catalysis. Angew Chem Int Ed. 2017;56:3080–84.

[88] Kato S, Saga Y, Kojima M, Fuse H, Matsunaga S, Fukatsu A, et al. Hybrid catalysis enabling room-temperature hydrogen gas release from n-heterocycles and tetrahydronaphthalenes. J Am Chem Soc. 2017;139:2204–07.

[89] a) Wang X, Zhu W, Liu Y. Tryptophan lyase (NosL): mechanistic insights into amine dehydrogenation and carboxyl fragment migration by QM/MM calculations. Catal Sci Technol. 2017;7:2846–56; b) Ji X, Liu W-Q, Yuan S, Yin Y, Ding W, Zhang Q. Mechanistic study of the radical SAM-dependent amine dehydrogenation reactions. Chem. Commun. 2016;52:10555–8.

Zhuofeng Ke, Yinwu Li, Cheng Hou and Yan Liu

10 Homogeneously catalyzed hydrogenation and dehydrogenation reactions – From a mechanistic point of view

Abstract: Homogeneously catalyzed hydrogenation/dehydrogenation reactions represent not only one of the most synthetically important chemical transformations, but also a promising way to renewably utilize the hydrogen energy. In order to rationally design efficient homogeneous catalysts for hydrogenations/dehydrogenations, it is of fundamental importance to understand their reaction mechanisms in detail. With this aim in mind, we herein provide a brief overview of the mechanistic understanding and related catalyst design strategies. Hydrogenations and dehydrogenations represent the reverse process of each other, and involve the activation/release of H_2 and the insertion/elimination of hydride as major steps. The mechanisms discussed in this chapter include the cooperation (bifunctional) mechanism and the non-cooperation mechanisms. Non-cooperation mechanisms usually involve single-site transition metal (TM) catalysts or transition metal hydride (TM-H) catalysts. Cooperation mechanisms usually operate in the state-of-the-art bifunctional catalysts, including Lewis-base/transition-metal (LB-TM) catalysts, Lewis-acid/transition-metal (LA-TM) catalysts, Lewis-acid/Lewis-base (LA-LB; the so-called frustrated Lewis pairs - FLPs) catalysts, newly developed ambiphilic catalysts, and bimetallic transition-metal/transition-metal (TM-TM) catalysts. The influence of the ligands, the electronic structure of the metal, and proton shuttle on the reaction mechanism are also discussed to improve the understanding of the factors that can govern mechanistic preferences. The content presented in this chapter should both inspire experimental and theoretical chemists concerned with homogeneously catalyzed hydrogenation and dehydrogenation reactions, and provide valuable information for future catalyst design.

Keywords: hydrogenation, dehydrogenation, mechanism, metal ligand cooperation, transition metal, Lewis acid, Lewis base, Frustrated Lewis pairs, ambiphilic, bimetallic

---

10.1 Introduction

Homogeneously catalyzed hydrogenation and dehydrogenation are widely used for the storage of H_2 in organic unsaturated compounds and the release of H_2 from saturated compounds, respectively. Homogeneously catalyzed hydrogenations/dehydrogenations, as powerful chemical transformations in chemical synthesis, arguably present the most extensively studied field in homogeneous catalysis [1]. The first examples can be traced back to 1938, when Calvin reported the homogeneous hydrogenations using transition metal (TM) compounds [2]. Subsequently, the reports on the ability of Wilkinson's catalyst to accomplish hydrogenations at room temperature under atmospheric pressures of H_2 led to the first period of prosperity for homogeneously catalyzed hydrogenations [3]. In order to increase the practical utility of hydrogenation methods, asymmetric hydrogenations were developed [4], and their significance was recognized with the award of the 2001 Nobel Prize in Chemistry to Ryoji Noyori for contributions to industrially relevant homogeneous catalysis. The remarkable progress during the past few decades has provided detailed information on key intermediates and the mechanisms underpinning homogeneously catalyzed hydrogenations and dehydrogenations. It is worth noting that the concept of bifunctional metal ligand cooperation (MLC) catalysis introduced by Noyori in the 2000s, has profoundly enriched the understanding of the mechanisms operative in homogeneously catalyzed hydrogenations [5].

Recently, catalyzed hydrogenations and dehydrogenations have experienced a renaissance, not least in part due to the global energy and environmental crisis that humanity currently faces [6]. In order to replace traditionally used fossil energy, the quest for sources of clean and sustainable energy is of the utmost importance. With its high energy capacity and nonpolluting character, hydrogen represents a promising prospective to solve this energy/environmental problem [7]. Traditional hydrogen-storage methods based on physical adsorption usually require harsh conditions and are still unable to completely tame the risk of explosion. Homogenous catalytic hydrogenations/dehydrogenations offer an attractive chemical alternative to the physical storage of H_2 [8]. Using homogenous catalysts, the energy inherent to H_2 can be stored and released from relatively small organic compounds (chemical fuels) via chemical bonds, which provides a safe method for the transportation and utilization of hydrogen energy.

Current state-of-the-art homogeneous hydrogenation/dehydrogenation catalysts have developed from non-cooperation TM systems to MLC systems. Besides traditional TM catalysts and transition metal hydride (TM-H) catalysts, Lewis base/transition metal (LB-TM) catalysts, and Lewis acid/transition metal (LA-TM) catalysts have been designed and employed for cooperatively catalyzed hydrogenations/dehydrogenations (Figure 10.1). Moreover, environmentally benign metal-free bifunctional catalysts, such as Lewis acid/Lewis base (LA-LB, so-called frustrated Lewis pairs – FLPs) catalysts and ambiphilic catalysts have emerged in the context of cooperative hydrogenations/dehydrogenations. In addition, the cooperation of TMs has also been reported for dimetallic hydrogenation/dehydrogenation catalysts. Since many

Non-cooperation types:

Cooperation (bifunctional) types:

L——M

TM cat.

LB⌣M

LB-TM cat.

LA⌣M

LA-TM cat.

L——M——H

TM hydride cat.

LA⌣LB

LA-LB (FLP) cat.

B⌣B

ambiphilic cat.

M⌣M

TM-TM cat.
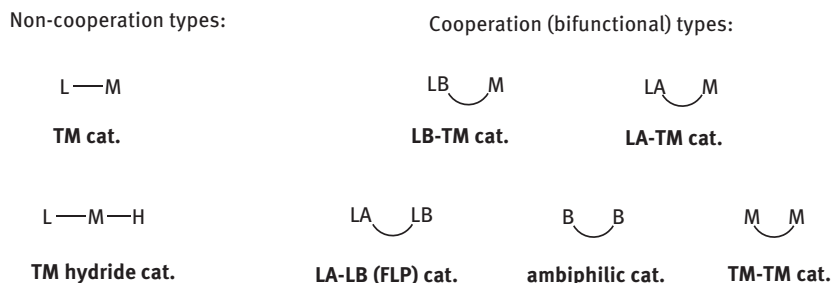
M = transition metals

Figure 10.1: Homogeneous non-cooperation and cooperation hydrogenation/dehydrogenation catalysts.

innovative strategies and mechanisms for catalytic hydrogenations have emerged, many of which are very different from the general understanding of several decades ago, a mechanistic overview of homogeneously catalyzed hydrogenations/dehydrogenations should be highly desirable.

The aim of this chapter is to discuss the current frontiers of the understanding of the cooperation mechanism in homogeneously catalyzed hydrogenations/dehydrogenations. For chronological purposes, we will begin with the traditional non-cooperation mechanism in TM systems, before we will focus our attention on cooperation mechanism in bifunctional systems, which should be inspiring for the catalysts design based on cooperative strategies. The mechanisms discussed in this chapter should be easily extended to the transfer hydrogenations/dehydrogenations, and dehydrogenations with hydrogen acceptors. With respect to asymmetric hydrogenations that are widely applied in organic synthesis, it should also be straightforward to understand the origin of the enantioselectivity based on the mechanistic diagrams presented in this chapter.

The general mechanism for homogeneously catalyzed hydrogen storage/production via hydrogenation/dehydrogenation is shown in Figure 10.2. Hydrogenation and dehydrogenation are reverse processes relative to each other. Hydrogenations involve the activation of H_2 and hydride insertion(s) into unsaturated compounds. Reversely, dehydrogenations involve the elimination of hydride(s) from saturated compounds

hydrogenation (hydrogen storage)

H_2 activation   **hydride insertion**

H_2 ⇌ *hydride(s) intermediate* ⇌ *saturated compound*
   Cat.   *unsaturated compound* / **Cat.**

H_2 release   **hydride elimination**

dehydrogenation (hydrogen production)
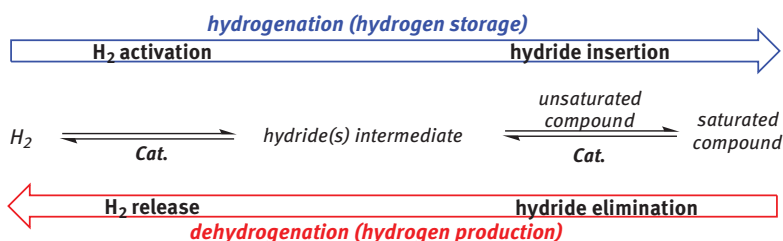
Figure 10.2: Homogeneously catalyzed storage (hydrogenation) and release (dehydrogenation) of H_2.

and subsequently release of H_2. Mechanistically speaking, the activation/release of H_2 and the insertion/elimination of hydride(s) are the two principal steps of these catalytic cycles, and both are tightly correlated. For the convenience of discussion, reaction mechanism(s) underpinning homogenously catalyzed hydrogenations/dehydrogenations can be classified according to the H_2 activation/release step. As summarized in Figure 10.3, homogeneous catalysts for hydrogenations/dehydrogenations include the traditional non-cooperation-type TM and TM-H catalysts, as well as the novel cooperation-type catalysts. Single-site TM catalysts usually operate via non-cooperation mechanisms that include the classical oxidative addition/reductive elimination mechanism, or the σ-bond metathesis (hydrogenolysis mechanism, as shown in Figure 10.3a (*cf.* Section 10.2). Cooperation-type catalysts usually contain two reactive sites for bifunctional catalysis. The cooperation mechanisms for LB-TM bifunctional catalysts are summarized in Figure 10.3b (*cf.* Section 10.3), the cooperation mechanisms for LA-TM bifunctional catalysts in Figure 10.3c (*cf.* Section 10.4), the LA-LB cooperation in metal-free FLP systems in Figure 10.3d (*cf.* Section 10.5), the ambiphilic cooperation mechanism for ambiphilic catalysts in Figure 10.3e (*cf.* Section 10.6), and the TM-TM cooperation mechanisms in Figure 10.3f (*cf.* Section 10.7). Furthermore, key factors governing the mechanistic preference will be discussed, including the role of the ligand, the electronic structure of the metal center, and the effect of proton shuttle.

10.2 Non-cooperation mechanisms

10.2.1 Oxidative addition/reductive elimination mechanism

Non-cooperation mechanisms for single-site TM catalysts include the classical oxidative addition/reductive elimination mechanism and the σ-bond metathesis (hydrogenolysis) mechanism (Figure 10.3a). The classical oxidation addition/ reductive elimination mechanism is depicted in Figure 10.4, using Wilkinson's catalyst $[(PPh_3)_3RhCl]$ as an example. The catalytic cycle starts with the coordination of H_2 to afford a typical dihydrogen complex, which quickly undergoes the oxidative addition to form a dihydride intermediate. Then, the substrate coordinates to the metal center for the subsequent hydride insertion. Finally, the reductive elimination furnishes the hydrogenated product under concomitant regeneration of the catalyst.

The σ→d donation and the d→σ* back-donation in the dihydrogen complex act as the driving force for the activation of H_2 in the catalytic cycle (Figure 10.5). The back-donation effect participates in two important steps in the catalytic cycle: (i) the d→σ* back-donation lowers the H-H bond order and thus facilitates the oxidation addition; (ii), the d→π* back-donation from the TM to the C = C double bond drives the hydride insertion. This mechanistic considerations thus impose two crucial prerequisites on the catalyst [9]: (i) the catalyst usually contains an electron-rich metal center, which

(a) Non-Cooperation

oxidative addition/reductive elimination

TM catalysts

σ-bond metathesis

TM-hyride catalysts

(b) LB-TM Cooperation

n-type MLC
M-L bond

n-type MLC
dissociative/pendant

non MLC
ligand innocent

n-type MLC
external LB

+ H₂

LB-TM catalysts

π type MLC
tautomerization
(de)aromatization

σ-type
synergetic MLC

(c) LA-TM Cooperation

p-type MLC
M-L bond

p-type MLC
dissociative/pendant

non MLC
ligand innocent

p-type MLC
external LA

+ H₂

LA-TM catalysts

π∗-type MLC
tautomerization
(de)aromatization

σ-type
synergetic MLC

(d) LA-LB (FLP) Cooperation

intramolecular
synergetic mechanism

intermolecular
synergetic mechanism

+ H₂

FLP catalysts

eletric field
mechanism

(e) Ambiphilic Cooperation

homolytic
mechanism

ambiphilic catalysts

heterolytic
mechanism

homolytic
mechanism

ambiphilic catalysts

heterolytic
mechanism

(f) TM-TM Cooperation

homolytic mechanism

heterolytic mechanism

+ H₂

TM-TM catalysts

oxidative addition

Figure 10.3: Mechanistic classification of homogeneously catalyzed hydrogenations/dehydro-genations according to the nature of the H_2 activation/release step: (a) non-cooperation mechanism (*cf*. Section 10.2); (b) LB-TM cooperation mechanism (*cf*. Section 10.3); (c) LA-TM cooperation mechanism (*cf*. Section 10.4); (d) LA-LB cooperation mechanism (*cf*. Section 10.5); (e) ambiphilic mechanism (*cf*. Section 10.6); (f) TM-TM cooperation mechanism (*cf*. Section 10.7).
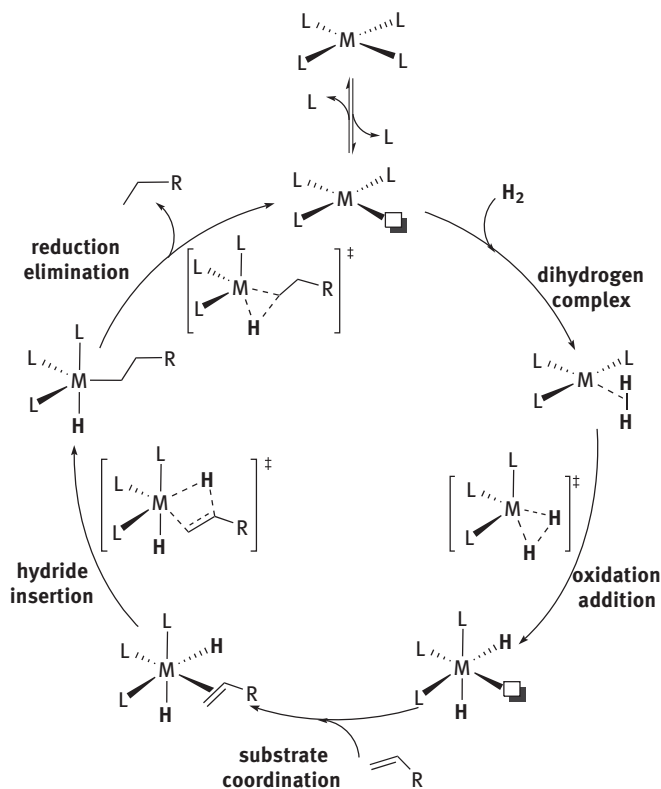
Figure 10.4: The oxidative addition/reductive elimination hydrogenation mechanism based on the Wilkinson's catalyst.
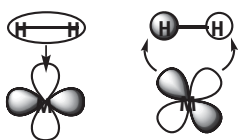
Figure 10.5: The σ→d donation and the d→σ* back-donation in the dihydrogen complex.

promotes the oxidative addition, and (ii) the presence of appropriate (hemi)labile ligands that facilitate the inner sphere reaction by dissociation to provide a vacant site.

10.2.2 σ-Bond metathesis mechanism

As another type of single-site TM catalysts, the TM-H catalysts generally prefer the σ-bond metathesis mechanism to activate/release H_2 (Figure 10.6). During the dehydrogenation, βhydride elimination yields the dehydrogenated product and regenerates the metal hydride complex. The corresponding reverse hydrogenation involves a hydride

Dehydrogenation
Hydrogenation

σ-bond metathesis

β-hydride elimination

M—H   YH-XH

Hydride insertion

YH-XH

Oxidative addtion/Reductive eliminaton
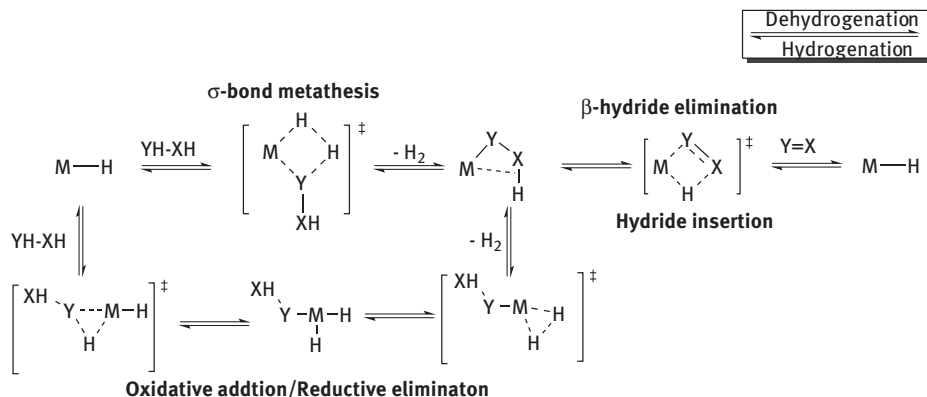
Figure 10.6: σ-Bond metathesis mechanism for the non-MLC hydride insertion/elimination.

insertion and the σ-bond metathesis with H_2 (also known as hydrogenolysis). It is worth noting that electron-rich TM centers may also oxidatively add into the X-H bond and reductively eliminate H-H during the dehydrogenation. In 1997, Leitner [10] and Sakaki [11] discussed mechanistic preferences between the oxidative addition/reductive elimination and the σ-bond metathesis mechanisms in the context of the catalytic hydrogenation of CO_2. Interestingly, the σ-bond metathesis mechanism proceeds via transition states that include either a four- or a six-membered ring structure (Figure 10.7).

four-membered ring   six-membered ring
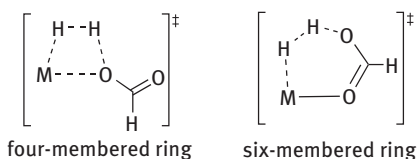
Figure 10.7: Transition states for σ-bond metathesis mechanism involving four- or six-membered ring structures.

10.3 LB-TM cooperation mechanisms

The LB-TM cooperation strategy is currently one of the most popular design strategies for homogenous hydrogenation/dehydrogenation catalysts [12]. The general LB-TM cooperation mechanism is depicted in Figure 10.8. The mechanism involves cooperation between the TM center and the LB functional site in the ligand during hydrogenation and dehydrogenation. Besides the d→σ⋆ back-donation, the LB functionality also simultaneously provides electron density to the σ⋆ orbital of H_2, which facilitates the heterolytic cleavage of H_2. This means that formally a hydride is transferred to the metal center and a proton is transferred to the Lewis base. The cooperation mechanism for the LB-TM catalysts are summarized in Figure 10.3b, including (1) the n-type MLC mechanism, which is based on cooperation between TM and the lone pair on the M-L bond
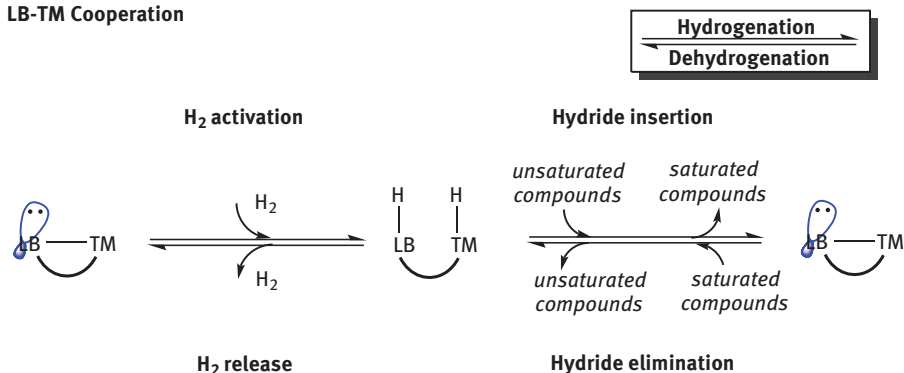
Figure 10.8: General hydrogenation and dehydrogenation mechanism for the LB-TM cooperation.

moeity, a dissociative/pendant LB, or an external LB; (2) the π-type MLC mechanism, which is also known as the (de)aromatization/tautomerization mechanism and based on cooperation between TM and the π-electrons in the ligand; (3) the σ-type MLC mechanism, which is based on cooperation involving the σ electrons; (4) the non-MLC mechanism, which involves an innocent ligand.

10.3.1 n-Type LB-TM cooperation mechanism

10.3.1.1 LB-TM cooperation mechanism on the M-L bond

In LB-TM systems, the M-L bond moiety usually bears an anionic ligand that can donate a lone pair of electrons. A representative example for this type of systems is Noyori's catalyst [13]. By introducing diamine or ethanolamine ligands [14], the amido ligand can participate in the hydrogenation via MLC mechanism (Figure 10.9). Under the influence of chiral ligands such as BINAP (2,2'-bis(diphenylphosphino)-1,1'-binaphthyl), high levels of enantioselectivity can be accomplished in such hydrogenations. The hydrogenation step proceeds via a typical outer-sphere MLC mechanism, which involves a transition state with a six-membered ring structure. In contrast, an inner-sphere hydride insertion mechanism, which would involve a dissociation of a ligand arm, is less feasible. Such a hypothetical mechanism involves arm opening/dissociation of the ligand arm, substrate coordination to the vacant coordination site at the metal center, insertion of the coordinated substrate the metal hydride bond and eventually release of the substrate. The H_2 activation step can proceed via transition states that involve either a four-membered or a six-membered ring structure assisted by proton shuttle.

Morris has developed earth-abundant LB-TM system for transfer hydrogenation, based on tetradentate PNNP ligand (N^1,N^2-bis(2-(diphenylphosphino)ethyl)-1,2-diphenylethane-1,2-diamine) (LB) and Fe (TM). Initially, the PNNP ligand should be deprotonated upon addition of a base to generate the reactive LB site [15]. Subsequently, the partially reduced complex should initiate the transfer hydrogenation via a stepwise
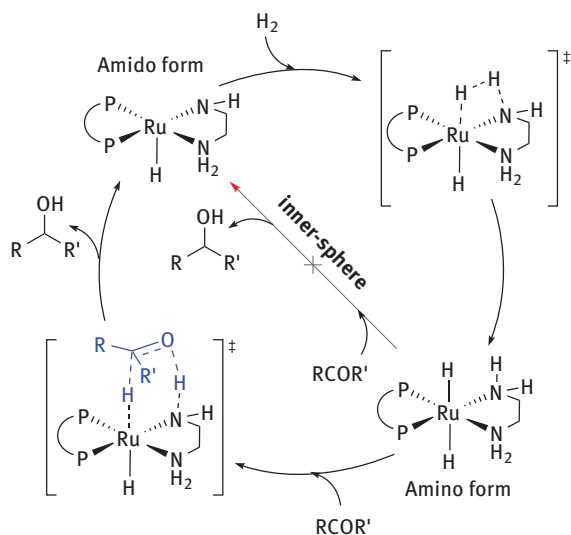
Figure 10.9: The n-typ LB-TM cooperation mechanism via the M-L bond in Noyori's catalyst.

bifunctional hydrogen transfer mechanism in an outer-sphere manner (PNNP-Fe, Figure 10.10) [16]. DFT calculations showed that the activation of the pre-catalyst is the rate-determining step and that the catalysis proceeds rapidly. With these mechanistic details in mind, Morris and co-workers designed a novel catalyst, in which one arm of the PNNP ligand is saturated to avoid any undesired pre-activation. The resulting iron catalyst achieved unprecedented turnover frequencies and even surpassed catalysts based on noble metals [17], which established the rational catalyst design paradigm based on a combination of theoretical and experimental results.
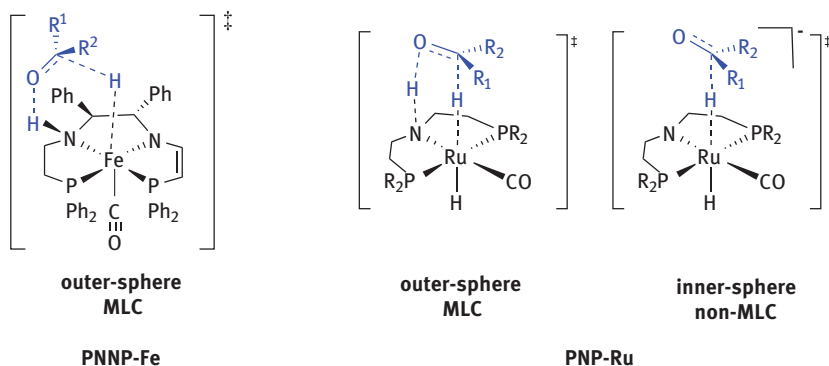
Figure 10.10: Outer-sphere MLC mechanism and inner-sphere non-MLC mechanism for PNNP-Fe and PNP-Ru systems.

Besides the outer-sphere MLC mechanism, it should be noted that an inner-sphere hydride elimination mechanism has also been proposed for the PNP-Ru system for dehydrogenation (PNP-Ru, Figure 10.10) [18]. In the inner-sphere mechanism, substrate directly interacts and reacts on the metal center, different from the case in the bifunctional outer-sphere mechanism.

10.3.1.2 LB-TM cooperation mechanism with a dissociative/pendant LB

LB-TM cooperation can also be achieved with a dissociative/pendant LB ligand. Bullock et al. have developed a series of earth-abundant TM catalysts bearing pendant amines for the electrochemical oxidation of H_2 [19]. Computational studies suggested an important role for the pendant amine for cooperatively catalyzed hydrogenations and dehydrogenations (Figure 10.11), which can be further assisted by water [19b, 20]. In the transition state depicted in Figure 10.11, the H_2 molecule is binding to the N atom of the pendant ligand on the one side and on the other side to a vacant coordination site of the metal center. Similar to the previously discussed systems, also here, the H_2 is activated by heterolytic cleavage and a hydride is transferred to the metal center and the basic ligand site is protonated.
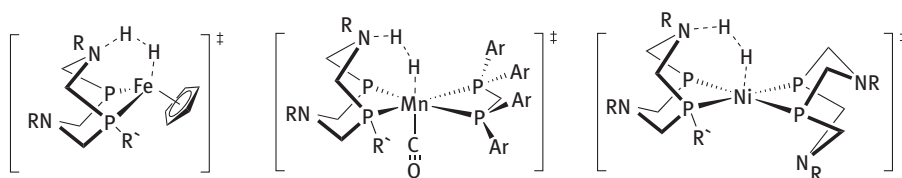
Figure 10.11: LB-TM mechanism with a dissociative/pendant LB.

A representative example for the LB-TM mechanism with a dissociative LB is the PyNN-Ru complex developed by Herzon et al (Figure 10.12). [21] During the hydrogenation of aldehydes, the amine arm of the tridentate PyNN ligand will dissociate under concomitant cleavage of H_2. Subsequently, the dissociated arm should participate in an MLC hydrogenation of the aldehyde, although the mechanistic details remain to be investigated theoretically.

10.3.1.3 LB-TM cooperation mechanism with an external LB

For stability purposes, several catalysts use tetradentate ligands as the basic catalyst platform. Without the additional vacant site, the MLC mechanism with an external LB is useful to facilitate the activation/release of H_2 (Figure 10.13). As external bases, amides [22], formates [23], bicarbonates [24], have been used. It should be noted that the hydride insertion/elimination step is possible without the cooperation of the external base. As shown in Figure 10.13, the hydride elimination step can either follow a α-H elimination (linear transition state; path a) or a β-H elimination (transition state with a
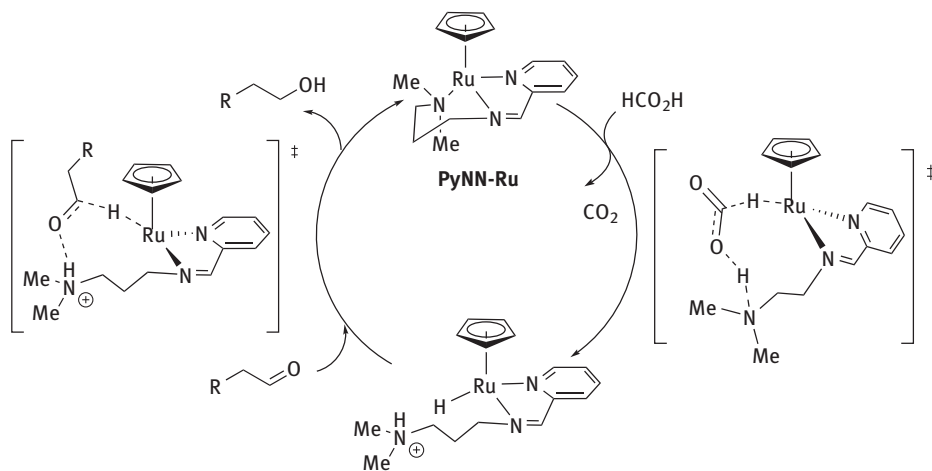
Figure 10.12: The LB-TM mechanism with dissociative LB using Herzon's system as an example.

four-membered ring structure; path b). In the transition state with a four-membered ring structure, the hydride transfer and the coordination of the substrate proceed simultaneously. In path c, the protonated LB cooperatively assists the hydride insertion.
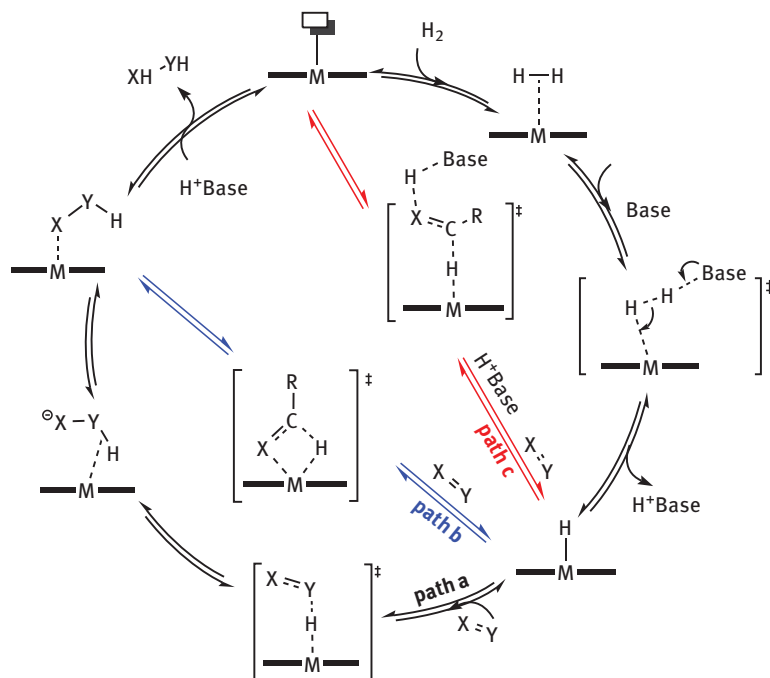
Figure 10.13: Hydrogenation and dehydrogenation via the MLC mechanism with an external LB.

10.3.2 π-Type LB-TM cooperation mechanism: (de)aromatization/tautomerization

One highly intriguing approach is the use of π-electrons as LBs in LB-TM cooperation systems, which widely expand the scope of ligand platforms for the design of LB-TM catalysts [12a]. A tautomerization is able to increase the basicity of the π electrons to enable the cooperation π electrons of TM center for hydrogenation/dehydrogenation. The reaction mechanism is accordingly also referred to as the tautomerization or (de) aromatization mechanism (if aromatic moieties are involved). Representative examples for such systems are the pyridine-based PNP and PNN pincer complexes that have been developed by Milstein (Figure 10.14) [25]. Although such catalysts have demonstrated unprecedented activity, the details of the underlying mechanism have been discussed controversially for a long time. Experimental studies have suggested an MLC-type H_2 activation/release step and an inner-sphere non-MLC hydride insertion/elimination step for the catalytic cycle (Figure 10.14, Left) [26]. Another experimental study has suggested higher activity for catalysts based on PNN relative to PNP pincer complexes. Subsequently, Wang et al. carried out a computational study on the dehydrogenative coupling of alcohols and amines, for which they proposed an outer-sphere bifunctional hydrogen-transfer mechanism [27].
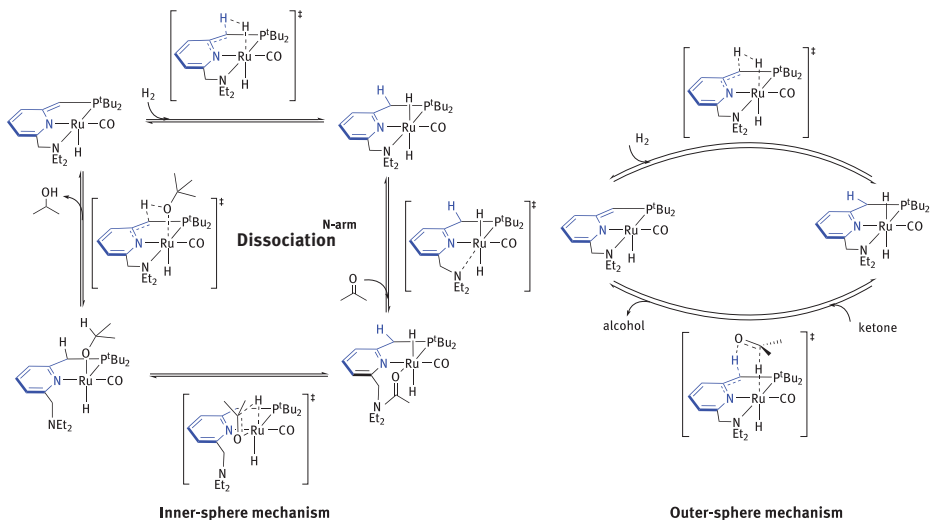
Figure 10.14: Inner-sphere (left) and outer-sphere (right) (de)aromatization/tautomerization MLC mechanisms using PNN-based LB-TM systems.

It should be noted that a (de)aromatization/tautomerization MLC mechanism via a Ru^{II}/Ru^{0} pathway has been proposed by Suresh et al. (Figure 10.15) [28]. Therein, a σ-bond metathesis step should initially release H_2 and generate the metal alkoxide
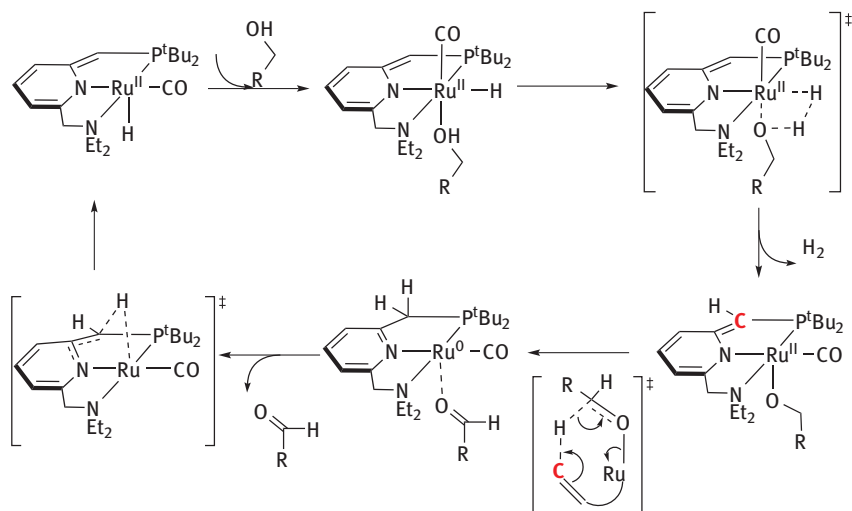
Figure 10.15: The (de)aromatization/tautomerization LB-TM cooperation mechanism via the Ru^{II}/Ru^{0} cycle.

complex. Subsequently, the π-electrons of the enamine would accept the β-hydrogen as a proton. Thus, the Ru^{II} metal center would be reduced to Ru^{0}. In the next step, the α-hydrogen relative to the imine moiety could thus act as a proton to oxidize Ru^{0} – Ru^{II} to regenerate the catalyst. It is noteworthy that the Ru^{II}/Ru^{0} MLC process is possible only when the isomerization of CO and hydride is energetically feasible.

Another system that operates via the aromatization/dearomatization mechanism is Shvo's catalyst and analogues (Figure 10.16) [29]. After the MLC-induced activation of H_2, the $η^4$-cyclopentadienone will transfer onto the anionic aromatic $η^5$-hydroxycyclopentadienyl ligand. In the subsequent MLC hydrogenation step, the anionic hydroxycyclopentadienyl ligand loses its aromaticity and the Ru^{II} center is reduced to Ru^{0}. Knölker's complex is an analogous catalyst, and hydrogenation reactions catalyzed by Knölker's complex have been studied by Casey and Guan [30]. Their mechanistic study, based on the deuterium isotope method and computational calculations, led them to propose a concerted MLC mechanism [30]. Subsequently, substitution effects and the chemoselectivity were discussed based on this MLC (de)aromatization mechanism [31].

10.3.3 σ-Type LB-TM cooperation mechanism

Although lower in energy, σ-bond electrons can also be involved in the LB-TM cooperation mechanism. The σ-type MLC proceeds via a σ-bond metathesis step, where the σ-bond electrons assist the activation/release of H_2 under concomitant cleavage/formation of the M-L bond. A typical ligand that operates via this mechanism is the phenyl ligand. In 2016, Wang et al. carried out a theoretical study on the dehydrogenation of
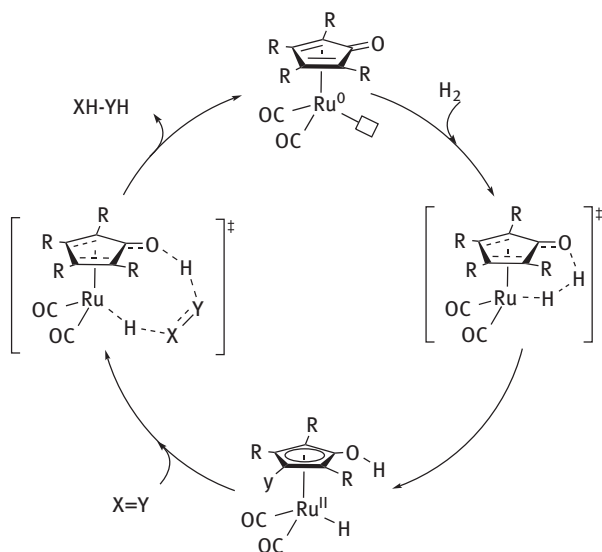
Figure 10.16: The (de)aromatization/tautomerization LB-TM cooperation mechanism using Shvo's catalyst as an example.

ammonia-borane catalyzed by the bis(phosphinite) pincer complex, PArP-Fe [32]. They proposed four different dehydrogenation mechanisms, and their results indicated that the σ-type LB-TM cooperation mechanism is favored (Figure 10.17). The rate-determining step is the MLC concerted dehydrogenation step via a six-membered ring transition state.

10.3.4 Ligand-innocent non-LB-TM cooperation mechanism

Despite the presence of LB ligands, LB-TM catalysts prefer in some cases a non-LB-TM cooperation mechanism. In such cases, the LB ligand acts as an innocent ligand for the hydrogenation and dehydrogenation. Szymczak reported an inner-sphere mechanism in dehydrogenation reactions catalyzed by an NNN-Ru complex [33]. Ke's theoretical study supported the notion that the NNN ligand remains innocent during the catalysis. The release of H_2 occurs via a σ-bond metathesis mechanism. With the vacant site produced by the H_2 release, the Ru center would rather promote the inner-sphere β-hydride elimination reaction, as shown in Figure 10.18. The NNN ligand does not function as a Lewis base, due to the lack of driving force in tautomerization process.

10.4 LA-TM cooperation mechanism

LA-TM cooperation is considered to be a novel reactivity mode for the activation of H_2 and hydrogenations/dehydrogenations. H_2 is activated by these systems via heterolytic
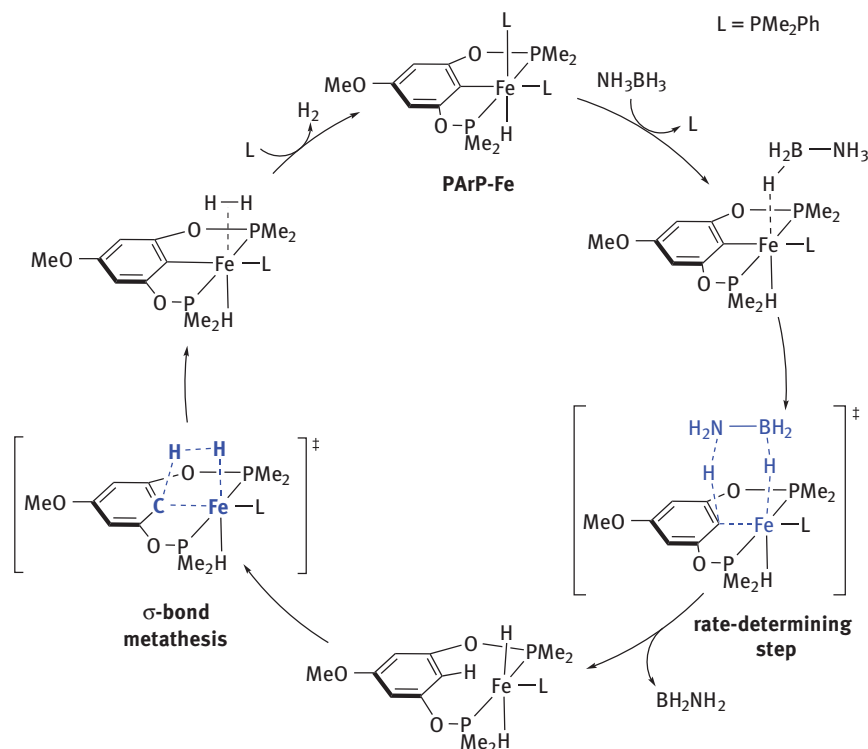
Figure 10.17: Dehydrogenation of ammonia-borane via the σ-type LB-TM cooperation mechanism for PArP-Fe catalyst.
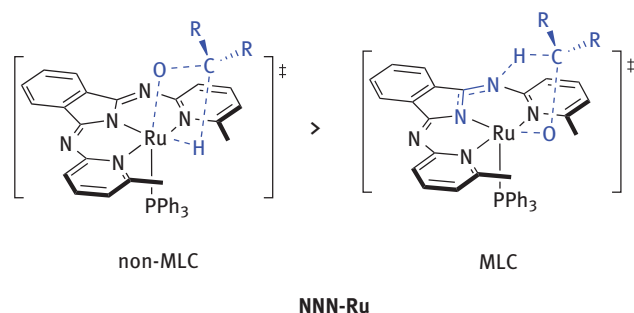
Figure 10.18: MLC (right) and non-MLC inner-sphere mechanism (left) for Szymczak's NNN-Ru catalyst.

bond cleavage. In contrast to the popular LB-TM system, LA-TM catalysts comprise a TM center and an electrophilic LA reactive site [34], in which the former acts as an electron donor, and the latter as an electron acceptor, to cooperatively facilitate the activation/ release of H_2 [35]. Therefore, electron-rich TMs, such as Fe [36], Co [37], Ni [38], Pd [39],

or Pt [40] in low valent state are usually chosen as the TM center to act as the nucleophilic partner in LA-TM systems. Although many electron-deficient elements/moieties could be used as the LA site, boron is currently the most commonly used. The LA reactive site has been incorporated into different ligand platforms, including nitrogen, sulfur, and phosphine ligands [41]. LA-TM catalysts that contain boron-phosphine pincer ligands are representative examples for hydrogenation/dehydrogenation systems (Figure 10.19).
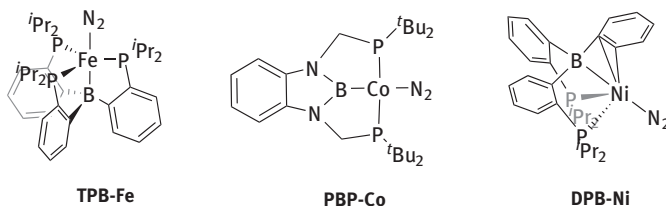
Figure 10.19: Representative LA-TM catalysts that contain boron-phosphine pincer ligands.

Compared to LB-TM cooperation, the LA-TM cooperation strategy has only been recently used for catalytic hydrogenations/dehydrogenations. Peters has reported that a DPB-Ni catalyst (DPB = diphosphine-borane) (Figure 10.19) can activate H_2 and efficiently hydrogenate alkenes at room temperature under atmospheric pressure [38]. The synergetic cooperation between the boron site and the TM center was suggested to be important. Later, based on this catalyst model, Ke and co-workers proposed the general mechanistic paradigm and the reactivity modes for the LA-TM cooperative activation of H_2 [42]. Similar to LB-TM, the LA-TM mechanisms can be subdivided into: (1) the p-type MLC, which involves a vacant p orbital on the M-L bond, a dissociative/pendant LA, or an external LA; (2) the π-type MLC, which involves an electrophilic conjugated moiety in the ligand; (3) the σ-type MLC, which proceeds via a simultaneous σ-bond dissociation; (4) the non-MLC mechanism, in which the LA ligand is innocent. A summary of the LA-TM MLC mechanisms is shown in Figure 10.3c, and the general hydrogenation/dehydrogenation mechanisms for LA-TM cooperation are depicted in Figure 10.20.

10.4.1 p-Type LA-TM cooperation mechanisms

10.4.1.1 M-L bond LA-TM cooperation mechanism

In the p-type LA-TM cooperation mechanisms, it is the vacant p orbital on the LA site that cooperates with the TM center during the activation/release of H_2. As shown in Figure 10.21a, this mechanism is most frequently operative for systems that contain a vacant p orbital on the LA atom of the M-L bond moiety. The heterolytic cleavage of H_2 can thus be facilitated on the M-L bond moiety by the vacant p orbital. Subsequently,

LA-TM Cooperation
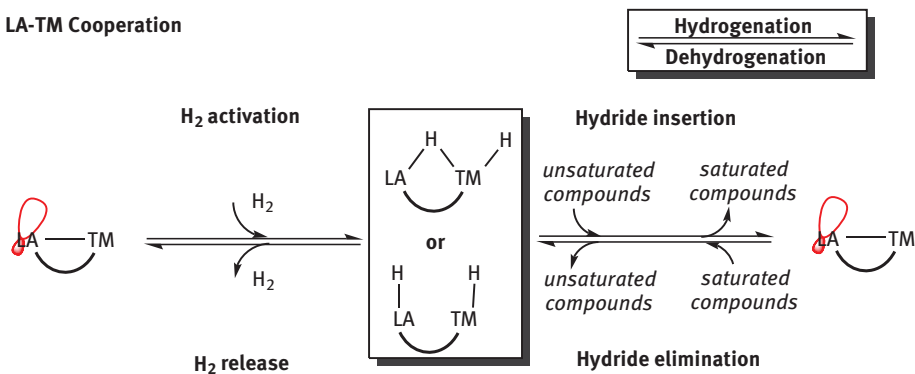
Figure 10.20: General hydrogenation/dehydrogenation mechanism for LA-TM cooperation.

the hydride interacts with the empty orbital on the LA site, while the proton engages with the d electrons of TM center (LB), which is oxidized after the cleavage of H_2. A representative system that prefers to operate via this M-L bond LA-TM cooperation mechanism is the PBP-Co catalyst shown in Figure 10.21a [37]. Therein, the boron atom is sp^2 hybridized, and datively coordinates to the TM center, leaving a vacant p orbital as the LA reactive site.

Figure 10.21: MLC Mechanisms of the p-type LA-TM cooperation.

10.4.1.2 LA-TM mechanism with a dissociative/pendant LA

The vacant orbital can also be created by the dissociation of the LA from the LA-TM dative bond, or by the introduction of a pendant LA into the ligand. As shown in Figure 10.21b, after the dissociation of the dative LA-TM bond, the LA exhibits a vacant orbital to assist the cleavage of H_2. In this dissociative mechanism, the H-H bond coordinates to the empty orbital of the LA, while the TM center donates d-electron density into the anti-bonding orbital of H-H. The dissociative LA-TM cooperation mechanism has been studied by Ke et al. using a DPB-Ni complex as a model catalyst (Figure 10.21b) [42], and their results showed that such a dissociative mechanism should not be very likely for this system due to the strong coordination interaction between boron and nickel. The dissociative LA-TM cooperation should be expected to proceed only in LA-TM systems with hemilabile ligands. LA-TM complexes bearing a pendant LA moiety have already been reported [43], and although these complexes represent promising examples for LA-TM cooperation via pendant LAs, their reactivity in catalyzed hydrogenations/dehydrogenations remains to be explored.

10.4.1.3 LA-TM cooperation mechanism with external LAs

Apart from the previously discussed intramolecular LA-TM cooperation, external LA also assists the activation/release of H_2 via an intermolecular manner. As shown in Figure 10.21c, a free external LA can use its already available vacant orbital to assist the activation of H_2 in cooperation with the TM center. This reaction mechanism is reminiscent of the dissociative LA-TM cooperation mechanism. However, it does not require the pre-dissociation of the LA. Recently, Wass and co-workers have discovered that the activation of H_2 can be accomplished by the cooperation between a palladium complex and $B(C_6H_5)_3$ as the external LA [44]. In this system, the palladium center serves as an electron donor to accept the proton, while boron acts as the electron acceptor binding to the hydride

10.4.2 σ-Type LA-TM cooperation mechanism

In addition to the p-type mechanism, the σ-type mechanism can also be found in the LA-TM system. Through a σ-bond metathesis transition state (Figure 10.22), the cleavage of H_2 occurs under concomitant cleavage of the LA-TM bond, followed by the coordination of the hydride and proton to the LA site and the TM center, respectively, and the low-valent TM center will be oxidized. For the DPB-Ni system [42], Ke et al. have revealed that this σ-type LA-TM cooperation represents a synergetic heterolytic mode. For LA-TM systems that do not contain readily available vacant p orbitals, or that exhibit a high energy penalty for the dissociation of the LA from the TM center, this σ-type LA-TM cooperation should be generally preferred over other mechanisms.

DPB-Ni system
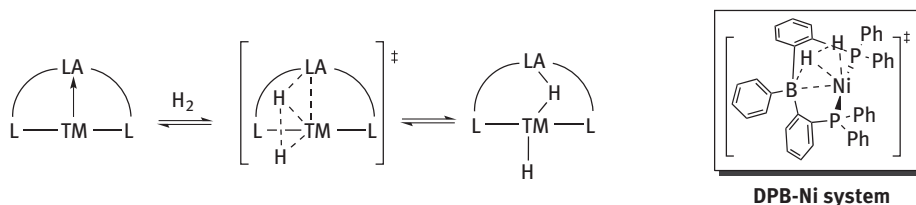
Figure 10.22: Mechanism of σ-type LA-TM cooperation via the synergetic heterolytic mode.

10.4.3 π*-Type LA-TM cooperation mechanism

Although experimental examples have not yet been reported, the π*-type coopera-
tion mechanism should theoretically be expected for LA-TM systems. In cases where
there is a conjugated moiety in the ligand that can tautomerize to a resonance
structure with a nucleophilic center, this conjugated moiety should theoretically be
able to act as a LA to cooperate with the TM center for hydrogenations/dehydrogena-
tions (Figure 10.23). It should be noted that the thermodynamic change for the
tautomerization is crucial for the desired π*-type LA-TM cooperation. This π*-type
strategy should be highly desirable for the design of bifunctional LA-TM systems in
the near future.
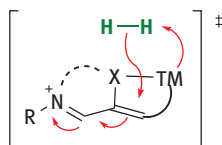
Figure 10.23: A proposed mechanism of the π*-type LA-TM cooperation.

10.4.4 Ligand-innocent non-MLC mechanism in LA-TM systems

In the non-MLC mechanism for LA-TM systems, the LA ligand remains innocent
during the activation/release of H_2. When the LA ligand is not involved in the
cooperation, the H_2 molecule tends to be homolytically activated via oxidative addi-
tion onto the metal center. Or, reversely, the release of H_2 occurs via the reductive
elimination of dihydride from the TM center. According to Ke's theoretical results,
this mechanism can be subdivided into the *fac*-homolytic mode and the *mer*-homo-
lytic modes [42]. In the *fac*-homolytic mode (Figure 10.24a), the activation/release of
H_2 occurs via a transition state, in which the reaction plane (∠H-TM-H) is arranged
perpendicularly to the LA-TM bond. Similar to traditional TM catalysts, the cleavage
of H_2 should be driven by the strong back-donation from the d electrons of the TM
center to the σ* orbital of H-H. In addition, as a typical feature for this mode, the LA
site that is perpendicular to the reaction plane (∠H-TM-H) stabilizes the transition

(a) *fac-* homolytic mode
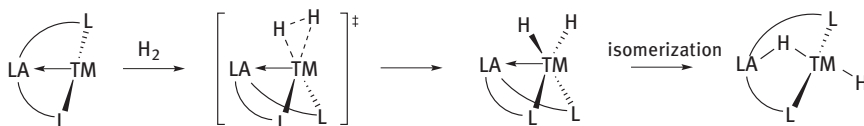
(b) *mer-* homolytic mode
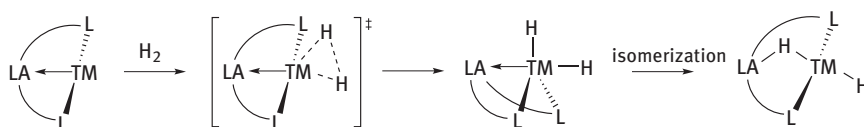
Figure 10.24: (a) The *fac*-homolytic and (b) the *mer*-homolytic modes for the ligand-innocent non-MLC mechanism in LA-TM systems.

state via interacting with the filled dz^2 orbital of the TM center. After the cleavage of H_2, a cis-dihydride intermediate is formed. In contrast, the activation/release of H_2 in the mer-homolytic mode (Figure 10.24b) proceeds through a transition state in which the LA-TM bond is in the reaction plane ($\angle$H-TM-H). The LA site usually interacts with the dx^2-y^2 orbital of the TM center, although the interaction varies in some cases depending on the geometry and the electronic structure of the LA-TM catalyst. Usually, the dihydride intermediate will further isomerize, transferring one of the metal hydrides to form an LA-μ-H-M bridging bond. This bridging hydride bond is a typical feature for the hydride intermediate in the LA-TM cooperation mechanism.

10.4.5 Hydrogenation/dehydrogenation mechanism in LA-TM systems

The metal hydride intermediates in LA-TM-catalyzed hydrogenations/dehydrogenations are special, as they contain, in contrast to the LB-TM systems, multiple hydrides and no protons. There is usually a unique bridging hydride in the LA-μ-H-M three-center bond of LA-TM systems. Due to the presence of the bridging hydrides, LA-TM catalysts operate via different mechanisms in hydrogenations/dehydrogenations. Paul and co-workers used a PBP-Co catalyst to investigate the inner-sphere and outer-sphere mechanism of the hydrogenation of alkenes with LA-TM systems [45]. The bridging and terminal hydrides cannot react easily with unsaturated bonds in a concerted fashion via an outer-sphere mechanism (Figure 10.25). In contrast, the concerted transfer of a hydride and proton to an unsaturated bond is feasible in LB-TM systems (Figure 10.8). In the inner-sphere mechanism, the unsaturated substrate X = Y initially coordinates with the TM center, followed by the hydride insertion into the X = Y. This hydride insertion step can proceed either via the insertion of the terminal hydride or via insertion of the bridging hydride (Figure 10.25). After the
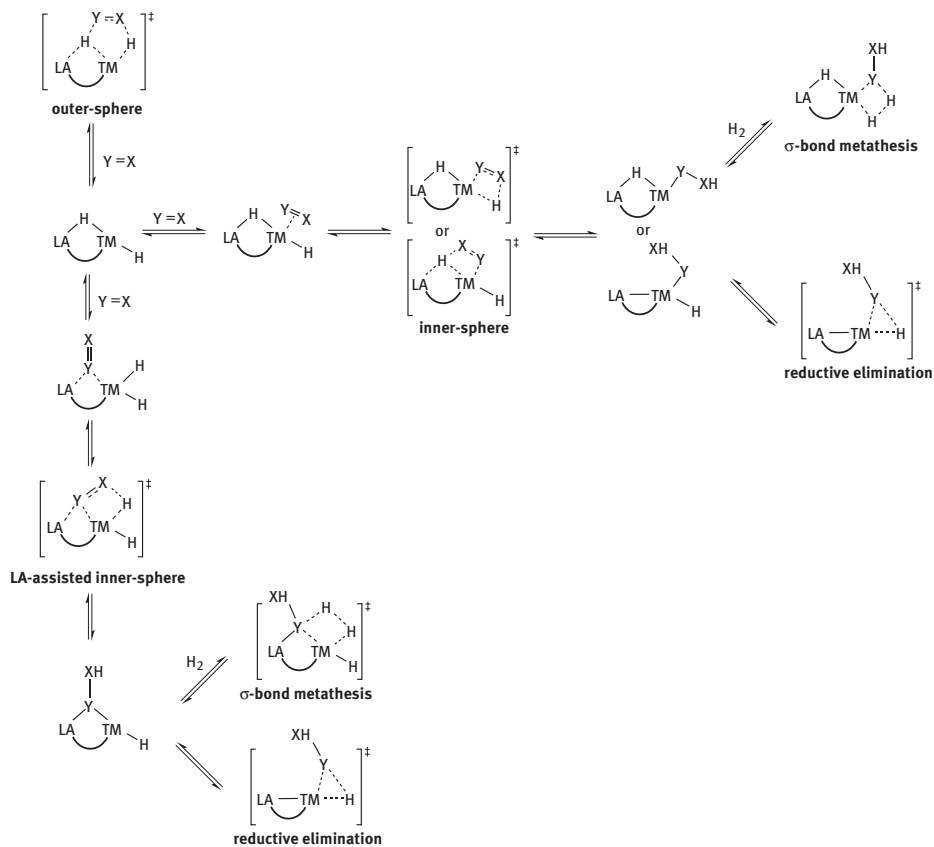
Figure 10.25: Hydrogenation/dehydrogenation mechanism in LA-TM cooperation systems.

hydride insertion, the reductive elimination of the −Y-XH and the hydride completes the hydrogenation cycle by releasing the saturated product and regenerating the LA-TM catalyst. On another reaction pathway, the −Y-XH ligand can react with another molecule of H_2 via a σ-bond metathesis step to produce the saturated product XH-YH and regenerate the metal hydride intermediate. If the unsaturated bond is polar, there should be another hydrogenation reaction pathway, the so-called LA-assisted inner-sphere hydride insertion, wherein the heteroatom of the unsaturated bond interacts with the LA site and activates the LA (Figure 10.25). The subsequent step can then proceed either via a reductive elimination or via a σ-bond metathesis to complete the hydrogenation cycle. The mechanistic schemes in Figure 10.25 should also be applicable to dehydrogenations or transfer dehydrogenations catalyzed by LA-TM catalysts [35]d]. Moreover, the reactivity difference between the bridging and the terminal hydrides should also be very interesting, as this may entail important consequences for the LA-TM cooperation mechanism for hydrogenations/dehydrogenations.

10.5 LA-LB cooperation (FLP) mechanism

Apart from catalysts that contain TMs, metal-free catalysts for homogeneously catalyzed hydrogenation/dehydrogenation reactions are becoming more and more attractive due to their environmental, economical, and practical merits [46]. Since the pioneering work of Stephan [46b], frustrated Lewis pairs (FLPs) have been developed into a promising class of metal-free catalysts for hydrogenations/dehydrogenations [47]. Typical bifunctional LA-LB catalysts are composed of electron-deficient LAs and electron-rich LBs. Representative LA-LB (FLP) catalysts are shown in Figure 10.26 [48]. As LAs and LBs prefer to form stable LA-LB adducts, FLP catalysts require particular structural features
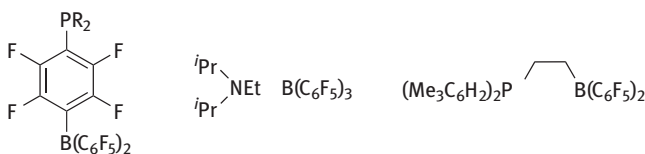
Figure 10.26: Representative LA-LB (FLP) catalysts.

in order to weaken or prevent the formation of strong LA-LB interactions, which leads to active LA LB sites that can be employed for hydrogenation/dehydrogenation reactions. In intermolecular FLP complexes, the LA/LB pairs generally contain sterically demanding groups to prevent the formation of stable LA-LB adducts. Moreover, groups with different electronic effects have been introduced into these systems in order to further improve the activity of the FLPs. In intramolecular FLPs, steric congestion, electronic properties, and geometric constraints play important roles for the reactivity of the catalysts. FLP catalysts exhibit typical LA-LB cooperation mechanisms for hydrogenations/dehydrogenations (Figure 10.3d), including inter-/intramolecular synergetic mechanisms and the proposed electric-field mechanism. The general hydrogenation/dehydrogenation mechanism for LA-LB (FLP) cooperation is depicted in Figure 10.27.

10.5.1 H_2 activation mechanisms in LA-LB cooperation systems

Two activation modes have been reported for the mechanism of the activation of H_2 in LA-LB cooperation systems: (i) the electron-transfer model, and (ii) the electric-field model (Figure 10.28). In the electron-transfer model, the σ-electrons in the σ orbital of H_2 can donate into the empty orbital of the LA, while the lone pair of electrons on the LB can donate into the σ* orbital of H_2. With the increased electron density in the σ* orbital, the H-H bond would be further activated. Given the synergetic impact of the empty orbital and the lone pair of electrons, such LA-LB cooperation systems can effectively activate H_2. Many mechanistic studies based on this process have been

LA-LB (FLP) Cooperation
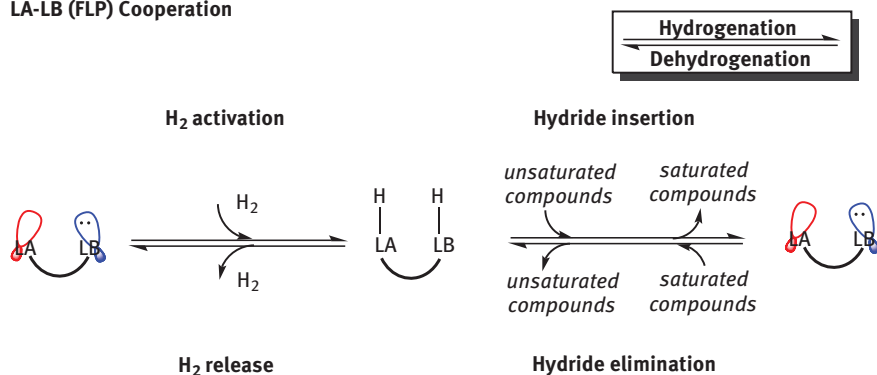
Figure 10.27: General hydrogenation/dehydrogenation mechanism for LA-LB (FLP) cooperation.

Electron-transfer model   Electric-field model
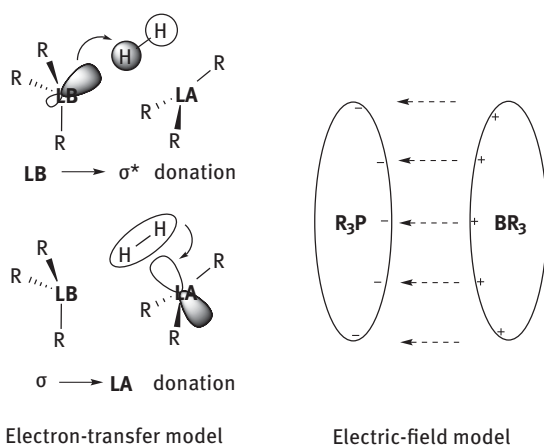
Figure 10.28: Electron-transfer model and electric-field model for LA-LB cooperation systems.

reported [49]. On the other hand, the electric-field model suggests that the electric-field created by the FLP should have great influence on the activation of H_2 upon its insertion into the reactive pocket between the LA and LB [50].

In LA-LB cooperation systems, the activation of H_2 can proceed via intermolecular or intramolecular mechanisms (Figure 10.29), which differ with respect to each other in the orientation of the H-H bond in the transition state. The representative intermolecular catalyst $Mes_2PCH_2CH_2B(C_6F_5)_2$ can activate H_2 reversibly [46b]. Grimme et al. have investigated typical intermolecular mechanisms (Figure 10.29a) based on the activation of H_2 by the intermolecular cooperation between $^tBu_3P$ and B $(C_6F_5)_3$ [50c]. It should be noted that in some cases the inclusion of H_2 into the FLP rather than the cleavage of H_2 cleavage may be the rate-determining step. For the intramolecular mechanism (Figure 10.29b), the steric hindrance of the FLP and the

(a) intermolecular mechanism

^{t}Bu$_3$P
+
B(C$_6$H$_5$)$_3$
$\xrightarrow{\text{H}_2}$
$\left[^t\text{Bu}_3\text{P} \text{--} \text{H} \text{--} \text{H} \atop \quad\quad \text{B(C}_6\text{H}_5)_3 \right]^{\ddagger}$
$\longrightarrow$
^{t}Bu$_3$PH $^+$
+
$^-$HB(C$_6$H$_5$)$_3$

(b) intramolecular mechanism

Mes$_2$P $\longrightarrow$ B(C$_6$F$_5$)$_2$
$\xrightarrow{\text{H}_2}$
$\left[\text{Mes}_2\text{P} \quad \text{B(C}_6\text{F}_5)_2 \atop \quad\quad \text{H} \text{--} \text{H} \right]^{\ddagger}$
$\longrightarrow$
H—B(C$_6$F$_5$)$_2$ $^-$ / Mes$_2$P$^+$ / H
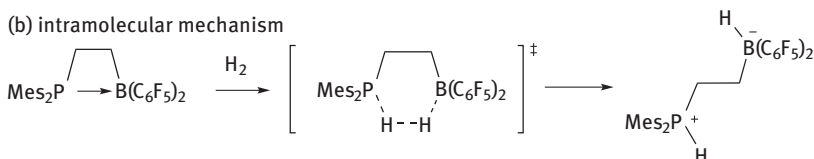
Figure 10.29: Intermolecular mechanism and intramolecular mechanism for the activation/cleavage of H$_2$ using LA-LB cooperation systems.

rigidity of the catalyst skeleton are considered important factors for the activation of H$_2$, which may influence the deformation energies of the substrate and catalyst from the reactants to the transition state stage.

10.5.2 Hydrogenation/dehydrogenation reaction mechanisms in LA-LB cooperation systems

The key intermediate of LA-LB systems for hydrogenations/dehydrogenations is composed of an LA-hydride group and an LB-proton group, which are similar to the intermediates in LB-TM systems. However, in contrast to TM centers, the LA or LB groups usually do not contain available vacant sites for the coordination of unsaturated substrates. Therefore, the inner-sphere mechanism should be relatively rare for LA-LB cooperation systems. The hydrogenations/dehydrogenations usually proceed in either a concerted or stepwise manner (Figure 10.30) [51]. In the concerted mechanism, the hydride insertion from the LA-hydride group to the substrate and the protonation by the LB-proton group occur simultaneously. In the stepwise mechanism, the reaction pathways should vary depending on the hydricity of the LA-hydride group and the pKa value of the pronated LB group. The stepwise reaction can start with the protonation of the substrate, before a proton-assisted hydride insertion occurs to complete the hydrogenation. Alternatively, the stepwise reaction may be initiated by a direct hydride transfer. The anionic group on the LA will be then deprotonated by the protonated LB group to yield the final product.

It is worth noting that the LA-LB cooperation mechanism can also occur between an LA catalyst and the substrate (LA-only catalysis). Some unsaturation substrates with a lone pair can act as an LB site to cooperate with the LA catalyst during the hydrogenation reactions. As show in Figure 10.31, the unsaturated substrate X = Y and the LA catalyst represent an intermolecular LA-LB pair and are thus able to activate H$_2$ cooperatively to afford an ion pair intermediate. In this intermediate, X = Y
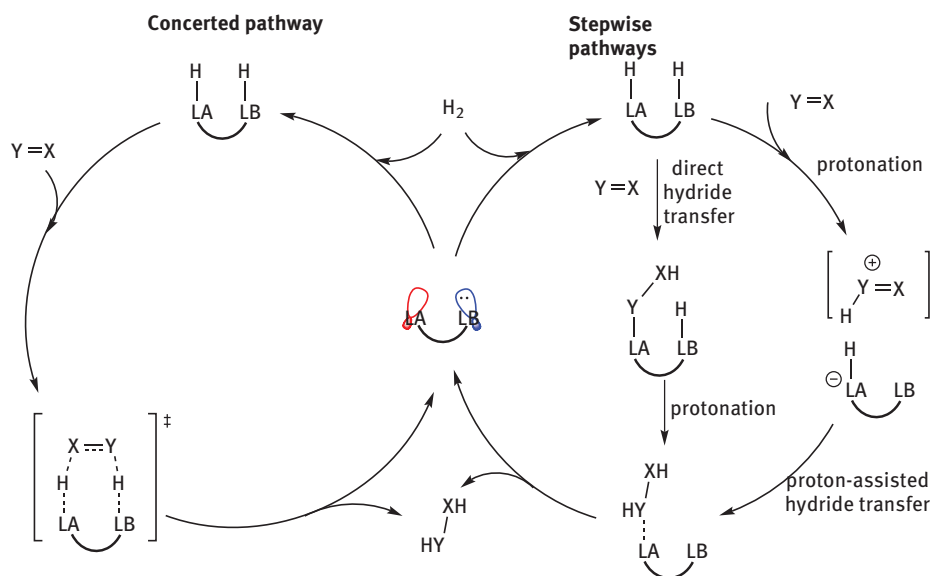
Figure 10.30: Concerted and stepwise mechanisms for hydrogenations via LA-LB cooperation.
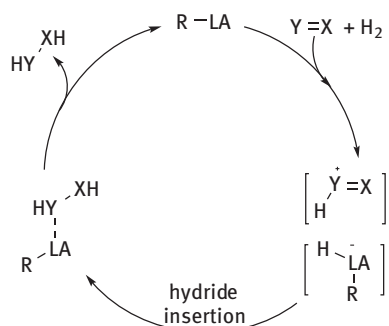
Figure 10.31: LA-LB cooperation mechanism in the absence of LB (LA-only catalysis).

is protonated and the LA is bound to the hydride. Subsequently, the hydride inserts into the protonated substrate, which yields the saturated product.

10.6 Ambiphilic mechanism

Compared to FLP catalysts, ambiphilic catalysts have emerged as another new type of metal-free bifunctional catalysts for the activation of H_2 [52]. In contrast to FLP catalysts, the bifunctional reactive sites of ambiphilic catalysts are identical. As shown in Figure 10.32, the di**E**yne or di**E**ene (E = Si, Ge, or Sn) compounds have been reported as

$R-E\equiv E-R$ **diEyne**

diEene

$E = Si, Ge, or Sn$

1,4,2,5-diazadiborinine

1,3,2,5-diazadiborinine

Li$_2$[DBA]
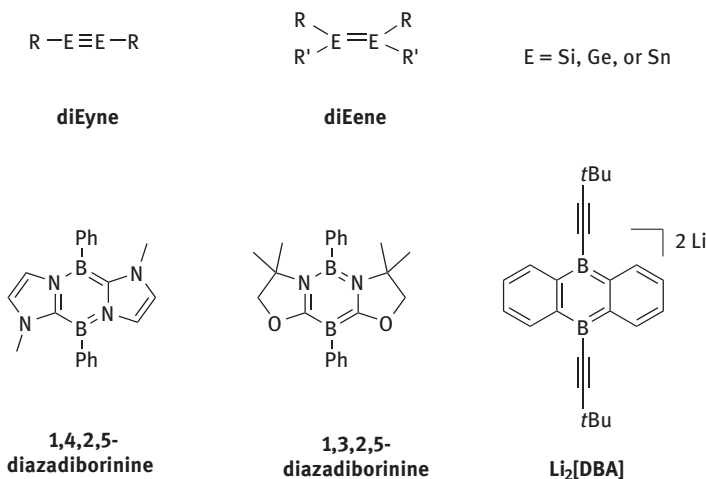
Figure 10.32: Representative ambiphilic catalysts.

potential catalysts for the activation of H$_2$ [52a, 53]. Some representative examples of ambiphilic boron-based catalysts containing boron atoms as the bifunctional reactive sites, e. g. 1,4,2,5-diazadiborinine, 1,3,2,5-diazadiborinine, and Li$_2$[DBA] complexes (DBA = 9,10-dihydro-9,10-diboraanthracene), are also shown in Figure 10.32[52b, 54]. By embedding the diborinine complex in a conjugated framework, one of the boron atoms can act as an LA, while the other can serve as an LB according to the resonance structures of the complex (Figure 10.3e). Ambiphilic catalysts have demonstrated their potential in the activation of H$_2$ [52, 53] and other small molecules. Although hydrogenation/dehydrogenation reactions using this type of compounds as catalysts have not been reported yet, the general mechanism for hydrogenations/dehydrogenations by ambiphilic cooperation can be theoretically envisioned (Figure 10.33).

Ambiphilic Cooperation

Hydrogenation
Dehydrogenation

H$_2$ activation

Hydride insertion

H$_2$ release

Hydride elimination
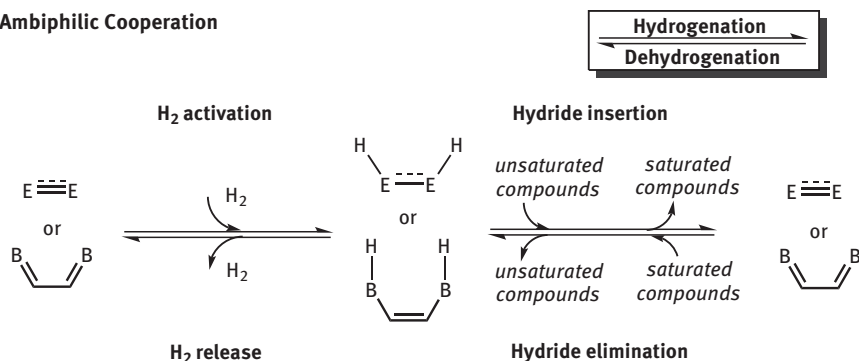
Figure 10.33: General hydrogenation/dehydrogenation mechanism for ambiphilic cooperation.

10.6.1 H$_2$ activation mechanism in ambiphilic systems

Due to the weak π-bond of di**E**yne or di**E**ene compounds, they show potential reactivity towards hydrogen activation. Their H$_2$ activation mechanisms exhibit interesting variation, due to the small HOMO-LUMO gap and the substituent effect. The di**E**yne or di**E**ene compounds with identical substituents generally activate H$_2$ in a homolytic cleavage manner (Figure 10.34a). The homolytic activation of H$_2$ can occur through either a *syn*-addtion pathway, or a *stepwise*-addition pathway. Interestingly, an *anti*-addition can also be possible as proposed by Inoue and Rieger [55]. Different substituents result in a polar π-bond in the di**E**yne and di**E**ene compounds, which may change the activation of H$_2$ into a heterolytic cleavage manner (Figure 10.34b).

(a) homolytic cleavage

(b) heterolytic cleavage

syn-addition   *stepwise*-addition   *anti*-addition   *syn*-addition   *stepwise*-addition   *anti*-addition
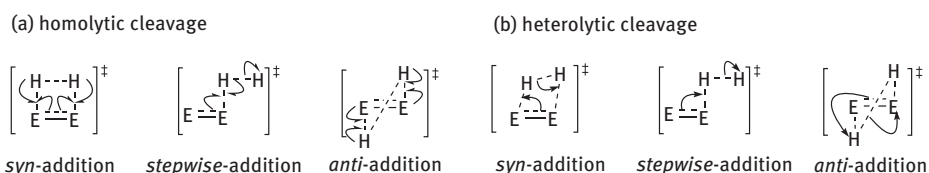
Figure 10.34: Ambiphilic cooperation mechanism for H$_2$ activation by di**E**yne or di**E**ene systems.

Boron-based ambiphilic moleclues provide a new electron-transfer model for the activation of H$_2$ [52b, 54]. Holthausen and Wagner reported that the HOMO and the LUMO of [DBA]$^{2-}$ (Figure 10.32) have the same local symmetries at the boron atoms, corresponding to the bonding and anti-bonding orbitals of H$_2$ molecule [52b]. As shown in Figure 10.35, the LUMO orbital of [DBA]$^{2-}$ mainly consists of two p* orbitals of boron atoms, which are antisymmetric with respect to the *C2* axial. With the same symmetry, the σ-bond of H$_2$ can well donate electrons to this LUMO orbital. On the other hand, the HOMO orbital of the ambiphilic catalyst is mainly composed of two p orbitals, which are symmetric with respect the *C2* axial. The anti-bonding orbital of H-H shows identical symmetry. Hence, the HOMO electrons can

HOMO ⟶ σ* σ ⟶ LUMO
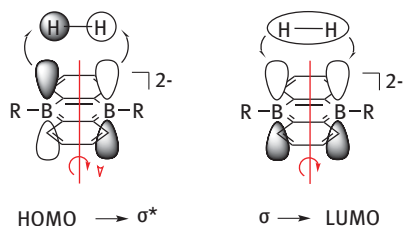
Figure 10.35: Electron-transfer model for the activation of H$_2$ by boron-based ambiphilic cooperation.

donate into the anti-bonding orbital of H_2, weakening the strong H-H bond. This synergetic effect of HOMO→σ* and σ→LUMO facilitates the activation of the H-H bond. Similarly to the situation in di**E**yne and di**E**ene systems, boron-based ambiphilic moleclues may also lead to the activation of H_2 via homolytic cleavage or heterolytic cleavage depending on the substituent effect.

10.6.2 Hydrogenation mechanism via ambiphilic cooperation

The hypothetically proposed mechanism proceeds in analogy to the one of the FLP systems. Either a concerted mechanism or a stepwise mechanism can be envisioned for the hydrogenations by ambiphilic systems. As show in Figure 10.36, the unsaturated substrate reacts with both of the B-H groups of the intermediate in one step. In

Concerted   Stepwise
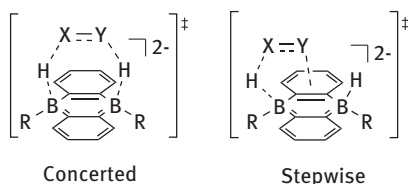
Figure 10.36: Proposed mechanism for hydrogenations catalyzed by ambiphilic systems.

the stepwise mechanism, the unsaturated substrate reacts with one B-H hydride in the first step. Then the conjugated framework is restored upon releasing a proton from the other B-H moiety to the substrate to complete the hydrogenation. However, further experimental and theoretical studies are required to better understand the mechanistic details of the ambiphilic cooperation in the hydrogenation/dehydrogenation reactions.

10.7 TM-TM cooperation mechanism

Homo- and heterobimetallic complexes bearing two TM centers are widely known, and the TM-TM cooperation mechanism is common in the activation of H_2 and hydrogenation reactions. The general hydrogenation/dehydrogenation mechanism for TM-TM cooperation is shown in Figure 10.37. Considering the vast variety of TM-TM systems, three predominate H_2 activation/release mechanisms have been classified: (1) a homolytic mechanism; (2) a heterolytic mechanism, and (3) an oxidative addition mechanism on one site (Figure 10.3f).
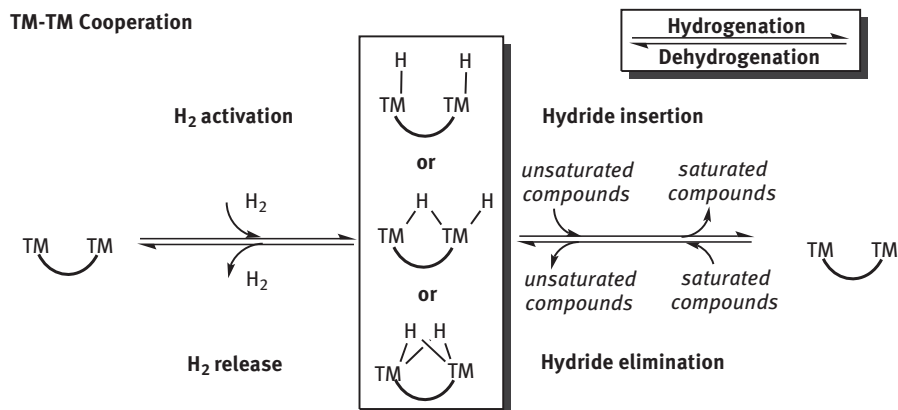
TM-TM Cooperation

Figure 10.37: General hydrogenation/dehydrogenation mechanism for TM-TM cooperation.

10.7.1 Homolytic mechanism via TM-TM cooperation

The homolytic mechanism is considered to be one possible mechanism in the activation of H_2 via TM-TM cooperation (Figure 10.38a). This mechanism is likely to occur within homobimetallic systems, such as porphyrin-Rh^{II} bimetalloradicals, which have been reported by Cui et al. [56]

(a) homolytic mechanism
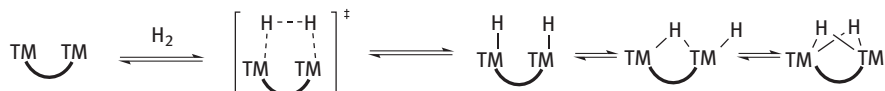
(b) heterolytic mechanism
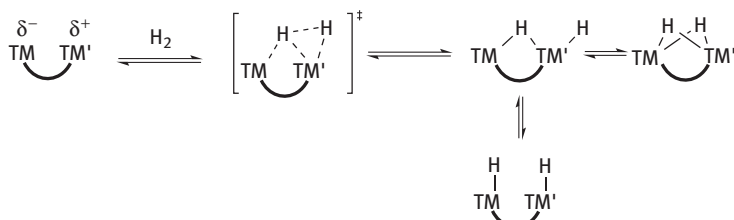
Figure 10.38: (a) Homolytic and (b) heterolytic H_2 activation/release mechanism via TM-TM cooperation.

10.7.2 Heterolytic mechanism via TM-TM cooperation

Compared with the homolytic mechanism, the heterolytic mechanism is more common in the activation of H_2 due to the abundance of heterobimetallic catalysts. In such heterobimetallic systems, one TM center acts as the electron donor, while the other acts as the electron acceptor to cooperatively activate H_2 (Figure 10.38b). Heterobimetallic TM-TM systems usually consist of complexes that contain two different TM atoms. For example, a Cu-Ru system has recently been reported to activate H_2 via a heterolytic mechanism [57], in which the Cu center acts as an LA to accept the H-H σ electrons, and the 4d electrons of Ru donate into the anti-bonding orbital of H_2. However, heterobimetallic TM-TM systems may also contain the same TMs, albeit in different valence states. For example, a heterolytic H_2 bond cleavage has been suggested based on calculated atomic charges in a mixed-valent diiridium complex [58]. Some cases of heterobimetallic TM-TM cooperation are very similar to the LA-TM cooperation, especially when one of the TM centers in the heterobimetallic complex exhibits characteristics of main group metals such as zinc [59].

10.7.3 Oxidative addition mechanism

The oxidative addition mechanism in TM-TM systems is similar to that in classical single-site TM systems. As shown in Figure 10.39, the activation of H_2 via the oxidative addition mechanism has been proposed for Ta-Ir heterobimetallic systems. The oxidative addition of H_2 at the Ir center results in the formation of the dihydride complex Ta-IrH$_2$ [60]. However, it should be noted that although the other TM center is not directly involved in the oxidation addition, it could assist the reaction via electron- or charge-transfer to the reactive TM center.
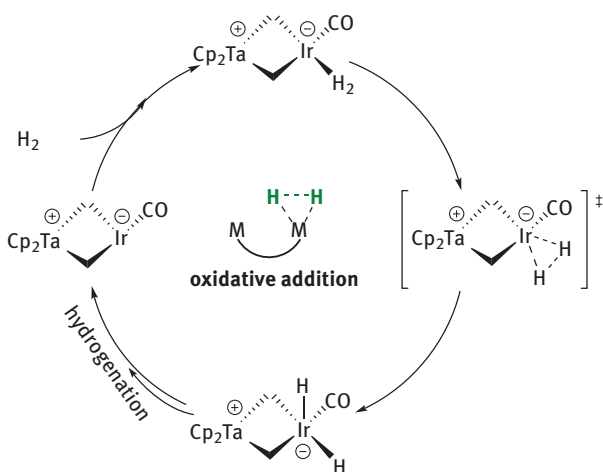
Figure 10.39: Oxidative addition mechanism of TM-TM cooperation system.

10.7.4 Hydrogenation/dehydrogenation mechanism in TM-TM systems

In comparison to the previously discussed activation of H_2, hydrogenation/dehydrogenation mechanisms via TM-TM cooperation are much more complicated. Firstly, the hydride intermediates comprise various isomers due to the flexible coordination on the TM-TM centers. As shown in Figure 10.37, the hydrides can (i) both be located at terminal positions, (ii) at terminal/bridging positions, or (iii) both are located at bridging positions. It should also be noted that the two M-H hydrides can adopt eclipsed, gauche, or staggered conformations with respect to each other, which adds even more structural complexity to the hydride intermediates. Secondly, both TM centers can provide a vacant site for the coordination of the unsaturated bond, which bring more possibility for the inner-sphere mechanism.

Similar to the LA-TM cooperation, hydrogenation/dehydrogenation reactions can proceed via a concerted outer-sphere mechanism (Figure 10.40a). However, different from the outer-sphere mechanism in the LA-TM systems, the TM-TM cooperation may lead to interesting redox processes that could endow one of the M-H moieties with proton reactivity upon reduction of the TM center(s). Accordingly, a concerted transfer of a hydride and a proton could be feasible for the outer-sphere mechanism in TM-TM cooperation systems.

Conversely, in the inner-sphere mechanism, the hydrogenations/dehydrogenations proceed in a stepwise fashion. The inner-sphere mechanisms are actually much more complicated as shown in Figure 10.40b, once the following considerations are taken into account: (1) the isomers of the hydride intermediates; (2) which TM center provides the vacant site for substrate; (3) is the hydride insertion preferred by the terminal hydride or the bridging hydride; (4) the possibility of double activation of the substrate by two TM centers. Moreover, for the subsequent step, σ-bond metathesis, migration/reductive elimination, and protonation mechanisms should be considered. What is certain, however, is that the mechanistic picture discussed here is far from comprehensive. Detailed mechanistic information is scarce in the literature, especially considering the mechanistic complexity of the TM-TM cooperation systems. Further experimental and theoretical studies are consequently highly desirable.

In addition, a dissociative mechanism is also possible for such TM-TM systems. The mechanistic paradigm is shown in Figure 10.40c, and is similar to the cooperative inner-sphere mechanism (Figure 10.40b). An example for a hydrogenation via a dissociative inner-sphere mechanism has been reported for an Ag-Ru cooperation system (Figure 10.41) [61]. The single-site reaction mechanism corresponds to the reaction pathway that the oxidative addition of H_2 occurs predominantly on one TM center as shown in Figure 10.40d. The other TM is either innocent or acts as a redox control partner. Redox control by two TM centers should endow TM-TM cooperation systems with properties that are significantly different from those of other cooperation systems.

(a) outer-sphere concerted hydrogenation mechanism
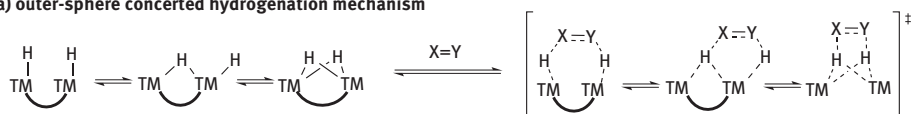
(b) inner-sphere mechanism

σ-bond metatheis

migration/redcutive elimination

protonation

(c) dissociative inner-sphere mechanism

proton shuttle
or
intermolecular

σ-bond metatheis

migration/redcutive elimination

protonation
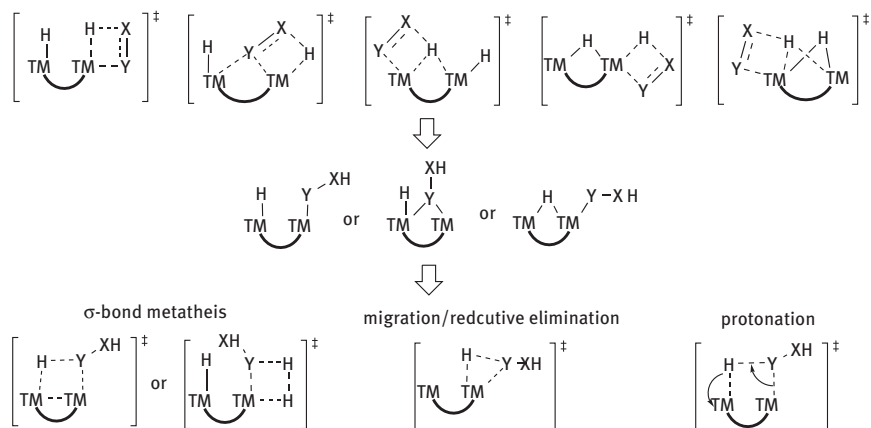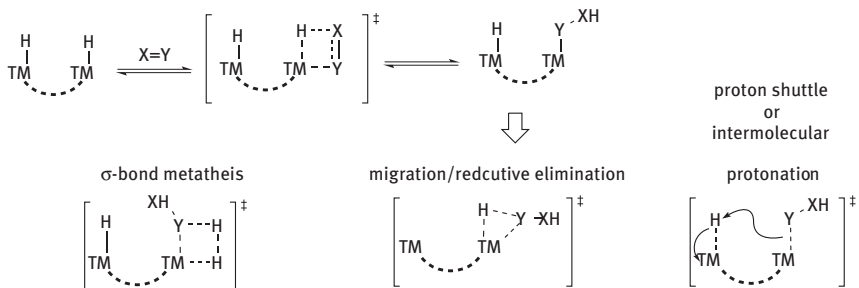
(d) one-stie mechanism
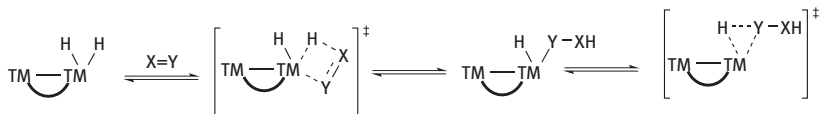
Figure 10.40: General hydrogenation/dehydrogenation mechanism in TM-TM cooperation systems.

Dehydrogenation reactions can be facilitated by the TM-TM cooperative mechanism. Bera et al. have prepared a diruthenium catalyst that is able to catalyze the acceptorless dehydrogenation of alcohols [62]. Using DFT calculations and kinetic
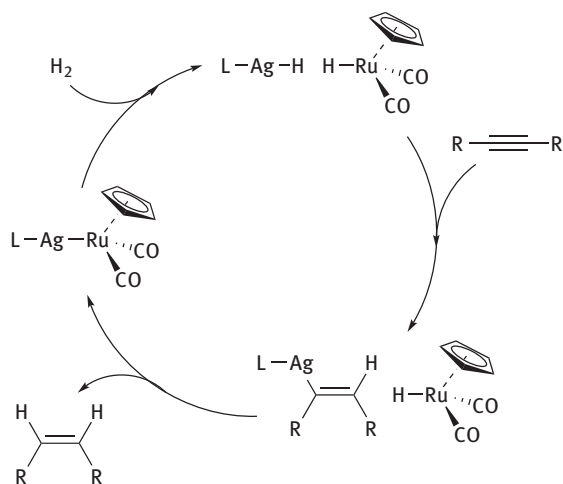
Figure 10.41: Hydrogenation via a dissociative inner-sphere mechanism in the Ag-Ru cooperation system.

isotope effect studies, a TM-TM cooperative mechanism was proposed for the dehydrogenation of these alcohols (Figure 10.42). In the dehydrogenation cycle, the alkoxide species firstly coordinates to the TM center and undergoes a β-hydride elimination, which should furnish the aldehyde. Then, the formed aldehyde will be released and the alcohol substrate will coordinate to the TM center. Then, the hydride abstracts the proton from alcohol to yield H_2, which has been suggested as the rate-determining step based on the results of computational and kinetic isotope effect studies.
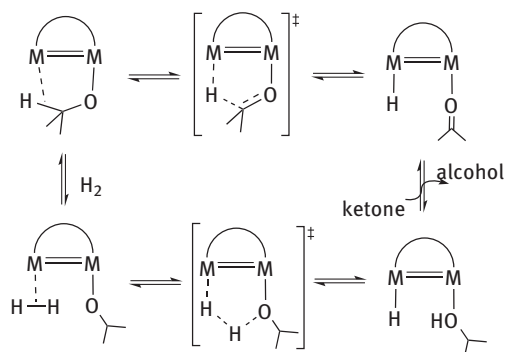
Figure 10.42: The TM-TM cooperative mechanism for dehydrogenation reactions.

10.8 Key factors governing the mechanistic preferences

10.8.1 The role of the metal and the ligand in MLC

The most important factor of the metal center in single-site TM, LB-TM, LA-TM, and TM-TM catalysts for the activation of H_2 is the d-backdonation effect (Figure 10.43). For example, Ke et al. have carried out a computational study on the effect of the
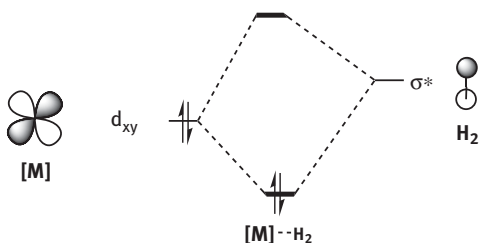
Figure 10.43: The d-backdonation effect.

metal based on Himeda's catalysts (Figure 10.44) [63]. The activity difference among the group 9 TMs (Co, Rh, and Ir) was attributed to their d-backdonation ability. With the TM center changing from Co to Rh and Ir, the energy of the back-donation is increased from 3.56 to 8.42 and 22.24 kcal/mol, respectively. This effect results in the elongation of the H-H bond distance 0.79, 0.80 and 0.85 Å, respectively. This indicates that the metal center have significant d-backdonation effect to the H_2, which explains well the experimentally observed order of activity.

metal	E(2) kcal/mol (dxy-a*)	bond length (Å) H-H
Ir	22.24	0.85
Rh	8.42	0.80
Co	3.56	0.79
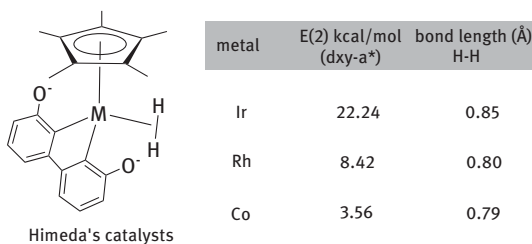
Himeda's catalysts

Figure 10.44: The d-backdonation effect from different TM center for Himeda's catalysts.

The electronic structure of the metal center has also a significant impact on the mechanistic preference of the catalysts. For MLC, a certain geometry is required in order to facilitate the cooperation. For example, an unusual inner-sphere non-MLC mechanism in the Co(II)-PNP system was theoretically investigated by Ke et al. [64] Their results suggested that the conventional MLC mechanism is not operative in this

Co(II)-PNP system, which is consistent with Hanson's experimental observations
[65]. As shown in Figure 10.45, in an MLC process, the metal hydride will be forced
from the *trans* position of the LB to the *cis* position, which leads to a drastic change in
the ligand field. The single filled $d_z{}^2$ orbital of the d^7 Co(II) center will become a strong
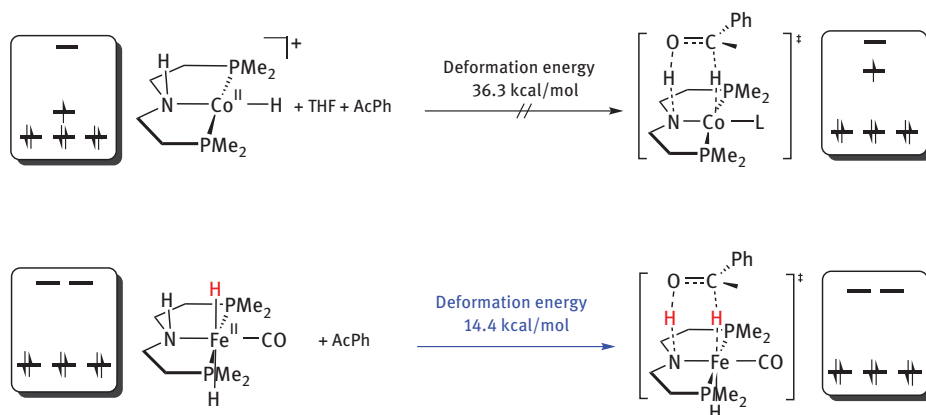
Figure 10.45: The deformation energy penalty due to the change in ligand field from reactant to
transition state for Co(II)-PNP and Fe(II)-PNP systems.

anti-bonding orbital in the transition state, which causes a high deformation energy
penalty (36.3 kcal/mol). In contrast, the Fe(II)-PNP system prefers a bifunctional MLC
mechanism without causing much deformation energy (14.4 kcal/mol). This is due to
the relatively small change of the ligand field of the six-coordinated Fe(II) center from
the reactant to the transition state. The influence of the deformation energy penalty
due to the change in ligand field from reactant to transition state should not only be a
crucial factor for governing mechanistic preferences of LB-TM systems, but also of
LA-TM and TM-TM systems.

Another important factor for the MLC mechanism is the driving force of the ligand
that takes part in the cooperation. When the catalyst operates according to the aroma-
tization/dearomatization mechanism, the driving force is normally provided by the
tautomerization of the pincer ligand. MLC cooperation was reported for PNN-Ru sys-
tems [12]a, [27]. Szymczak observed, however, an inner-sphere non-MLC mechanism in
the NNN-Ru system [33]. DFT studies on the mechanistic preferences (MLC vs inner-
sphere non-MLC) of these two complexes bearing structural similar pincer ligands were
performed by Ke et al. [32, 66] As shown in Figure 10.46, the calculated results indicated
that the NNN-Ru pincer complex chooses the inner-sphere non-MLC mechanism due to
an unfavorable tautomerization on the NNN ligand (anti-aromatic transformation).
Conversely, the PNN-Ru catalyst prefers the MLC mechanism due to the favorable
tautomerization on the PNN ligand (aromatic transformation). The tautomerization
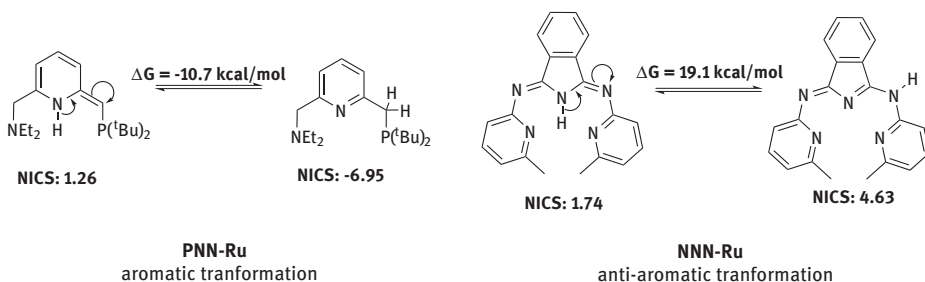
Figure 10.46: The aromatic driving force for the π-type LB-TM cooperation mechanism: (de) aromatization.

driving force of the ligand should thus constitute a general rule to understand the MLC mechanism in order to advance the rational catalyst design based on cooperation strategies.

10.8.2 Proton shuttle

The proton shuttle mechanism refers to a proton transfer mode that involves a bridging molecule (substrate or solvent) to transfer a proton. For example, the outer-sphere bifunctional hydrogenation (six-membered ring) may involve a bridging molecule (highlighted in red in Figure 10.47) as a proton shuttle to form a larger eight-membered ring [67]. This is preferred especially for reactive sites that are remote relative to the metal hydride. Similarly, the deprotonation of the -Y-XH ligand proceeds via a four-membered ring transition state. In the proton shuttle mechanism,
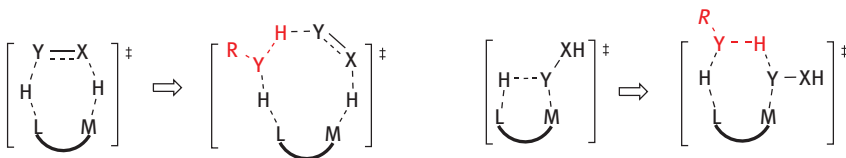
Figure 10.47: The proton shuttle mechanism.

an extra RYH molecule can participate in the proton transfer to form a six-membered ring transition state. However, it should be noted that the proton shuttling mechanism is a double-edged sword: on the positive side, this approach can release high levels of strain and decrease the deformation energy of the transition state, which can lower the activation free energy; on the negative side, this process involves an entropy penalty to incorporate an extra molecule in the transition state. Moreover, an extra molecule as a proton shuttle may cause steric hindrance. These factors should be taken into consideration when evaluating the proton shuttle mechanism.

10.9 Concluding remarks

After several decades of development, the introduction of different cooperation mechanisms as novel strategies has led to a renaissance of homogenously catalyzed hydrogenation and dehydrogenation reactions. This novel cooperation catalysis will play an increasingly important role in the development of efficient, environmentally benign, controllable, and scalable homogeneous hydrogenation/dehydrogenation systems that may help to solve challenging synthetic problems as well as problems associated with energy supply and environmental impact.

Firstly, the synergetic effect via cooperation mechanisms should be helpful to advance the catalyst development by replacing precious metals with non-precious metals. Moreover, metal-free catalyst can be envisioned to eventually replace metal catalysts for homogeneous hydrogenation/dehydrogenation reactions. Secondly, novel cooperation mechanisms may capitalize from the combination of reactive sites, which should enrich the toolbox for catalyst design, allow expanding reaction scopes, and thus improve the chemoselectivity, regioselectivity, and enantioselectivity of hydrogenation/dehydrogenation reactions.

The mechanistic paradigms in this chapter have covered state-of-the-art of homogeneous cooperation catalysts for hydrogenation/dehydrogenation reactions. Among them, the MLC mechanisms for LB-TM systems are relatively well studied. Many mechanistic variations have been proposed or documented by experimental and computational studies. More efforts should focus on earth-abundant TM centers for industrial applications. In contrast, the LA-TM cooperation mechanisms are not well explored. In LA-TM systems, the LA accepts an electron pair and the TM donates electron(s) cooperatively, which should allow to access new types of transformations and new reactive intermediates for bifunctional catalysis. The exploration of new types of reactivity and hydrogenation/dehydrogenation applications are highly desirable. For the metal-free LA-LB mechanism, a substantial body of information has been obtained due to extensive work on FLP-catalyzed reactions. However, the development of FLP protocols for (de)hydrogenations with low catalyst loadings, broad functional group tolerance, and high levels of selectivity remain to be addressed. The recently emerged mechanism for ambiphilic cooperative hydrogenations/dehydrogenations still requires substantial investigation, especially in the context of hydrogenations/dehydrogenations or the electrocatalytic use of H_2.

Rational catalyst design is crucial to achieve high activity and selectivity. The understanding of mechanistic paradigms should be used to systematically study important factors in catalyzed hydrogenation and dehydrogenation reactions in order to establish relationships between structural factors and activity/selectivity. With increase of computational ability and accuracy, theoretical methods may offer valuable information on mechanisms and important factors that govern catalytic preferences. Together with the efforts of experimental and computational studies, the mechanistic understanding should thus continue to contribute to the development of

novel strategies and reactivity modes for the design of homogeneous catalysts for hydrogenation and dehydrogenation reactions.

References

[1]   (a) De Vries JG, Elsevier CJ. The handbook of homogeneous hydrogenation. Weinheim: Wiley-VCH, 2007; (b) Sanfilippo D, Rylander PN. in Ullmann's Encyclopedia of Industrial Chemistry, 2009.

[2]   Calvin M. Homogeneous Catalytic Hydrogenation. Trans Faraday Soc 1938;34:1181–91.

[3]   (a) Crabtree RH, Felkin H, Morris GE. Cationic iridium diolefin complexes as alkene hydrogenation catalysts and the isolation of some related hydrido complexes. 1977;141:205–15; (b) Hoveyda AH, Evans DA, Fu GC. Substrate-directable chemical reactions. Chem Rev. 1993;93:1307–70.

[4]   (a) Knowles WS, Sabacky MJ. Catalytic asymmetric hydrogenation employing a soluble, optically active, rhodium complex. Chem Commun. 1968;0:1445–46; (b) Knowles WS, Sabacky MJ, Vineyard BD, Weinkauff DJ. Asymmetric hydrogenation with a complex of rhodium and a chiral bisphosphine. J Am Chem Soc. 1975;97:2567–68; (c) Horner L, Siegel H, Büthe H. Asymmetric Catalytic Hydrogenation with an Optically Active Phosphinerhodium Complex in Homogeneous Solution. Angew Chem, Int Ed. 1968;7:942–42; (d) Miyashita A, Yasuda A, Takaya H, Toriumi K, Ito T, Souchi T, Noyori R. Synthesis of 2,2'-Bis(diphenylphosphino)-1,1'-binaphthyl (BINAP), an Atropisomeric Chiral Bis(triaryl)phosphine, and Its Use in the Rhodium(I)- Catalyzed Asymmetric Hydrogenation of a-(Acylamino)acrylic Acids,. J Am Chem Soc. 1980;102:7932–34.

[5]   Noyori R, Yamakawa M, Hashiguchi S. Metal-ligand bifunctional catalysis: A nonclassical mechanism for asymmetric hydrogen transfer between alcohols and carbonyl compounds. J Org Chem 2001;66:7931–44.

[6]   Pimentel D, Hurd LE, Bellotti AC, Forster MJ, Oka IN, Sholes OD, et al. Whitman, R. J. Food production and the energy crisis. Science 1973;182:443–49.

[7]   Barreto L, Makihira A, Riahi K. The hydrogen economy in the 21st century: a sustainable development scenario. Int J Hydrogen Energy 2003;28:267–84.

[8]   Eberle U, Felderhoff M, Schüth F. Chemical and Physical Solutions for Hydrogen Storage. Angew Chem, Int Ed 2009;48:6608–30.

[9]   Osborn JA, Wilkinson G, Mrowca JJ. in Inorg Synth. John Wiley & Sons, Inc., 2007: 67–71.

[10]   Hutschka F, Dedieu A, Eichberger M, Fornika R, Leitner W. Mechanistic Aspects of the Rhodium-Catalyzed Hydrogenation of CO2 to Formic AcidA Theoretical and Kinetic Study. J Am Chem Soc 1997;119:4432–43.

[11]   Musashi Y, Sakaki S. Theoretical Study of Rhodium(III)-Catalyzed Hydrogenation of Carbon Dioxide into Formic Acid. Significant Differences in Reactivity among Rhodium(III), Rhodium(I), and Ruthenium(II) Complexes. J Am Chem Soc 2002;124:7588–603.

[12]   (a) Gunanathan C, Milstein D. Metal–Ligand Cooperation by Aromatization–Dearomatization: A New Paradigm in Bond Activation and "Green" Catalysis. Acc Chem Res 2011;44:588–602; (b) Khusnutdinova JR, Milstein D. Metal-Ligand Cooperation. l Angew Chem Int Ed Engl. 54:12236–73; (c) Werkmeister S, Neumann J, Junge K, Beller M. Pincer–Type Complexes for

Catalytic (De)Hydrogenation and Transfer (De)Hydrogenation Reactions: Recent Progress. Chem Eur J. 2015;21:12226–50.

[13] Noyori R, Kitamura M, Ohkuma T. Toward efficient asymmetric hydrogenation: Architectural and functional engineering of chiral molecular catalysts. Proc Natl Acad Sci U S A 2004;101:5356–62.

[14] (a) Noyori R, Hashiguchi S. Asymmetric Transfer Hydrogenation Catalyzed by Chiral Ruthenium Complexes. Acc Chem Res. 1997;30:97–102; (b) Noyori R, Ohkuma T. Asymmetric Catalysis by Architectural and Functional Molecular Engineering: Practical Chemo- and Stereoselective Hydrogenation of Ketones. Angew Chem, Int Ed. 2001;40:40–73; (c) Phillips SD, Fuentes JA, Clarke ML. On the NH Effect in Ruthenium-Catalysed Hydrogenation of Ketones: Rational Design of Phosphine-Amino-Alcohol Ligands for Asymmetric Hydrogenation of Ketones. Chem Eur J. 2010;16:8002–5.

[15] Morris RH. Exploiting Metal-Ligand Bifunctional Reactions in the Design of Iron Asymmetric Hydrogenation Catalysts. Acc Chem Res. 2015;48:1494–502.

[16] Prokopchuk DE, Morris RH. Inner-Sphere Activation, Outer-Sphere Catalysis: Theoretical Study on the Mechanism of Transfer Hydrogenation of Ketones Using Iron(II) PNNP Eneamido Complexes. Organometallics. 2012;31:7375–85.

[17] Zuo WW, Lough AJ, Li YF, Morris RH. Amine(imine)diphosphine Iron Catalysts for Asymmetric Transfer Hydrogenation of Ketones and Imines. Science 2013;342:1080–83.

[18] Alberico E, Lennox AJJ, Vogt LK, Jiao HJ, Baumann W, Drexler HJ, et al. Unravelling the Mechanism of Basic Aqueous Methanol Dehydrogenation Catalyzed by Ru-PNP Pincer Complexes. J Am Chem Soc. 2016;138:14890–904.

[19] (a) O'Hagan M, Shaw WJ, Raugei S, Chen ST, Yang JY, Kilgore UJ, et al. Moving Protons with Pendant Amines: Proton Mobility in a Nickel Catalyst for Oxidation of Hydrogen. J Am Chem Soc. 2011;133:14301–12; (b) Ho MH, O'Hagan M, Dupuis M, DuBois DL, Bullock RM, Shaw WJ, Raugei S. Water-assisted proton delivery and removal in bio-inspired hydrogen production catalysts. Dalton Trans. 2015;44:10969–79.

[20] Chen XY, Ge HY, Yang XZ. Newly designed manganese and cobalt complexes with pendant amines for the hydrogenation of CO2 to methanol: a DFT study. Catalysis Sci Technol. 2017;7:348–55.

[21] Zeng M, Li L, Herzon SB. A Highly Active and Air-Stable Ruthenium Complex for the Ambient Temperature Anti-Markovnikov Reductive Hydration of Terminal Alkynes. J Am Chem Soc. 2014;136:7058–67.

[22] Gao H, Chen L, Chen J, Guo Y, Ye D. A computational study on the hydrogenation of CO2 catalyzed by a tetraphos-ligated cobalt complex: monohydride vs. dihydride. Catalysis Sci Technol. 2015;5:1006–13.

[23] Urakawa A, Jutz F, Laurenczy G, Baiker A. Carbon dioxide hydrogenation catalyzed by a ruthenium dihydride: A DFT and high-pressure spectroscopic investigation. Chem-Eur J. 2007;13:3886–99.

[24] Marcos R, Xue L, Sánchez-de-Armas R, Ahlquist MSG. Bicarbonate Hydrogenation Catalyzed by Iron: How the Choice of Solvent Can Reverse the Reaction. ACS Catal. 2016;6:2923–29.

[25] Zhang J, Leitus G, Ben-David Y, Milstein D. Facile conversion of alcohols into esters and dihydrogen catalyzed by new ruthenium complexes. J Am Chem Soc. 2005;127:10840–41.

[26] Poverenov E, Gandelman M, Shimon LJW, Rozenberg H, Ben-David Y, Milstein D. Pincer "Hemilabile" Effect. PCN Platinum(II) Complexes with Different Amine "Arm Length". Organometallics. 2005;24:1082–90.

[27] Li H, Wang X, Huang F, Lu G, Jiang J, Wang Z-X. Computational Study on the Catalytic Role of Pincer Ruthenium(II)-PNN Complex in Directly Synthesizing Amide from Alcohol and Amine: The Origin of Selectivity of Amide over Ester and Imine. Organometallics. 2011;30:5233–47.

[28] Sandhya KS, Suresh CH. Autotandem Aromatization–Dearomatization Pathways for PNP–RuII–Catalyzed Formation of Imine and Hydrogen from Alcohol and Amine. Organometallics. 2013;32:2926–33.

[29] (a) Conley BL, Pennington-Boggio MK, Boz E, Williams TJ. Discovery, Applications, and Catalytic Mechanisms of Shvo's Catalyst. Chem Rev 2010;110:2294–312; (b) Karvembu R, Prabhakaran R, Natarajan K. Shvo's diruthenium complex: a robust catalyst. Coord Chem Rev. 2005;249:911–8.

[30] Casey CP, Guan HR. Cyclopentadienone Iron Alcohol Complexes: Synthesis, Reactivity, and Implications for the Mechanism of Iron-Catalyzed Hydrogenation of Aldehydes. J Am Chem Soc. 2009;131:2499–507.

[31] (a) Lu X, Zhang Y, Turner N, Zhang M, Li T. Using computational methods to explore improvements to Knolker's iron catalyst. Org Biomol Chem. 2014;12:4361–71; (b) Lu X, Cheng R, Turner N, Liu Q, Zhang M, Sun X. High Chemoselectivity of an Advanced Iron Catalyst for the Hydrogenation of Aldehydes with Isolated C=C Bond: A Computational Study. J Organic Chem. 2014;79:9355–64.

[32] Hou C, Zhang Z, Zhao C, Ke Z. DFT Study of Acceptorless Alcohol Dehydrogenation Mediated by Ruthenium Pincer Complexes: Ligand Tautomerization Governing Metal Ligand Cooperation. Inorg Chem. 2016;55:6539–51.

[33] Tseng K-NT, Kampf JW, Szymczak NK. Mechanism of N,N,N-Amide Ruthenium(II) Hydride Mediated Acceptorless Alcohol Dehydrogenation: Inner-Sphere ß-H Elimination versus Outer-Sphere Bifunctional Metal–Ligand Cooperativity. ACS Catal. 2015;5:5468–85.

[34] (a) Inagaki F, Matsumoto C, Okada Y, Maruyama N, Mukai C. Air-Stable Cationic Gold(I) Catalyst Featuring a Z-Type Ligand: Promoting Enyne Cyclizations. Angew Chem, Int Ed. 2015;54:818–22; (b) Amgoune A, Bourissou D. sigma-Acceptor, Z-type ligands for transition metals. Chem Commun. 2011;47:859–71; (c) Braunschweig H, Dewhurst RD. Transition metals as Lewis bases: "Z-type" boron ligands and metal-to-boron dative bonding. Dalton Trans. 2011;40:549–58.

[35] (a) Nesbit MA, Suess DLM, Peters JC. E-H Bond Activations and Hydrosilylation Catalysis with Iron and Cobalt Metalloboranes. Organometallics. 2015;34:4741–52; (b) Devillard M, Bouhadir G, Bourissou D. Cooperation between Transition Metals and Lewis Acids: A Way To Activate H-2 and H-E bonds. Angew Chem, Int Ed. 2015;54:730–32; (c) MacMillan SN, Harman WH, Peters JC. Facile Si-H bond activation and hydrosilylation catalysis mediated by a nickel-borane complex. Chem Sci. 2014;5:590–97; (d) Tanoue K, Yamashita M. Synthesis of Pincer Iridium Complexes Bearing a Boron Atom and Pr-i-Substituted Phosphorus Atoms: Application to Catalytic Transfer Dehydrogenation of Alkanes. Organometallics. 2015;34:4011–17; (e) Kwan EH, Kawai YJ, Kamakura S, Yamashita M. A long-tethered (P-B-P)-pincer ligand: synthesis, complexation, and application to catalytic dehydrogenation of alkanes. Dalton Trans. 2016;45:15931–41.

[36] Fong H, Moret ME, Lee Y, Peters JC. Heterolytic H-2 Cleavage and Catalytic Hydrogenation by an Iron Metallaboratrane. Organometallics. 2013;32:3053–62.

[37] Lin TP, Peters JC. Boryl-Mediated Reversible H-2 Activation at Cobalt: Catalytic Hydrogenation, Dehydrogenation, and Transfer Hydrogenation. J Am Chem Soc. 2013;135:15310–13.

[38] Harman WH, Peters JC. Reversible H-2 Addition across a Nickel-Borane Unit as a Promising Strategy for Catalysis. J Am Chem Soc. 2012;134:5080–82.

[39] Schindler T, Lux M, Peters M, Scharf LT, Osseili H, Maron L, et al. Synthesis and Reactivity of Palladium Complexes Featuring a Diphosphinoborane Ligand. Organometallics. 2015;34:1978–84.

[40] Barnett BR, Moore CE, Rheingold AL, Figueroa JS. Cooperative Transition Metal/Lewis Acid Bond-Activation Reactions by a Bidentate (Boryl)iminomethane Complex: A Significant Metal-Borane Interaction Promoted by a Small Bite-Angle LZ Chelate. J Am Chem Soc. 2014;136:10262–65.

[41] (a) Owen GR. Functional group migrations between boron and metal centres within transition metal-borane and -boryl complexes and cleavage of H-H, E-H and E-E' bonds. Chem Commun. 2016;52:10712–26; (b) Bouhadir G, Bourissou D. Complexes of ambiphilic ligands: reactivity and catalytic applications. Chem Soc Rev. 2016;45:1065–79; (c) Li Y, Zhang J, Shu S, Shao Y, Liu Y, Ke Z. Boron-based Lewis Acid Transition Metal Complexes as Potential Bifunctional Catalysts. Chin J Org Chem. 2017;0:0–0.

[42] Li YW, Hou C, Jiang JX, Zhang ZH, Zhao CY, Page AJ, et al. General H-2 Activation Modes for Lewis Acid-Transition Metal Bifunctional Catalysts. ACS Catal. 2016;6:1655–62.

[43] Toure M, Chuzel O, Parrain J-L. Synthesis and structure of Ag(I), Pd(II), Rh(I), Ru(II) and Au(I) NHC-complexes with a pendant Lewis acidic boronic ester moiety. Dalton Trans. 2015;44:7139–43.

[44] Forrest SJK, Clifton J, Fey N, Pringle PG, Sparkes HA, Wass DF. Cooperative Lewis Pairs Based on Late Transition Metals: Activation of Small Molecules by Platinum(0) and B(C6F5)(3). Angew Chem, Int Ed. 2015;54:2223–27.

[45] Ganguly G, Malakar T, Paul A. Theoretical Studies on the Mechanism of Homogeneous Catalytic Olefin Hydrogenation and Amine-Borane Dehydrogenation by a Versatile Boryl-Ligand-Based Cobalt Catalyst. ACS Catal. 2015;5:2754–69.

[46] (a) Xu BH, Kehr G, Frohlich R, Wibbeling B, Schirmer B, Grimme S, et al. Reaction of Frustrated Lewis Pairs with Conjugated Ynones-Selective Hydrogenation of the Carbon-Carbon Triple Bond. Angew Chem, Int Ed. 2011;50:7183–6; (b) Welch GC, Juan RRS, Masuda JD, Stephan DW. Reversible, metal-free hydrogen activation. Science. 2006;314:1124–6; (c) Spies P, Schwendemann S, Lange S, Kehr G, Frohlich R, Erker G. Metal-free catalytic hydrogenation of enamines, imines, and conjugated phosphinoalkenylboranes. Angew Chem, Int Ed. 2008;47:7543–6; (d) Greb L, Ona-Burgos P, Schirmer B, Grimme S, Stephan DW, Paradies J. Metal-free Catalytic Olefin Hydrogenation: Low-Temperature H2 Activation by Frustrated Lewis Pairs. Angew Chem, Int Ed. 2012;51:10164–8; (e) Chase PA, Welch GC, Jurca T, Stephan DW. Metal-free catalytic hydrogenation. Angew Chem, Int Ed. 2007;46:8050–3.

[47] (a) Stephan DW, Erker G. Frustrated Lewis pairs: metal-free hydrogen activation and more. Angew Chem Int Ed Engl. 2010;49:46–76; (b) Stephan DW. Frustrated Lewis pairs: from concept to catalysis. Acc Chem Res. 2015;48:306–16; (c) Erker G, Stephan DW. Frustrated Lewis Pairs I Uncovering and Understanding. 2013:332.

[48] (a) Chase PA, Welch GC, Jurca T, Stephan DW. Metal-Free Catalytic Hydrogenation. Angewandte Chemie. 2007;119:8196–9; (b) Sumerin V, Schulz F, Nieger M, Leskelä M, Repo T, Rieger B. Einfache heterolytische H2-Aktivierung mit Aminen und B(C6F5)3. Angew Chem. 2008;120:6090–2; (c) Momming CM, Fromel S, Kehr G, Frohlich R, Grimme S, Erker G. Reactions of an intramolecular frustrated Lewis pair with unsaturated substrates: evidence for a concerted olefin addition reaction. J Am Chem Soc. 2009;131:12280–9.

[49] (a) Hamza A, Stirling A, Rokob TA, Papai I. Mechanism of Hydrogen Activation by Frustrated Lewis Pairs: A Molecular Orbital Approach. Int J Quantum Chem. 2009;109:2416–25; (b) Paradies J. Metal-free hydrogenation of unsaturated hydrocarbons employing molecular hydrogen. Angew Chem Int Ed Engl. 2014;53:3552–57; (c) Rokob TA, Papai I. Hydrogen activation by frustrated lewis pairs: insights from computational studies. Top Curr Chem. 2013;332:157–211.

[50] (a) Rokob TA, Hamza A, Stirling A, Papai I. On the mechanism of B(C6F5)3-catalyzed direct hydrogenation of imines: inherent and thermally induced frustration. J Am Chem Soc. 2009;131:2029–36; (b) Rokob TA, Hamza A, Stirling A, Soós T, Pápai I. Turning Frustration into Bond Activation: A Theoretical Mechanistic Study on Heterolytic Hydrogen Splitting by Frustrated Lewis Pairs. Angew Chem. 2008;120:2469–72; (c) Schirmer B, Grimme S. Electric field induced activation of H2–can DFT do the job?. Chem Commun (Camb) 2010;46:7942–44; (d) Grimme S, Kruse H, Goerigk L, Erker G. The mechanism of dihydrogen activation by frustrated lewis pairs revisited. Angew Chem Int Ed Engl. 2010;49:1402–05.

[51] Chase PA, Jurca T, Stephan DW. Lewis acid-catalyzed hydrogenation: B(C6F5)3-mediated reduction of imines and nitriles with H2. Chem Commun. 2008;0:1701–3.

[52] (a) Spikes GH, Fettinger JC, Power PP. Facile activation of dihydrogen by an unsaturated heavier main group compound. J Am Chem Soc. 2005;127:12232–33; (b) von Grotthuss E, Diefenbach M, Bolte M, Lerner HW, Holthausen MC, Wagner M. Reversible Dihydrogen Activation by Reduced Aryl Boranes as Main-Group Ambiphiles. Angew Chem, Int Ed. 2016;55:14067–71.

[53] (a) Peng Y, Brynda M, Ellis BD, Fettinger JC, Rivard E, Power PP. Addition of H(2) to distannynes under ambient conditions. Chem Commun. 2008;0:6042–44; (b) Hadlington TJ, Hermann M, Li JY, Frenking G, Jones C. Activation of H-2 by a Multiply Bonded Amido-Digermyne: Evidence for the Formation of a Hydrido-Germylene. Angew Chem, Int Ed. 2013;52:10199–203.

[54] (a) Liu L, Chan CL, Zhu J, Cheng CH, Zhao YF. Stability, Reactivity, Selectivity, Catalysis, and Predictions of 1,3,2,5-Diazadiborinine: Computational Insight into a Boron-Boron Frustrated Lewis Pair. J Org Chem. 2015;80:8790–95; (b) Wu D, Ganguly R, Li YX, Hoo SN, Hirao H, Kinjo R. Reversible [4+2] cycloaddition reaction of 1,3,2,5-diazadiborinine with ethylene. Chemical Science. 2015;6:7150–55; (c) Wu D, Kong LB, Li YX, Ganguly R, Kinjo R. 1,3,2,5-Diazadiborinine featuring nucleophilic and electrophilic boron centres. Nature Commun. 2015;6; (d) Wang BL, Li YX, Ganguly R, Hirao H, Kinjo R. Ambiphilic boron in 1,4,2,5-diazadiborinine. Nature Commun. 2016;7.

[55] Wendel D, Szilvasi T, Jandl C, Inoue S, Rieger B. Twist of a Silicon-Silicon Double Bond: Selective Anti-Addition of Hydrogen to an Iminodisilene. J Am Chem Soc. 2017;139:9156–59.

[56] Cui W, Wayland BB. Activation of C-H/H-H Bonds by Rhodium(II) Porphyrin Bimetalloradicals. J Am Chem Soc. 2004;126:8266–74.

[57] Karunananda MK, Mankad NP. Heterobimetallic H2 Addition and Alkene/Alkane Elimination Reactions Related to the Mechanism of E-Selective Alkyne Semihydrogenation. Organometallics. 2017;36:220–27.

[58] Gray TG, Veige AS, Nocera DG. Cooperative Bimetallic Reactivity: Hydrogen Activation in Two-Electron Mixed-Valence Compounds. J Am Chem Soc. 2004;126:9760–68.

[59] Riddlestone IM, Rajabi NA, Lowe JP, Mahon MF, Macgregor SA, Whittlesey MK. Activation of H2 over the Ru-Zn Bond in the Transition Metal-Lewis Acid Heterobimetallic Species [Ru(IPr)2(CO) ZnEt]+ J Am Chem Soc. 2016;138:11081–84.

[60] (a) Hostetler MJ, Bergman RG. Synthesis and reactivity of Cp2Ta(CH2)2Ir(CO)2: an early–late heterobimetallic complex that catalytically hydrogenates. J Am Chem Soc. 1990;112:8621–23; (b) Zhang Y, Roberts SP, Bergman RG, Ess‡ DH. Mechanism and Catalytic Impact of Ir–Ta Heterobimetallic and Ir–P Transition Metal/Main Group Interactions on Alkene Hydrogenation. ACS Catal. 2015;5:1840–49.

[61] Karunananda MK, Mankad NP. E-Selective Semi-Hydrogenation of Alkynes by Heterobimetallic Catalysis. J Am Chem Soc. 2015;137:14598–601.

[62] Dutta I, Sarbajna A, Pandey P, Rahaman SMW, Singh K, Bera JK. Acceptorless Dehydrogenation of Alcohols on a Diruthenium(II,II) Platform. Organometallics. 2016;35:1505–13

[63] Hou C, Jiang J, Zhang S, Wang G, Zhang Z, Ke Z, et al. Hydrogenation of Carbon Dioxide Using Half-Sandwich Cobalt, Rhodium, and Iridium Complexes: DFT Study on the Mechanism and Metal Effect. ACS Catal. 2014;4:2990–97.

[64] Hou C, Jiang J, Li Y, Zhang Z, Zhao C, Ke Z. Unusual non-bifunctional mechanism for Co-PNP complex catalyzed transfer hydrogenation governed by the electronic configuration of metal center. Dalton Trans. 2015;44:16573–85.

[65] Zhang G, Hanson SK. Cobalt-catalyzed transfer hydrogenation of C=O and C=N bonds. Chem Commun. 2013;49:10151–53.

[66] Hou C, Jiang J, Li Y, Zhao C, Ke Z. When Bifunctional Catalyst Encounters Dual MLC Modes: DFT Study on the Mechanistic Preference in Ru-PNNH Pincer Complex Catalyzed Dehydrogenative Coupling Reaction. ACS Catal. 2016;7:786–95.

[67] Qu S, Dang Y, Song C, Wen M, Huang K-W, Wang Z-X. Catalytic Mechanisms of Direct Pyrrole Synthesis via Dehydrogenative Coupling Mediated by PNP-Ir or PNN-Ru Pincer Complexes: Crucial Role of Proton-Transfer Shuttles in the PNP-Ir System. J Am Chem Soc 2014;136:4974–91.

Index